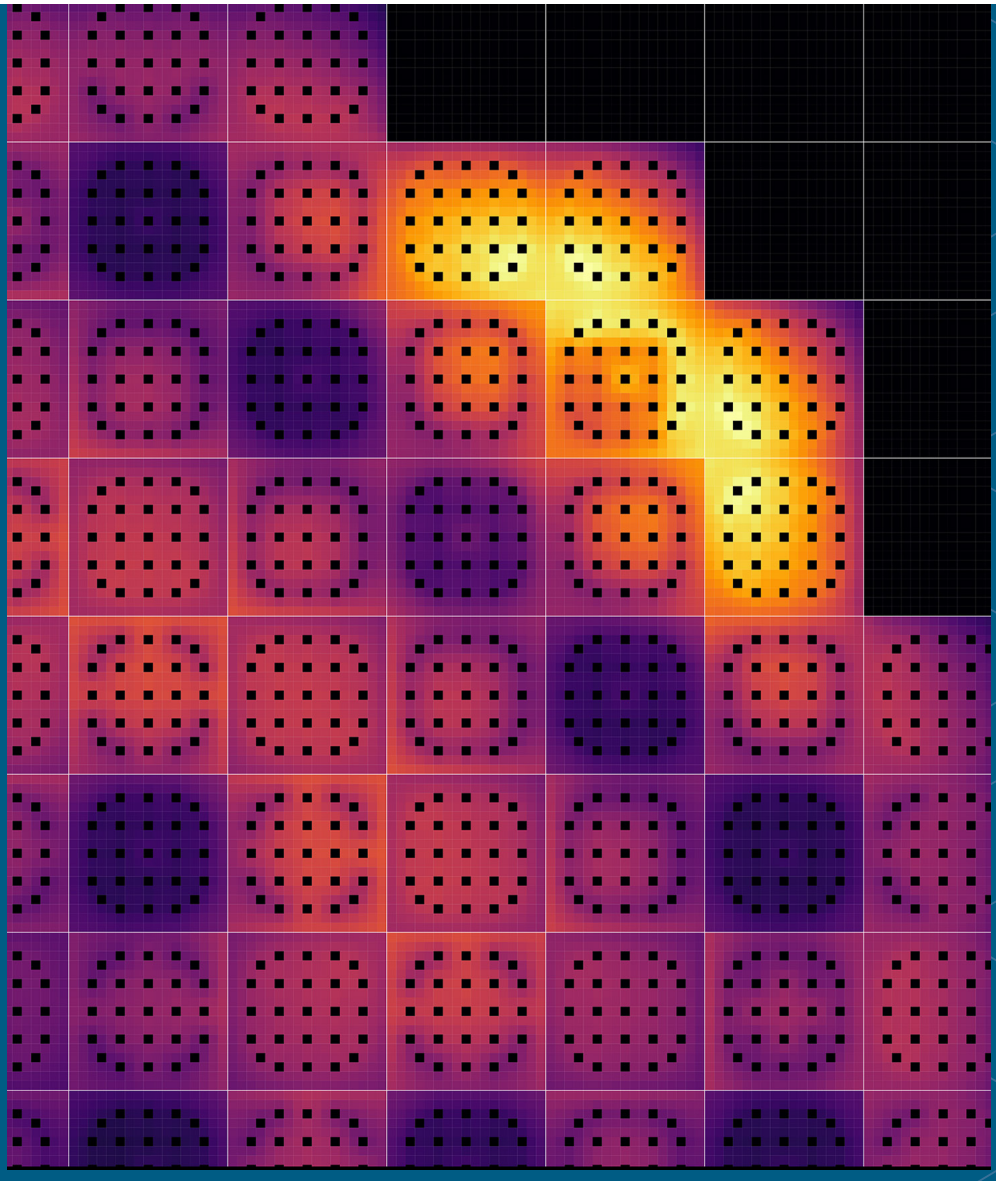

VTT

beyond
the obvious

SAFIR2022 – The Finnish Research Programme on Nuclear Power Plant Safety 2019–2022

Interim Report

Jari Hämäläinen | Vesa Suolanen (eds.)

VTT TECHNOLOGY 383

VTT TECHNOLOGY 383

SAFIR2022 – The Finnish Research Programme on Nuclear Power Plant Safety 2019–2022

Interim Report

Jari Hämäläinen & Vesa Suolanen (eds.)

VTT

ISBN 978-951-38-8743-8

VTT Technology 383

ISSN-L 2242-1211
ISSN 2242-122X (Online)
DOI: 10.32040/2242-122X.2021.T383

JULKAISIJA – PUBLISHER

VTT
PL 1000
02044 VTT
Puh. 020 722 111
https://www.vtt.fi

VTT
P.O. Box 1000
FI-02044 VTT, Finland
Tel. +358 20 722 111
https://www.vttresearch.com

Preface

The Finnish Research Programme on Nuclear Power Plant Safety 2019–2022, SAFIR2022, continues a series of Finnish national research programmes in nuclear energy that started in 1989. The programmes were initially carried out separately in the fields of operational aspects of safety (YKÄ 1990–1994, RETU 1995–1998) and structural safety (RATU 1990–1994, RATU2 1995–1998, OHA 1995–1998), and then in combined programmes (FINNUS 1999–2002, SAFIR2003–2006, SAFIR2010 2007–2010, SAFIR2014 2011–2014, SAFIR2018 2015–2018). Simultaneously research has been carried out in the national nuclear waste management programmes (KYT2022 runs in parallel with SAFIR2022).

SAFIR2022 consists of four main research areas: (1) Overall safety and systemic approach to safety; (2) Reactor safety; (3) Structural safety and materials; and (4) Research infrastructure. Research has been carried out in 36 projects that are guided by eight reference groups. The research results of the projects are published in scientific journals, conference papers and research reports.

The programme management structure consists of the Management Board, four steering groups managing the research areas, eight reference groups, and programme administration. SAFIR2022 Management Board has representatives of the Radiation and Nuclear Safety Authority (STUK), the Ministry of Economic Affairs and Employment (MEAE), Fennovoima Oy, Fortum, Teollisuuden Voima Oyj (TVO), Technical Research Centre of Finland Ltd (VTT), Lappeenranta-Lahti University of Technology (LUT), Aalto University (Aalto), Tampere University (TAU) and the Swedish Radiation Safety Authority (SSM).

Research in the programme has been carried out by VTT, LUT, Aalto, Finnish Meteorological Institute (FMI), Finnish Institute of Occupational Health (FIOH), TAU and RISE Research Institutes of Sweden. A few subcontractors have also contributed to the work in the projects.

This report has been prepared by the programme management in cooperation with the project leaders and project staff.

More information on SAFIR2022 can be found on the programme website http://safir2022.vtt.fi

Contents

1. Introduction

In accordance of the Finnish Nuclear Energy Act, the objective of SAFIR2022 National Nuclear Power Plant Safety Research programme 2019-2022 is to ensure that should new matters related to the safe use of nuclear power plants arise, the authorities possess sufficient technical expertise and other competence required for rapidly determining the significance of the matters.

National research programmes on nuclear safety have had a significant role in the maintenance of expertise and the training of new experts. Since 1990 the programmes (YKÄ & RATU 1990–1994, RETU&RATU2 1995–1998, OHA 1995-1998, FINNUS 1999–2002, SAFIR 2003–2006, SAFIR2010 2007–2010, SAFIR2014 2011-2014 and SAFIR2018 2015-2018) have had a total volume of 172 M€ and 1374 person years.

The total volume of the SAFIR2022 programme has been 6,8 M€ (46 person years) and 6,4 M€ (43 person years) in 2019 and 2020, respectively. The main funding organisations during 2019-2020 were the Finnish State Waste Management Fund (VYR) with 8,6 M€ and the Technical Research Centre of Finland Ltd (VTT) with 2,6 M€. Research has been carried out in 36 projects. The results are utilised by the Radiation and Nuclear Safety Authority (STUK), Teollisuuden Voima Oyj (TVO), Fortum, Fennovoima Oy and the Swedish Radiation Safety Authority (SSM), in addition to the research organisations carrying out the projects. However, international co-operation is involved in most of the projects and thus the results are also more widely utilised.

VYR funding is collected from the Finnish utilities Fennovoima, Fortum and TVO based on their MWth shares in Finnish nuclear power plants (units in operation, under construction, and in planning phase according to the decisions-in-principle). In addition to VYR and VTT, other key organisations operating in the area of nuclear safety also fund the programme.

SAFIR2022 Management Board was nominated in August 2018. It consisted of representatives of STUK, the Ministry of Economic Affairs and Employment (MEAE), Fennovoima, Fortum, TVO, VTT, Aalto University (Aalto), Lappeenranta-Lahti University of Technology (LUT). In 2019 the Management Board was completed with a representative of SSM.

SAFIR2022 has four main research areas that are managed by *the steering groups* (SG1-SG4): SG1 Overall safety and systemic approach to safety, SG2 Reactor safety, SG3 Structural safety and materials and SG4 Research infrastructure

(see http://safir2022.vtt.fi/ and [3]). The research areas were defined in the SAFIR2022 Framework plan [1] as follows.

The *Overall safety and systemic approach to safety* (SG1) collects a wide range of nuclear safety research areas that overarch between several topics, as well as topics affecting the nuclear power plant as a whole. Such topics include the concept of overall safety itself, organisational issues, automation architecture, control room design and operations, human factors, external hazards, safety and security interfaces, electrical systems, setting the safety requirements, and controlling the plant design throughout its lifetime.

Reactor safety (SG2) research focuses on the development of experimental and computational methods aimed at ensuring that a nuclear facility and its systems are able to implement the safety requirements set for them. The research questions focus on the fundamental safety aspects and on an understanding of the behaviour of nuclear fuel, plant processes and plant systems in both normal and abnormal situations, including phenomena relevant to accident progression and the resulting consequences. In addition to general method development for complex physical phenomena, the tools need to be validated and the uncertainties managed. Important topics are also severe accident analysis and management, internal and external hazards, including the fire risks analysis and phenomena related to the climate change and fuel research. (In the beginning of the programme, the topics related to fire risks and climate phenomena were included in SG1 area.)

The aim of research on *Structural safety and materials* SG3 is to increase knowledge that supports the long-term and reliable use of the nuclear power plants, particularly with respect to matters involving the integrity of barriers or material issues that affect the reliability of the safety functions. The research targets the ageing phenomena of the existing devices and structures and the correctly timed management of their progress. Attention is also paid to the utilisation of structure- and device-specific ageing information and the operative capability of the devices and structures in exceptional conditions. The research topics include ageing (metallic, concrete, polymer, water chemistry, automation systems), non-destructive testing (NDT, metallic and concrete), structural safety analysis, preparation for new technologies and new material solutions.

Research infrastructure SG4 related research is funded in on order to ensure modern research facilities and equipment. Domestic infrastructure is vital for the maintenance and enhancement of national competences. It is also useful for leveraging international experimental capabilities for national needs. The safety assessment of nuclear power plants requires deep knowledge about physical processes taking place inside the plant systems, structures, and components. Such knowledge ultimately rests on representative experimentation and physical modelling. A similar understanding is also needed for the assessment of operational safety and plant ageing. Up-to-date research capabilities should satisfy the needs of both existing and future power plants and other nuclear facilities. The strong infrastructure development phase in the SAFIR programmes started with the development of VTT research capabilities realising the VTT Centre for Nuclear Safety. The next phase will be to continue the development of thermal hydraulic facilities at LUT University.

The SAFIR2022 programme's planning group, nominated by the MEAE in November 2017, defined the following mission for national nuclear safety programmes:

> *National nuclear safety research aims at high national nuclear safety assessment capability. It develops and creates expertise, experimental facilities as well as computational and assessment methods for solving future safety issues in close cooperation with competent international partners.*

The vision of SAFIR2022 was defined as follows:

> *The SAFIR2022 research community is a vigilant, internationally recognised and strongly networked competence pool that carries out research on topics relevant to the safety of Finnish nuclear power plants on a high scientific level and with modern methods and experimental facilities.*

The Framework Plan [1] describes the research to be carried out in SAFIR2022 that essentially also covers the themes of the preceding SAFIR2018 programme [2].

During the first half 2019–2020 of the SAFIR2022 programme period, research was carried out under the guidance of eight *reference groups*:

1. Overall safety and organisation
2. Plant level analysis
3. Reactor and fuel
4. Thermal hydraulics
5. Mechanical integrity
6. Structures and materials
7. Severe accidents
8. Research infrastructure.

The results achieved by all SAFIR2022 projects in each year and the summaries of the research plans for the next year are reported in the annual reports and plans (see, e.g., [4] and [5]).

Table 1 shows the actualised costs and volumes of SAFIR2022 projects in 2019–2020.

Table 1. SAFIR2022 projects 2019–2020.

Project	Acronym	Participating organisations	Total funding (k€)		Volume in person years 2019–2020
			2019	2020	
1. Overall safety and systemic approach to safety					
Building operational readiness of control room crews: preparing for the unexpected	BORS	VTT, FIOH	132	137	2,3
Co-simulation model for safety and reliability of electric systems in flexible environment of NPP	COSI	VTT, Aalto	165	151	2,4
New developments and applications of PRA	NAPRA	Aalto	217	201	2,7
Development of framework for justification of overall safety	OSAFE	VTT, LUT	92	98	1,4
Participative development for supporting human factors in safety	PARSA	FIOH, VTT	121	88	1,6
Predicting extreme weather, sea level and atmospheric dispersion for nuclear power plant safety	PREDICT	FMI	236	205	4,1
Safety and security assessment of overall I&C architectures	SEARCH	VTT, Aalto	370	369	6,2
Uncertainty management in fire risk analyses	URAN	VTT, Aalto	220	219	3,7
Effective improvement of leadership and safety culture	EPIC**	VTT		57	0,4
2. Reactor safety					
Analytical severe accident research	ANSA	VTT	269	209	3,1
Coupled analysis of transient scenarios	CATS	VTT	200	163	2,7
CFD methods for reactor safety assessment	CFD4RSA	VTT	195	197	2,4
Interdisciplinary fuels and materials	INFLAME	VTT	243	183	3,0
Developing the working arms of Kraken, the next generation computational framework for reactor design and licensing analyses	LONKERO	VTT	253	255	4,4
Mitigation and analysis of fission products transport	MANTRA	VTT	162	123	1,5
Passive heat exchanger experiments	PAHE	LUT	127	126	2,2
PWR PACTEL tests	PATE	LUT	234	205	3,4
Radiation shielding and criticality safety analyses	RACSA	VTT	181	170	2,6
Sparger separate effect tests	SPASET	LUT	166	128	2,5
Safety through thermal-hydraulic analyses and co-operation	THACO	VTT	228	220	3,2
Enhanced multi-physics calculation capabilities for fuel behaviour and reactor analyses	EMBER**	LUT		29	0,3

Project	Acronym	Participating organisations	Total funding (k€)		Volume in person years 2019–2020
			2019	2020	
Fuel microstructure and radium solubility	PORA**	VTT		100	0,8
3. Structural safety and materials					
Additive manufacturing in nuclear power plants	AM-NPP	VTT, Aalto, LUT	94	72	1,3
Advanced materials characterisation for structural integrity assessment	AMOS	VTT	137	167	1,9
Critical studies in support of the ageing management of NPP concrete infrastructure	CONAGE	VTT, Aalto	152	143	2,0
Modelling of aged reinforced concrete structures for design extension conditions	CONFIT	VTT, TAU	116	86	1,0
Effect of long-term operation on aging and environmentally assisted cracking of nuclear power plant component materials	ELIAS	VTT, Aalto, TAU	135	75	1,4
Extended lifetime of structural materials through improved water chemistry	ELMO	VTT	193	194	2,2
Fatigue and evolving assessment of integrity	FEVAS	VTT, Aalto	183	147	2,1
Non-destructive examination of NPP primary circuit components, machine learning and reliability of inspection	RACOON	VTT, Aalto	132	189	2,6
Safety criteria and improved ageing management research for polymer components exposed to thermal-radiative environments	SAMPO	VTT, RISE	184	190	2,0
Fatigue management for LTO	FATIMA**	VTT		116	0,6
4. Research infrastructure					
Barsebäck RPV material used for true evaluation of embrittlement	BRUTE	VTT	370	382	4,7
Infrastructure development at LUT safety research laboratory	IDEAL	LUT	448	466	5,1
Participation in Jules Horowitz Reactor project - towards first criticality in 2022	JHR2022	VTT	136	129	1,4
Pre-emptive reduction of radiological laboratory legacy waste	LAB-WAST*	VTT	309		1,9
0. Programme administration					
SAFIR2022 Administration	ADMIRE	VTT	373	437	2,0
		Total	**6772,7**	**6425,9**	**89,3**

The costs of ADMIRE are for periods 1.1.19–31.3.20 and 1.1.20–31.3.21. The costs include subcontracted small study projects (100 k€ per year) and value-added tax 24%.
*) Project carried out only during in 2019.
**) Project started from 2020 (EPIC, EMBER, PORA and FATIMA).
PORA project reports to KYT2022 programme (see http://kyt2022.vtt.fi/).

Financial and statistical information

The total volume of the SAFIR2022 programme in 2019–2020 was 13,2 M€ and 89 person years. The funding partners were VYR with 8,569 M€, VTT with 2,551 M€, LUT University with 0,554 M€, Aalto University with 0,279 M€, NKS with 0,315 M€, SSM with 0,115 M€ and Halden Reactor Project in-kind with 0,106 M€. In addition to their shares of the collected VYR funding, Fortum, TVO and Fennovoima directly funded specified projects with 0,080 M€, 0,065 M€ and 0,030 M€, respectively. Several other partners funded different projects by 0,543 M€ in total. The funding proportions of the major funding partners are illustrated in Figure 1.

The costs structure of the projects is shown in Figure 2. The personnel costs make up the major share.

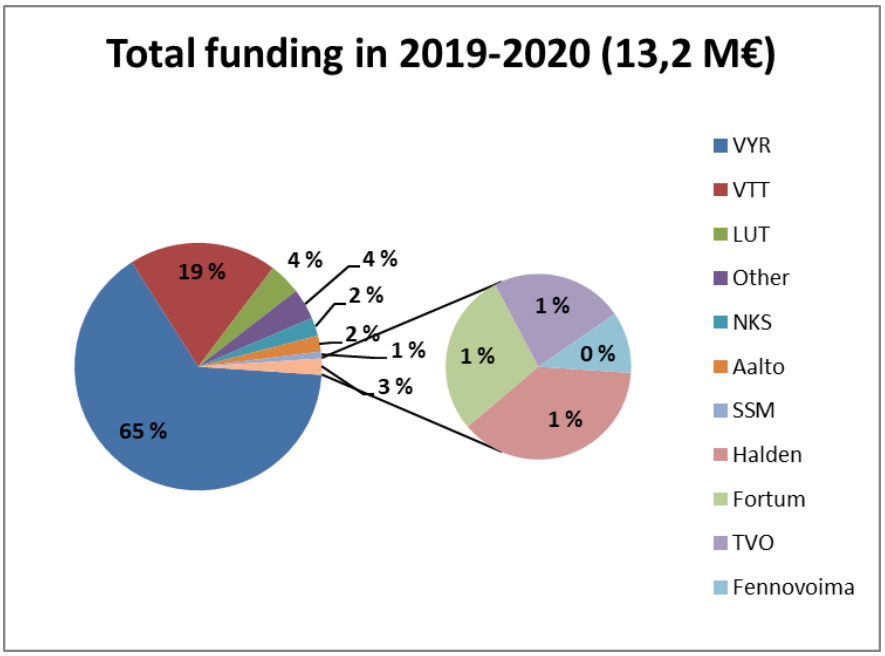

Figure 1. Funding of the SAFIR2022 programme in 2019–2020.

Figures 3–5 show the funding and volumes of SAFIR2022 research areas in 2019–2020. In the area Research infrastructure (SG4) the share of person-years was lower than the share of total funding because of infrastructure investments (Figures 3–4). In SG1 and SG2 the shares of the person-years were bigger and in SG3 slightly smaller than the shares of the total funding, respectively.

The total funding of the research projects decreased from 6,4 M€ in 2019 to 6,0 M€ in 2020 which can be seen in Figure 5. However, the total funding of SG3 area projects still slightly increased.

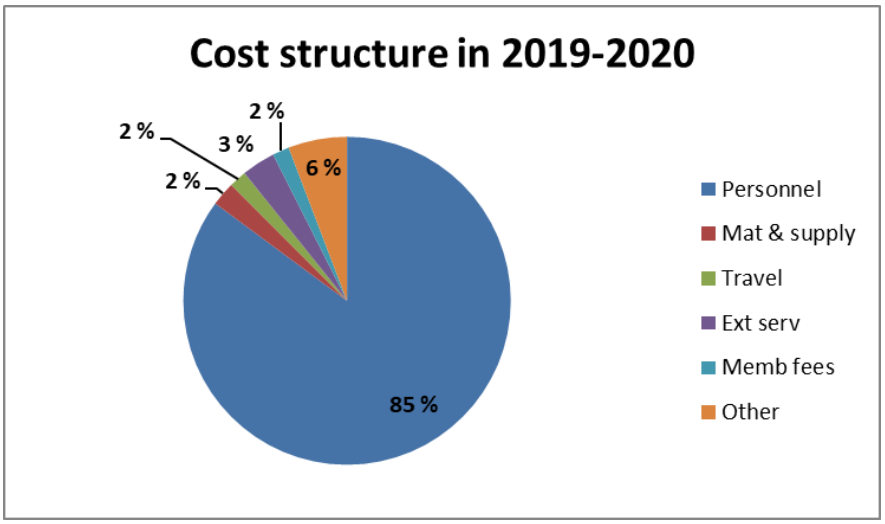

Figure 2. Cost structure of SAFIR2022 in 2019–2020.

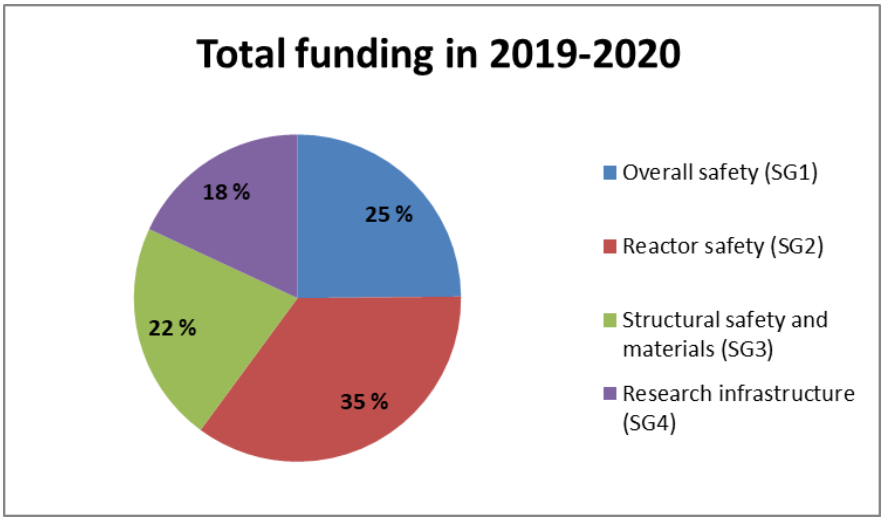

Figure 3. Division of funding to the research areas in 2019–2020.

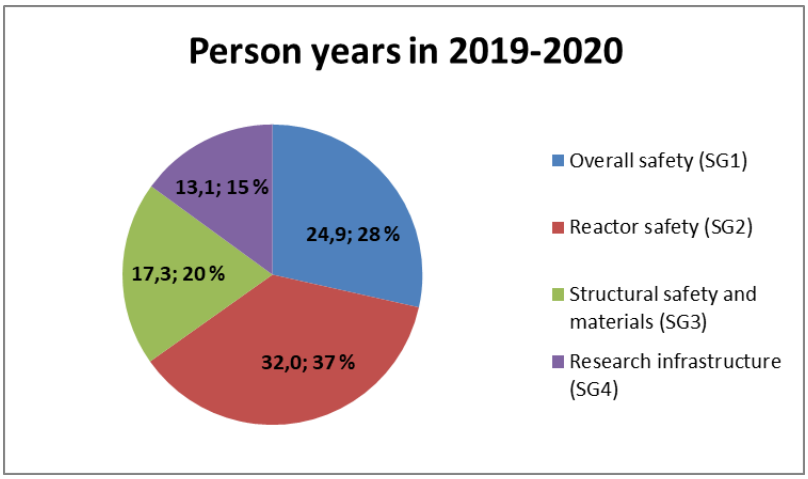

Figure 4. Volumes of the research areas in 2019–2020.

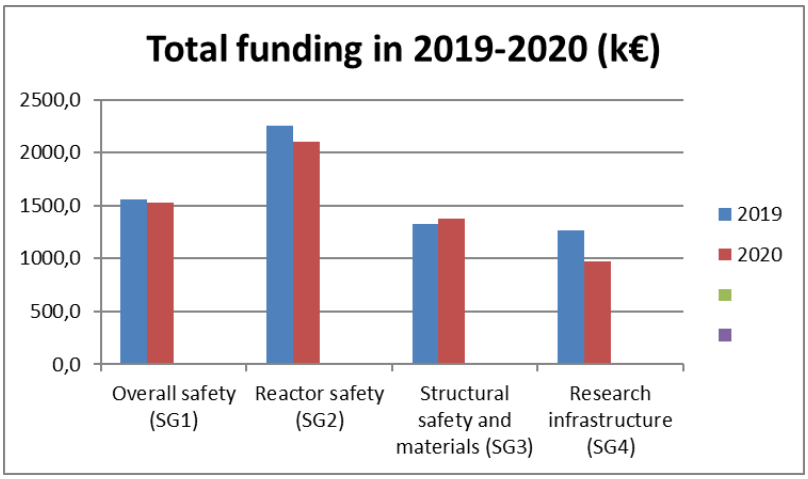

Figure 5. Total funding of the research areas in 2019–2020.

The projects of the programme have produced 345 publications and 86 other deliverables (“Others”) in 2019–2020 (Table 2). Major part of the publications consisted of public research reports and conference articles. A total of 48 scientific journal articles were made. The average number of publications in the research projects was 3,9 per person year (“Others” excluded), and the average number of scientific journal articles was 0,6 per person year. The projects had different scopes and there were also clear differences in the number of publications between the projects even when the project volumes are taken into account. Some projects also mainly published the results as research reports that allow more extensive reporting and are useful for the end-users of the results of certain research areas.

Table 2. Publications in the SAFIR2022 projects in 2019–2020.

Projects	Volume (person years)	Publications					
		Research reports	Scientific journal articles	Conference articles	Theses	Others	Total
Total	**89,3**	**195**	**48**	**77**	**25**	**86**	**431**
BORS	2,3	2	1	6	1	5	**15**
COSI	2,4	5	1	0	1	2	**9**
NAPRA	2,7	13	1	2	0	0	**16**
OSAFE	1,4	1	1	1	1	3	**7**
PARSA	1,6	0	1	2	0	8	**11**
PREDICT	4,1	1	6	7	5	11	**30**
SEARCH	6,2	3	4	7	2	2	**18**
URAN	3,7	7	4	0	1	1	**13**
EPIC**	0,4	0	0	2	0	0	**2**
ANSA	3,1	5	1	0	0	9	**15**
CATS	2,7	7	0	0	1	4	**12**
CFD4RSA	2,4	10	3	3	0	1	**17**
INFLAME	3,0	8	0	5	1	9	**23**
LONKERO	4,4	2	2	10	0	5	**19**
MANTRA	1,5	6	4	1	0	2	**13**
PAHE	2,2	5	0	0	0	0	**5**
PATE	3,4	8	1	0	0	0	**9**
RACSA	2,6	6	3	5	0	3	**17**
SPASET	2,5	4	2	1	1	0	**8**
THACO	3,2	6	1	1	1	0	**9**
EMBER**	0,3	1	0	0	0	0	**1**
PORA**	0,8	2	0	0	0	1	**3**
AM-NPP	1,3	5	1	0	0	0	**6**
AMOS	1,9	8	0	0	0	0	**8**
CONAGE	2,0	12	0	4	1	0	**17**
CONFIT	1,0	2	1	1	0	0	**4**
ELIAS	1,4	3	1	6	0	2	**12**
ELMO	2,2	8	2	0	2	0	**12**
FEVAS	2,1	3	2	6	2	0	**13**
RACOON	2,6	4	4	0	1	3	**12**
SAMPO	2,0	12	0	0	0	0	**12**
FATIMA**	0,6	0	0	2	0	0	**2**
BRUTE	4,7	15	1	1	1	3	**21**
IDEAL	5,1	5	0	2	3	0	**10**
JHR2022	1,4	4	0	1	0	10	**15**
LABWAST*	1,9	7	0	1	0	2	**10**
ADMIRE	2,0	5	0	0	0	0	**5**

*) Project carried out only during the year 2019.
**) Project started from the year 2020.

Altogether 23 higher academic degrees were obtained in the research projects in 2019-2020: 10 Doctoral degrees and 13 Master's degrees (Table 3).

Table 3. Academic degrees obtained in the projects in 2019–2020.

Project	Doctor	Master
BORS		1
COSI		1
OSAFE		1
PREDICT	4	1
SEARCH	1	1
URAN	1	
CATS		1
INFLAME		1
THACO		1
SPASET	1	
CONAGE		1
ELMO		2
FEVAS	2	
RACOON		1
BRUTE		1
IDEAL	1	

Structure of the report

This report describes on the main results of the projects during 2019–2020. Chapters 2–9 include summaries of the projects in the eight reference groups of SAFIR2022. More detailed statistical information of the programme and lists of project publications can be found in the annual reports on SAFIR2022 website.

Acknowledgements

The results of the SAFIR2022 programme during the first half 2019–2020 period have been produced by all who have been involved in the research projects. Their work is highly esteemed.

The contributions of project managers and researchers that form the essential contents of this report are acknowledged with gratitude.

The work of the persons in the Management Board, the steering groups and the reference groups that has been carried out with the expense of their own organisations is highly appreciated.

Jari Hämäläinen and Vesa Suolanen

References

[1] National Nuclear Power Plant Safety Research 2019-2022. SAFIR2022 Framework Plan. Publications of the Ministry of Economic Affairs and Employment, Energy 22/2018. 101 p. ISBN: 978-952-327-314-6. http://urn.fi/URN:ISBN:978-952-327-314-6 (available on http://safir2022.vtt.fi/).

[2] Hämäläinen, J. & Suolanen, V. (eds.) SAFIR2018 – The Finnish Research Programme on Nuclear Power Plant Safety 2015-2018. Final Report. VTT, Espoo, 2019. VTT Technology 349. 498 p. ISBN 978-951-38-8682-0 (available on http://safir2018.vtt.fi/).

[3] SAFIR2022 – The Finnish Research Programme for Nuclear Power Plant safety 2019-2022. Operational Management Handbook. 2019. 19 p + 26 app. http://safir2022.vtt.fi/.

[4] Hämäläinen, J. & Suolanen, V. (eds) SAFIR2022 Annual Report 2019. Research Report VTT-R-00311-20. 127 p + 47 app (available on http://safir2022.vtt.fi/).

[5] Hämäläinen, J. & Suolanen, V. (eds) SAFIR2022 Annual Plan 2020. Research Report VTT-R-00312-20. 51 p (available on http://safir2022.vtt.fi/).

2. Overall Safety and Organisation

2.1 Building operational readiness of control room crews (BORS)

Jari Laarni[1], Satu Pakarinen[2], Hanna Koskinen[1], Marja Liinasuo[1], Kristian Lukander[2], Tomi Passi[2], Tuisku-Tuuli Salonen[1]

[1]VTT Technical Research Centre of Finland Ltd
P.O. Box 1000, FI-02044 Espoo

[2]Finnish Institute of Occupational Health
P.O Box 40, FI-00032 TYÖTERVEYSLAITOS

Abstract

The BORS project investigates operator work practices from the perspective of human-system interfaces, procedures, operators' resources for action and skills training. Our aim is to advance and deepen our understanding of resilience skills, operators' work practices and cognitive processes in complex incidents and severe accidents. To that aim, we conducted simulator tests that are unique in a sense that they are either performed in a new kind of environment (i.e., virtual control room) or that they address topics that have not been widely studied (e.g., stress management in complex incidents). The results suggest that some signs of operational resilience were identified in these studies supporting the view that operators are able to mobilize new work practices to promote task execution in demanding operational situations. Based on our results, methods, tools, guidance, and training activities can be developed for the promotion of operators' resilience skills that expand their resources for action in case of severe accidents and other demanding situations.

Introduction

The BORS project investigates operator work practices from the perspective of human-system interfaces (HSIs), procedures, operators' resources for action and skills training. First, our aim has been to further our understanding of operator work practices and cognitive processes in complex incidents and severe accidents. To that aim, we conducted simulator tests that are unique in a sense that they were either performed in a new kind of environment (i.e., virtual control room) or that they address topics that have not been widely studied (e.g., stress management in complex troubleshooting). Second, our aim has been to study to procedure use practices and promote resilience skills in procedure execution by conducting a large-scale simulator study, in which both prose- and flowchart-based incident procedures were used. Third, our aim has been to develop an analysis framework for the identification of resilience skills that enable intelligent use of procedures. The analysis

framework is based on the identification of critical functions and their interactions by using the Functional Resonance Analysis Method (FRAM; Hollnagel, 2012).

Application of virtual reality technology in evaluation and training

Virtual reality (VR) technology provides new opportunities for operator training and HSI design and evaluation. Two examples are given from our recent research, one addressing complex troubleshooting in a virtual control room (VR CR), another reviewing literature on VR-based field operator training.

Complex troubleshooting in a virtual reality control room

We studied how an immersive 3D environment can be used in simulator studies to better understand operator performance in complex incidents (Figure 1; see also Laarni et al., 2020). For example, our aim was to better understand the cognitive processes in detecting, identifying and diagnosing incidents in a VR CR. The VR-environment was based on 3D models that were created into the Unity design environment. We applied a special kind of headset enabling a seamless blend between the central high-resolution and a larger lower-resolution display. Two operator crews participated in the main test, and one crew in the pilot test. There were four brief incidents in which the operators had to detect and identify a malfunction and start to manage it; in a longer run, a sudden fire in the main control room (MCR) was simulated, forcing the crew to walk to the Emergency CR. After each trial, the operators were interviewed, and they had to describe what they had done, what information they had used and what hypothesis they had made about the cause of the malfunction.

Crews were able to detect all the malfunctions apart from one, and conduct the critical operations to stabilize the power process. They were also able to propose diagnostic hypotheses about the cause of the malfunction and make plans on how to test these hypotheses. Overall, the crews estimated that they performed slightly slower in VR than in a physical simulator. Also, the operations were sometimes performed in different order than normally, and sometimes the critical information was also observed from another source than in a physical simulator. Some signs of behavioural resilience were identified. For example, the operators collaborated more actively than normally, and sometimes they coordinated their activities in novel ways.

Overall, the virtual CR created a realistic and immersive experience. All in all, the symptoms of simulator sickness were quite mild, but the experiences of Spatial Presence scores were only moderate, and they were even lower than in our previous studies, in which a different VR headset was used. The system in the present study had defects that compromised the user experience as compared to the earlier version, which could not be compensated by improved resolution and other useful features of the new system. In terms of systems usability, both positive and negative

comments were given. According to the system usability questionnaire, the headset was quite comfortable to wear, communication was smooth due to the fact that it did not occur through headsets, and it was easy to learn to navigate through the VR CR. On the negative side, action possibilities were quite limited, and even though resolution was improved as compared to our earlier studies, it still was not good enough for reading from a distance.

Figure 1. The physical simulator environment with three participants. The virtual CR is shown on a laptop screen located on the table.

Virtual-reality based field operator training

In nuclear power plants (NPPs), field operators make inspections and perform operations outside the main control room, and also collaborate with MCR operators in different plant states. With emerging virtual technology, new opportunities for field operator training have become available. We conducted a literature review to get an overview on how virtual training can be utilized to improve training of field operators, and also collaboration with the MCR operators.

Typically, virtual reality utilizes a wearable device, that is a VR headset comprising a stereoscopic head mounted display, hand-held controllers and motion tracking. In VR, the virtual 3D world is provided to the user, and the user can interact and move physically within the virtual environment. In our review, a broad definition of the term VR is used, as the solutions reported in the research literature vary considerably in technical maturity, level of interactivity, and how they are applied in training.

VR can be applied for different forms of field operator training: they can be used in training of fault, incident and accident management in collaboration with MCR operators, in training of maintenance work and work process planning, in training of radiation visualization and hazard detection, and in training of physical safety.

The majority of the studies concerning field operator training shows clear learning effects as compared to before training or no training. When VR training is compared to traditional methods of training the evidence suggests some advantage for VR solutions over traditional forms of training. On the other hand, some studies (Nystad et al., 2002; Sebok et al., 2002) indicate that also within the VR training, it is of crucial importance how the training is organized and aligned with the training goals.

Taken together, the results of the review suggest that VR is a promising tool for field operator training. VR training has both its prospects and limitations. Positive effects depend on how plant facilities and functions have been implemented in VR. If the virtual CR accurately replicates the target system and its functions, the user is able to build accurate mental models, transfer the learned skills to actual work, and has an overall positive learning experience. Other things that may contribute to training results are the degree of autonomy and active participation (versus passive viewing) assigned to the trainee, the level of support and guidance from the instructor, and the trainee's familiarity with the task content.

All in all, even though VR solutions have become more and more in common in entertainment industry and consumer market, there is plenty of room for development in the fields of education and training. In the future, with the technological maturation and increasing availability of training solutions, VR training is likely to become more common in the nuclear domain, and especially in field operator training.

Promoting operational readiness through procedures

In nuclear domain, it is not possible to anticipate all possible operative situations when designing HSIs, procedures and training, and therefore, arriving to the optimal solution in these situations requires flexible thinking and problem solving. To put it another way, there is always a tension between work-as-imagined and work-as-done. HSIs and procedures are designed based on the designers' view of the work of operative personnel - which is only partly grounded on the work-as-done. We have investigated this tension from both vantage points: by analysing the management of a complex incident together with process experts and procedure designers in focus group settings, and by conducting a simulator study in which operator crews had to detect, diagnose and correct malfunctions in a training simulator.

FRAM method in procedure development

Intelligent use of procedures can be thought of as one of the skills supporting operational readiness of MCR crews (Norros et al., 2014; Savioja et al., 2014). These skills are not something that lie exclusively in the operators' mind, but they are emergent phenomena and they are interacting with other resources and skills. Procedures can be thought as resources for action, but since they cannot guarantee safety as such, people need skills to apply them successfully.

We developed an analysis framework for the identification of resilience skills enabling intelligent use of procedures (see also Laarni et al., 2020). An analysis of critical functions and their interaction was carried out by using the FRAM methodology (Hollnagel, 2012). Data was collected by focus groups, interviews and video-based observations. Our results suggest that the FRAM methodology can be successfully applied to the analysis of proceduralized activity. A two-stage approach was shown to be fruitful: We first create an overview FRAM model (shown in Figure 2 in Finnish) describing the main activities of the task from the perspective of the nuclear process, and after that, we create a more detailed description, looking at the task from CR operator roles' perspective.

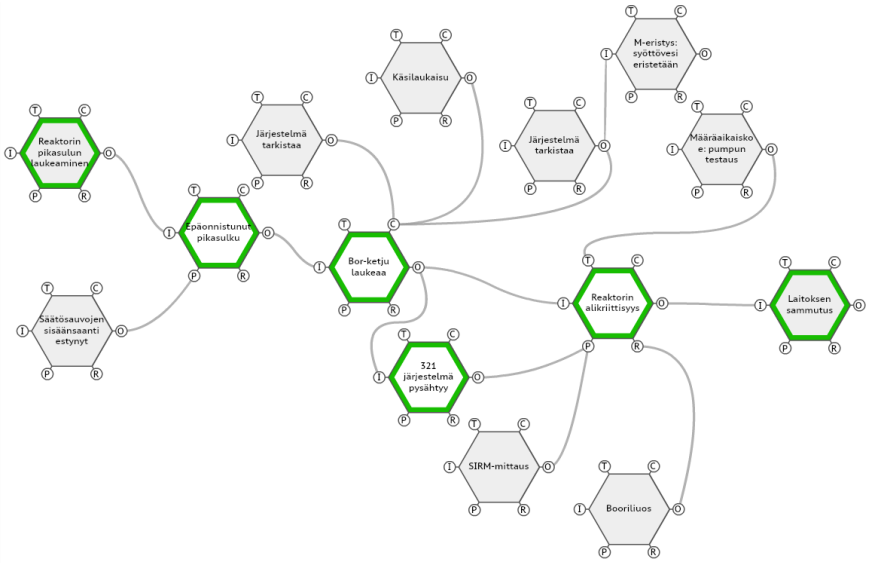

Figure 2. A simplified FRAM model (in Finnish). The model was developed by a free software tool named the FRAM Model Visualizer (http://functionalresonance.com/FMV/index.html).

We were able to identify some potential variability of the functions, which was mainly related to the communication and collaboration between operators and between operators and personnel in the field. When comparing the variability in performance, predicted by the FRAM and observed in simulator runs, we found that the method was able to identify some sources of variability.

Process experts and procedure designers thought that FRAM might be useful in the early stages of procedure design, and especially in designing procedures for novel situations. However, it was also thought that FRAM is perhaps more useful in work analysis than in procedure design.

Overall, formal methods provide structure and guidance for the development of procedures, and FRAM, as one example of these methods, may have added value in the development of procedures also in nuclear domain.

Simulator study on promotion of operational readiness through procedures

We conducted a simulator study to explore in more detail the tension between work-as-imagined and work-as-done, and the skills that are needed to reconcile the gap between these two. A total of 14 NPP operator crews participated. Two scenarios were included in the study, a minor incident (Loss of one coolant pump) and a major incident (Failed reactor shutdown), in which there is a risk for a serious accident. One of the main strengths of the study is that operator performance was investigated both by subjective (i.e., interviews and questionnaires) and objective (i.e., observations and recordings of psychophysiological signals) quantitative and qualitative methods. By using multiple sources of data and multiple approaches to analyse the data it is possible to increase validity and credibility of findings.

Most of the crews acted in a quite consistent way, and performance was high in both simulator runs. A considerable variation in performance times was, however, observed. For most of the crews, communication and collaboration between operators was fluent. However, the amount and quality of communication varied quite much between crews, and some communication breakdowns were identified.

Clear and systematic differences were found in the workload and stressfulness between the two scenarios. Both the experienced task load and psycho-physiologically measured stress were higher in Failed reactor shutdown –incident than in Loss of one coolant pump –incident (Figure 3). Within the scenarios, the levels of stress were higher during the initial diagnosis and stabilization phases where several critical operations are conducted. The stress also reduced as soon as the incidents had been successfully managed. Differences in the levels of stress between operator roles were small. Possibly, the shift supervisors' and reactor operators' greater experience compensate for their higher task demands as compared with the turbine and auxiliary panel operators.

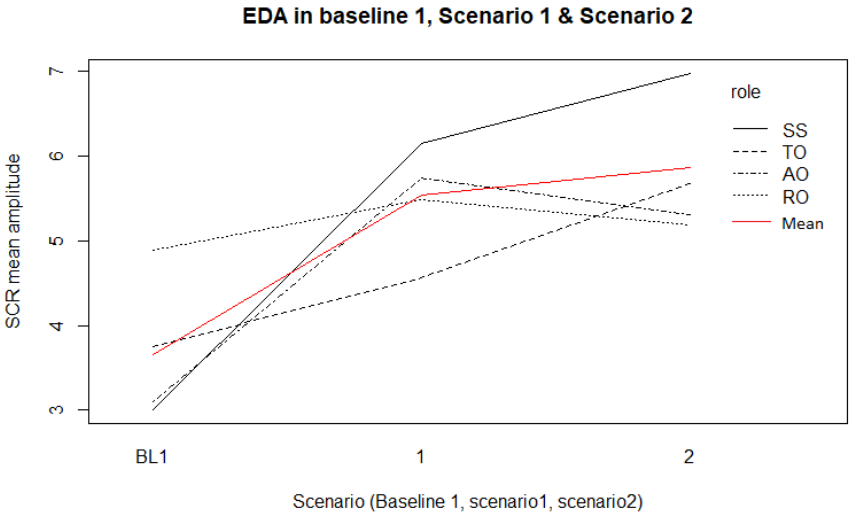

Figure 3. Interaction plot depicting skin conductance response (SCR) during baseline, and Scenario 1 and 2. BL1 = baseline 1; 1 = Scenario 1; 2 = Scenario 2. SS = Shift supervisor; RO = Reactor operator; TO = Turbine operator; AO = Auxiliary operator; EDA = electrodermal activity.

Self-reported situation awareness (SA) was clearly lower for the more challenging scenario for all crews. Two crews reported lower SA during the Failed reactor shutdown incident than the other crews, indicating that they had more serious problems in accomplishing the more complex situation. There was a highly significant negative correlation between self-reported overall SA and dimensions of self-reported workload. The results indicate that the higher the operator's workload was, the lower his/her awareness of the overall situation.

Scores for the four dimensions of self-reported teamwork (Coordination, Communication, Leadership and Time management) were also significantly lower for the more demanding scenario. Differences between the four dimensions were small, however. There was a significant negative correlation between Coordination and Time management and all dimensions of self-reported stress and workload. There was also a significant negative correlation between Communication and all dimensions of self-reported workload except Performance dimension. These results indicate that stress and excessive workload have a far-reaching negative effect on teamwork, which in turn may hamper task performance.

Reactor operators differed in how they devoted their attention to different user interfaces and other objects in the simulator environment. Proportionally, they paid more attention to computer displays of their workstation, procedures and other operators than to other information sources (e.g. some sections of the operator desk). Higher glance rate to procedures was associated with higher levels of situation understanding, indicating that active/proactive use of procedures is associated with better SA. On the other hand, longer glances to other operators and to the rightmost

section of the reactor operator's desk including, e.g., interfaces for manual control rod operation and reactor status monitoring, was associated with lower levels of SA (especially, understanding what to do in order to achieve a safe and stable process state).

There was quite much variation in procedure use practices between crews. On the other hand, procedures were applied quite fluently, indicating that usage practices are quite stable in each crew. In Failed reactor shutdown –incident the experts' evaluation of procedure usage was associated with performance time: the higher the scores the faster the crew completed the incident. According to interviews, the operators are satisfied with the present procedures irrespective of the format. When one option has to be chosen among several alternatives, operators preferred the prose format. One reason for the operators' preference can be that they are familiar with the present procedures, and the procedures are good enough for the operating purposes.

Applications

Based on our research, methods, tools, guidance and training activities can be developed for promotion of operators' resilience skills that expand their resources for action in demanding operational situations. Firstly,we have developed a concept for a retrospective video-based think- and reason-aloud process tracing method for operator training purposes. In this method, video showing both gaze direction and psychophysiological recordings are presented to the operator. Video from the test will be presented twice, in the first presentation the operator is instructed to think and reason-aloud what he/she was thinking during the session on the basis of the gaze-direction video; in the second presentation he/she is asked to describe his/her feelings (feel-aloud) during the session.

Secondly, our aim is to build a framework for resilience skills training for nuclear domain. In addition to lectures, it consists of workshops in which existing resilience skills and their interdependencies as well as constraints and restraints are identified, novel actions are introduced and their potentials are elaborated. A basic idea is to mobilize trainees themselves to expansive, participatory development of their work practices and conditions through three kinds of activities: first, potentials for cultivation of practices are recognized and existing skills are identified; second, possible work constraints and restraints are identified; and third, actions are recognized that makes it possible to reduce or increase the need for the use of particular resilience skills (Saurin et al., 2012).

Summary and conclusions

We conducted a simulator study in a VR CR to investigate the build-up of situation awareness in incident situations, operators' mental states and activities during complex troubleshooting and variation of operator workload and stress at different phases of task execution. We also conducted an extensive simulator study, in which

both prose-based and flowchart-based incident procedures were used. Some signs of negative effects of increased stress and work load and decreased situational awareness were detected during demanding situations. On the other hand also indicators of operational resilience, such as creative collaborative problem solving and fluent change in behaviour strategies to realign with changing conditions, were identified in these studies supporting the view that operators are able to mobilize new work practices to promote task execution in demanding operational situations.

Acknowledgement

The authors would like to thank all the designers, the simulator trainers and the operators involved in our studies.

References

Hollnagel, E. 2012. FRAM: The Functional Resonance Analysis Method: Modelling Complex Socio-technical Systems. Burlington: Ashgate.

Laarni, J., Liinasuo, M., Pakarinen, S., Lukander, K., Passi, T., Pitkänen, V. & Salo, L. 2020. Building Cognitive Readiness and Resilience Skills for Situation Assessment and Diagnostic Reasoning in a VR CR. In: Stephanidis C., Antona M. (eds.) HCI International 2020 - Posters. HCII 2020. Communications in Computer and Information Science, vol 1225. Cham: Springer.

Laarni, J., Tomminen, J., Liinasuo, M., Pakarinen, S. & Lukander, K. (2020). Promoting Operational Readiness Through Procedures in Nuclear Domain. In: Harris D., Li WC. (eds.) Engineering Psychology and Cognitive Ergonomics. Cognition and Design. HCII 2020. Lecture Notes in Computer Science, vol 12187. Cham: Springer.

Norros, L., Liinasuo, M. & Savioja, P. 2014. Operators' orientations to procedure guidance in NPP process control. Cognition, Technology & Work 16, 487–499.

Nystad, E., Drøivoldsmo, A., & Sebok, A. 2002. Use of radiation maps in a virtual training environment.

for NPP field operators. HWR-681). Halden, Norway: OECD Halden Reactor Project.

Savioja, P., Norros, L., Salo, L. & Aaltonen, I. 2014. Identifying resilience in proceduralized accident management activity of NPP operating crews. Safety Science 68, 258-274.

Saurin, T. A. & Wachs, P. 2018. Modelling interactions between procedures and resilience skills. Applied Ergonomics 68, 328-337.

Sebok, A., Nystad, E., & Droivoldsmo, A. 2002. Improving safety and human performance in maintenance and outage planning through virtual reality-based training systems. In: Proceedings of the IEEE 7th Conference on Human Factors and Power Plants. IEEE.

2.2 Development of framework for justification of overall safety (OSAFE)

Juhani Vihavainen[1], Juhani Hyvärinen[1], Mikko Turunen [1], Marja Ylönen[2], Kim Björkman[2]

[1] LUT, University
P.O. Box 20, FI-53851 Lappeenranta

[2] VTT Technical Research Centre of Finland Ltd
P.O. Box 1000, FI-02044 Espoo

Abstract

The general objective of the OSAFE project (2019-2022) is to advance (the understanding of) nuclear power plant safety and security, i.e., overall safety by applying a set of methods (risk-informed, graded approach, safety culture, defence-in-depth, institutional strength-in-depth, system modelling) and improving of these methods for the purposes of safety assessment and safety justifications e.g. in the context of operating plant's electric systems and the new technologies, such as SMRs. OSAFE project focused in 2020 on two different tasks: Small Modular Reactors (SMRs) from the perspective of design, and semantic modelling in the context of non-baseload operations. We will present here the research on SMRs.

The specific goal regarding SMRs was to study the safety systems of U.S. EPR and NuScale SMR design and compare these with each other based on the analysis of their Design Control Documents. The results of this assessment show that U.S. EPR implements more safety systems as compared to a simple and compact NuScale design. NuScale Power Module design implements an integrated primary circuit, which utilizes natural circulation to cool the reactor core. U.S. EPR design requires forced circulation with Main Coolant Pumps to create sufficient coolant flow to remove heat from the reactor core. Additionally, emergency heat removal systems are passive in NuScale design as opposed to more complex active heat removal systems in U.S. EPR design.

Introduction

There is a growing interest in the SMRs in Finland and globally. This interest derive partly from the need to find ways to decrease carbon emissions. For instance EU's ambitious goal to obtain carbon-free Europe by 2050 is one driver for SMRs. However, there are several uncertainties related to SMRs, such as challenges regarding licensing and safety justifications.

The goal in OSAFE project regarding SMRs was to examine the SMRs and related requirements and challenges for nuclear safety justification. Emphasis was on assessment of design features. Impact of SMR safety features to the demonstration

of compliance of plant safety requirements. SMRs are considered as an interesting option for electricity and heat production. They are expected to be easier to build and to operate under certain site conditions. The smaller size of the reactor offers interesting safety features, notably in terms of residual heat removal and size of containment structure. In addition, passive systems for heat removal are introduced to most of the SMR designs right from the beginning.

The differences in the safety features between normal Light Water Reactor and Light Water SMR may have an impact on the demonstration of compliance of plant safety requirements for SMR. Analysis on how easily SMR can fulfil the current safety requirements and its effects to the licensing process was an important topic worth investigating. Suitable SMR concept is investigated, applying ORSAC methodology, and find on what safety functions natural and inherent processes can be or are being credited to implement safety functions, instead of dedicated safety systems.

Overall safety of the SMRSs from a functional Defence-in-Depth viewpoint

The specific goal regarding SMRs was to study the safety systems of U.S. EPR and NuScale SMR design and compare these with each other by researching their Design Control Documents. The objective was to create a comprehensive framework for the overall safety of SMRs from a functional Defence-in-Depth (DiD) point of view.

The starting point of this assessment was the proposal of overall safety concept based on the functional Defence-in-Depth principle developed by International Atomic Energy Agency (IAEA). This concept contains Normal Operation (NO) and Anticipated Operational Occurrences (AOOs) are defined as Operational States, while Design Basis Accidents (DBAs) and Design Extension Conditions (DECs) without significant fuel degradation and with core melting are defined as Accident Conditions (Figure 1).

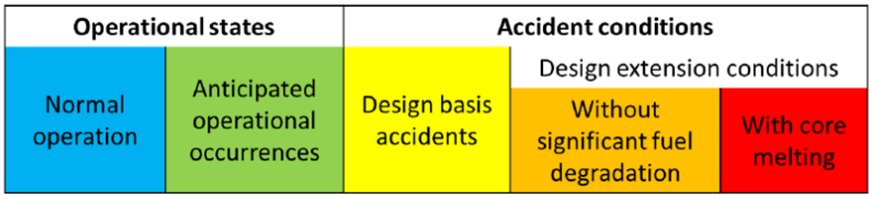

Figure 1. Functional Defence-in-Depth concept developed by IAEA.

The overall safety concept was developed further by combining the main safety functions and the functional DiD concept developed by IAEA (Figure 2). The front-line safety systems were attached to the DiD frame by adding the three main safety functions: 1) subcriticality, 2) heat removal and 3) containment functions. The

subcriticality refers to control of reactor power containing the capability to shut down the reactor. The heat removal refers to fuel heat removal and cooling that is proportionate to the reactor power. The containment refers to confinement of radioactive materials inside closed systems, or capability to isolate the containment, maintain it leak-tight, and also prevent leakages from process systems carrying radioactive materials. To the new presentation of the overall safety concept two main support functions were attached: power supply and HVAC. Power supply refers to emergency power supply, to power safety features of the plant including control room. The HVAC refers to heating, ventilation and cooling to maintain operating conditions in safety equipment rooms.

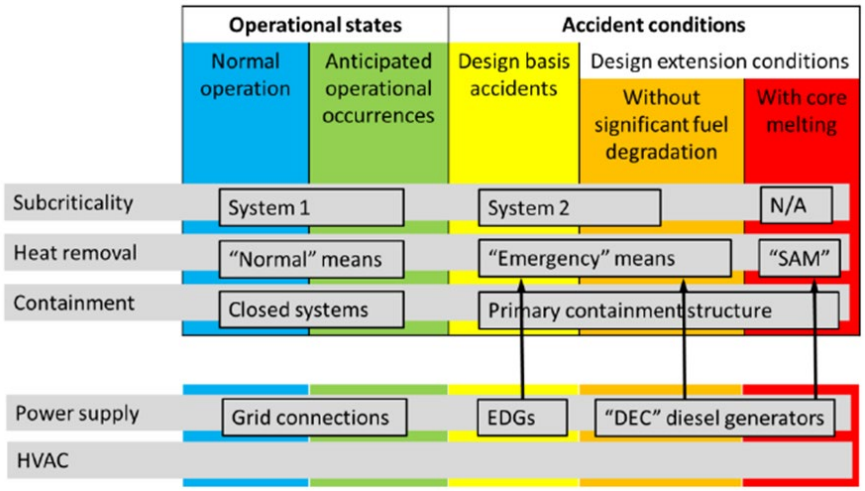

Figure 2. Main safety and support functions and functional Defence-in-Depth concept by IAEA combined.

The developed concept was then used by analysing the front-line safety systems of two different nuclear power plants and comparing them to get a better understanding of the overall safety for Small Modular Reactors. The first facility representing large power reactor was an Evolutionary Pressurized Reactor (EPR) originally designed by Areva NP. The actual EPR concept had been modified and implemented to a U.S. EPR design. The second facility representing SMR concept was NuScale, which is a Pressurized Water Reactor (PWR) with an integrated primary circuit designed by NuScale Power. The main reason to end up to the comparison of these designs was because U.S. NRC is the governing authority for both NuScale and U.S. EPR. They are designed through the same set of regulatory requirements. In addition, the majority of the technical details are public and available online from Agencywide Documents Access and Management System (ADAMS).

The systematic analysis and going through the documentation material concluded first the creation of large template of 5 x 5 matrix, where front-line safety

systems and support systems were placed to their respective positions for both studied designs separately. The observations were made that there were certain interdependencies between safety systems, which were credited in more than one DiD levels. Example of resulting NuScale template is presented in Figure 3. In NuScale design, some systems are shared between modules and these systems are indicated by a blue font in Figure 3. Decay Heat Removal System (DHRS) is designed to remove decay and residual heat from the reactor core and to retain RCS inventory in the RPV. DHRS provides residual heat removal and decay heat removal during AOOs, DBAs and DECs, and especially during non-LOCAs when the normal secondary side cooling is unavailable or otherwise not used. DHRS has safety-related functions during both Operational States and Accident Conditions.

	Operational States		Accident Conditions		
	Normal Operation	Anticipated Operational Occurrences	Design Basis Accidents	Design Extension Conditions	
				Without significant fuel damage	With core melting
Subcriticality	CVCS	CVCS			"N/A"
	CRA	CRA	CRA		
	Soluble boron				
	Gadolinia				
Heat removal	SG → Condenser → CWS → Atmosphere	SG → Condenser → CWS → Atmosphere			
	RCCWS → SCWS → Atmosphere	RCCWS → SCWS → Atmosphere			
		ECCS → CNV → UHS	ECCS → CNV → UHS	ECCS → CNV → UHS	
		SG → DHRS → UHS	SG → DHRS → UHS	SG → DHRS → UHS	
			RPV → CNV → UHS	RPV → CNV → UHS → Atmosphere	RPV → CNV → UHS → Atmosphere
				CFDS	
Containment	Closed piping (RCPB)	Closed piping (RCPB)	RPV	RPV	
	RSVs → CNV	RSVs → CNV			
		CIVs	CIVs	CIVs	
Power supply	TG				
		EDSS	EDSS		
			BPSS	BPSS	
HVAC	CRVS	CRVS	CRHS	CRHS	
	RBVS	RBVS			

Figure 3. The major operating systems as well as front-line safety systems implemented in NuScale placed on the functional Defence-in-Depth template.

The results of this assessment show that U.S. EPR implements more safety systems as compared to a simple and compact NuScale design. NuScale Power Module design implements an integrated primary circuit, which utilizes natural circulation

to cool the reactor core. U.S. EPR design requires forced circulation with Main Coolant Pumps to create sufficient coolant flow to remove heat from the reactor core. Additionally, emergency heat removal systems are passive in NuScale design as opposed to more complex active heat removal systems in U.S. EPR design. Table 1 shows the gathered information of how many safety systems combinations and support systems have safety-related functions between different levels of defence in both facilities.

Table 1. The number of safety system combinations and support systems that have safety-related functions between different levels of defence.

Number of safety system combinations and support systems	AOOs	DBAs	DECs
U.S. EPR	17	21	15
NuScale	12	9	8

References

Hyvärinen Juhani, Kauppinen Otso-Pekka, Vihavainen Juhani. 2016. Overall Safety Conceptual Framework – ORSAC. Final Report Revision 1, December 20, 2016. Lappeenranta University of Technology.

STUK. 2019. Guide YVL B.1. Safety design of a nuclear power plant. Regulatory Guides on Nuclear Safety (YVL). Available: http://www.finlex.fi/data/normit/41774- YVL_B.1e.pdf.

Turunen, M. 2020. Overall safety of small modular reactors. Master thesis. LUT University. http://urn.fi/URN:NBN:fi-fe2020120499439.

U.S. NRC. 2020a. Design Certification Applications for New Reactors. Available: https://www.nrc.gov/reactors/new-reactors/design-cert.html [viewed 8.9.2020].

U.S. NRC. 2020b. Final Safety Evaluation Report for the NuScale standard plant design. Available: https://www.nrc.gov/docs/ML2023/ML20231A804.pdf.

2.3 Participative development for supporting human factors in safety (PARSA)

Anna-Maria Teperi[1], Mikael Wahlström[2], Arja Ala-Laurinaho[1], Kaupo Viitanen[2], Timo Kuula[2]; Ilkka Asikainen[1], Vuokko Puro[1]

[1] Finnish Institute of Occupational Health (FIOH) P.O. Box 40, FI-00032 Helsinki

[2] VTT Technical Research Centre of Finland Ltd
P.O. Box 1000, FI-02044 Espoo

Abstract

New ways to commit and motivate personnel, and to develop competence, work practices and new learning are necessary for safety in the nuclear domain. The change forces facing nuclear industry are aging personnel and technology, new technologies and new ways of organizing work at nuclear power plants. This further emphasizes the relevance of art and practice of human factors, which aims for participative development (PD) with human-centered frameworks and models.

PARSA project develops, applies and evaluates measures and tools to improve working practices, work process knowledge and mutual co-operation with shared situational awareness across organizational levels and units, aligning PD approach. Case studies are conducted in the context of nuclear maintenance.

PARSA uses video-based reflection and collaborative work process analysis as methods, and conducts a critical inquiry to nuclear spesific human performance tools, with applicative targets. The aim is synergy among theoretical frameworks and practical implications, to have a shared view of needs, measures and prerequisites of PD in the nuclear industry, to improve safety.

Introduction

New ways to commit and motivate personnel, and to develop competence, work practices and new learning are necessary for safety in the nuclear domain, which is facing several changes in its functional environment. New technologies, new ways of organizing and structuring work at nuclear power plants (NPP), aging personnel and technology, and recruiting new generation to positions of operators and other experts challenge the resilience and capabilities of nuclear personnel and organisations (MEE, 2018; Wahlström, 2021). Modern threats, such as pandemics, also affect management and operations at NPPs, as well as regulative changes. On the other hand, the nuclear industry has attracted increased interest in climate change debat, due to its benefits of producing climate-friendly electricity, and its share of reducing CO2 emissions in the world (Wahlström, 2021). This further emphasizes the relevance of constanct improvement of the nuclear industry, in which art and practice of human factors (HF) potentially offer innovative ways of action.

The operative personnel and experts themselves are essential in enabling transition and development of organising work and knowledge (Boreham, 2002). Supporting good safety climate and participative decision making are critical in NPPs, to provide energy in a sustainable manner. In high-reliability organizations, front-line employees´ suggestions and concerns enable the early identification of potential problems that might have catastrophic consequences (Dekker, 2015). Despite this, previous research has mostly focused on person-centered antecedents of participation and, to a lesser extent, the importance of contextual factors at work and organisations (Silla, Gracia, Peiro, 2020).

Researchers, too, can be of assistance in knowledge sharing, in providing a context for mutual learning and development, by modelling work assignments, sharing ideas, understanding demands and needs of operative work and finding solutions, as focused on design thinking and co-creation, for example (Teperi, 2021). Theoretical and methodological groundings of learning studies, work, organizational and social psychology and other collaborative research, combined with the emphasis on safety, provides a fascinating setting for this kind of developmental research.

The PARSA project aims to define needs and prerequisities of PD, and to apply, test and improve capability of PD, by close evaluation of current work processes and practices in NPPs. We aim to improve accurate models and tools for participative orientation at work and in safety management. We aim for reframing and improving new ways of action, guidance, operational practices and practical solutions that promote organizational learning and good working practices and modelling tacit knowledge in nuclear operations. The case studies are scoped and implemented in maintanance operations of NPPs.

The entity of PARSA project is depicted in Figure 1.

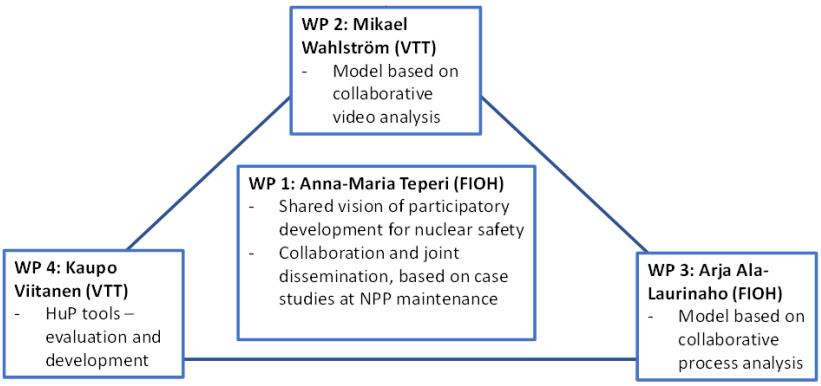

Figure 1. Four workpackages and their basic aims at the PARSA-project.

Synergy and coordination – brigde building between academy and industry

Building bridge between scientific work and industry has high relevance in the nuclear industry, which has ultimate goal for safety. Human Factors (HF)-focused frameworks and models may facilitate this kind of 'bridge-building' by means of PD, which is embedded in HF thinking. The core intention is to be aware of operative voice, for example weak signals, which could inhibit learning or be potential risks at maintaining or improving safety in NPPs. For the solid background, the need for mutually shared views applies also synergy and learning between academy and industry, and collaboration among theoretical frameworks represented by researchers of the field.

Nuclear industry is facing several demands in its functional environment such as changes in regulation, energy policy with e.g. critical audience, aging vs. modernization of technology and maintaining competence. Former generations with grand tacit knowledge are retiring and new generation is coming to the field. New health risks such as pandemias may emerge, affecting nuclear organizations and ways to work (Huttunen, Aurela, Melkas, Avolahti, 2012; MEE, 2018; SAFIR2022 Supplement).

In baseline interviews of PARSA in 2019, we found specified needs at maintenance in NPPs, such as organizational changes, increased awareness and need to respond to business pressures, restructuring of technical support services and variety of leadership and management styles, related to a mixture of management orientations as more experienced and new generation leaders are working at the field. This setting places also new challenges and possibilities for HF research, practice and development, to facilitate PD which produces new competence and practical solutions for supporting nuclear safety in future.

Spesifically, there is a need to have a shared, conceptualized and clearly summarized view of the current state and development needs of the ways, how to support implementation of PD procedures, to improve nuclear safety.

We aim for synergy and collaboration with two targets. First, we aim to offer forums and co-operation structures with NPPs, STUK and other key actors and researchers at the field, to share lessons learnt from the NPP study cases to relevant partners, to 'speed up' organizational and systemic learning. This serves contacts between science and practice, and between business and authority.

Second, based on scientific ponderings and case studies of the substudies of PARSA, we will formulize a shared vision of the needs, measures and prerequisites for creating PD approach, to improve safety in the nuclear industry.

The practical benefits and outputs are improved practices for work development and learning practices in NPPs, which is also useful for regulator at their basic task. Scientific contribution is to create new knowledge and theoretical view of prerequisites and benefits of PD as a part of safety management at the technologically driven and proceduralized nuclear industry.

Tacit knowledge understanding and new learning through video-based reflection

We have introduced the method of video-based collaborative reflection method for maintenance personnel. The idea is that learning takes place as the workers observe their own work practices from the video recording. This allows that the workers can discuss what could be done differently and what was done right by watching the events that took place during the activities. The idea on using video in the development of expertise at the nuclear domain draws from a strong line of research made at Électricité de France (EDF) by Lahlou (2010) and others (Le Bellu & Lahlou, 2010; Fauquet-Alekhine et al. 2018). We aim at transferring this line of research into Finland and developing it by using prominent Finnish research traditions. In particular, this relates to the way in which the researchers could facilitate the video-observation sessions with the workers. Overall, in addressing the requirement of high-quality research in SAFIR2022, we synthesize established lines of study: work on interpretive-practice (Norros, 2004; Savioja, et al., 2014; Norros, 2018; Wahlström et al., 2018), use of first-person camera for uncovering tacit knowledge line work developed at EDF (Lahlou, 2010) as well as workplace learning developed especially in the change laboratory tradition in Finland (Engeström, 2001). Figure 2 provides a visual illustration of the developmental method.

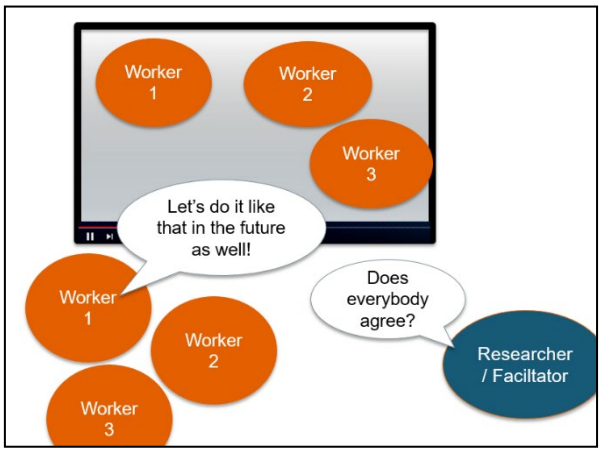

Figure 2. Basic idea of the self-confrontation method.

In 2019, it was agreed that maintenance workers' heavy lifting activities during yearly maintenance (outage) could be video-taped for training and learning purposes. The selected case was the lifting of reactor shield unit, as it is one of the critical tasks during the yearly outage, and lifting accidents could lead to serious consequences. The operating organization collected the video data on this heavy-lifting task and first version of guidelines for video-based session was created in collaboration with the researchers and NPP personnel.

Based on the analysis and first experiences about the method, five main purposes for video-based reflection was recognized:

- *before lifting operations* for refreshment training,
- *after lifting operations* for reviewing & reflecting group activity,
- *after incident* (abnormal, emergency) for reviewing & reflecting group activity and finding immediate reasons for incident,
- procedure development,
- general heavy-lifting training for new workers.

The first guidelines were aimed at *after lifting operations*, meaning that the video session would be organised soon after the lifting and outage with the people involved in the lifting. A test session based on these guidelines was organized at the end of the reporting period. The results of this session suggest, that all the five purposes are relevant in the maintenance context. Furthemore, the most relevant could be the video session for *before lifting operations,* to be organised just before the heavy-lifting task. The video reflection would then help the lifting personnel to prepare for the task together. Utilising video material in *after incident* situation and *heavy-lifting training* was also seen as especially relevant. The next step in 2021 would be to create guidelines related to all five purposes and to organize a session for *before lifting operations* for the next outage.

Additionally, initial guidelines for choosing the safety-critical maintenance task and implementing the video-based method were created. The video method's connection with existing HU tools pre-job briefing and post-job review was also preliminary reviewed and will be further investigated as part of the collaboration between substudies of PARSA. The results of video-based reflection could possibly be utilized in pre-job briefings, and post-job reviews could give input to video sessions. The ultimate goal would be that the power plant personnel would utilize the video-based reflection methods by themselves as practical tools for improving organisational learning.

Organizational learning through collaborative work process analysis

Collaborative Work Process Analysis (WPA) (Leppänen, 2001; Leppänen, Hopsu, Klemola & Kuosma, 2008) is a method that facilitates building of work process knowledge and shared understanding of work. It aims to increase the participants' ability to see the work process as an entity and to encourage them to take an active role in improving and developing the process. In this case, we introduce WPA in NPP maintenance to analyse work processes, their critical phases, interfaces and collaboration needs, to support organizational learning, knowledge sharing as well as safety and improvement of work.

Shared understaning of work and processes supports system and human resilience by improving ability to anticipate and learn both at every-day-operations as well as at more demanding situations (Hollnagel 2014). Understanding work as a

system requires good conceptual and theoretical knowledge applied to the specific work context and work situation. *Work process knowledge* (Kruse, 1986, Boreham 2002) refers to understanding of the work system as a whole, including e.g. understanding work processes, the interdependencies of activities in different departments, work roles, and organizational culture. Work process knowledge is constructed in the course of solving problems and contradictions at work through combining the practical experience (know how) with the theoretical knowledge.

Sandberg (2000) and Norros (2004) further explain how situatively appropriate action in work depends on an actor's way of experiencing or making sense his work. The actor's *conception of work (*Sandberg, 2000) affects crucially to which knowledge and skills the actor is actually using for the accomplishment of the tasks. A key characteristic of the more comprehensive conceptions is the more profound understanding of the interactions and interdependencies of the object of work, covering also more phases of work, compiled into a coherent entity to be acted on as a whole. Norros (2004), in turn, has used the concepts of *core task* and *habits of action* in explaining the differences of situated actions of different actors. The core task denotes the result-critical content of work that the actors should take into account to achieve the objective of the work; the more accurate and comprehensive their conception of the core task is the better they can judge the various situations and decide for the appropriate actions in them. Interpretative habits of actions (vs. reactive) promote the construction of a comprehensive picture of the events and their dynamics, and thus enhance the situatively appropriate action.

The core of the WPA is the sharing of knowledge and experiences of the participants. Through dialogues, the theoretical and practical knowledge of the participants are combined to form shared local concepts and theory of work – to form shared work process knowledge. The method is based on steered discussions, and the participants work in different kinds of groups to analyze their work processes, ways of action, materials, products and co-operation as well as problems and development needs related to the these. In this project, we use a modified version of the method, developed in safety critical air traffic management, and futher used e.g. in aviation maintenance (Teperi et al 2019).

Based on preliminary interviews (n=9) and discussions in a planning workshop with NPP nuclear maintenance and plant operations participants (n=10) in 2019, the first WPA workshops were decided to focus on disturbance cases and collaboration between different actors. In Spring 2020, a two-day work process analysis with five groups of operative personnel and a half-a-day workshop accompanied with other experts and organizational levels was organized (altogether n=20). Four different disturbance cases were analyzed and collaboration between different actors depicted. Also development needs were identified, and three proposals were selcetd for further planning. The second set of work process analysis was conducted on autumn 2020. Focus was on collaboration between Engineering, Operations and Maintenance departments to form a unified view of modification processes. First, representatives of each function (n=8) analysed a case example of scheduling a compressor change, and then results and development proposals were further discussed in evaluation workshop (n=16).

In both WPA processes, the selected proposals had to with securing accurate information for all partners and in IT systems. Especially, WPA of 'Modifications' highlighted the importance of shared situation awareness across different activities, and proposals to enhance it were made.

A draft of the booklet to guide conduction of work process analysis in NPPs has been written, including lessons learned from the method utilization with NPP1. These lessons concern e.g. criteria of selecting a relevant case for WPA, selecting participants, and focusing also success factors of the work processes.

HUP tools development: benchmarking and critical inquiry

We have also focused on reflecting the underlying assumptions, limits and possibilities of human performance tools (HU tools) as a method for improving nuclear safety. HU tools are a diverse set of good working practices originated from various industrial contexts. They are usually applied in operational context by shop-floor workers (especially maintenance and control room). The most commonly used HU tools include Pre-job Briefing, Post-job Review, STAR Principle (Self-Checking), Peer Checking, Independent Verification and Clear Communication (Oedewald, Skjerve, Axelsson, Viitanen, & Bisio, 2015). Detailed descriptions of HU tools, instructions regarding when to use them and what kind of behaviors to avoid are provided for nuclear industry practitioners in U.S. Department of Energy Human Performance Improvement Handbook, Volume 2 (DoE, 2009).

There is quite little prior scientific work done specifically on HU tools. The NKS/SAFIR2014 project HUMAX (Oedewald et al., 2015, 2014; Skjerve & Axelsson, 2014) conducted in 2013-2014 is likely to be the most extensive study carried out on this topic. HUMAX examined questions such as what are the expected, experienced and measured benefits of HU tools, how maintenance personnel perceives HU tools and how to successfully implement the tools. Apart from the insights from HUMAX, there exists a lot of potentially relevant knowledge on analogous tools and programs, but it is scattered due to the inconsistent use of concepts and labels in the literature, in different industrial contexts and in different scientific disciplines. For instance, some HU tools may have direct counterparts in other industries, but under different aliases.

We elaborate the basis and assumptions of HU tools based on previous research and further examination of HUMAX data. Case studies are conducted to collect new empirical data, integrating insights from other PARSA work packages.

In 2019, a book chapter[1] was written describing the most common HU tools in the nuclear industry, and typical challenges and potential success factors regarding their implementation and application based on available literature (Viitanen, 2021). The book chapter concluded that implementation process plays a crucial role of successful introduction of HU tools. HU tools serve different purposes, have

[1] Viitanen, Kaupo. "Human Performance Tools as a Part of Programmatic Human Performance Improvement." In: *Human Factors in the Nuclear Industry*, 107–26. Elsevier, 2021. https://doi.org/10.1016/B978-0-08-102845-2.00006-5.

different implementation considerations, strengths, and weaknesses. Their benefit is not only error reduction, but they also provide support for task performance and potentially increase system resilience and improve safety culture.

In 2020, case studies at Olkiluoto and Loviisa were prepared. Both case studies were planned to examine pre-job briefings and post-job reviews. The selection of these topics was motivated by the experienced challenges in implementing post-job reviews in the nuclear power companies. Data collection in Olkiluoto during 2020 outage (observations and interviews) was cancelled due to COVID-19 situation. Journal article manuscript draft prepared in 2019 was further elaborated, to be submitted in 2021.

In 2021, the main activity is Loviisa case study, which involves document analysis of pre-job briefing and post-job review feedback data. Content analysis is performed on the data, e.g., to identify what topics emerge during pre-job briefings and post-job reviews. Possibilities to observe HU training at Loviisa will be reviewed depending on COVID-19 situation. Depending on COVID-19 situation, observations and/or interviews will be conducted during outages either at Olkiluoto or at Loviisa. In addition, video data collected in WP2 is planned to be used as an additional data source to elaborate how HU tools are used during heavy lifts, and how to possibly integrate video-based reflection process with pre-job briefings and post-job reviews. Furthermore, at least one joint workshop will be held jointly among PARSA substudies (aligning Figure 1) to examine how HU tools relate to the process analysis conducted in WP3.

Summary and conclusions

The PARSA project has aimed to apply, test and improve participative development (PD) at work by conducting case studies at the nuclear maintenance units. PD approach is deeply embedded in Human Factors (HF) science and practice, to realize human-centered thinking and practices for better system performance, safety and well-being. Our specific focus has been on self-reflection skills and evaluation of working practices, and on facilitation of organizational learning and mutual co-operation among and across organizational levels and units.

PARSA has used video-based reflection and collaborative work process analysis as methods, and conducted a critical inquiry to nuclear spesific human performance tools, ‘good working practices’, with applicative targets.

The practical implications of PARSA are producing a training concept, guidelines and booklets to be used by NPPs, to reframe workplace learning, good working practices, as well as mutual communication and organizational learning procedures. The scientific contribution is made by offering new information and conceptualizations regarding needs, measures and prerequisites of PD to improve safety in the highly proceduralized nuclear industry, as well as other safety critical fields and industries. PARSA results can be utilized by NPPs, regulatory bodies and design organizations. New tools and practices are immediately exploitable by NPPs and the Finnish regulator.

References

Boreham, N., 2002. Work process knowledge in technological and organizational development. In: Boreham, N., Samurcay, R., Fisher, M. (eds). Work process knowledge. Routledge, London, pp. 1-14.

DoE. 2009b. Human Performance Improvement Handbook Volume 2, Human Performance Tools for Individuals, Work Teams, and Management. Department of Energy Washington, DC: Government Printing Office.

Engeström, Y. 2001. Expansive learning at work: Toward an activity theoretical reconceptualization. *Journal of education and work*, *14*(1), 133-156.

Fauquet-Alekhine, Philippe and Le Bellu, Sophie and Buchet, Marion and Bertoni, Jérôme and Bouhours, Guillaume and Daviet, Frédéric and Granry, Jean-Claude and Lahlou, Saadi. 2018. *Risk assessment for subjective evidence-based ethnography applied in high risk environment: improved protocol.* Advances in Research, 16 (3). pp. 1-15.

Hollnagel E. 2014. Safety-I and Safety-II: The Past and Future of Safety Management. Farnham, UK: Ashgate.

Huttunen, R., Aurela, J., Melkas, E., Avolahti, J. 2012. Kansallisen ydinenergia-alan osaamistyöryhmän raportti. Työ- ja elinkeinoministeriön julkaisuja. Energia ja ilmasto 2/2012.

Kruse, W. 1986. On the necessity of labour process knowledge. In: Schweitzer, J. (ed.) (1986). Training for a Hu-man Future, Weinheim, 188-193.

Lahlou, S. 2010. Digitization and transmission of human experience. Social science information, 49(3), 291-327.

Le Bellu, S., & Lahlou, S. 2010. Comment capter le savoir incorporé dans un geste métier du point de vue de l'opérateur?. ISDM: Informations, Savoirs, Décisions, Médiations, (36).

Leppänen, A. 2001. Improving the mastery of work and the development of the work process in paper production. Industrial Relations, 56:3, 579-605.

Leppänen A., Hopsu L., Klemola S. & Kuosma E. 2008. Does multi-level intervention enhance work process knowledge? Journal of Workplace Learning, 20, 416-430.

MEE. 2018. National Nuclear Power Plant Safety Research 2019-2022. SAFIR2022 Framework Plan. Publications of the Ministry of Economic Affairs and Employment of Finland. 22/2018. Helsinki.

Norros, L. 2004. Acting under uncertainty: The core-task analysis in ecological study of work. Espoo: VTT.

Norros, L. 2018. Understanding acting in complex environments: Building a synergy of cultural-historical activity theory, Peirce, and ecofunctionalism. Mind, Culture, and Activity, 25(1), 68-85.

Oedewald, P., Skjerve, A. B., Axelsson, C., Viitanen, K., & Bisio, R. 2015. Human performance tools in nuclear power plant maintenance activities - Final report of HUMAX project (No. NKS-328). NKS.

Oedewald, P., Skjerve, A. B., Axelsson, C., Viitanen, K., Pietikäinen, E., & Reiman, T. 2014. The expected and experienced benefits of Human performance tools in nuclear power plant maintenance activities - Intermediate report of HUMAX project (No. NKS-300). NKS. Retrieved from http://www.nks.org/scripts/getdocument.php?file=111010112048626.

SAFIR2022 Supplement. 2020. SAFIR2022 – Supplement to the Framework Plan for 2021 Call.

Sandberg, J. 2000. Understanding human competence at work: an interpretative approach. Academy of Management Journal 43:1, 9-25.

Savioja, P., Norros, L., Salo, L., & Aaltonen, I. 2014. Identifying resilience in proceduralised accident management activity of NPP operating crews. Safety Science, 68, 258-274.

Silla, I., Gracia, F. J., & Peiró, J. M. 2020. Upward Voice: Participative Decision Making, Trust in Leadership and Safety Climate Matter. Sustainability, 12(9), 3672.

Skjerve, A. B., & Axelsson, C. 2014. Human-Performance Tools in Maintenance Work - A Case Study in a Nordic Nuclear Power Plant (No. NKS-321). NKS. Retrieved from http://www.nks.org/scripts/getdocument.php?file=111010212620555.

Teperi, A-M., Asikainen, I., Ala-Laurinaho, A., Valtonen, T., Paajanen, T. 2019. Modeling Safety Criticality in Aviation Maintenance Operations to Support Mastery of Human Factors. Springer International Publishing AG, part of Springer Nature 2019. P. M. F. M. Arezes (Ed.): AHFE 2018, AISC 791, pp. 1–11, 2019. https://doi.org/10.1007/978-3-319-94589-7_32.

Teperi, A-M. 2021. Utilizing design thinking for renewal of safety management practices in the nuclear industry. 2021. In: Teperi, A-M., Gotcheva, N. Human Factors in the Nuclear Industry. A Systemic Approach to Safety. 1st

Edition. Elsevier, Woodhead Publishing. https://doi.org/10.1016/B978-0-08-102845-2.00006-5.

Viitanen, K. Human Performance Tools as a Part of Programmatic Human Performance Improvement. In: Teperi, A-M. & Gotcheva, N. 2021: Human Factors in the Nuclear Industry. A Systemic Approach to Safety. 1st Edition. Elsevier, Woodhead Publishing. Elsevier, 2021. https://doi.org/10.1016/B978-0-08-102845-2.00006-5.

Wahlström, M., Seppänen, L., Norros, L., Aaltonen, I., & Riikonen, J. 2018. Resilience through interpretive practice – A study of robotic surgery. Safety Science, 108, 113-128.

Wahlström, B. 2021. Human factors in nuclear power: Reflections from 50 years in Finland. In: Teperi, A-M., Gotcheva, N. Human Factors in the Nuclear Industry. A Systemic Approach to Safety. 1st Edition. ISBN: 9780081028452. Elsevier, Woodhead Publishing. https://doi.org/10.1016/B978-0-08-102845-2.00006-5.

2.4 Effective improvement of leadership and safety culture (EPIC)

Kaupo Viitanen, Nadezhda Gotcheva, Merja Airola

VTT Technical Research Centre of Finland Ltd
P.O. Box 1000, FI-02044 Espoo

Abstract

EPIC develops knowledge and approaches that support effective improvement of nuclear safety through leadership and safety culture. The project is divided into two work packages: methodical safety culture improvement, and characterization of leadership activities. The first work package systematically models how safety culture improvement activities are performed in nuclear power companies, focusing on the work of the safety culture experts. The second work package identifies good leadership practices within a selection of managerial or supervisory contexts at nuclear power companies.

Introduction

Safety culture was introduced after the Chernobyl accident to help understand the social and organizational aspects of nuclear safety. Safety culture draws from the concept of organizational culture, which refers to the pattern of shared basic assumptions learned through adaptation, and the espoused values and artefacts that reflect and influence the basic assumptions (Guldenmund, 2000; Schein, 1985). In the nuclear industry, safety culture is defined as “the assembly of characteristics and attitudes in organizations and individuals that establishes that, as an overriding priority, nuclear plant safety issues receive the attention warranted by their significance” (IAEA, 1991, p. 1). Good safety culture is expected in nuclear industry and licensees are required to implement systematic safety culture improvement activities to assure good safety culture (e.g., IAEA, 2016; STUK, 2019).

Leadership is a fundamental characteristic of a strong safety culture (IAEA, 2016, 2006, 1991; WANO, 2013). GSR Part 2 defines leadership for safety as “the use of an individual’s capabilities and competences to give direction to individuals and groups and to influence their commitment to achieving the fundamental safety objective and to applying the fundamental safety principles, by means of shared goals, values and behaviour” (IAEA, 2016, p. 2). Leadership activities influence culture and are critical for directing the organizational attention and resources to continuous improvement of safety (e.g. Barling et al., 2002; Clarke, 2013; Donovan et al., 2016; Flin and Yule, 2004; Krause, 2005). After the Fukushima Daiichi accident in 2011, leadership for safety has received increased international attention and has been more explicitly included in the requirements for licensees (e.g., IAEA, 2016; STUK, 2019).

Despite extensive scientific research done in the area of (safety) leadership and safety culture (for reviews, see e.g., Donovan et al., 2016; Fleming et al., 2018; van Nunen et al., 2018), many questions related to development of leadership and culture for safety still remain open. These open questions include: what approaches and methods nuclear facilities can use for safety culture improvement, how to assess the impact of such activities, how leadership (e.g., management walkarounds, leading with example, etc.) activities can be applied for safety culture improvement, and how to ensure their effectiveness.

EPIC is planned as a three-year project (2020–2022). The general objective of EPIC is to develop knowledge and approaches that support effective[2] improvement of leadership and safety culture. The effectiveness of leadership and safety culture improvement activities is viewed from a multi-level perspective (sociotechnically, Rasmussen, 1997; and culturally, Schein, 1985). Such an approach acknowledges that leadership activities and safety culture improvement initiatives can influence phenomena at different levels of culture (e.g., artefacts, behaviour, attitudes, norms, basic assumptions), and at different levels of the sociotechnical system (e.g., organizational, social, individual or technological level).

Specific project objectives include modelling the best practices of methodical safety culture improvement and safety leadership activities in Finnish power companies. The research study results in a framework describing effective approaches to methodical safety culture improvement (WP1), as well as a model characterizing safety leadership best practices observed in selected contexts (WP2). The outcomes of the study are expected to support the design and evaluation of effective nuclear safety improvement through culture development and leadership activities.

Methodical safety culture improvement (WP1)

Methodical safety culture improvement is done according to a systematic or established procedure, and with a planned and target-oriented approach (cf. YVL A.3 314). It requires applying a systemic approach. Nuclear power companies have implemented methodical safety culture improvement in their organizations, for example, by means hiring experts in social sciences and implementing safety culture programs. Safety culture improvement has therefore become an organizational function, to be ensured by the top management, and whose implementation is supported by safety culture experts.

The ways in which safety culture improvement function has been implemented show some variability, even between Finnish power companies. EPIC examines the different approaches to implement safety culture improvement, and the practices and methods considered to be effective. This is achieved by systematically modelling safety culture work in all Finnish power companies using document analysis and safety culture expert workshops. For this purpose, EPIC develops a methodical

[2] By “effective” we refer to improvement that is “successful in producing a desired or intended results” (Lexico.com definition) and that has a positive influence on nuclear safety

safety culture improvement framework, which is then used as a reference to collect experiential data from power companies.

Implementation of an organizational function is assumed to follow a Deming cycle (plan-do-check-act, ISO, 2015). Furthermore, because organizational culture emerges from the activities of the whole organization – and cannot be managed only by experts – it is assumed that to be effective, safety culture improvement function is extensively connected to all other organizational functions. Therefore, examining the approaches to implement safety culture improvement function involves modelling how the nuclear power companies implement phases of Deming cycle for safety culture improvement, and how other organizational functions are involved in each of the phases. In addition, the modelling process involves identifying the history and motivation (e.g., significant turning points) of safety culture work, as well as examining how safety culture experts and the power companies conceptualize safety culture. Figure 1 summarizes the modelling framework.

For each of the main themes (conceptualization, organizing, planning, implementation, assessment) of the methodical safety culture improvement framework, a list of items have been developed based on existing industry guidelines, scientific literature, as well as previous work done by the EPIC research team (e.g., Viitanen et al., 2018a, 2018b, 2017). The items are then reviewed based on power company documentation, and together with power company experts. As of early 2021, the draft version of the framework contains approximately 60 items[3]. A series of workshops begun in late 2020 with Finnish nuclear power companies during which data has been collected based on the framework. The draft framework has been observed to provide a good reference for modelling safety culture work. Based on the experiences of these workshops with power companies, development needs of the framework were identified. Some items still need to be added and some existing ones require further clarification. The workshops with power companies continue during 2021.

[3] Examples of items include:
What safety culture models are used for assessment/improvement? What advantages and disadvantages do they have? [conceptualization]
Is there a separate unit or division responsible for safety culture development? What does the unit do? How does its organizational positioning affect its work? [organizing]
How do you choose what safety culture activities are implemented? What are the key success factors for choosing good selection of safety culture activities? [planning]
What kind of safety culture improvement activities are conducted? What effects have you observed that are the result of safety culture work? What do you attribute them to? [implementation]
How is safety culture assessed? Which of the methods you use to assess and monitor safety culture do you find most useful, and why? [assessment]

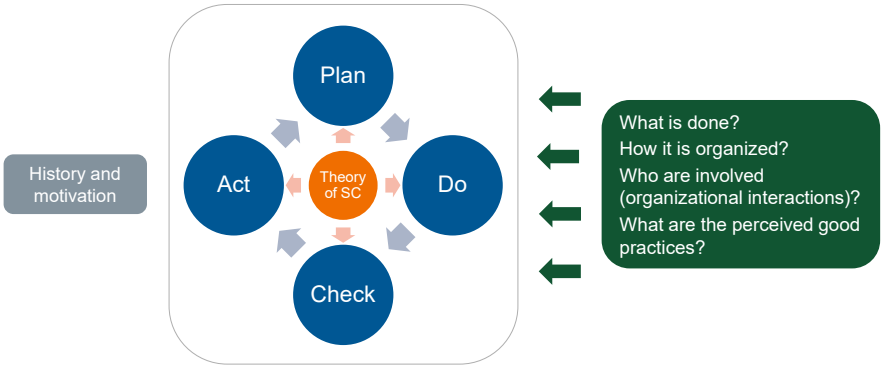

Figure 1. Illustration of the structure of the framework used for safety culture improvement function modelling.

Characterizing safety leadership in Finnish nuclear industry (WP2)

International requirements have recognized effective leadership as critically important for ensuring long-term safety performance of nuclear power organizations (e.g., IAEA, 2016). However, despite the global nature of the nuclear industry, what is considered good leadership may vary from one country to another. Moreover, the actual intended impacts and unintended consequences of leadership activities in the organizations may remain elusive. Sometimes leaders perform activities, which are seen as good but may have negative effects in the long-term. There is a need for a thorough understanding of the characteristics of leadership in the Finnish nuclear industry, and to gain a general in-depth knowledge on how to improve leadership for safety and managerial decision-making, specifically in light of the IAEA's GSR Part 2 requirements (IAEA, 2016, pp. 7–8).

EPIC addresses this need by identifying how safety leadership activities in selected contexts enhance safety culture, and by identifying the preconditions for good safety leadership, best practices and observed challenges. The project carries out focused case studies on leadership in all Finnish nuclear power companies. Leadership contexts were selected together with power companies and they include: case A (operational decision-making process and the related meeting practices), case B (management observation tours) and case C (safety leadership best practices of supervisors during daily work).

Our approach involves reflecting the data from multiple theoretical perspectives. First, nuclear industry expectations for leadership and its outcomes (e.g., behavioural or cultural change) serve as the baseline (e.g., GSR Part 2, Harmonized Safety Culture Model). Due to the general nature of how leadership is described in the nuclear industry documents, we complement them with additional models or approaches to leadership. Leadership style maturity model (Watts and Paciga, 2011) is utilized to characterize the extent to which leadership activities cover all

relevant aspects of the sociotechnical approach to safety, including technical leadership (focus on technology), systematic leadership (focus on processes and systems), systemic leadership (focus on people), and unitive leadership (focus on integration and alignment of human, technology and organization). Organizational tensions and contradicting goals approach (Reiman, 2015; Reiman et al., 2015) is utilized to identify the types of (contradicting) roles safety leaders may assume. Finally, national cultural characteristics (e.g., Hall, 1976; Hofstede, 1984; Trompenaars and Hampden-Turner, 1997) of the leadership activities are considered. These perspectives are summarized in Figure 2.

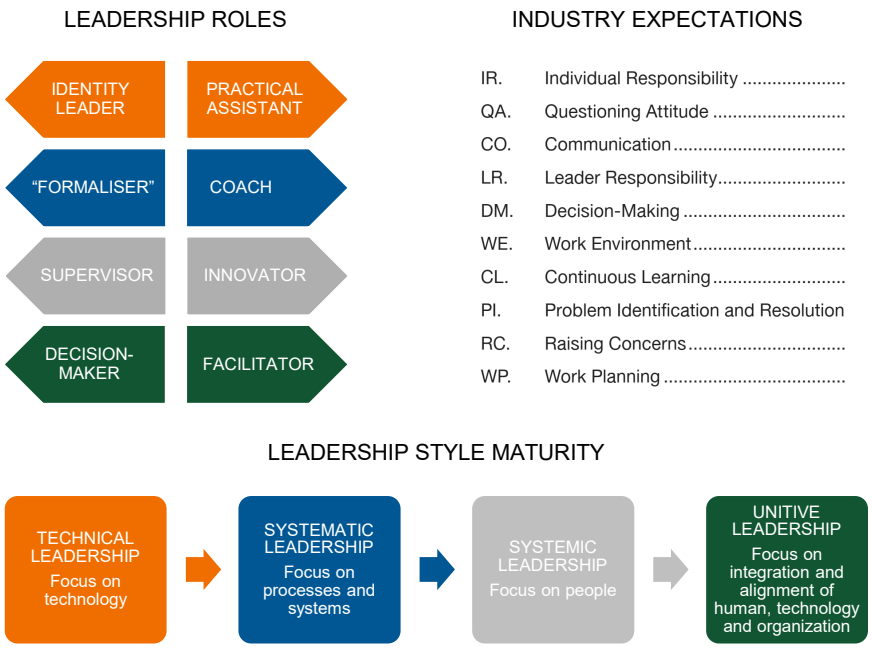

Figure 2. Summary of the perspectives used to examine leadership within EPIC.

In 2020, data collection (interviews and document analysis) and analysis related to case A (ODM process and the related meeting practices) was performed. It was observed that it was relatively easy to identify place case A findings within the safety culture and leadership models chosen. This suggests that the data analysis approach is practical. Using the analysis approach, we could identify a variety of leadership activities that work well (i.e., that support the ODM process and that facilitate safety culture).

In case B, observation tour register analysis and document analysis was performed. Open feedback field of the observation tour register was analysed by categorizing findings based on their polarity (negative, positive), inclusion of "people

leadership" issues as well as other relevant themes. Case B continues with interviews of observers and employees planned for early 2021.

As part of EPIC research study, a gap analysis (literature review) between nuclear industry requirements related to safety leadership and scientific literature on safety leadership was performed[4]. The analysis focused specifically on the safety leadership role and responsibilities of senior management. The analysis was not able to identify from safety leadership literature many empirical studies related to GSR Part 2 requirements 2:3.1b ("Acknowledging that safety encompasses interactions between people, technology and the organization") and 2:3.1d ("Establishing that decisions taken at all levels take account of the priorities and accountabilities for safety"). The analysis concluded that the study of senior management is challenging and recommended that facilitating the collaboration between research organizations and senior managers in nuclear facilities is one of the key factors to drive further the scientific study of leadership, as well as to assist practitioners in fulfilling the latest requirements on leadership and management for safety.

Summary

EPIC research study aims to identify effective leadership and safety culture improvement practices in Finnish nuclear industry. During the first year of the project (2020), the project started empirical case studies in all three Finnish nuclear power companies, as well as developed frameworks and data analysis approaches. The findings can be utilized by Finnish power companies (and other nuclear organization) in their activities to improve nuclear safety by means of leadership and safety culture development.

Empirical data collection and analysis continues in 2021. Dissemination to practitioners (research project report and final seminar) as well as academic audience (conference and/or journal articles) are planned for 2022.

References

Barling, J., Loughlin, C., Kelloway, E.K., 2002. Development and test of a model linking safety-specific transformational leadership and occupational safety. J. Appl. Psychol. 87, 488–496. https://doi.org/10.1037//0021-9010.87.3.488

Clarke, S., 2013. Safety leadership: A meta-analytic review of transformational and transactional leadership styles as antecedents of safety behaviours. J. Occup. Organ. Psychol. 86, 22–49. https://doi.org/10.1111/j.2044-8325.2012.02064.x

[4] Gotcheva & Airola: Leadership for Safety in Literature and International Requirements: Preliminary Gap Analysis at Senior Management Level. Presented at the IAEA online workshop on Systemic Approach to Safety, 7-10 December 2020.

Donovan, S.-L., Salmon, P.M., Lenné, M.G., 2016. Leading with style: a literature review of the influence of safety leadership on performance and outcomes. Theor. Issues Ergon. Sci. 17, 423–442. https://doi.org/10.1080/1463922X.2016.1143986

Fleming, M., Harvey, K., Cregan, B., 2018. Safety culture research and practice: A review of 30 years of research collaboration. J. Appl. Biobehav. Res. 23, e12155. https://doi.org/10.1111/jabr.12155

Flin, R., Yule, S., 2004. Leadership for Safety: Industrial Experience. Qual. Saf. Health Care 13, 45–51. https://doi.org/10.1136/qshc.2003.009555

Guldenmund, F.W., 2000. The nature of safety culture: a review of theory and research. Saf. Sci. 34, 215–257. https://doi.org/10.1016/S0925-7535(00)00014-X

Hall, E.T., 1976. Beyond culture. Anchor Books, Garden City, N.Y.

Hofstede, G., 1984. Culture's Consequences: International Differences in Work-Related Values. SAGE Publications.

IAEA, 2016. Leadership and Management for Safety (No. GSR Part 2). International Atomic Energy Agency, Vienna, Austria.

IAEA, 2006. Application of the Management System for Facilities and Activities (Safety Guide No. GS-G-3.1). International Atomic Energy Agency, Vienna, Austria.

IAEA, 1991. INSAG-4. Safety Culture (No. 75- INSAG-4), Safety Series. International Atomic Energy Agency, Vienna, Austria.

ISO, 2015. ISO 9001: 2015 - Quality Management Systems - Requirements. International Organization for Standardization.

Krause, T.R., 2005. Leading with safety. John Wiley & Sons, Hoboken, New Jersey.

Rasmussen, J., 1997. Risk management in a dynamic society: a modelling problem. Saf. Sci. 27, 183–213. https://doi.org/10.1016/S0925-7535(97)00052-0

Reiman, T., 2015. Turvallisuusasiantuntijoiden roolit, toimintatavat ja tarvittavat kyvyt ja taidot, VTT Technology. VTT Technical Research Centre of Finland, Espoo.

Reiman, T., Rollenhagen, C., Pietikäinen, E., Heikkilä, J., 2015. Principles of adaptive management in complex safety–critical organizations. Saf. Sci., WOS2012 71, Part B, 80–92. https://doi.org/10.1016/j.ssci.2014.07.021

Schein, E.H., 1985. Organizational culture and leadership. Jossey-Bass Publishers, San Francisco.

STUK, 2019. YVL A.3 Leadership and management for safety. Säteilyturvakeskus, Helsinki, Finland.

Trompenaars, F., Hampden-Turner, C., 1997. Riding the Waves of Culture: Understanding Diversity in Global Business. Nicholas Brealey Publishing.

van Nunen, K., Li, J., Reniers, G., Ponnet, K., 2018. Bibliometric analysis of safety culture research. Saf. Sci. 108, 248–258. https://doi.org/10.1016/j.ssci.2017.08.011

Viitanen, K., Gotcheva, N., Rollenhagen, C., 2017. Safety Culture Assurance and Improvement Methods in Complex Projects – Intermediate Report from the NKS-R SC_AIM (No. NKS-381). NKS.

Viitanen, K., Gotcheva, N., Rollenhagen, C., Reiman, T., 2018a. Safety Culture Assurance and Improvement Methods in Complex Projects – Final Report from the NKS-R SC_AIM (No. NKS-405). NKS.

Viitanen, K., Reiman, T., Rollenhagen, C., Gotcheva, N., 2018b. Mapping methodical change in safety culture. Presented at the Probabilistic Safety Assessment and Management conference, Los Angeles, USA.

WANO, 2013. Traits of a Healthy Safety Culture (No. PL 2013-01). World Association of Nuclear Operators.

Watts, G., Paciga, J.J., 2011. Conscious Adaptation: Building Resilient Organizations.

3. Plant Level Analysis

3.1 Co-simulation model for safety and reliability of electric systems in a flexible environment of NPP (COSI)

John Millar[1], Poria Divshali[2], Sergio Motta[2], Pasi Laakso[2], Timo Korvola[2], Matti Lehtonen[1]

[1]Aalto University
P.O. Box 15500, FI-00076 Espoo

[2] VTT Technical Research Centre of Finland Ltd
P.O. Box 1000, FI-02044 Espoo

Abstract

This interim report summarises the progress achieved thus far in the COSI project (the time of writing is February, 2021). Essentially, a co-simulation model has been developed that interfaces a Nuclear Power Plant (NPP) with its internal electrical network, which has already producing some interesting results, some of which have already been reported in D.1.1 and published. A scaled down first version of the Finnish transmission network has been modelled that has interfaced successfully with a simplified version of the internal electrical network, and some preliminary simulation results have been attained. The main challenges are implementing changes in the Apros modelling of the NPP, including endowing it with a time resolution commensurate with that required to model faults in the power system and getting the full co-simulation model running, i.e., the Apros modelling of the NPP and the Matlab Simscape models of the full internal NPP electrical network and a sufficient model of the external Finnish transmission network.

The authors are mindful of the computational burden and lack of efficacy in over-developing the transmission model. The main goal of the third year of the project is to improve the existing model to be fit for purpose and utilize it to investigate events in the internal network and transmission network that are most likely to adversely impact the NPP. To this end a simulation matrix is being developed so that we can most efficiently harness the resources we have available in the third year of this project. Preliminary simulations produced in report D.2.2 at the end of 2021 show promise, although it would be unwise to over-interpret these preliminary results.

Introduction

The general objective of this project is to study safety design principles of electrical systems, with the focus on the topics considered most relevant to the stakeholders in terms of plant level safety, systems safety, and component safety design.

The COSI project is tasked with developing a multi-physics simulation model which interfaces the internal electric power system of an NPP and the external high voltage transmission system with a thermomechanical operation model including the reactor physics and automation, for example, Apros. Such a model must encompass the entire chain of electrical systems, enabling a structured approach for the evaluation of possible common cause failures and the design principles of electrical systems in the existing and future NPPs, and small modular reactors including flexible operation. The simulation platform will be utilized for evaluating the adequacy and balance of the safety requirements of the electrical systems in an NPP during faults and disturbances.

Electrical systems perform various functions in an NPP, and they are required for the operation of many safety systems. In normal operation, all electrical systems are connected at the high voltage level, which creates the potential for common cause failures due to faults in the plant internal or external power system. In fact, several such incidents have been reported.

An overvoltage is a condition where the voltage applied to a component exceeds its design, for example, its insulation level. Overvoltages are classified into two types, depending on the length of the condition. Shorter events are known as transient overvoltages, while longer events are power frequency overvoltages. NPPs are generally considered to be well protected against transient overvoltages. However, the same is not true for power frequency overvoltages. The common causes of power frequency overvoltages are ground faults, reactive power imbalances and voltage control issues. In the Forsmark event in 2006, the generator voltage controller compensated the low voltage during a prolonged short circuit condition, and caused an overvoltage when the fault was disconnected. According to the literature, electrical transients may not have been adequately considered in the original design or later modifications of plants. However, no other similar incidents seem to have been reported.

An open phase condition (OPC) occurs when one or two of the three phases are disconnected. Typical reasons are mechanical failures of conductors or breakers. An OPC may cause significant phase imbalance downstream of the fault, and the level of imbalance is strongly affected by any downstream transformers and different load types. Many OPC analyses found in the literature focus on analysing or simulating the electrical behaviour of a single component or the entire electrical system of a plant. Typical components analysed are transformers and induction motors. Theoretical calculations, computer simulations and laboratory measurements have been found to agree reasonably well. However, analyses of entire electrical systems appear to be somewhat limited, in three respects. First, most simulations use very simple models of the loads, where small loads are aggregated into larger units and all loads are modelled as constant or using a simple mathematical relationship. Second, the simulations only consider electrical effects, ignoring any potential dynamics or feedback from electrical protection or the thermomechanical system. Finally, even time-domain simulation studies appear to be most interested in steady-state behaviour rather than transient effects. In OPC analysis, dynamic temporal effects

are important, because the key question is whether motors trip, overheat or keep running until the fault is cleared.

Subsynchronous oscillations (SSO) comprise several related conditions where components in the electrical system interact in an oscillatory manner. They are divided into two traditional types and one more recently discovered type, depending on which devices participate in the interaction. In subsynchronous resonance (SSR), the oscillation occurs between a synchronous generator and a series compensated power line, while with subsynchronous torque interaction (SSTI), a synchronous generator interacts with an actively controlled device in the grid. Sub-synchronous control interaction (SSCI) occurs when an actively controlled generator (e.g., a wind turbine) interacts with a series compensated power line. Subsynchronous oscillations cause significant stresses on electrical and mechanical parts of the system because the amplitude of the oscillation will increase until something gives way. The turbine generator shaft is usually the weakest link in an interaction that involves a synchronous generator. Generator shaft damage is expensive to repair, and flying debris resulting from shaft failure could hypothetically affect safety systems in an NPP. An SSR first occurred at the Mohave coal power plant in 1970. Since then, it has been researched extensively, and SSO analyses are a routine part of HVDC, series compensation and power plant projects. Typical studies include mathematical analyses and electrical simulations. Simulations in particular are a more useful tool than before due to increased computational resources. SSO has been studied in nuclear power plant generators, as NPPs typically have large turbine generators that are susceptible to SSOs. However, it does not appear to have been considered from a nuclear safety perspective before, and neither have its potential effects on the thermomechanical system. Three particularly relevant conditions (power frequency overvoltages, open phase conditions and subsynchronous oscillations) were selected for in-depth analysis. Based on the literature review and analyses, these three conditions were recommended for simulation in the COSI project, although from the vantage-point at the beginning of 2021, we are forced to consider whether the transmission system model will be adequate for a credible investigation into subsynchronous oscillations - at least this is unlikely in 2021.

Existing electrical simulation studies have not considered thermomechanical system feedback effects and other transient dynamics in much detail. Most of the NPPs in Finland use Apros as the main simulation tool for the thermomechanical and automation process. However, since Apros cannot simulate the detailed electrical system events, e.g., unsymmetrical faults such as single-phase faults in the electric system, detailed electrical power system models are simulated using other simulation tools. In these circumstances, the interaction of the electrical system and the thermomechanical system tends to be neglected, which indeed motivates the aim of WP1 in the COSI project, the design of the architecture of the co-simulation platform for an NPP, which is the subject of the next section. The following sections will summarize the modelling progress in each of the domains and some preliminary base-line results will be presented, along with the direction of future work.

Platform Architecture

As stated above, the aim of WP1 in the COSI project is to design the architecture of the co-simulation platform for NPP. The co-simulation platform provides the opportunity to simulate the interaction between detailed models implemented in different simulation tools. In this platform, the master program is developing using the Matlab (or Python). Apros will be the Open Platform Communications (OPC) server and the master program is the OPC client for connecting to Apros. The master program connects to other power system simulators using the appropriate protocol, which depends on the simulator's features. In this architecture, the master program, MATLAB, delivers the mechanical model of APROS to the power system simulators. In the same way, the master program delivers the electrical model of power system simulators to APROS. The power system simulators can consist of the various tools used for simulations, such as PowerFactory, Simulink, etc. The challenge of building the architecture of the COSI co-simulation platform covers the data exchange layout among simulators, data exchange intervals, time step handling, the protocol of data exchange between simulators and the initialising of simulators. The proposed co-simulation architecture for the COSI platform is shown in Figure 1, [1].

Following the architecture design in 2019, WP1 has developed the first version of the co-simulation platform in 2020. The master program, in principle, coordinates the domain-specific simulation tools. At present it connects to Apros using an Open Platform Communications (OPC) data connection. The FMI-Compliant Interface developed based on TCP/IP protocol could be used in the future for PSCAD, for instance.

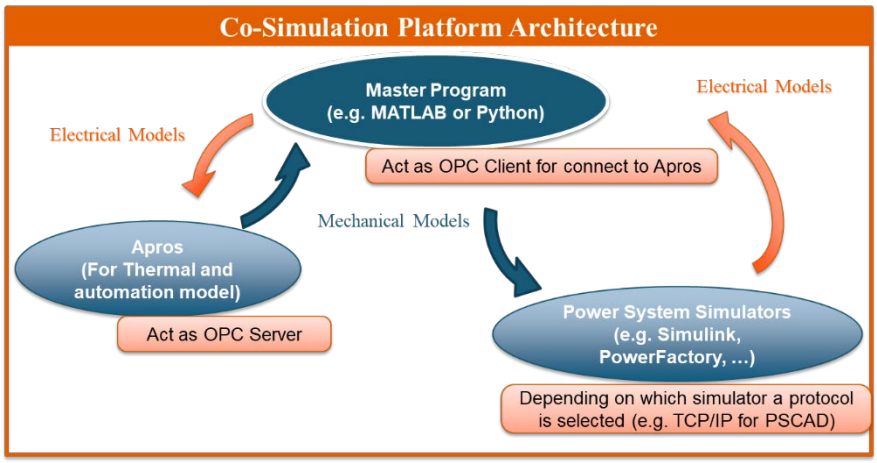

Figure 1. The co-simulation architecture for the COSI platform.

To verify the co-simulation platform, small thermomechanical and electrical models have been used. The electrical model includes a generator, which through a unit

transformer is connected to the high voltage grids and through an auxiliary transformer provides energy for three large motors. The generator is coupled to a turbine shaft and the motors are coupled to: the basic pump, motor pump, and common pump in Apros. The simulation results show that the co-simulation works well. All involved tools have their normal usage environment available that can be used to view simulation results and allow the user to edit and change the settings in all simulators simultaneously. This enables the model and tools that are developed in each domain-specific simulator to be used directly by their respective domain expert, while the co-simulation platform can analyse the interaction of these different domains without simplifying the models of any of the domains.

First Implementation of the Co-simulation Platform

WP2 implemented a real NPP model using the developed co-simulation platform. Although the co-simulation in the small model works well, with the complete NPP model the co-simulation faced some challenges when trying to integrate the generator from the electrical simulator to the turbine/shaft from Apros. There is a conflict when there is more than one generator, as Apros calculates the frequency of the electrical system and writes over what was written from the electrical simulator. This conflict will be resolved this year. The Master Program has several main sections/functions, as reported in D.1.1 [2], where the detailed code is also given:

- Set Co-simulation parameters
- Define Input Layout
- Create Data Structure and OPC HOST
- Initialising
- Co simulation loop
- Data exchange
- Progress report and plot results

Naturally, the co-simulation requires several parameters, including the co-simulation time range, the time-step of each simulator, the names of the Simulink files containing the internal and external grid models, and the name of the file and variable indicating where to save the initial data, which facilitates computation times by starting the fault simulations from steady-state initial conditions (it takes some time for the steady-state to be achieved in a large system).

Data regarding the turbine-generator sets and the various types of Motor-Pumps must also be provided, as there are various options to be chosen from. User instructions for the Apros and Simulink/Simscape models and the Master Program itself have also been developed.

The results from the first simulations have highlighted that the existing simplification assumptions and neglecting the interaction between the electrical system and thermomechanical system can misrepresent the electrical and thermomechanical behaviour during an electrical fault, shown in the first part of the results section. The other, as yet minor, achievement of the project thus far is a successful coupling of

a simplified transmission network model with a simplified model of the NPP's internal electoral network, but without full thermo-mechanical modelling of the NPP itself. The results give some faith that the Simulink/Simscape platform is suitable at least for a scaled-down model of the transmission grid, but significant research results have not yet been attained, and the transmission model will require some further development to have some credibility.

The following figures show the various models that have so far been developed. Figure 2 is a simplified (for publication purposes) version of the Apros thermomechanical modelling of the NPP. Figure 3 is a simplified (also for publication purposes) version of the NPP's internal electrical network, and Figure 4 is a highly simplified model of Fingrid's transmission network. Although overly simplistic, Figure 4 represents a pragmatic first step, given that this modelling has had the least research time devoted to it, and that it is sufficient to test the potential efficacy of the full co-simulation approach.

Whilst there are challenges with suitable time steps and some file conflict between the Apros and Simulink platforms, which will be soon resolved, the COSI project has already achieved some promising results, including, from the more mature parts of the project, publishable material that has raised some interest. This will now be outlined in brief, as [1], [2] and [3] are readily available, and relate the work done so far in more detail.

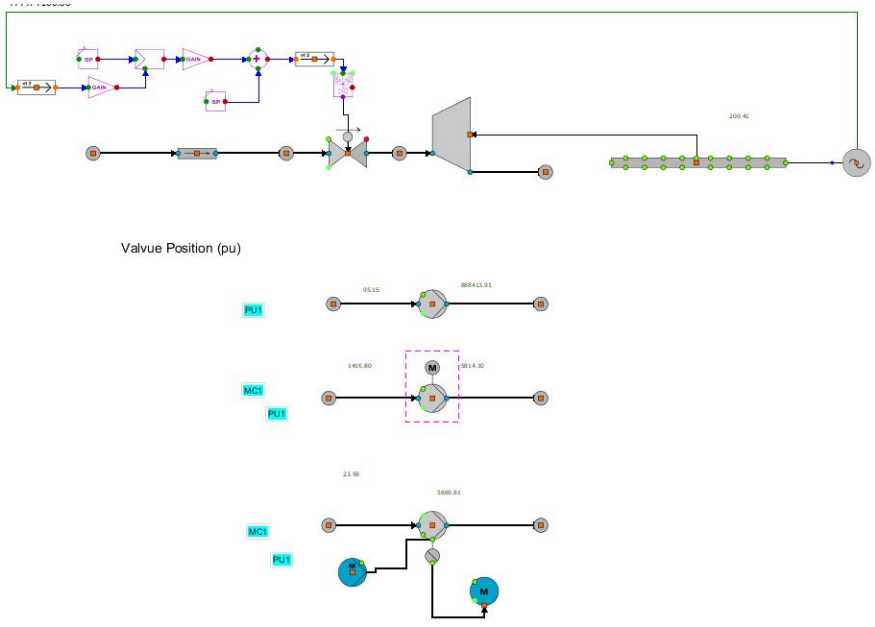

Figure 2. Apros model used in the published test cases.

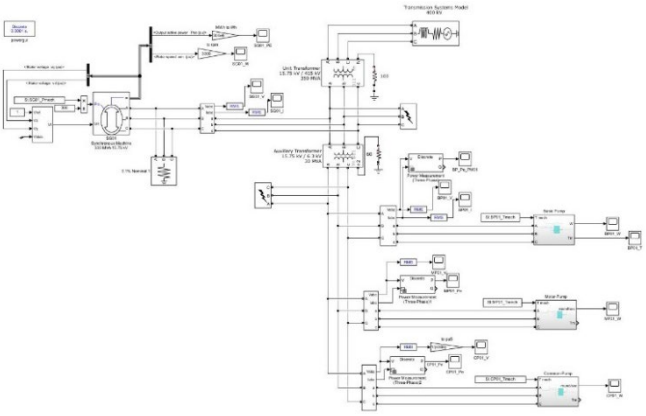

Figure 3. The Simulink/Simscape simplified model of the NPP's internal network.

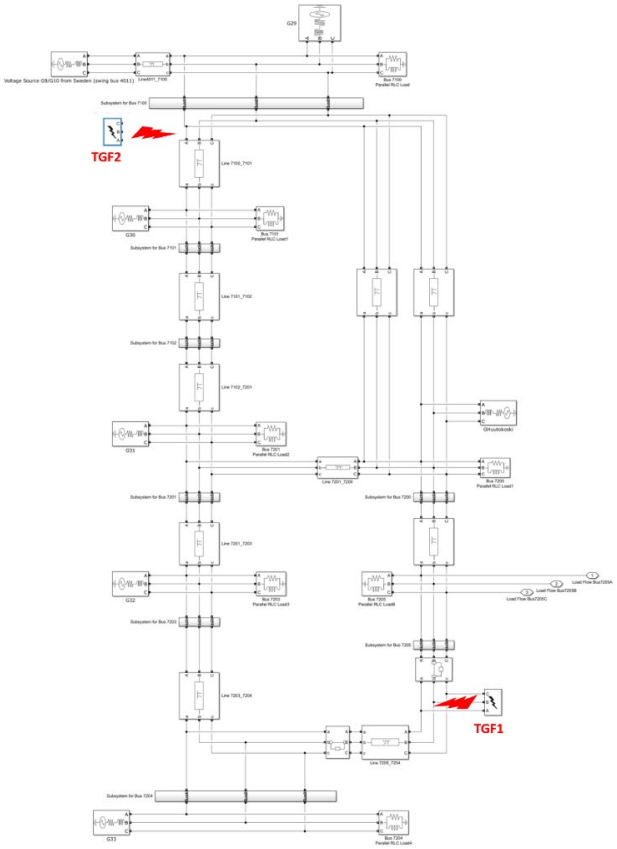

Figure 4. The preliminary 8-node simplification of the Finnish transmission network taken, with significant modifications, from the 57-node Nordic model.

Results

The most notable result from D.1.1 is shown in Figure 5, which indicates that co-simulation (a coupling of the models in Figures 2 and 3) reveals instability in the motor-pump set when subject to a single-phase fault, whereas without the thermo-mechanical modelling (Figure 3 on its own), the simulation misses this potentially critical behaviour. Whilst protection is likely to operate before the red lines deviate from the blue in Figure 5, the figure clearly indicates that the two models are not equivalent, justifying the incorporation of full thermomechanical modelling of the NPP in simulations.

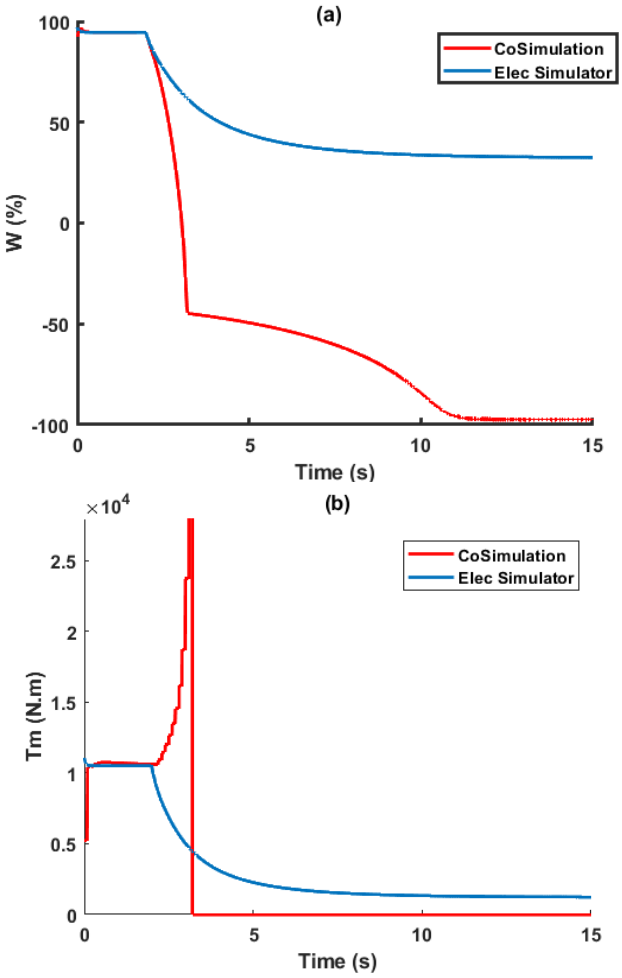

Figure 5. Simulation without co-simulation indicates stability of the motor-pump set whereas co-simulation (coupling with the thermomechanical system) reveals otherwise.

Rather than reproducing simulations published elsewhere, we refer the reader to [1] and [2].

The other achievement thus far in the project is the combination of the models in Figs. 3 and 4, where the single node Thevenin equivalent shown in the top right of Figure 3 is replaced by the simplified model of the Finnish transmission grid, where the interface is via the 3 phase connectors at the bottom right of Figure 4. The 8-node transmission model is based on a Nordic 57 node model [4], with reference to data used in a more comprehensive model in Nina Helistö's master's thesis [5], published generation data from [6], consumption data derived from time series data from [7] allocated to the nodes (very approximately…) to create maximum winter and minimum summer load scenarios, as shown in Table 1, [3].

Table 1. Generation [5] and demand data [6] used in baseline simulations involving transmission grid model.

	Adjusted winter						
	P_G29	1201.83	MW	2019 Finnish time series data from Fingrid			
	PloadBus7100	1341	MW		**Consumption**	**Generation**	
	QindLoadBus7100	250	Mvar	**Minimum**	5413.1	3932.1	MVA
				Maximum	14665	11331	MVA
	P_G30	1090.93	MW				
	PloadBus7101	3341	MW				
	QindLoadBus7101	590	Mvar				
					P_GHuutokoski	1048.83	MW
	P_G31	1090.93	MW		PloadBus7200	300	
	PloadBus7201	2800	MW		QindLoadBus7200	40	
	QindLoadBus7201	450	Mvar				
	P_G32	3315.33	MW		P_G34	1014	MW
	PloadBus7203	2800	MW		PloadBus7205	300	MW
	QindLoadBus7203	450	Mvar		QindLoadBus7205	30	Mvar
			P_G33	2568.83	MW		
			PloadBus7204	3600	MW		
			QinLoadBus7204	500	Mvar		
Adjusted winter							
Aggregate Generation		**11330.7**	MW				
Aggregate Demand		**14665.07**	MVA				

Line lengths and types were refined by reference to Fingrid published data [7] and a geographical data base [8]. The modelling is at least running, and some confidence has been gained by it giving a similar response to a 3-phase short-circuit (without protection operating) as the Thevenin equivalent, meaning, in that respect at least, the model shown in Figure 4 behaves as well as the node in the top right corner of Figure 3.

The results for this base-line simulation are shown in Figure 6.

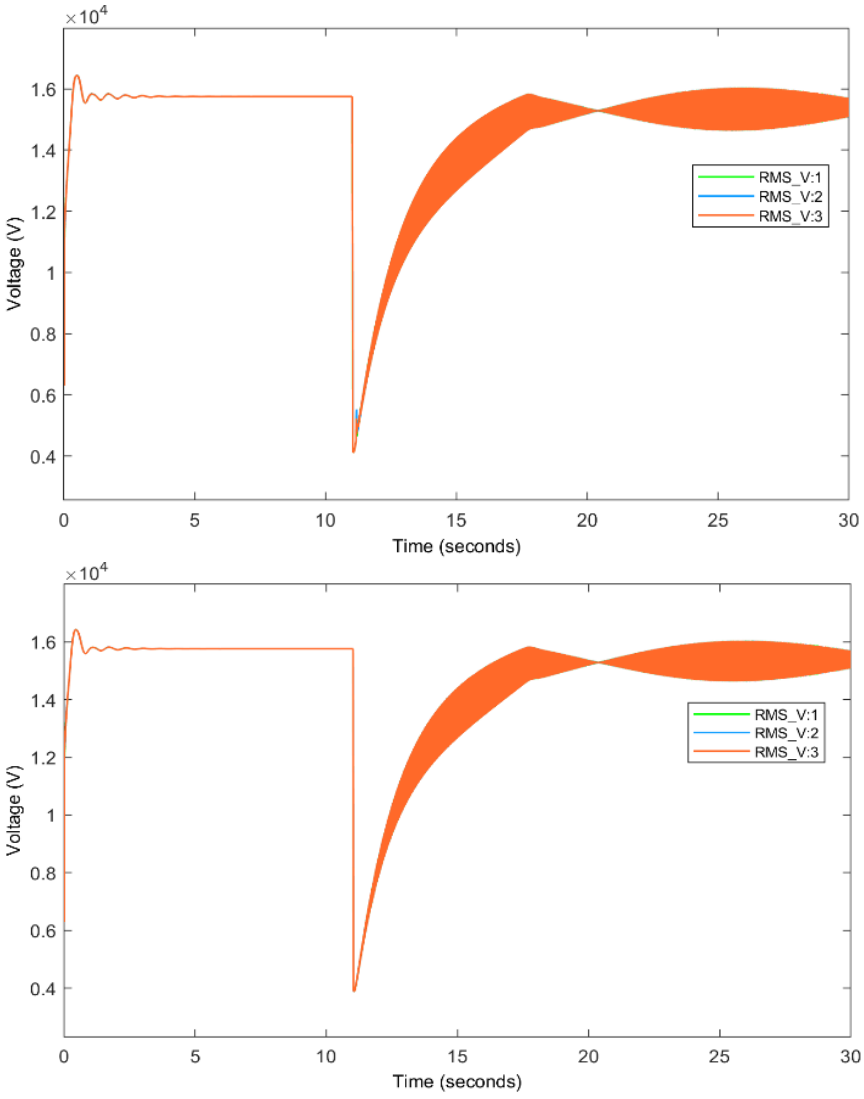

Figure 6. Initial transient voltage response (before the model reaches a steady-state condition) and the voltage response after a 3-phase short circuit on the feeders connecting the simplified co-simulation model with transmission model – the 8-node model on the left and the single Thevenin equivalent node model on the right [3].

What a distributed model can achieve that a single node cannot, has been hinted at in simulations found in [3], and the next section outlines the next steps to be taken.

Next Steps

There are small bugs that need resolving, including the earlier mentioned file writing conflicts and time-step issues. There seem to be some issues with trying to replace voltage sources with basic synchronous generators in Simscape, which is not a show-stopper for this year's simulations, but nevertheless would be good to resolve. Whilst we have been advised and have resolved not to attempt a rigorous and complete model of the Finnish transmission system this year, we will have to check our assumptions and add a few nodes to make the model credible for the work under focus.

An NDA will soon allow Aalto access to the full internal electrical model of the NPP, but Aalto will not have access to the Apros modelling of the thermonuclear model of the specific NPP under investigation. Therefore, it has been determined that a simulation matrix will be developed and that Aalto will run simulations with the transmission model interfaced in Simscape with the model of the internal electrical grid of the NPP but without the Apros model to ascertain the scenarios most likely to be of interest for full modelling. VTT will then carry out a subset of the simulations for full investigation with the entire co-simulation model. This would seem to be a suitable division of labour. The first draft of the simulation matrix from the 2021 COSI project plan is reproduced in Table 2 of this document, with the fault positions marked in Figure 7. Note that we will need simulations to verify whether or not scenarios are 'not interesting to simulate'.

Table 2. Different fault types and fault locations suggested for the fault-based studies. Cases marked in green are preliminarily identified as priorities, and cases without any marks are identified as not interesting to simulate.

		LG	LL	LLG	LLLG	OPC (1 phase)	OPC (2 phase)
Faults in External Grid (off-site)	Location 1	✓	✓	✓	✓	✓	✓
	Location 2	✓	✓	✓	✓	✓	✓
	Location 3	✓	✓	✓	✓	✓	✓
Faults in Internal Grid (on-site)	Location 4	✓	✓	✓	✓	✓	✓
	Location 5					✓	✓
	Location 6	✓	✓	✓	✓	✓	✓
	Location 7	✓	✓	✓	✓	✓	✓

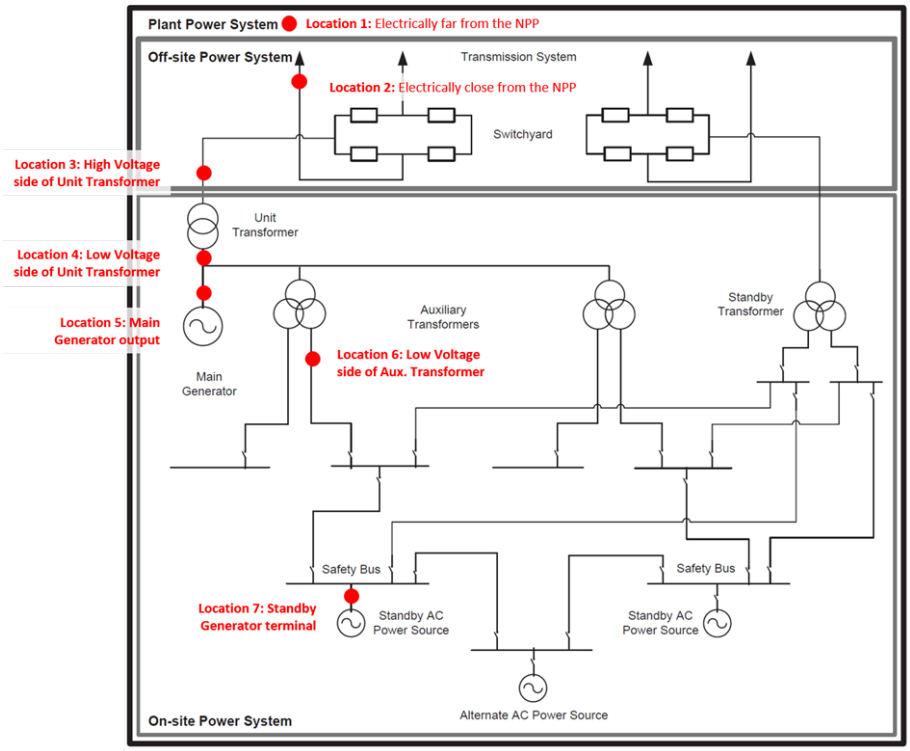

Figure 7. Preliminary indication of possible fault locations on both on-site and off-site (transmission) systems.

Summary and Conclusions

Putting it simply, thus far we have succeeded in coupling the Apros model in Figure 2 with the model of the internal electrical network shown in Figure 3, which has been reported in D.1.1 [2] and published in [1], and in coupling the models of the internal network and the external transmission network (Figure 3), as reported in D.2.2 [3]. There are some issues, as mentioned above, with time-steps, file conflicts and some as yet unresolved anomalies with Simscape. These challenges are part of research, and the parties in VTT and Aalto are keen to get on with the research!

It remains to be seen how much having a model of the actual transmission network changes the results of the simulations of the impact of faults in the internal network on the NPP. Thus far these simulations have simply used a Thevenin equivalent (single node) equivalent of the transmission network. The addition of the transmission model to the co-simulation platform will enable the assessment of how close to the NPP transmission grid faults might impact the functioning of the NPP, and conversely, how far from the NPP faults within the NPP might impact the transmission grid and all that is connected to it. We will rely on the steering group members

and Fingrid to advise us on the range of faults that might occur in the transmission grid and in the NPP, and how quickly circuit breakers operate, their selectivity, and the chance that they may malfunction. It is expected that we should be able to follow up the publication [1] with another this year, depending on what we find.

References

[1] Divshali, P., Laakso, P., Hänninen, S., Millar, J. & Lehtonen, M. 2021. “Electrical and Thermomechanical Co-simulation Platform for NPP”, Energies, 14, x. https://doi.org/10.3390/xxxxx, Accepted for publication.

[2] Divshali, P., Hänninen, S., Laakso, P., Korvola, T. & Millar, J. 2020. “The COSI Project, D1.2. Description of the simulation platform”, VTT Research Centre of Finland.

[3] Millar, J., Divshali, P. & Laakso., 2021. “SAFIR-COSI WP2 report: D2.2: Baseline simulation results”, Aalto University publication series SCIENCE + TECHNOLOGY, 1/2021, ISSN: 1799-490X, http://urn.fi/URN:ISBN:978-952-64-0252-9.

[4] Zorgrafos, Dimitrios. 2019. "Power System Inertia Estimation and Frequency Response Assessment“, Doctoral thesis, Kungliga Tekniska Högskolan, Stockholm, December. http://kth.diva-portal.org/smash/get/diva2:1369967/FULLTEXT01.pdf.

[5] Helistö, N. 2012. "Suomen kantaverkon mallintaminen tehonjakolaskentaa varten", Master’s thesis, Helsinki University of Technology, Espoo, Finland.

[6] Finnish generation data, downloaded from https://energiavirasto.fi/toimitusvarmuus#voimalaitosrekisteri on September 4, 2020.

[7] Fingrid’s Open Data portal: https://data.fingrid.fi/en/dataset?keywords_en=Real+time+data

[8] Kantaverkko 1.1.2020 Voimajohdot, downloaded from https://www.epressi.com/media/userfiles/107305/1551708488/kantaverkon-nimeaminen-johdot-ja-asemat-2020-luonnos.pdf.

[9] Maanmittauslaitos karttapaikka: https://asiointi.maanmittauslaitos.fi/karttapaikka/

3.2 New developments and applications of PRA (NAPRA)

Ilkka Karanta, Kim Björkman, Atte Helminen, Terhi Kling, Timo Korhonen, Marja Liinasuo, Tero Tyrväinen

VTT Technical Research Centre of Finland Ltd
P.O. Box 1000, FI-02044 Espoo

Abstract

NAPRA aims at generating new knowledge about various topical issues in probabilistic risk assessment (PRA).

The Finnish seismic PRA practices have been compared with international ones.

A simulation-based event tree model has been developed for a cable room fire scenario; the model offers several advantages over a probabilistic fire model. The event tree includes an operation time model, which is used for gaining timing information of fire detection, fire brigade actions, and other human actions. The reliability of sprinkler systems has been studied concerning both available literature and a case study.

The PRA of long time windows has been considered from many viewpoints in the Nordic PROSAFE project. A Finnish pilot model of spent fuel pool, utilizing simulation-based event trees, has been developed and compared with other advanced PRA methods used by Swedish research partners; the resulting fuel damage frequencies are quite comparable. A human reliability analysis (HRA) model for the pilot that handles both recoveries and repairs has been constructed.

Human reliability in dynamic contexts has been studied through a literature review, operator interviews and a stakeholder survey.

PRA of systems involving digital subsystems has been studied together with five foreign research partners in an OECD/NEA WGRISK initiated benchmark study called DIGMAP. Each participant has modelled the same reactor protection system (RPS) with their own approach. The results demonstrate the importance of identification of common cause failure groups, and of the diversity (or lack of it) of the RPS.

A stakeholder survey concerning the methods, uses and applications of failure tolerance analysis (FTA) has been conducted. The survey clarified the present status of FTA in Finland, the role and purpose of FTA, and the connections between FTA and PRA. An FTA example analysis has been carried out, illustrating the FTA process and highlighting how some parts of FTA could be conducted.

A literature study on the PRA of small modular reactors (SMR) has been conducted. The main issues in applying PRA to SMRs concern the handling of passive safety features, and modelling and analysis of multi-module plants.

Introduction

The general objective of NAPRA (2019-2022) is to develop methods and analyses for probabilistic risk assessment (PRA) of nuclear facilities. It encompasses most PRA research carried out in SAFIR2022. Despite decades of development, there still exist room for improvement in PRA methods and methodology. A case in point is the need to account for the dynamicity of accident scenarios and human involvement in them. New developments such as the need to take long accident progression time windows into account pose challenges to PRA. Emerging technologies, such as small modular reactors, bring modelling and analysis issues that must be addressed for credible PRAs. The key challenge of NAPRA is to address – and within resource constraints, to contribute to – a wide-ranging and topical mix of PRA research themes that are relevant and interesting from the Finnish nuclear safety point of view.

PRA is by its nature multidisciplinary, and aims at a holistic understanding of risks that the system under consideration is subjected to. This is reflected in the different work packages of NAPRA that is 1) developing methods for and understanding of external and internal hazards and their impact on nuclear facilities, 2) considering the issues with and select and apply methods for the analysis of accidents with long time windows and of humans and crews working in dynamic contexts, 3) exploring the features and problems related to the reliability assessment of systems containing digitalized subsystems, and their role in PRA, and 4) dealing with the challenges of such emerging fields as multi-unit and site-level PRA, and the PRA of small modular reactors.

Hazards

Typically, a significant portion of core damage risk comes from external and internal hazards (OECD 2014; OECD 2015). Therefore, it is important that the hazard analyses, estimated frequencies and modelling of the consequences of hazards are sufficiently realistic. To achieve this, proper integration of deterministic and probabilistic hazard analyses is needed. In addition, it is important to analyse human behaviour in hazard scenarios.

The Finnish seismic PRA procedure has been outlined and compared with international practices (Helminen 2020). The outline is shown in Fig. 1. The international reference considered was a draft technical opinion paper (OECD 2019) that represents the technical opinion consensus of risk analysts and experts in OECD NEA member countries concerning seismic PRA for nuclear facilities. Based on the comparison, and discussions with the PRA experts of Fennovoima, differences and potential topics for more detailed research were identified. The following two were identified as central: connecting risk significance and fragility analysis of systems, structures and components (SSC); and developing general seismic PRA modelling principles. The following three were also identified as interesting: more detailed

study of seismic HRA; failure correlation and seismic grouping of SSCs; assumptions applied to the seismically induced LOCAs, fires and floods.

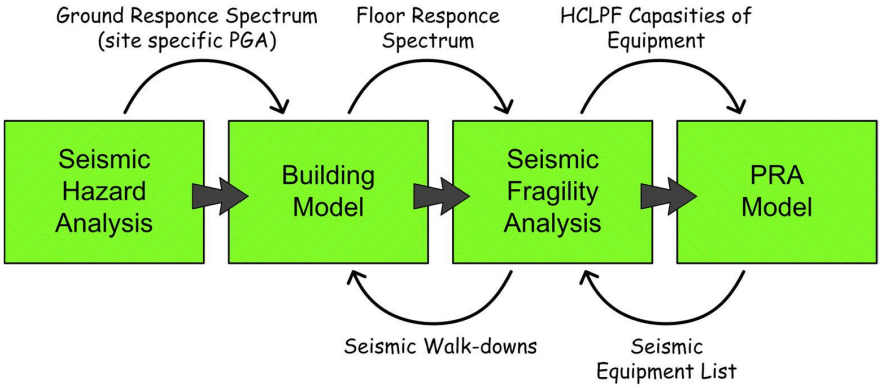

Figure 1. An outline of the Finnish seismic PRA procedure.

We have implemented an old nuclear power plant cable room fire scenario (Hostikka et al. 2012) in a new tool, simulation-based event tree of FinPSA (Tyrväinen et al. 2020b, Tyrväinen et al. 2021b). Simulation-based event trees are event trees with user-written computation scripts that calculate probabilities of event tree branches and possibly other variable values; a module in the FinPSA code implements this functionality (VTT 2019). The scenario concerns a fire occurring in a cable room that contains both power and instrumentation and control (I&C) cables of two redundant subsystems. The cables of the subsystems are physically separated in a multilevel metallic cable tray system. In the places where the cables of different subsystems are near each other, mechanical shield plates have been installed between the cable trays. The cables are the primary fire load in the room, and the power cables are the most probable source of ignition. In the study, the ignition was assumed to occur in one subsystem, and the analysis aimed at estimating cable damage probability in the other subsystem.

The main components of the model are the event tree, Monte Carlo fire simulations, and a stochastic operation time model for firefighting. Fire simulations from the old case study (Hostikka et al. 2012) were utilised. In that study, 200 fire simulations were performed separately using deterministic Fire Dynamics Simulator (FDS) (McGrattan et al. 2013), 100 for the case with sprinklers operating and 100 for the case with sprinklers failed. To get a representative sample, the Excel-based Probabilistic Fire Simulator (PFS) (Hostikka & Keski-Rahkonen 2003) was used for generating the inputs to FDS with Latin hypercube sampling. The random variables included the location of the initial fire, the size of the initial fire, properties of power cables and concrete, and the response of the sprinkler system (if working). For each simulation, the time was determined when the temperature of the insulating material of the cables reaches critical temperature; it is assumed that the cables fail in this temperature. There is some uncertainty on what the critical temperature of a cable

is, two alternative critical temperatures, 180 °C and 215 °C, were used in the analysis. Results of the fire simulations were imported to FinPSA as vectors (Tyrväinen et al. 2020b). The relevant variables imported were the detection time, cable damage time and time when firefighting conditions become intolerable.

The stochastic operation time model is implemented in FinPSA scripts in eight parts corresponding to different operational phases, including fire detection, guard centre actions, control room actions and fire brigade actions. The event tree is presented in Figure 2. The FinPSA model was simulated 10000 times. For each individual fire simulation and operation time simulation, it was checked whether the fire brigade was able to suppress the fire before cable damage. Furthermore, it was checked whether the firefighting conditions (temperature, visibility, heat radiation) were tolerable when the fire brigade arrived in the room. The results calculated using FinPSA are approximately same as the results calculated by the old tool, PFS, but FinPSA offers better model structure, better readability and better maintainability than PFS.

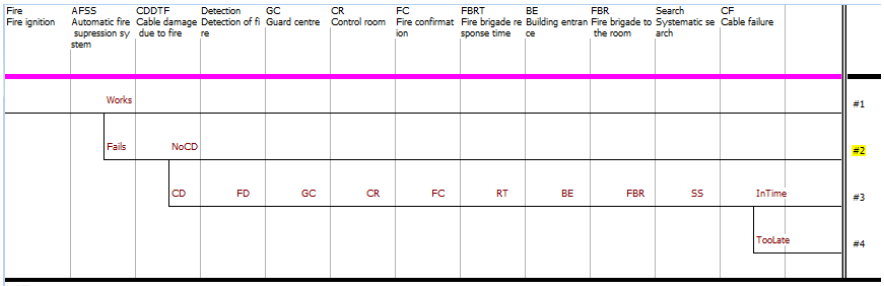

CF

```
function real TooLate
  $ Operation time from the detection to the beginning of the systematic search is calculated
  t_oper = t_co+t_v
  if t_cr < t_gc+t_rt+t_be+t_re then
  begin
    t_oper = t_oper+t_gc+t_rt+t_be+t_re
  end
  else
  begin
    t_oper = t_oper+t_cr
  end
```

Figure 2. Simulation-based event tree model for cable room fire scenario including stochastic operation time model for firefighting.

We also performed further analyses with the old fire simulations. It was found that the cable fires were of two different types (Figure 3). Small fires (less than 1 GJ of released energy, occurrences about 40 % of all simulated cases) are local fires that do not spread, and burn out by themselves before cable damage. Large fires (more than 10 GJ of released energy, occurrences a little more than 50 % of simulated cases) spread along the cable trays horizontally and/or vertically. Almost all small fires are initiated at the cable trays that are close to the ceiling, whereas larger fires are initiated at lower cable trays.

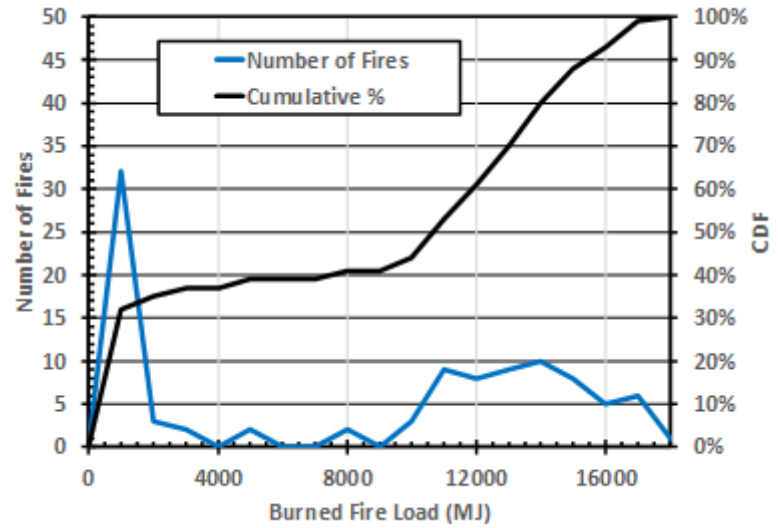

Figure 3. The frequency distribution of energy released in a fire in the cable room fire simulations.

An example of fire simulation results is presented in Figure 4. The picture represents the time “visibility lost” (too much smole) criterion is yielded as a function of the time when cable temperature reaches 215 °C (critical temperature, see above). These two quantities are highly correlated with each other, and thus the time when cable temperature reaches a certain level can be used as a proxy for the time when it becomes difficult for the fire brigade to extinguish the fire – equipment may be needed for breathing, and a heat camera is needed for locating the fire. Furthermore, this correlation is not sensitive to height at which smokiness has been estimated. Another thing that can be seen from the figure is that cable damage occurs in this scenario typically in less than 30 minutes (1800 seconds). Within this time, the fire should be detected, the fire brigade alarmed, the fire brigade entered the cable room door and the power cables in the room de-energized. From operation time simulations it seems that this available time is usually too short for the fire brigade to extinguish the fire before cable damage.

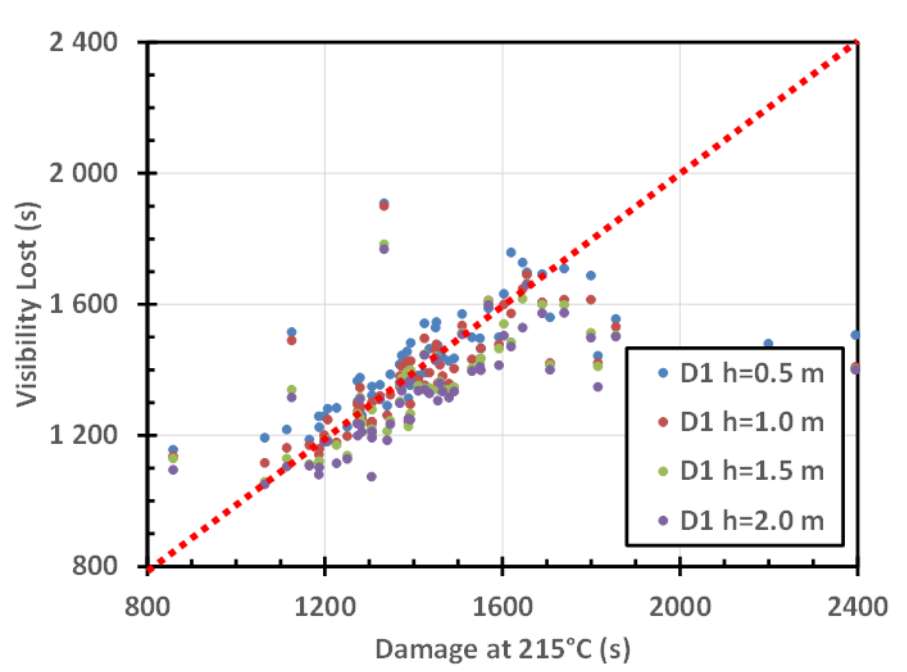

Figure 4. The time "Visibility lost" criterion is yielded as a function of the time when cable temperature reaches 215 °C in the cable room fire simulations.

A large number of uncertainties have been identified for the cable room fire PRA study. The uncertainties are related to fire simulation parameters, interpretation of fire simulation results, fire simulation model itself, computation methods, time delays of firefighting actions and reliability of the automatic suppression system. The significances of different uncertainties have been assessed according to possibilities. Most of the uncertainties have been assessed to have a small significance for the results. The most significant uncertainties are related to some fire simulation parameters (particularly time of maximum heat release rate), reliability of the automatic suppression system and some central firefighting actions.

We have studied reliability analysis of sprinkler systems by reviewing previous analyses found in the literature and conducting a simplified fault tree analysis for a generic wet pipe system (Tyrväinen et al. 2021b). Such reliability analyses have been quite rare or at least not published. Collection of sufficient amount of failure data for sprinkler system components is necessary for credible reliability analysis.

Probabilistic risk assessment with long time windows

PRA models are mostly very simplified with regard to mission times of safety functions, timings of events and repairs of components (Tyrväinen et al. 2020a). Typically, a mission time of 24 hours is assumed for most safety functions in level 1

PRA. The Fukushima nuclear power plant accident however pointed out that it might be relevant to consider longer time windows in some accident scenarios. In addition, spent fuel pool accidents typically last at least several days. In such long accident scenarios, it is important to model recoveries and component repairs, because there is lots of time to perform them and without crediting the repairs the results would be very conservative. Also, existing human reliability analysis methods have mainly been developed for shorter time windows, and the static PRA methodology has limited capability to represent long-lasting accident scenarios, which are dynamic in nature. There are also other issues related to long time windows, such as how to specify mission times and success criteria, that needed clarification. Due to these issues, a Nordic project called “Prolonged available time and safe states” (PROSAFE), funded partially by NKS and NPSAG, was implemented in 2019-2020 in cooperation with Swedish and Norwegian research partners.

Literature review and stakeholder survey on long time windows

Two surveys were carried out in PROSAFE, a literature survey and a stakeholder survey (Tyrväinen et al. 2020a). The topics encompassed by the surveys included safe state, acceptance criteria, success criteria, mission time, HRA methods (especially regarding long time window), and crediting recoveries and repairs.

The issue of safe, stable state (SSES) is of importance in PRA, because reaching one within the mission time (time window of the analysis) is a prerequisite for considering that core damage (PRA level 1) or large release (PRA level 2) has been avoided; otherwise a judgmental modelling decision has to be made (e.g. extending the mission time to a point where stable safe state is reached, see (IAEA 2016)). Quite different definitions of SSESs have been provided in guidance documents. Some refer to performance of safety systems, some to the state of the reactor, some to value ranges of certain physical quantities, and some are combinations of two or more of these. One definition addressed only reactor coolant system conditions. Only one quantitative criterion was found in guidance documents, and even that was mentioned in only one document. The definitions were short and open to interpretation. The answers to the stakeholder survey tended to give more concrete definitions of SSES than the guidance documents: for example, subcriticality and water supply for 24 hours are mentioned. For spent fuel, sufficient cooling to maintain stable temperature and subcriticality are referred to.

The basis for success criteria seems to be the avoidance of core damage within the time window considered, and sometimes also reaching a SSES. They may be defined as “Criteria for establishing the minimum number or combinations of systems or components required to operate, or minimum levels of performance per component during a specific period of time, to ensure that the safety functions are satisfied” (ASME 2009). There are several different types of success criteria, e.g. for different safety functions. Typically, thermohydraulic analyses are used to develop them. Success criteria are based on the idea that the state of the reactor remains acceptable in all scenarios, for example that maximum fuel cladding

temperature remains below 1204 °C. In the survey, all organizations stated that more realistic consideration of time-related dependences of success criteria can benefit PRA, especially for long time windows; now only two organizations have considered change of success criteria over time, for one case each.

Mission time may be defined as “the time period that a system or component is required to operate in order to successfully perform its function” (ASME 2009). For many safety systems, this is the time it takes to bring the plant to a safe, stable state; deterministic safety analyses can be used to estimate how long that takes. Mission times are usually set by the analysts, but in reality, they may vary greatly depending on the role of the safety system, the scenario, and the accident sequence (e.g. what other safety systems are available). Mission time analysis is closely connected to success criteria analysis, and for example same thermohydraulic calculations may be used in both. The mission time for success criteria is typically set to 24 hours (PRA level 1) and 48 hours (PRA level 2). In the survey it turned out that longer mission times than those mentioned are considered for shutdown states and spent fuel pool analyses; shorter mission times are used by some organizations in loss of offsite power scenarios and for batteries.

Recovery means using alternative equipment or means to perform a safety function (e.g. core cooling) when primary equipment fails, or the use of alternative means to utilize equipment that has not responded as required. For example, opening doors to promote room cooling when HVAC system fails is a recovery action. Repair, in turn, means the elimination or mitigation of faults that caused a system, structure or component to fail, and bringing it to operable state. From the PRA point of view, recovery and repair (R/R) pose two problems: how to assess the probability that R/R is conducted successfully within the allowable time, and how to model R/R in the PRA model. R/R performance data is rarely available especially concerning the extremely stressful circumstances of an ongoing accidents, and therefore the best available R/R data often comes from expert judgment; also models of R/R may be constructed to obtain success probability estimates. R/R failure is usually taken into account in the fault tree level or event tree level. It can also be taken into account in the sequence and minimal cut set levels. Most organizations that responded to the survey model some recovery actions. Repairs are usually considered only in long mission time scenarios (e.g. level 2 PRA and spent fuel pool PRA). The respondents model R/R in PRA either as separate basic events or as included in the probabilities of basic events; one organization told that they have a fault tree for repair events, and it appears as a section in an event tree.

PRA model of spent fuel pool

We have developed a simulation-based event tree modelling approach for spent fuel pool (Tyrväinen et al. 2021a). It integrates deterministic spent fuel pool behaviour and probabilistic analysis. The spent fuel pool water level and temperature are calculated in the simulations at every time point of interest, e.g., when a make-up system is started or fails. The time windows for probabilistic analysis are

dynamically calculated based on the current spent fuel pool conditions. For example, the mission time of a make-up system is calculated based on how long it takes to reach the safe state, i.e., the water level is normal, and the spent fuel pool cooling system is back in operation. Durations of manual actions, repair times and failure times are drawn from probability distributions to determine accident progression timings on each simulation cycle.

We have analysed two spent fuel pool accident scenarios, transient and loss of offsite power (LOOP), using the simulation-based event tree approach. The analysis has been performed based on a fictive and simplified static PRA model created for the PROSAFE project. The simulation-based event trees have been used to quantify top minimal cut sets of the static PRA model more realistically. The simulation-based event tree for LOOP is presented in Figure 5. Repair modelling decreased the fuel damage frequency quite a lot compared to the static model. The importance of human failure events increased in the results. The importance of components and failure modes with short repair times decreased in the results. Dynamic treatment of mission times had also some impact on the results, which is seen as decreased importance of failure to run events in the LOOP case. The results were more or less consistent with those calculated by other methods, I&AB and enhances event/fault tree method, used by PROSAFE partners, even though there were some differences in the assumptions and inputs (Tyrväinen et al. 2021a).

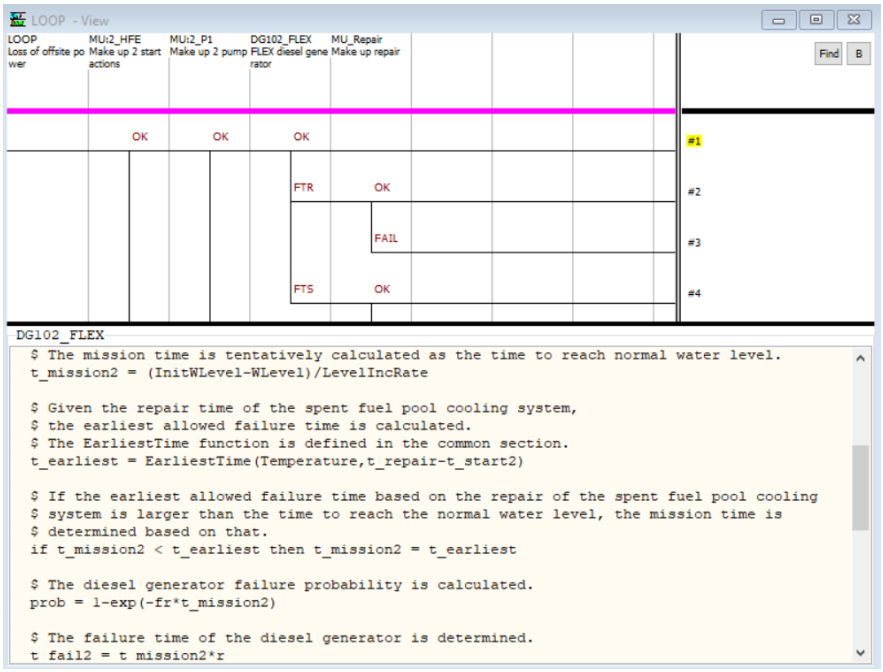

Figure 5. Simulation-based event tree for loss of offsite power scenario of a spent fuel pool.

Long time windows affect also human reliability analysis. In short time window scenarios (with a time span of 24 hours), repairs of systems, structures or components, or even recoveries need not be taken into account because it may be assumed that there is too little time for them. However, when there is longer time available, there is time for repairs and recoveries, and taking them into account helps avoiding unnecessary conservatism in results. Another factor that long available time windows influence is that there is ample time in each task for both diagnosis and all necessary actions. This affects human error probability (HEP) estimates in two ways. First, the stress level of whoever are conducting the activities (operators in the case of operator actions and usually also in the case of recoveries, so-called field men in the case of repairs) are lower than they would be when available times are short. Second, there is enough time to recover from memory lapses and other factors that may have led to human errors. Both of these diminish the HEPs. However, HRA of repairs poses some issues of its own. First, the repairs are conducted by mechanics (often called 'field men') and not by operators; it is uncertain to what extent the HEP estimates that usually describe operator performance are generalizable to this worker group. Second, task analyses of repair tasks may not be available, and they have to be constructed. Third, equipment failures are usually noticed by the operators, and they call in the mechanic; thus, there are elements of crew effects in every repair task. Also human activities related to the deployment and use of mobile (FLEX) equipment – pumps, diesel generators, hoses – were considered, although only FLEX diesel generators were eventually taken into the HRA model.

We conducted human reliability analyses for the two scenarios (transient, LOOP) described above. Three tasks were modelled, all of them post-initiator tasks: deployment of the second redundancy of the main SFP cooling system, deployment of make-up system 1 before uncovered fuel, deployment of make-up system 2 before uncovered fuel. Also three repair tasks were considered: repair of the main SFP cooling system before boiling (repair items: pump stopping, heat exchanger failure), repair of make-up system 1 before uncovered fuel (repair item: pump failure), repair of make-up system 2 before uncovered fuel (repair items: FLEX diesel generator failure and pump failure). The method used was the human reliability analysis procedure (Swain 1987) of the Accident Sequence Evaluation Program (ASEP). It turned out that ASEP is easy to learn and follow. It is also easy to apply to repairs, once the required repair actions are known for each repair task. The results were reasonably well in line with those obtained by Swedish partners with different methods. We also constructed a recovery model in the form of an event tree for each task.

Dynamic human reliability analysis

The research in HRA, excluding the research on long time window HRA described in the previous section, has concentrated on dynamic HRA. Thus far, a literature study, a stakeholder survey, and an empirical study have been conducted.

Dynamic HRA literature review

The literature study of dynamic HRA (Liinasuo et al. 2020) considers dynamicity, related to human performance from psychological and risk analysis viewpoints. The cognitive psychology of dynamic features in human behaviour is discussed in the framework of perceptual cycle theory, and its applications in retrospective accident analysis and identification of causal relationships that account for human error. Also dynamical situations at the plant and its surroundings, and their effects on humans at the plant, are briefly considered.

An effort was made in the study to clarify the meaning and definition of dynamic HRA by taking a look at the existing literature from this point of view. The conceptions of what dynamic HRA is vary. Apparently, what makes HRA dynamic is either the phenomena considered in the HRA, or the methods used. On the phenomena side, dynamicity means that besides the current situation, things that happened earlier internally (mental states) or externally (development of situation, changes in physical environment) affect human performance and error proneness; for example, people may cling to their earlier interpretation of the situation despite new information that challenges that information. However, when talking about HRA in a dynamic context, the phrase 'dynamic HRA' is not necessarily used. Also causality between cognitive factors and operator behaviour can be regarded to be a part of this concept. On the method side, dynamic HRA methods primarily mean methods that are based on the modelling and simulation of human cognitive processes, human communication etc. To incorporate internal and external dynamic factors and thus to increase accuracy in risk modelling, it has been proposed that virtual operator models should be integrated with virtual plant models.

Conventional HRA methods (THERP, SPAR-H etc.) used today are static in two senses: 1) they do not handle well internal states and cognitive processes of humans, and 2) their task structure is static, consisting of a fixed set of tasks. It has been predicted that a shift from static to dynamic HRA will occur along transition from fixed models (static fault and event trees) to models based on direct simulation of accident sequences (dynamic PRA, also integrated deterministic and probabilistic safety assessment IDPSA) (Boring & Rasmussen 2017).

Cognitive modelling and simulation are usually conducted on platforms called cognitive architectures. The term means both hypothetical structures that provide a mind and how they work together, and their computer implementations. ACT-R and SOAR are some prominent cognitive architectures. Cognitive modelling and simulation can also be performed on general-purpose discrete simulation platforms such as Saint. Also human performance modelling methods can be used, such as GOMS which is meant for estimating the time spent in physical and mental actions required in a given task. Crew modelling combines the cognitive processes of individuals with communication and coordination; its methods often combine HRA with cognitive modelling, and include for example ADS-IDAC, PROCOS, SHERPA, PHOENIX and IDHEAS. Agent modelling and simulation can be used as an approach to both modelling and analysis of both individuals and crews.

Dynamic HRA empirical studies

Dynamic HRA was also studied in two empirical studies (Liinasuo et al. 2021). The first one was a survey to find out how familiar Nordic HRA professionals are with the dynamic HRA concept; what their opinions and experiences on it are; and what further research on it would be interesting or important. Six Finnish and Swedish human reliability analysis experts from five different organizations replied to the query. All respondents were PRA specialists, with HRA being a part of their work. In general, the respondents' view is that the greatest potential benefit of dynamic HRA is increased realism. On the other hand, they emphasized that deployment of dynamic HRA methods should not lead to increased complexity of models and workload in analysis, because resources available for HRA are limited and the models are already complex. Dynamicity is involved in long time windows and annual maintenance break scenarios, among others. The respondents identified also several interesting future research topics.

The second study was an interview of main control-room operators to shed light on dynamic HRA related phenomena qualitatively, in the form of asking operators' opinions on error possibility in various operational, possibly error-prone situations in the main control room. The questions included examples of dynamic situations, for example "imagine that you have been in a hurry the same day but now the hurry has been over for a while" and "imagine a situation where you earlier made an error". The interviewees were asked, on a five-point scale, to assess whether the error possibility increases, remains the same, or decreases. There was only a small number of interviewees – six in all, including two shift supervisors, two reactor operators, and two turbine operators – limiting the conclusions to be made. However, even this small sample provided a lot of information and variation, which can also reflect the true variation, possibly realised also with a larger sample. The results appear possible and true. Whether this is the case, calls for a new study with more interviewees.

Digital I&C reliability and risk analysis

Despite of significant research efforts, there is still no international consensus on PRA modelling methods for digital I&C systems. Therefore, digital I&C has been modelled in overly simplified and conservative manner in most PRAs currently. Challenges include particularly modelling and quantification of software failures, modelling of fault-tolerant features, postulation of common cause failures and common cause failure parameter estimation. It should be noted that these issues are not only relevant for PRA but also in the deterministic safety demonstration, which includes e.g. fault tolerance analyses.

We have participated in an OECD/NEA WGRISK task DIGMAP, which is an international benchmark study on PRA modelling digital I&C (Shin et al. 2019). In DIGMAP, six participants have prepared PRA models for a fictive reactor protection system (RPS) (Tyrväinen 2020), and the modelling approaches and results have

been compared. VTT's modelling approach was to use simple fault trees and to perform complex computations in background. The approach was selected because it did not seem practical to handle all CCF combinations of large common cause failure (CCF) groups explicitly in the PRA model. All RPS related basic events in the model are CCFs that cause one or multiple safety functions to fail. CCFs were modelled separately for different modules and for application software, system software and hardware. CCF combinatorics and probabilities were calculated using separate spreadsheets. The top fault tree for one signal is presented in Figure 6.

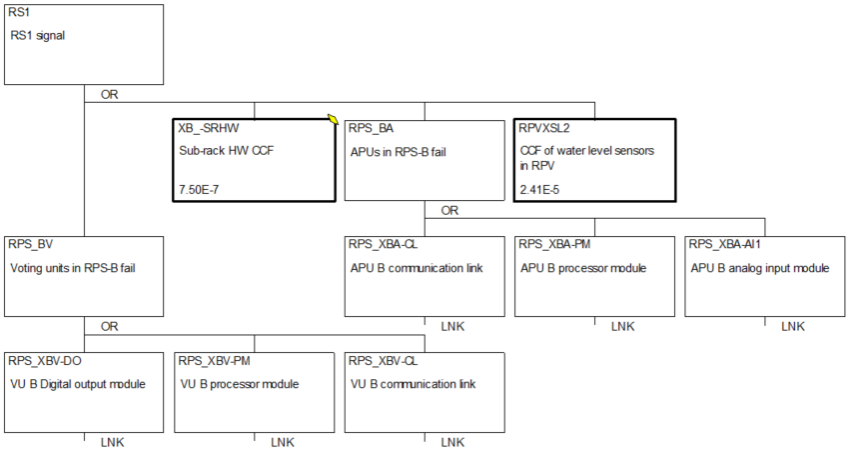

Figure 6. Fault tree for RS1 signal in VTT's model.

The DIGMAP project particularly has demonstrated the importance of understanding the diversity of the reactor protection systems (or lack of it) and the identification of common cause failure groups. Both high level and low level modelling approaches were used among DIGMAP participants, but the level of modelling detail did not really have impact on the overall results. Both approaches have their benefits and drawbacks, and the most suitable approach can also depend on the application. It has to be noticed that the development of a compact PRA model for digital I&C requires quite detailed background calculations and good modelling skills, i.e. there is no easy shortcut. Large CCF groups were technically the most challenging modelling issue of the project that caused some differences in the results. It was found that one has to be very careful when using simplifying workarounds.

Failure tolerance analyses

Failure tolerance analysis (FTA) is a framework to organize individual analyses aimed at demonstrating that a nuclear power plant (NPP) design and construction fulfils failure tolerance requirements set forth in YVL guides – perhaps most prominently in YVL B.1 (STUK 2019), but also for example in D.3 and E.11. This is a new

requirement meaning that not many examples of such analyses exist and there are several open issues how failure tolerance analyses should be performed. Some of these issues are common to PRA. In principle, PRA may support FTAs, and FTA may support PRAs.

Informally put, failure tolerance means that a failure cannot spread across the system: the system will fill safety requirements even though some parts of it have failed. Several issues in dealing with failure tolerance in different contexts led STUK to develop a more holistic approach that STUK has named failure tolerance analysis (Humalajoki & Niemelä 2018). These issues were, for example, that there had been overlapping work, gaps that no analysis covered, boundaries between and acceptance criteria of analyses were unclear, and there were difficulties in getting a clear picture of failure tolerance at the plant level.

Individual analyses that can be utilized in FTA include, for example, failure modes and effects analysis (FMEA), common cause failure (CCF) analysis, redundancy and diversity analyses, interface analysis, hazard analyses, and analyses of spurious I&C actuations. For example analysis of spurious actuations can be performed with several analysis methods.

Stakeholder survey

In 2019, we carried out a survey among stakeholders to clarify the main issues related to FTA and the role of PRA as a part of it (Karanta & Björkman 2020). All Finnish stakeholders (Fennovoima, Fortum, STUK, TVO) responded to the survey.

The experience in conducting FTA varies from company to company. Fennovoima's conduct of FTA is related to the construction license application. Fortum has conducted FTA for plant modifications, and to the scope of the modifications only. TVO has conducted a top-level FTA for Olkiluoto 1 and 2, failure modes and effects analysis (FMEA) for PRA, and certain other analyses for some systems; for Olkiluoto 3, several systems have been analysed in the FTA framework.

Concerning the role of PRA in YVL B.1, STUK stated that "the purpose of YVL B.1 is to assure that the systems, structures and components (SSC) in an NPP are correctly designed and dimensioned, so that the SSCs have enough capacity and functionality to perform their function for scenarios they are intended to operate in". On the other hand, "PRA does not deal with physical design errors. Instead, PRA assumes that systems are correctly dimensioned so that they fulfil their tasks if SSCs are functional. Thus, the role of PRA in revealing design errors is quite limited. In short, the role of PRA is not related to functionality, but to the reliability of maintaining the functionality as designed." STUK also lists 12 YVL B.1 requirements where PRA can be used. This is a small number remembering that there are hundreds of requirements in YVL B.1. Fortum also sees PRA's role in YVL B.1 as limited, because those of its requirements that they have addressed (with FTA) are deterministic by nature. Fennovoima and TVO see PRA's role as somewhat larger; in TVO's view, analysis of dependencies between failures and consequences on plant level is so complex that modelling techniques of PRA may come in handy.

Concerning the role of PRA in FTA, STUK notes that “PRA shall be used in the definition of design extension condition B. Otherwise PRA is not applicable to failure analyses”. STUK justifies this by noting that PRA models are simpler than failure analyses. On the other hand, failure analysis results can be and are used in PRA, and “it is nearly impossible to perform PRA without FTA”.

Fortum sees that PRA may be useful in justifying certain configurations when FTA shows that all deterministic requirements are not fulfilled, if the risk significance is low enough. Fortum further notes that it is beneficial to keep PRA independent (of FTA), to gain insights from different viewpoints.

TVO sees reuse possibilities of FMEA and CCF analyses that have already been conducted in PRA (this reuse possibility was also noted by Fortum). TVO stresses especially the central role of FMEA to both FTA and PRA.

To summarize, the most important result of the survey is that PRA is not a promising approach to support FTA. On the other hand, failure tolerance analysis results have important uses in PRA.

A failure tolerance analysis example

Many of the approaches used in an FTA are well established, e.g. failure modes and effects analysis and common cause failure analyses. To study the applicability of less established methods to support FTA analyses we developed a simplified example case for a FTA and performed some example computations.

The example case dealt with a fictive boiling water reactor (BWR) the description and model of which were developed in the DIGREL project (Authén et al. 2015). The system considered in this example is a cooling division of the BWR and its safety I&C system.

In the study, our main emphasis was on application possibilities of model checking. The main steps of the FTA process were taken from an Microsoft Excel worksheet provided by STUK. The analyses illustrated in the example were

- common cause failure (CCF) analysis of sensors. This covered CCF analysis of sensors in three failure modes. The example case concerned if a single CCF could prevent the emergency feedwater (EFW) and emergency core cooling (ECC) systems from performing their functions following a specific initiating event. The analysis was performed by directly dealing with the systems involved, without any particular method.
- diversity analysis of frontline and backup safety functions related to process equipment (pumps, valves etc.). Diversity analysis is an analysis for identifying potential common cause failure groups from various similarity clues (e.g. two components serve the same or similar functional role, the components have the same manufacturer etc.) and inferring the need (or not) of improving diversity by considering the consequences of the common cause failure if it occurred in some scenarios. The example analysis was carried out concerning the diversity attributes of two motor valves of the cooling train.

- failure tolerance of one I&C system single failure analysis (N+1, N+2). In the N+1 case the idea is that if N systems are needed for a specific function, N+1 systems should be provided because one may be assumed to fail (similarly in the N+2 case one is assumed to fail and the other unavailable e.g. due to maintenance). Two reactor protection systems (RPS-A and RPS-B) that control the cooling train were considered. A recently developed model checking approach (Pakonen & Buzhinsky 2019) was applied to verify that the N+1 and N+2 criteria were satisfied concerning certain properties of the RPSs. A design error was discovered in this fictive BWR design.
- analysis of active failures of separated I&C entities. We analysed if spurious activation of the EFW or the ECC system of the division is possible. We used model checking, and the general property checked was “a response of the system shall be preceded by a valid request”, for example coolant injection by ECC is preceded by extremely low coolant level in the reactor pressure vessel. Six specific properties derived from this general property. It was found that without any failures in the I&C system, both ECC and EFW worked with all the signals (as one would expect from a correct design); however, when there was a single failure in the I&C system, four out of the six properties were not satisfied.

Also analysis of allocation of signals from/to I&C systems, analysis of CCF between frontline and backup safety I&C, analysis of failure propagation, analysis of priorities of commands were treated briefly. For example, the analysis of command priorities could be conducted very simply because considering only one division made things very simple (only two signals between which to prioritize).

Based on the results model checking is a viable and promising approach to conduct, support and complement different analyses in FTA (Björkman & Karanta 2021).

Multi-unit and site-level PRA, PRA of small modular reactors

SMRs are a novel approach to nuclear reactor design, and practical experience about them is as of yet non-existent. This poses challenges to PRA of SMRs. PRA tool, method and risk metric development is needed to account for the SMR reliability and the uncertainties related to SMR risk. Especially methods to handle passive features and multi-module issues in PRAs should be investigated or enhanced. In 2019 we reviewed the literature related to SMR PRA (Björkman & Tyrväinen 2019). Several approaches have been suggested for passive system reliability modelling. Either traditional methods are used or dynamic methods (mainly dynamic event trees) are suggested for accounting for unique features of SMR risk. SMR risks have also been considered from level 2 and 3 perspective.

Applications

The PRA research conducted in NAPRA is related to applications on three levels. Some of the results may be directly applied, some others support the PRA efforts of Finnish nuclear stakeholders, and yet others provide groundwork for improving and enhancing application-oriented PRA research.

In seismic PRA, the identified research topics could on their part serve as a basis for bringing Finnish seismic PRA up to the level of recent international developments. The constructed fire PRA model provides an example of how to conduct fire PRA in a way that to a reasonable level takes into account the dynamic nature of fire progression and its effects on safety, utilizes the results of physical fire models and models of fire brigade action, and yet at the same time is simple to implement and cost-effective to run.

When PRA is conducted on spent fuel pools, it is important to take into account the long time windows in order to get realistic results. Long time windows may also come about in some scenarios that concern NPP units. When the need or will to consider long time windows in plant PRA arise, the results of the PROSAFE project offer both information on several relevant issues, and methodological support to carry out the analyses in practice.

Dynamic HRA literature review results will be useful when dynamic HRA efforts are started. Needs or strong motivation for this may emerge if conducting risk or accident analyses in a dynamic manner – for example, integrating human actions, plant response and risk considerations in a set of dynamic simulation models. An important class of dynamic HRA methods involve cognitive and crew simulation. Need for simulation-based approaches may emerge when HRA is needed for the assessment of novel equipment and systems (for example, a new type of reactor); then main control room simulators, operators or even a plant are not available, but cognitive simulation models may produce HRA results that are sufficient for the design phase. Cognitive simulation may also be used when empirical data (such as MCR simulator results) is not available and is impracticable to produce; for example, it is impracticable to carry out simulator experiments involving NPP operators for long time window scenarios as the operators would have to be involved for several days, and it is also impracticable to get sufficient data utilizing operators when the human error in question occurs very rarely (and so perhaps hundreds of thousands of simulator runs would be needed).

The results of the stakeholder survey concerning failure tolerance analysis are directly applicable by the NPP companies of Finland. It is presumable that both STUK's views on FTA and other companies' experiences in conducting it are of interest to them. The small example FTA may be used as an approachable introduction to the philosophy and issues of FTA, and it may also give some ideas on how to conduct the analyses. The FTA case example may serve as a short introduction to some FTA issues, or as a source of ideas on how to conduct FTA.

There is considerable interest in small modular reactors in the Finnish energy sector, and STUK has taken the stand that it will require PRA for these kind of plants, too. The literature study on the PRA of SMRs may serve as a one-stop source of

issues related to this topic, and thus help PRA experts the have to conduct PRA on this type of NPP.

Conclusions

Probabilistic risk assessment is in a state of flux caused by developments in nuclear technology, in PRA methodology and in nuclear safety. On the technological side, the digitalization of nuclear facilities poses challenges to risk analysis which methods based solely on probability theory seem ill-equipped to solve. Small modular reactors and other modern developments have raised the need to develop further subdomains of PRA where generally accepted standard solutions do not yet exist, such as multi-module or site-level PRA and the PRA of passive safety features. On the methodological side, calls for greater realism in e.g. fire PRA and level 2 PRA have led to the development of dynamic PRA, development of dynamic HRA, and tighter integration of deterministic and probabilistic analyses, all of which are still to a large extent works in progress. On the nuclear safety side, lessons from the Fukushima accident have forced the reconsideration of PRA subfields that had not received wide attention previously such as PRA with long time windows and PRA of spent fuel storage. There is also a trend towards seeing risk assessment and management on a holistic, systemic level where PRA is just one of the available and useful approaches, and needs to be put into context in order to find its role in the big picture.

NAPRA project, as its predecessors in the SAFIR framework, is an attempt to address PRA issues in a way that would lead to contributions to the field itself, introduction of recent developments to the Finnish context, use of research results in PRA practice, and increasing PRA expertise in Finland. These efforts will continue to the greatest extent possible.

The need for development of PRA or, more generally, mathematical and quantitative approaches to risk analysis that address the uncertainties involved, is increasing. In addition to the issues stated above, there are also other development catalysts that may shape the field in the future. Calls for better quality of PRA and increased plausibility of its results point to a more scientific approach to PRA, including improvements of verification and validation of models and their results. Need of cost-effectiveness in these work-intensive analyses points to the increasing role of automated PRA modelling. Such issues, and other issues relevant to nuclear safety in Finland and other Nordic countries, can be addressed in the next SAFIR programme whose preparations will be started also concerning PRA in the remaining period of SAFIR2022. We hope to identify relevant research topics for the next programme in cooperation with Finnish and Nordic stakeholders, so that the theoretical and practical objectives of Finnish PRA research may be satisfied in the future.

References

ASME. 2009. PRA standard: ASME/ANS RA-Sa-2009 Standard for Level 1/Large Early Release Frequency Probabilistic Risk Assessment for Nuclear Power Plant Applications. American Society of Mechanical Engineers 2009.

Authén, S., Holmberg, J.-E., Tyrväinen, T., Zamani, L. 2015. Guidelines for reliability analysis of digital systems in PSA context – Final Report. Roskilde: Nordic nuclear safety research (NKS). NKS-330. 103 p.

Björkman, K. & Karanta, I. 2021. A simple failure tolerance analysis case study for a fictive boiling water reactor. Espoo: VTT. VTT Research Report VTT-R-00038-21.

Björkman, K. & Tyrväinen, T. 2019. Probabilistic risk assessment of small modular reactors - Literature review. Espoo: VTT. VTT Research Report VTT-R-01041-19.

Boring, R. L., & Rasmussen, M. 2017. GOMS-HRA: A method for treating subtasks in dynamic human reliability analysis. Risk, Reliability and Safety: Innovating Theory and Practice - Proceedings of the 26th European Safety and Reliability Conference, ESREL 2016, Walls, Revie & Bedford eds, London: Taylor and Francis, 956-963.

Helminen, A. 2020. International and Finnish Practices on Seismic Probabilistic Risk Assessment. Espoo: VTT. VTT Research Report VTT-R-00023-20. 9 p.

Hostikka, S. & Keski-Rahkonen, O. 2003. Probabilistic simulation of fire scenarios. Nuclear Engineering and Design 224, 301-311.

Hostikka, S., Kling, T., Paajanen, A. 2012. Simulation of fire behaviour and human operations using a new stochastic operation time model. 11th International probabilistic safety assessment and management conference & the annual European safety and reliability conference (PSAM11 & ESREL 2012), Helsinki, 25-29 June, 2012. 10 p.

Humalajoki, P. & Niemelä, I. 2018. NPP failure analyses in Finland. Probabilistic Safety Assessment and Management PSAM 14, September 2018, Los Angeles. 8 p.

IAEA. 2016. Attributes of full scope level 1 probabilistic safety assessment (PSA) for applications in nuclear power plants. IAEA-TECDOC-1804, Vienna: International Atomic Energy Agency.

Karanta, I. & Björkman, K. 2020. A survey on the use of PRA to support failure tolerance analysis. Espoo: VTT. VTT Research Report VTT-R-00192-20.

Liinasuo, M., Karanta, I. & Kling, T. 2020. Dynamic human reliability analysis (HRA) - a literature review. Espoo: VTT. VTT Research Report VTT-R-00193-20. 27 p.

Liinasuo, M., Karanta, I. & Kling, T. 2021. Dynamic human reliability analysis – A stakeholder survey and an empirical study. Espoo: VTT. VTT Research Report VTT-R-00189-21. 33 p.

McGrattan, K., McDermott, R., Weinschenk, C., Overholt, K., Hostikka, S. & Floyd, J. 2013. Fire Dynamics Simulator User's Guide, Sixth edition. Gaithersburg: National Institute of Standards and Technology. NIST special publication 1019. 262 p.

OECD. 2014. Probabilistic safety assessment (PSA) of natural external hazards including earthquakes, NEA/CNRA/R(2014)9. Paris: OECD Nuclear Energy Agency. 47 p. + app. 357 p.

OECD. 2015. International workshop on fire probabilistic risk assessment (PRA), NEA/CSNI/R(2015)12. Paris: OECD Nuclear Energy Agency. 51 p. + app. 400 p.

OECD. 2019. Seismic Probabilistic Safety Assessment for Nuclear Facilities. CSNI Topical Opinion Paper, No. 2, Nuclear Energy Agency, OECD, 2019-05-27 Draft.

Pakonen, A., Buzhinsky, I. 2019. Verification of fault tolerant safety I&C systems using model checking. In 2019 IEEE International Conference on Industrial Technology (ICIT) (pp. 969-974). Piscataway: IEEE Institute of Electrical and Electronic Engineers.

STUK. 2019. Safety design of a nuclear power plant. Guide YVL B.1, Radiation and Nuclear Safety Authority, 15.06.2019, 67 p. + app. 6 p.

Shin, S.M., Porthin, M., Tyrväinen, T., Mueller, C., Piljugin, E., Stiller, J., Quatrain, R., Demgne, J., Brinkman, H., Nararajan, V., Picca, P., Gordon, J., Sedlak, J. & Jaros, M. 2019. An international joint research to explore the method for digital I&C reliability assessment: OECD/NEA DIGMAP. Asian Symposium on Risk Assessment and Management (ASRAM2019), September/October 2019, Gyeongju, Korea. 8 p.

Swain, A.D. 1987. Accident Sequence Evaluation Program human reliability analysis procedure. Washington, DC: Sandia National Laboratories for the U.S. Nuclear Regulatory Commission. NUREG/CR-4772.

Tyrväinen, T. 2020. Probabilistic risk model of digital reactor protection system for benchmarking, Espoo: VTT. VTT Research Report VTT-R-01028-19. 19 p. + app. 6 p.

Tyrväinen, T., Karanta, I., Kling, T., He, X., Olofsson, F., Bäckström, O., Massaiu, S., Sparre, E., Eriksson, C., Cederhorn, E. & Authén, S. 2020a. Prolonged available time and safe state. Roskilde: Nordic nuclear safety research (NKS). NKS-432. 116 p.

Tyrväinen, T., Karanta, I., Kling, T., He, X., Olofsson, F., O., Massaiu, S., Sparre, E., Eriksson, C., Cederhorn, E. & Authén, S. 2021a. Prolonged available time and safe state. Roskilde: Nordic nuclear safety research (NKS). NKS-444. 165 p.

Tyrväinen, T., Kling, T. & Korhonen, T. 2020b. Analysis of cable fire scenario with simulation-based event tree. Espoo: VTT. VTT Research Report VTT-R-01302-19. 22 p.

Tyrväinen, T., Korhonen, T. & Kling, T. 2021b. Extensions to cable room fire PRA study and method. Espoo: VTT. VTT Research Report VTT-R-01545-20. 38 p.

VTT Technical Research Centre of Finland Ltd. 2019. FinPSA – Tool for promoting safety and reliability. https://www.simulationstore.com/finpsa (link accessed 25.1.2021)

3.3 Predicting extreme weather and sea level for nuclear power plant safety (PREDICT)

Kirsti Jylhä, Ulpu Leijala, Carl Fortelius, Taru Olsson, Mika Rantanen, Olle Räty, Jani Särkkä, Karoliina Hämäläinen, Marko Laine, Anna Luomaranta, Jani Räihä, Milla Johansson, Minna Rantamäki

Finnish Meteorological Institute (FMI)
P.O. Box 503, FI-00101 Helsinki

Abstract

The safety management over the life cycle of a nuclear power plant requires probability estimates of exceptional weather and sea level conditions in the current and future climate. We studied the occurrence of sea-effect coastal snowfall and high sea level as a single event or jointly with heavy precipitation. High wind speeds as an object of probabilistic weather forecasting were also considered. Atmospheric conditions favouring sea-effect snowfall were detected to occur most often in the western coast of Finland. Passing extratropical cyclones (low air pressure systems) were found to induce compound heavy rain and high sea level events. Synthetically generated low-pressure systems appeared as a promising tool for studies of extreme sea levels. Bayesian hierarchical modelling of sea level extremes reduced the range of uncertainty in their return level estimates. Probabilistic weather forecasts bring more confidence on decision making in case of nuclear emergency.

Introduction

The Finnish regulatory guides require that the design of a nuclear facility shall take into consideration abnormally high and low sea water levels and a number of exceptional meteorological phenomena (Guide YVL B7, 2019). Furthermore, meteorological data affecting dispersion of radioactive releases in the atmosphere shall be known (Guide YVL C4, 2019). Accordingly, the main topics of the PREDICT project (https://en.ilmatieteenlaitos.fi/predict) are: 1) extreme weather events in a changing climate; 2) extreme sea level; and 3) forecasts of extreme weather and sea level events. The motivation for the 3rd topic in PREDICT was to improve abilities to forecast relevant extreme weather and marine phenomena, thus providing early warning and time for countermeasures.

The research on extreme weather and sea level aims to improve the reliability of estimates about the likelihood of exceptional single and co-occurring weather and sea level events in the surroundings of the Finnish nuclear power plant (NPP) sites (Jylhä et al. 2018). Impacts of climate change also need to be considered. Globally, 2011–2020 was the warmest decade on record (WMO, 2021). In Finland, the year 2020 was warmer than ever recorded, and the same was true for the period May-August in 2018 (FMI, 2018, 2021). In January 2019, the Aapeli storm broke the

record for highest average wind speed in Finnish sea areas, and storm-force gusts were measured even inland (FMI, 2019a). Also a new wave height record in the Central Bothnian Sea was achieved (FMI, 2019b). In February 2020, a record-high sea level (135 cm over mean water) was observed at the Rauma tide gauge. Although it is not possible to attribute a single event, such as an exceptionally warm summer, to anthropogenic increases in greenhouse gas emissions (Trenberth et al. 2015), it is evident that human induced long-term trends in the mean values affect the probabilities of occurrence of values near both ends of the frequency distributions, depending also on potential changes in the variance or shapes of the distributions.

In 2019–2020, we have i) clarified how frequently intense coastal snowfall cases have occurred in the past; ii) assessed joint probabilities of intense precipitation and high sea level; iii) evaluated the uncertainty in the estimates of exceptionally high sea levels; and iv) focused on simulated low-pressure systems and sea level extremes. Finally, the goal of the work related to v) forecasting extreme events was to exploit the potential of state-of-the-art numerical weather prediction (NWP) systems for the benefit of safe and economical nuclear power production.

Climatology of intense coastal snowfall in the past

Typical conditions favouring formation of sea-effect snowfall include 1) ice-free sea surface which acts as a constant source of energy and moisture into the atmosphere, 2) a thick layer (> 1 km) of cold air over the sea and 3) wind which blows from a suitable direction over the ice-free sea. When these prerequisites are met, the vertical temperature difference and the moisture flux from the sea surface generate strong rising air motion and convective precipitation (Markowski and Richardson, 2010). Depending on the mean wind direction, excess sea-effect snowfall may occur over land near the coastline, as happened in Merikarvia in 2016 (Olsson et al. 2017).

During 2016-2018, case studies had been performed with a numerical weather prediction model (HARMONIE-AROME), reanalysis data (ERA5), radar reflectivity images and gridded observational data (FMIClimGrid, Aalto et al. 2016, Luomaranta et al. 2019). These case studies concerned the sea-effect snowfall event in Merikarvia (Olsson et al. 2017, Olsson et al. 2018) and four known cases from the recent past (Olsson et al. 2020). Based on Olsson et al. (2018), we found that ERA5 reanalysis data could be suitable for sea-effect snowfall studies.

In PREDICT in 2019-2020, we have focused on testing the detection criteria for sea-effect snowfall events in Finland. Criteria presented for the Swedish east coast (Jeworrek et al. 2017) were taken as a starting point. These criteria were modified according to four case studies made with HARMONIE-AROME (Olsson et al. 2020). The main modifications concerned obviously the wind direction, but also the 10 m wind speed threshold was decreased from 10 m/s to 7 m/s. The refined criteria were: sea-surface temperature higher than 0°C, temperature difference between sea-surface and 850 hPa atmospheric level higher than 13°C, boundary layer height over

1000 m, daily total snowfall at least 1.5 mm (as liquid), 10 m wind speed at least 7 m/s, directional wind shear between 700 hPa and 975 hPa atmospheric levels under 60° and wind direction towards inland (ranging from easterlies to northerlies along the Finnish coastline).

The refined criteria were first tested with regional climate model (RCA4) data for 2000–2010 and were found suitable for sea-effect snowfall detection in Finland (Olsson et al. 2020). In 2020, the same criteria were applied to a 40-year long period of ERA5 data, covering 1979–2018. Two to eight snow band days, on average, were found around the Finnish coastal areas annually. Coastal precipitation and snow depth changes over land were identified from the daily gridded climate dataset for Finland (FMIClimGrid) during the detected snow band days. The annual number of favourable days for coastal sea-effect snowfall to occur was highest in western coast of Finland (Fig. 1). Also the largest daily increase (67 cm) in snow depth was observed in the same area. Otherwise the largest daily increases in snow depth were between 25 cm and 36 cm. The most favourable months for sea-effect snowfall were November, December and January but inter-annual variations were large. No statistically significant trends in the annual frequency were found during 1979–2018.

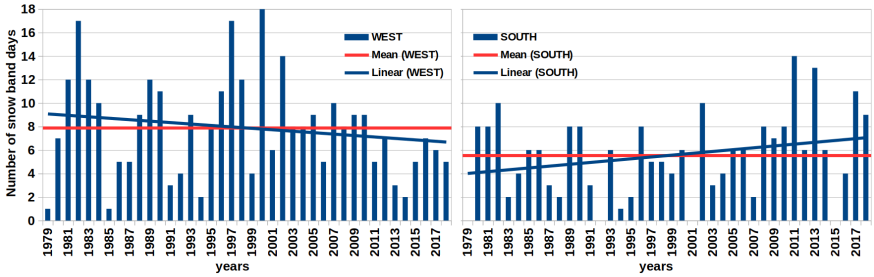

Figure 1. Annual (September to May) number of favourable days to produce sea-effect snowfall in western and southern coastal areas of Finland in 1979–2018 according to ERA5. The daily mean number of snow band days in 1979–2018 is shown by the red line and the linear trend by the blue line.

Characteristics of joint heavy rain and high sea level events

When heavy precipitation occurs simultaneously with a high sea level, they induce greater risk for coastal flooding than if the hazards occur in isolation. The co-occurrence of these hazards is a fairly common phenomenon which happens from time to time on the Finnish coast. Previous studies have investigated the long-term variations and trends of sea level (e.g., Johansson et al. 2001) or precipitation (e.g., Irannezhad et al. 2014) alone, but any comprehensive studies of joint occurrence of these hazards (hereafter compound events) have not been performed earlier in Finland.

This research was initiated in 2019 by investigating the climatology and variation of compound events using tide gauge observations and station-based precipitation

data (Räihä et al. 2020). One of the main results was that while the daily sea level is on average highest in December, the highest daily precipitation typically occurs in summer and autumn (Fig. 2). Thus, Räihä et al. (2020) concluded that compound events occur mainly between September and February and their probability is highest in November or December.

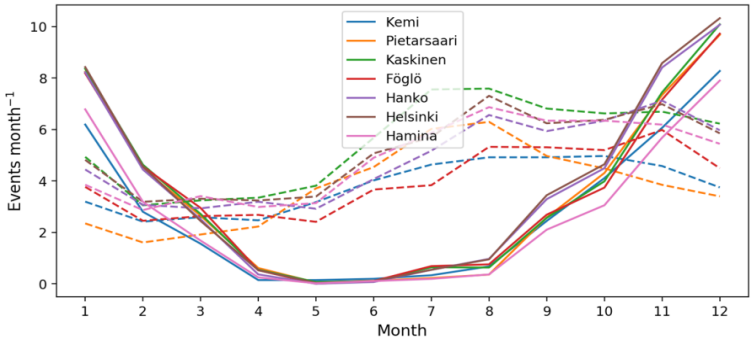

Figure 2. Monthly mean number of days when the maximum sea level is at least half of the warning level of a high sea level (solid lines) and the precipitation amount is at least 4.5 mm (dashed lines) near the tide gauges in 1960-2018 (in Pietarsaari since 1961). Figure adapted from Räihä et al. (2020).

The study of the compound events was continued in 2020 (Rantanen et al. 2020). As a revision to the work of Räihä et al. (2020), more tide gauge observations and gridded precipitation data were used. Furthermore, several additional aspects of compound events were investigated, including (i) long-term trends and interannual variability of the compound events, (ii) synoptic situations leading to the compound events and (iii) underlying atmospheric circulation patterns which typically favour the occurrence of compound events.

We found that the frequency of compound events has increased during the 1961–2019 study period, and in particular in the Bothnian Bay where the positive trend of the compound events was also statistically significant on an annual basis. According to the analysis, the increasing trend was linked to a more positive phase of North Atlantic Oscillation (NAO) during the recent decades. As expected, we found that the passing extratropical cyclones is the main cause for the compound events. When the total annual number of compound events in all tide gauges was considered, we found that Scandinavian pattern (SCAND) is the most controlling circulation pattern. During its negative phase, SCAND features a large low pressure area over Scandinavia, which is supportive of high cyclonic activity in Fennoscandia and thus high number of compound events.

The method and the results from Rantanen et al. (2020) will be reported in a peer-reviewed publication. This work has already started and will continue in 2021.

Uncertainty in the exceptional sea level estimates

Coastal flood hazard estimates accompanied with uncertainty ranges provide a valuable tool for the society and decision makers to prepare for the flooding events and to be able to design coastal areas in an effective and safe manner. Estimation of occurrence probabilities of sea level extremes is complex due to the limited amount of data on extreme events. This also causes major uncertainties in the related estimates, which need to be properly accounted for. Previous studies have provided important information on coastal flood risks in Finland (e.g. Leijala et al. 2018; Pellikka et al. 2018), but more work is needed to improve uncertainty quantification and statistical modelling of sea level extremes on the Finnish coast.

Work on this task started in 2019 in two ways. Firstly, we investigated how different extrapolation methods affect the probability estimates of the short-term sea level variations in the present climate on the Finnish coast. We also conducted stationarity studies to reveal potential trends and changes in the sea level distributions with time, including comparison of the probability distributions for time periods 1929–1958 (I), 1959–1988 (II) and 1989–2018 (III) based on 4-hour interval observations. Tentative results related to the studies on extrapolation techniques and stationarity were summarized in Leijala et al. (2020a), and the outcomes were separately demonstrated at the three Finnish NPP sites (Leijala et al. 2020b). Secondly, we initiated studies on utilizing statistical modelling on sea level extremes and took part in a benchmark exercise organised by OECD/NEA. The exercise consisted of a set of synthetic tests, which were designed for comparing different approaches to modelling extremes and quantifying the related uncertainties. We applied Bayesian analysis methods in this work (Räty and Laine, 2019), which formed the basis of the subsequent methodological development.

In 2020, the statistical modelling studies were deepened and extended to cover real-world data. Theoretical return levels of annual sea level maximum were calculated at twelve tide gauges on the Finnish coast using a Bayesian hierarchical modelling approach. We used the generalised extreme value (GEV) distribution as the basis of our model and tested four hierarchical descriptions, which pool information across the tide gauges, for the GEV parameters. In the simplest one, the tide gauge specific GEV parameters were assumed to come from the same joint Gaussian hyper distribution (denoted as Common in Fig. 3). In the rest of the models, GEV parameters were modelled using the distance with respect to the Kemi tide gauge as a covariate (Linear, Spline and GP (Gaussian process) in Fig. 3). Tide gauge specific fits (denoted as Separate in Fig. 3) were used as the baseline when assessing the performance of the hierarchical models. All models were fitted using R and Stan probabilistic programming languages (Stan Development Team, 2020a; 2020b).

The initial results were reported in Räty et al. (2020). An example is provided for two tide gauges in Fig. 3, which demonstrates the added value of hierarchical modelling approach. In particular, the uncertainty range of GEV parameters tends to be narrower for the hierarchical models compared to the individual fits. Overall, the four hierarchical models provide similar GEV parameter estimates. Also, differences in theoretical return level estimates obtained from the separate and hierarchical fits

are small for relatively common extremes (e.g. 50-year return level), but become more visible when very rare events (e.g. 1000-year return level) are considered (Fig. 3, panels b-c and e-f).

Future research will address how to take non-stationarity in the extremes into account and how physical covariates such as circulation indices could be used to explain the temporal variability in sea level extremes.

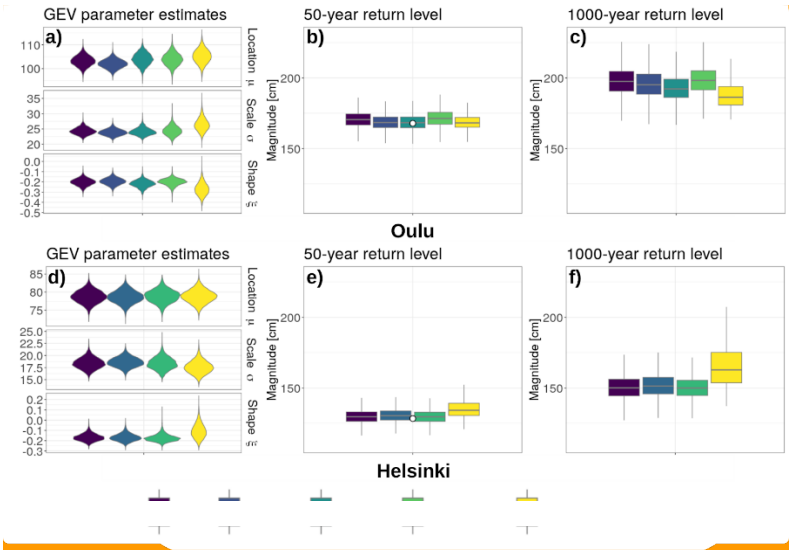

Figure 3. Posterior distributions of (left) GEV parameters and the corresponding (middle) 50-year and (right) 1000-year return level estimates of sea level height (cm) at Oulu and Helsinki for the four hierarchical models and tide gauge specific fits. Note that the linear model was not applied at the Helsinki tide gauge.

Simulated low-pressure systems and sea level extremes

Because time series of sea level records are relatively short, return level estimates corresponding to return periods of 100 years or longer tend to exceed the observed sea level extremes. The physical factors leading to these extremes can be studied by simulating the effect of large-scale wind storms to the sea levels. In the Baltic Sea, short-term sea level variations are caused by atmospheric factors (wind, air pressure) and internal sea level oscillations. The highest extremes are related to large-scale wind storms created by low-pressure systems (cyclones). The local sea level extremes are sensitive to the properties of the low-pressure systems. By investigating how these properties affect the sea level at the coast, we seek for the parameters that give rise to the highest maxima.

In 2019, the study was initiated by developing a numerical method that generates low-pressure systems (Räihä et al. 2019). The spatial variation of air pressure at the sea level is described using a Gaussian distribution. One can adjust the

parameters of the low-pressure system, such as the maximum depth of the air pressure anomaly, size of the system, velocity and direction of propagation (see an example in Fig. 4). Estimates for these parameters were studied using ERA5 meteorological reanalysis data 1989-2018. In 2020, the method was used to simulate the sea level variations induced by different low-pressure systems. From the simulation results, we got the first preliminary estimates for the highest sea levels at the three Finnish NPP locations (Särkkä et al. 2020). The methodology developed and tested in 2019-2020 appeared to be suitable for further studies of extreme sea levels.

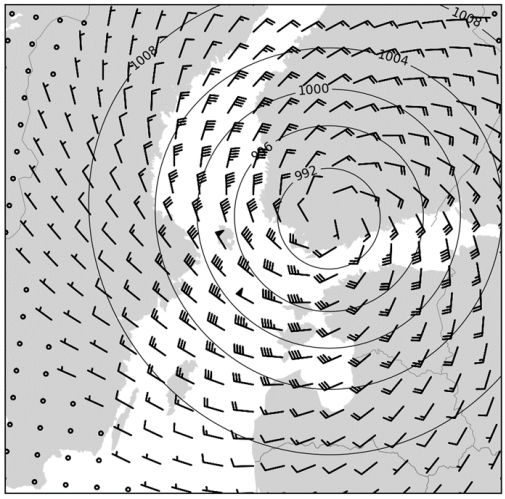

Figure 4. An example of a simulated low-pressure system to study extreme sea levels on the Baltic Sea coast. Contours represent sea level air pressure (hPa) and wind barbs represent the wind direction and speed at the height of 10 m. A full barb is added for each 10 knots (about 5 m/s) and a half barb for each 5 knots.

Assessment of probabilistic weather forecasts

The Finnish Meteorological Institute supplies the weather and dispersion information required in radiation accidents for the use of radiation and rescue authorities. Global weather prediction models provide probabilistic forecasts up to 15 days. From these long term forecasts a first impression related to weather events can be obtained. While moving closer to the actual event time, the importance of a higher resolution ensemble prediction system is emphasized. The operational probabilistic weather forecasting system MEPS (Meteorological co-operation – Ensemble Prediction System) provides more detailed structures of the weather 60 hours ahead than the global models do. The higher resolution and probabilistic approach brings more confidence on decision making in case of nuclear emergency.

Based on probabilistic verification scores we can say that the regional high resolution MEPS adds value to the mean wind and wind gust forecasts. In comparison

to global models, the high resolution model MEPS is able to produce a larger ensemble spread approaching the mean RMS error (Fig. 5), which is a desirable feature. The ensemble spread reflects the width of the ensemble and the range of the possible outcomes. To cover the full ensemble forecast uncertainty the spread should be as large as the mean RMS error. For the 3h accumulated precipitation, not as large an improvement by the high resolution model was seen as for transient and mean wind speeds. However, a closer investigation between the different precipitation thresholds showed that MEPS has higher skill to detect and predict small rain showers.

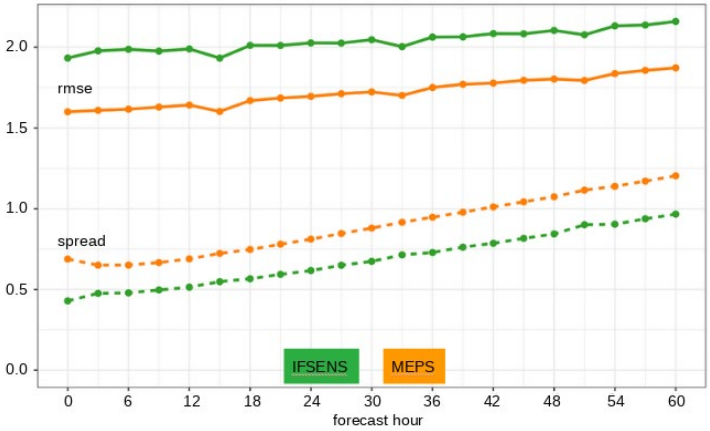

Figure 5. Ensemble Spread and skill (RMS error) for 10 m wind speed (m/s). Global model IFS-ENS: green. High resolution limited area model MEPS: orange. Verification period 1. Sep - 30. Nov. 2020.

A strong low pressure, which was named Liisa at FMI, hit Finland on Thursday 19th November 2020. It left in total 121 000 households without electricity mainly due to fallen trees severing power lines. The case study of Liisa showed how MEPS was able to forecast very realistically the structure of the convective line with good precision in timing and shape (Fig. 6).

The ensemble forecasts take into account the uncertainty associated with the location and timing of a wind storm or heavy precipitation. However, the likelihood of an event occurrence is dependent on the model skill, which depends on initial conditions and methods used to generate the ensemble. Future work to improve the probabilistic forecast MEPS is to try to enlarge the ensemble spread by perturbing model parameters. The Stochastically Perturbed Parametrizations (SPP) scheme includes 14 parameters that can be perturbed in MEPS: 7 for clouds and microphysics, 3 for turbulence and 4 for radiation. This method has already been proven to be able to inflate the spread for the global IFS-ENS model (Ollinaho et al. 2017) and the expectations for MEPS are high.

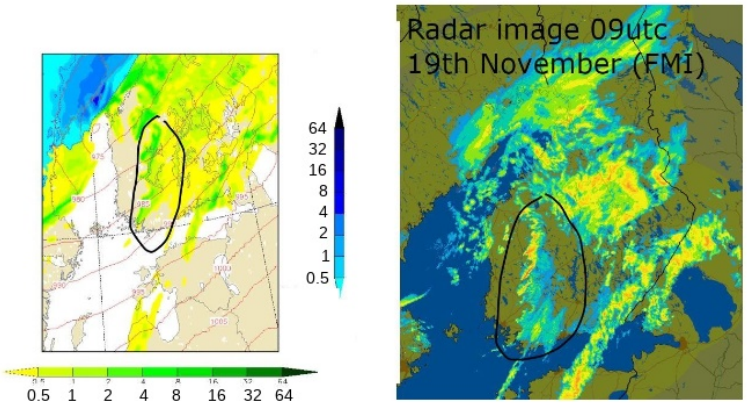

Figure 6. On the left: MEPS control run 19th November 2020 at 06 UTC, forecasted instantaneous precipitation (mm/hour) valid at 09 UTC. On the right: Finnish Meteorological Institute's radar image (an observation) of precipitation at the same time. The convective line of interest is marked with a circle in both images.

Summary and conclusions

The general objective of PREDICT is to develop and maintain research expertise and methods needed for assessing probabilities of occurrence of safety-relevant single and compound extreme weather and marine events. The project aims to provide information that can be applied for the determination of the design basis for new NPP units, for probabilistic risk assessments of new and existing NPPs, and for periodic safety reviews of existing NPPs. The study topics of the project include statistics of sea-effect coastal snowfall; characteristics of joint heavy rain and high sea level events; uncertainty in the exceptional sea level estimates; influences of properties of low-pressure systems (cyclones) on sea levels; and probabilistic weather forecasts.

The main findings of PREDICT in 2019-2020 are given below:

- Conditions favouring sea-effect snowfall were analysed to occur most often in the western coast of Finland, in coherence with actual observations.
- Joint heavy rain and high sea level events are typically caused by passing extratropical cyclones. Most of these compound events occur during a positive North Atlantic Oscillation period.
- Bayesian hierarchical modelling of sea level extremes in the Finnish coastal region reduced the range of uncertainty in the estimated distribution parameters, in comparison to the tide gauge specific fits.
- A sea level model, with input data from synthetically generated low-pressure systems, appeared as a promising tool for studies of extreme sea levels.
- A probabilistic approach and increasing spatial resolution in weather forecasting bring more confidence on decision making in case of nuclear emergency.

Acknowledgement

In addition to the funding granted by the State Nuclear Waste Management Fund in Finland (VYR), the studies of sea-effect snowfall have been partly finalized by the Finnish Cultural Foundation, Satakunta Regional Fund, and by the Finnish Meteorological Institute (FMI). ERA5 reanalysis data were downloaded online through the web interface of the Climate Data Storage (CDS) of the Copernicus Climate Change Service (C3S).

References

Aalto, J., Pirinen, P. & Jylhä, K. 2016. New gridded daily climatology of Finland: permutation-based uncertainty estimates and temporal trends in climate. *Journal of Geophysical Research – Atmospheres*, 121, 3807–3823.

FMI, 2018: The summer from May to August was warmer than ever in recorded history. Finnish Meteorological Institute Press release archive, 6.9.2018; https://en.ilmatieteenlaitos.fi/press-release/656561883

FMI, 2019a: Aapeli storm marked the beginning of a cold January. FMI Press release 7.2.2019; https://en.ilmatieteenlaitos.fi/press-release/872470162

FMI, 2019b: Wave height records in the Baltic Sea. FMI Scientific themes; 1.3.2019; https://en.ilmatieteenlaitos.fi/wave-height-records-in-the-baltic-sea

FMI, 2021. 2020 – warmest year since Finland started keeping records. FMI Press release 12.1.2021. https://en.ilmatieteenlaitos.fi/press-release/3j2EOkB0jThiRSUOo7Gj37

Guide YVL B7, 2019. Provisions for internal and external hazards at a nuclear facility. Radiation and Nuclear Safety Authority (STUK).

Guide YVL C4, 2019. Assessment of radiation doses to the public in the vicinity of a nuclear facility. Radiation and Nuclear Safety Authority (STUK).

Hersbach, H., Bell, B., Berrisford, P., Hirahara, S., Horányi, A. et al. 2020. The ERA5 global reanalysis. *Quarterly Journal of the Royal Meteorological Society*, 146, 1999–2049.

Irannezhad, M., Marttila, H. & Kløve, B. 2014. Long-term variations and trends in precipitation in Finland. *International Journal of Climatology*, *34*, 3139-3153.

Jeworrek, J., Wu, L., Dieterich, C., & Rutgersson, A. 2017: Characteristics of convective snow bands along the Swedish east coast. *Earth System Dynamics*, 8, 163–175.

Johansson, M., Boman, H., Kahma, K.K. & Launiainen, J. 2001. Trends in sea level variability in the Baltic Sea. *Boreal Environment Research*, 6, 159-180.

Jylhä K, Kämäräinen, M., Fortelius, C., Gregow, H., Helander, J. et al. 2018. Recent meteorological and marine studies to support nuclear power plant safety in Finland. *Energy*, 165 (A), 1102-1118.

Leijala U., Johansson M. M. & Pellikka H. 2020a. Analyzing the extrapolation techniques and uncertainty related to the coastal flood risk estimates in Finland. PREDICT/SAFIR2022 deliverable D2.3.1 in 2019, Finnish Meteorological Institute.

Leijala U., Johansson M. M. & Pellikka H. 2020b. Analysing the extrapolation techniques and uncertainty related to the coastal flood risk estimates in Finland - Implications to Finnish Nuclear Power Plant (NPP) sites. PREDICT/SAFIR2022 deliverable D2.3.2 in 2019, Finnish Meteorological Institute.

Leijala U., Björkqvist J.-V., Johansson M. M., Pellikka H., Laakso L. & Kahma K.K. 2018. Combining probability distributions of sea level variations and wave run-up to evaluate coastal flooding risks. *Natural Hazards and Earth System Sciences*, 18, 2785-2799.

Luomaranta, A., Aalto, J., Jylhä, K. 2019. Snow cover trends in Finland over 1961–2014 based on gridded snow depth observations. *Int J Climatol*. 39: 3147–3159.

Markowski, P. & Richardson, Y. 2010. Mesoscale Meteorology in Midlatitudes, John Wiley & Sons, Ltd, 407 pp.

Ollinaho, P., Lock, S.J., Leutbecher, M., Bechtold, P., Beljaars, A. et al. 2017. Towards process-level representation of model uncertainties: stochastically perturbed parametrizations in the ECMWF ensemble. *Quarterly Journal of the Royal Meteorological Society*, *143*, 408-422.

Olsson, T., Perttula, T., Jylhä, K. & Luomaranta, A. 2017. Intense sea-effect snowfall case on the western coast of Finland. *Adv. Sci. Res*., 14, 231-239.

Olsson, T., Post, P., Rannat, K., Keernik, H., Perttula, T., Luomaranta, A. et al. 2018. Sea-effect snowfall case in the Baltic Sea region analysed by reanalysis, remote sensing data and convection-permitting mesoscale modelling. *Geophysica*, 53, 65-91.

Olsson, T., Luomaranta, A., Jylhä, K., Jeworrek, J., Perttula, T. et al. 2020. Statistics of sea-effect snowfall along the Finnish coastline based on regional climate model data, *Adv. Sci. Res*., 17, 87–104.

Pellikka H., Leijala U., Johansson M. M., Leinonen K. & Kahma K. K. 2018. Future probabilities of coastal floods in Finland. *Continental Shelf Research*, 157, 32–42.

Rantanen M., Jylhä K., Särkkä J., Leijala U. & Räihä J. 2020. Characteristics of joint heavy rain and high sea level events. PREDICT/SAFIR2022 deliverable D1.2.1 in 2020, Finnish Meteorological Institute.

Räihä J., Kämäräinen M., Jylhä K. & Särkkä J. 2019. A method for generating synthetic low-pressure systems to support studies of sea level extremes. PREDICT/SAFIR2022 deliverable D2.4.1 in 2019, Finnish Meteorological Institute.

Räihä J., Leijala U., & Jylhä K. 2020. Co-occurrence of heavy precipitation and high sea level. PREDICT/SAFIR2022 deliverable D1.2.1 in 2019, Finnish Meteorological Institute.

Räty O. & Laine M. 2019. OECD/NEA Benchmark on External Events Hazard Frequency and Magnitude Statistical Modelling. PREDICT/SAFIR2022 deliverable D1.3.1 in 2019, Finnish Meteorological Institute.

Räty. O., Laine M., Leijala U., Särkkä J. & Johansson M. M. 2020. Bayesian hierarchical modeling of sea level extremes in the Finnish coastal region. PREDICT/SAFIR2022 deliverable D2.1.1 in 2020, Finnish Meteorological Institute.

Stan Development Team, 2020a. RStan, the R interface to Stan, http://mc-stan.org/, r package version 2.21.2.

Stan Development Team, 2020b. Stan Modeling Language Users Guide and Reference Manual, Version 2.25, http://mc-stan.org/.

Särkkä J. & Räihä J. 2020. Sea level simulations using synthetic low-pressure systems. PREDICT/SAFIR2022 deliverable D2.2.2 in 2020, Finnish Meteorological Institute.

Trenberth, K. E., Fasullo, J. T., Shepherd, T. G. 2015. Attribution of climate extreme events. *Nature Climate Change*, 5, 725–730.

WMO, 2021. 2020 was one of three warmest years on record. Press Release Number: 14012021, published 15 January 2021. https://public.wmo.int/en/media/press-release/2020-was-one-of-three-warmest-years-record

3.4 Safety and security assessment of overall I&C architectures (SEARCH)

Antti Pakonen[1], Jarmo Alanen[1], Igor Buzhinsky[2], Atte Helminen[1], Joonas Linnosmaa[1], Timo Malm[1], Polina Ovsiannikova[2], Nikolaos Papakonstantinou[1], Valeriy Vyatkin[2]

[1]VTT Technical Research Centre of Finland Ltd
P.O. Box 1000, FI-02044 Espoo

[2]Aalto University, Department of Electrical Engineering and Automation
P.O. Box 15500, FI-00076 Aalto

Abstract

The objective of SEARCH (2019–2022) is to develop methods and tools for assessing technical design solutions related to overall instrumentation and control (I&C) system architectures. A particular focus is on trade-offs between requirements related to safety, dependability and security. We also aim to broaden the scope in which formal methods can effectively be used to verify properties on how the I&C systems operate as a whole.

In the first two project years, SEARCH has developed models and methods for early hybrid assessment of safety and security of overall I&C architectures. In addition, we have further developed methods of performing software model checking, accounting for hardware failures and communication delay. We have also developed a practical tool for explaining counterexamples.

Introduction

The overall I&C system architecture of a nuclear power plant must fulfil the Defence-in-Depth (DiD) principle—there have to be successive levels of protection independent of each other. In theory, the architecture could be designed in a way where I&C systems on each level would have their own instrumentation and human-system interfaces, and no system would communicate across the DiD layers. Such a design, however, is not only prohibitively costly, but potentially less safe in terms of complexity, operability or maintainability. As a result, the overall I&C architecture needs to be optimised, meaning that the requirements on separation are deliberately relaxed (see Figure 1).

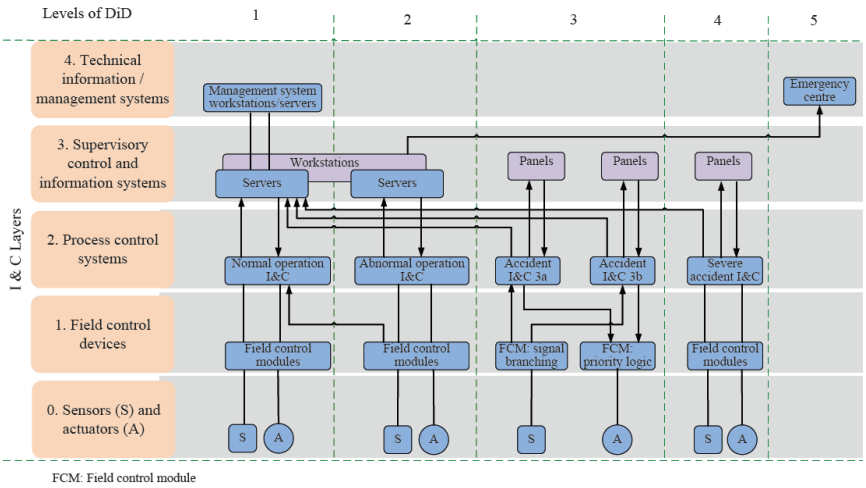

Figure 1. The separation of DiD layers can be compromised when the overall I&C architecture is optimised (IAEA 2018).

To ensure that key requirements for safety are still achieved by the optimised design, we need a suitable combination of deterministic and probabilistic safety analyses. The architecture needs to be constantly re-assessed during the design lifecycle, as new details about the plant and the I&C systems become available (IAEA 2018). Cybersecurity also needs to be addressed from the start. We also need to ensure that the computer security measures do not overtly compromise other vital aspects (IEAE 2028), in particular safety, but also availability.

A formal verification method called model checking has been used in the Finnish nuclear industry to assess I&C application software design. However, it is currently not easy to combine all the features and properties of real-world system in formal models (IAEA 2015). The industrial acceptance of such methods has also been slowed by the lack of user-friendly, graphical tools (IAEA 2015), and the difficulty in expressing non-functional requirements, in particular.

In the first two project years, the SEARCH project has developed models, methods and tools for analysing the safety and security of early I&C architectures. We have also broadened the way model checking can be applied, by developing methods to verify both software and hardware specific aspects against both functional and non-functional requirements. Furthermore, we have developed new, user-friendly tools for better understanding the analysis results that model checking tools produce.

To properly evaluate the proposed methods and tools, we have built practical demonstrations based on actual industrial data: the early I&C architecture of Hanhikivi-1, and the models that VTT has built in over a decade of practical model checking projects for STUK, Fortum and Fennovoima.

DiD assessment of I&C architectures

Hybrid safety-security modelling and assessment

Safety and security of complex critical infrastructures are very important principles for economic, environmental, and social reasons. Although safety and security have different foci, in many areas they overlap with each other, and actions to advance the other activity in complex system can have implications for the other. The complexity of these systems introduces difficulties in the identification of safety and security risks that emerge from interdisciplinary interactions and dependencies. Modern systems have become increasingly complex, leading to unintended vulnerabilities to both nominal mishaps and mishaps imposed by an attacker. The discovery of safety and security design weaknesses late in the design process can lead to increased costs, additional system complexity and delays to the deployment of the system. Safety and security system capabilities are currently often evaluated independently using separate assessments and specific methods that are performed by specialized experts at different system design phases. The methodologies we have developed in SEARCH attempt to introduce hybrid models including both safety and security concepts that can support a concurrent safety and security assessment at an early design phase.

In (Papakonstantinou et al. 2019), we developed an interdisciplinary model-driven method and a prototype tool for hybrid DiD assessment of early complex systems. Instead of focusing on removing vulnerabilities, we assumed that a determined attacker can always find a way to penetrate defence. The method can assess basic safety and security design principles (e.g., redundancy, separation, diversity, security zones) concurrently, and provide feedback in early system design. To support the security assessment of complex systems the UML profile proposed for safety assessment in (Papakonstantinou et al. 2017) was extended with security concepts of facility functions, security levels, authorization levels, computer and facility security zones, conduits and physical gates. Based on this modelled set of safety and security attributes, the developed prototype tool can assess aspects of the safety and security DiD capabilities of an early design. The four steps needed for the proposed combined early safety and security assessment are:

- Step 1: Develop the multidisciplinary dependency model of the system focusing on interdisciplinary connections (dependencies between disciplines).
- Step 2: Add the known safety and security aspects (safety/security system components and attributes).
- Step 3: A software tool automatically assesses the safety and security capabilities of the system based on a set of safety and security rules.
- Step 4: Safety/security engineers and system engineers evaluate the feedback of step 3. Use the results to improve the system design. If changes are done, return to step 3.

The results can be then used to identify errors, improve the design and cut costs before a formal human expert inspection. We demonstrated the tool on a case study of an early conceptual design of a fuel cooling pool system of a nuclear power plant.

In another effort in SEARCH, in order to support and combine multidisciplinary modelling and assessment, we have developed, together with the AUTOPORT (Business Finland) project team, a model-driven methodology for a hybrid Reliability, Availability, Maintainability, Safety and Security (RAMMS) risk assessment. This work enhances and extends our safety risk assessment ontology and data model, originally developed as a part of our System Engineering Artefact Model (SEAModel) (Tommila & Alanen 2015), to also support security and dependability engineering.

To create such a hybrid risk assessment ontology, we first needed to harmonize some basic concepts between dependability, safety and security. The harmonisation results are shown in Table 1.

Table 1. Harmonised basic concepts between safety, security and dependability.

Safety	**Security**	**RAM**	**Harmonised term**
Fault	Vulnerability	Fault	**Imperfection**
Hazard	Threat	Loss scenario	**RAMSS hazard**
Harm	Impact	Loss	**Negative impact**
Protective measure	Countermeasure	Improvement measure	**Risk control**

Using these harmonised terms, we created a hybrid risk assessment ontology, which supports creation of a structured work item (artefact) storage (such as a database), with traceability links, of the input and output work items related to the risk assessment activity. This RAMSS ontology is presented in Figure 2.

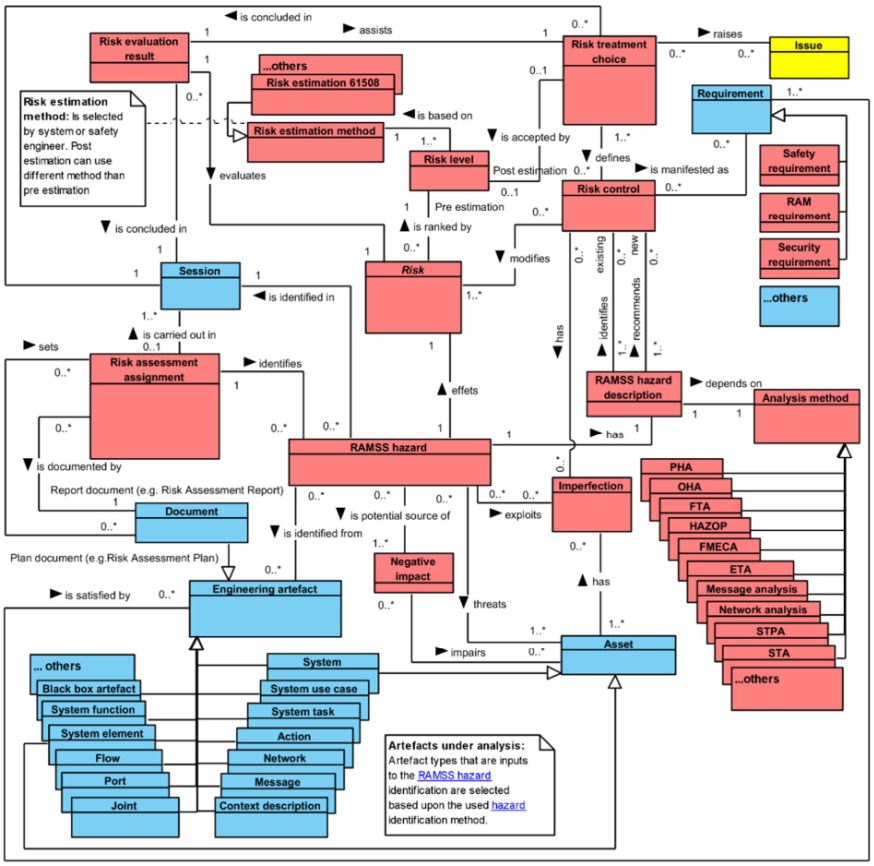

Figure 2. RAMSS risk assessment ontology. The risk assessment related artefact types are with red colour, the blue ones are general systems engineering artefact types, and the yellow artefact is a project management related artefact.

The RAMSS risk assessment ontology should support any risk analysis method, but we wanted also to create a SEAModel compatible ontology for an early nuclear I&C cybersecurity risk assessment called Security Threat Assessment (STA). The idea was not to define a new cybersecurity risk assessment procedure, but an ontology and the derived data model, which can be used in the context of any typical security risk assessment procedures, such as the ones presented in ISO 31000 or IEC 62443-3-2. The STA data model is presented in Figure 3.

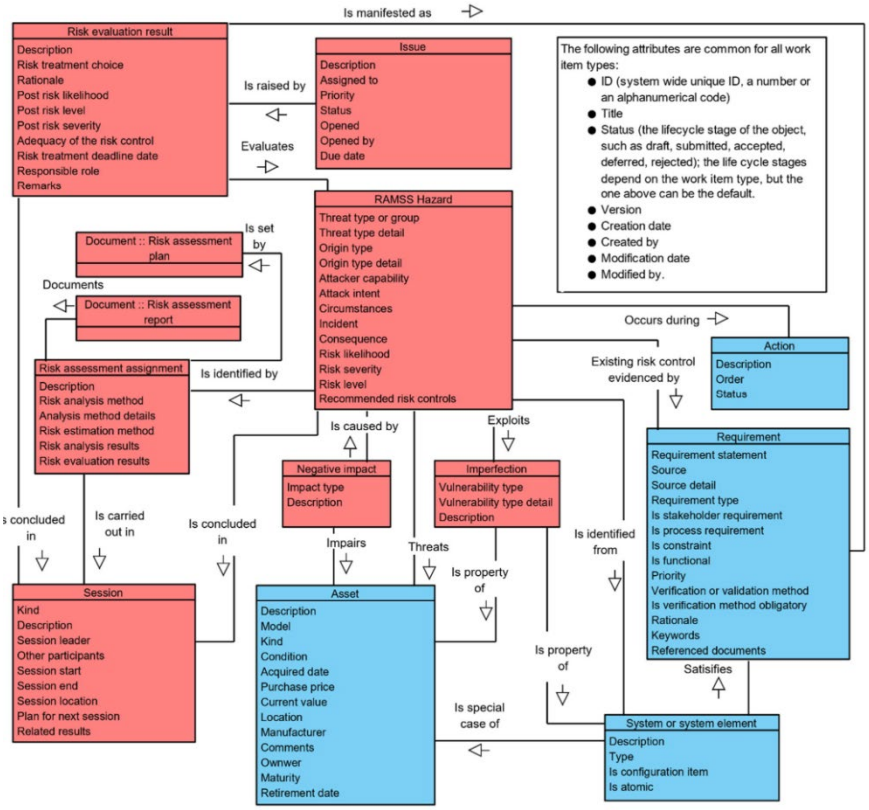

Figure 3. Data model for STA artefacts and their relations.

We also implemented the STA data model onto the Polarion REQUIREMENTS requirements management tool and demonstrated the models with an I&C related security threat case (a threat to lose fuel pool cooling due to an attack by a malicious IT service person).

Early DiD assessment of I&C architectures – a practical demonstration

In collaboration with Fennovoima, we have developed proof-of-concept algorithms and a prototype tool (see Figure 4) for early assessment of DiD-related I&C design properties. We built a demonstration using Hanhikivi-1 project data (text documents, spreadsheet, and functional diagrams) on safety functions, I&C systems, and the system's interfaces and classifications.

We then defined checks based YVL and plant specific requirements on safety classification, functional separation, communication independence, diversity, and failure tolerance. We checked both plant-level requirements, and then the system-

specific requirements elaborated based on them, trying to identify any conflicts. Utilising the MS Visio diagram importer developed in another SEARCH task (see below), we also identified interfaces between systems based on diagram signals between safety functions, and then crosschecked that information against interfaces as specified by the other documents.

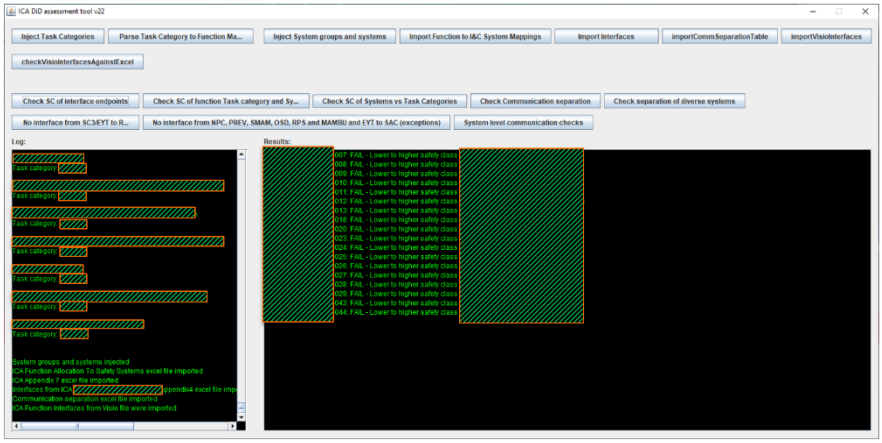

Figure 4. A prototype tool listing detected communication separation requirement violations (FH-1 project data masked).

Our prototype tool correctly identified several already known issues related communication direction, failure tolerance and diversity. Some of the issues had to do with deliberate design decisions—e.g., prioritisation logic can only be implemented in higher safety class system if communication from a lower safety class is allowed as an exception. The tool also produced several false positive results, since the function allocation did not differentiate if the system(s) provided the measurement, performed the logic, or carried out the actuation. We also pointed out that some relevant information (e.g. communication direction in interfaces) was not explicitly defined.

In 2021, we aim to use the lessons learned in the case study to develop formal modelling techniques for analysing DiD properties.

Review of Architecture Description Languages

Supported by in-kind participation from OECD Halden Reactor Project (run by Institute for Energy Technology (IFE)), SEARCH reviewed and studied the use of Architecture Description Languages (ADL) in I&C architecture modelling and analysis to enable Model-Based System Engineering (MBSE) in design and assessment. ADLs can enable the modelling of both hardware and software aspects of systems and components, supporting the “plant-as-a-whole” approach.

We started in (Hauge et al. 2019) with a systematic survey of the literature identifying current model-based techniques, methods, and approaches that can support

the assessment of safety and security in the early system stages like the concept stage, architecture or early design stages, as well as support the building of confidence that both of those quality factors are satisfactorily addressed early. The selected search strings generated an initial set of 178 papers, illustration of the categorisation of the research fields is shown in Figure 5. The most mature and promising direction for further exploration of model-based approaches supporting safe and secure DI&C design was represented by papers that used the AADL (Architecture Analysis and Description Language) as its basis.

Figure 5. Relevant research fields of safety and security papers supporting model-based assessment with the proportional shares of each, based on the literature review of (Hauge et al. 2019).

Other objective was to study the use of ADLs for standardized and structured ways to model the overall I&C architecture, a set of selected DiD related requirements of the dependencies formed with the connections between systems, and automatic assessment of the fulfilment of those requirement using the model. In (Linnosmaa et al. 2020) we studied the capabilities of AADL against this goal. We first specified an example case for a part of an overall I&C architecture (including safety functions, safety classes, DiD levels and I&C systems) loosely based on the APR-1400 design. In addition, we crafted some basic separation related DiD requirements based the Finnish YVL guides. We then studied the AADL version 2.2 and an open source tool called OSATE2 to model and assess the system.

The graphical version of the AADL model of the case architecture is shown in Figure 6. The shown AADL counterparts for overall I&C architecture components were selected to best fit their needed scope. The components we chose were:

- I&C system: AADL component *System*
- DiD level of the I&C system: AADL component *Custom property set*
- Safety class of the I&C system: AADL component *Custom property set*
- Safety function: AADL component *Process*
- DiD level of the safety function: AADL component *Custom property set*
- Safety class of safety function: AADL component *Custom property set*
- Connection between systems: *Connections* to an AADL component *Bus*

We demonstrated that even though AADL may not a standardized components or methods for modelling a system at the level of overall architecture, it still offers support for modelling the primary components.

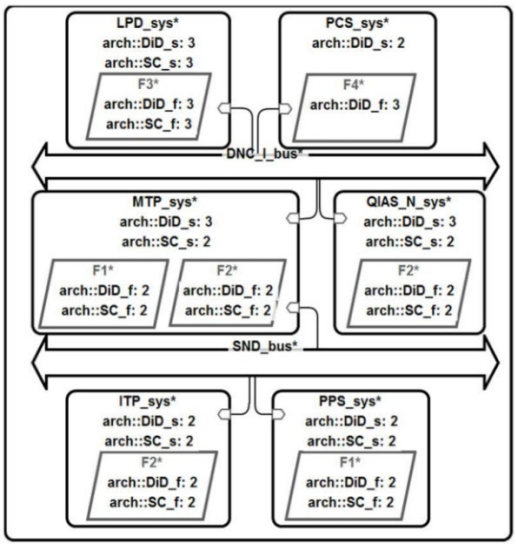

Figure 6. Diagram view of the AADL overall I&C architecture OSATE (Linnosmaa et al. 2019).

However, we did not find a way to express our wanted requirements using the standard AADL notation, at least not in a way we could have analysed their fulfilment. We did gather a set of promising analyses from literature based in various annexes to the language, which could be used to expand the model to offer more DiD related assessment capabilities. To conclude, the AADL components are more geared towards specifying the physical decomposition of a single system.

In (Sechi et al. 2020), the focus was shifted a little to focus studying early stage architecture modelling and safety assessment of a single system under modernization. Our case was the Halden Safety Fan (HSF), which is an initiative to research model-based design, assurance and digitalization of old analogy emergency ventilation system based on the real system part of the Halden research reactor in Norway. Digitalization steps, in general, include establishing a concept description, the development and safety assessment plans, system requirements specification, risk analysis and safety assessment report. It is an interesting possibility for researchers to get hand-on experience working with real-life equipment and the related documentation.

As the whole HSF initiative is still at an early stage, our work included also defining some of the properties for HSF case, for example describing the overall functions of the system, the main sub-systems and components, and the interconnections between these. We also started to outline the functional behaviour of the

system. Based on our system descriptions we modelled the structural aspects (standard AADL) and non-nominal behaviour (AADL error modelling annex EMV2) of the system. AADL and the tool OSATE, offered constructs for effective composition and linking of specification parts. The information of a specific part can be focused on one place but can be accessed from many places. The navigation within a model is not constricted to linear navigation, from the textual representation, different kinds of graphical diagrams are generated and linked to allow navigation to any part of the specification quickly. A system defined with OSATE2 includes clear syntax and semantics allows for automatic or semi-automatic analysis such as FHA, FTA, FMEA. We used FTA to find minimum cutsets for redundant train failure state of the system. We also used this information to inject a failure in a dynamic process model modelled with APROS.

To summarise, AADL offers easy to use language constructs to support the extension of the standard AADL ("common") model for both safety and security analysis and assurance activities using annexes. Two examples of relevant extensions are the EMV2 with a focus on error modelling and the Resolute assurance case language for AADL. Furthermore, tool support for any language extension is possible in OSATE2 by developing the necessary plugin, that is well supported.

Project SEARCH also included expert participation in three virtual HRP Workshops under the general topic of "Safety of Digital Instrumentation and Control Systems". The workshop facilitated sharing knowledge across application sectors in order to learn about the state-of-the-art and best practices applicable to the nuclear power plant domain. The findings and conclusions of these workshops has been reported in (Esnoul et al. 2020). In conclusion, the workshop participants identified support for the overarching assertion "*It is technically feasible within the state-of-the-art to provide reasonable assurance that a digitally implemented safety function will be performed as intended. Such reasonable assurance will not require diverse design means of performing the same safety function or one with an equivalent effect*". Additionally, the discussions helped identify issues experienced in current practice, obstacles to adoption of better approaches, and opportunities for future collaborative research.

Formal verification methods and tools

I&C hardware issues in model checking

Certain safety functions of I&C systems are designed to be fault tolerant. Checking fault tolerance formally requires hardware failures to be formally modelled in addition to the I&C logic. Due to the focus of SEARCH on overall reliability assessment, we decided to extend our previous results (Pakonen & Buzhinsky 2019) obtained at the end of the SAUNA project (SAFIR 2018) to support connected implementations of more than one safety function.

In our recent works (Buzhinsky & Pakonen 2019; Buzhinsky & Pakonen 2020a), we allow safety functions to correspond to one or more *I&C systems*, and allow each

I&C system to have several *divisions*, such that all the components (*units*, which perform computations, and connections between them) of the system are duplicated in each division. The typical assumption of failure tolerance is the *single failure tolerance* criterion: the safety functions must work correctly with arbitrary failures in any single division.

The structure of the most comprehensive case study that we considered is shown in Figure 7. It consists of one non-safety system, the process automation system (PAS), and three safety systems: the protection system (PS), the safety automation system (SAS), and the priority and actuator control system (PACS). These systems correspond to three functions: normal operation, preventive protection and reactor protection. The relation between the systems and the safety functions is shown in Figure 8. We developed this case study based on the U.S. EPR NPP materials (Areva 2012; Areva 2013) and our own invention, and tried to make the implementations of units realistically detailed.

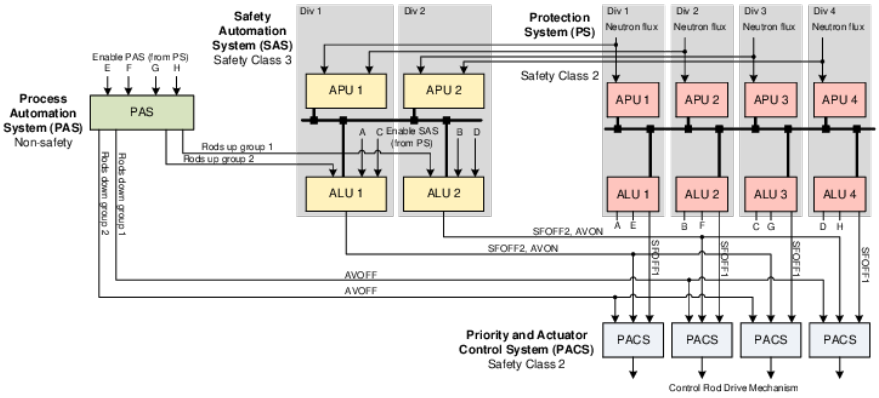

Figure 7. Case study for failure tolerance model checking (Buzhinsky & Pakonen 2020a).

Our approach to failure modelling extends the one proposed in (Pakonen & Buzhinsky 2019). As before, we perform model checking in NuSMV (Cimatti et al. 2002), model the elements of the system in MODCHK (Pakonen at al. 2013), remove unit/division pairs that do not influence the temporal property to be verified, and in particular examine only one divisions of the verified unit. To support the structural assumptions mentioned above, some other aspects of the approach were refined.

First, we made the processing of symmetries in the overall model automatic. We will refer to the pair of an assignment of failure division(s) and the selected division of the unit whose property must be verified as a *configuration*. Previously, when we dealt with only one redundant system, we used the facts that the implementations of the units in all the divisions of this system are identical and the connections between the units are symmetric (which is the case for the PS in Figure 7) to only consider one configuration during model checking as verification outcomes for other configurations would be necessarily identical. However, when the structure of the

system becomes as complex as the one shown in Figure 7, and when different systems are allowed to have failures in different divisions, it is no longer apparent which configurations are equivalent. To solve this problem, we developed an approach that computes the *domination relation* between configuration: configuration A dominates configuration B if the verification outcome of A is at least as reliable as the one of B (i.e., any positive outcome for A implies a positive outcome for B). Once this relation is computed, it is sufficient to model-check a subset of configurations that dominates all possible configurations under the considered failure assumption. An example of a matrix of such a relation is shown in Figure 9.

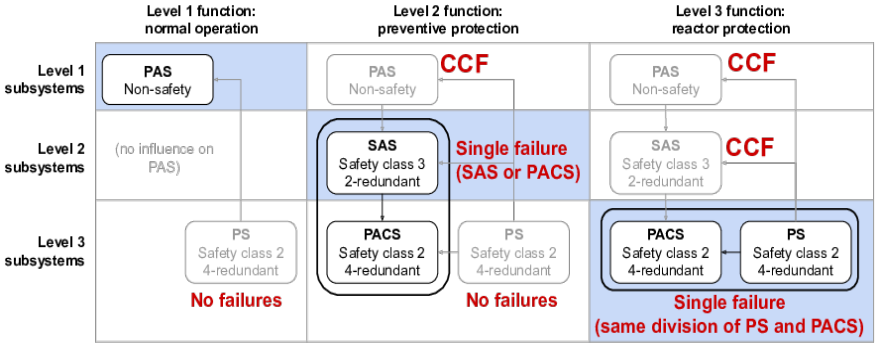

Figure 8. Connections between the systems and the safety functions, and the used failure criteria (Buzhinsky & Pakonen 2020a). “CCF” stands for a common cause failure (modelled as a failure in all the divisions).

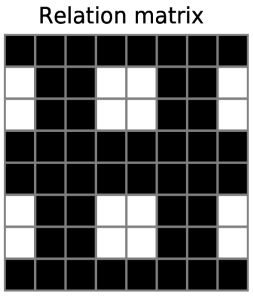

Relation matrix	Failing divisions	Viewpoint
	PAS: 1, PS: none, SAS: 1	PACS, division 1
	PAS: 1, PS: none, SAS: 2	PACS, division 1
	PAS: 1, PS: none, SAS: 1	PACS, division 2
	PAS: 1, PS: none, SAS: 2	PACS, division 2
	PAS: 1, PS: none, SAS: 1	PACS, division 3
	PAS: 1, PS: none, SAS: 2	PACS, division 3
	PAS: 1, PS: none, SAS: 1	PACS, division 4
	PAS: 1, PS: none, SAS: 2	PACS, division 4

Figure 9. Matrix of the domination relation when verifying temporal properties of the outputs of the PACS (“viewpoint”) related to preventive protection (Buzhinsky & Pakonen 2020a). Here, out of eight possible configurations, it is sufficient to model-check any single configuration that corresponds to a black row in the matrix.

Second, we agreed on several conventions regarding the temporal properties to be verified. Formulation of some temporal properties becomes non-trivial due to the following problems: (1) for each temporal property, verification may potentially be performed for several configurations, meaning that the divisions of the components

to be verified become known only after symmetry analysis; (2) the divisions where failures are possible also become known only after symmetry analysis; (3) we only model failures on connections between the units. To solve the first problem, when referring to the concrete divisions of the components in a temporal property, we utilize a division placeholder, which will be replaced by the index of the actual division to be verified after symmetry analysis. To solve the second problem, when we need to express a property that refers to multiple divisions of the system, we use only AND, OR and other counting operations over all the divisions. The results of these operations do not depend on the order of their arguments, and thus on the divisions selected for failure injection. To solve the third problem, we avoid temporal properties referring to the internal variables of the units. It is in principle possible to verify temporal properties that do refer to these variables, but then they need to be carefully checked to be meaningful.

Third, we have found that a mere optimization of the model of a failure injection blocks, which are inserted on the connections of the model in the divisions that may be affected by failures, notably decreases the model checking time. Essentially, the optimized version of the failure block is a mere replacement of the failing signal with a nondeterministically generated value. However, we have also found that the use of such a simple model may lead to false positive results when model-checking computation tree logic (CTL) properties. For a subclass of such properties that expresses the possibility of a Boolean output to produce both values in the future (AG-EF properties), we have enhanced the failure model to restore the reliability of verification.

In parallel to the work on failure modelling, we used the presence of communication modelling in our approach to support one more aspect of real-world systems: we also accounted for communication delays between the components and their asynchrony. We tried two techniques: the one developed previously (Pakonen & Buzhinsky 2019), where discrete-time delay blocks may nondeterministically delay the signals between the components of the system, and a new approach based on real-time modelling of delays (Buzhinsky & Pakonen 2020b) in the nuXmv model checker.

In the new approach, we modelled each unit of the system as a timed automaton (Alur & Dill 1994) that operates cyclically, making a step once per a fixed time duration. Executions of different units are not necessarily synchronous. In addition, we modelled the buffers between the units that store the data which has not yet been received. These buffers model the delays by being able to hold the old version of the received signal for a duration within a specified range. Figure 10 shown an example of a timeline in the real-time model of the PS.

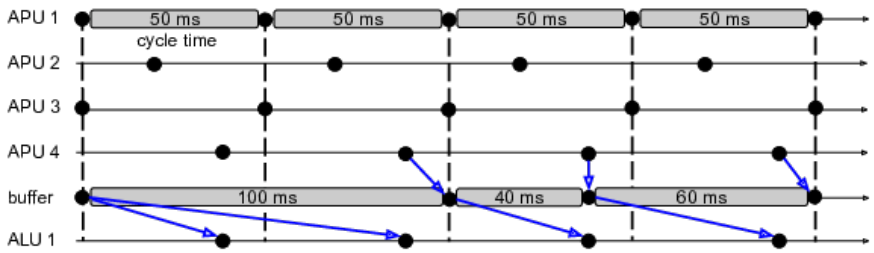

Figure 10. Example of a timeline of the PS in a timed nuXmv model (Buzhinsky & Pakonen, 2020b). Blue arrows show the information flow from APU 4 to ALU 1.

In most of our experiments, we focused on the situation of modelling hardware failures, but not delays and asynchrony. In this failure-only setting, we succeeded in verifying the system shown in Figure 7 with model checking algorithms based on binary decision diagrams (BDDs). Our experiments encompassed three failure scenarios shown in Figure 8, and also an artificial scenario where the single failure criterion was applied to all the subsystems of our case study independently. Checking a single temporal property took up to several seconds.

The situation of both failures and delays being modelled is more challenging. With the basic, cycle-based delay modelling, BDD-based algorithms usually no longer terminate within reasonable (i.e., several hours) time limits, but incomplete bounded model checking (BMC) handles such situations well. To evaluate the real-time communication modelling approach (Buzhinsky & Pakonen 2020b), we only included the PS into the overall model. On such a reduced case study, we found that BMC is again successful, and in addition a small fraction of properties can be verified by a complete model checking algorithm (IC3). Finally, the real-time communication modelling approach opens the opportunity of verifying temporal properties with explicitly specified time durations (e.g., required response time), but we found such properties more computationally complex to verify than regular ones.

Explanation of counterexamples

While model checking it is an efficient instrument for detecting failures in I&C logics, finding a particular problem location in a model or its specification can still be a daunting task. Overall, model checking tools take the formal model of the system and its specification as input and produce a counterexample as output if the latter is violated. In our case, the system is represented as a NuSMV function block diagram and its properties are formulated using linear temporal logic (LTL). We define a state of the system as a list of all the system variables with their values at a particular discrete time step. Thus, a counterexample is a sequence of such states where the specification fails, starting from the initial one. At the same time, a counterexample is a mere table of values that lacks information about the system structure, contains dozens of variables, and requires pen and paper to be analysed.

Therefore, we developed Oeritte, a tool for visual counterexample analysis that combines a technique for counterexample explanation using the LTL property that was developed during SAFIR2018 (Pakonen et al. 2018) with highlighting of possible failure paths in the diagram of the system.

We define *an assignment* as a value of a variable at a particular discrete time step. As an LTL formula failure can be explained through a set of assignments of the variables included in it (Pakonen et al., 2018), we can decompose the process of explaining the false outcome of the LTL formula to the one of explaining a number of individual assignments in the counterexample. We can then focus on explaining a single assignment, called an explanation target. Informally, a *cause* of a target is a set of assignments of the system variables such that it is possible to infer the target by applying logical inference starting from these assignments and proceeding in the direction of information flow through function blocks. A cause is *inclusion-minimal* if it contains no subset of assignments that satisfy the statement above. Thus, to *explain the target* is to find the union of all of its inclusion-minimal causes.

In order to find such causes, we, first, decomposed the system into a net of interconnected atomic blocks that represent atomic operators (e.g., +, -, *, ∨, ∧) or simple functions (e.g., counting, conditional operators, delays) and have a finite number $n > 1$ of inputs and one output. Then, for each of these blocks, we defined a function that explains their outputs. We also defined an explanation function for a connection between blocks, which, basically, states that a cause of the end assignment of the connection is its start assignment at the same step. Now, to explain the target in the function block diagram, we developed a recursive algorithm that searches for causes of the assignments included in every next found cause starting from the explanation target and terminating in the assignments of the variables that belong to system inputs or lack incoming connections. We implemented the algorithm in a tool with graphical user interface, Oeritte.

In 2020, we formulated a theoretical base under our definitions and proved that the result of the algorithm corresponds to a union of all the inclusion-minimal causes. We also removed some of the restrictions on input files, allowing explanation in the diagrams with several levels of hierarchy (or, speaking in terms of NuSMV, that include nested modules). To enhance user experience, we implemented an automatic visual connection of the cause of the LTL formula with the variables in the diagram.

The graphical user interface of Oeritte is shown in Figure 11. A tooltip with the variable name appears when the cursor hovers over any of the squares (called *pins)* on the sides of the blocks that correspond to their input and output variables. Blocks with the single input or output pin on the left and right sides of the diagram represent the interface of the current diagram. Lines connecting module inputs and outputs are connections between the variables. The area to the left of the diagram provides information about the LTL formula being analysed. There exist two formula evaluation views, i.e., the one depicted in Figure 11(i) – parsing tree view, and the other from (Pakonen et al. 2018). Oeritte incorporates two kinds of explanation techniques: the cause identification algorithm (Pakonen et al. 2018) for LTL formula failures and individual assignment explanation, described above. The result of the

latter, which includes all the minimal causes for the target, is depicted in the diagram in the form of highlighted pins and connections in between.

In Figure 11, the elements of the user interface are marked with the letters in red circles:

a) two main tabs for the project settings and the working environment;
b) counterexample represented as a table of values;
c) a list of counterexample steps (a click on one evaluates the diagram according to the step chosen);
d) FBD visualisation (diagram area);
e) if the diagram contains modular blocks, it is possible to open their internal nets of blocks in separate tabs;
f) diagram zoom buttons;
g) all failed properties for the system (it is possible to dynamically switch between several formulas);
h) possible evaluation views of the chosen LTL property;
i) the evaluation of the chosen LTL property in a parsing tree view;
j) a button that initialises the LTL formula explanation process as described in (Pakonen et al. 2018);
k) assignments of the variables from the LTL formula that form its cause;
l) assignments that belong to the input interface of the current diagram and are a part of a cause.

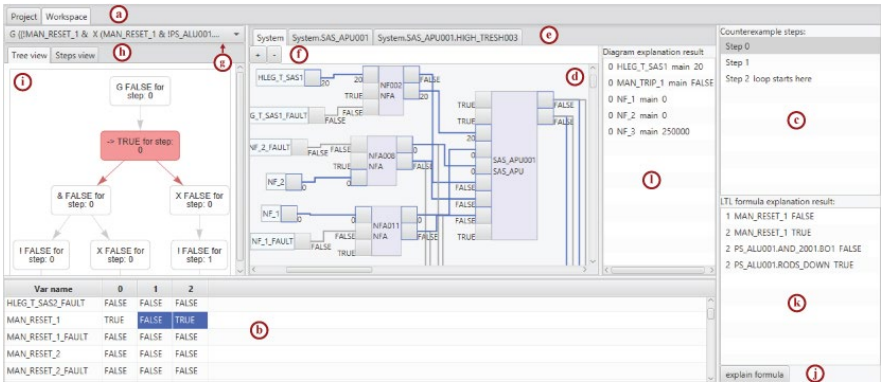

Figure 11. Main view of the counterexample explanation tool Oeritte.

As our most recent case study, we used a semi-fictitious I&C application logic (Buzhinsky. & Pakonen 2020a) partly based on the U.S. EPR protection system (Areva 2012; Areva 2013) encoded in NuSMV. We consider this system to be of an industrial size as it contains approximately 650 lines of code describing 20 different function block types and 32 function block instances. For this system, we verified the formula saying that the “rods down” command shall be deactivated when the safety criterion is satisfied, and the operator issues a manual reset. The property was violated and the counterexample for it had three steps, each of which contained

values of all 375 system variables. The visual counterexample explanation revealed the situation where the value of the variable of the system was locked in its active state, therefore, preventing the “rods down” command to be deactivated. Figure 12 shows the example of a graphical explanation received by the analyst when searching for a cause of variable RODS_DOWN being active at counterexample step zero.

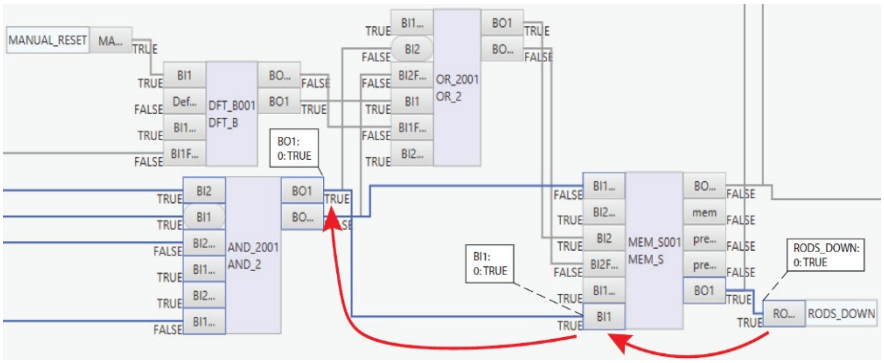

Figure 12. An example of the explanation of the variable RODS_DOWN at step 0 of the counterexample. Red arrows show the direction of the attention of the analyst.

Model-to-model translation

VTT’s model checking work is supported by the graphical front-end MODCHK (Pakonen et al. 2013), but the analyst still has to manually recreate the application logic (function block diagram), even if the diagram is already available in some electronic format. A lot of the research in model translation is based on the assumption that the logic is based on the IEC 61131-3 standard, but nuclear vendors rely on closed, non-standard languages (Pakonen et al. 2021). The source code is not usually available, and third parties only have access to diagrams as PDF or MS Office files. We therefore created a methodology (Pakonen et al. 2020) for transforming generic I&C diagrams into an intermediate UML model, which in turn supports transformations to target formats like IEC 61131-3 PLCOpen XML, or the input language of the NuSMV model checker. On one hand, 61131-3 supports interoperability with a range of different engineering and analysis tools. On the other hand, many nuclear domain specific features we need to capture (signal validity, allocation of logics to physical devices, graphical layout of the diagrams) are not inherently supported by the standard, so our UML metamodel maintains those aspects in the intermediate model.

MS Visio is used in basic design by companies like Framatome (Teleperm XS block diagrams) or Atomproekt (Hanhikivi-1 NPP functional diagrams) (Pakonen et al. 2020). We therefore demonstrated the methodology by importing exemplar diagrams from MS Visio, and then generating the inputs file for both NuSMV and a generic I&C development tool based on IEC 61131-3 (Codesys).

In developing the MS Visio importer, we ran into several issues, since Visio does not use the kinds of proper semantics or syntax checks that a proper I&C engineering tool would. In our exemplar diagrams, we noticed connections that only look as such (but actually float), connections wires drawn in the “wrong” direction, and groups of components that only look like a single component. In the transformations based on Visio’s XML file format, some connections had to therefore be deduced based on “proximity” on the diagram.

In the end, even if a transformation is not able to capture every aspect of the original logic, the analyst would benefit from having even a part of a complex logic automatically generated in the model checking tool. Errors or omissions made in the transformation would most likely be revealed trough the resulting counterexamples.

Extending the model checking tool portfolio

Since 2008, the open-source model checker NuSMV has been successfully used by VTT in practical industry projects to detect I&C software design issues (Pakonen et al. 2020). However, one of the limitations that NuSMV imposes is that models of I&C application logics containing analog signal processing logics have to be abstracted, as NuSMV only allows integer variables and simple math. Analysts need to carefully simply such logics, and some types of logics cannot be modelled with reasonable accuracy at all.

The developers of NuSMV have also released a model checker called nuXmv. One of the advanced features of nuXmv is that it supports infinite-state models, which in practice means real number variables. The research question we sought to answer was: does the improved capability come at a prohibitive computational cost?

To evaluate the scalability of nuXmv infinite-state algorithms, we first collected eleven real-world industrial NuSMV models of I&C applications with analog logic. The models came from three different plant projects, with three different companies responsible for the application logic design. We then remodelled the logics using NuSMV, by remodelling the basic function blocks containing math, and changing the integer model variables to real number variables. Then, we compared the time it took to verify the NuSMV model against the different algorithms that nuXmv provides.

In most of the cases, the IC3 algorithm performed very well, and was faster than NuSMV. The overall fastest method was IC3 invariant checking, but only a limited number of generally interesting properties can be expressed as invariants.

The verification results did not change, in the sense that the checks produced the same results for both the finite-domain and infinite-domain case. It can therefore be argued that the simplifications used by VTT in NuSMV analyses are a reasonable approach at practical verification. Still, it is clear that nuXmv outperforms NuSMV, and discussions are underway between VTT and nuXmv developers about terms for commercial use.

Co-use of model checking and probabilistic safety assessment

Probabilistic Safety Assessment (PSA) is a well-established convention in the nuclear industry. PSA complements deterministic methods like model checking by determining the probability of failure of systems that constitute the overall architecture (IAEA 2018). However, digital I&C PSA remains a challenge, and it is generally agreed that there is a lack of a common basis for quantifying software reliability (IAEA 2015).

In the SAFIR2018 project SAUNA, we developed ways to co-use the methods so that model checking would benefit from PSA. One option we experimented with was to use PSA to limit the set of postulated component failures when introducing hardware failures to model checking (Björkman & Pakonen 2019).

In SEARCH, we shifted the focus to ways how model checking could benefit PSA. We collected the 57 design issues VTT had by then detected in practical model checking customer projects in the Finnish nuclear industry. We defined the failure mode and possible systems level end effect(s) of each issue. We then compared the results against the I&C software failure modes and end effects for PSA found in the literature (Helminen & Pakonen 2020).

Table 2. Examples of software design issues with non-trivial failure modes and end effects. See (Helminen & Pakonen 2020) for the complete list.

Suggested failure mode	Notes on possible system level end effect(s) and relevance to PSA
Indecisive / conflicting output state	Safety function may be limited.
Fluctuating output state	A failure mode that might endanger a component protection function. Not likely modelled in PSA.
Incorrect control parameter	Incorrect setpoint due to incorrect internal system state. More analysis would be needed to recognize the failure mode(s) and potential end effects(s) for PSA.
N/A	Control function related. Not modelled in PSA.
N/A	Periodic test fails, no effect on plant operation.
N/A	Redundant systems can be put to test mode simultaneously. More analysis would be needed to recognize the failure mode(s) and potential end effect(s) for PSA.

For most of the 57 real-world issues, it was possible to assign a failure mode based on a common taxonomy (OECD/NEA/CSNI 2015). For some issues, it was difficult to assign a specific failure mode, or see any direct relevance to PSA. Based on some issues, we suggested new software failure modes: (1) indecisive / conflicting output state, (2) fluctuating output state, or (3) incorrect control parameter (Helminen & Pakonen 2020). Table 2 lists examples of issues where the classification or the relevance to PSA was non-trivial.

In general, if some design inconsistency is found using model checking, the issue can be fixed (if the cost of redesign is justifiable). Once found and fixed, a fault might no longer be relevant in PSA. Still, information about the existence or non-existence of design faults increases the confidence on system reliability. Since software failures, in particular, are hard to predict, model checking can provide valuable support for software reliability estimation (Helminen & Pakonen 2020).

References

Alur, R. & Dill, D. L. 1994. A theory of timed automata. Theoretical Computer Science, vol. 126, no. 2, pp. 183–235.

Areva. 2012. U.S. EPR Protection System, Technical ReportANP-10309NP, Revision 4. [Online]. Available: https://www.nrc.gov/docs/ML1216/ML121660317.html.

Areva. 2013. U.S. EPR Final Safety Analysis Report. [Online]. Available: https://www.nrc.gov/reactors/new-reactors/design-cert/epr/reports.html.

Björkman, K. & Pakonen A. 2019. Coupling model checking and PSA: a case study. Proceedings of the 29th European Safety and Reliability Conference (ESREL 2019), Hannover, Germany, Sep 22-26, pp. 2789-2796.

Pakonen, A., Buzhinsky, I. & Vyatkin, V. 2018. Counterexample visualization and explanation for function block diagrams. Proceedings of 2018 IEEE 16th International Conference on Industrial Informatics (INDIN), Porto, Portugal, July 18-20, pp. 747-753.

Pakonen, A. & Buzhinsky, I. 2019. Verification of fault tolerant safety I&C systems using model checking. 20th IEEE International Conference on Industrial Technology (ICIT), February 13–15, 2019, Melbourne, Australia, pp. 969–974. IEEE.

Buzhinsky, I. & Pakonen, A. 2019. Model-checking detailed fault-tolerant nuclear power plant safety functions. IEEE Access, vol. 7, 2019, pp. 162139–162156.

Buzhinsky, I. & Pakonen, A. 2020a. Symmetry breaking in model checking of fault-tolerant nuclear instrumentation and control systems. IEEE Access, vol. 8, 2020, pp. 197684–197694.

Buzhinsky, I. & Pakonen, A. 2020b. Timed model checking of fault-tolerant nuclear I&C systems. 18th IEEE International Conference on Industrial Informatics (INDIN). July 20–23, 2020, Warwick, UK, pp. 159–164. IEEE.

Cavada, R., Cimatti, A., Dorigatti, M., Griggio, A., Mariotti, A., Micheli, A., Mover, S., Roveri, M. and Tonetta, S., 2014, July. The nuXmv symbolic model checker. In International Conference on Computer Aided Verification, pp. 334–342. Springer, Cham.

Cimatti, A., Clarke, E., Giunchiglia, E., Giunchiglia, F., Pistore, M., Roveri, M., ... & Tacchella, A. 2002. NuSMV 2: An OpenSource tool for symbolic model checking. In International Conference on Computer Aided Verification, pp. 359–364. Springer, Berlin, Heidelberg.

Esnoul, C., Gran, B. A., Simensen, J. E., Olsen, S. A., Sarshar, S., Karpati, P. & Gao, X. 2020. Workshops proceedings: the state-of-the-art to assure a digital safety system. HWR-1288. OECD Halden Reactor Project. Institutt For Energiteknikk (IFE). Halden, Norway. 30 p. + app. 69 p.

Hauge, A. A., Linnosmaa, J., Fredriksen, R. & Sechi, F. 2019. Safety and security in DI&C design – systematic literature study. HWR-1247. OECD Halden Reactor Project. Institutt For Energiteknikk (IFE). Halden, Norway. 40 p.

Helminen, A. & Pakonen, A. 2020. Potential applications of model checking in probabilistic risk assessments. VTT Research Report VTT-R-00017-20, VTT Technical Research Centre of Finland. 13 p.

IAEA 2015. Technical Challenges in the Application and Licensing of Digital Instrumentation and Control Systems in Nuclear Power Plants. IAEA Nuclear Energy Series, No. NP-T.13.

IAEA 2018. Approaches for Overall Instrumentation and Control Architectures of Nuclear Power Plants. IAEA Nuclear Energy Series, No. NP-T-2.11.

Linnosmaa, J., Pakonen, A., Papakonstantinou, N. & Karpati, P. 2020. Applicability of AADL in modelling the overall I&C architecture of a nuclear power plant. Proceedings of the 46th annual conference of the IEEE Industrial Electronics Society (IECON 2020), Singapore, October 18-21, pp. 4337-4344.

OECD/NEA/CSNI 2015. Failure modes taxonomy for reliability assessment of digital I&C systems for PRA, OECD/NEA Working Group RISK report NEA/CSNI/R(2014)16.

Pakonen, A., Biswas, P. & Papakonstantinou, N. 2020. Transformation of non-standard nuclear I&C logic drawings to formal verification models. Proceedings of the 46th annual conference of the IEEE Industrial Electronics Society (IECON 2020), Singapore, October 18-21, pp. 697-704.

Pakonen, A., Buzhinsky, I. & Björkman, K. 2021. Model checking reveals design issues leading to spurious actuation of nuclear instrumentation and control systems. Reliability Engineering & System Safety 205, 107237.

Pakonen, A., Mätäsniemi, T., Lahtinen, J. and Karhela, T., 2013. A toolset for model checking of PLC software. In 2013 IEEE 18th Conference on Emerging Technologies & Factory Automation (ETFA), pp. 1–6. IEEE.

Papakonstantinou, N., Tommila, T., O'Halloran, B., Alanen, J. & Van Bossuyt, D.L. 2017. A model driven approach for early assessment of defence in depth capabilities of complex sosiotechnical systems. Proceedings of ASME 2020 International Design Engineering Technical Conference & Computers and Information in Engineering Conference (IDECT/CIE 2020), Saint Louis, MO, USA, August 16-19. 10 p.

Papakonstantinou, N., Linnosmaa, J., Bashir, A. Z., Malm, T. & Van Bossuyt, D. L. 2019. Early combined safety – security defence in depth assessment of complex systems. Proceedings of the 66th Reliability and Maintainability Symposium (IEEE RAMS 2020), Palm Springs, CA, USA. January 27-30. 7 p.

Sechi, F., Hauge, A. A., Sirola, M., Olsen, S. A., Linnosmaa, J. & Sarshar, S. 2020. Early stage safety assessment using a system model as input. HWR-1287. OECD Halden Reactor Project. Institutt For Energiteknikk (IFE). Halden, Norway. 36 p. + app. 53 p.

Tommila, T. & Alanen, J. 2015. Conceptual model for safety requirements specification and management in nuclear power plants. Espoo: VTT. VTT Technology 238. 120 p. + app. 26 p.

3.5 Uncertainty management in fire risk analyses (URAN)

Jukka Vaari[1], Alexandra Tissari[1], Nikhil Verma[1], Simo Hostikka[2]; Morteza Gholami Haghighi Fard[2]

[1]VTT Technical Research Centre of Finland Ltd
P.O. Box 1000, FI-02044 Espoo

[2]Aalto University
P.O. Box 11000, FI-00076 AALTO

Abstract

A pyrolysis modelling approach was expanded to full-scale simulation of a cable tray fire. Earlier experimental thermogravimetric analysis (TGA) and cone calorimeter results were used to construct the pyrolysis model. For model validation, data form the CFSS-1 experiment of the OECD/NEA PRISME 2 project was used.

A state-of-the-art methodology for the simulation of the cable cone calorimetry with FDS wass proposed in this study. Cable geometry was modelled with cubic obstructions using the new 3D heat transfer (HT3D) and 3D pyrolysis (PYRO3D) routines of the FDS.

Effects of ageing on the thermal decomposition process of polyethylene using united-atom MD simulations were studied. Qualitatively, ageing had a very little effect on the shape and position of the simulated TGA curves, suggesting essentially no effect of ageing on pyrolysis of polyethylene.

Introduction

Electrical equipment is one of the most probable cause of fire in nuclear power plants (NPP): almost half of the fire events in NPPs reported in the OECD FIRE Database have been caused by electrical equipment (OECD 2015). Although cables have been reported to act as the fire initiator only in approximately 5 percent of the reported fires, a fire initiating at a different source may spread to cables as well. As there is typically hundreds of kilometres of electrical cables in NPPs (OECD 2018), they pose a significant fire load.

CFD-based fire simulations are routinely used for fire PRA and FHA analyses in nuclear power plants. The uncertainty of these simulations arises from three sources: model uncertainty, input uncertainty, and the user effect. Input uncertainty refers to the uncertainty of boundary and initial conditions in a real fire scenario, and it particularly concerns the problem of simulating fire spread. The modeller already faces a considerable challenge in trying to find a suitable pyrolysis reaction mechanism, and associated kinetic parameters, for fresh materials. An additional component to the uncertainty comes through ageing, which may affect both the physical and chemical composition of the materials.

URAN-project covers three main themes: modelling tool development and validation, uncertainty quantification of fire models and molecular dynamics investigation of aging effects. The first two themes will involve active participation to OECD PRISME 3 -project and utilization of the results. The third theme links the project to the other proposed SAFIR 2022 projects and applied and fundamental research projects outside the program.

Pyrolysis based fire spread model for cable trays

Cables present a major potential fire source in nuclear power plants despite the use of flame retardant materials. OECD/NEA PRISME programs have previously studied the effect of different cable materials, cable arrangements and ventilation systems on the fire propagation, providing new information on the fire behaviour of cables.

Most of the full-scale CFD cable tray simulations have used prescribed descriptions of the fire or semi-empirical or empirical flame spread models to predict the fire heat release rate. However, pyrolysis models have been successfully used to simulate cables in small- and bench-scale experiments. Matala and Hostikka (2011) developed pyrolysis models for two polyvinyl chloride (PVC) cables using small-scale and bench-scale experimental data. Simulation results were validated against experimental results with good agreement.

In this work, the pyrolysis modelling approach was expanded to full-scale simulation of a cable tray fire. The experimental thermogravimetric analysis (TGA) and cone calorimeter results reported by Mangs and Hostikka (2013) were used to construct the pyrolysis model. The simplified cable is assumed to consist of four different materials in seven different layers. The structure of the simplified cable is symmetric with respect to the centreline of the material. It is assumed that the layers from external side to the centre are sheath, filler, insulation and copper. A schematic visualization of the simplified cable structure is shown in Figure 1. Thicknesses of the material layers are in proportion to each other in the figure. In the cone calorimeter simulation, thicknesses of the layers are assumed to be 1.8 mm for insulation material in total, 5.8 mm for the sheath material in total, 2.4 mm for the filler material in total and 0.8 mm for the copper.

Reaction paths were formed for polymeric cable components using the principles presented by Matala and Hostikka (2011). It was assumed that each of the materials initially consist of single component each. The components in the virgin material are referred to as Sheath component 1, Insulation component 1 and Filler component 1. The yields of reactions and the names of residue components are shown in Table 1. All reactions happen in parallel and in a single step.

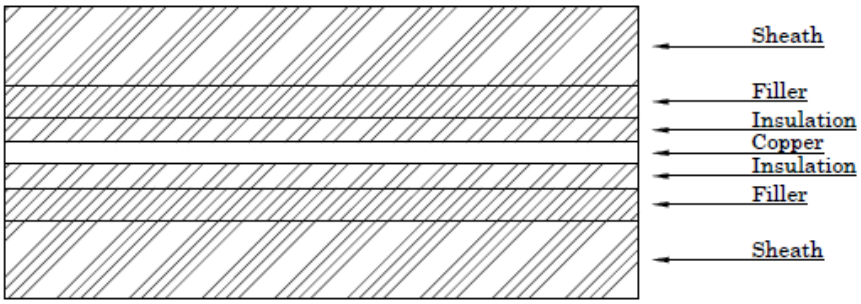

Figure 1. Schematic visualization of the simplified cable structure. Thicknesses of the material layers are in proportion to each other.

Table 1. Yields of reactions and residue components.

Component	Fuel (%)	Inert gas (%)	Residue (%) (residue component)
Sheath component 1	25	29	46 (Sheath component 2)
Sheath component 2	23	3	74 (Sheath component 3)
Sheath component 3	-	29	71 (Char)
Insulation component 1	19	26	55 (Insulation component 2)
Insulation component 2	16	2	82 (Insulation component 3)
Insulation component 3	-	26	74 (Char)
Filler component 1	12	12	76 (Filler component 2)
Filler component 2	4	1	95 (Filler component 3)
Filler component 3	-	3	97 (Filler component 4)
Filler component 4	3	34	63 (Char)

Table 2. Kinetic parameters of the polymeric cable components.

Component	A (1/s)	E (J/mol)	N (-)
Sheath component 1	$7.0 \cdot 10^{32}$	$3.8 \cdot 10^{5}$	2.4
Sheath component 2	$2.0 \cdot 10^{31}$	$4.6 \cdot 10^{5}$	2.2
Sheath component 3	$1.2 \cdot 10^{31}$	$6.0 \cdot 10^{5}$	2.0
Insulation component 1	$3.9 \cdot 10^{21}$	$2.5 \cdot 10^{5}$	1.1
Insulation component 2	$1.8 \cdot 10^{37}$	$5.6 \cdot 10^{5}$	4.8
Insulation component 3	$4.0 \cdot 10^{24}$	$5.0 \cdot 10^{5}$	2.9
Filler component 1	$2.2 \cdot 10^{27}$	$3.1 \cdot 10^{5}$	3.0
Filler component 2	$4.2 \cdot 10^{39}$	$5.7 \cdot 10^{5}$	3.6
Filler component 3	$7.1 \cdot 10^{22}$	$4.5 \cdot 10^{5}$	3.0
Filler component 4	$1.2 \cdot 10^{42}$	$2.6 \cdot 10^{5}$	3.3

Kinetic parameters are required to simulate the material decomposition. A typical approach to find kinetic parameters is to compare simulated TGA to experimental TGA, and attempt to find parameters that result in the smallest possible difference between the simulations and experiments. TGA was simulated with FDS, version 6.7.1, using the method proposed in the FDS User Guide (McGrattan et al. 2019).

An open source optimization tool PyroPython (Sikanen 2019) was used for parameter optimization. The kinetic parameters are given in Table 2. Heats of combustion and heats of reaction for polymeric cable components and thermal parameters for char were estimated using a cone calorimeter simulation and data from cone calorimeter experiments. In the cone calorimeter experiments an external flux of 50 kW/m^2 was used.

The simulated cable tray fire was the CFSS-1 experiment from the OECD/NEA PRISME 2 project (Zavaleta et al 2018). The geometry used for the simulations is visualized in Figure 2. The cable trays are located in the middle of the computational domain. The computational domain has height of 10 meters, width of 6 meters and depth of 2.4 meters. The domain boundaries are positioned far enough from the fire source ensuring that the boundaries do not disturb either the flow or the combustion process. The numerical mesh consisted of regular hexahedral cells. The edge length of these cells was 5 cm in the vicinity of the fire and 10 cm elsewhere.

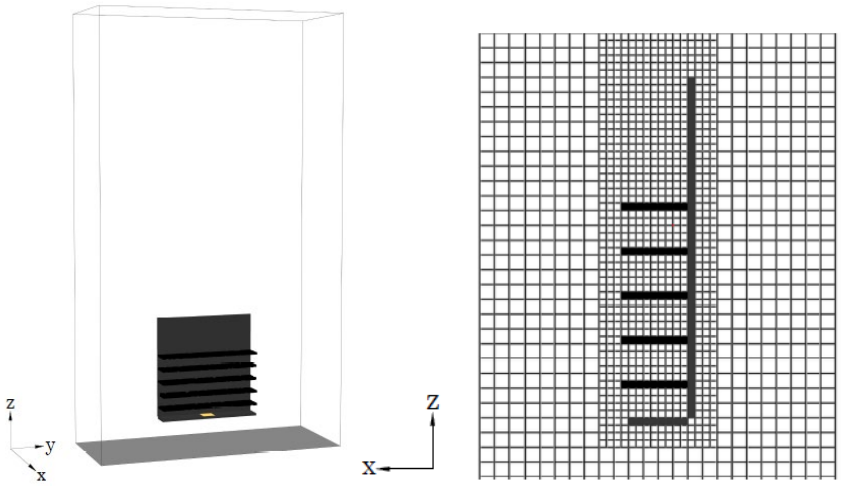

(a) (b)

Figure 2. (a) The simulation domain. (b) Detail from the numerical grid. The refinement around the trays continues to the top boundary of the domain.

The FDS software requires that geometries conform to the rectilinear numerical grid. This limits the accuracy of geometrical descriptions of objects with complex shape. Cable trays are often represented as single solid geometries, which causes issues in simulating fire spread as the passage of hot gases through the trays is blocked. Here, a stochastic approach for making the simplified cable tray geometry containing openings is introduced. First, based on the tray volume and the amount cables in the tray, a computational estimate is made for how many openings are required in the CFD cable tray geometry. A distribution of openings, conforming to the

numerical grid, is then automatically generated by repeating the procedure several times. Finally, selected opening configurations are used for fire spread simulations.

Five simulations were conducted using the same opening fraction but different tray geometries (opening distributions). The experimental and simulated heat release rates are shown in Figure 3, and the flame spread in Figure 4. It can be observed that the fire growth phase before 120 seconds is quite well captured in all of the simulations. The maximum heat release rate is overpredicted by 11 to 17 %, with the average overprediction of 14 %. The predicted heat release rate peaks occur 30 to 70 seconds before the experimental peak. The decay phase between 300 and 500 seconds is very similar between the simulations and the experiment. The predicted fires extinguish after approximately 600 seconds, whereas the experimental fire was maintained until more than 1200 seconds had passed.

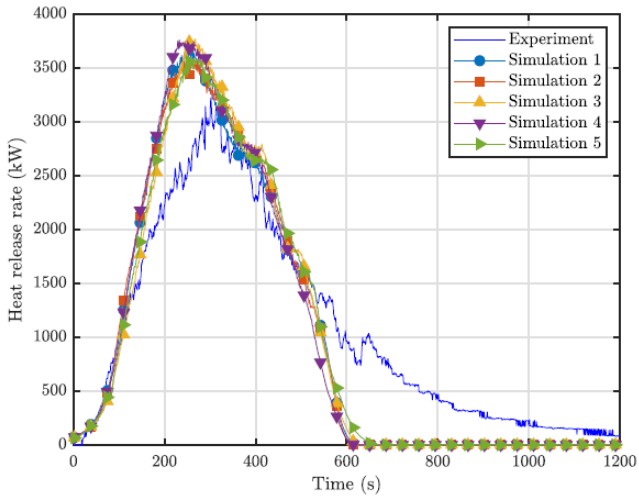

Figure 3. Experimental and simulated heat release rate.

Fire propagated faster in the full-scale simulations than in the corresponding experiments. In comparison, the heat release rate and mass consumption were predicted more accurately in the cone calorimeter simulation. It is considered possible that approximating the cables as a continuum is more suitable for modelling fire propagation in tight arrangements and leads to too high propagation rate in loose arrangements. Another aspect which could partially explain this difference is that in full-scale simulation the exposed cable area was parametrically increased, whereas in the bench-scale simulation it was not. Based on the sensitivity study, changing the area adjustment parameter has a significant effect on the results. Furthermore, the pyrolysis model used in this work is based on a very limited set of experimental data, which could limit its predictive capability.

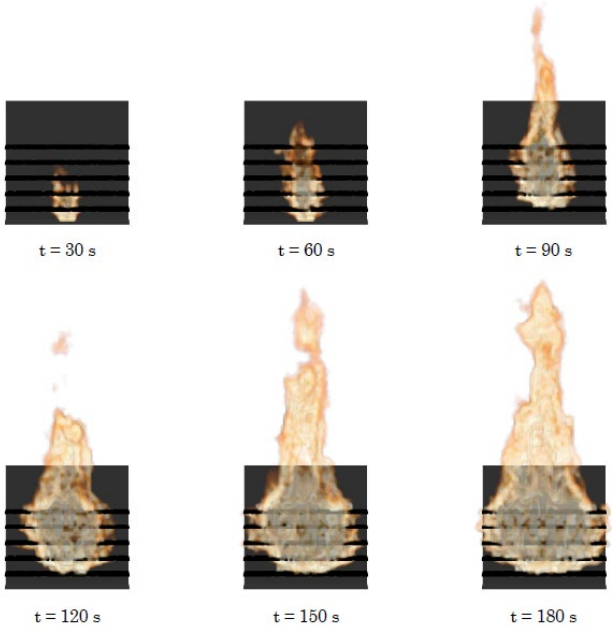

Figure 4. Flame spread every 30 seconds until 180 seconds in simulation 1.

Next generation of cable fire models

The heat conduction and pyrolysis model of the FDS software was developed to a 3D formulation by Bruns et al. (2018). This model has the potential to work better for simulation of thermal degrading materials, while integrating perfectly with the parallel computing capabilities of the FDS. This new method retains reasonable accuracy, in terms of mass conservation and surface temperature, when a complete solid material is introduced in the solution domain. Since 3D heat conduction formulation translates into being closer to the physical phenomena, simulation of pyrolyzing material via this method may be more logical compared to the one-dimensional pyrolysis assumptions.

FDS uses a cubic grid for its simulations, whereas the electrical cables are cylindrical. The geometrical concept behind this study is to investigate whether we are able to model a cable geometry with various cubic obstructions using the new 3D heat transfer (HT3D) and 3D pyrolysis (PYRO3D) routines of the FDS. Figure 5 shows the fundamental proposition for modeling the geometry of a single electrical cable. Numerous little cubic solid materials can be put adjacent to each other in order to represent the geometry of a cylindrical cable.

A state-of-the-art methodology for the simulation of the cable cone calorimetry with FDS is proposed in this study. Following the conventional hierarchy of cone calorimetry modeling, the Thermo-Gravimetrical Analysis (TGA) experiments of individual cable components are modeled with a one-dimensional pyrolysis and heat

transfer method for each layer of the cable. This one-dimensional TGA modeling choice owes to the fact that micro-scale tests of the components are usually performed for a specimen which has greater face area compared to the thickness of the sample, enforcing the degradation process mainly through the direction of the sample thickness. The geometry of the actual cable is constructed using a multitude of solid cuboids bundled together to form a substitution for the cylindrical shape of the cable. Attempts have been made to create the most similar layout to the actual cross-section of the cable, in an effort for addressing the geometrical deficiencies of the conventional models. Subsequently, a model that represents the three-dimensional pyrolysis and heat transfer within the cable degrading in a cone calorimetry setup is established.

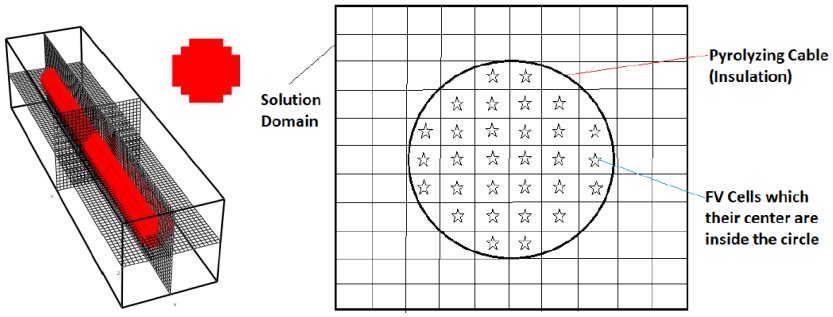

Figure 5. Geometry model for 3D pyrolysis of electrical cable.

Three different setups for modeling the cone calorimetry experiments are investigated (Figure 6). In the first setup, referred as Cone Model 1 from here onward, the solution domain consists of two particular volumes. The lower volume (20x3x20 mm^3) where the cable (longest width 18mm) exists is the location where mainly pyrolysis reactions occur. The upper volume (40x3x26 mm^3) is representative of the free space under the hood of the cone calorimetry, where pyrolysis gases burn. In the cable structure, black, grey, dark blue, and gold colors represent the obstructions of the sheath, filler, insulation, and metallic conductors, respectively.

This model decision was made to account for the symmetrical effects of the neighboring cables which were not included in the geometry of the model. Two boundaries shown by the teal color are having no heat transfer to prevent them from contributing to radiation. Two radiation panels are modeled horizontally right on top of the cable. The temperature of these panels are set such that the topmost point of the cable surface is exposed to a 50kW=m_2 radiative heat flux. Open boundaries shown in Figure 6 act as either make-up air providers or the hood exhausts. y_{min} and y_{max} surfaces of the domain possess mirror boundary conditions to account for the (approximately) symmetry of the physics over the length of the cable.

Two other cone calorimetry setups are also investigated in this study, referred as Cone Model 2 and 3. For Cone Model 2, the response of the material (in terms of

degradation speed) to altering the position of the radiation panels is examined. In Cone Model 3, the effects of rotating the cable by 90 degrees are analyzed.

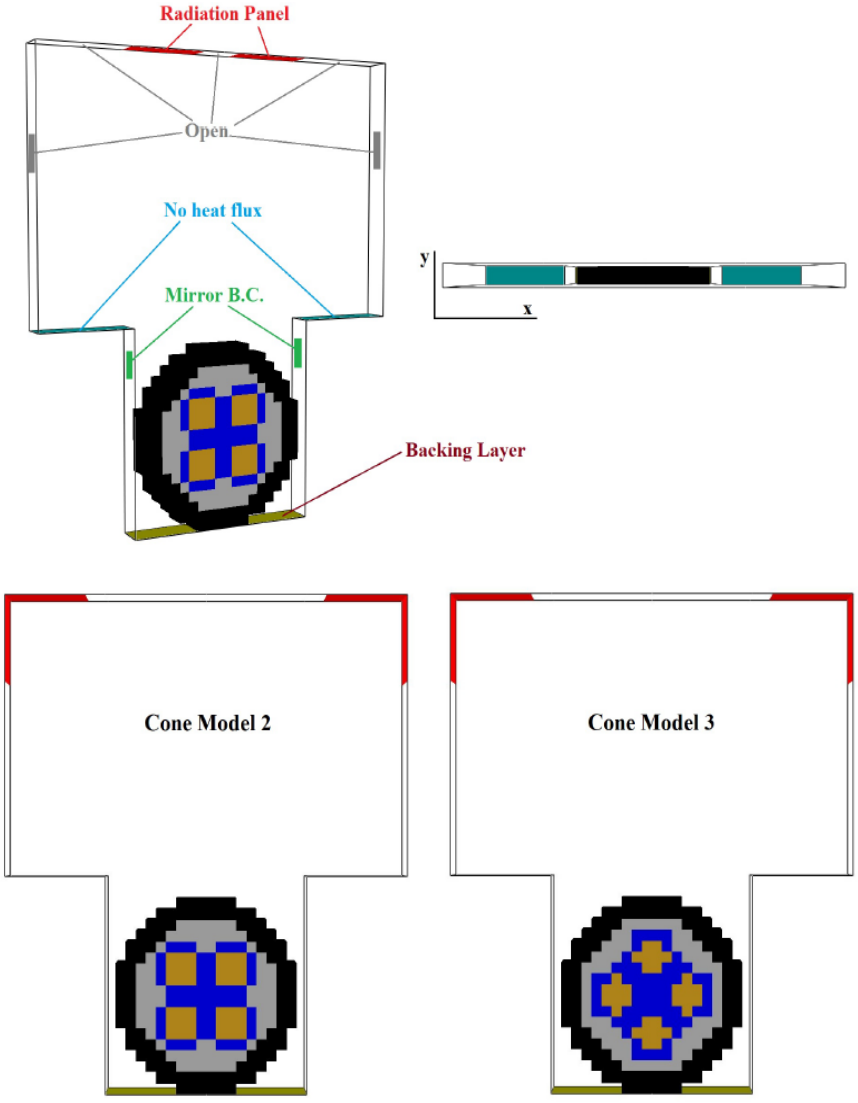

Figure 6. Geometry and boundary conditions of the cone calorimeter models.

Figure 7 compares the mass loss rate per unit are results of three Cone Models against the experimental results. Two major peaks can be observed in the MLRPUA curve of the experimental data; one at the first few seconds of the tests (referred as the First Peak), and another at about t = 650s (referred as the Second Peak). The

last experimental data point is at time t = 1348s. Nonetheless, simulations were continued to t = 3000 s. The Cone Model 1 was able to roughly capture the trend of the experimental data up until 1348s, however, not all of the cable materials were consumed by that time. Another severe degradation begins at about 1650 seconds of the simulation time (referred as the Third Peak). Figure 7 also compares the total heat release rate per unit area results of the Cone Models. The results are not impeccably following the trend of the experimental curve, in particular for the Third-Peak. Adjustment of the HRR curve requires further optimization of the components heats of combustion.

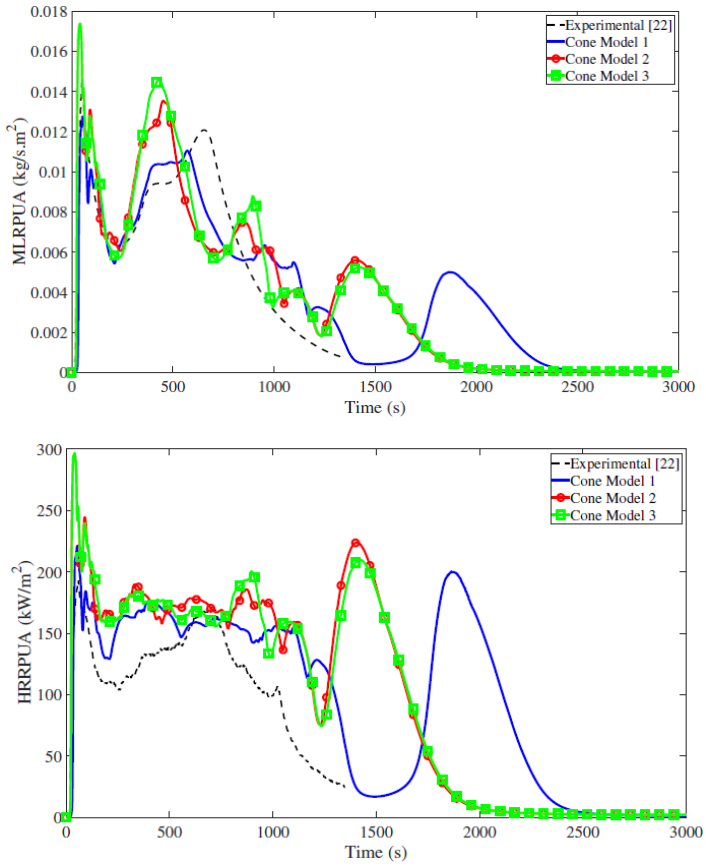

Figure 7. Comparison of the total mass loss rate (top) and heat release rate (bottom) per unit area for the three cone models.

Manually optimized thermal parameters were able to approximately capture the trend of the experimental mass loss rate curve until the time when the cone calorimetry test was finished. However, a significant amount of unconsumed materials was observed in the model at that simulation time. This may be due to two reasons.

Firstly, the cable materials may not degrade in the cone calorimeter by following their pyrolysis path in TGA. This means that plausibly more char material would have been produced in the presence of air in the cone calorimeter, which needs further investigation on reaction kinetics. Secondly, the estimated thermal parameters in the cone model may not have been optimized sufficiently. The set of thermal parameters were not able to reproduce the heat release rate curve properly.

The effect of the change of the radiation panel position was found significant in accelerating the cable degradation. The model is substantially sensitive to the portion of the cable surface which is receiving the radiation heat flux. In contrast, the change of the orientation of the cable did not vary the results notably.

Thermal decomposition of aged materials

Existing experimental research reveals conflicting evidence on the effect of ageing on the burning properties of polymers. VTT reports VTT-R-02816-14 (SAFIR2014 project LARGO) and VTT-R-04401-15 (SAFIR2018 project FIRED) concluded that aging would not significantly change the fire risk related to cable materials. However, the radiative aging experiments reported in VTT-R-05490-16 (FIRED) found some changes in the cone calorimeter results, particularly decreased time to ignition, increased peak heat release rate (HRR), and increased effective heat of combustion. This work concluded that the topic should be studied further. The extensive literature review by Vahabi et al. (2015) concluded that due to the wide range of ageing conditions, polymers, and flame retardants, ageing can lead to a decrease, no change, or even an increase in flame retardancy. In addition, the review found that irradiation generally increases the peak HRR in cone calorimeter experiments, but no definitive explanation could be given.

In FIRED, we started the ground-breaking research of using Reactive Molecular Dynamics (RMD) to predict the kinetic parameters needed for flame spread. The idea in reactive molecular dynamics is to simulate chemical reactions within a classical MD framework, but using an interaction potential between atoms that has been formulated and trained such that chemical connectivity changes between atoms are possible. The ReaxFF potential (van Duin et al. 2001), used in FIRED, is a sophisticated and versatile potential for RMD. While computationally significantly cheaper than quantum mechanical calculations, it is still much more expensive than traditional classical MD potentials where connectivity remains fixed.

Recently, we have performed MD modelling of crystallisation, cross-linking, and bond-scission of polyethylene using an approach, where each CH_2 repeat unit is described as one particle. While this united-atom approach has been known for some time, we have modified the approach to include chemical reactivity.

In this work, we have performed united-atom MD simulations of thermal decomposition of fresh and aged polyethylene in order to look for effects of ageing on the thermal decomposition process. The focus is entirely on the polymer matrix, so that additives, anaerobic ageing, radiation, and humidity are not considered. The simulations were performed using the MD software LAMMPS (Plimpton 1995). Chemical

bonding and van der Waals interactions between particles were described by the TraPPE-UA force field (Martin and Siepmann 1999). Additives (antioxidants, plasticizers, fire retardants, colorants, fillers, etc) are not considered. The main chemical modifications for the base polymeric materials due to ageing involve chain scissions and cross-linking reactions. The hypothesis for this study is that the modifications to the molecular weight distribution by these reactions inherently lead to changes in the burning properties.

The MD model was built to include the main mechanisms of the free-radical pyrolysis scheme for polyethylene, which are random scission, unzipping, and back-biting (Poutsma 2003). To validate the model, we employed experimental data from the study by De Witt and Broadbelt (2000). They studied isothermal decomposition of polyethylene at 420 ºC, measuring the yields of decomposition products (all gaseous products plus solid-state decomposition products up to a carbon number of 34) at conversions 0.05, 0.21, and 0.34. The MD simulation of the data involved a a polydisperse system with a weight-averaged mean chain length of 9000 repeat units and a dispersity of 1.79. It was prepared by first generating a random-walk MD model for a single chain of 90000 repeat units long, followed by random scission of 17 bonds. The dispersity deviates from a value of 2 because of the statistically small number of scissions.

Figure 8 presents the comparison of experimental and simulated data as the logarithm of the molar product yield vs the carbon number. Experimental data for carbon numbers 6 and 7 is missing due to experimental reasons. Data for the lowest conversion at high carbon numbers suffers from poor resolution. However, linearity of the plot for conversions 0.21 and 0.34 shows that for carbon numbers 8 to 30, the random scission mechanism is in effect. Clear deviation from linearity is seen in the data for carbon numbers 1-6, indicating that unzipping and back-biting effects are important, and they significantly increase the yields of these light species compared to pure random scission mechanism.

Regarding the random scission process, the simulated results for high carbon numbers show a linear trend on a logarithmic scale, but for each conversion the slope of the simulated data is smaller compared to experiments. Two explanations could be proposed. First, a general feature of the logarithmic plot is that the slope of the plot increases as a function of conversion. Therefore, it is possible that there is an unintended mismatch between the experimental and simulated conversions due to uncertainty in estimating the conversion. Second, the radical transfer processes may affect bond scission probabilities tens of bonds from the chain end, and taking all of these processes into account in modeling (Levine and Broadbelt 2009) can quite accurately reproduce the experimental data, suggesting that the slope is sensitive to the details of the reaction mechanism.

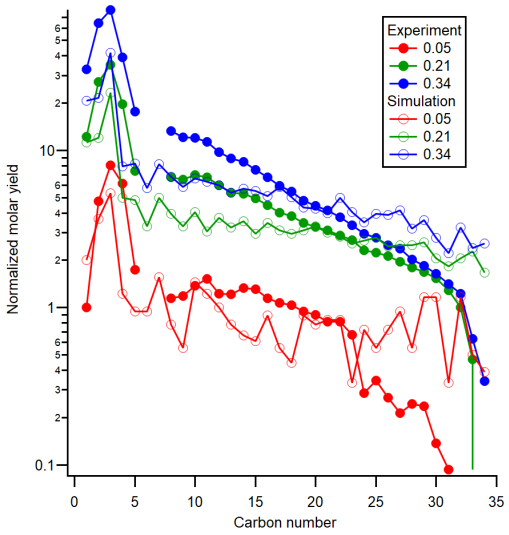

Figure 8. Experimental and simulated product yields for three conversions.

We then used the united-atom MD model for simulating TGA curves for fresh and aged PE and XLPE systems listed in Table 3. The results are presented in Figure 9 for a heating rate of 3 K/ps. The general conclusion from the results is that neither the degree of aging, nor the degree of cross-linking have any significant effect on the results. There is a slight tendency of the TGA curves to move towards lower temperatures as a function of ageing, which might be an indication of better burning, but the effect is very small. It follows therefore that ageing is not expected to have a notable effect on the burning properties of an aged base polymer. It should be stressed, however, that this result only concerns the base polymer, and not the possible additives.

Table 3. PE and XLPE systems used in this work for studying the effect of ageing.

Linear PE			XLPE, gel fraction 0.71			XLPE, gel fraction 0.85		
Broken bonds		M_n	Broken bonds		M_n	Broken bonds		X_g
num-ber	%		num-ber	%		num-ber	%	
182	0.06	637	355	0.12	679	367	0.12	0.60
365	0.12	459	566	0.19	459	566	0.19	0.30
570	0.19	349	1065	0.36	261	1054	0.35	0.06
765	0.26	285	1784	0.59	161			
1079	0.36	219	2258	0.75	129			

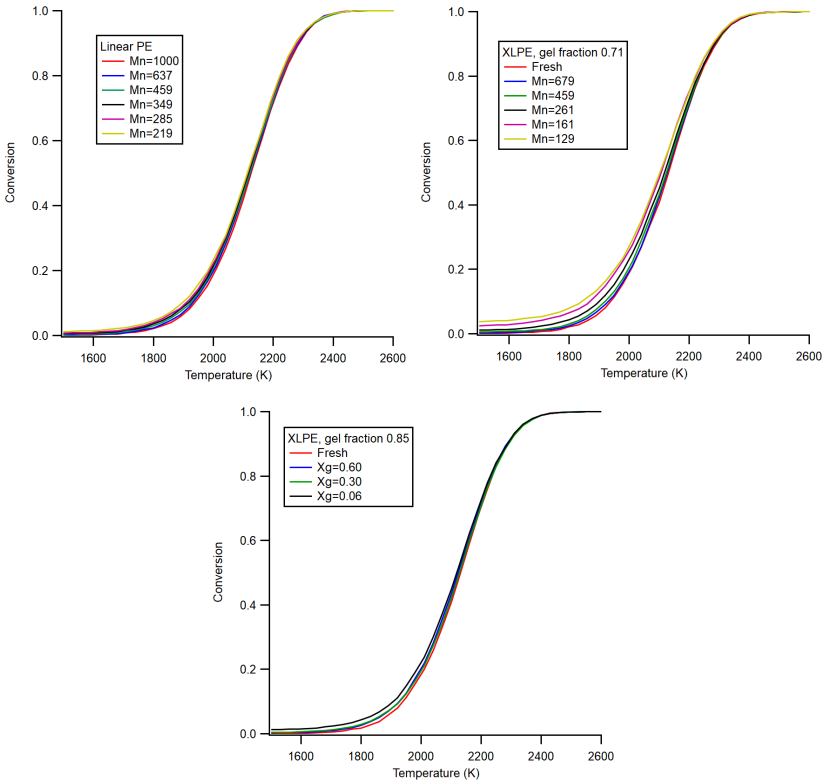

Figure 9. Simulated TGA curves for aged PE and XLPE systems (for explanation of the legends, see Table 1) at 3 K/ps heating rate.

We also performed an isoconversional analysis for selected fresh and aged systems in order to quantitatively check the effect of ageing on the pyrolysis kinetics. Specifically, the systems were the fresh linear PE and the aged PE with Mn=219, and fresh XLPE with a gel fraction of 0.71, and aged XLPE with Mn=129. Figure 10 presents the conversion-dependent activation energies for these cases. The results indicate a slight increase (about 2 kcal/mol) of the activation energy due to ageing. Again, the effect of ageing is next to non-existent, but if real, it would suggest that ageing makes the pyrolysis process more difficult, suggesting reduced burning. This result runs contrary to the conclusion drawn from Figure 9, and currently it is not clear how these two results should be understood together. More work would be required to resolve the controversy, possibly using systems that are much more radically (and perhaps unphysically) aged so that the effects on the shape of the TGA curves and on the activation energies would become more pronounced. Nevertheless, for the moment the main conclusion from Figures 9 and 10 remains that the effect of ageing on the pyrolysis behaviour of PE and XLPE is minimal.

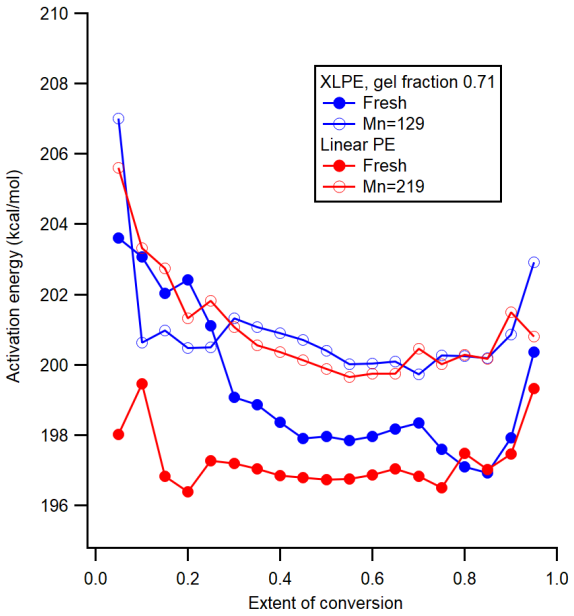

Figure 10. Conversion-dependent activation energies for selected fresh and aged systems.

References

Bruns, M., McDermott, R., Benkorichi, S., & Hostikka, S. 2018. Development of 3D pyrolysis in FDS. Spring Technical Meeting of the Eastern States Section of the Combustion Institute, State College, USA.

De Witt, M.J. & Broadbelt, L.J. 2000. Binary Interactions between High-Density Polyethylene and 4-(1-Naphthylmethyl)bibenzyl during Low-Pressure Pyrolysis. Energy & Fuels vol. 14 pp. 448-458.

Levine, S.E. & Broadbelt, L.J. 2009. Detailed mechanistic modeling of high-density polyethylene pyrolysis: Low molecular weight product evolution. Polymer Degradation and Stability vol. 94 pp. 810-822.

Mangs J. & Hostikka, S. 2013. Experimental characterization of the MCMK cable for fire safety assessment. VTT Research Report VTT-R-06873-12.

Matala A. & Hostikka, S. 2011. Pyrolysis modelling of pvc cable materials. In: Fire Safety Science, International association for firre safety science, pp 917-930, DOI 10.3801/IAFSS.FSS.10-917.

Martin, M.G. & Siepmann, J.I. 1999. Novel configurational-bias Monte Carlo method for branched molecules. Transferable potentials for phase equilibria. 2. United-atom description of branched alkanes. The Journal of Physical Chemistry B vol. 103 pp. 4508-4517.

McGrattan, K., Hostikka, S., Floyd, J., McDermott, R. & Vanella, M. 2019. Fire Dynamics Simulator Technical Reference Guide Volume 1: Mathematical Model - NIST Special Publication 1018-1 Sixth Edition. Tech. rep., Office of Nuclear Regulatory Research.

OECD. 2015. Collection and Analysis of Fire Events (2010-2013) - Extensions in the Database and Applications. Fire Project Report. Committee on the Safety of Nuclear Installations (CSNI), NEA/CSNI/R(2015)14. URL https://www.oecd-nea.org/nsd/docs/2015/csni-r2015-14.pdf

OECD. 2018. Investigating Heat and Smoke Propagation Mechanisms in Multi-Compartment Fire Scenarios. Final Report of the PRISME Project, Committee on the Safety of Nuclear Installations (CSNI), NEA/CSNI/R(2017)14. URL https://www.oecd-nea.org/nsd/docs/2017/csni-r2017-14.pdf

Plimpton, S. 1995. Fast parallel algorithms for short-range molecular dynamics. Journal of Computational Physics vol. 117 pp. 1–19.

Poutsma, M.L. 2003. Reexamination of the Pyrolysis of Polyethylene: Data Needs, Free-Radical Mechanistic Considerations, and Thermochecmical Kinetic Simulation of Initial Product-Forming Pathways. Macromolecules vol. 36 pp. 8931-8957.

Sikanen, T. 2019. PyroPython (version 0.01) [Computer software]. URL https://github.com/PyroId/PyroPython

Vahabi, H., Sonnier, R. & Ferry, L. 2015. Effects of ageing on the fire behaviour of flame-retarded polymers: a review. Polymer International vol. 64 pp. 313-328.

van Duin, A.C.T, Dasgupta, S., Lorant. F & Goddard III, W.A. 2001. ReaxFF: a reactive force field for hydrocarbons. Journal of Physical Chemistry A vol. 105 pp. 9396-9409.

Zavaleta P. & Audouin, L. 2018. Cable tray fire tests in a confined and mechanically ventilated facility. Fire and Materials 42(1):28-43, DOI 10.1002/fam.2454

4. Reactor and Fuel

4.1 Coupled analysis of transient scenarios (CATS)

Ville Sahlberg, Anitta Hämäläinen, Hanna Räty, Veikko Taivassalo, Rebekka Komu

VTT Technical Research Centre of Finland Ltd
P.O. Box 1000, FI-02044 Espoo

Abstract

System code TRACE and reactor analysis code PARCS were adopted into use, including transient analyses with coupled TRACE-PARCS and participation of two young experts in a PARCS training course. Master's thesis on sensitivity and uncertainty analysis of transient calculations was completed in 2019. In 2020, these developments were combined by adapting the VTT's uncertainty and sensitivity analysis tool Sensla for use with the newly adopted TRACE-PARCS.

A PWR core with a blocked fuel assembly was analysed with porous-CFD simulations. Due to the blockage, coolant exceeded its saturation point in a small part of the core. Thus, handling conditions where steam bubbles form is necessary for modelling blocked assemblies and an important future research topic.

Introduction

The objective of the project is to develop the modelling of transient events and accidents so that we can give more reliable answers to the safety requirements set in the YVL guides. To achieve this, CATS utilizes computational transient analysis tools that have been in use for decades, adopts new independent analysis tools into use as well as participates in the complete renewal of the VTT's reactor analysis system as a part of the ongoing effort to develop the Kraken computational platform. An important part of the project is generating and maintaining expertise for transient analysis calculations.

The focus in CATS is to further improve the analysis of transient scenarios using coupled thermal-hydraulics and reactor core modelling. The researched areas include both the computational tools as well as uncertainty and sensitivity analyses of the modelling. In addition, CATS includes exploratory research topics such as porous computational fluid dynamics (CFD) modelling of transient scenarios. These aid in developing both the modelling tools and the modelling expertise of future.

Plant modelling with neutronics coupling

The transient behaviour of reactor cores have been traditionally modelled at VTT by the in-house reactor dynamics codes TRAB3D [1] and HEXTRAN [2]. These are coupled to the system code SMABRE [3] to form a toolset for deterministic analysis of transient scenarios. However, there is an ongoing work at VTT to develop a new simulation framework Kraken [4] for reactor analysis. This includes developing and adopting a new generation of simulation tools for Kraken. As a part of this development process, it was decided that Kraken needs an independent system code for transient analyses. This is especially important for providing an alternative for the use of Apros [5] or the system code SMABRE, where an independent alternative is needed. It was decided that the system code TRACE [6] is very suitable for this role. It is an independent tool which can be used for modelling LOCA cases as well as other transients and accidents. A significant goal of CATS is the comprehensive adoption of the system code TRACE into use producing expertise in use of TRACE.

The adoption of TRACE was hastened in 2019 as a TRACE model for VVER-1000 was received from Karslruhe Institute of Technology. However, the model had several shortcomings and the initial work with TRACE was on modifying the model. Standalone TRACE was used for uncertainty and sensitivity analysis work. In 2020, two young experts participated in NRSHOT-PARCS nuclear reactor simulator hands-on training online course. The course topics included training on the reactor analysis core PARCS [7] and on coupling TRACE and PARCS.

After this, coupled TRACE-PARCS was used for transient analysis of a coolant pump transient from Kalinin-3 benchmark [8]. The pressure boundary conditions of the VVER-1000 model were replaced with a control system for primary pressure and pressurizer water level. The substitution of the previous core model for a new PARCS model was straightforward and the nodalization between TRACE and PARCS is shown in Figure 1.

Figure 1. The mapping between the TRACE and PARCS models. TRACE nodes are mapped with different colors and the numbering corresponds to assembly numbering in PARCS.

However, one noticed downside of TRACE-PARCS is that it can only handle a single control rod material at a time while the benchmark provided material specifications for two control rod materials. The transient was simulated with all control rods consisting of the first control rod material, boron carbide. Then the calculations were repeated with boron carbine replaced by dy-ti materials. The effect of this limitation on control rod materials is presented in Figure 2.

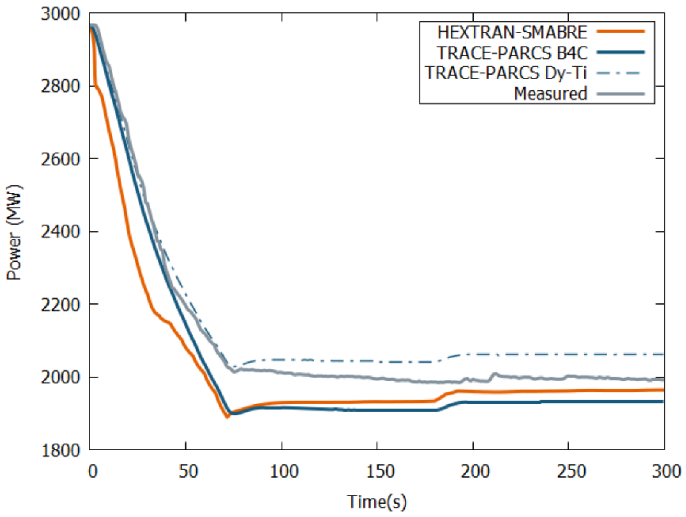

Figure 2. Total power from HEXTRAN-SMABRE and TRACE-PARCS calculations for the coolant pump transient of Kalinin-3 benchmark, compared to measurements.

Most importantly, during the TRACE-PARCS simulation work, several issues and bugs were found from standalone PARCS and coupled TRACE-PARCS. Majority of these concerned hexagonal VVER-type geometries and resolving them would be important for accurate modelling of VVERs. These errors were reported to the developers of TRACE and PARCS and fixes to these issues will be delivered to all users of TRACE and PARCS in future code versions. Given that the goal of the TRACE-PARCS work in CATS is long-term adoption of TRACE as a comprehensive and effective tool, identifying significant issues with TRACE-PARCS and obtaining fixes for them is a resounding success.

Steam line nodalization

As a part of mapping potential future research topics, the effect of nodalization on boiling water reactor (BWR) steam line modelling was analysed [9]. Transient analysis calculations of BWR overpressurization transient were calculated with TRAB3D as a stand-alone calculation as well as with TRAB3D coupled with system code SMABRE. The calculations were compared to past measurements of the transient.

New nodalization models were tested and analysed to see if a more dense nodalization would improve SMABRE's modelling of pressure waves in the BWR steam line.

It was observed that SMABRE doesn't reproduce the measured pressure waves. This holds with both sparse and dense nodalization. The built-in BWR steam line model in stand-alone TRAB3D did not reproduce the measured pressure waves either. For full conclusiveness, the same calculations should be repeated with the process simulation and system code Apros in the future. This would confirm information on the applicability of the current system codes for modelling long BWR steam lines. The results of the simulation runs with different nodalizations are presented in Figure 3.

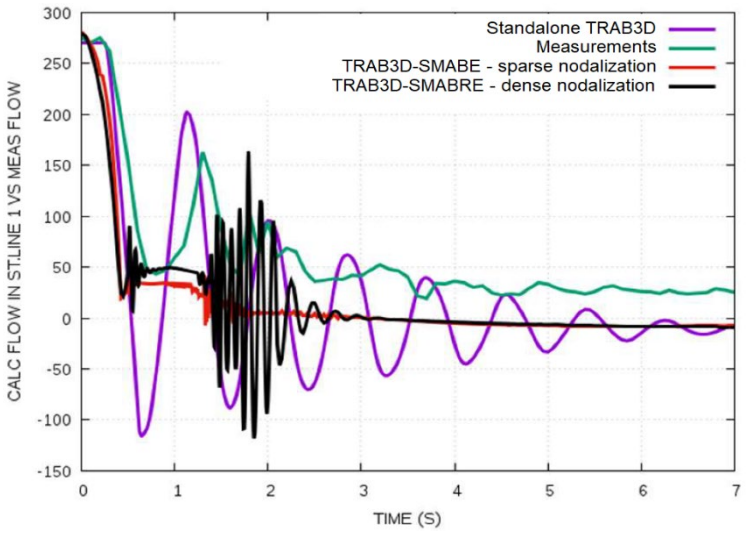

Figure 3. Simulation results of the BWR overpressurization transient and the measured data. A plot of flow in the steam line 1 during the transient.

Uncertainty and sensitivity analysis

For comprehensive deterministic analyses, an additional layer of sensitivity and uncertainty analysis is needed on top of reactor dynamics simulation capabilities. Uncertainty and sensitivity analysis is an irreplaceable part of best estimate modelling and simulation. By analysing different uncertainties, the most impactful variables and parameters of deterministic analyses can be found. This ensures more reliable answers to the safety requirement questions.

Rebekka Komu completed her Master's Thesis [10] on uncertainty and sensitivity analysis of nuclear reactor core and thermal-hydraulic system models in 2019. The thesis examined a coolant pump transient from Kalinin-3 VVER benchmark. Analyses were performed for a separate code model with HEXTRAN, for a thermal-

hydraulics model with TRACE (Figure 4) and for a coupled core and system model with HEXTRAN-SMABRE (Figure 5). VTT's own uncertainty and sensitivity analysis tool Sensla was used for simulations with HEXTRAN-SMABRE and DAKOTA tool was used for stand-alone TRACE simulations.

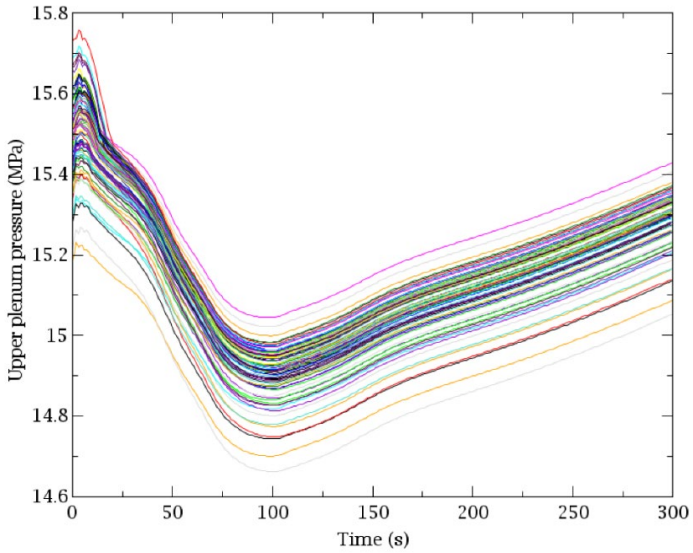

Figure 4. Upper plenum pressure in the TRACE sensitivity runs.

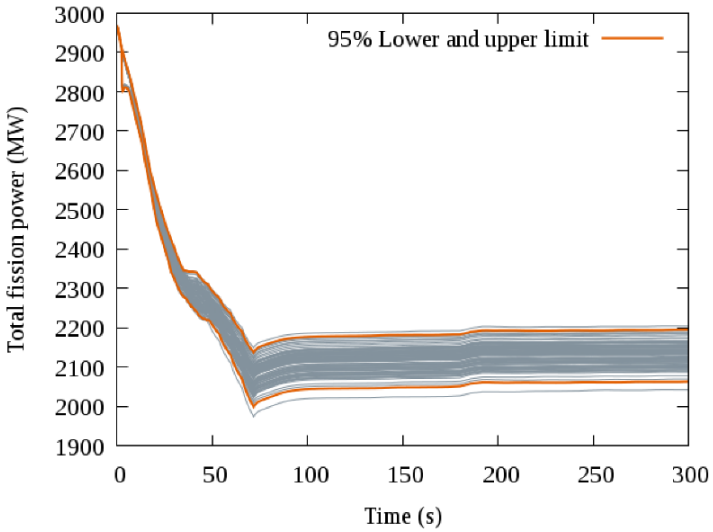

Figure 5. Total fission power with 95% intervals for HEXTRAN-SMABRE runs with their parameter set varied according to the first examined variation scenario.

In 2020, these developments in uncertainty and sensitivity analysis were combined with the efforts in adopting TRACE-PARCS. The previously used sensitivity analysis tool for TRACE was not capable of comprehensive uncertainty and sensitivity analysis for the coupled TRACE-PARCS code system. Thus, Sensla was expanded for use with TRACE-PARCS and the first sensitivity analyses using TRACE-PARCS with Sensla were performed [11]. This was a continuation and replication of the earlier work using HEXTRAN-SMABRE. In addition, a partial rank correlation coefficient calculation routine external to Sensla was developed and taken into use (Figures 6 and 7). This increased the extent of uncertainty and sensitivity analyses that can be performed with both TRACE-PARCS and HEXTRAN-SMABRE.

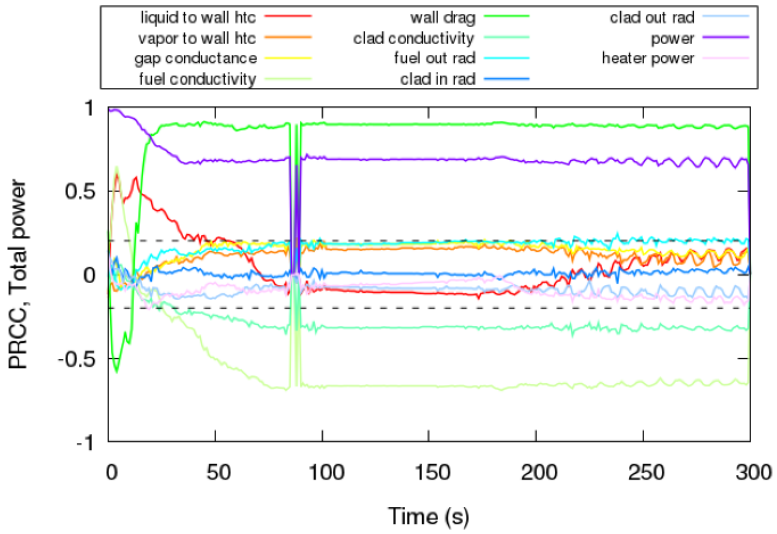

Figure 6. Partial rank correlation coefficients between the reactor power and various simulation parameters in the coolant pump transient from Kalinin-3 benchmark. Results from TRACE-PARCS calculations.

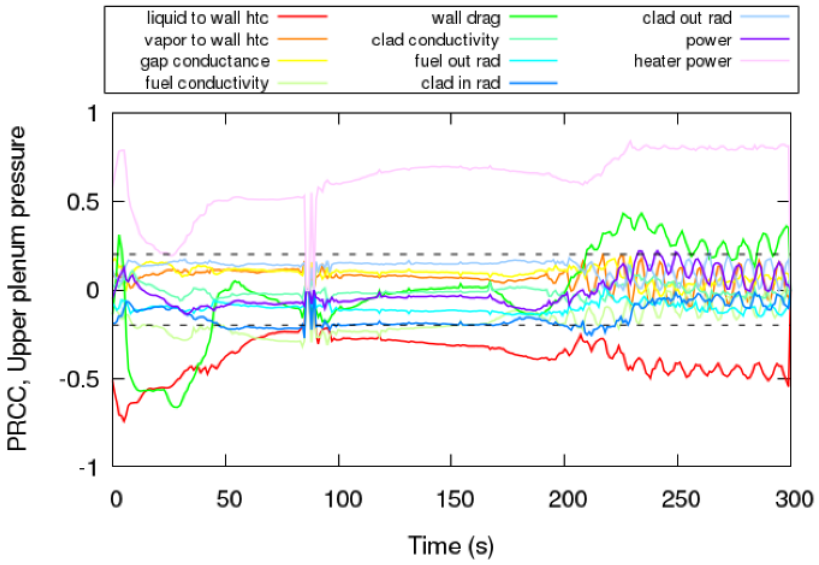

Figure 7. Partial rank correlation coefficients between upper plenum pressure and various simulation parameters in the coolant pump transient from Kalinin-3 benchmark. Results from TRACE-PARCS calculations.

Thermal margin calculation methodology

Literature review and expert analysis of state of the art approaches to thermal margin calculation was performed in 2019 [12]. In total, approaches from more than ten different organizations with significant experience in reactor analysis were examined (Table 1). A distinct need to develop a comprehensive approach for calculating thermal margins for the simulation framework Kraken was identified. The trend in published material was away from traditional hot channel methodology and towards more detailed modelling. The VTT's FINIX code [13] was identified as a very suitable fuel performance module for such multi-physics applications. However, given that more accurate thermal margin calculations require a higher fidelity calculation, there is a need for higher resolution solution from neutronics and thermal hydraulics as well. Given the computationally very intensive natures of higher fidelity thermal hydraulic solvers, the conclusion of the analysis was that currently computational resources limit the direct applicability of pin-by-pin and subchannel level modelling. Approaches with flexible geometry structure are advised, with high modelling resolution only near points of interest.

Table 1. List of organizations and codes examined for thermal margin calculation methodology.

Organization	Codes
AREVA/FRAMATOME	ARCADIA
CASI (US DOE)	VERA-CS, MPACT+CTF
GRS	QUABOX/CUBBOX-ATHLET
HZDR	DYN3D
IRSN, CEA	HEMERA
KI	BIPR-8A -ATHLET
KIT	DYN3D, PARCS, TRACE, RELAP5, SUBCHANFLOW
OKB Gidropress	KORSAR/GP
PSI	S3K/PARCS, TRACE, COBRA-TF
Studsvik scandpower	SIMULATE-3K, TRACE, VIPRE, ENIGMA
VTT	TRAB3D, HEXTRAN, TRAB

Porous CFD modelling and core clogging

Exploratory research in CATS aims to highlight shortcomings of current modelling tools and to examine the limitations of high fidelity approaches for transient calculations. For 2019-2020, the examined case for porous CFD modelling has been a blockage in a fuel assembly in an European Pressurised Water Reactor (EPR) core. The EPR primary loop is modelled with the system code SMABRE, the neutronics of the reactor core with the reactor dynamics code TRAB3D and the thermal hydraulics of the reactor pressure vessel and the reactor core with the porous CFD software PORFLO [14][15]. This division is presented in Figure 8 and a closeup of the PORFLO mesh in Figure 9.

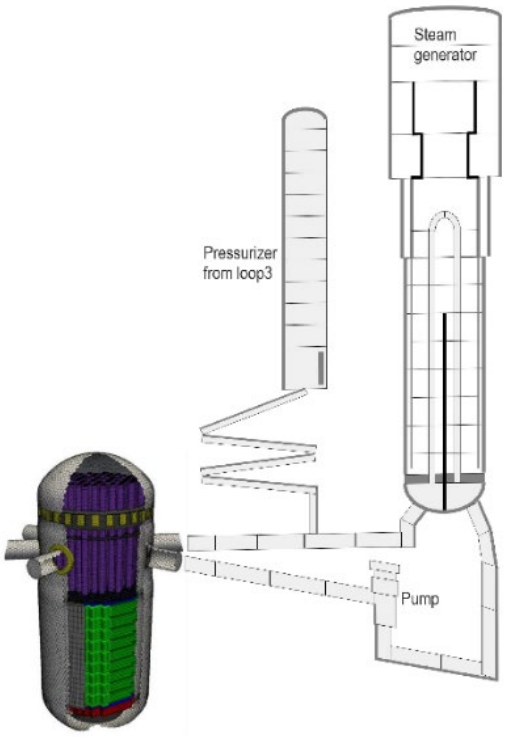

Figure 8. Nodalization of a single EPR primary loop for SMABRE and schematic representation of the couplings between SMABRE and PORFLO models.

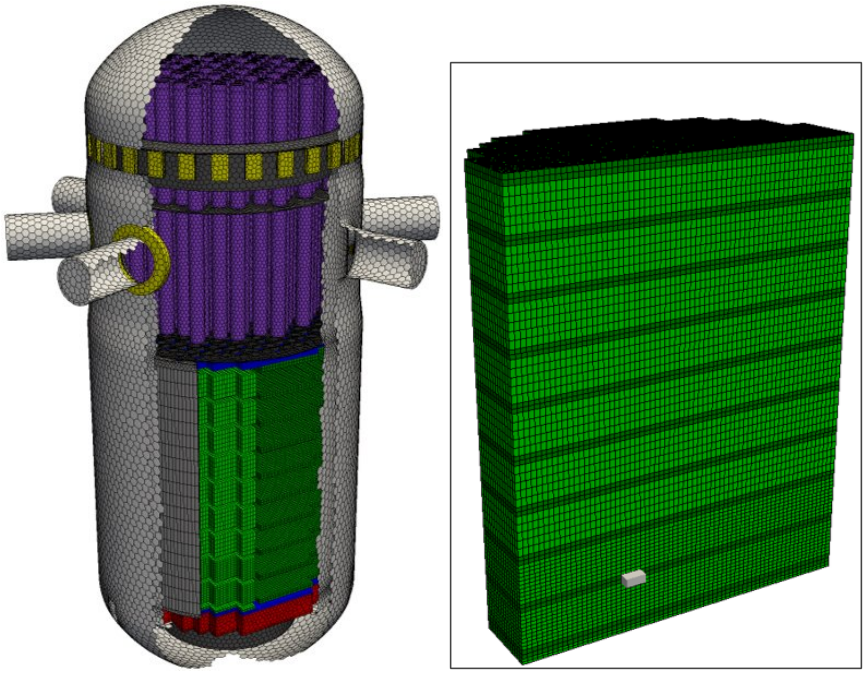

Figure 9. A closeup of the computational mesh for the porous CFD calculation. The clogged spacer grid is visible as a gray slate in the cross-sectional view of the reactor core.

The blockage has the cross-sectional area of a single assembly and represents a clogged spacer grid. The blockage locally restricts the flow of coolant. The blockage is partially porous, but has a hiher resistance to flow than the surrounding area. Compared to a corresponding case with no blockage, coolant temperature rises more at the location of the blockage, as expected. Above the blockage, the coolant flow rate returns close to the unblocked case flow rate (Figure 10). Together with mixing, this reduces the influence of the blockage higher up in the core and in the upper plenum. However, the coolant temperature still rises above its saturation point in a small area of the core (Figure 11). It is worth noting that these results should not be considered representative of any specific EPR. The computational model was based on publicly available material for different EPRs planned to be built in different countries.

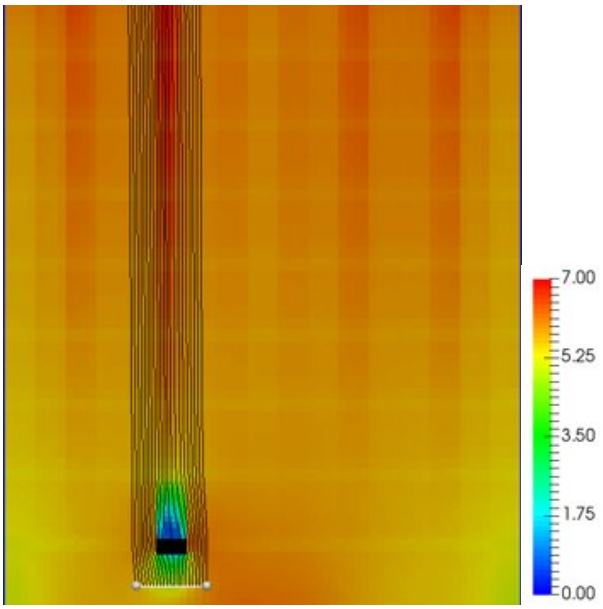

Figure 10. Velocity (m/s) and streamlines of the coolant flow around the blockage.

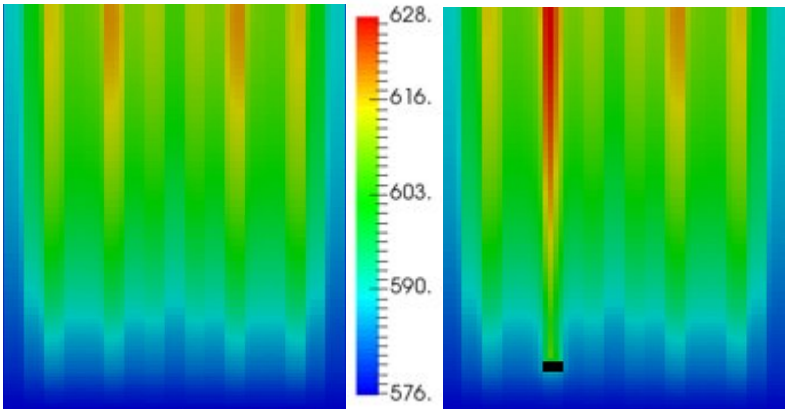

Figure 11. The temperature of the coolant (K) in normal operation (left) and with a blockage (right). The temperature of the coolant rises past the saturation point after the blockage.

International co-operation

Cooperation and information exchange on VVER safety within the AER framework together with other countries which use VVER reactors is an important part of the international co-operation and networking in the CATS project. In 2019, the AER

working group D meeting was organized as a joint meeting with the OECD/NEA Rostov-2 Benchmark meeting in Munich, Germany. Ville Sahlberg attented both of these meetings and the location for the next AER working group D meeting was agreed to be Finland [16]. The importance of the Finnish AER members to the AER community was recognized as no other agreeable location aside Finland was found for the next meeting. Unfortunately, in 2020 the global covid-19 pandemic led to the cancellation of the meeting. Hanna Räty participated in a remote meeting of the AER Scientific Council annual meeting in 24.11.2020.

Participation in the meetings of the NEA Working Party on the Scientific Issues of Reactor Systems (WPRS), is also within the scope of CATS. WPRS is responsible for the organization of the reactor dtynamics benchmarks among other activities. Participation in NEA working groups and benchmarks is important for validating methods used in transient analysis. Elina Syrjälahti attended the OECD/NEA WPRS & Expert Groups meetings in February 2019 in Paris, France [17].

The adoption of the system code TRACE and the reactor analysis code PARCS have created a new avenue of international cooperation for the CATS project. Multiple issues and bugs were found from both standalone PARCS as well as from TRACE-PARCS during project work. These issues were reported to the developers of TRACE and PARCS and have consistently resulted in fixes and updates for these computational tools. This co-operation of CATS and the developers of TRACE and PARCS benefits all Finnish actors who wish to use them as independent analysis tools as well as the whole international TRACE-PARCS user community.

Summary and conclusions

The CATS project produced a considerable amount of non-tangible results in 2019-2020 through training of new experts in the use of TRACE and the adoption of TRACE-PARCS as a proper reactor analysis tool. The impact of identifying and reporting several significant issues with VVER modelling with TRACE-PARCS remains to be seen. Historically, hexagonal geometries and VVER models have been among the less used features of TRACE-PARCS. However, if modelling of VVER-type power plants with TRACE increases in the future, then the global impact of identifying these issues early and thoroughly can be significant.

CATS is and remains at the forefront of examining new ways to model transient scenarios. While porous CFD simulation of a blocked assembly as a part of a PWR is at the limits of modern modelling capability, that is also the limit where new qualitative insights can be found.

Acknowledgements

We thank the development teams of the system code TRACE and the reactor analysis code PARCS for their cooperation with the CATS project.

References

[1] Kaloinen, E and Kyrki-Rajamäki, R. “TRAB-3D, a new code for three-dimensional reactor dynamics," in CD-ROM Proceedings of ICONE-5, 5th International Conference on Nuclear Engineering. Nuclear Advances through Global Cooperation, Nice, France, May 26-30 1997.

[2] Kyrki-Rajamäki, R. “Three-dimensional reactor dynamics code for VVER type nuclear reactors," Technical Research Centre of Finland, DrTech Thesis. VTT Publications 246, 1995.

[3] Miettinen J. and Hämäläinen A, “Development and Validation of the Fast Running Thermohydraulic Model SMABRE for Simulator Purposes," ICONE-8: Eight International Conference on Nuclear Engineering. Baltimore, USA, 2-6 April, 2000 [CD-ROM]. New York: American Society of Mechanical Engineers. Paper ICONE8-8188, 12 p. ISBN 0791819922.,2000.

[4] Valtavirta V., Hovi V., Loukusa H., Rintala A., Sahlberg V., Tuominen R., Leppänen J., ”Kraken – An upcoming Finnish reactor analysis framework”. International Conference on Mathematics and Computational Methods Applied to Nuclear Science and Engineering, M and C 2019. United States, 25th-29th August 2019. Pages 786-795.

[5] Webpages of Apros Process Simulation Software. http://www.apros.fi/en/

[6] Office of Nuclear Regulatory Research, 2009. TRACE V5.0 Theory Manual. Field Equations, Solution Methods, and Physical Models. USNRC, Washington, DC.

[7] Webpages of Purdue Advanced Reactor Core Simulator (PARCS) https://engineering.purdue.edu/PARCS.

[8] Tereshonok, V. et al. Kalinin-3 coolant transient benchmark – switching-off of one of the four operating main circulation pumps at nominal reactor power specification- First Edition 2008.

[9] Hämäläinen, A., “BWR overpressurization transient and SMABRE steam line dynamics”, VTT Technical Research Centre of Finland, Research report VTT-R-01296-19.

[10] Komu, R., “Uncertainty and Sensitivity analysis for Nuclear Reactor Core and Thermal-Hydraulic System Models”. Master’s Thesis, University of Oulu, 2019.

[11] Komu, R., “Implementing the uncertainty and sensitivity analysis tool Sensla for TRACE-PARCS”, VTT Technical Research Centre of Finland, Research report VTT-R-00048-21.

[12] Räty, H., “On the methodology of calculating thermal margins”, VTT Technical Research Centre of Finland, Research report VTT-R-00197-20.

[13] Ikonen, T., Loukusa, H., Syrjälahti, E., Valtavirta, V., Leppänen, J., & Tulkki, V. Module for thermomechanical modeling of LWR fuel in multiphysics simulations. Annals of Nuclear Energy, 111–121, 2014.

[14] Ilvonen M., Hovi V. and Taivassalo V., 3D Core thermal hydraulics with the PORFLO code – turbulence modelling and porous medium with porosity steps, in proceedings of 22nd International Conference on Nuclear Engineering ICONE-22, Prague, Czech Republic, July 7-11, 2014.

[15] Taivassalo, V., “Feasibility study on the applicability of TRAB3D-PROFLO-SMABRE in analyses of core clogging in a PWR”, VTT Technical Research Centre of Finland, Research report VTT-R-00195-20.

[16] Sahlberg, V., Travel report, AER working group D meeting and OECD/NEA Rostov-2 Benchmark meeting, 24.-27.6.2019, Munich, Germany.

[17] Syrjälahti, E., Travel report, OECD/NEA WPRS & Expert groups meeting, 19.-22.2.2019, Paris, France.

4.2 Interdisciplinary fuels and materials (INFLAME)

Janne Heikinheimo, Henri Loukusa†, Asko Arkoma, Jussi Peltonen, Caitlin Huotilainen, Konsta Sipilä, Rami Pohja, Sami Penttilä, Teemu Kärkelä

VTT Technical Research Centre of Finland Ltd
P.O. Box 1000, FI-02044 Espoo

†currently working elsewhere

Abstract

The INFLAME project focuses on nuclear fuel behaviour during its irradiation in a nuclear reactor, including steady-state, transient and design basis accident conditions. The behaviour of nuclear fuel is studied both by means of modelling and experiments. In the first part of the project, the modelling items of fuel behavior in reactivity-initiated accident (RIA) conditions has included CABRI international program pre-test simulations, and an RIA sensitivity analysis with Sobol' variance decomposition method. Code development work has continued with the in-house fuel performance module FINIX.

In the experimental work packages of the project, both cladding and pellet experimental studies have been performed. On the part of cladding, cladding creep testing, autoclave testing and steam furnace testing capabilities have been developed and some of the material characterization and performance tests for conventional and accident tolerant cladding concepts done. On the part of the pellet, experimental capabilities at the VTT Centre for Nuclear Safety have been developed, and iodine release experiments performed for CsI doped CeO_2 pellets.

One DSc thesis was finalized in 2020 based on the fuel thermochemical behavior analyses made in this and the preceding SAFIR fuel projects, and one Master's thesis work is ongoing.

Introduction

Nuclear fuel is the most central physical element of the nuclear reactor, as the energy used in power production is produced within the fuel. Nuclear fuel in light water reactors (LWR) currently in operation consists of ceramic uranium oxide fuel pellets within a metallic cladding tube. The cladding tube, and in some sense the fuel pellet, act as the first release barriers of radioactivity in accidental conditions. Nuclear fuel performance modeling is used to predict fuel behavior and thus ensure both efficient and safe operation of nuclear power plants, where one of the most important issues is to ensure the integrity of the cladding. For most accurate modeling of nuclear fuel, close connection between modeling and experiments must be maintained. The INFLAME project contains both experimental and modelling work packages, and the

objective is to have close contact between the experimental and theoretical research during the project for maximum impact.

In the INFLAME project, several current issues regarding fuel behavior under irradiation are investigated. These include integral fuel behavior modeling and participation to international research projects from which data for validation can be obtained, as well as experimental work on both fuel cladding and pellets.

Design basis accident analyses

In addition to normal operation of nuclear power plants, several other design basis scenarios must be taken into account in nuclear safety analysis. The YVL guides, i.e., the Regulatory Guides on Nuclear Safety of STUK (STUK, 2019) classify these as:

(i) anticipated operational occurrences,
(ii) postulated accidents, and
(iii) design extension conditions.

Of postulated accidents, the reactivity-initiated accident (RIA) and loss-of-coolant accident (LOCA) are the two main types of accidents considered in fuel performance analyses.

The LOCA analyses performed in 2019 were related to pre-calculations of a planned hotcell LOCA test of a VVER rodlet tested previously in Halden IFA-789.

In an RIA, the reactivity of the core or part of it is abruptly increased, inducing a sharp power pulse. The event may cause fuel rod failures and consequent release of radioactive material to the coolant. The shattered fuel pellet fragments give rise to steam generation. In the worst case, this initiates a pressure pulse which can damage the surrounding fuel assemblies and possibly the whole core. The extremely narrow time scale of the reactivity-initiated accident, in the order of tens of milliseconds, sets additional demands on fuel modelling codes. For detailed thermomechanical modelling of fuel rod during RIA, VTT applies the SCANAIR computer program, developed by the French research organization IRSN. Models in SCANAIR are specifically developed for modelling RIAs.

In the current YVL guides, RIA-relevant enthalpy limits for loss of fuel rod integrity and fuel melting are stated. These historical figures may not be applicable for the fuels currently operated in the reactors. Over the years, the fuel burnup has increased, making the cladding more brittle and susceptible to failure in RIA. In several countries, including USA and France, RIA criteria are currently being revised.

In the OECD/NEA CABRI International Project (CIP), the CABRI research reactor in France has been refurbished and equipped with a water loop for RIA testing. The experimental campaign was begun with the CIP-Q test in 2018, and is expected to continue during the course of this project. Information obtained from CIP will be used to improve knowledge on the behavior of current fuel materials in RIAs, taking into account the confidentiality limitations of the CIP data. The first CABRI International Project (CIP) Analytical Group Meeting was participated in 2020 and the

results reported during the annual VTT review of international fuel research projects held as a half-day seminar. VTT participated in the pre-calculations of CIP1-2B and CIP3-1R with SCANAIR, and the preceding steady-state operation histories were simulated with the VTT-ENIGMA code. CIP1-2B test will use a high burnup UO_2 fuel with M5 cladding to study especially the boiling crisis and fission gas contribution to the cladding loading. CIP3-1R test focuses on PCMI failure and fuel ejection.

During years 2010–2019, OECD/NEA/CSNI Working Group on Fuel Safety (WGFS) organized a series of RIA fuel codes benchmarks, Phases 1-3. As an in-kind item to fulfil the requirements of the SCANAIR license agreement, VTT participated in 2019 in a writing group which summarised the three phases into a single document.

SCANAIR in-kind work of 2020 consisted of calculation of 1st order (main effect), 2nd order and total effect sensitivity indices with the Sobol' variance decomposition method for a fresh fuel case from the OECD/NEA RIA fuel codes benchmark Phase 2 (OECD/NEA, 2017). The existing Python and Matlab scripts by Ikonen and Tulkki (2014) were extended for SCANAIR. In the analysed case, the interaction effects were found to be negligible (2nd order indices were close to zero). Figure 1 shows a comparison of 1st order and total effect sensitivity indices with the correlation coefficients for cladding axial elongation. Total of nine outputs were studied, and the sensitivity indices were calculated at the time of maximum value of each output quantity. The varied parameters are shown in x-axis on figure 1.

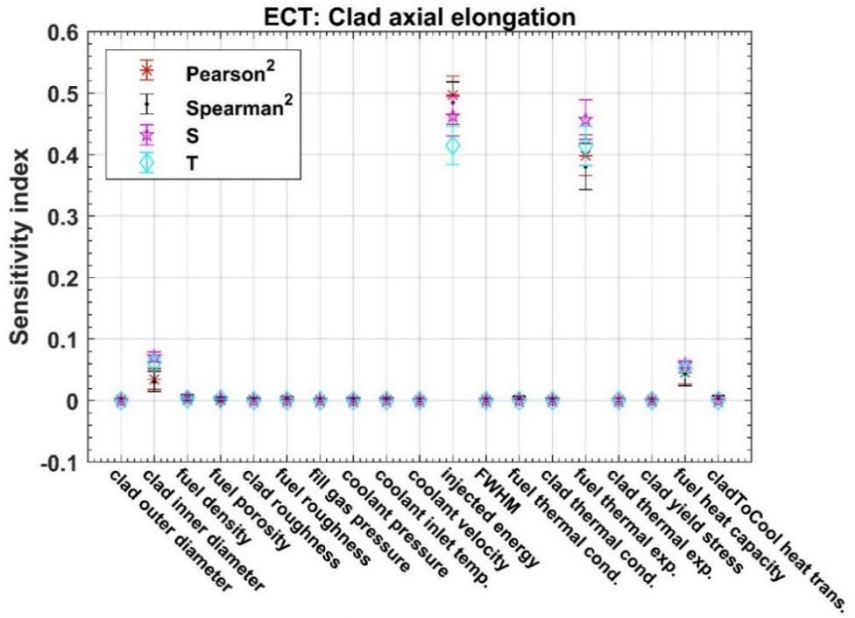

Figure 1. Comparison of 1st order and total effect sensitivity indices with correlation coefficients for cladding axial elongation. The first order Sobol' indices "S" are close to the total effect indices "T" indicating that the underlying model is additive.

FINIX development

From initial basic modelling of the temperature distribution in fuel, FINIX currently can model many mechanical phenomena in fuel cladding, such as elastoplasticity and creep, and many complex phenomena in the pellet, such as fission gas release, pellet densification and swelling. The approach of the development of FINIX is to be as simple, in modelling and in usage, so that the code may find applications in a wide range of other codes. This is in contrast to many other multiphysics codes that strive for information in utmost detail from all possible sources to perform mechanistic predictions (e.g. BISON), or others that are simple models intended to be implemented only within a certain code (Pizzocri et al., 2020).

In the years 2019-2020, the vast majority of effort put into FINIX has focused on enabling its performance in coupled applications. As such, two methods of FINIX restart were introduced with which the I/O of all of the FINIX data structures either via binary or ASCII files are possible, and as such the wrapper software SuperFINIX can run multiple FINIX simulations in steps at the same time while transferring files between FINIX simulations and the rest of the solvers in the Kraken calculation framework currently developed in the LONKERO project.

Improvements were done in error reporting and input checking functionality. Option to change rod internal gas contents within a simulation and the possibility to use cmake to compile the code were added. Other improvements consisted of implementations of new cladding material (FeCrAl), modified thermal property models for analysis of erbia-doped fuel pellets, modified cladding models for stress and strain, bug fixes, and computational optimizations. Figure 2 shows cladding inner surface temperature in CABRI REP-Na1 RIA test with FINIX, FRAPCON and FRAPTRAN with different variations in the base irradiation and transient modelling.

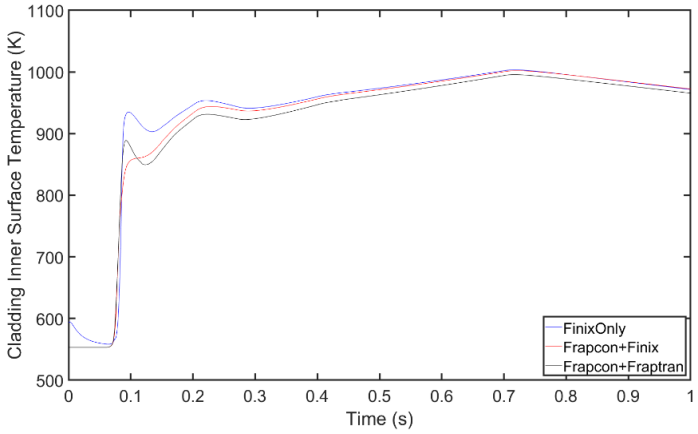

Figure 2. Cladding inner surface temperature in CABRI REP-Na1 RIA test with different code systems: base irradiation with FRAPCON and transient with FRAPTRAN as a reference, and base irradiation with FRAPCON or FINIX when transient is calculated with FINIX.

Modelling of Jules-Horowitz Reactor with Serpent

The research visit to CEA Cadarache was postponed due to the VTT travel ban caused by COVID. The original date of the secondment period was in the beginning of October. In January 2021 the project began in Finland, with the primary goalpost being the development of initial Serpent model for JHR. This model will be used for benchmarking purposes between Tripoli-4, MCNP and Serpent, after which the studies on the neutronic designs of JHR testing devices will be commenced. Among other topics, the optimization of OCCITANE experimental device will be performed with the Serpent model by calculating estimates for the spectrum ratio, fast neutron flux and gamma heating associated with the device. Figure 3 depicts the initial attempt at modelling JHR geometry with Serpent by utilizing the French GADGET-input script, whereas figure 4 depicts the relative capture cross section of JHR core with homogenized and simplified fuel rod assembly.

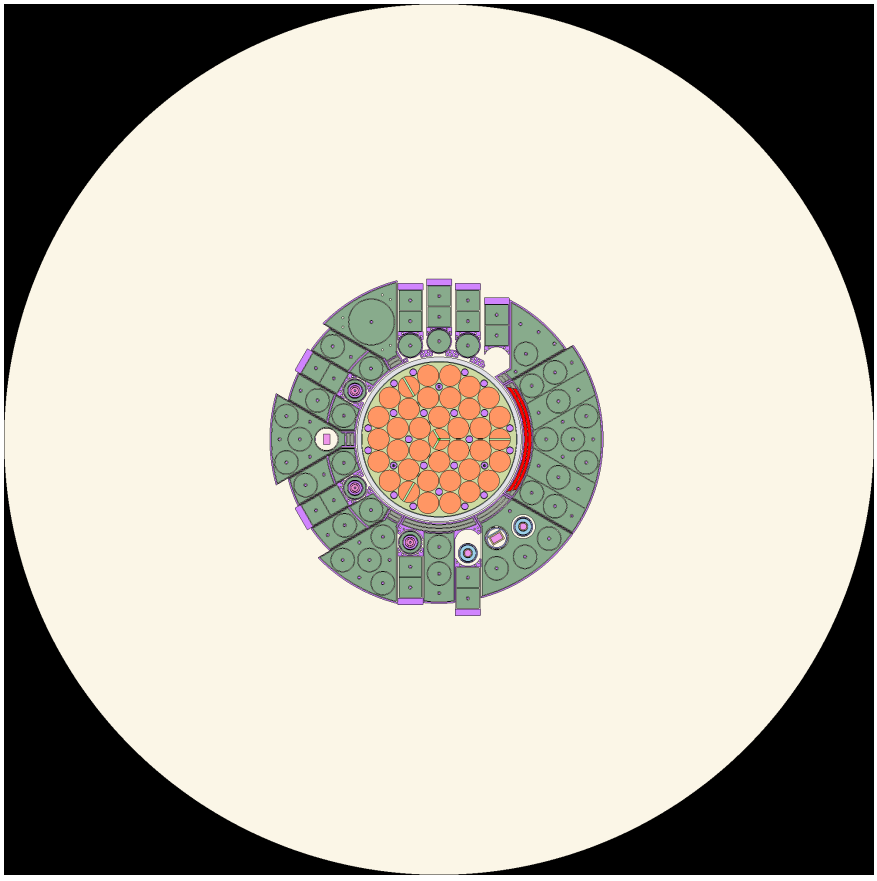

Figure 3. The initial attempt at modelling JHR geometry with Serpent by utilizing the French GADGET-input script.

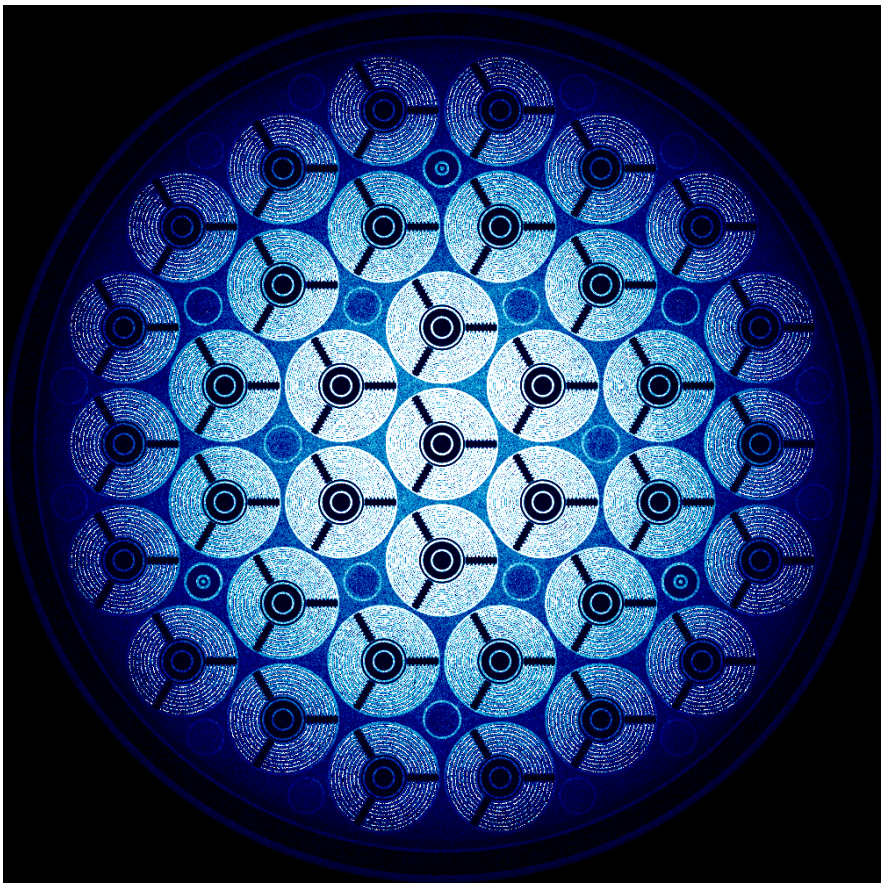

Figure 4. The relative capture cross section of JHR core with homogenized and simplified fuel rod assembly.

Mechanical tests

Creep, due to high temperature, stresses, radiation or a combination of these, is a significant degradation mechanism for nuclear fuel cladding during reactor operation and repository conditions. The fuel cladding material creep propagation may be affected also by other factors, e.g. waterside corrosion and hydrogen pick-up. ATF claddings, such as austenitic stainless steels and oxide dispersion strengthened (ODS) alloys, are designed to exhibit better creep resistance than zirconium-based alloys, which are widely used in currently operating light water reactors (Massey et al., 2016).

Creep testing of cladding materials is typically performed using internal pressure tests for thin-walled samples at elevated temperature. Although very significant creep is not expected for most ATF cladding types at normal operation conditions,

the current situation is that there is still inadequate amount of data available on the strain evolution in axial and hoop direction during creep.

A device for mechanical creep testing is already in use at VTT. In this project, the device will be used to perform creep tests on available advanced cladding material samples. At the first stage in 2019, the thermal creep experiments were carried out with DIN 1.4970 type austenitic stainless steel claddings. In 2020, experiments continued with transient tests using DIN 1.4970 stainless steel. Tests were done with alternating pressure, hoop-axial pressure ratio and temperature.

The creep tested specimen was visually inspected and measured before and after the test (figure 5). No signs of significant damage were found from the specimen during the visual inspection and the dimension measurements did not indicate any significant creep evolution, e.g. ballooning in the middle of the gauge section.

The creep-to-rupture behaviour of the specimen was assessed using the Larson-Miller modelling method. Figure 6 shows the hoop (circumferential) stress versus Larson-Miller parameter correlation for data from literature (Cautaerts et al., 2017), earlier VTT test data and the result of the test performed in 2020 (at 500°C) together with Larson-Miller predictions and scatter bands of the assessed data. Because the latest test was performed with load transients, time weighted average hoop stress (364 MPa) was calculated for consumed creep exposure. The test was interrupted before rupture after 7359 h at the hoop stress level of 392 MPa. The model predicts that the creep to rupture for the test would have been 37178 h if the hoop stress of 392 MPa would have been maintained until the rupture. However, the increased axial stress level (due to additional axial load by the bellows) compared to the situation where the stress state would have been emerging solely from the internal pressurewould have probably shortened the remaining time to a creep rupture.

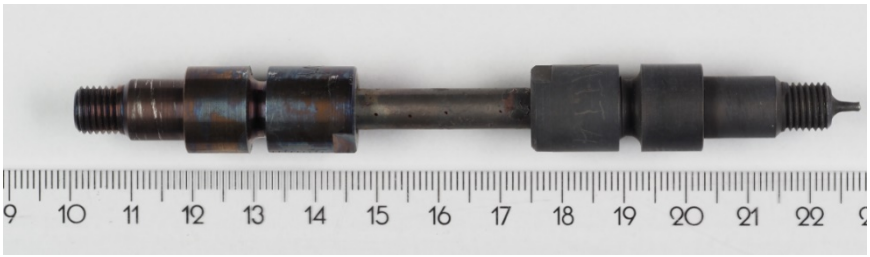

a)

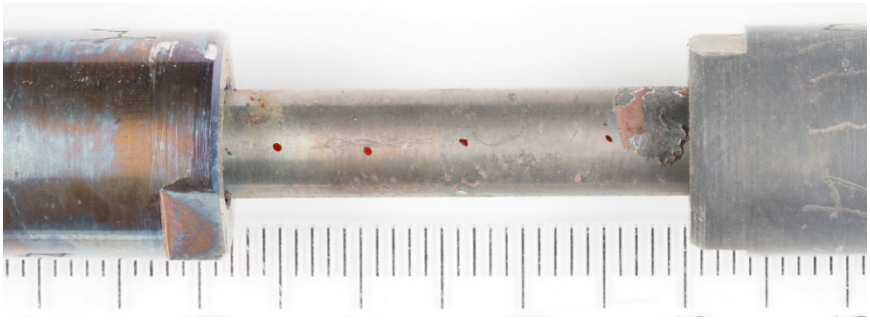

b)

c)

Figure 5. The creep specimen with length measurement in a) red dots indicating the diameter measurement locations in b) and black dots indicating the diameter measurement locations in c).

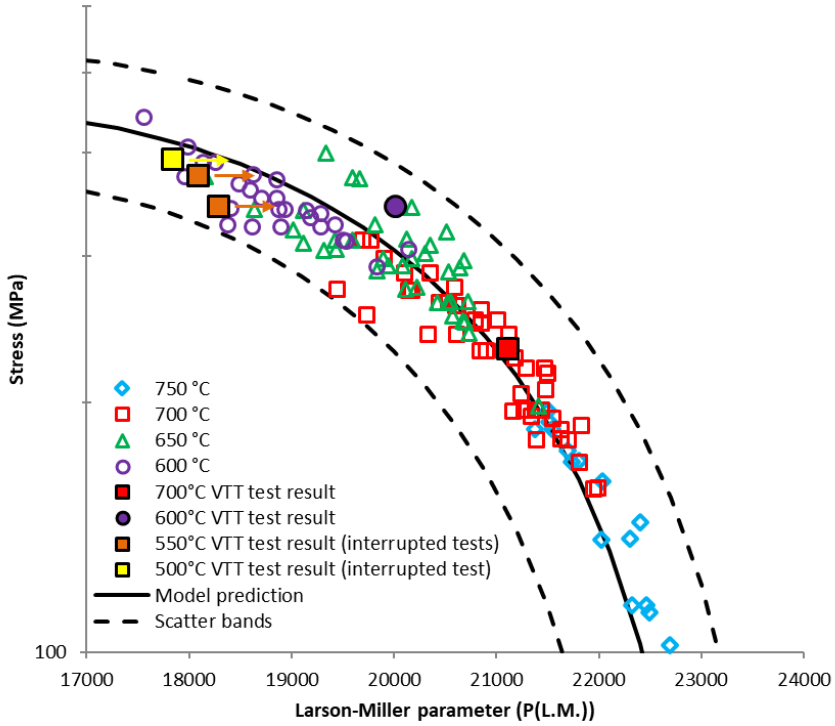

Figure 6. The hoop stress versus Larson-Miller parameter correlation for DIN 1.4970 material with data from literature (Cautaerts et al., 2017), earlier VTT test data and the result of the test performed in 2020 (at 500°C) together with Larson-Miller predictions and scatter bands of the assessed data.

Autoclave oxidation tests

VTT has developed a high temperature recirculation loop that has been previously used to study the corrosion of steam generator (SG) tubes under normal operating conditions (Huotilainen et al., 2018). The high temperature hot recirculation loop (figure 7) will be adapted to simulate the relevant environment, in terms of thermal-hydraulic conditions and primary coolant chemistry, for fuel cladding. The effect of neutron irradiation will not be studied nor simulated with the high temperature hot recirculation loop. The oxide's behavior and growth will be monitored by online electrochemical measurements, such as electrochemical impedance spectroscopy (EIS) and linear polarization. EIS is a powerful technique for evaluating corrosion processes and providing invaluable data concerning the oxide, electrolyte and electric double layer properties.

A hot loop for testing material samples in controlled water chemistry and online oxidation measurement with electrochemical impedance spectroscopy already exists at VTT. However, the available heat flux over the sample in the existing device

was only comparable to a low linear heat generation rate of the fuel. In 2019, the autoclave equipment was updated so that a linear heat generation rate of over 20 kW/m could be achieved with the apparatus. This makes possible for testing cladding materials in conditions relevant to a nuclear power reactor. The testing apparatus was verified by experiments on E110 cladding alloy material at around 300 °C. The impedance measurement performed well and the growth of the oxide layer could be distinguished from the test results. The connection of the impedance results to the oxide layer thickness were studied with the equivalent circuit models. Boiling conditions were also investigated, and coolant boiling could also be distinguished from the impedance measurements, extending the applicability of the method.

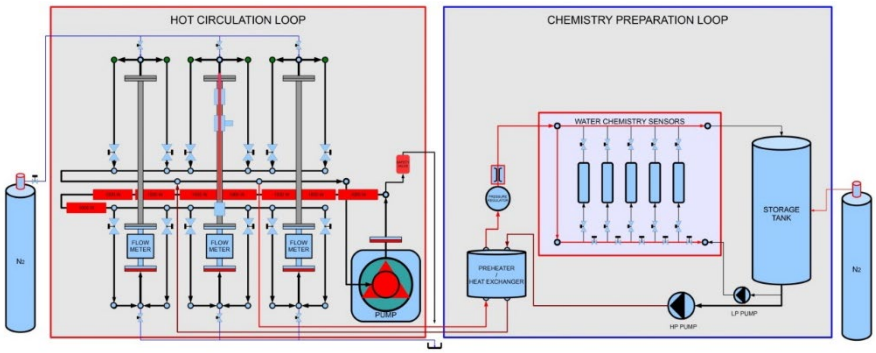

Figure 7. Schematic illustration of the high temperature hot recirculation loop (left side) and chemistry preparation loop (right side) used in this study.

Steam furnace oxidation testing

High temperature steam testing are being performed for the selected ATF cladding materials in this part of the project. Cladding exposures are performed at different temperatures (1000–1600 °C) for different exposure times/experiment durations (from minutes to hours) to produce data on the oxidation of the tested materials with high temperature steam furnace system in VTT's Research Hall (figure 8). The test specimens will be characterized using Light Optical Microscope (LOM) and Scanning Electron Microscope (SEM) techniques, and the oxidation products will be analyzed using SEM-EDS (energy dispersive spectroscopy). Test data is used for oxidation process modelling. Data on the oxide layer can also be obtained with glow discharge optical emission spectroscopy (GDOES), if necessary. The data can be used to improve the prediction capabilities of simulations in accident analyses and to increase understanding of accident evolution. Although the aim is to improve the cladding behavior in accident conditions, the materials are also studied to verify that the new claddings are not inferior compared to zirconium alloys during normal operation. A deeper understanding on oxidation mechanisms is created together with tests in normal LWR operating conditions. The exposure tests in LWR conditions

are continued, with focus based on the most promising cladding solutions. Steam test samples are further characterized and modelling of oxide film thickness and hydrogen content as a function of depth is performed with the mixed-conduction model. Additional hydrogen pickup and desorption tests will be performed to gain a better understanding of uptake mechanisms and the behavior of hydrogen in traditional and ATF cladding materials. The project will promote collaboration between industry and research institutes under the IAEA umbrella. Especially Canadian Nuclear Laboratories (CNL), Massachusetts Institute of Technology (MIT) and Westinghouse are the key partners to developed ATF cladding materials further. The essential part of this activity is to contribute in round-robin testing of new cladding material solutions within a new IAEA Coordinated Research Project (CRP) named Testing and Simulation for Advanced Technology and Accident Tolerant Fuels (ATF-TS). The scope is to test potential ATF cladding solutions in numerous international institutes with identical tests parameters.

Hot steam testing is a viable method for investigating the oxidation characteristics of cladding materials. Tests are performed at temperatures between 1200 and 1600 °C with variable exposure time, which gives data on oxidation behavior. This data can further be used in model development and validation. The technique is especially good for screening materials and for improved understanding of the oxidation mechanisms, but also for investigations under LOCA conditions.

VTT participated in the IAEA coordinated research program ACTOF (Analysis of Options and Experimental Examination of Fuels for Water-Cooled Reactors with Increased Accident Tolerance) with steam furnace oxidation testing of several advanced cladding materials in the past years. The results obtained at VTT in the research program were published in an IAEA TECDOC. In 2020, the experiments in steam environment continued for Zr-based coated claddings held at 1200 °C for 30 min. The coatings were pure Cr, CrN, CrAl. The behaviour of these coatings was worse than expected: some of the coatings were ripped off from the cladding tubes as shown in figure 9. The tests with the same materials will continue in 2021 with reduced exposure times. The tests aim at a new round-robin exercise for ATF cladding materials under fresh IAEA ATF-TS CRP.

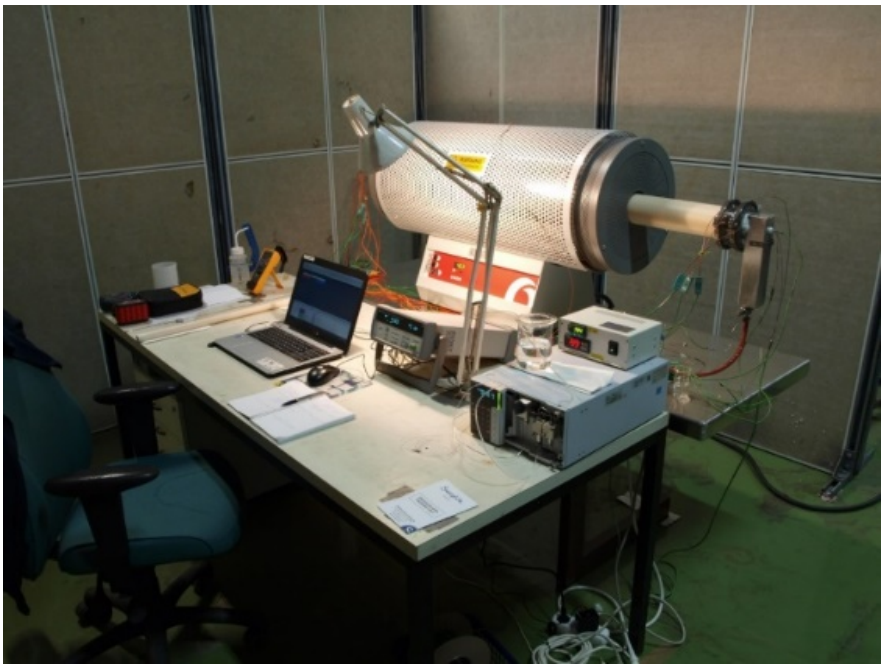

Figure 8. High temperature steam furnace system in VTT's Research Hall.

Figure 9. CrAl coated Zr-tube exposed at 1200 °C up to 30 min in flowing steam.

Pellet annealing test equipment

The influence of chemical processes on the in-pile behavior of nuclear fuel is not very well understood. With increasing burnup, various chemical phenomena take place in the fuel rod, such as diffusion of fission products, formation of separate solid phases from an initially homogeneous material and vaporization of volatile elements from fuel. These chemical processes influence not only the material properties of the fuel but also of the cladding via gas phase diffusion and especially during hard contact between the pellet and the cladding. The possibility of damage to fuel due to pellet-cladding interaction (PCI) is a complex process involving both mechanical stress and active chemical processes. For example, iodine forms gaseous zirconium iodide (ZrI_4) which erodes the cladding and aids stress corrosion cracking (Cox, 1990). Additionally, in case of a defective fuel rod or in accident conditions, the chemical and physical properties determine the release behavior of radionuclides from the fuel.

An annealing furnace was obtained in 2019 for future testing of pellet materials at VTT (figure 10). During the course of the project, the furnace was tested at the VTT Centre for Nuclear Safety. A remote controller system was established for the furnace and temperature calibration tests were performed in 2020. The heating series up to 1700 °C is illustrated in figure 11.

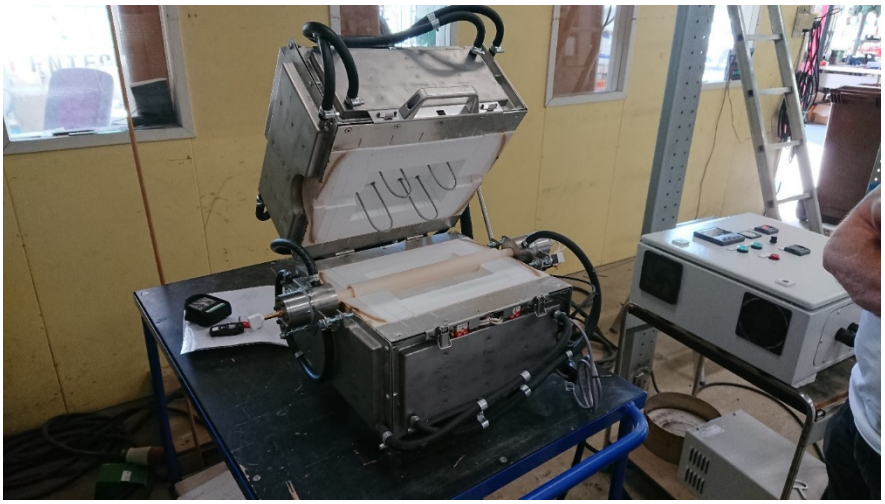

Figure 10. Furnace opened prior to the acceptance tests. The $MoSi_2$ resistive heating elements are attached to the furnace top cover. The sample tube lies on the bottom part of the furnace.

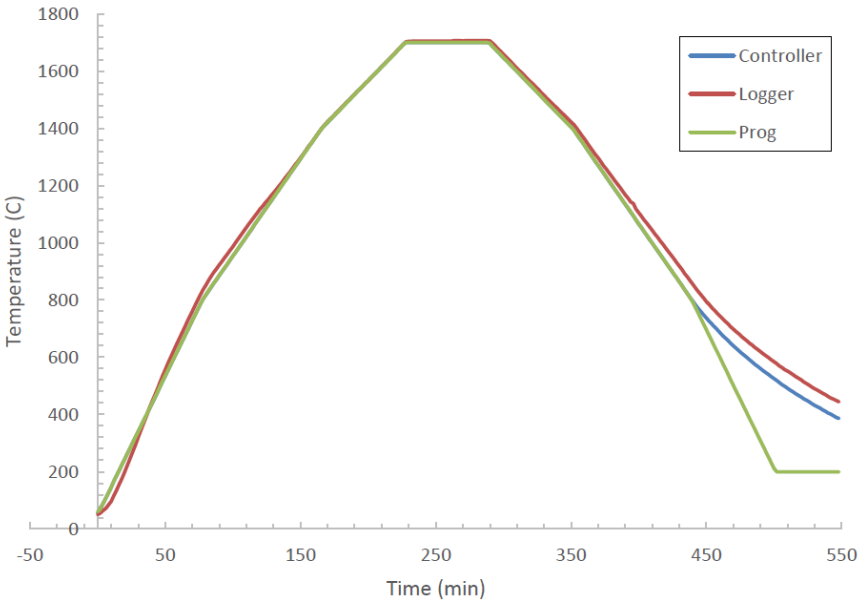

Figure 11. Temperature evolution during the programmed temperature cycle. The target temperature was 1700 °C and the ramp rate below 800 °C was 10 °C/min, at 800 °C < T < 1400 °C, 7 °C/min, and at 1400 °C < T < 1700 °C, 6 °C/min. The final temperature was 200 °C. The temperature cycle "Prog" was followed with the "Controller" thermocouple. The actual temperature inside the specimen tube was measured with a separate thermocouple "Logger".

Non-radioactive CeO_2 has been previously applied in fuel pellet related experiments due to the same crystallographic structure and similar mechanical properties as UO_2 (García-Ostos et al., 2016; Khafizov et al., 2019; Pakarinen et al., 2015; Yablinsky et al., 2015). In this study, we applied CeO_2 powder as surrogate material for UO_2. The CeO_2 powder was mixed with CsI powder and pressed into pellets. Annealing experiments were performed for non-sintered and SPS sintered pellets.

In 2020, the first tests for CsI doped CeO_2 pellets were performed at high temperatures, and iodine and particle release were monitored. Sample for the calibration measurements was prepared with a cylindrical die and applying compression of 6 kN. The sample contained 30w% of CsI and 70w% of CeO_2 powder. First, two sample pellets were annealed to 1100 °C and cooled down. Iodine and particle measurements were applied during the heating cycle. The same samples were heated again to 1300 °C, while applying iodine and particle measurements. Iodine release from the samples during the second heating cycle is presented in figure 12. The goal was to observe sensitivity limits for the iodine on-line measurements as well as monitor iodine release during conventional sintering procedure. The second set of samples were sintered with the spark plasma sintering device. The samples contained 1mol% of CsI and they were sintered at 900 °C, 1000 °C and 1100 °C. Annealing experiments for iodine release were performed up to 1500 °C while

monitoring iodine and particle release via their transport through the experimental setup. The densities of the samples were 0.70%, 0.75%, and 0.76% of the theoretical maximum density, respectively. The spark plasma sintering procedure of the pellets and the density measurements were performed at Charles University (Czech Republic).

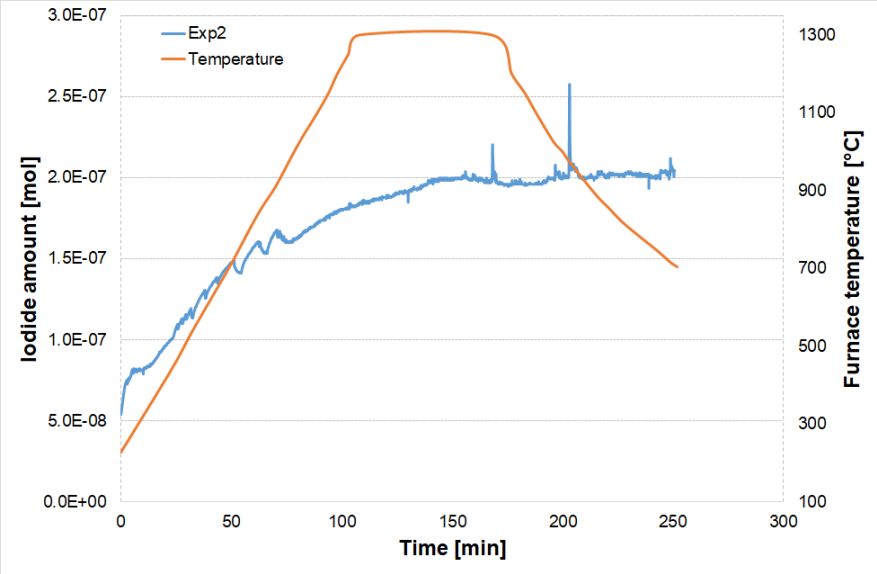

Figure 12. Calculated amounts of iodide from the measured voltage with the ISE at 25 °C as a function of experiment duration (heating,stabilisation and cooling phases).

References

Cautaerts, N., Delville, R., Dietz, W., Verwerft, M., 2017. Thermal creep properties of Ti-stabilized DIN 1.4970 (15-15Ti) austenitic stainless steel pressurized cladding tubes. Journal of Nuclear Materials 493, 154–167. https://doi.org/10.1016/j.jnucmat.2017.06.013

Cox, B., 1990. Pellet-clad interaction (PCI) failures of zirconium alloy fuel cladding - A review. Journal of Nuclear Materials 172, 249–292. https://doi.org/10.1016/0022-3115(90)90282-R

García-Ostos, C., Rodríguez-Ortiz, J.A., Arévalo, C., Cobos, J., Gotor, F.J., Torres, Y., 2016. Fabrication and characterization of CeO2 pellets for simulation of nuclear fuel. Nuclear Engineering and Design 298. https://doi.org/10.1016/j.nucengdes.2015.12.026

Huotilainen, C., Ikäläinen, T., Peltonen, S., Saario, T., Sipilä, K., 2018. In-situ monitoring of stainless steel AISI 316L corrosion behavior under PWR secondary side thermal hydraulic and heat transfer conditions, in: 21st Inter-National Conference on Water Chemistry in Nuclear Reactor Systems.

Khafizov, M., Pakarinen, J., He, L., Hurley, D.H., 2019. Impact of irradiation induced dislocation loops on thermal conductivity in ceramics. Journal of the American Ceramic Society 1–10. https://doi.org/10.1111/jace.16616

Massey, C.P., Terrani, K.A., Dryepondt, S.N., Pint, B.A., 2016. Cladding burst behavior of Fe-based alloys under LOCA. Journal of Nuclear Materials 470, 128–138. https://doi.org/10.1016/j.jnucmat.2015.12.018

Ikonen, T., Tulkki, V., 2014. The importance of input interactions in the uncertainty and sensitivity analysis of nuclear fuel behavior. Nuclear Engineering and Design, Vol. 275, pp. 229-241.

OECD/NEA, 2017. Reactivity-initiated Accident Fuel-rod-code Benchmark Phase II: Uncertainty and Sensitivity Analyses. NEA/CSNI/R(2017)1.

Pakarinen, J., He, L., Hassan, A.-R., Wang, Y., Gupta, M., El-Azab, A., Allen, T.R., 2015. Annealing-induced lattice recovery in room-temperature xenon irradiated CeO2: X-ray diffraction and electron energy loss spectroscopy experiments. Journal of Materials Research 30, 1555–1562. https://doi.org/10.1557/jmr.2015.13

Pizzocri, D., Barani, T., Luzzi, L., 2020. SCIANTIX: A new open source multi-scale code for fission gas behaviour modelling designed for nuclear fuel performance codes. Journal of Nuclear Materials 532, 152042. https://doi.org/https://doi.org/10.1016/j.jnucmat.2020.152042

STUK, 2019. Nuclear fuel and reactor, 15.3.2019, YVL B.4, https://www.stuklex.fi/en/ohje/YVLB-4 (visited 19 Feb 2021)

Yablinsky, C.A., Devanathan, R., Pakarinen, J., Gan, J., Severin, D., Trautmann, C., Allen, T.R., 2015. Characterization of swift heavy ion irradiation damage in ceria. Journal of Materials Research 30, 1473–1484. https://doi.org/10.1557/jmr.2015.43

4.3 Developing the working arms of Kraken, the next generation computational framework for reactor design and licensing analyses (LONKERO)

Ville Valtavirta

VTT Technical Research Centre of Finland Ltd
P.O. Box 1000, FI-02044 Espoo

Abstract

The aim of LONKERO a four year excellence project is to build a next generation computational framework for reactor analysis that can be used for deterministic safety analyses when the current generation of Finnish tools based on e.g. the TRAB3D and HEXTRAN sequences are eventually retired.

LONKERO started from individual new generation Finnish solver modules for reactor core physics, such as the Serpent Monte Carlo neutronics code, the Ants nodal neutronics code, the FINIX fuel behavior module and the Kharon porous medium thermal hydraulics solver.

In two years LONKERO has nurtured Kraken from these individual solvers into a respectable reactor core simulator capable of modelling multiple operating cycles of large light water reactors (LWRs) and small modular reactors (SMRs) while automatically evaluating licensing relevant data such as power peaking, control rod reactivity worths, reactivity feedback coefficients and shutdown margins.

Modularity and the internal cross validation of reduced order solvers with high fidelity have been two large design goals that have threaded their way through the first two years of Kraken's life. This has been demonstrated in SMR core level problems where the solution can be obtained both with continuous energy Monte Carlo and few-group nodal diffusion based calculation sequences.

The initial results for the two-operating-cycle experimental benchmark BEAVRS show that Kraken can predict detector maps for operating reactors at an accuracy comparable to current industry leaders. The project moves to transient modelling for its second half.

Introduction

The excellence project LONKERO answers the need stated in the SAFIR2022 Framework Plan regarding the development of a new set of advanced codes for reactor and nuclear power plant analysis. The focus in LONKERO is especially on developing a new computational reactor analysis framework leveraging the new generation of Finnish solvers for reactor core physics such as the Serpent Monte Carlo particle transport code, the Ants nodal neutronics code and the FINIX fuel behaviour module. This *Kraken*-framework is developed in LONKERO for future use in deterministic safety analyses of current and upcoming reactor concepts.

Furthermore, Kraken is to be usable as a research and design tool that can be applied to a wide variety of reactor core related research problems including the design of new reactor concepts.

Kraken needs to be able to conduct steady state, operating cycle and transient analyses both at the core level and coupled to system codes that model the feedback of the power plant itself. Achieving this goal in only four years when starting from separate solver codes in various states of development requires a significant amount of effort. Furthermore, the benchmarking and validation of the different capabilities of Kraken also need to be started as soon as the implementation of each capability is finished.

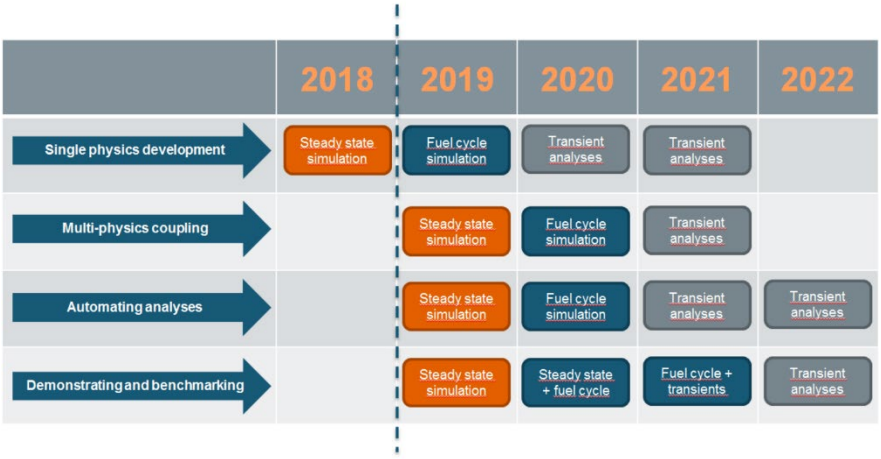

Figure 1. A high level overview of the four year plan for the development, demonstration and benchmarking of the Kraken framework.

In order to manage the construction of a complete reactor simulator in such a tight schedule, a rapid development pace has been set in the LONKERO project. An overview of this development schedule is given in Figure 1: The first year of the project focused on the coupled reactor core level solution in steady state while the second year had its focus in creating a core simulator capable of operating cycle simulations. Years 2021 and 2022 focus on extending Kraken's capabilities to transient analyses, initially at the core level and then coupled to a system code.

One of the design goals for the Kraken framework was to construct the framework in a modular fashion so that the solver for one core physics can be swapped to another with minimal effect on the other solvers and on the simulation model as a whole. This enables the verification of reduced order solutions (e.g. nodal diffusion neutronics) against high fidelity solutions of the same physics (e.g. Monte Carlo neutronics) without having to change the simulation models for the two other physics (thermal hydraulics and thermal mechanics). Figure 2 shows a schematic of the planned couplings for the Kraken framework: Solver modules for the three reactor

core physics (neutronics, thermal hydraulics and thermal mechanics) are coupled together via a reactor core level interface to create a core simulator. This core simulator is further coupled with system codes in the future in order to simulate transients with system level feedbacks. While Kraken is mainly built on the new generation of Finnish solvers, the coupling to existing national and international state-of-the-art solvers is also enabled by the design choices.

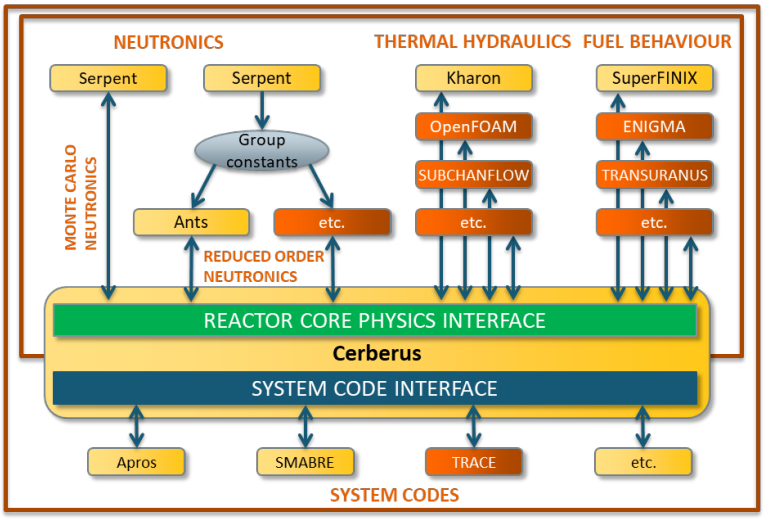

Figure 2. A schematic representation of the plans for the completed Kraken framework. Finnish solver modules developed at VTT are shown in yellow, while potential state-of-the-art third party solvers to be coupled are shown in orange.

At the beginning of the four-year excellence project, the individual core physics solver modules were available in various states of development, but could not be used together to solve the coupled problem between neutronics, coolant flow and fuel behaviour. Therefore, the first goal of the project was to establish a common communication syntax between the solvers and the multi-physics driver module Cerberus and implement basic communication capabilities in the individual solver modules.

Establishing the main solver modules and a common communication syntax

The common communication syntax between the solvers was established as the first task of the project in early 2019 followed by the implementation of basic communication capabilities in the individual solver modules. This work also involved constructing data structures for the exchanged data fields on various spatial data meshes in a manner that allowed flexible solution transfers between the different solvers. The initial choice and implementation of the basic communication

capabilities laid the foundation for executing the coupled calculations in a flexible and efficient manner.

Designing and developing the reactor core level fuel behaviour module SuperFINIX

At the start of the project, two out of three core physics had their own core level solvers: the core level neutronics could be solved either by Serpent or Ants and the core level thermal hydraulics could be solved by Kharon. The fuel behaviour solution, however intended to rely on FINIX, which only models a single fuel rod. In the past, FINIX was used in coupled calculations through a direct integration to the neutronics solver such as Serpent or HEXTRAN. Taking such an approach with Kraken, however, would run counter to the modular structure of the framework and would mean that separate couplings would need to be built between each neutronics solver and each (future) fuel behaviour solver, instead of simply implementing a single coupling between each solver module and Cerberus, the central multi-physics driver.

In order to achieve the modular structure of the framework, a separate core level fuel behaviour module, *SuperFINIX*, was created, which receives the boundary conditions for the core-level fuel behaviour solution, i.e. core level power and thermal hydraulics fields from Cerberus and distributes this data to the individual fuel rod level. The actual fuel behaviour solution is handled by however many tens, hundreds or thousands of individual FINIX solvers are required to cover each modelled fuel rod.

As it was clear that the framework's modularity would allow the users to choose neutronics and thermal hydraulics solvers with various different resolutions, i.e. tools with nodal/channel level or pin/subchannel level or even intra-pin/CFD level resolutions, SuperFINIX would need to be able to receive and supply data at various fidelities. While the actual fuel behaviour solution is always done at the individual rod level with a (r,z) power distribution inside the fuel rod and resulting in a (r,z) temperature distribution inside the fuel rod, the coupled neutronics and thermal hydraulics solvers may not be able to use the data at this resolution. Thus, SuperFINIX needs to handle the averaging of the data to rod, subassembly and assembly levels in a consistent manner. Similarly, SuperFINIX must be able to receive power distributions at assembly, subassembly, rod and intra-rod levels and distribute this data to individual FINIX solvers in a consistent manner.

This variable-fidelity capability was demonstrated in a conference article where SuperFINIX was coupled to Serpent via Cerberus at three different fidelities, exchanging data

1. At the assembly level.
2. At the pin-level.
3. At the pin-radial level.

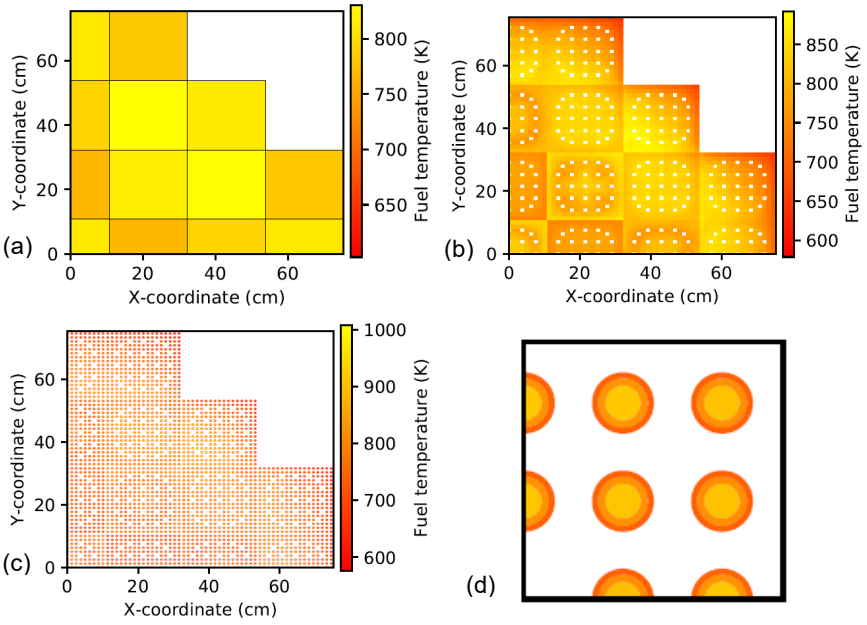

Figure 3. An SMR core level fuel temperature solution obtained from SuperFINIX at three different fidelities: (a) Assembly averaged. (b) Rod averaged. (c) Radial distributions inside rods. (d) Detail from radial distributions.

This is illustrated in Figure 3 where the fuel temperature fields supplied by SuperFINIX at the three levels are shown. The flexibility is inherent for SuperFINIX in the sense that temperature fields can be requested from SuperFINIX at any level and the level of coupling does not need to be pre-specified, but could even change during the calculation. This should also pave way to e.g. direct in-line hot-channel analyses, where the fuel assembly with the highest power is modelled at a higher level of detail.

Establishing coupled calculation sequences for steady state

Once the core level solver modules were ready and the communications syntax for solver initialization, field transfers and solution updates was established and implemented, the actual construction of coupled calculation sequences for steady state was very straightforward.

The multi-physics driver Cerberus has been designed to allow the user to easily establish new coupled calculation sequences and such sequences can be implemented either through plaintext input-files, in which the participating solvers, the coupled fields and the general solution flow are defined. However, to offer powerful extendability, Cerberus was written as a Python package, which means that users

and developers can actually access the solvers, coupled fields and many control variables of the solvers from normal Python code through Cerberus. This allows the quick construction of even complex coupled calculation sequences.

Two coupled sequences were quickly established, the high-fidelity neutronics sequence Serpent-Kharon-SuperFINIX and the reduced order neutronics sequence Ants-Kharon-SuperFINIX. Due to the modular design of the framework, the Kharon and SuperFINIX models could typically be shared by the reduced order and high-fidelity neutronics sequences, meaning that only the neutronics solver and model was swapped when moving from one sequence to the other.

Licensing relevant data evaluated with the steady state calculation sequences

In order to constantly evaluate the achievement of the goals of the LONKERO project, the use of Kraken to the evaluation of licensing relevant data was begun as soon as the steady state sequences were established. The capabilities of Kraken were chosen to be demonstrated at an SMR core level calculation, which would allow the use of both calculation sequences to solving the problem. The high computational cost of Monte Carlo neutronics practically excludes its use from most hot-full-power calculations in the context of large LWRs.

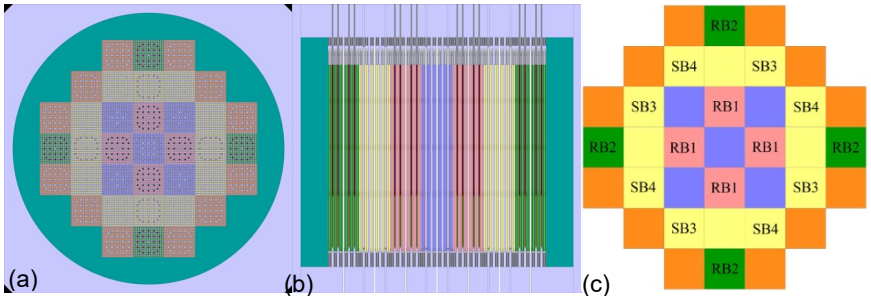

Figure 4. Geometry of the SMR core level progression problem. (a) Horizontal plot from the Serpent model. (b) Vertical plot from the Serpent model. (c) Location of regulating (RB) and shutdown (SB) control rod banks.

The SMR core was constructed by combining core level data from the NuScale FSAR and detailed geometry and material information from the BEAVRS benchmark. The core geometry in Figure 4 shows the core loading designed with scoping calculations using the Ants-based coupled sequence. The different colours of the assemblies correspond to different uranium enrichments and the placement of regulating and shutdown control rod banks is indicated clearly.

Several interesting pieces of data were evaluated with the two calculation sequences including reactivity feedback coefficients, control rod bank worths and shutdown margins. This work was documented in one special assignment and one conference article.

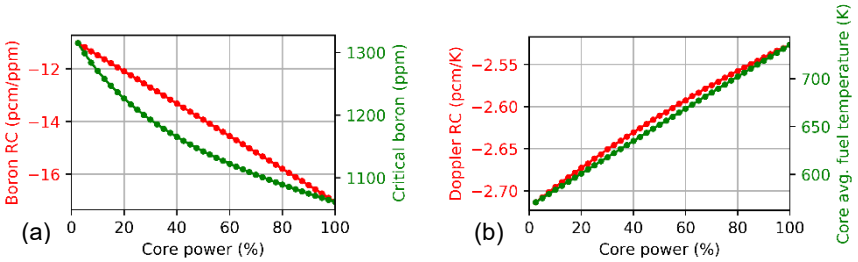

Figure 5. Two reactivity coefficients calculated with the Ants-Kharon-SuperFINIX for the SMR core at various power levels. (a) Boron reactivity coefficient (red) and critical boron (green). (b) Doppler reactivity coefficient (red) and core average fuel temperature (green).

As an example of the calculated reactivity coefficients, Figure 5 shows the boron and Doppler reactivity coefficients evaluated using the Ants-based calculation sequence at various power levels between zero power and full power. As the Ants-based sequence produces results at the seconds-to-minutes timescale, it is possible to calculate such variations at a large number of different power levels or with various core loading patterns.

Both calculation sequences were used in calculating the reactivity worths of the different control rod groups at cold zero power, hot zero power and hot full power states. The results, shown in Table 1 indicated a good agreement between the two calculation sequences, even though the main intent of the work was only to demonstrate the capability for such calculations.

Table 1. Reactivity worths of control rod groups of the SMR core at cold zero power (CZP), hot zero power (HZP) and hot full power (HFP) conditions. The one sigma statistical uncertainty for the Serpent results is 4 pcm.

	CZP			**HZP**			**HFP**		
	Ants	**Serpent**	**A–S**	**Ants**	**Serpent**	**A–S**	**Ants**	**Serpent**	**A–S**
RB1	861	874	–13	1974	2012	–38	2084	2221	–137
RB2	2094	2092	+2	2218	2161	–57	2290	2285	+5
SB3	2592	2597	–5	3547	3559	–12	3612	3697	–85
SB4	2592	2596	–4	3547	3560	–13	3612	3703	–91

As with reactivity coefficients, the Ants-based calculation sequence could easily and quickly be applied to evaluating such data using different variations as in Figure 6, which shows the available reactivity worth of regulating bank 1 as a function of the momentary insertion height of the bank as well as at different power levels.

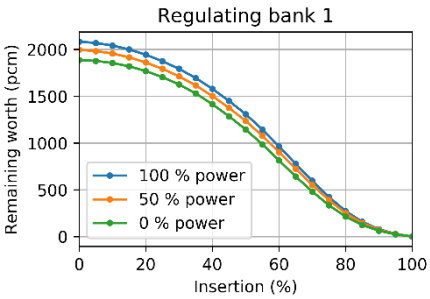

Figure 6. Available reactivity worth of regulating group 1 at different insertions at different reactor power levels. Evaluated with Ants-Kharon-SuperFINIX.

One additional application, which was also demonstrated in the SMR case was the evaluation of shutdown margins, including the separate effects coming from fuel cooling, the limitation of the highest worth control rod assembly (CRA) being stuck etc. Table 2 shows the short term hot shutdown and long term cold shutdown margins for the SMR core evaluated by the Ants-based calculation sequence.

Table 2. Shutdown margin for the SMR core. Evaluated with the Ants based calculation sequence from hot full power and critical boron.

Parameter		**(pcm)**
1.	Total available CRA worth at HFP	18187
2.	Effect of power dependent insertion limits at HFP	332
3.	Highest worth CRA stuck	5317
4.	Power defect (short term cooling)	662
5.	Long term cooling	924
6.	Xenon decay	2353
7.	Net margin for hot shutdown (1. – 2. – 3. – 4.)	11876
8.	Net margin for long term shutdown (7. – 5. – 6.)	8599

Overall, this first demonstration proved that in addition to offering the basic coupled solution to the reactor core-level coupled problem, Kraken could be used to producing licensing relevant derivative data with little additional effort. The realisation of the modularity design goal of Kraken was tested when the same SuperFINIX and Kharon models were used both with Ants and Serpent neutonics solutions.

Validating the Serpent-Ants neutronics calculation chain using experimental data from the BEAVRS first cycle startup tests

While the SMR level demonstration showed that Kraken can provide coupled steady state solutions to reactor core level problems and while the Serpent and Ants based sequences were generally in good agreement, the whole problem was completely computational and could not offer validation for the capability of Kraken to accurately offer solutions to real world problems.

The BEAVRS benchmark was chosen as the case in which the steady state and operating cycle modelling of Kraken would be validated against experimental data. BEAVRS offers data from the first two operating cycles of a commercial US PWR and is widely used for reactor simulator validation around the world.

As a first step in the validation process, Kraken was used to model the zero power physics tests conducted at the beginning of the first operating cycle. At zero power, this was especially a test of the two-step neutronics calculation chain Serpent-Ants involving the generation of few-group constants for Ants by Serpent and the nodal diffusion solution to the reactor core level neutronics by Ants.

Table 3. Serpent and Serpent-Ants results for critical boron concentrations (ppm). Serpent one sigma uncertainty is approximately 0.5 ppm.

	Estimates			Differences		
	Ref.	Serpent	Ants	S–R	A–R	A–S
ARO	975	967	965	–8	–10	–3
D in	902	905	902	+3	+0	–3
C, D in	810	809	804	–1	–6	–6
A, B, C, D, in	686	673	667	–13	–19	–6
A, B, C, D, S_E, S_D, S_C in	508	486	476	–22	–32	–9
Mean of $\lvert X - Y \rvert$				9.4	13.5	5.3
RMS of X – Y				12.1	17.4	5.9

The predictions of Serpent and Serpent-Ants for critical boron concentrations and control rod bank worths at different points of the physics tests control rod insertion sequence are shown in Table 3 and Table 4, respectively. As Serpent is used both for generating the group constants for Ants and for directly calculating the full core solutions, the Ants prediction can be compared both to the measured values and the Serpent prediction. While the comparison to experimental data includes many uncertainties such as those coming from nuclear data and measurement accuracy, the comparison between Ants and Serpent is free of all such sources of uncertainty and directly reflects the capability of the reduced order neutronics to reproduce the solution of the high-fidelity neutronics.

Comparing Serpent and Ants results to the measured values, a good agreement can be seen both in critical boron concentrations and in control bank worths. The RMS differences in critical boron between calculated and experimental are below 20 ppm and the RMS differences in predicted vs. measured control bank worths are around 20 pcm, which is very small.

Table 4. Serpent and Serpent-Ants results for control rod bank worths (pcm). Serpent one sigma uncertainty is approximately 5 pcm.

	Estimates			Differences		
	Ref.	Serpent	Ants	S–R	A–R	A–S
D in from ARO	788	785	800	–3	+12	+15
C in from prev.	1203	1247	1235	+44	+32	–12
B in from prev.	1171	1206	1203	+35	+32	–3
A in from prev.	548	527	514	–21	–34	–13
S_E in from prev.	461	488	483	+27	+22	–5
S_D in from prev.	772	767	776	–5	+4	+9
S_C in from prev.	1099	1105	1093	+6	–6	–12
Mean of $\lvert X - Y \rvert$				20.1	20.4	10.0
RMS of X – Y				25.1	23.6	10.8

While the critical boron concentration is a wholly global parameter, the prediction of control bank worths can be considered to also offer some information on the accuracy of the spatial flux solution. However, in order to obtain a better estimate on whether the Ants flux solution could be considered spatially accurate, an additional computational comparison was made between Serpent and Ants for the predicted power distribution.

Both Serpent and Ants were used to evaluate assembly, quarter assembly and pin power distributions for the unrodded (all-rods-out) and rodded (7 banks in) core configurations. Experimental data is practically never available at this level of fidelity without major uncertainties, which means that such computational validation without the uncertainties resulting from nuclear data libraries, measurement conditions etc. is of great importance.

In this computational validation of the power distribution predicted by Ants, a very good agreement was observed between few-group nodal diffusion (Ants) and continuous energy Monte Carlo (Serpent). The RMS difference in predicted assembly and quarter assembly powers between Serpent and Ants was below 1.0 % for both unrodded and rodded cores and the RMS difference in predicted pin powers was at the 1.3 % for the unrodded and 1.7 % for the rodded core.

Figure 7 shows the Serpent predicted pin power distribution in the rodded core and the difference in the pin powers predicted by Serpent and Ants. The largest

differences in predicted pin powers can be seen in the rodded assemblies and at the core periphery.

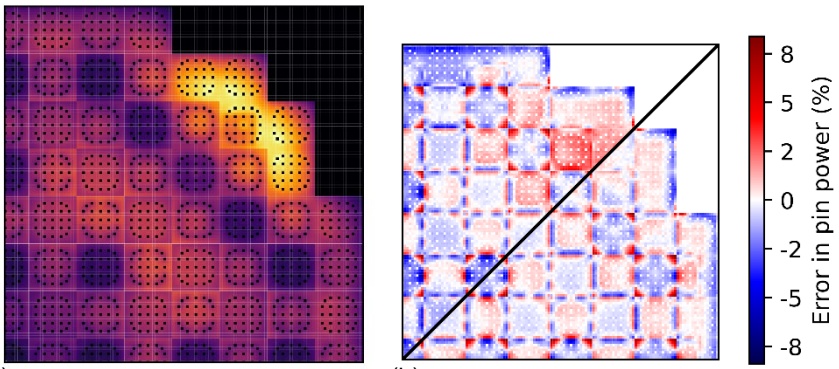

Figure 7. Results from computational validation for pin power predictions at hot-zero-power of the BEAVRS core in the beginning of cycle 1 (seven control rod banks inserted). (a) Serpent predictions for pin powers. (b) Pin power errors (Ants/Serpent - 1)*100% including (top left) and cleaned of (bottom right) assembly power errors.

The BEAVRS HZP validation for Kraken was first presented as a conference article in and then as an invited journal article. The results for both experimental and computational validation were very good and served as the baseline of the maximum level of agreement that could be hoped for in any future full power and operating cycle comparisons in the context of the BEAVRS benchmark. If the predictions would have been poor in the hot-zero-power case or when compared against the most fair reference available, i.e. Serpent full core solution, no good agreement could be hoped for the operating cycle analyses. The achieved level of agreement, however, raised high hopes for the quality of Kraken's solution to the actual operating cycles of the BEAVRS benchmark.

Establishing coupled calculation sequences for fuel cycle simulations

The year 2020 marked the shift from simply establishing the basics of Kraken's coupled calculation features to actually constructing a reactor core simulator that could handle operating cycle simulations with fuel shuffling. The solution flow in the coupled calculations needed to include the time-integration of the individual solvers to the next point on the operating cycle. The individual solvers also needed to be able to restart some of their data from an earlier simulation to model the shuffling of fuel between operating cycles.

The solvers for the different core physics were at very different levels of readiness for calculations including depletion. Kharon, as a thermal hydraulics code was not affected by the accumulation of fuel burnup at all and while SuperFINIX needed to

be extended to the accumulation of burnup for the individual fuel rods, such capabilities already existed in FINIX. For Ants, however, the burnup capabilities needed to be implemented in 2019 and major development efforts were devoted into developing a group constant model that could reproduce the neutron interaction parameters of each calculation node very well at various momentary and historical conditions.

Constructing a reactor core simulator capable of fuel cycle simulations

The powerful capabilities of the Cerberus Python package were leveraged in writing a reactor simulator program that could handle operating cycle simulations with Serpent-Kharon-SuperFINIX and Ants-Kharon-SuperFINIX. The design goal of modularity was kept clear when constructing the reactor simulator so that changing the neutronics solver from Serpent to Ants or vice versa did not necessitate any changes to either the Kharon or SuperFINIX models or the reactor simulator setup itself.

A significant amount of control logic and intelligence was implemented to the reactor simulator so that it could control the reactivity of the reactor with various different approaches while being able to keep track of e.g. the power peaking in the reactor core. Control rod based reactivity control could also aim for the flattest possible power distribution achievable with the user imposed limits to control rod movement. Secondary reactivity control measures could be chosen by the user to allow for stretch-out at the end-of-cycle through iteration of critical system power, critical inlet temperature or critical inlet mass flux.

The evaluation of various distributed and uniform reactivity coefficients, control rod worths and shutdown margins was fully automated and implemented as an optional part of the normal operating cycle simulation.

Licensing relevant data evaluated with the core simulator over a whole operating cycle

As with the steady state sequences, the capabilities of the reactor core simulator were demonstrated in an SMR core level problem. This allowed the solution of the same operating cycle both with the Serpent and Ants based calculation sequences and would demonstrate both the modularity and the possibility of internal computational verification, both of which are design goals of Kraken.

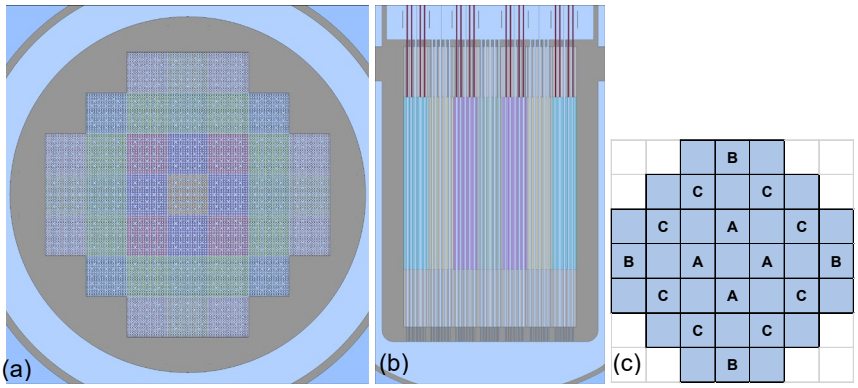

Figure 8. Geometry of the SMR core level progression problem for operating cycle simulations. (a) Horizontal plot from the Serpent model. (b) Vertical plot from the Serpent model. (c) Location of the three control rod banks A, B and C.

The reactor core used in the operating cycle demonstration was based on an early design of a Finnish district heating reactor developed at VTT, shown in Figure 8. The core was simplified in some ways, e.g. the spacer grids were omitted and the control rods only contained a single absorber zone, but overall the core can be considered to be a rather realistic low temperature SMR core.

Boron based long term reactivity control was chosen for this study as the control rod based criticality search is much slower to conduct with Serpent and was deemed too cumbersome for the demonstration. In addition to simply simulating the operating cycle until end-of-cycle at zero boron, various derivative data was evaluated and compared at many points of the operating cycle. The Ants-based sequence was so fast that the evaluation of reactivity feedback coefficients etc. was conducted in-line during the operating cycle simulation, whereas with Serpent this option was not used (although it could have been) and the simulator was restarted to several (but not all) points during the operating cycle for the evaluation of such data.

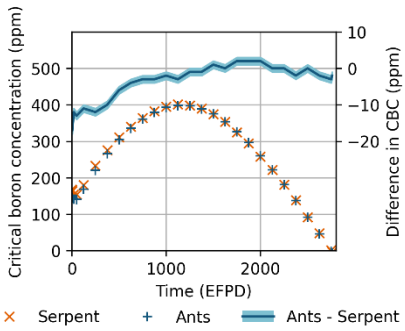

Figure 9. Critical boron concentrations predicted by Serpent and Ants based calculation sequences for the first operating cycle of the SMR core. One-sigma uncertainties included for Serpent.

Both Serpent-Kharon-SuperFINIX and Ants-Kharon-SuperFINIX managed the simulation of the operating cycle admirably. The boron letdown curves predicted by both sequences for the cycle are shown in Figure 9. The agreement between the two sequences is very good, with the differences staying below 20 ppm. The presence of erbium as a burnable absorber in the fuel is seen as an increase in the fuel reactivity up to 1250 EFPD. The cycle lengths and maximum boron concentrations predicted by the two sequences are in a very good agreement.

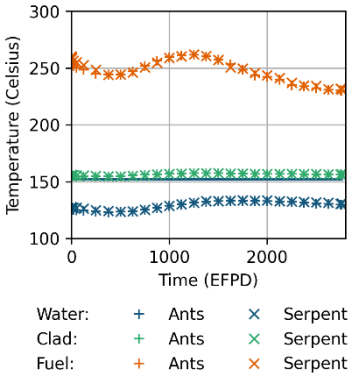

Figure 10. Maximum temperatures of coolant, cladding and fuel during the operating cycle of the SMR core. A solid blue line indicates the saturation temperature of water at the system pressure.

The maximum temperatures of the coolant, fuel and cladding are easily obtained from the simulator. Figure 10 shows such temperatures predicted by the Ants and Serpent based sequences. A very good match between the two sequences can be seen, although it should be noted that the fuel behaviour solution here used one

representative rod per fuel assembly and the agreement in fuel temperatures might not be as good if each rod in the reactor core would have been modelled individually.

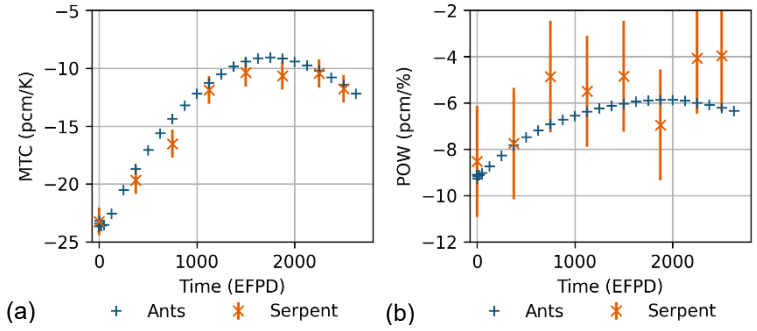

Figure 11. Two reactivity feedback coefficients evaluated with Ants and Serpent based calculation sequences. One-sigma uncertainties included for Serpent. (a) The moderator temperature coefficient, evaluated based on an uniform perturbation to the inlet temperature. (b) Total power coefficient evaluated based on a distributed perturbation to the core power distribution.

The evaluation of reactivity feedback coefficients with Monte Carlo neutronics is rather costly and obtaining a low statistical uncertainty is difficult without significant computational effort. Figure 11 shows two reactivity feedback coefficients evaluated with the Serpent and Ants based calculation sequences and while a good agreement can be seen between the two sequences, the statistical uncertainty especially in the power reactivity coefficient is large.

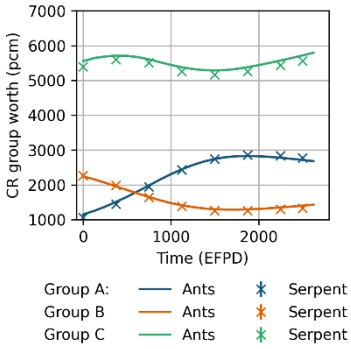

Figure 12. Reactivity worths of the control rod groups evaluated by Ants and Serpent based sequences during the operating cycle of the SMR core. Instantaneous reactivity worth from hot-full-power all-rods-out configuration.

The reactivity worths of the control rod groups are evaluated by the core simulator if requested by the user. Figure 12 shows the reactivity worths predicted by Serpent and Ants based sequences and again, a good agreement between the two can be observed. The Ants-based sequence slightly overpredicts the reactivity worth of group C compared to the Serpent based sequence, but practically no differences are seen in the worths of groups A and B.

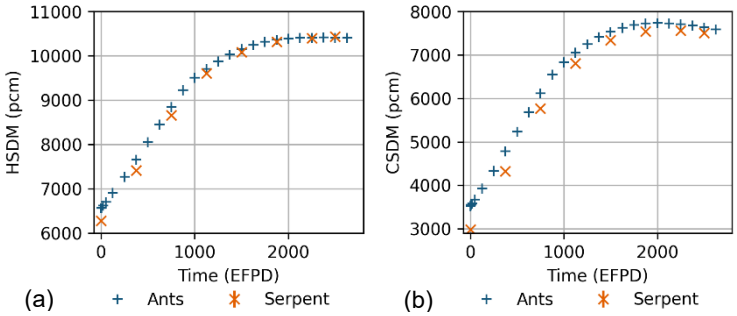

Figure 13. Hot (a) and cold (b) shutdown margins evaluated by Ants and Serpent based sequences during the operating cycle of the SMR core.

The shutdown margins are also automatically evaluated if requested including

1. The instantaneous hot subcriticality after the shutdown of the chain reaction, but before the decay of xenon or cooling of core below the inlet temperature.
2. The long term cold subcriticality after the xenon has decayed and the core has cooled to room temperature and pressure.

The highest worth control assembly (CRA) is automatically located and left “stuck” when evaluating the shutdown margins. The shutdown margins evaluated by the two calculation sequences for the hot and cold shutdown states are shown in Figure 13. In the hot shutdown margin, small differences can be seen at the beginning of the cycle that can be contrasted to the differences in the predicted critical boron. In the cold shutdown margin, however a clear overprediction by Ants can be seen, likely resulting from the fact that separate cold-zero-power group constants have not been included in the library used in the study.

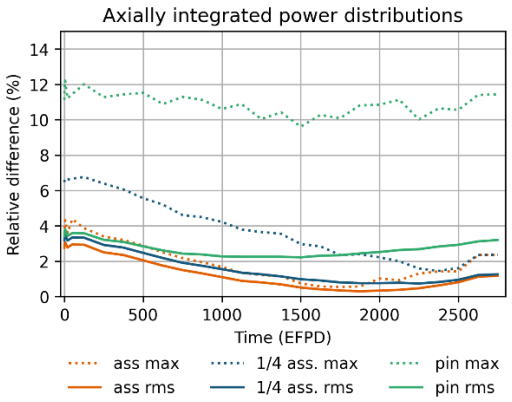

Figure 14. Maximum and RMS relative differences in predicted radial power distributions between the Ants and Serpent based sequences during the operating cycle of the SMR core.

Finally, comparisons of the power distributions predicted by the two calculation sequences at different parts of the operating cycle (shown in Figure 14) indicate larger differences than were seen in the BEAVRS HZP computational validation, which may result of the small heavily reflected reactor core. The differences in the assembly and quarter assembly power distributions decrease as the accumulation of burnup provides a negative feedback on the differences in the power distribution. As Serpent accumulates burnup on pin level and Ants on the quarter assembly level, a decrease of a similar magnitude is not seen in the pin powers.

The studies related to the first operating cycle of this low temperature SMR core provide a comprehensive demonstration of the application of Kraken to operating cycle simulations with in-line or restart based evaluation of various licensing relevant data. Furthermore, the modularity of Kraken was demonstrated by using the same reactor simulator model and the same Kharon and SuperFINIX models with both neutronics solvers. As the same data can be easily evaluated with reduced order and high-fidelity solvers, the use of high-fidelity solvers to the verification and computational validation of reduced order solvers becomes feasible even in the context of hot-full-power operating cycle simulations. The very good agreement between Serpent and Ants based calculation sequences does serve as computational validation of the Serpent-Ants two-step calculation chain in hot-full-power conditions when burnup and operational history effects are included.

The results from this study have been submitted to the ANS M&C conference.

Validation of the steady state and operating cycle simulation capabilities using data from the first two operating cycles in the BEAVRS benchmark

The true test for most of the work of LONKERO 2019 and LONKERO 2020 came in the form of modelling the first two operating cycles of the BEAVRS benchmark and predicting the boron letdown curve and also the fission chamber measurements made at various points over the initial operating cycles. The work required the application of much that was implemented and learned over the first half of the project including:

- Generation and parametrization of a full set of group constants for Ants by Serpent including:
    - Fuel and reflector group constants covering all fuel assembly and burnable absorber configurations present during the operating cycles.
    - Feedback to group constants from momentary temperatures, densities and boron concentrations.
    - Effects of burnup and local historical conditions on the group constants.
- Coupled burnup calculation for the first operating cycle using Ants, Kharon and SuperFINIX following the very complex operating history of the first cycle.
- Reactor reloading for the second cycle including:
    - 64 fresh assemblies.
    - 129 spent assemblies shuffled in the core.
        - Borosilicate absorbers removed after first cycle.
- Coupled burnup calculation for the second operating cycle following the somewhat more regular operating history of the second cycle.
- Restarts of the reactor simulator to the points during the operating cycles at which detector maps were measured.
- Prediction of responses of fission chamber detectors passed through the instrumentation tubes of various assemblies in the reactor core.

This validation effort faced most of the actual challenges of modelling real reactor operation as that was by definition the content of the benchmark. If Kraken could manage the BEAVRS benchmark with reasonable accuracy, the first two years of the project could be considered a success.

While the final journal article of this validation is still being compiled it is already clear that Kraken performed very well in this comparison against experimental data.

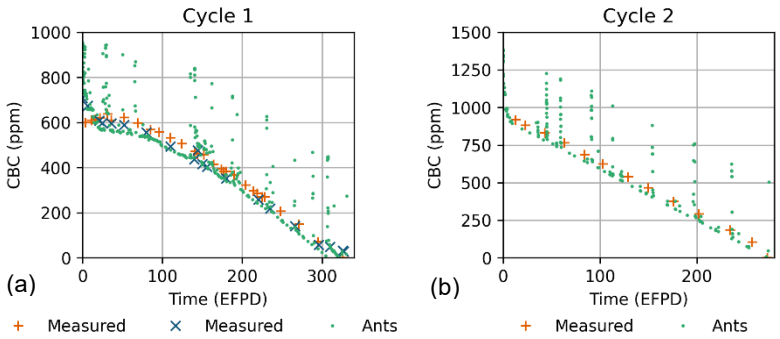

Figure 15. The measured boron letdown curves for the two cycles of the BEAVRS benchmark and prediction by the Ants-based calculation sequence of Kraken.

Figure 15 shows the measured and calculated boron letdown curves for the two operating cycles. The complex operating power history can be clearly seen as many periods of reactor shutdown and low power operation reflected as higher spikes in the momentary critical boron conditions calculated by Ants. The agreement between Kraken and the measured critical boron concentrations (CBCs) is very good, albeit Kraken tends to underpredict the CBC by a small fixed margin, which is not too concerning considering the experimental and modelling uncertainties present.

As noted earlier, critical boron concentrations are a global parameter that may be quite easy to match with experimental data by accident. The benchmark also includes actual detector maps measured from the core at different assemblies at various points over the two operating cycles. This data contains additional uncertainties, with several maps being measured during changing power, boron, control rod and xenon conditions and the measurement data showing a large diagonal tilt over the reactor core especially during the first operating cycle. The occurrence of such a tilt in a generally symmetric core is not explained in the benchmark, which is why it also includes detector data, from which the tilt has been corrected in postprocessing and this data is typically used in the validation of reactor simulators using symmetric reactor models.

As the detector measurements contain many sources of uncertainties, the results of current industry and scientific leaders such as Studsvik Scandpower using CMS5], UNIST using a reactor simulator based on the STREAM neutron transport code and Los Alamos National Laboratory using the VERA core simulator developed in the DoE CASL project were used as reference points when estimating the performance of Kraken in predicting detector maps.

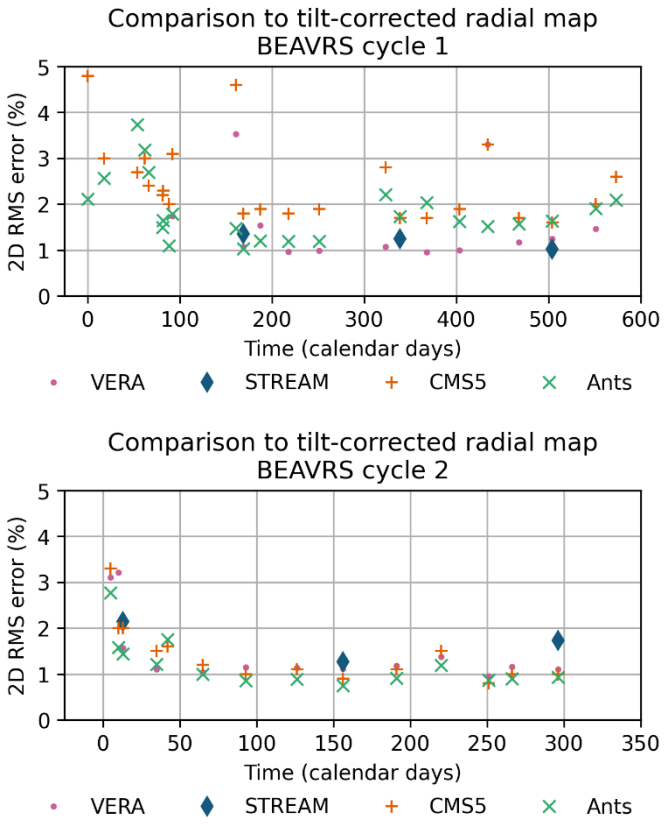

Figure 16. The 2D RMS errors when comparing calculated results to measured detector maps. Various industry and scientific leaders and Kraken (Ants).

The 2D RMS errors in the detector map predictions are shown in Figure 16 for VERA, STREAM, CMS5 and Kraken (Ants). It is evident that Kraken predicts the 2D detector map with the same level of accuracy as the current industry leader CMS5 and performs favourably against neutron transport codes such as STREAM and VERA even though the nodal diffusion used by Ants in this study cannot, by definition, resolve the neutron flux to the same fidelity as transport solvers.

The results of this BEAVRS validation should still be considered preliminary and are being collected into a journal article which will also include comparisons against the 3D maps reconstructed from the detector measurements. Nevertheless, even these initial results show that Kraken is not simply a research tool but offers an actual reactor core simulator that can be applied to real operating reactors with good expectations for the accuracy of the computational predictions.

Summary

In two years, the Kraken framework has evolved from an idea on paper and a few individual solvers to a full-fledged reactor core simulator that can model actual operating cycles of real reactors with a level of accuracy comparable to current industry leaders. In addition to a significant development effort, the demonstration and validation of Kraken has also been in forefront of the LONKERO project.

In addition to developing the framework as a whole, LONKERO has focused on the extending the nodal neutronics solver Ants with all of the capabilities required to achieve such coupled simulations. Some more specific research topics have also been visited such as the implementation of microdepletion capabilities in the Serpent-Ants calculation chain, which can be used to predict the concentrations of individual nuclides in individual materials (fuel, cladding, etc.) in the Ants nodal neutronics code even though such material information is generally homogenized out of the nodal models.

The first two years of LONKERO can be considered to achieve the ambitious goals set in the project plan, which raises the expectations for the latter two years that focus on transient modelling without and with coupling to system codes.

4.4 Radiation shielding and criticality safety analyses (RACSA)

Pauli Juutilainen, Eric Dorval, Silja Häkkinen

VTT Technical Research Centre of Finland Ltd
P.O. Box 1000, FI-02044 Espoo

Abstract

The scope of the RACSA project contains applications related to particle transport outside of the actual reactor core. More accurately, it covers photon transport for radiation shielding applications, reactor dosimetry and criticality safety. The focus with the photon transport has been on the validation process of the previously developed functionalities in the Serpent Monte Carlo code. The capability of Serpent to model complicated geometries, such as laboratory facilities, has also been further tested.

Reactor dosimetry capabilities are being continuously extended and improved. Validation has been a major part of dosimetry efforts too, as an ambitious verification and validation effort has been undertaken by calculating both computational and experimental benchmark problems in accordance with the guidelines of the U.S. NRC Regulatory Guide 1.190. A total of 2 calculational and 3 experimental problems were modelled, yielding very satisfactory results. Modelling of these problems required copious amounts of coding work, in combination with the use of Serpent's built-in variance reduction techniques. Moreover, work was started on the development of a brand-new transport solver specially conceived for the needs of practical reactor dosimetry.

Considering the criticality safety, the long-time process to construct a validation package for fresh fuel criticality safety analyses has continued. In addition to increasing the number of modelled critical experiments, a similarity evaluation tool based on sensitivity and uncertainty analysis methodology has been implemented for Serpent. It should facilitate the selection of suitable cases for each validation run. The suitability of Serpent for burnup credit applications has also been improved.

Introduction

The radiation shielding in the project name refers to both analyses of human exposure of ionising radiation and reactor dosimetry, in which the tolerance of the reactor pressure vessel and other components close to the reactor core are exposed to high-energy neutron irradiation. Criticality safety studies, comprising the third pillar of the project, focus on ensuring that the nuclear fuel never goes critical. The common factor of these fields is particle transport outside of reactor core, even though the practical computational methods required in modelling them may vary rather significantly. However, the effort put to the development of the Serpent Monte Carlo

code (Leppänen et al, 2015a) over the years in various research projects has made the code capable of modelling all these phenomena to varying extent. In addition to the mere development, these features should also be validated, which is one of the major objectives of the RACSA project. Currently, validation effort is particularly required for the photon transport and dosimetry functionalities, as well as fuel depletion calculations for criticality safety analyses requiring the use of burnup credit.

In terms of radiation shielding, photon transport model is needed when exposure to gamma radiation is evaluated in a given configuration of radiation source and shielding elements. It is also needed in the energy deposition modelling, but it is outside the scope of RACSA activities. Practically all the physical phenomena affecting the photon transport had been implemented before SAFIR2022 programme began, but little validation had been done. In order to fill the gap, two sets of gamma shielding benchmarks with experimental data have been calculated.

The capability of Serpent to model complex geometries has been tested with the hot-cells of the VTT Centre for Nuclear Safety (CNS) as a demonstration environment. The capability of reading CAD-based geometry model and utilize the variance reduction techniques in the transport calculation are the Serpent features at specific test in such calculations.

During the previous SAFIR programme, the reactor dosimetry activities were strongly labelled by changes in personnel, due to which the work on the topic mainly aimed at building new expertise. However, along with that, the usability of some legacy tools were improved. Additionally, the first test with Serpent for dosimetry applications were conducted. In the RACSA project, the focus has been strongly on validating Serpent for the dosimetry applications. Work for a new, reduced-order deterministic dosimetry code has been initiated. The purpose of such a code is to allow faster calculations than Monte Carlo codes can perform, for situations in which the ultimate accuracy is not the primary objective.

The validation package for criticality safety analyses has been under development over several years. Its purpose is to enable the user to define the systematic bias between the computational platform and the real world such that a sufficient computational safety margin can be defined for a target configuration whose subcriticality must be ensured. In practice, this requires a large number of benchmark critical experiments modelled for the code to be used. Additionally, tools are required to run and process the modelled cases and select the most suitable ones for each validation run, as the experiments should be neutronically similar to the target application. The package has been constructed for Serpent and MCNP (Werner et al, 2018).

Utilizing the concept of burnup credit, or taking into account the reduced reactivity of irradiated fuel, requires validation of the fuel depletion calculation and the criticality calculation of the irradiated fuel in its storage configurations. These are somewhat more difficult tasks than the validation suite for fresh fuel configurations, since much less applicable experimental data is available. In order to improve the usability of Serpent for such analyses, the impact of the uncertainties in nuclear fission yield and decay data on the criticality calculations of a spent fuel configuration has been assessed.

Radiation shielding

The implementation of a photon transport mode in the Serpent Monte Carlo code first began outside of the SAFIR projects with the original target to account for gamma heating in coupled multi-physics simulations (Leppänen et al, 2015b). Since then, the photon transport mode has been developed to the level where it is capable of modelling all the relevant photon interactions, related to primary and secondary gamma radiation (Kaltiaisenaho, 2020a).

As an important part of shielding applications, variance reduction methods have been implemented to Serpent (Leppänen, 2019). Also known as non-analog Monte Carlo method, such methodology is practically necessary when the particle population differs significantly in various parts of the modelled configuration. This is obviously the case or at least the primary and only target of all shielding configurations. The reactor dosimetry (more on it below) is an other field of applications where variance reduction tehcniques are required.

The method development has been mostly frozen in the RACSA project and the focus has been on validating and testing these previously developed functionalities. In case of gamma transport, the validation efforts have been based on the shielding benchmark presented in the Shielding Integral Benchmark Archive Database (SINBAD, Kodeli et al, 2006) and International Criticality Safety Benchmark Evaluation Project (ICSBEP, OECD/NEA 2019).

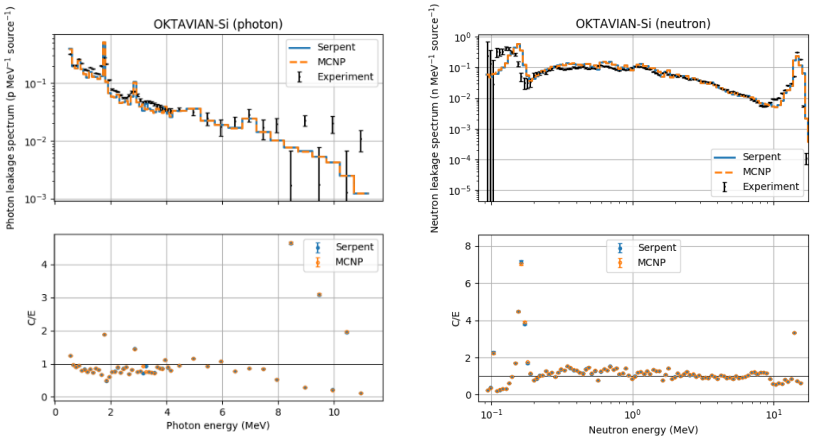

Figure 1. Photon (left) and neutron (right) leakage spectra in silicon shielding. The flux are presented in figures above, and the C/E ratios below.

The coupled neutron-photon transport mode was applied when the OKTAVIAN benchmark from SINBAD was calculated (Kaltiaisenaho, 2020b). The OKTAVIAN facility uses the D-T fusion reaction to generate neutrons with an energy distribution peaking at around 14 MeV. In order to create the neutron beam, the deuterons were

accelerated and driven into a solid titanium–tritium target, which was placed at the centre of the spherical material assemblies. These various materials acted as shield and the leakage of neutrons and photons through it was measured. The experiments were computationally repeated with Serpent 2.1.32 and MCNP-6.2 (Werner et al, 2018). ENDF/B-VII.1 neutron cross-section data was used. In all cases the agreement between the codes was rather good, but when compared to the experimental results, the agreement strongly depended on the shielding material. As an example, neutron and photon spectra in silicon and the related calculated vs. measured ratios are depicted in Figure .

Serpent's photon transport and coupled neutron-photon transport routines have been further validated by calculation of two benchmarks ALARM-CF-FE-SHIELD-001 and ALARM-CF-PB-SHIELD-001 (Häkkinen, 2020). The benchmarks describe measurements of a Cf-252 source through six different sized iron (radius 10 - 35 cm) and three different sized lead (radius 10 - 30 cm) spheres. Photon and neutron spectra were calculated at 3R distance from the source with a development version of Serpent 2.1.32 and MCNP6.2, where R is the sphere radius. Serpent calculations were compared to MCNP calculations and measurement results. The Serpent and MCNP calculations applied the same neutron cross section files, namely ENDF/B-VII.1, but the Serpent calculations were also repeated with thew JENDL-4.0 cross sections in order to see the effect of cross section library on the results. The photon libraries used in Serpent and MCNP calculations were both based on ENDF/B-VII.1. As an example of the results, Figure 2 and Figure 3 present the neutron and photon spectra through a 20 cm radius iron sphere and the difference between Serpent calculations and measurement results (C/E) with measurement uncertainties.

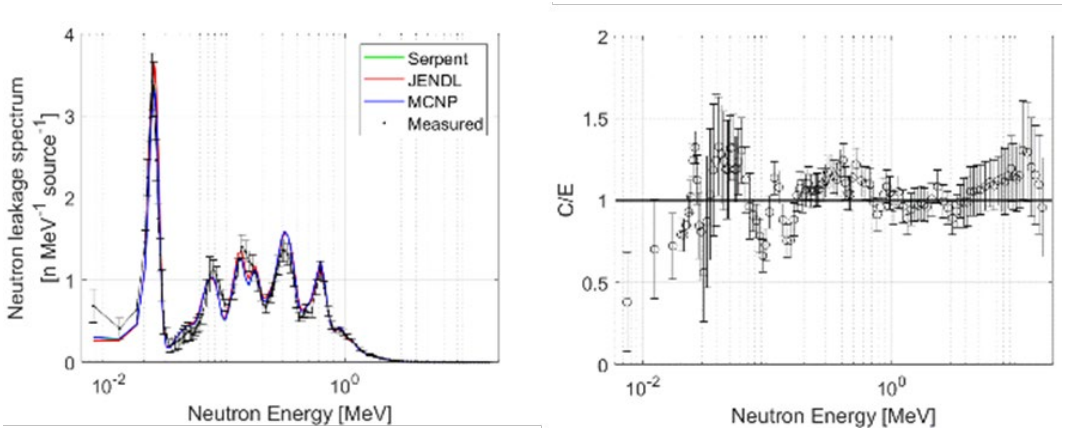

Figure 2. Neutron spectrum through a 20 cm radius iron sphere. JENDL stands for Serpent calculations with JENDL-4.0 cross section library.

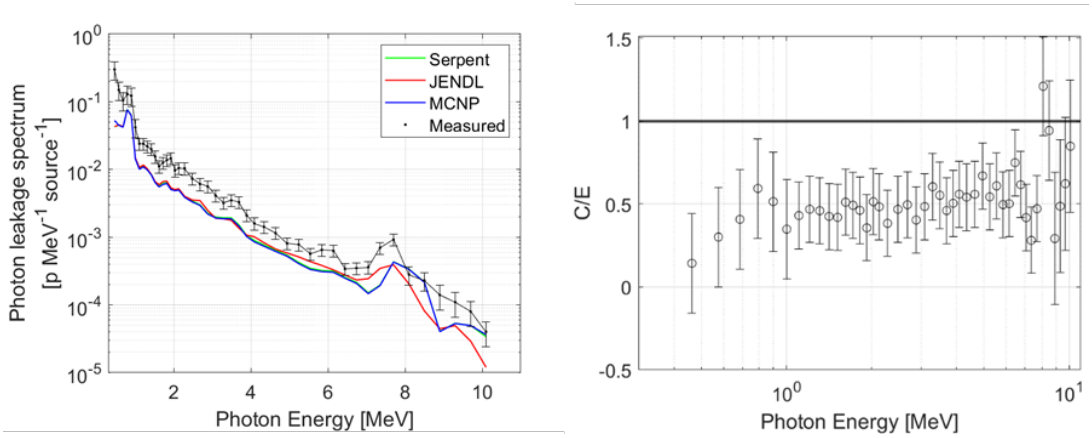

Figure 3. Photon spectrum through a 20 cm radius iron sphere. JENDL stands for Serpent calculations with JENDL-4.0 cross section library.

Overall, the Serpent calculated spectra followed the shape of the measured spectra fairly well. For the iron spheres, the neutron spectrum calculated by Serpent and MCNP results agreed mostly within 2 % below 4 MeV and the photon spectrum mostly within 3 %. For the lead spheres, the neutron spectrum calculated by the two codes agreed mostly within 1.5 % with energies 0.04–4.0 MeV. Differences in the photon spectrum through the 10 cm radius lead sphere were mostly below 5 % and for the larger spheres below 10 % except at higher photon energies above 6.5 MeV. The neutron cross section library had a clear effect on the results.

The currently distributed Serpent version 2.1.31 was also compared to the development version (Häkkinen, 2021). The differences between the two versions were mostly related to Gaussian Energy Broadening which was performed with the development version but is not possible in the currently distributed Serpent version. Some differences of the order of 3 % between the photon spectra of the two Serpent versions were observed for the two larger lead spheres with radius 20 and 30 cm. This may be related to differences in the coupled neutron-photon transport routines in the two code versions. The photons through the largest lead spheres are almost entirely born in neutron reactions in the lead sphere.

The applicability of Serpent for shielding analyses in complex geometries such as laboratories and power plant areas has been tested using the sample storage vault of the VTT CNS hot-cell as a demonstration case. The calculations will be published in a conference paper (Leppänen and Jokipii, 2021). A CAD model was constructed on the geometry and imported to Serpent. In addition to calculations, dose rate measurements were performed, with the photons emitted from Co-60 and Mn-54 sources. Since the conference is yet to come, the results are not presented here into more detail than it turned out that with the applied accuracy of material properties, geometry description and detectors the disagreement between the calculations and the measurements was generally rather significant. Valuable

information was also obtained on the performance of the global variance reduction (GVR) methodology in heavy shielding configurations.

Reactor dosimetry

In the field of reactor dosimetry, previous years have been characterized by changes in personnel and the subsequent need to train new recruits in a vast field that spans over experimental as well as computational aspects. In the computational domain, the main training goal has systematically been to get up to speed with the use of legacy computer programs used for activation and neutron fluence calculations, such as PREVIEW (Wasastjerna, 1991), or for spectrum adjustment, such as LSL-M2 (Stallman, 1986).

Once the required skills in the use of these legacy codes were acquired, it became repeatedly evident that new approaches to training new dosimetry practitioners should be adopted. On one hand, although source-code-level understanding is needed for maintenance purposes, several old legacy codes are not easily accessible to new practitioners. On the other hand, continuously increasing computing capabilities have promoted the development of modern computer codes which are also finding their way into the reactor dosimetry domain. In particular, the Monte Carlo code Serpent 2 (Leppänen et al, 2015a) has extended its scope of applications to reactor dosimetry (Viitanen and Leppänen, 2016) thanks to the incorporation of new variance reduction techniques (Leppänen et al, 2016, Leppänen, 2019).

Prior to the widespread use of Serpent 2 for dosimetry applications, it needs to be verified and validated. The verification is carried out in the form of code-to-code comparisons, whereas the validation is carried out by calculation of experimental dosimetry benchmarks. It was decided to carry out this effort following well established guidelines (U.S. NRC, 2001). A total of seven benchmark problems were identified for validation purposes in RACSA. Most benchmark specifications were sourced from the SINBAD database (Kodeli et al, 2006).

In spite of the high accuracy of modern Monte Carlo codes, considerable running times are still needed in order to attain low statistical uncertainties. In several cases, this consideration makes them not directly suitable for the modelling of long and complex irradiation histories. In such irradiations, spatial and spectral changes in the neutron source (as well as possible depletion of activation products) need to be captured via time-dependent calculations. In an attempt to preserve much of the accuracy of Serpent whilst exploiting the fast running times associated with deterministic methods, a hybrid approach will be adopted in RACSA. The rationale is to generate integral response data with Serpent 2 in the form of multi-group response matrices. This data is then read and put to use in a dedicated deterministic solver, to be developed from scratch.

International cooperation in the field of reactor dosimetry mainly takes place in the form of participation in meetings periodically organized by the European Group on Reactor Dosimetry (EWGRD), as well as in the International Symposium on Reactor Dosimetry (ISRD), organized by the same Committee.

Validation of Serpent for dosimetry applications

Four benchmarks were calculated. A related manuscript was prepared (Dorval, 2020a), and accepted for participation in the ISRD-17. Originally envisaged to be held in May 2020, the Symposium was postponed due to the Covid-19 pandemic. In consequence, the results to be presented there cannot be reproduced in this report before the Symposium is held. Instead, modelling details and general indications about the overall quality of the results will be provided here.

Two computation benchmark models were used for verification purposes. The original models were developed for the MCNP code (Pelowitz, 2003), and kindly facilitated by one of the original authors. Both models correspond to 3-D PWR cores with standard core loading pattern (STD), and partial length shield assemblies (PLS). The neutron source was specified in the form of pin-wise, energy- and height-dependent distributions. The representation of this, as well as other complex fixed sources to be used throughout the validation of Serpent 2, necessitated the development of a new, flexible, 2-level, geometry-agnostic neutron source routine. The main features of the neutron source options implemented are given in Table 1.

Table 1. Fixed neutron source options available in the new routine.

1st level (assembly)	2nd level (pin)	Pin type	Axial	Angular	Energy
Cartesian, hexagonal	Cartesian, hexagonal	Square, (hollow) cylindrical, rectangular, (bent) MTR plate	Piece-wise constant	isotropic	Histogram, Watt fission spectrum, Maxwell fission spectrum

Several alternatives were explored in Serpent for the transport of fission neutrons to the reactor pressure vessel: cell importances with energy cut-off, weight windows, and a combination of weight windows with delta-tracking and peripheral assembly simplifications. Although all modelling approaches yielded similar results (and, in particular, in excellent agreement with MCNP), the adoption of a simplified geometry, combined with delta-tracking and weight windows was remarkably more computationally efficient. This was enabled by the development of the new source routine, which is completely independent of the underlying problem geometry.

The other two benchmarks to be presented in ISRD-17 are experimental, namely Pool Critical Assembly-Pressure Vessel Facility (PCA); and the H.B. Robinson-2 (HBR-2) Pressure Vessel Dosimetry Benchmark. Both models are 3-D, but in particular the latter is particularly challenging given the complexity of the geometry, the time-dependent neutron source; and the need to compute ex-vessel activation results, which pose a severe challenge for the variance reduction techniques. The importance maps generated by Serpent for these benchmarks are presented as superimposed tones ranging from blue (low importance) to red (high importance,

where the activation detectors are located), as depicted in Figure 4 and Figure 5. Also due to the postponement of ISRD-17, the final results cannot be published yet. The agreement with experiment was very satisfactory.

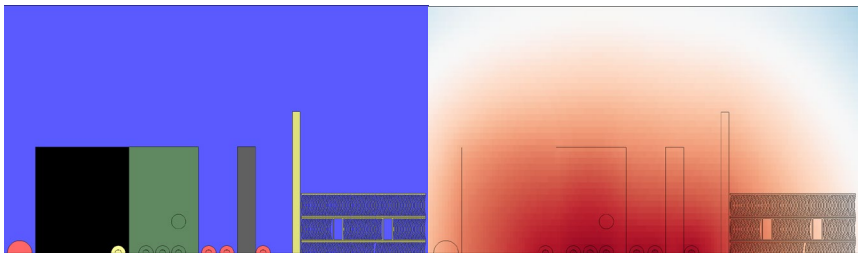

Figure 4. PCA benchmark geometry (left) and superimposed importance map (right).

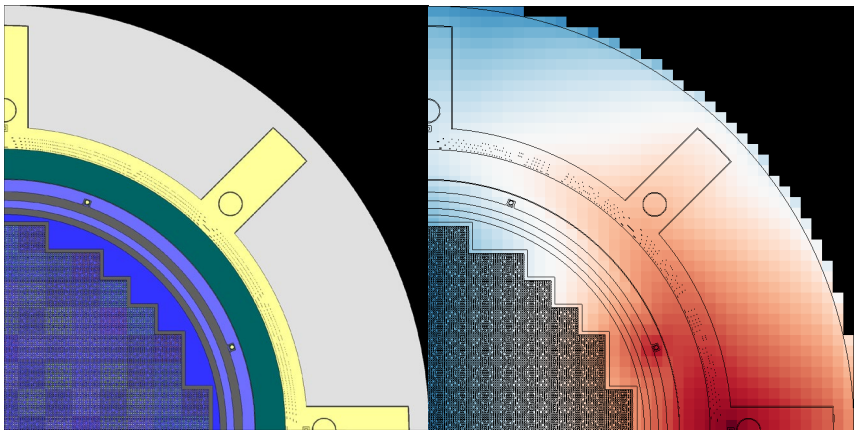

Figure 5. HBR-2 benchmark geometry (left) and superimposed importance map (right).

A fifth benchmark problem was calculated with Serpent in 2020, namely NESDIP-2. This (experimental) facility features a conversion plate attached to the beam line of the NESTOR research reactor. The facility and results of the benchmark are presented in Figure 6.

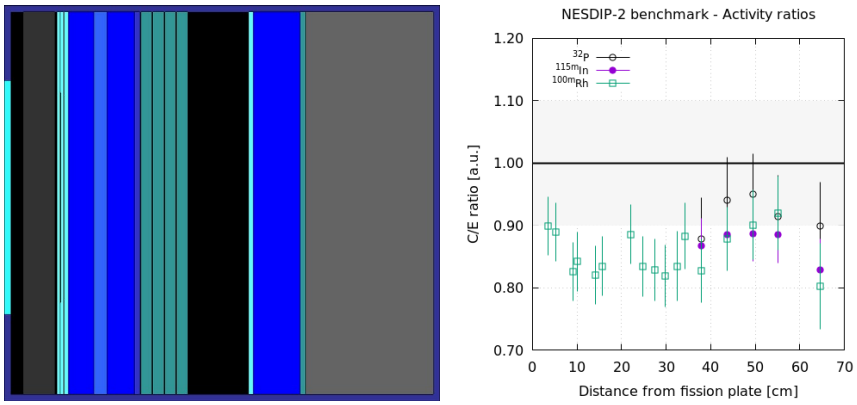

Figure 6. Top view of the NESDIP-2 facility (left) and calculated-to-experimental ratios (right) for different reactions at several distances from the conversion plate.

The C/E ratios in Figure 6 are systematically below unity. This result, however, is consistent with other work (Milocco et al, 2013) which points to the fact that the absolute calibration used in fission source determinations.

Pertaining the development of the new solver for reactor dosimetry applications, a response-matrix formalism was chosen, and all the necessary routines for the generation of response-matrix data were already implemented in Serpent 2 and documented (Dorval, 2020b). As schematized in Figure 7, the rationale is to decompose a dosimetry problem domain into a series of single nodes coupled by interface currents. Every node has its own embedded mesh. This mesh can be of different types, and in practice is chosen in order to capture the main geometrical features of the reactor model.

A new dedicated solver is being developed. This deterministic solver reads the data generated by Serpent at node level (in three dimensions), and takes care of coupling currents and solving both local (node-wise) and global (core-wise) problems for time-dependent neutron sources supplied as snapshots along an arbitrary irradiation history. The development of this solver is the main focus of the 2021 dosimetry task in RACSA. It is expected that at some point the same benchmark problems calculated with Serpent can be exploited towards the validation of the new solver.

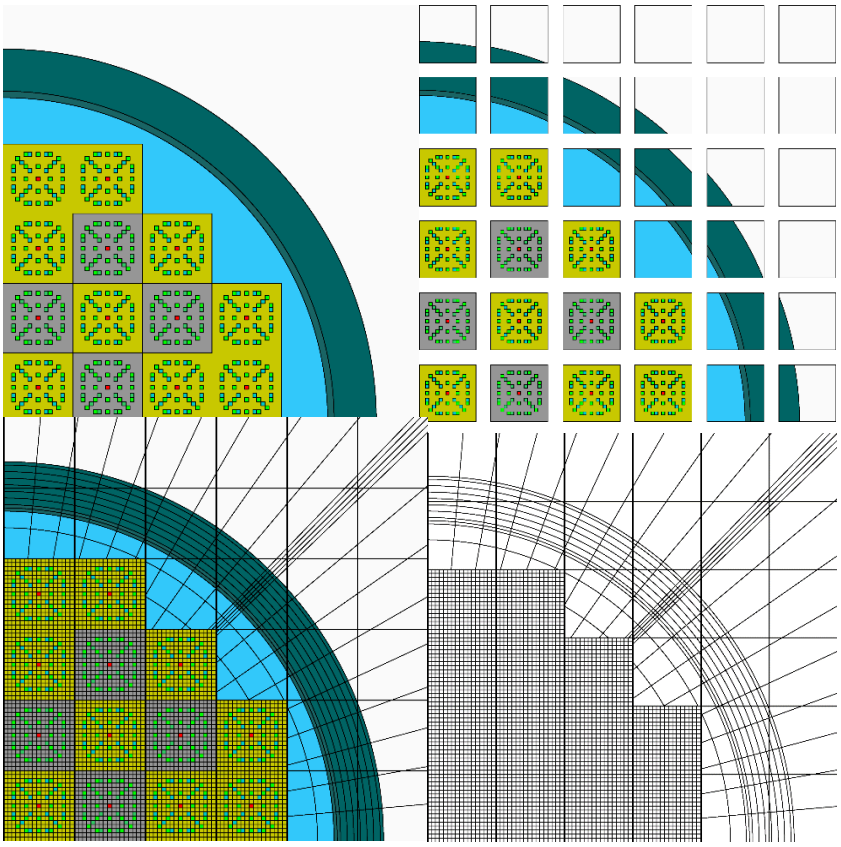

Figure 7. Partition of a problem domain (top left) into blocks connected by interface currents (top right). By application of a mesh-in-box concept at node level, the original prob-lem is solved onto a computational mesh (bottom left) which is chosen in order to capture the main geometrical features of the model (bottom right).

Criticality safety

The activities related to criticality safety conist of the construction of the validation package for analyses with fresh fuel or reasonable fresh-fuel assumption and developing capabilities to utilize burnup credit in criticality safety studies concerning spent fuel.

The validation package has been constructed for Monte Carlo codes Serpent and MCNP in order to make them applicable tools for criticality safety analyses. The package is required when a criticality safety analysis is to be done for a given target application using either of the two codes in order to determine the systematic bias of the computing platform. The concept of platform in this case covers the

combination of the code and the cross-section data library versions, as well as the hardware and operating system as minor components to be calibrated.

In order to determine the bias, a large number of critical experiments, documented in the ICSBEP Handbook (OECD/NEA, 2019), needs to be modelled for the code that is to be used. It is a time-consuming task to carefully write such a large set of inputs modelling each experiment, even though the work has been contributed by a few partner organizations from which VTT has received a considerable amount of inputs. However, the generally accepted guidelines and regulations state that no inputs from other organisations should be taken into use without review, which somewhat limits the benefit of obtaining inputs from elsewhere.

In addition to the number of experiments, the diversity of the host facilities matters, as the experiments should be as independent of each other as possible. The requirement reduces the effective size of the package to some extent, since many of the experiments have been performed in a relatively small group of research facilities. Moreover, the experiments used for validation should be similar to the target application in terms of the neutronic environment.

Over the previous SAFIR programmes, the main emphasis has been in constructing new inputs (or reviewing those obtained from other organisations) and a Perl script has been written to run the calculations and perform the statistical post-processing for the selected cases. Previously, the selection of suitable cases was merely based on the guidelines, such as (Dean and Tayloe, 2001), which ultimately relied on expert judgement.

During the RACSA project, sensitivity and uncertainty (S/U) method -based approach has been studied. The approach is based on the assumption that the experiment and application are similar to each other, if the multiplication factor k_{eff} is similarly sensitive to same nuclear data perturbations. The similarity is evaluated with the correlation coefficient c_k: the closer to unity it is, the more similar the cases are. The evaluation of c_k is based on the sensitivity profiles of each configuration for all relevant combinations of nuclides and reaction types (fission, capture, fission neutron yield, etc.) and the uncertainty estimation of the nuclear data provided in the covariance data libraries. The same sensitivity evaluation methodology is used in MCNP (Kiedrowski et al, 2011) and Serpent (Aufiero et al, 2015).

First, such studies were performed with the recently acquired MCNP-6.2 package (Werner et al, 2018) that contains a criticality safety analysis tool called Whisper (Kiedrowski et al, 2015), including a set of MCNP inputs for criticality safety experiments from ICSBEP Handbook. Using the sensitivity evaluation functionality of MCNP, Whisper ranks the modelled experiments to similarity order against the target application and selects a suitable number of experiments that are finally used to define the computational safety margin. The suitable number in this context depends on the similarity level of the available experiments.

Whisper also has a functionality to identify the experiments that might be of lower quality in terms of experimental accuracy and evaluated uncertainty in k_{eff}. However, it is emphasised in the literature that the method is not fully error-proof, but it can suggest high-quality benchmark to be excluded and lower-quality cases accepted.

Therefore, the traditional benchmark rejection methods utilizing trend analysis with respect to various parameters should still be kep in the toolbox.

The similarity evaluation was also implemented to function with Serpent (Juutilainen and Valtavirta, 2021). As mentioned above, sensitivity evaluation functionality has been previously implemented to Serpent (Aufiero et al, 2015), but some effort was required to make it compatible with the covariance data file. The test calculations were made with the same SCALE 44-group covariance data based on ENDF/B-VII.0 as used by the MCNP-Whisper sequence. Since the methodology and covariance data are the same, Serpent and Whisper should produce c_k's close to each other when compared to the same target application which was a VVER-1200 assembly in these studies. Figure 8 shows that when compared the experiments that have an input for both MCNP and Serpent, the relative difference in c_k's was mostly below 1 %. It can be seen that for a few individual experiments the relative difference is larger, which suggests that the input models are not equal and should therefore be examined to detect the likely-existing errors (to be done later in the project).

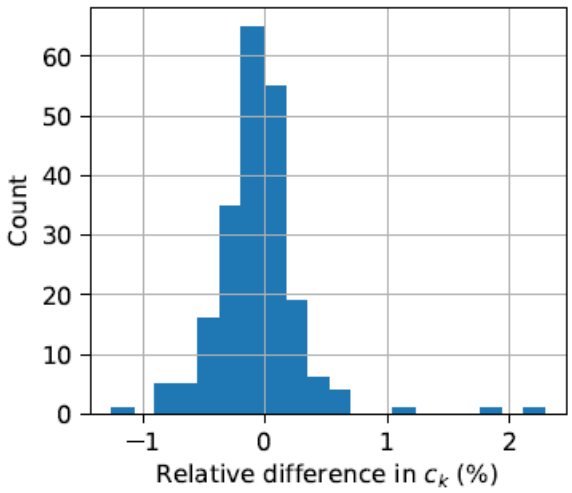

Figure 8. Histogram of relative differences of correlation coefficients determined by Serpent and MCNP-Whisper -sequence (Serpent/MCNP - 1)*100 %

Some work has also been performed to improve the suitability of Serpent for criticality safety analyses with burnup credit. When the decreased reactivity of irradiated fuel is to be credited, the calculations contain some additional uncertainties compared to criticality safety analyses for spent fuel and they must be accounted for in the analysis. The work in RACSA so far has concentrated on the uncertainties in burnup calculation due to the uncertainties in nuclear data.

More accurately, a study was performed to determine the impact of nuclear fission yield and decay data uncertainties on the criticality of spent fuel (Juutilainen,

2020). Burnup calculation was performed for a VVER-440 assembly with a small amount of burnable absorber (Gd) in an infinite 2D geometry. In these calculations, a new fission yield and decay data sampling method implemented to Serpent was used (Rintala, A. 2020). The calculations were repeated 300 times. All of these rounds used fission yield and decay data sampled in the beginning of the calculation. The sampling is based on the estimated uncertainty of the data provide in the library. Log-normal distribution is assumed for the uncertainty.

Following the burnup calculations, the multiplication factor k_{eff} was calculated at several decay steps up to millions of years. The decay period was calculated for all 300 variations of sampled nuclear data in an infinite 2D geometry, where the spent fuel assembly was surrounded by layers of iron copper and water, thus mimicking the final disposal conditions. The calculations were performed for discharge burnup levels from 5 to 20 MWd/kgU, since the low-burnup fuel is naturally the limiting factor in criticality safety studies. One of the notable features in final disposal criticality safety assessments is the fact that after the initial decrease in the spent fuel reactivity, the fraction of fissile nuclides increases over the first few tens of thousands of years so that care is needed to find the moment for the maximum k_{eff}. Figure 9 provides an example of the k_{eff} curve family and the histogram of k_{eff} values at the reactivity top roughly 20,000 years after the end of irradiation, when the discharge burnup was 10 MWd/kgU. Generally, the k_{eff} deviation understandably increased along with higher discharge burnup.

Another Serpent burnup calculation performed within the RACSA project is related to the benchmark planned by the OECD/NEA Working Party of Nuclear Criticality Safety (WPNCS). The benchmark has not been officially started, but Serpent was used to calculate the exercise with the drafted specifications, based on a 15 x 15 assembly with 4.1 wt-% UO_2 fuel and without any burnable absorbers. Infinite 2D geometry is assumed and a slightly simplified irradiation history is applied. A plain fuel depletion calculation has been planned for the first phase of the benchmark, whilst the impact of nuclear data uncertainties are supposed to be considered in the later phase. So far, similarly to the above-described case, nuclear fission yield and decay data sampling has been applied for Serpent calculations and repeated 300 times. Additionally, 20 repeated calculations have been performed to account for the statistical uncertainty of the Monte Carlo method. As an ultimate goal of the benchmark, also the impact of cross-section data uncertainties are going to be studied. This is yet to be done with Serpent.

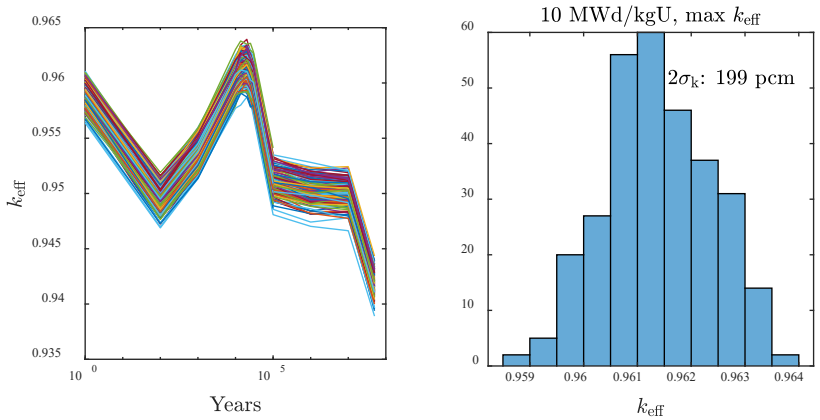

Figure 9. Following the discharge burnup of 10 MWd/kgU, 300 k_{eff} curves with sampled nuclear data as a function of time (left) and the distribution of k_{eff} values at the reactivity peak 20,000 years after discharge (right).

References

Aufiero, M., Bidaud, A., Hursin, M., Leppänen, J., Palmiotti, G., Pelloni, S. & Rubiolo, P. 2015. A collision history-based approach to sensitivity/perturbation calculations in the continuous energy Monte Carlo code SERPENT. Annals of Nuclear Energy. Volume 85. Pages 245-258. 2015. https://doi.org/10.1016/j.anucene.2015.05.008.

Dean, J. C. and Tayloe, R. W. 2001. Guide for Validation of Nuclear Criticality Safety Calculational Methodology. Technical report, U.S. Nuclear Regulatory Commission, 2001.

Dorval, E. 2020a. Validation of the Serpent 2 Monte Carlo code for reactor dosimetry applications. Abstract accepted for participation in the 17th Symposium on Reactor Dosimetry (ISRD-17), Lausanne, Switzerland. Postposed due to the Covid-19 pandemic.

Dorval, E., 2020b, On the generation of reponse-matrix data with Serpent 2. VTT Research report VTT-R-01489-20.

Häkkinen, S. 2020. Serpent 2 Validation for Radiation Shielding Applications. 29th International Conference Nuclear Energy for New Europe. September 7-10, 2020. Portoroz, Slovenia.

Häkkinen, S. 2021. Serpent 2 Validation for Radiation Shielding Applications. Submitted to Journal of Nuclear Engineering and Radiation Science.

Juutilainen, P. 2020. Impact of the fission yield and decay data uncertainties on the multiplication factor after irradiation. VTT Research report VTT-R-00251-20.

Juutilainen, P., Valtavirta, V. 2021. Status of the criticality safety validation package in 2020. VTT Research report VTT-R-00179-21.

Kaltiaisenaho, T. 2020a. Photon transport physics in Serpent 2 Monte Carlo code. Computer Physics Communications. Volume 252. https://doi.org/10.1016/j.cpc.2020.107143.

Kaltiaisenaho, T. 2020b. Validation of the coupled neutron-photon transport in Serpent 2 with OKTAVIAN benchmarks. VTT Research report VTT-R-00005-20.

Kiedrowski, B.C., Brown, F.B. & Wilson, P.P.H. 2011. Adjoint-Weighted Tallies for k-Eigenvalue Calculations with Continuous-Energy Monte Carlo. Nuclear Science and Engineering, 168(3):226–241, 2011.

Kiedrowski, B.C., Brown, F.B., Conlin, J.L., Favorite, J.A., Kahler, A.C., Kersting, A.R., Parsons, D.K., & Walker, J.L. 2015. Whisper: Sensitivity/Uncertainty-Based Computational Methods and Software for Determining Baseline Upper Subcritical Limits, Nuclear Science and Engineering, 181:1, 17-47, DOI: 10.13182/NSE14-99

Kodeli, I., Sartori, E. & Kirk, B. 2006. SINBAD - Shielding Benchmark Experiments - Status and Planned Activities, Proceedings of the ANS 14th Biennial Topical Meeting of Radiation Protection and Shielding Division, Carlsbad, New Mexico (April 3-6).

Leppänen, J., Pusa, M., Viitanen T., Valtavirta, V. & Kaltiaisenaho, T. 2015a. The Serpent Monte Carlo code: Status, development and applications in 2013. Ann Nucl Energy, 82:142–150.

Leppänen, J., Hovi, V., Ikonen, T., Kurki, J., Pusa, M., Valtavirta, V. and Viitanen, T. 2015b. The Numerical Multi-Physics project (NUMPS) at VTT Technical Research Centre of Finland. Ann. Nucl. Energy, 84 (2015) 55-62.

Leppänen, J., Viitanen, T. & Hyvönen, O. 2017. Development of a Variance Reduction Scheme in the Serpent 2 Monte Carlo Code. Proceedings of M&C 2017 - International Conference on Mathematics & Computational Methods Applied to Nuclear Science & Engineering, Jeju, Korea, April 16-20, on USB.

Leppänen, J. 2019. Response Matrix Method–Based Importance Solver and Variance Reduction Scheme in the Serpent 2 Monte Carlo Code. Nucl Technol, 205:1416–1432.

Leppänen, J., Jokipii, M. 2021. Radiation Shielding Calculations at VTT Centre for Nuclear Safety Using the Serpent 2 Monte Carlo Code. Submitted to ANS M&C 2021 - The International Conference on Mathematics and Computational Methods Applied to Nuclear Science and Engineering. Raleigh, North Carolina. October 3–7, 2021.

Milocco, A., Trkov, A. & Kodeli, I. 2013. Quality Assessment of Evaluated Experiments Nesdip-2, Nesdip-3, Janus-1, Janus-8. 22nd International Conference Nuclear Energy for New Europe, Slovenia.

OECD/NEA. 2019. International Handbook of Evaluated Criticality Safety Benchmark Experiments. NEA/NSC/DOC(95)03.

Pelowitz, D. (Ed.). 2013. MCNP6^{TM} User's Manual, LA-CP-13-00634 Rev. 0.

Stallman, F. 1986. LSL-M2: A Computer Program for Least-Squares Logarithmic Adjustment of Neutron Spectra. Technical Report NUREG/CR-4349, Oak Ridge National Laboratory. (Additional unpublished manual provided with version 2.0).

U.S. NUCLEAR REGULATORY COMMISSION (NRC), 2001. Regulatory Guide 1.190 - Calculational and dosimetry methods for determining pressure vessel neutron fluence.

Viitanen, T. & Leppänen, J. 2016. Calculating Neutron Dosimeter Activation in VVER-440 Surveillance Chains with Serpent. 26th Symposium of AER on VVER Reactor Physics and Reactor Safety, Helsinki.

Wasastjerna, F. 1991. PREVIEW, a Program for Calculation of Pressure Vessel Irradiation in the Loviisa Reactors. VTT Technical Report YDI110/91.

Werner, et al. 2018. MCNP6.2 Release Notes. Los Alamos National Laboratory. Report LA-UR-18-20808 (2018).

4.5 Enhanced multi-physics calculation capabilities for fuel behaviour and reactor analyses (EMBER)

Ville Rintala, Heikki Suikkanen

LUT University
P.O. Box 20, FI-53851 Lappeenranta

Abstract

The recently developed coupled neutronic and fuel performance calculation capabilities at LUT University are extended within EMBER to obtain a comprehensive, yet light-weight calculation framework for multi-physics reactor analyses. During the planned duration of three years, the project aims to deepen the level of the current coupling between neutronics, burnup and fuel behaviour, complete the framework via integration of a core thermal hydraulic solver and finally establish transient analysis capabilities. During the first year of the project, coupling between the Monte Carlo neutronics solver Serpent and the fuel behaviour solver TRANSURANUS was extended with the possibility to use nuclide concentrations calculated by Serpent in TRANSURANUS as part of the coupled calculation. Necessary modifications and additions were implemented to the coupled calculation driver program Kytkin and a new nuclide data interface was developed and implemented in TRANSURANUS to allow reading-in external nuclide information. The functioning of the nuclide interface was verified with a test calculation.

Introduction

Computer codes applied for reactor design, operation and safety analyses aiming to accurately predict the behaviour of a reactor need to account for the relevant feedbacks between the various processes, including core neutronics and burnup, thermal hydraulics and fuel behaviour. Although coupled codes considering these feedbacks have been developed and used for decades, advances in the computing power and availability of computer hardware make it feasible to use physically more correct but computationally expensive calculation approaches, such as Monte Carlo neutronics, for best-estimate analyses at an increasingly larger scale, also considering couplings between multiple physics; even for more industry-like applications (Ferraro et al. 2019). Even if still computationally too demanding to be used in routine analyses, this type of multi-physics tools can be used to address specific issues and quantify the effect of various simplifications and approximations that more traditional approaches typically need to resort to, thus also confirming whether such approximations actually are conservative or not.

EMBER ultimately aims at reducing uncertainties in reactor and fuel analyses via development of advanced multi-physics calculation capabilities that will account for the reactor core neutronics and thermal hydraulics, and fuel behaviour and burnup.

These are most typically solved by separate dedicated solvers that range from fast-running simulator-type solvers to computationally expensive best-estimate tools. To account for feedbacks, the separate solvers are coupled to exchange data and iterate a multi-physics solution. Such coupled calculation capabilities between existing neutronic, fuel behaviour and thermal hydraulic solvers are developed and extended in EMBER.

The project extends the recently developed coupled neutronic and fuel performance calculation capabilities at LUT University (Suikkanen et al. 2020) by increasing the level coupling between already coupled solvers, by adding new solvers to the calculation system to account for thermal hydraulic feedback and to provide transient calculation capabilities. The results of EMBER should prove useful in analyses aiming to determine limits for the safe operation of reactors and in criticality safety analyses including the related burnup credit calculations as well as in considerations related to the final disposal of spent fuel.

Overall work plan and objectives

Launched in 2020, the work in EMBER is planned to be completed in three years. During the first year, the previously developed coupled calculation capabilities between the fuel behaviour solver TRANSURANUS and the reactor physics solver Serpent are extended by implementing capabilities to transfer nuclide data solved by Serpent to be utilized in the fuel behaviour simulation conducted by TRANSURANUS. In 2020, the coupled calculation framework will be complemented by integrating a core thermal hydraulic solver to provide a solution for the coolant conditions, to be utilized by the other two solvers. In 2022, the vision is to extend the capabilities of the coupled calculation framework to transient analyses.

EMBER is a light-weight project, each year focusing on the development of a single major feature or capability to the calculation framework. Thus, the project only consists of two work packages; the first containing all the development work while the second is devoted to project management and international collaboration tasks.

Existing calculation framework

The coupled calculation system developed at LUT currently consists of the Monte Carlo reactor physics burnup calculation code Serpent 2 and the 1.5D fuel performance code TRANSURANUS. The coupling is external and based on exchanging output data between the solvers via ASCII files. A separate driver program written in Perl handles the execution of the two solvers, exchange of data and monitoring of convergence. Existing functionalities of the two solvers are utilised, such as the multi-physics interface of Serpent and the capability to read-in external radial power distributions in TRANSURANUS. In basic use, no source code modifications are needed to the currently up-to-date versions of either of the two solvers. While sacrificing some computational performance when compared to more integrated coupled code systems, this light-weight coupling approach is considered

straightforward to maintain and deploy into use as it requires no special versions of the solvers or installation of additional frameworks.

The coupling between Serpent and TRANSURANUS is realized by means of an external driver program written in Perl. This program executes the coupled solvers in correct sequence and processes the output data of either solver into a format that can be used as an input by the other. In its current state, the LUT calculation system is designed for burnup calculations that progress as a series of steady state steps. The general solution flow of a coupled calculation is shown in Figure 1. Suikkanen et al. 2020 provides further details of the calculation framework.

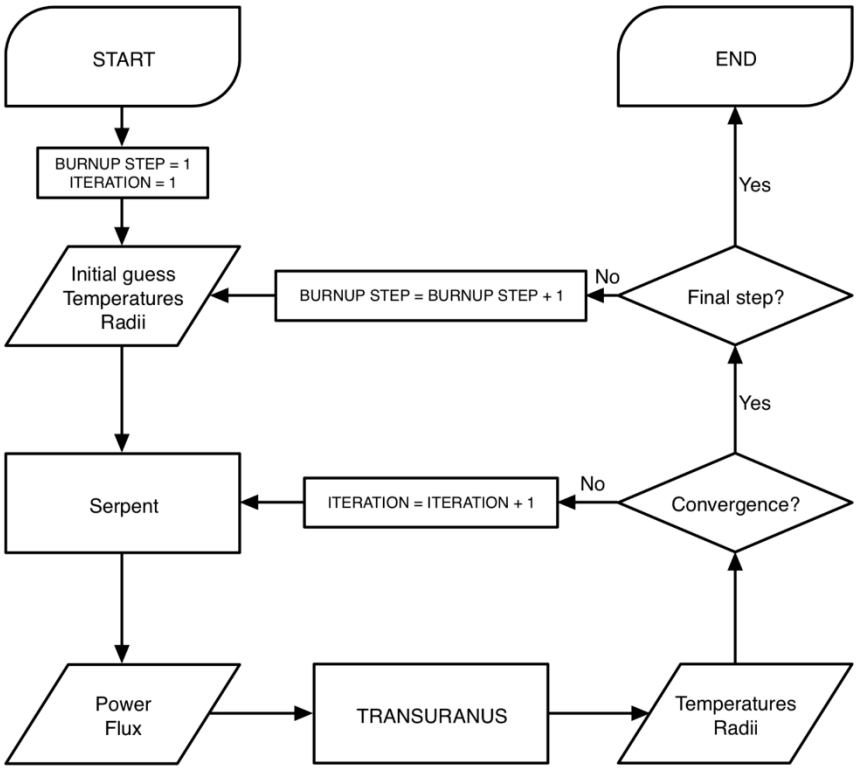

Figure 1. Flowchart of the LUT coupled calculation system (Suikkanen et al. 2020).

Extension of the Serpent – TRANSURANUS coupling

Capability to utilise nuclide concentrations calculated by Serpent in TRANSURANUS were developed to further deepen the level of coupling and increase its usefulness especially as a special tool in fuel behaviour analyses. A major part of the work was to design an interface to TRANSURANUS, through which such external data could be imported. While regular out-of-the-box data output was sufficient to

export data from Serpent, new subroutines were needed for the coupled calculation driver program Kytkin to handle the data flow.

The design requirement for the data interface was to be able to import nuclide inventory data provided by an external solver, Serpent in this case, for all of the calculation nodes in the fuel rod model. Despite being primarily intended for importing nuclide data, it should be relatively straightforward to extend the capabilities of the data interface for importing practically any node-wise data. The data interface was implemented as a new subroutine in TRANSURANUS which is executed when specified in the input file. In such a case, TRANSURANUS will then, during the fuel rod simulation, read in an additional input file containing nuclide data. The current implementation was developed for coupled calculations using the LUT calculation system and thus it is expected that TRANSURANUS is run in a restart mode one burnup step at a time, between which the nuclide data file is updated with new data calculated by Serpent. At this stage, the data interface is applied for bringing in Serpent-calculated fission product data during a coupled Serpent-TRANSURANUS fuel rod calculation. TRANSURANUS considers the gaseous fission products xenon, krypton, caesium and neodymium; creation of which would normally be calculated by a separate sub-routine at each calculation node. This subroutine was now modified to read the nuclide increments from the data structure of the data interface instead.

The developed data interface capability in TRANSURANUS was verified by performing calculations with and without the interface. First, a regular TRANSURANUS simulation was performed with a fuel rod irradiated for one cycle. At each macro time step the created xenon, krypton, caesium and neodymium concentrations at each calculation node were extracted and written to a file. In the second step, this data was processed into a format that the data interface can read, thus producing a nuclide file for each macro step interval. Another TRANSURANUS run was then performed, which, instead of solving the fission product concentrations, read the data from the external nuclide files and used this data within the subroutine handling the creation of fission products. Thus, comparing the standard run and the one utilizing the output from the standard run, but provided through the interface, it would be expected that more or less identical results for the created fission products between the cases would be obtained if the interface functions as intended. This was confirmed to be the case as can be observed from Figure 2.

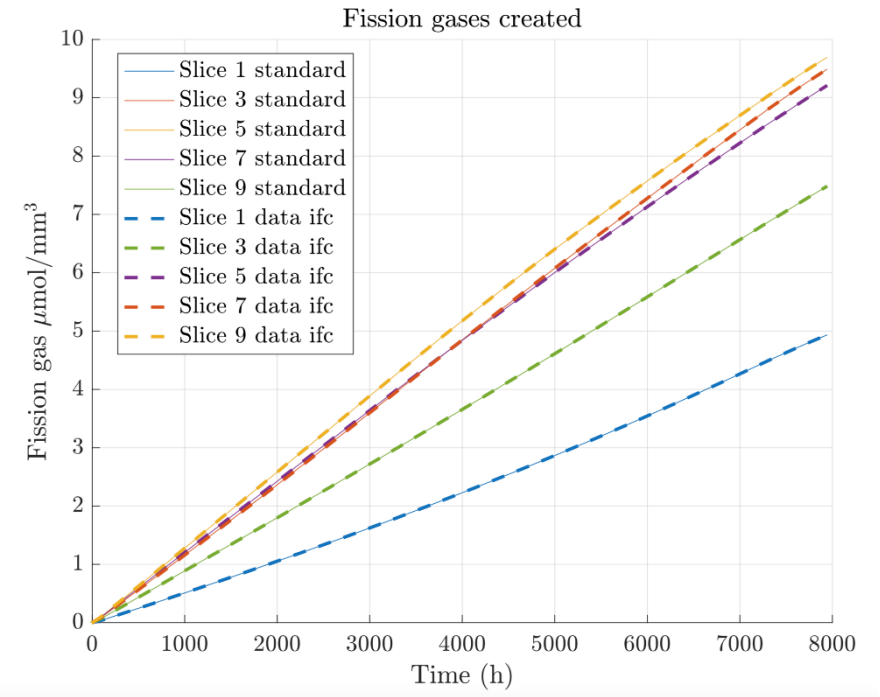

Figure 2. Verification of the nuclide data interface.

New features were implemented to the coupled calculation driver program Kytkin to allow reading Serpent nuclide output, handling the nuclide data and writing this data to the format used by the TRANSURANUS data interface. Output of Serpent depletion calculations, that is, the concentrations of various nuclides are obtained for prespecified volumetric bins. In addition to figuring out the bins corresponding to specific regions of the fuel rod, mapping and interpolation of the data to correct TRANSURANUS nodes needed to be developed. This is illustrated in Figure 3.

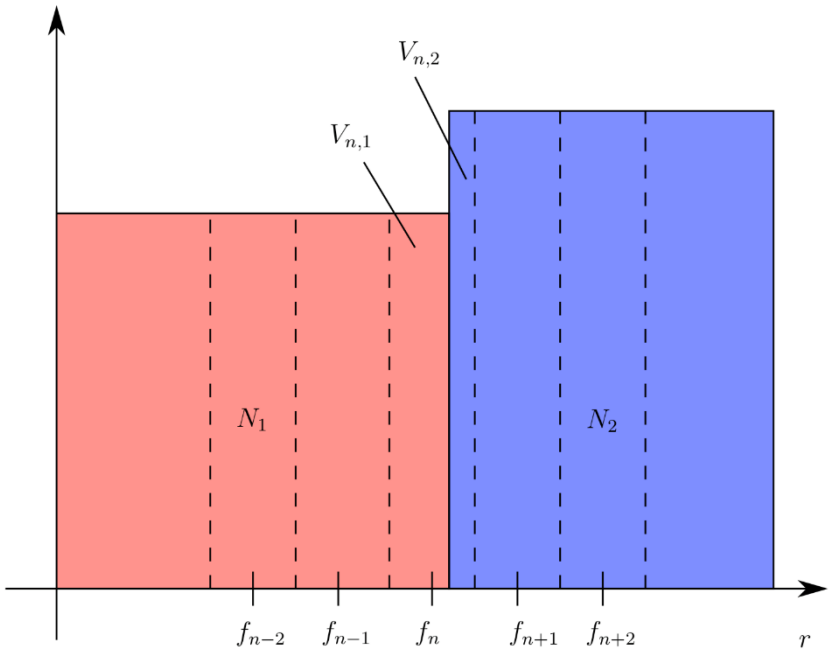

Figure 3. Arbitrary position in fuel pin. Serpent burnup zones (coloured) with atomic densities N1 and N2. Volumes $V_{n,1}$ and $V_{n,2}$ are used in calculation of volume fractions of the local volume of TRANSURANUS calculation node f_n.

Summary and conclusion

The coupled calculation framework of LUT was extended with the transfer of nuclide data from Serpent to the fuel behaviour solver TRANSURANUS during a coupled calculation between the two. The data interface implemented to TRANSURANUS for reading-in external nuclide data was verified to function as intended by performing test calculations. The developed capabilities are expected to reduce uncertainties in fuel behaviour analyses via more accurate neutronic and depletion solution and also facilitate the inclusion of additional fission products in the fuel behaviour simulations. Work continues by demonstrating the nuclide transfer capabilities in a realistic calculation case aiming to quantify the effect of the physically more correct neutronic and depletion solution on the fuel behaviour simulation results. Also, during 2021 a core thermal hydraulic solver will be integrated to the coupled calculation framework, thus completing it for steady-state and fuel depletion calculations.

Acknowledgement

The authors acknowledge Fortum Oyj for providing fuel history data for use in testing the developed calculation capabilities. The authors wish to thank collaborators at

JRC ITU Karlsruhe (Dr. Paul van Uffelen and Dr. Arndt Schubert) for providing feedback and ideas regarding the developed analysis capabilities.

References

Ferraro, D., Garcia, M., Imke, U., Valtavirta, V., Leppänen, J., Sanchez-785 Espinoza, V., 2019. Serpent/SCF pin-level multiphysics solutions for the VERA Fuel Assembly benchmark. Annals of Nuclear Energy 128, 102–114.

Suikkanen, H., Rintala, V., Schubert, A. & Van Uffelen, P. 2020. Development of coupled neutronic and fuel performance analysis capabilities between Serpent and TRANSURANUS. Nuclear Engineering and Design 359, 110450.

5. Thermal Hydraulics

5.1 CFD methods for reactor safety assessment (CFD4RSA)

Timo Pättikangas[1], Ville Hovi[1], Juho Peltola[1], Veikko Taivassalo[1], Jouni Syrjänen[1], Tommi Rämä[2], Timo Toppila[2]

[1]VTT Technical Research Centre of Finland Ltd
P.O. Box 1000, FI-02044 Espoo

[2]Fortum Power and Heat Oy
P.O. Box 100, FI-00048 FORTUM

Abstract

The overall objective of the CFD4RSA project is to improve the usability and reliability of Computational Fluid Dynamics (CFD) calculations in nuclear Reactor Safety Assessment. The work consists of four Work Packages, where topics that are important in safety assesment are studied. First, the reliability of coupled CFD-Apros calculations is investigated in the modelling of postulated accident scenarios. Second, uncertainty quantification methods in CFD calculations are tested and taken into use. Third, coarse-mesh CFD models are developed for reactor pressure vessel. Fourth, thermal stratification in pressure suppression pools of BWRs is studied.

Introduction

Computational Fluid Dynamics (CFD) is gradually becoming more important in Nuclear Reactor Safety (NRS) assessment. Increasing computing power and better understanding of the uncertainties and limitations of CFD methods are making use of CFD in NRS more appealing. Emerging coarse-mesh CFD methods reduce the computational cost of CFD but on the other hand increase the need of model development. In the CFD4RSA project, some of the topics, where CFD is most useful for safety assessment, are developed and validated.

Recently two important reports have been published on the use of CFD for Nuclear Reactor Safety (NRS) assessment. The reports were written by the NEA Committee on the Safety of Nuclear Installations (CSNI), which consists of CFD experts of regulators and research centers. Additional input was given by CFD experts, for instance, from EDF and AREVA. The NEA/CSNI reports list problems in NRS assessment, where use of CFD would be useful. First one of the reports focusses mainly on topics, where single-phase CFD calculations could be used (Smith et al., 2014). The second report mainly discusses topics, where multiphase CFD calculations would be useful (Bestion, et al., 2014). The different Work Packages of the

CFD4RSA project have been chosen on the bases of these reports and national interests.

In WP1, coupled CFD–Apros simulations are performed, where an Apros model of a generic VVER-440 nuclear power plant has been coupled with CFD model of one of the pressurizer or steam generator of the plant. Novel two-way coupling of the Apros and CFD models has been tested for the simulation of transient following Main Steam Line Break in the plant.

In WP2, uncertainty quantification of CFD calculations is addressed. Traditionally, uncertainty of CFD simulations has been assessed by performing a few simulations by varying the mesh size, time step, boundary conditions, turbulence models or some model coefficients. Recently, more systematic approaches on the uncertainty quantification in CFD has been tested in international benchmarks. In WP2, these approaches are reviewed and tested in application relevant to nucclear reactor safety.

In WP3, coarse-mesh CFD models for reactor pressure vessels are developed and validated. The SAFIR2022 Framework Plan points out that one of the challenges of CFD calculations is the large computational cost. Therefore, methods that are computationally less expensive are needed. The coarse-mesh CFD methods provide three-dimensional analysis for situations, which cannot be properly described with lumped parameter models. In the coarse-mesh approach, the computational cost is smaller than in traditional CFD calculations, but some additional modelling of the flow is necessary.

WP4 will consist of studies of heat transfer in a fuel rod bundle of a boiling water reactor. The boiling models of ANSYS Fluent will be compared to the boiling models implemented in OpenFOAM at VTT. The NUPEC BWR full-size fine-mesh bundle test (BFBT) benchmark will be used as the test case. This Work Package will start in 2021, and it will not be discussed in more detail in this report.

In WP5, CFD and Apros tools for the analysis of the thermal stratification of pressure suppression pools of BWRs are developed and validated. It has been suggested that in the Fukushima accident the pressure suppression pool of one of the reactors was thermally stratified (Jo et al., 2016). At the Royal Institute of Technology (KTH), an Effective Heat Source (EHS) and Effective Momentum Source (EMS) model has recently been developed for the description of the thermal stratification, when steam is injected into a pressure suppression pool through sparger or vent pipe (Gallego-Marcos, 2018; Gallego-Marcos et al., 2018). In WP5, the EHS/EMS model will be implemented into the ANSYS Fluent CFD code. In addition, the possibility of implementing an EHS/EMS based model to the lumped parameter/system code Apros will be tested.

Coupled CFD-Apros simulations loss-of-feedwater transient

Coupled CFD-Apros simulation of the pressurizer of a generic VVER-440 plant was performed by using commercial Apros Co-simulation Tool for CFD with domain decomposition method. The pressurizer was modelled with ANSYS Fluent CFD code

and the rest of the plant was modelled with the Apros system code. In addition, the CFD model measurements were coupled to automation process of the system code. Loss-of-feedwater transient was calculated, where the two-way interaction of the pressurizer and the rest of the plant is fairly complicated. The Apros model of the plant controls the spray and heaters during the transient depending on the water level in the pressurizer. The couplings of the model are illustrated in Figure 1.

A postulated loss-of-feedwater scenario was simulated with the coupled model and the results were compared with stand-alone Apros results. All in all, the models behaved very similarly considering the compared quantities of pressurizer pressure, spray mass flow rate, mass flow rate at the surge line, mass transfer rate, liquid level and relative heater power. The progression of the transient was also almost identical, with only a few seconds of delay between the events. This suggests that the coupling tool works as planned but also that there is no specific need for 3D pressurizer model but 1D model is good enough in this postulated transient.

The Apros Co-simulation Tool for CFD is generic and user configurable for different coupling scenarios: flow coupling, wall and volume heat transfer coupling, measurement coupling and Fluent script language coupling. Therefore, the coupling tool can also be used to provide 3D details of other main components of NPP, such as steam generators.

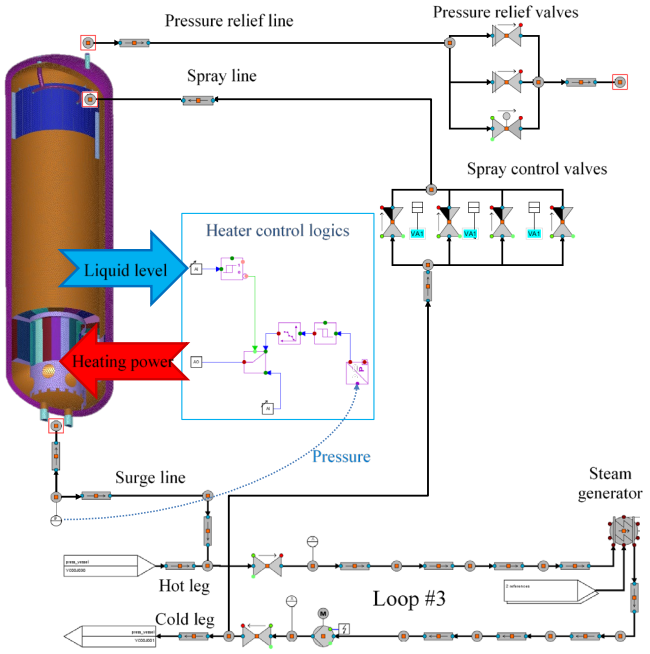

Figure 1. Coupling of CFD model of pressurizer with Apros model of a generic VVER-440 nuclear power plant.

Uncertainty Quantification in CFD

Computational simulations are a way to ensure the fulfilment of safety regulations and thus the safe operation of nuclear power plants. Quantification of calculation uncertainties and sensitivities improves the confidence to the simulation results. Within system thermal hydraulics (NEA, 2011), best estimate methods complemented with uncertainty analysis have been used for quite some time. Within CFD in nuclear reactor safety applications, however, efforts on uncertainty analyses have been initiated just during recent years (Bestion, 2018; NEA, 2016). The main field of application of Uncertainty Quantification (UQ) in CFD is expected to be mixing problems (NEA, 2016).

As a first step of minimizing uncertainties in CFD simulations, a set of guidelines were established by a writing group of WGAMA. The resulting Best Practice Guidelines (BPG) for the Use of CFD in Nuclear Reactor Safety Applications (NEA 2007, 2014) provide recommendations for conducting CFD simulations, including the selection of models and numerical options. BPG may be used to limit the number of uncertain parameters included to the uncertainty analysis (e.g., when strong arguments in favour of best numerical options are found in BPG). Phenomena Identification and Ranking Table (PIRT) is recommended in the BPG in order to help distinguishing the relevant parameters. In PIRT, the analysed scenario is divided into smaller segments (phenomena, process, inputs), and these are then ranked based on expert judgement and/or sensitivity studies.

Uncertainties in CFD simulations arise from various sources that may be interlinked. These are, e.g. (NEA, 2016):

- Numerical solutions (discretization, convergence)
- Singularities in the solution of Navier-Stokes equations for momentum, mass and energy conservation
- Solution schemes for turbulence: Reynolds averaged Navier-Stokes (RANS) equations, Large Eddy Simulation (LES) model
- Description of physical phenomena: missing physics in the models
- Choice between various physical and numerical models; user effect
- Boundary conditions, initial state and assumptions on the geometry
- Scaling uncertainty when applying the code to a different geometry compared to its validation domain (e.g. power reactor vs. test conditions)

The uncertainty quantification was studied by using the GEMIX experimental facility for turbulent mixing of two different liquids as the test case. The GEMIX experiment is located at the Laboratory of Thermal Hydraulics of the Paul Scherrer Institute in Switzerland. Recently, NEA/OECD Benchmark was arranged, where experiments of turbulent mixing of liquids were modelled with CFD calculations (Fokken et al., 2017). The main goal of the exercise was to study the possibility of uncertainty quantification of the CFD results for nuclear reactor safety analysis. The turbulent mixing is important in many nuclear reactor safety applications, such as mixing of hot and cold water and mixing of hydrogen with air and steam.

In the GEMIX experiment, mixing of hot and cold water was studied, where the density difference between the liquids is important. The experimental geometry is shown in Figure 2. The GEMIX facility consists of two rectangular channels separated with a splitter blade. The water flows from the two channels are mixing after the splitter blade. The flow velocity, turbulence kinetic energy and liquid density were measured at different distances in the downstream direction from the tip of the splitter blade.

In the experiment, the cold water was modelled with water-sucrose mixture and the hot water with pure water. The density difference between the hot and cold water was only one percent.

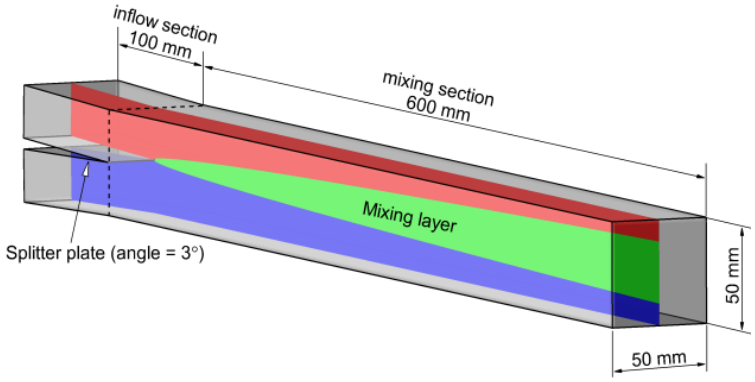

Figure 2. Set-up of the GEMIX turbulent mixing experiment (Fokken et al., 2017).

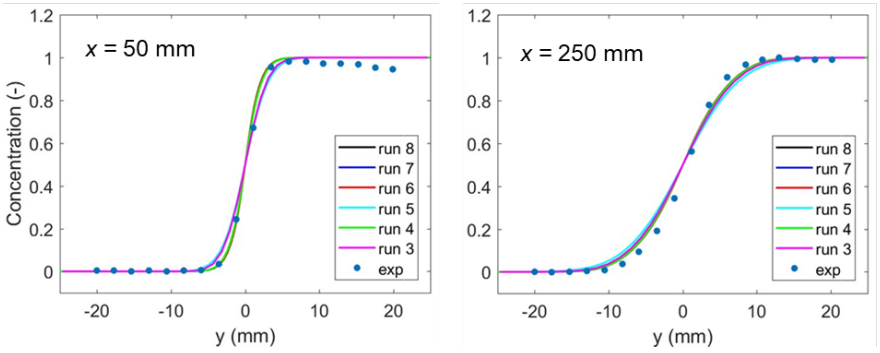

Figure 3. Mass fraction of pure water in the mixing channel at two different distances from the tip of the splitter blade. Results of simulations are compared to experimental results.

In Figure 3, the mass fraction of pure water is shown. The differences between the models are largest near the blade tip at x = 50 mm. It was found that k-ε model with wall functions and wall-resolve RSM k-ε model provide results that differ from other model combinations. These two models predict lower-gradient slopes for the mass

fraction compared to other models. The calculated results for the mass fraction are fairly close to the measured values.

The ASME V&V method for uncertainty quantification was studied in the frame of the GEMIX benchmark. In the GEMIX benchmark and many other CFD calculations, the turbulence model is a major source of model uncertainty. The input uncertainty was also significant because the inlet boundary condition was most important.

Coarse-mesh CFD models for pressure vessels

In the development of coarse-mesh models for pressure vessels, the NuScale SMR reactor was used as test case. The physical models and properties used in the present simulations are still largely place holders that to demonstrate functionality of the computational model and are not yet quantitatively representative of real life.

The computational mesh consists of approximately 910 000 polyhedral cells and some of the components are explicitly described in the mesh, while others will be represented by porous regions modelled as stationary phases. Figure 4 illustrates the computational geometry and the mesh.

An Ants neutron transport model for the NuScale reactor core was provided by the SAFIR2022 project LONKERO. In the axial direction, the Ants domain extends the whole length of the fuel assemblies, including the bottom and top end pieces. In the radial direction, it includes all the fuel assemblies and the heavy reflector. Each fuel assembly is represented with a single node in the radial direction and with 31 nodes in the axial direction.

In the current form, the nuclear cross section data used in the Ants model does not include feedbacks from the thermal-hydraulic state. Therefore, a single multiphysics iteration is sufficient to produce a stationary state, provided that the thermal-hydraulic solution has converged to a steady state. The Ants model is configured for full-power operation (160 MWth).

Contours of selected properties are plotted on multiple cross sections of the pressure vessel in Figure 5. Starting from the top left corner, these are: solid volume fraction [-], steam volume fraction [-], (liquid) water temperature [K], power density (from the Ants model) [W/m3], liquid vertical velocity [m/s], magnitude of the drag force exerted on the liquid phase [N/m3], absolute pressure [Pa], and saturation temperature [K].

The solid phase represents the porous structures that are not explicitly described in the mesh. These structures include the reactor core, heavy reflector, upper core plate, control rod assemblies and their guide tubes, guide tube plate, heat exchanger, and pressurizer heating elements. The pressure drop associated with these structures has been modelled with anisotropic interphase drag forces. The magnitude of these drag forces for the liquid phase are shown Figure 5.

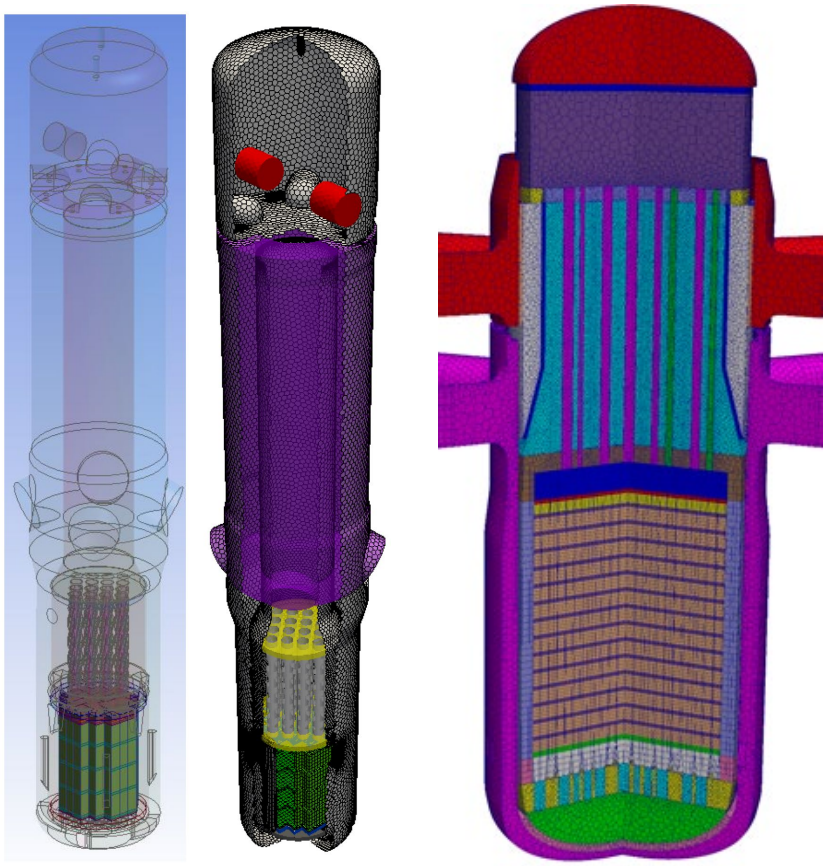

Figure 4. Coarse-mesh CFD model for the NuScale SMR reactor (left) and VVER-1000 reactor (right).

The coarse mesh models were also applied to the VVER-1000 reactor, which was selected because of the experimental data available. Exercise 1 in Phase 2 of the VVER-1000 Coolant Transient Benchmark (V1000CT-2), also known as the VVER-1000 vessel mixing problem (Kolev et al., 2010a), was chosen as the test case. In this exercise, the primary objective was to test the capability of the thermal-hydraulics models to reproduce the single-phase mixing in a reactor pressure vessel. The exercise is based on experiments in the Kozloduy-6 reactor and its purpose is to study thermal-hydraulics with given boundary conditions for the pressure vessel and with a pre-described power distribution. The benchmark was modelled by seven groups with various CFD codes and by five groups with system-code type methods (Kolev et al., 2010b).

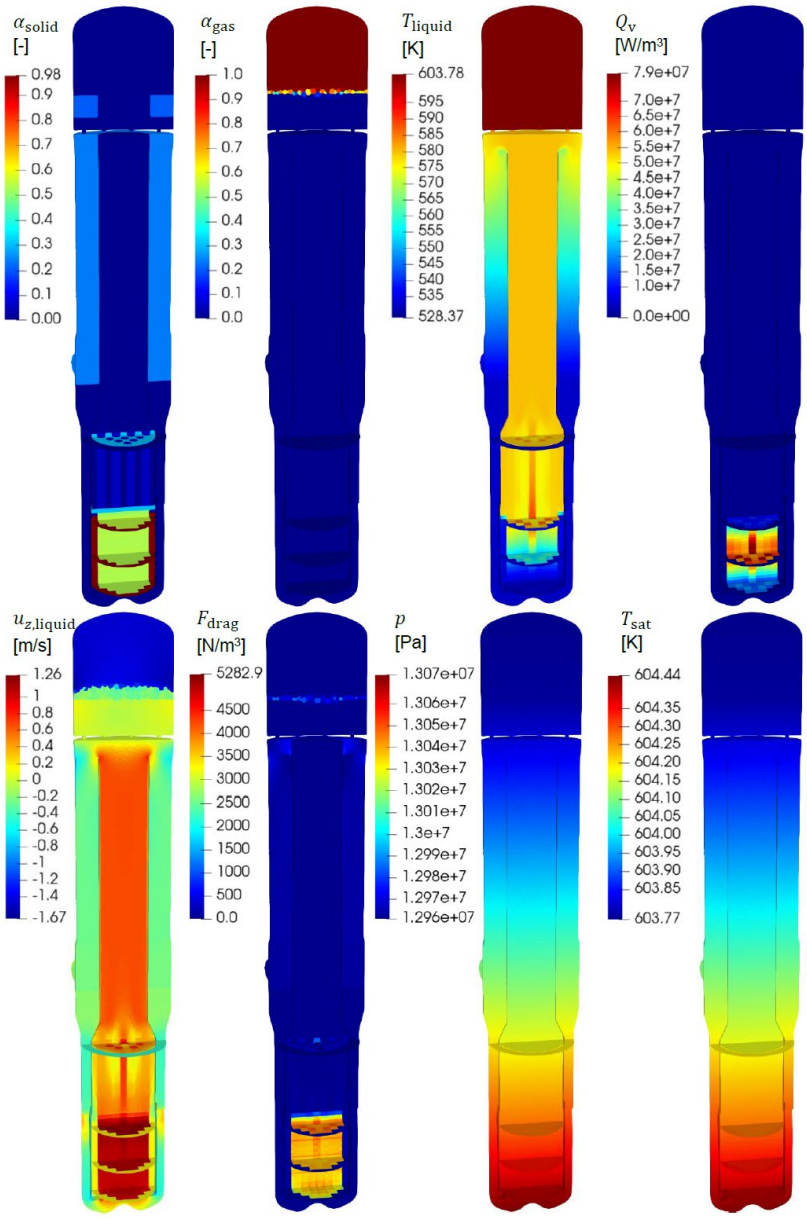

Figure 5. Coarse-mesh CFD calculation of NuScale reactor at full power. Starting from the top left corner: solid volume fraction [-], steam volume fraction [-], (liquid) water temperature [K], power density (from the Ants model) [W/m3], liquid vertical velocity [m/s], magnitude of the drag force exerted on the liquid phase [N/m3], absolute pressure [Pa], and saturation temperature [K].

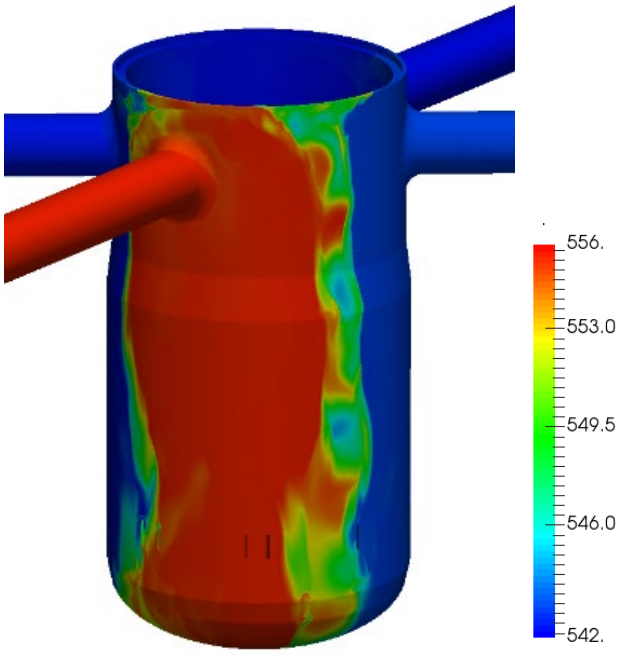

Figure 6. Instantaneous coolant temperature (K) in the downcomer of VVER-1000 Coolant Transient Benchmark.

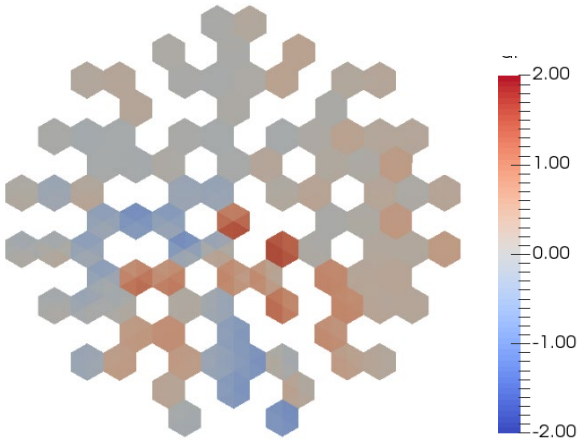

Figure 7. Difference (K) between the computed and experimental coolant temperatures at the core inlet for the final state. The computational values were obtained with the macroscopic *k-ε* model and with the coarse mesh.

In the turbulence modelling, the *k-ω* model was tested due to the poor performance of the standard k-ε model in modelling mixing and swirl. The k-ω model should be better in predicting flow in a boundary layer with an adverse pressure gradient. The Shear Stress Transport (SST) version was selected, because it should not be as sensitive to freestream as the standard *k-ω* model and it has been calibrated to accurately reproduce separation from surfaces.

An example of the simulation result is shown in Figure 6. A stable solution was not obtained and computed fields fluctuate as a function of time. The time-dependent results of RANS models are sometimes considered as URANS results also in cases where a turbulence model should represent all fluctuations (e.g. Hart 2016). The theoretical base of this approach is not solid, but transient simulations with the RANS models require less computing than the real URANS model.

Simulations with coarse mesh were performed and the calculated temperatures were compared to the measurements. Figure 7 shows the difference between the numerical results and measurements for the core inlet temperature. The modelling approach was found to be largely mesh-independent and even the coarse mesh with the cold legs can be used as long as the inlet boundary conditions are obtained reliably.

CFD simulations of separate effect tests of condensation

In a Boiling Water Reactor (BWR), the operation of the pressure suppression pool is affected by thermal stratification and mixing phenomena. In particular, thermal stratification can be important in different hypothetical Loss-Of-Coolant-Accident (LOCA) scenarios, where steam line breaks inside the containment or during station blackouts.

At the Royal Institute of Technology (KTH), the behavior of the pressure suppression pool has been studied during a steam injection through blowdown pipes and spargers. Effective Heat Source (EHS) and Effective Momentum Source (EMS) models have been developed to predict the long-term thermal behavior of the pool (Gallego-Marcos, 2018; Gallego-Marcos et al., 2018). At KTH, the EHS/EMS models have been implemented in the GOTHIC code.

At the LUT University, a set of experiments with spargers have been performed in the PPOOLEX facility. The experiments were mainly focused on the oscillatory bubble regime, and exploratory tests were done in chugging and stable jet regimes. The experimental data was used by KTH to address important phenomena governing the pool behavior and validate the computational models. A small-scale Separate Effect Facility (SEF-POOL) was built to measure directly the effective momentum induced by steam injection through a sparger. The experiments enabled the development of the effective momentum source correlations at KTH.

At VTT, one of the SEF-POOL experiments was simulated with CFD calculations. In the simulations, the reactingTwoPhaseEulerFoam solver was used. The simulation results were compared with pressure measurements and high-speed video from the experiment.

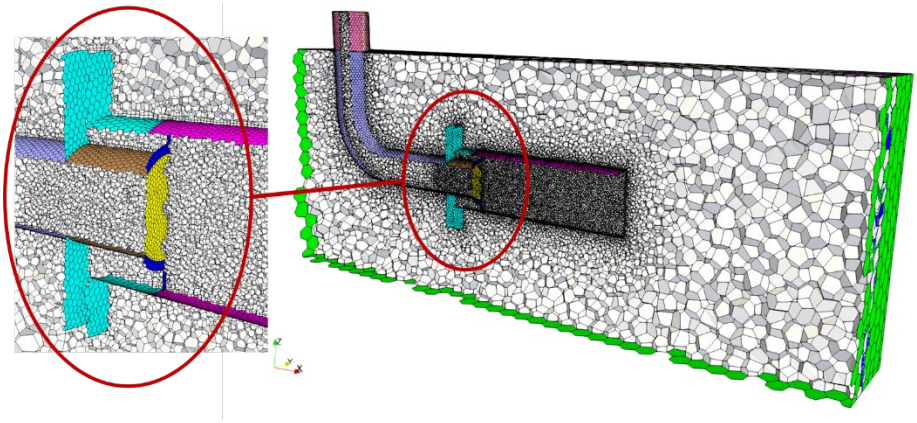

Figure 8. CFD mesh for the SEF-POOL separate effect test facility of LUT, where steam is blown into a water pool.

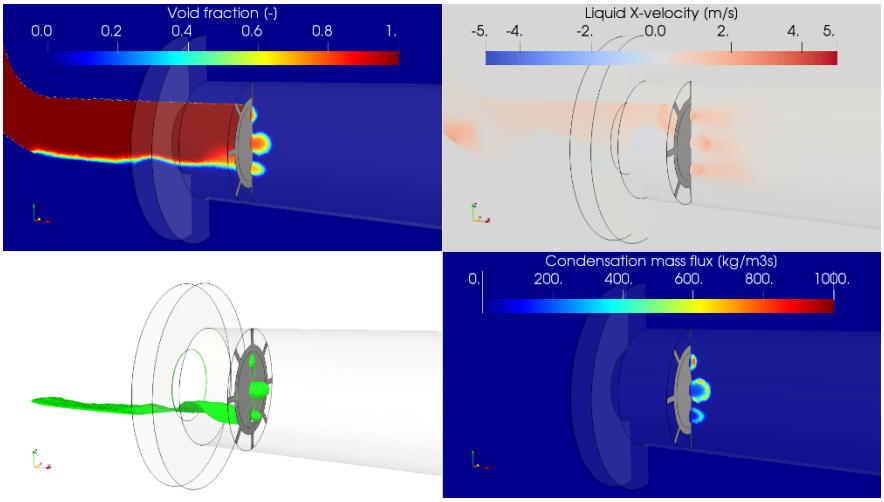

Figure 9. Formation and condensation of steam bubbles in the nozzle region during one chugging period. The frames shown are void fraction, horizontal velocity of liquid, iso-surface of void fraction and condensation mass flux.

The CFD model of the separate effect test facility is shown in Figure 8. In the model, steam is injected downwards into the vertical pipe, which bends to horizontal direction. A steel plate with three orifices (∅16mm) is located at the end of the horizontal section. Steam flows through the orifices into the polycarbonate tube. The tube is submerged in a box filled with water. Some water can also flow from the box into the polycarbonate tube through the flange connecting the steam line to the polycarbonate tube.

In Figure 9, an example of bubble formation at the orifices and following condensation is shown. The void fraction can be seen in the top left frame and iso-surface of void fraction in the bottom left frames. A steam bubble is condensing in the orifice at the center of the plate. One can see that the bubbles in the top and bottom orifice are not synchronous with the bubble in the center orifice. The average period of chugging in all three orifices is approximately Δt = 21 ms. During chugging some water penetrates through the orifices into the inlet pipe, and some water can be seen flowing around on the bottom of the inlet pipe.

The condensation mass flux is shown in the bottom right frame of Figure 9. The highest values of the condensation mass flux are more than 2000 kg/m^{3}s, which occur at the beginning of the collapse of steam bubble. Typical flow velocities of the liquid in front of the orifices are approximately 1…3 m/s.

The SEF-POOL tests and PPOOLEX stratification experiments of the SPASET project have been used by KTH in the development and validation of Effective Heat Source (EHS) and Effective Momentum Source (EMS) models (Gallego-Marcos, 2018; Gallego-Marcos et al., 2018). At VTT, implementation of corresponding approach in the Apros system code has been studied. The conclusion of the work has been that the EHS/EMS model is not directly applicable in Apros LP modelling, but could be maybe utilized in the stratification calculation when using the Apros thermalhydralic model. However, the concern was that the Apros thermalhydralic model applies 1D flow solution, whereas the EHS/EMS model is delevoped to be coupled with 2D or 3D flow solver.

In the Apros studies, stratification modeling capability of Apros was investigated by using 1D thermalhydralic model with so-called pseudo-2D nodalisation. The PPOOLEX stratification test SPA-T3 was simulated. The sensitivity studies included, e.g., the effect of nodalisation concept, loss coefficient, direction of momentum transfer from steam source, discretization scheme and steam mass flow during the pool mixing phase.

The simulation results show that the pool stratification phase was predicted well with the 2-column nodalisation used. Sufficiently dense nodalisation was needed to capture the real sharp stratification because the temperature was calculated as function of the solved enthalpy, which still represents the average enthalpy of node. The best agreement with experiment was obtained when using the higher order discretisation scheme for enthalpy solution and the larger loss coefficient for the horizontal branches than for the vertical ones.

The Apros results also showed that the pool mixing phase could not be predicted reasonably. If the nodalisation was very coarse, pool mixing took place, but it was then mostly caused by numerical diffusion or inaccuracy in modelling the real sharp stratification thermocline.

Sensitivity study showed that a significant increase in steam mass flow (and momentum) did not improve the predicted pool mixing. Therefore, implementation of the EHS/EMS model in Apros would not probably solve alone the deficiencies found in the mixing calculation.

References

Bestion, D., Anglart, H., Mahaffy, J., Lucas, D., Song, C.H., Scheuerer, M., Zigh, G., Andreani, M., Kasahara, F., Heitsch, M., Komen, E., Moretti, F., Morii, T., Mühlbauer, P., Smith, B.L., Watanabe, T., 2014. Extension of CFD Codes Application to Two-Phase Safety Problems – Phase 3, NEA/CSNI/R(2014)13, November 2014, http://www.oecd-nea.org/nsd/docs/2014/csni-r2014-13.pdf

Bestion, D., 2018. BEPU methods using CFD codes - progress made within OECD-WGAMA CFD activities. ANS Best Estimate Plus Uncertainty International Conference (BEPU 2018), Lucca, Italy, May 13-18, 2018.

Cutrono Rakhimov, A., Visser, D.C., Komen, E.M.J., 2018a. Uncertainty quantification method for CFD applied to the turbulent mixing of two water layers. Nuclear Engineering and Design, Vol. 333, pp. 1-15.

Fokken, J., Krohn, B., Kapulla, R., Ničeno, B., Prasser, H. M., Badillo, A., 2017. OECD/NEA CFD-UQ Benchmark Exercise: CFD Prediction and Uncertainty Quantification of a GEMIX mixing layer test. Final Report, Laboratory of Thermal Hydraulics, Paul Scherrer Institute, Switzerland.

Gallego-Marcos, I., 2018. Steam condensation in a water pool and its effect on thermal stratification and mixing, Doctoral Thesis, KTH School of Engineering Siences, Stockholm, Sweden, 87 p.

Gallego-Marcos, I., Kudinov, P., Villanueva, W., Kapulla, R., Paranjape, S., Paladino, D., Laine, J., Puustinen, M., Räsänen, A., Pyy, L., and Kotro, E., 2018. Pool stratification and mixing induced by steam injection through spargers: analysis of the PPOOLEX and PANDA experiments, Nuclear Engineering and Design **337**, 300–316.

Hart, J., 2016. Comparison of turbulence modeling approaches to the simulation of a dimpled sphere. Procedia Engineering 147 (2016) 68 – 73.

Jo, B., Erkan, N., Takahashi, S., Song, D., Sagawa, W., Okamoto, K., 2016. Thermal stratification in a scaled-down suppression pool of the Fukushima Daiichi nuclear power plants, Nuclear Engineering and Design **305**, 39–50. https://doi.org/10.1016/j.nucengdes.2016.05.017

Kolev N.P., Aniel, S., Royer, E., Bieder, U., Popov, D., Topalov, Ts., 2010a. VVER-1000 Coolant transient benchmark Phase II (V1000CT-2), Vol. 1, Final specifications of the VVER-1000 vessel mixing problem, NEA/NSC/DOC (2007)22, OECD.

Kolev, N.P., Spasov, I., Royer, E., 2010b. VVER Coolant Transient Benchmark: Phase 2 (V1000CT-2), Summary Results of Exercise 1 on Vessel Mixing. Simulation, NEA/NSC/DOC (2010)10, Paris, OECD.

NEA, 2007. Best practice guidelines for the use of CFD in nuclear reactor safety applications. NEA/CSNI/R(2007)5.

NEA, 2011. BEMUSE Phase VI Report, status report on the area, classification of the methods, conclusions and recommendations. NEA/CSNI/R(2011)4.

NEA, 2016. Review of Uncertainty Methods for Computational Fluid Dynamics Application to Nuclear Reactor Thermal Hydraulics. NEA/CSNI/R(2016)4.

Smith, B.L., Andreani, M., Bieder, U., Ducros, F.,Graffard, E., Heitsch, M., Henriksson, M., Höhne, T., Houkema, M., Komen, E., Mahaffy, J., Menter, F., Moretti, F., Morii, T., Mühlbauer, P., Rohde, U., Scheuerer, M., Song, C.-H., Watanabe, T., Zigh, G., with additional imput from Archambeau, F., Bellet, S., Bestion, D., Boyd, C.F.,Krepper, E., Muñoz-Cobo, J.M., Simoneau, J.-P., 2014. Assessment of CFD Codes for Nuclear Reactor Safety Problems – Revision 2, NEA/CSNI/R(2014)12, January 2015, http://www.oecd-nea.org/nsd/docs/2014/csni-r2014-12.pdf

5.2 Passive heat exchanger experiments (PAHE)

Vesa Riikonen, Virpi Kouhia, Joonas Telkkä, Lauri Pyy

LUT University
P.O. Box 20, FI-53851 Lappeenranta, Finland

Abstract

The objective of the project was to improve understanding of the AES-2006 design PHRS-C passive heat removal system and to generate data for code validation. Carefully designed experiments are the most reliable way to obtain fundamental understanding and reliable data of the phenomena. Data can be used in the development and validation of system and CFD codes for the safety analyses of nuclear power plants.

Introduction

The main aim of the project was to ensure the operation and efficiency of the AES-2006 design PHRS-C passive heat removal system in accident and transient situations of nuclear power plants and to generate data for code validation. The goal was to identify physical mechanisms that can reduce performance or prevent the functioning of the loop, to help recognizing conditions in which the functioning of the system could be endangered and to suggest ways assuring the operation. Especially, flow oscillations in two-phase conditions were a topic of interest.

Different organizations can use data in the development and validation of system and CFD codes for the safety analyses of nuclear power plants. Computer analyses are needed also in the planning of the experiments as well as in post analyses to help understanding the physics in the experiments.

The project carried out research on topics relevant to the safety of Finnish nuclear power plants on a high scientific level and with modern methods and experimental facilities. It maintained and extended the research expertise needed for the experimental work and generated data for the validation of computational tools.

PASI facility

The AES-2006 design PHRS-C passive heat removal system is designed to operate without an external power source and to rely on relatively small gravitational pressure differences. The system operates at low near atmospheric pressure, meaning that it is susceptible to boiling oscillations due to large water-steam density difference. While oscillating flow may be an efficient heat removal mechanism, it may cause dynamic loads and consequent fatigue on system piping, containment penetrations, pipe supports, and associated vessels.

The PASI facility (Kouhia et al., 2018, 2020) is a one-loop model of an open passive containment cooling system. The applicable reference system for the PASI test facility is the passive containment heat removal system of the AES-2006 type pressurized water reactor. The design height scale of the PASI facility versus the reference system is 1:2. PASI (Figure 1) consists of a steam system, an open natural circulation system, and measurement and data acquisition systems. To the original design of the facility the higher sparger and water pool have been designed and installed.

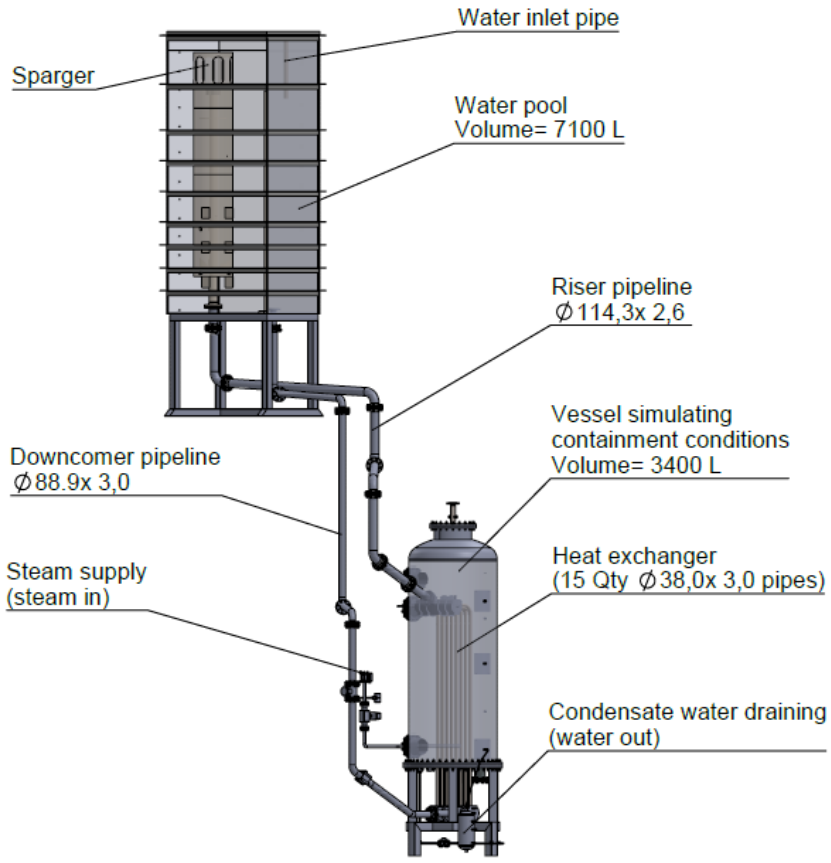

Figure 1. General view of the PASI test loop.

Natural circulation experiment

Seven characterizing experiments were performed with the PASI test facility in 2018 with the original low sparger and water pool (Kouhia, Riikonen, 2018, Kauppinen, 2019). One of these experiments was the natural circulation experiment, which was

performed to characterize the basic facility operation modes. Flow oscillations were observed in the experiment, which ended before the system reached quasi-steady two-phase flow conditions. It was expected that the oscillations would even out when the temperature in the system increases to the saturation temperature of the water pool. This was tested with a new natural circulation test in 2019 (Telkkä, Riikonen, 2019). Pre-test calculations with APROS were done with the PASI simulation model provided by VTT (Kolehmainen, 2018) to find experiment parameters.

In the experiment, the loop mass flow rate fluctuated strongly with the average oscillation frequency of about 0.01 Hz (Figure 2). The oscillation continued approximately for one hour, until the end of the experiment. Hence, the assumed attenuation of the flow oscillation was not achieved in this experiment.

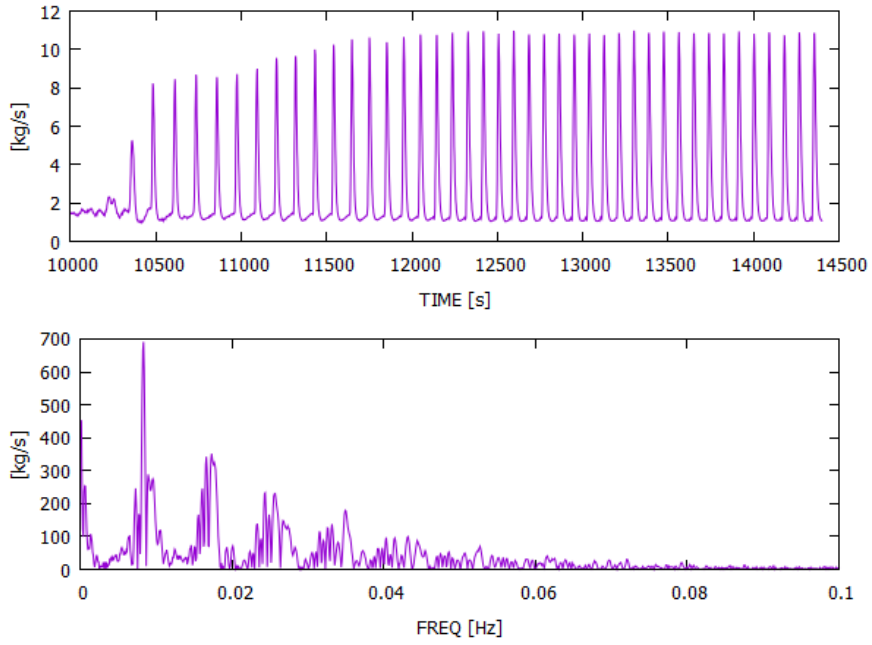

Figure 2. Flow oscillation period of the experiment and the results of the Fourier analysis for that period.

Experiments for VTT projects

In SAFIR2022, VTT proposed projects (THACO and CFD4RSA) where APROS-Fluent simulations are used for calculating the operation of the PASI facility. A test series with PASI was needed to fulfil these needs. In 2019 the tests were planned with VTT (Riikonen et al., 2019). The new experiments required some additional instrumentation and facility modifications to the vessel simulating containment

conditions. Specific goal was to produce as high-quality data as reasonable possible for APROS-Fluent simulation needs of VTT.

Two experiments were carried out with the high sparger and water pool (Telkkä, Pyy, Riikonen, 2020). In the first experiment, the goal was to observe the natural circulation behavior of the PASI facility under different steam mass flow rates to the containment and how much condensate can be collected from the bottom of the containment vessel and from the walls of the containment vessel. In the second experiment the heat losses from the containment were under investigation.

It was possible to measure the amount of condensate from the heat exchanger part of the containment where the bulk amount of condensate was created. The wall condensation was minimal (Figure 3). Most of the time it was below the measurement range of the smallest available flow measurement device.

Undesired stratification of temperatures in the containment was observed (Figure 4). The stratification was most likely due to the condensate in the bottom of the containment. A small layer of condensate will be always kept in the bottom of the vessel to ensure that pressure is not lost from the containment when draining the line.

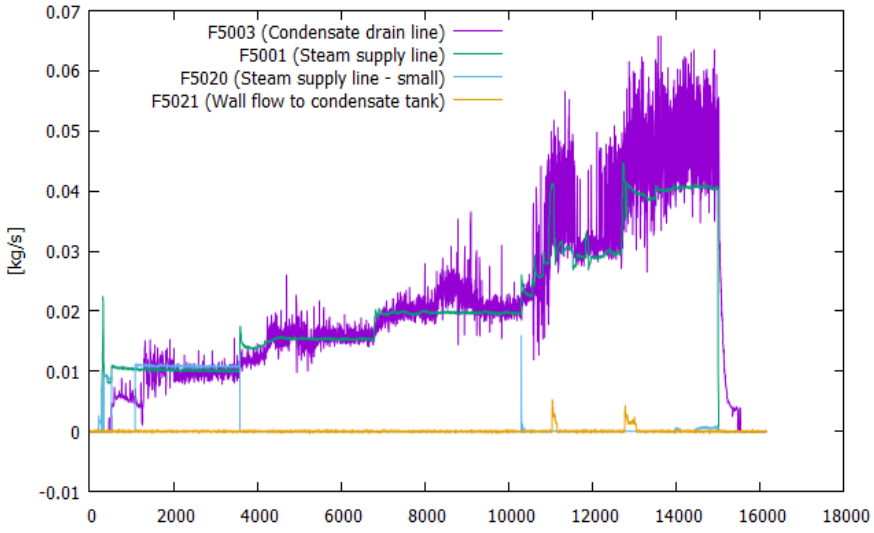

Figure 3. Mass flow rates for condensate drain line and wall flow in relation to steam supply line flows.

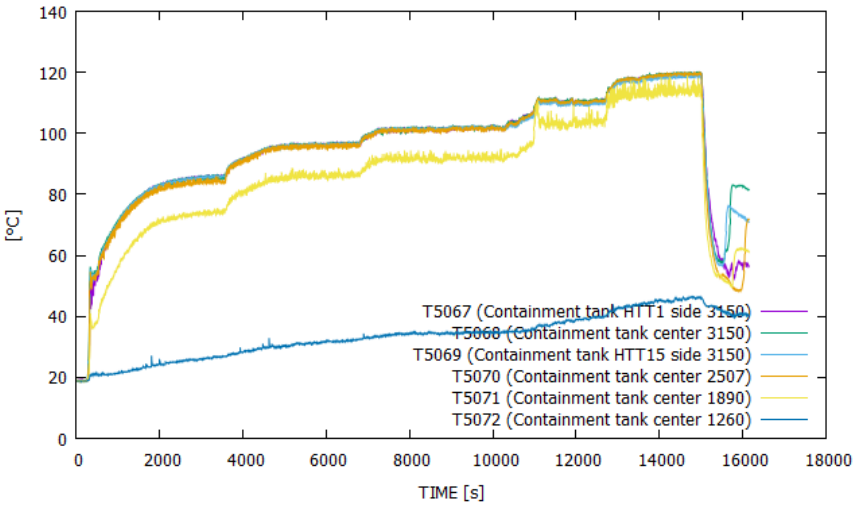

Figure 4. Temperatures inside the containment at different elevations.

The uncertainties in the defined heat losses and heat capacities of the PASI facility are relatively high. There is not any single source for the uncertainties. Mostly those are rising from the approximations made for the analysis and from the uncertainties in the measurements. The most significant source of uncertainty is the flow measurements. An additional heat loss experiment was carried out to clarify the situation. In this experiment, the loop was empty, and the vessel was heated up without steam supply but using electrical heaters inside the vessel instead.

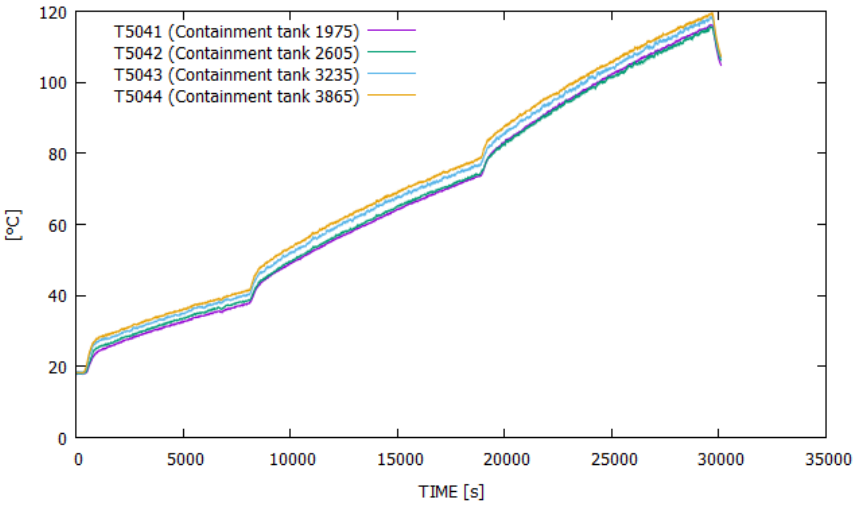

Figure 5. Temperatures at different elevations inside the containment tank.

Only minor temperature stratification inside the containment vessel was observed (Figure 5). Concerning the inner and outer wall temperatures, the temperature was clearly higher at the lowest elevation compared with the other elevations. The containment tank temperature at the lowest elevation was closer to the wall temperatures compared to the situation at the topmost elevation.

Acknowledgement

The Finnish Research Program on Nuclear Power Plant Safety 2019–2022 (SAFIR2022) has provided funding for the SAFIR2022 PAHE project. The authors are grateful for the support of this research task.

References

Kauppinen O-P, TRACE model of PASI test facility. PAHE 1/2019, Research Report, LUT University, Nuclear Engineering, 2019, Lappeenranta.

Kolehmainen, J., Apros simulations of the PASI characterizing experiments. Research report, VTT-R-04602-18.

Kouhia V., Riikonen V., Telkkä J., Partanen H., Räsänen A., Kauppinen O-P., Kotro E., Saure I., Tielinen K., Karppinen J., General description of the PASI test facility, second edition. INTEGRA 5/2018, Technical Report, Lappeenranta-Lahti University of Technology LUT, Nuclear Engineering, 2018, Lappeenranta.

Kouhia V., Riikonen V., PASI facility – characterizing experiments. INTEGRA 3/2018, Research Report, Lappeenranta University of Technology, Nuclear Engineering, 2018, Lappeenranta.

Kouhia, V., Riikonen, V., Kauppinen, O.-P., Telkkä, J., Hyvärinen, J., 2020. PASI – A TEST FACILITY FOR RESEARCH ON PASSIVE HEAT REMOVAL. Article in the proceedings of the International Topical Meeting on Advances in Thermal Hydraulics 2020 (ATH 2020).

Riikonen V., Purhonen H., Kauppinen O-P., Kouhia V., Telkkä J., Räsänen A., Kotro E., Tielinen K., PASI test plans. PAHE 2/2019, Research Report, LUT University, Nuclear Engineering, 2019, Lappeenranta.

Telkkä J., Pyy L., Riikonen V., PASI tests for VTT projects. PAHE 1/2020, Research Report, LUT University, Nuclear Engineering, 2020, Lappeenranta.

Telkkä J., Riikonen V., PASI natural circulation test NC-03. PAHE 3/2019, Research Report, LUT University, Nuclear Engineering, 2019, Lappeenranta.

5.3 PWR PACTEL tests (PATE)

Vesa Riikonen, Virpi Kouhia, Lauri Pyy

LUT University
P.O. Box 20, FI-53851 Lappeenranta, Finland

Abstract

The objective of the project is to improve the understanding of thermal hydraulic system behavior of EPR type PWRs by performing integral effects tests with PWR PACTEL (Kouhia et al., 2019). Carefully designed experiments are the most reliable way to obtain fundamental understanding and reliable data of the phenomena. Data can be used in the development and validation of computer codes for the safety analyses of nuclear power plants. Performing experiments not only requires the hardware and programs controlling the devices and gathering data, but also the knowledge of the system behavior. Computer analyses are needed in the planning of the experiments as well as in post analyses to help understanding the physics in the experiments.

Introduction

The PWR PACTEL facility has been designed and constructed in LUT University to gain experience on the behavior of EPR type PWRs and to study unique EPR accident management procedures. The research has been focused on different phenomena in the main circulation loops and vertical steam generators. Finland has participated also in the OECD/NEA PKL Phase 4 project with PWR PACTEL experiments. The education of experts on EPR specific issues and the preservation of expertise on experimental research are the major tasks of the PWR PACTEL related research.

A part of the international efforts in enhancing the reactor safety is the OECD projects. Finland participated in the OECD/NEA PKL Phase 4 project. Most of the OECD countries using nuclear power are participating in the PKL projects. The OECD/NEA PKL Phase 4 experiments investigated safety issues relevant for current PWR plants as well as for new PWR design concepts by means of systematic parameter studies on thermal hydraulic phenomena and transient tests under postulated accident scenarios. Finland and LUT provided two integral tests and one reference test (impact of nitrogen on cool-down/heat removal) with the PWR PACTEL facility. The OECD/NEA PKL Phase 4 project ended in autumn 2020. LUT is participating also in the OECD/NEA ETHARINUS project through the SAFIR2022 PATE project. The project began on 1.12.2020.

Most of the organizations participating in the OECD PKL Phase 4 Project were doing analytical work with thermal-hydraulic codes. In 2018 a TRACE model of the PKL facility was made in the SAFIR2018 INTEGRA project. The model has been

used in simulations of the selected PKL experiment (Kauppinen, 2019) in the OECD/NEA PKL Phase 4 project.

The main aim of the project is to ensure the operation of safety related systems or the efficiency of the procedures in accident and transient situations of nuclear power plants. An integral test facility, such as PWR PACTEL, offers a good possibility to carry out tests that supplement test campaigns in the other facilities or make independent tests to study phenomena relevant to the safety of EPR type nuclear power plants. As a result, counterpart-like tests give information of parameter effects such as a smaller scaling ratio or a higher pressure level (PWR PACTEL/PKL) when certain operator actions or system activation set points are used. LUT can make post analyses of the PWR PACTEL experiments to help understanding the physics in the experiments if needed. LUT can participate also in the analytical work of the experiments with the PKL facility for educational purposes with the TRACE simulation model of the PKL facility.

The project carries out research on topics relevant to the safety of Finnish nuclear power plants on a high scientific level and with modern methods and experimental facilities. It enhances the Finnish nuclear safety assessment capability for solving future safety issues as they appear. It maintains and extends the research expertise needed for the experimental work and produces data for the validation of computational tools.

The project has a significant international connection through the OECD/NEA PKL Phase 4 and OECD/NEA ETHARINUS projects training new researchers and familiarizing them with international networking, as well as developing their skills in communicating their research.

PWR PACTEL facility

The PWR PACTEL test facility is designed for safety studies related to thermal hydraulics of the PWRs with EPR type vertical steam generators. The facility consists of a reactor pressure vessel model, two loops with vertical steam generators, a pressurizer, and emergency core cooling systems including nitrogen-driven accumulators.

The loops and steam generators of the EPR style construction enable the PWR and EPR related experimental research. The reactor pressure vessel model in PWR PACTEL comprises a U-tube construction modeling the downcomer, lower plenum, core, and upper plenum. The core is not a direct model of the reference EPR core. The core rod bundle consists of 144 electrically heated fuel rod simulators arranged in three parallel channels. The heated length of the core is about 2 m shorter than in the EPR core. However, the center of the core is at the correct elevation. The core can be powered by a maximum of 1 MW electric power supply. The maximum core power corresponds roughly to the scaled residual heating power of the EPR reactor. The total height of the PWR PACTEL pressure vessel model corresponds to the pressure vessel height of EPR. The volume ratio between the pressure vessels in PWR PACTEL and EPR is about 1/405. The pressurizer is shorter than in

EPR. The volume ratio between the pressurizers of PWR PACTEL and EPR is 1/562. The two primary loops with vertical steam generators are fully representative for PWR applications. Each loop has a steam generator of 51 full size inverted U-tubes with five different tube heights, a hot leg, and a cold leg with a pump. The height of the steam generators is approximately 1/4 of the height of the steam generators in the EPR plant. The heat transfer area of the heat exchange tube bundles and the primary side volume of each steam generator scale down to the ratio of 1/400. The general view of the PWR PACTEL test facility is presented in Figure 1.

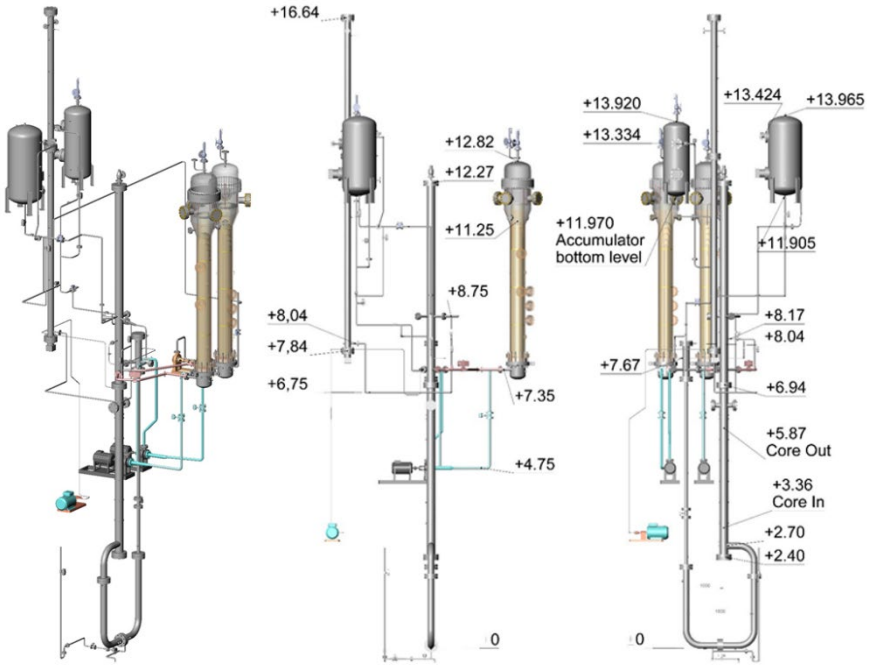

Figure 1. General view of the PWR PACTEL facility.

The instrumentation in the facility comprises temperature, pressure, pressure difference, and flow transducers. The core power, the power of the heaters in the pressurizer, and the power of the main circulation pumps are measured also. Signals from the measurement instruments are recorded with the National Instruments Compact FieldPoint distributed I/O system and then converted into engineering units using appropriate conversion equations and factors. Some parameters such as mass flow rates and liquid levels require calculation of the single-phase coolant density based on the local pressure and fluid temperature information using steam tables. The experiment data are checked manually. Data are reviewed for anomalous readings and mutually compared with readings of nearby instruments.

Nitrogen experiments

Finland participated in the OECD/NEA PKL Phase 4 project. The experiments investigated safety issues relevant for current PWR plants as well as for new PWR design concepts by means of systematic parameter studies on thermal-hydraulic phenomena and transient tests under postulated accident scenarios. The test topics had been arranged according to the two focus areas implemented into the experiments: parametric studies on thermal-hydraulic procedures for model development and validation of T/H system codes and experimental verification of cool-down procedures and operation modes for different incidents and accidents.

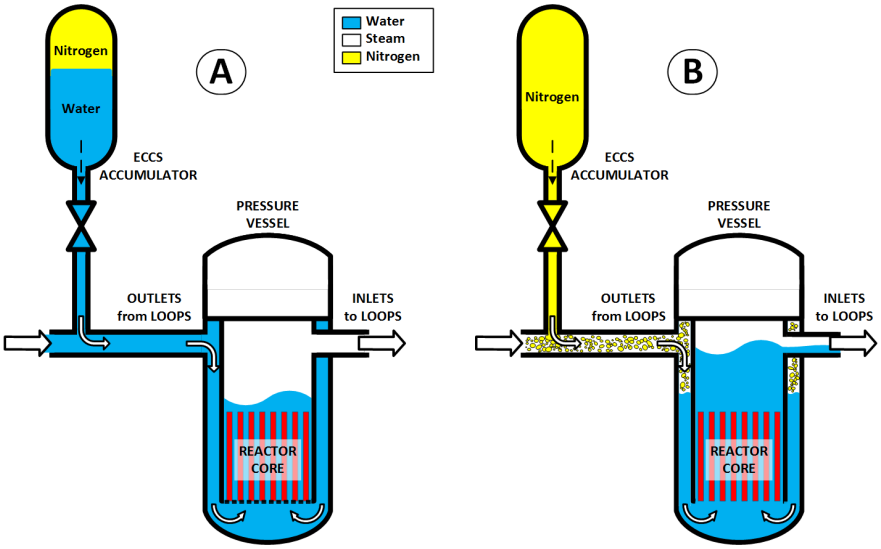

Figure 2. Anticipated behavior of the reactor cooling system during LOCA when nitrogen in the accumulator is released to the primary side.

In the OECD/NEA PKL Phase 4 project three PWR PACTEL experiments (Riikonen, 2019) were performed in 2018 and 2019. The PWR PACTEL tests complemented the PKL experiment(s) on IB/SB-LOCA. The experiments were planned in co-operation with the project partners. In the earlier PWR PACTEL experiments (Riikonen et al., 2018) studying the effect of nitrogen in LOCA, the piston effect of nitrogen (Figure 2) was studied. In these experiments, the line between the upper plenum and downcomer was open and the break location near the downcomer. Therefore, nitrogen escaped through the break and no clear piston effect was observed. In the PWR PACTEL experiments of the OECD/NEA PKL Phase 4 project, the break location was near the steam generator and the effect of the line between the upper plenum and downcomer was tested. The experiments required a reference experiment where nitrogen was not released to the primary system. Two experiments

where nitrogen was released to the primary system, were carried out in 2019 in SAFIR2022 PATE project.

The earlier PWR PACTEL nitrogen experiments with a hot leg break (Riikonen et al., 2018) showed that the accumulator nitrogen could stop the primary side depressurization and cause a core heat up at reactor pressure above or very close to a typical low-pressure safety injection shut-off head. To map the range of the pressures at which the decoupling of the primary and secondary side pressures takes place more testing is needed, as a function of the break size, the number of the accumulators injecting (nitrogen mass) and the number of the steam generators participating in the secondary side depressurization (volume available for nitrogen). The main goal of these nitrogen effect tests is to map the full range of the pressures at which the decoupling of the primary and secondary side pressures takes place and to generate data for the code validation of system thermal hydraulic codes. Pre-test simulations with APROS were done to plan the experiments. In the pre-test simulations the effect of break size and suitable break sizes in the experiments were studied.

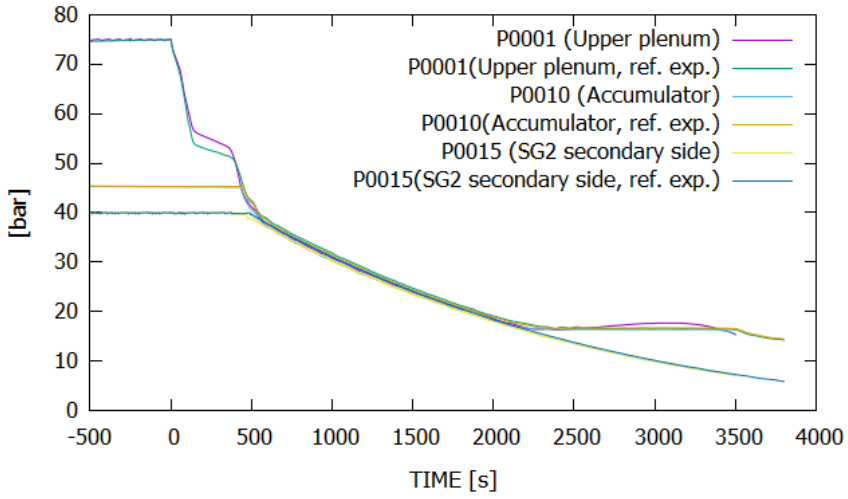

Figure 3. Pressures in the primary and secondary sides and accumulator.

The first test to investigate the effect of the number of steam generators on the system was carried out in 2020 (Kouhia, Riikonen, 2020). In this experiment only one loop was used. The overall system behavior was as in the reference experiment with two loops. The progression of the main parameters was similar and the main event timings were relatively close to each other in the experiments, though the transient proceeded slightly faster with one loop. The core heat-up started slightly earlier and the amount of water in the pressure vessel and loop was at times located slightly differently between the experiments. As the accumulator nitrogen release period started the primary pressure decrease stopped. The results showed that the

transient with either one or two loops and steam generators connected to the system had a similar effect on the overall appearance of the decoupling of the pressures, the pressure value level when the decoupling appeared, and the length of that period (Figure 3).

The results of the tests on nitrogen effects are used for ensuring the computational capabilities in predicting the effect of nitrogen in the accumulator injection in plant analyses. The test data can be used in the development and validation of computer codes for the safety analyses of nuclear power plants.

Inadvertent opening of the pressurizer SV with a simultaneous opening of the MSRT valves experiments

An inadvertent opening of the pressurizer pilot operated safety valve with a simultaneous spurious full opening of the valves in the main steam relief trains influences the departure from nucleate boiling ratio in the beginning of a loss-of-coolant accident. At the same time the primary system is cooled down. This affects the core temperature and DNBR, but the magnitude of the effects is not clear. The goal of the experiments was to clarify the effect of the fast secondary side cooldown. The experiments were planned in co-operation with TVO in 2019 (Riikonen, Pyy, 2019). Pre-test simulations with APROS were done to get initial insight on the conditions during the experiment procedures.

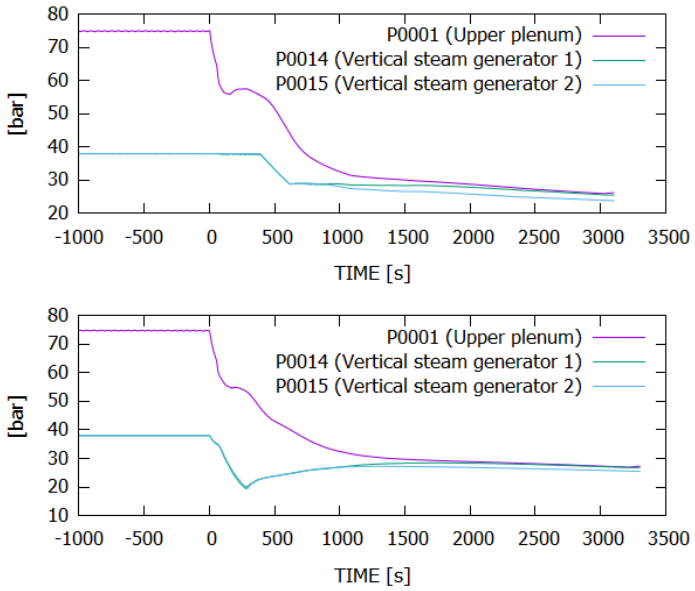

Figure 4. Pressures in the primary and secondary sides.

Two experiments were performed (Riikonen, Pyy, 2020). In the first experiment opening of one pressurizer safety release valve was assumed. The second experiment was similar but the main steam relief valves were assumed to open at the same time as one pressurizer safety release valve. The general system behavior was similar in both experiments. The core temperatures never increased above the initial values. At the end, the core temperatures stabilized and decreased slowly.

The results of the experiments are used for clarifying the effect of the fast secondary side cooldown. The subject is relevant to validate I&C fault analysis. The test data can be used in the development and validation of computer codes for the safety analyses of nuclear power plants.

Simulations of PWR PACTEL nitrogen experiment

The APROS code version 6.08.23 was used in the post-test simulation of one PWR PACTEL nitrogen experiment, which was performed in the OECD/NEA PKL Phase 4 project. The simulation model of the PWR PACTEL facility utilizes the 6-equation thermal-hydraulic model of the APROS code. The PWR PACTEL simulation model includes the main parts of the facility: the whole primary side, the secondary sides of the steam generators and the ECCS as needed. The geometry is modelled moderately detailed, and the measurement elevations of the facility are considered thoroughly in the nodalization. The simplified scheme of the simulation model used in this simulation task is shown in Figure 5. The dense nodalization in the actual simulation model is not fully visible in the figure. The utilized process components include more than one node in the calculation level and the division into nodes is not fully representative.

In general, this calculation task with the APROS code showed comparable results compared to the measured data (Kouhia, 2020). The overall trends and events during the transient were predicted comparable. Yet, some discrepancies were found, connected to some local parameter values and the manometric behavior between the simulation and experiment results. The accumulator injection period was slightly prolonged in the simulation. The nodalization choices affected the mixing and parameter trends for example in the downcomer top parts. The accumulator model needed modification considering the efficiency of the liquid heat transfer by increasing the multiplication factor from the default value to a value of 9.5 in this case. The transient calculation with nitrogen content involved is at certain periods consuming the computer CPU time and prolonging the overall calculation time. The maximum time step needs to be decreased to a small value at times to avoid divergence problems.

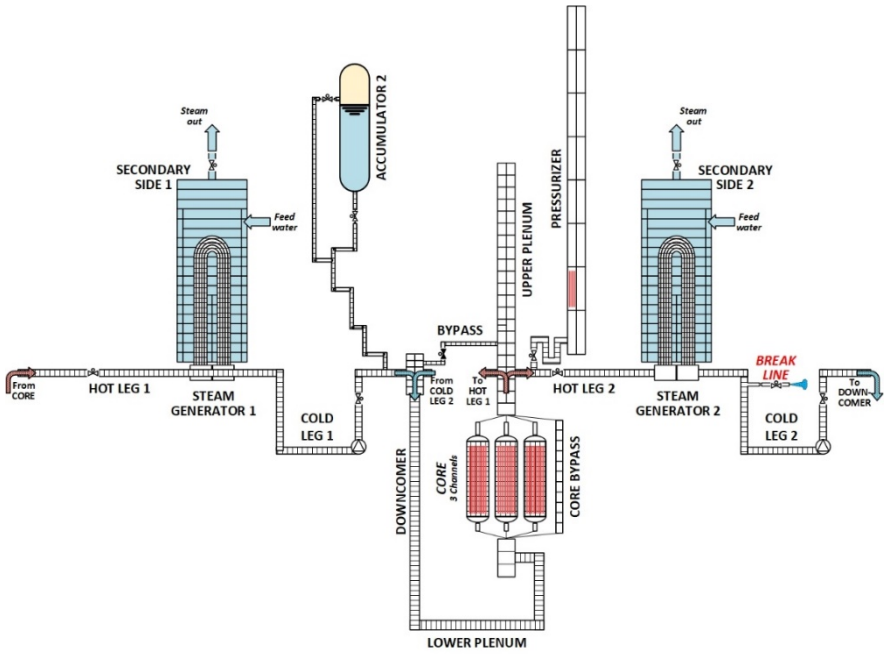

Figure 5. Schematic view of the PWR PACTEL simulation model for the APROS code.

TRACE calculations of PKL i2.2 run 3

In the OECD/NEA PKL Phase 4 project, the experiment results were analyzed by the organizations participating in the project. Extensive computational efforts were used in the OECD/NEA PKL Phase 4 project to analyze the transients ran in the test facilities and to transfer the data to the reactor scale. With the TRACE simulation model of the PKL facility LUT participated also in the analytical work of the experiments with the PKL facility.

At LUT University, the TRACE model of the PKL test facility was constructed in the SAFIR2018 INTEGRA project in 2018. In the SAFIR2022 PATE project in 2019, the TRACE model was tested by calculating one transient test of the PKL facility (Kauppinen, 2019). The TRACE model of the PKL facility was constructed by using the Symbolic Nuclear Analysis Package (SNAP) and the calculations of the PKL i2.2 run 3 test were performed with the TRACE version of 5.0 patch 5. Figure 6 presents the TRACE model of the PKL test facility. The model includes all the main components of the facility, i.e., the reactor pressure vessel, pressurizer, four loops with steam generators and primary coolant pumps, steam generator secondary sides, and accumulators. The pressure drops and heat losses of the model are adjusted according the PKL experiment results.

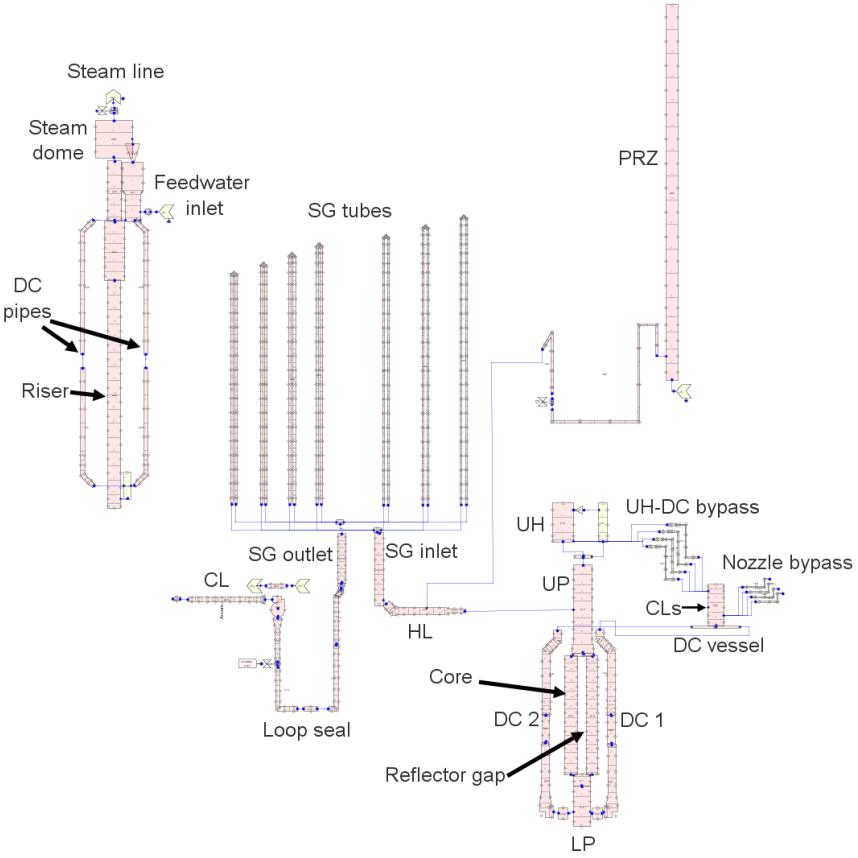

Figure 6. TRACE model of the PKL test facility. Only the reactor pressure vessel and Loop 2 with the pressurizer and steam generator secondary side are presented. All four loops are modelled similarly.

The calculated test was PKL test i2.2 run 3 which is an IBLOCA experiment. In the test the break located in the horizontal part of the cold leg in Loop 1. The break was oriented upwards, and the break size was 17 % of the cold leg flow area. The HPSI and LPSI systems were injecting in the cold leg of Loop 3. Two of the eight PKL accumulators were active; one injecting to the cold leg of Loop 2 and one in the cold leg of Loop 3.

The calculated initial conditions were mostly well predicted by TRACE. Also, the general progression of the transient was relatively well predicted, even though there were some discrepancies between the calculation and test. The leaked water mass was overestimated in the calculation. The direct outflow of the ECC water through the break seemed to be overestimated due the simple nodalization in the downcomer top part. The LPSI injection started much earlier in the calculation than in the test since the primary side pressure dropped at the lower level compared to the test.

TRACE did not predict the core heat-up while in the test two small core temperature excursions occurred: at the beginning of the transient before the HPSI injection and at the beginning of the accumulator injection. Also, there were discrepancies in the steam generator outlet collector and secondary side temperatures between the test and calculation.

During the TRACE calculations, the adjustments of the k-factors at the break throat, at the edges of the cold legs and downcomer, and at the accumulator injection line orifice were done for improving the model prediction. These adjustments improved the prediction of the leaked mass, the behavior of the primary side pressure, the accumulator injection flow rate, and the core cladding temperature behavior during the accumulator water injection.

Acknowledgement

The Finnish Research Program on Nuclear Power Plant Safety 2019–2022 (SAFIR2022) has provided funding for the SAFIR2022 PATE project. The OECD/NEA PKL Phase 4 project was performed with the financial support of the Finnish Research Programme on Nuclear Power Plant Safety (SAFIR2018 and SAFIR2022) and the partners participating in the OECD/NEA PKL Phase 4 project.

The authors are grateful for their support to all the financiers of this research task, OECD Nuclear Energy Agency (NEA), the members of the SAFIR2018 and SAFIR2022 Reference Group 4, and the members of the Program Review Group and the Management Board of the OECD/NEA PKL Phase 4 project. The data from the experiments in the OECD/NEA PKL Phase 4 project is available to the NEA member countries via their CSNI representative organizations three years after the end of the project.

References

Kouhia V., Simulation of PWR PACTEL Nitrogen Experiment NCG-23 with APROS, Research Report, PATE 5/2019, LUT University / Nuclear Engineering, 2020, Lappeenranta.

Kouhia V., Riikonen V., PWR PACTEL Nitrogen Experiment NCG-30, Research Report, PATE 1/2020, LUT University / Nuclear Engineering, 2020, Lappeenranta.

Kouhia V., Riikonen V., Partanen H., Räsänen A., Kauppinen O-P., Telkkä J., Pyy L., Tielinen K., General Description of the PWR PACTEL test facility – fourth edition, Technical report, PATE 1/2019, LUT University / Nuclear Engineering, 2019, Lappeenranta.

Kauppinen O-P., TRACE calculations of PKL i2.2 run 3, Research Report, PATE 6/2019, LUT University / Nuclear Engineering, 2019, Lappeenranta.

Riikonen V., The PWR PACTEL nitrogen experiments in the OECD/NEA PKL Phase 4 project, Research Report, PATE 2/2019, LUT University / Nuclear Engineering, 2019, Lappeenranta.

Riikonen V., Pyy L., Plans for the PWR PACTEL inadvertent opening of SV and MSRT tests, Research Report, PATE 3/2019, LUT University / Nuclear Engineering, 2019, Lappeenranta.

Riikonen V., Pyy L., PWR PACTEL experiments of inadvertent opening of SV and MSRT, Research Report, PATE 2/2020, LUT University / Nuclear Engineering, 2020, Lappeenranta.

Riikonen V., Kouhia V., Kauppinen O-P., Sjövall H., Hyvärinen J., Experimental observation of adverse and beneficial effects of nitrogen on reactor core cooling, Nuclear Engineering and Design 332 (2018) 111–118, https://doi.org/10.1016/j.nucengdes.2018.03.027.

5.4 Sparger separate effect tests (SPASET)

Markku Puustinen, Antti Räsänen, Lauri Pyy, Eetu Kotro, Kimmo Tielinen,
Giteshkumar Patel, Elina Hujala

Lappeenranta-Lahti University of Technology LUT
School of Energy Systems
Nuclear Engineering
P.O. Box 20, FI-53851 Lappeenranta

Abstract

The Sparger Separate Effect Tests (SPASET) project has increased knowledge of small-scale phenomena affecting the effective heat and momentum sources during steam injection through spargers. The effect of pool water sub-cooling, a transition from sub-sonic to sonic flow conditions, injection nozzle chamfer, and multi-hole injection on the effective momentum have been studied. The experiment results have been utilized in the development and validation of the simplified effective heat source (EHS) and effective momentum source (EMS) models proposed by KTH. They are also being used at LUT and VTT in the improvement of the computational fluid dynamics (CFD) models related to direct contact condensation (DCC).

Introduction

Steam injection through spargers induces heat, momentum, and mass sources that depend on the steam injection conditions and can result in thermal stratification or mixing of the pressure suppression pool (PSP). The development of thermal stratification in the PSP is of safety concern since it reduces steam condensation capacity of the pool, increases the pool surface temperature, and thus leads to higher containment pressures, compared with completely mixed pool conditions. A realistic evaluation of the steam condensation capacity of the PSP in different thermal stratification scenarios is therefore important and additional data on pool behaviour are needed for validation of computer models and realistic evaluation of safety margins.

The SPASET project has contributed to the validation of simulation tools, i.e. CFD codes such as ANSYS Fluent and OpenFOAM and system codes such as Apros, by increasing knowledge of small-scale phenomena affecting the effective heat and momentum sources during steam injection through spargers. The experiment results have been utilized for the evaluation of the simulation models in the SPASET project itself at LUT as well as in the related CFD4RSA project at VTT and in Nordic co-operation research efforts between LUT, VTT and KTH.

Prediction of the long-term thermal behaviour of a large water pool during steam injection through blowdown pipes and spargers with CFD codes is time-consuming and requires lots of computational capacity because the associated DCC phenomenon needs to be solved. The simplified EHS and EMS models would reduce the

needed computational capacity. The premise of these models is that due to the difference in spatial and time scales between the DCC phenomena and large pool behaviour, only the integral effects of DCC on the pool should be modelled. These effects are defined as heat and momentum sources, which determine the large-scale pool circulation and temperature distribution.

Validation of the EHS/EMS models has been done using experimental data from the drywell-wetwell suppression pool facility (PPOOLEX) and the separate effect facility (SEF-POOL) at LUT, Finland, and the PANDA facility at PSI, Switzerland [Li et al., 2014, Li et al., 2018, Gallego-Marcos et al., 2018a, Gallego-Marcos et al., 2018b, Gallego-Marcos et al., 2019a, Gallego-Marcos et al., 2019b, Gallego-Marcos et al., 2018c]. The validated models have been applied to the full-scale analysis of a Nordic BWR PSP during a steam injection through spargers [Gallego-Marcos et al., 2019c]. The results show that strong thermal stratification of potential safety importance can develop in the pool during prototypic steam injection conditions. The analysis results suggest that further development of the EHS/EMS correlations and computational models is necessary to enable modeling of regimes and conditions, which have not yet been studied in experiments, but are critically important and can completely change the PSP stratification and mixing behaviour.

LUT has studied the suitability of the large interface condensation and interfacial area models of the OpenFOAM code for steam injection through spargers in the SPASET project [Patel et al., 2019, Patel et al., 2020]. VTT has implemented the EHS/EMS models in the ANSYS Fluent code by using user-defined functions and performed simulations of DCC and thermal stratification experiments of LUT in a related CFD4RSA project [Pättikangas et al., 2018, Pättikangas, 2020]. Also, VTT has studied the possibilities to implement the approaches based on the EHS/EMS model in the Apros system code.

A combined experimental/analytical/computational program has been carried out during the SPASET project. With experiments in the SEF-POOL facility, a database for the development, improvement, and validation of numerical simulation models has been generated. Sophisticated, high-frequency measurements and high-speed video cameras have been used to get detailed enough data.

SEF-POOL test facility

The reference system for the SEF-POOL facility is an SRV sparger pipe of a BWR plant. Hence, the facility is designed in such a way that discharge of steam through injection holes at the sparger lower end into sub-cooled pool water can be simulated representatively [Tielinen et al., 2018]. The goal of the tests is to define the effective momentum for a given steam condensation regime, particularly for the oscillatory bubble regime. For this purpose, the design of the test facility is such that the effective momentum (liquid force carried by the condensate liquid) can be directly measured with a force sensor or it can be calculated based on measured steam momentum (steam force at the injection hole) (Figure 1).

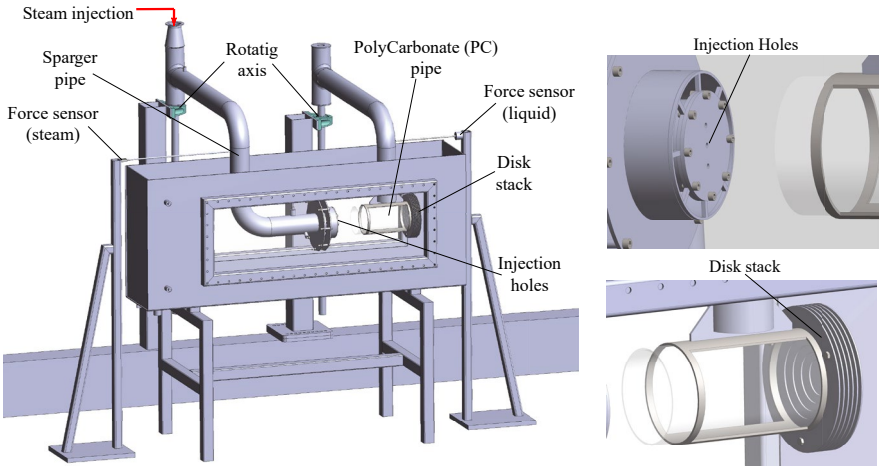

Figure 1. General view of the SEF-POOL facility configuration where the propulsion volume (PC pipe) is independent and attached to its own support arm.

For helping to recognize different flow regimes and for obtaining the bubble diameter as a function of time, the test facility allows high-speed video recordings of the DCC of steam through a window on the sidewall of the pool. The high-speed camera system consists of two monochromatic Phantom Miro M310 cameras. The maximum resolution is 1280x800 px, but in practise the picture area is cropped to increase the maximum amount of the images the internal memory can hold, thus increasing the total time of the recordings. The imaging system has evolved during the project and in the tests conducted in 2020 stereo viewing perspective, i.e. both cameras were in an angle towards the pool, was applied. Besides, the calibration procedure was improved by shifting from separate calibration images to recording a calibration video consisting in theory of thousands of calibration images.

An air injection system has been built for generating bubbles into the pool for visualizing flow fields. Figure 2 shows a stereo view of a cloud of rising small air bubbles generated with the system in a stagnant pool, i.e. there was no steam injection into the pool at that moment.

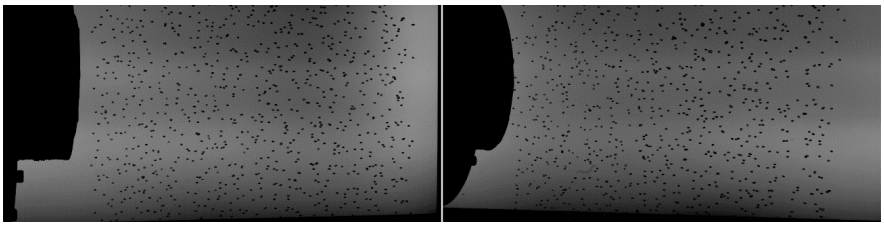

Figure 2. Cloud of intentionally generated air bubbles for tracking liquid movements in the SEF-POOL facility.

SEF-POOL tests

In BWRs, the development of thermal stratification or mixing during steam injection through spargers can affect the performance of the PSP. Prediction of the effective momentum induced by the oscillatory bubble regime is necessary for the modelling of the pool behaviour. To directly measure the effective momentum an extensive test series has been run in the SEF-POOL facility at LUT [Puustinen et al., 2019, Gallego-Marcos et al., 2019b, Puustinen et al., 2020, Puustinen et al., 2021]. Data on the characteristics of small-scale phenomena affecting the effective heat and momentum sources have been provided.

Effect of pool water sub-cooling on the effective momentum, effective momentum in the transition regime, i.e. effect of transition from sub-sonic to sonic flow conditions, effective momentum at mass fluxes higher than 300 kg/m^{2}s, the effect of nozzle chamfer and multi-hole injection have been studied in 2019-2020. Particular interest in the 2020 tests was in capturing good-quality high-speed camera stereo recordings of the steam jet behaviour and jet entrainment visualized with the help of air bubbles injected into the pool. Oscillatory bubble, partly the oscillatory cone jet, and partly the stable jet regimes have been the covered flow modes in the tests.

Steam injection into the initially highly subcooled pool in sub-sonic and sonic regimes revealed that both the Jacob and Mach number have a significant effect on the effective momentum coefficient C (i.e. the ratio of the liquid momentum rate to the theoretical value of the momentum rate of steam). Figures 3 and 4 present the time-averaged steam mass flow rates, force values, and pool temperatures from the tests done in sub-sonic and sonic conditions, respectively. In the sub-sonic case, the measured force curve has a low gradient shape during the initial phase of the test when the pool water is highly sub-cooled. In the sonic case, the measured force jumps more directly upwards as soon as the steam injection is started.

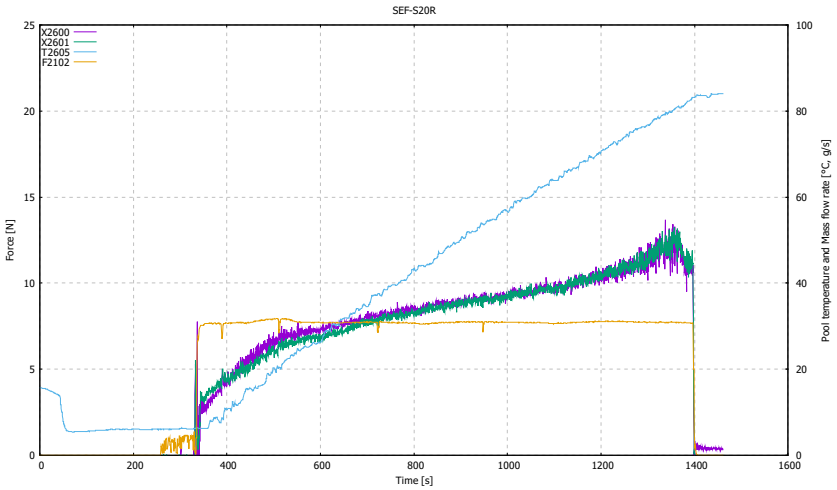

Figure 3. Measured forces (X2600, X2601), flow rate (F2102) and pool temperature (T2605) with sub-sonic steam injection into a highly sub-cooled water pool.

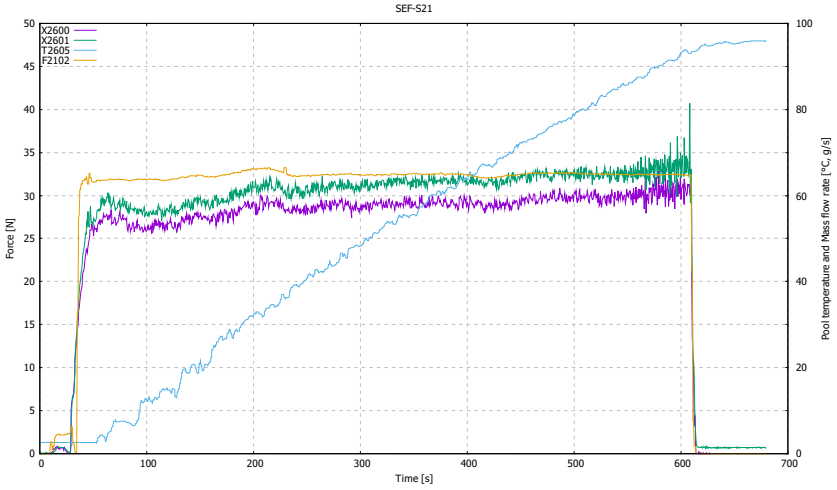

Figure 4. Measured forces (X2600, X2601), flow rate (F2102) and pool temperature (T2605) with sonic steam injection into a highly sub-cooled water pool.

Practically all the injection holes in plant spargers are drilled with chamfers, i.e. the outlet edge of the injection hole is specifically shaped. The effect of the chamfered injection hole was studied in the 2019 tests in SEF-POOL. The injection plate used in those tests was manufactured so that a 125° chamfer on the outlet edge of the 16 mm orifice was formed. The chamfer effect on the effective momentum magnitude was found to be almost insignificant both in the sub-sonic and sonic regime when compared to reference tests done with straight holes.

In the 2020 tests, steam injection through a three-hole plate seemed to produce slightly larger force measurement values than injection through a single-hole plate with the same steam mass flux. In addition, in the three-hole case, the measured force curve reached its peak value at the pool temperature of about 60 °C and then turned very slightly downwards while in the single-hole case the peak occurred at the pool temperature of about 80 °C.

As the sub-cooling of the pool water decreases, the size of the forming steam bubbles increases (Figure 5). The high-speed video clips reveal that at low sub-cooling detached bubbles can move a long distance from the injection hole and allow the formation of a new bubble before they collapse. Close to saturation conditions a new developing bubble can catch up with the previous detached bubble, which has not condensed completely yet, collide with it, and even merge with it.

Both in the single-hole and three-hole tests done with the smallest steam injection rate, incomplete condensation occurred as the pool temperature approached saturation conditions. The forming steam bubbles were large and they started to rise upwards due to buoyancy forces even when they were still attached to the injection plate. The detached bubbles continued the rising movement and seemed to reach the pool surface before they collapsed. In these cases, the steam flow velocity was so small that the forming steam bubbles slowed down and were unable to travel horizontally far from the injection plate. Instead, the buoyancy forces took control and started to lift the bubbles upwards.

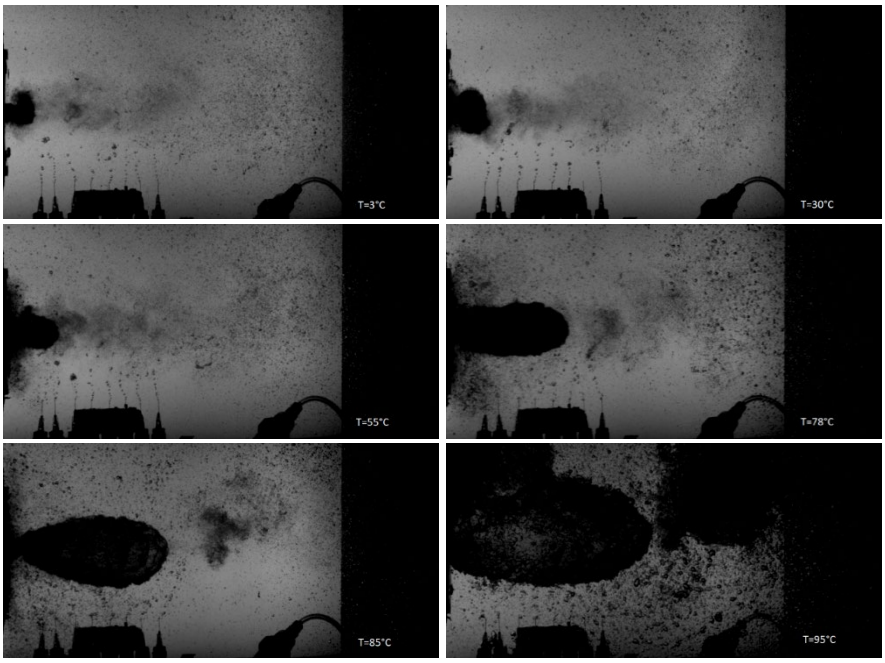

Figure 5. Effect of pool water temperature on the size of forming steam bubbles.

The most important outcome of the 2020 tests was the successful refining of the air bubble generator configuration and the high-speed camera set-up so that KTH can effectively use their in-house tools in the analysis of the recordings for tracking the movement of the air bubbles and thus ultimately assess the liquid velocity and the amount of jet entrainment.

OpenFOAM simulations and pattern recognition algorithm

The SEF-INF2 test was chosen as the reference case for the CFD simulations. In the test, the saturated vapour was injected by using an orifice of a diameter of 16 mm. A 2D-axisymmetric geometry containing a 1° sector of the whole SEF-POOL facility was generated including the condensation pool around the PC pipe. Two grid refinements (1 mm and 2 mm) were used in the PC pipe uniformly to study the effect of grid density on DCC rates. All the simulations were obtained by employing the compressible two-phase solver 'reactingTwoPhaseEulerFoam', which is based on the Eulerian-Eulerian two-fluid approach of the OpenFOAM-7 CFD code. The Rayleigh-Taylor Interfacial (RTI) area model of Pellegrini et al. was included for the interfacial area modeling [Pellegrini et al., 2015]. The interfacial heat transfer between steam and water was modelled by using the Nusselt number formulation of the Coste continuous model of Coste [Coste, 2004]. Flow turbulence was solved by employing the $k - \varepsilon$ turbulence model.

The results showed that the velocity boundary condition yielded incorrect behaviour of the steam-water interface in the PC pipe. A pressure inlet boundary condition was suitable for this case and provided the average mass flow rate measured in the test. The formation and condensation of the bubbles were visible in the OpenFOAM simulations of the SEF-POOL test (Figure 6). The steam plume length and bubble size qualitatively were smaller in the 1 mm grid case than in the 2 mm grid case. The denser grid enlarged the total interfacial area, which increased the total DCC rate in the simulations. However, it is difficult to draw any further conclusions based on the simulated short transient. A longer simulated transient is needed to analyse the validity of the DCC and interfacial area models in sparger cases.

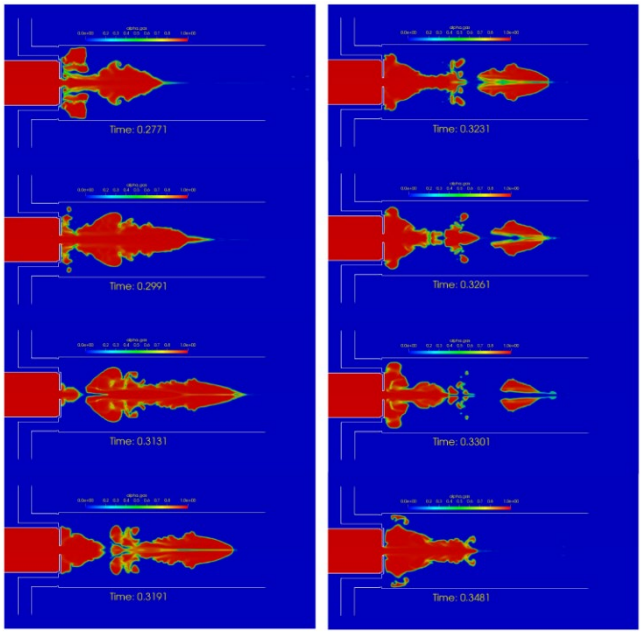

Figure 6. Instantaneous volume fraction fields showing the second bubble formation and condensation in the OpenFOAM simulation with 1 mm uniform grid size.

The same test was simulated with the 3D domain. The results show that a bubble formed at the sparger orifice and detached from there (Figure 7). It travelled forward oscillating and finally condensed rapidly in the pool water. The steam bubble condensed inside the PC pipe. In the 3D simulation, the first bubble formation, and its detachment took a little longer time than in the 2D-axisymmetric simulations. Also, the total interfacial area and bubble volume in the 3D simulations were smaller than in the 2D-axisymmetric simulations.

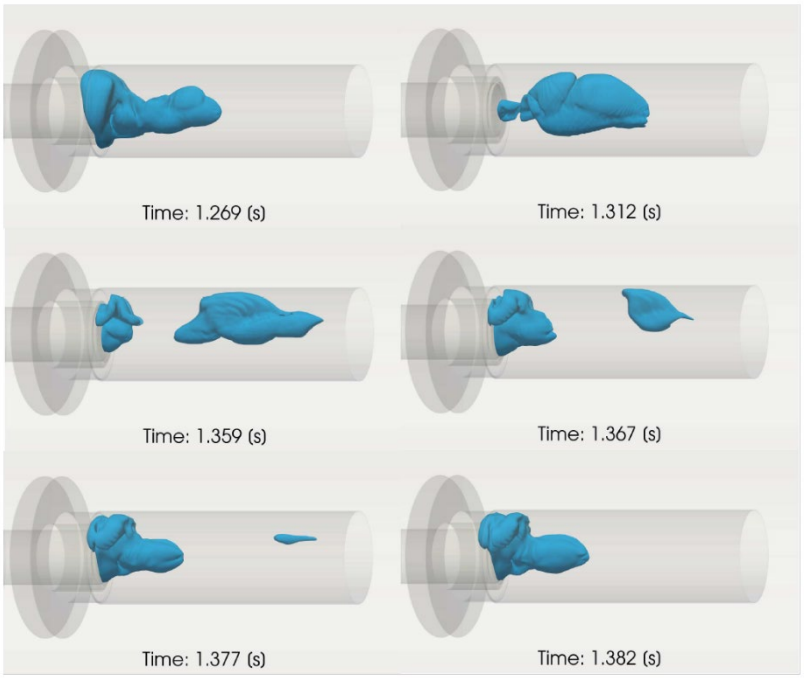

Figure 7. Instantaneous volume fraction fields showing the formation and condensation of a steam bubble in the 3D OpenFOAM simulation of the SEF-INF2 test.

Image analysis and pattern recognition have great potential in thermal-hydraulic research. The image analysis algorithm developed at LUT has been improved to cover cases where multiple bubbles travel at the same time in the frame being analysed and it now seems to work well with multiple bubbles tracking their whole lifetime (Figure 8). After constructing the tracks of the bubbles, different properties of the bubbles can be evaluated, such as mean bubble lifetime, the mean time difference between the bubble formations, the corresponding bubble formation frequency, surface velocities, and accelerations to different directions in the 2D plane. The algorithm was applied to the SEF-INF2 video recordings and the instantaneous volume fraction field images of the 2D simulation results. The modified pattern recognition-based image analysis algorithm represented the real bubble shape better than before. It yielded a good total bubble volume of the 2D-axisymmetric case with the 2mm grid size.

With suitable video recordings, the algorithm can be used with pipe flows too. Surface velocity and acceleration estimations at arbitrary angles give important knowledge, for example of the direction in which the condensation of the steam bubble begins, and will thus be a good aid for CFD validation purposes.

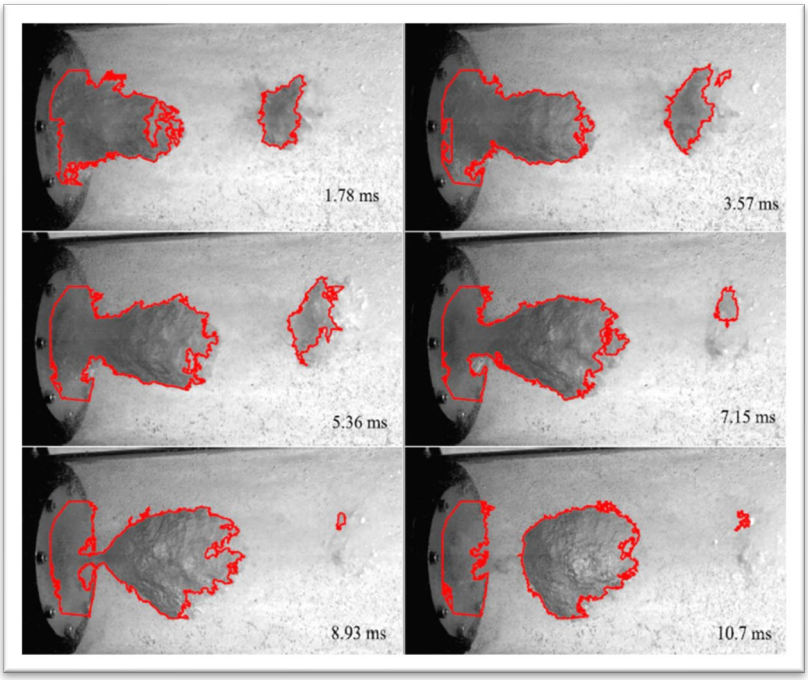

Figure 8. Application of pattern recognition algorithm to the SEF-INF2 test. Recognized steam bubble boundaries are marked as red.

Summary and conclusions

The SPASET project (2019-2020) has contributed to the validation of the simplified EHS/EMS models by increasing knowledge of small-scale phenomena affecting the effective heat and momentum sources during steam injection through spargers. Tests in the SEF-POOL at LUT have also supported the validation effort of the DCC and interfacial area models of CFD codes as well as the implementation of the EHS/EMS models to the Apros system code.

The effect of pool water sub-cooling, the transition from sub-sonic to sonic flow conditions, injection nozzle chamfer, and multi-hole injection on the effective momentum have been studied in 2019-2020. Good-quality high-speed camera stereo recordings of the steam jet behaviour and jet entrainment visualized with the help of air bubbles injected into the pool have been captured. KTH can effectively use their in-house tools in the analysis of the recordings for tracking the movement of the air bubbles and thus ultimately assess the liquid velocity and the amount of jet entrainment.

OpenFOAM simulations of the SEF-POOL tests have been performed by using both 2D-axisymmetric and 3D geometries. The effect of interfacial area modeling has been studied by implementing the Rayleigh-Taylor Interfacial (RTI) area model

of Pellegrini et al. (2015) The simulated 3D transient showed that the total DCC rate, interfacial area, and bubble volume were smaller in the 3D simulation than in the 2D-axisymmetric simulations. The improved pattern recognition-based image analysis algorithm has been successfully applied for tracking multiple steam bubbles at the same time for their whole lifetime. The algorithm was also applied to the instantaneous volume fraction field images of the 2D simulation results. The improved algorithm represented the real bubble shape better than before and yielded a good total bubble volume of the 2D-axisymmetric case with the 2mm grid size.

Acknowledgement

NKS and SSM have given financial supported for the work done under the SPASET project.

References

Coste, P. 2004. Computational Simulation of Multi-D Liquid-Vapor Thermal Shock with Condensation. Proceedings of ICMF'04, Yokohama, Japan, May 30 - June 4, 2004.

Gallego-Marcos, I., Villanueva, W., Kudinov, P. 2018a. Modelling of Pool Stratification and Mixing Induced by Steam Injection through Blowdown Pipes. Annals of Nuclear Energy 112 (2018), https://doi.org/10.1016/j.anucene.2017.10.019.

Gallego-Marcos, I., Kudinov, P., Villanueva, W., Kapulla, R., Paranjape, S., Paladino, D., Laine, J., Puustinen, M., Räsänen, A., Pyy, L., Kotro, E. 2018b. Pool Stratification and Mixing Induced by Steam Injection through Spargers; Analysis of the PPOOLEX and PANDA Experiments. Nuclear Engineering and Design 337 (2018), https://doi.org/10.1016/j.nucengdes.2018.07.004.

Gallego-Marcos, I. 2018c. Steam Condensation in a Water Pool and its Effect on Thermal Stratification and Mixing. Doctoral thesis, KTH Royal Institute of Technology, School of Engineering Sciences (SCI), Physics, Nuclear Engineering (2018), URN: urn:nbn:se:kth:diva-238732.

Gallego-Marcos, I., Kudinov, P., Villanueva, W., Kapulla, R., Paranjape, S., Paladino, D., Laine, J., Puustinen, M., Räsänen, A., Pyy, L., Kotro, E. 2019a. Pool Stratification and Mixing Induced by Steam Injection through Spargers; CFD Modelling of the PPOOLEX and PANDA Experiments. Nuclear Engineering and Design 347 (2019), https://doi.org/10.1016/j.nucengdes.2019.03.011.

Gallego-Marcos, I., Villanueva, W., Kudinov, P., Puustinen, M., Räsänen, A., Tielinen, K., Kotro, E. 2019b. Effective Momentum Induced by Steam Condensation in the Oscillatory Bubble Regime. Nuclear Engineering and Design 350 (2019), https://doi.org/10.1016/j.nucengdes.2019.05.011.

Gallego-Marcos, I., Grishchenko, D., Kudinov, P. 2019c. Thermal Stratification and Mixing in a Nordic BWR Pressure Suppression Pool. Annals of Nuclear Energy 132 (2019), https://doi.org/10.1016/j.anucene.2019.04.054.

Li, H., Villanueva, W., Puustinen, M., Laine, J., Kudinov, P. 2014. Validation of Effective Models for Simulation of Thermal Stratification and Mixing Induced by Steam Injection into a Large Pool of Water. Science and Technology of Nuclear Installations. Volume 2014, Article ID 752597.

Li, H., Villanueva, W., Puustinen, M., Laine, J., Kudinov, P. 2018. Thermal Stratification and Mixing in a Suppression Pool Induced by Direct Steam Injection. Annals of Nuclear Energy 111 (2018), https://doi.org/10.1016/j.anucene.2017.09.014.

Patel, G., Hujala, E., Tanskanen, V., Puustinen, M. 2019. OpenFOAM Simulations and Pattern Recognition Analysis of the SEF-POOL Tests. Lappeenranta University of Technology, School of Energy Systems, Nuclear Engineering, Research Report SPASET 2/2019.

Patel, G., Hujala, E., Puustinen, M. 2020. CFD Simulations and Pattern Recognition Analysis of the SEF-POOL Tests. Lappeenranta University of Technology, School of Energy Systems, Nuclear Engineering, Research Report SPASET 2/2020.

Pellegrini, M., Naitoh, M., Josey, C., Baglietto, E. 2015. Modeling of Rayleigh-Taylor Instability for Steam Direct Contact Condensation. The 16th International Topical Meeting on Nuclear Reactor Thermal Hydraulics (NURETH-16), Chicago, IL, August 30 - September 4, 2015.

Puustinen, M., Laine, J., Räsänen, A., Kotro, E., Tielinen, K. 2019. SEF-POOL Tests. Lappeenranta: Lappeenranta-Lahti University of Technology LUT. School of Energy Systems. Nuclear Engineering. Research Report INSTAB 1/2018.

Puustinen, M., Räsänen, A., Kotro, E., Tielinen, K. 2020. SEF-POOL Tests on Small-Scale Phenomena of Steam Discharge into Sub-Cooled Water. Lappeenranta: Lappeenranta-Lahti University of Technology LUT. School of Energy Systems. Nuclear Engineering. Research Report SPASET 1/2019.

Puustinen, M., Räsänen, A., Kotro, E., Tielinen, K., Pyy, L. 2021. SEF-POOL Tests on Jet Entrainment. Lappeenranta: Lappeenranta-Lahti University of Technology LUT. School of Energy Systems. Nuclear Engineering. Research Report SPASET 1/2020.

Pättikangas, T., Hovi, V. 2018. CFD Simulation of Condensation of Vapor Jets. Research Report VTT-R-00993-18, Espoo, 2018.

Pättikangas, T. 2020. CFD Analysis of Pressure Suppression Pool by Using Effective Heat and Momentum Source Models. Research Report VTT-R-00228-20, Espoo, 2020.

Tielinen, K., Räsänen, A., Kotro, E., Saure, I., 2018. General Description of SEF-POOL Test Rig. Lappeenranta University of Technology, School of Energy Systems, Nuclear Engineering, Research Report INSTAB 2/2017.

5.5 Safety through thermal-hydraulic analyses and cooperation (THACO)

Seppo Hillberg, Tatu Hovi, Ismo Karppinen, Joona Kurki, Joona Leskinen, Ari Silde, Marton Szogradi, Jarno Hiittenkivi, Robert Airaksinen

VTT Technical Research Centre of Finland Ltd
P.O. Box 1000, FI-02044 Espoo

Abstract

The first two years of THACO project have been heavily influenced by the OECD/NEA's new Rod Bundle Heat Transfer (RBHT) project. In 2019, as the new experimental data was not yet released, the work on this subject started by calculation of older RBHT experiments with both Apros and TRACE. In 2020, the new RBHT open-phase experiment data was available and it focused on the impact of rod peak power, inlet subcooling and most notable, different reflooding rates and types such as oscillatory reflooding. These cases were also calculated with Apros and TRACE. Machine learning and BEPU analysis were used in the Apros analysis and the model was made ready for the 2021 blind phase code benchmark.

Additionally, PASI (LUT), PKL and FIX-II facility experiments have been calculated within the first two years. International cooperation in various OECD/NEA's and U.S. NRC's programs is heavily represented in the project.

Introduction

THACO is a project focusing on improving nuclear safety, mainly by increasing the reliability of thermal-hydraulic deterministic safety analyses of light water nuclear power plants. In particular, the focus is on the continued validation of analysis tools for system-scale safety assessment, knowledge transfer and education of new experts. A large part of the project is focused on international and domestic cooperation projects, which contribute to obtaining crucial validation data for the research project, and also to knowledge transfer between organizations.

Main part of the analysis work is carried out with, and related to, the system-scale safety analysis tool Apros that has been developed in Finland in cooperation between VTT and Fortum, and that is currently used in safety analysis work both at the regulatory side and by Finnish utilities Fennovoima, Fortum and TVO. Another code used in lesser extent in the project is the U.S. NRC's system code TRACE. This code provides a suitable benchmark in the validation process as an independent, widely used and well-validated safety analysis tool.

The project comprises of three work packages: the first including the analysis work and the second international cooperation. The third work package contains only participation fees of international programs.

Assessment of Apros and TRACE against RBHT reflooding experiments

Rod Bundle Heat Transfer (RBHT) calculations began in 2019 with both Apros and TRACE calculations (Leskinen & Hovi 2020). Experiments 1143, 1096, 1196, 1108 and 1383 were calculated and the results were compared against the corresponding experimental data. The interest in these experiments was related to the new OECD/NEA RBHT project but, as the new data project data was not yet available, older experiments were calculated in preparation for the soon expected open and benchmark cases. The experiments are listed Table 1, model data in Figures 1 and 2, and quench front propagation results in Figure 3.

Table 1. Summary of the experiments calculated with Apros and TRACE.

	Experiment index				
Run condition	**1143**	**1096**	**1196**	**1108**	**1383**
Upper plenum pressure [MPa]	0.138	0.138	0.276	0.138	0.276
Initial peak clad temperature [°C]	870.85	759.85	870.85	759.85	759.85
Rod peak power [kW/m]	2.3	1.31	2.3	1.31	1.31
Flooding rate [m/s]	0.1524	0.0254	0.1524	0.0254	0.0254
Inlet subcooling [°C]	83	11	53	83	11

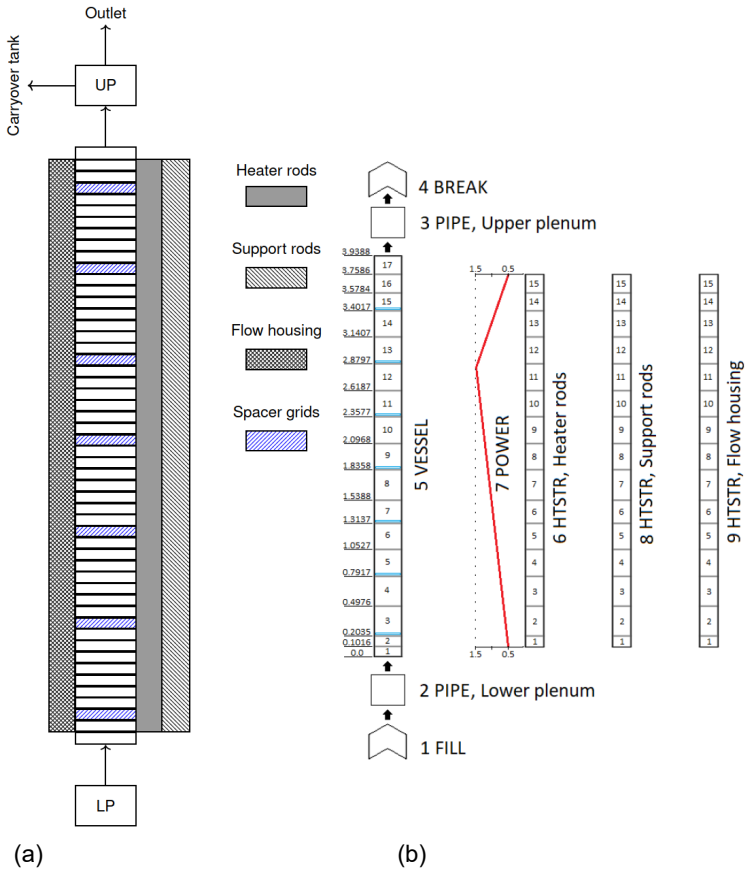

Figure 1. (a) Apros and (b) TRACE nodalizations of the RBHT test section.

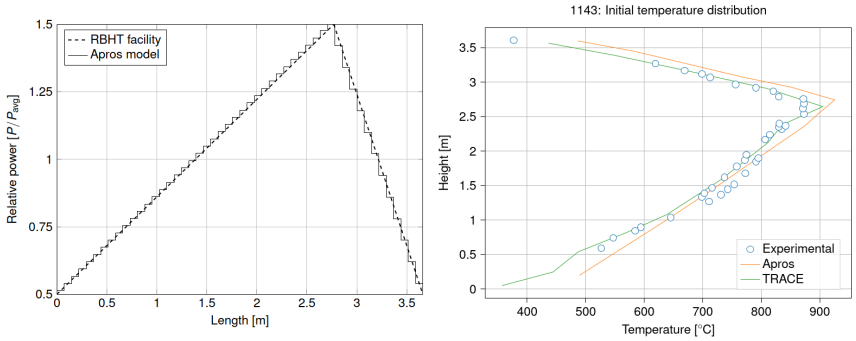

Figure 2. (a) Axial power distribution and (b) initial temperature distribution in one of the tests.

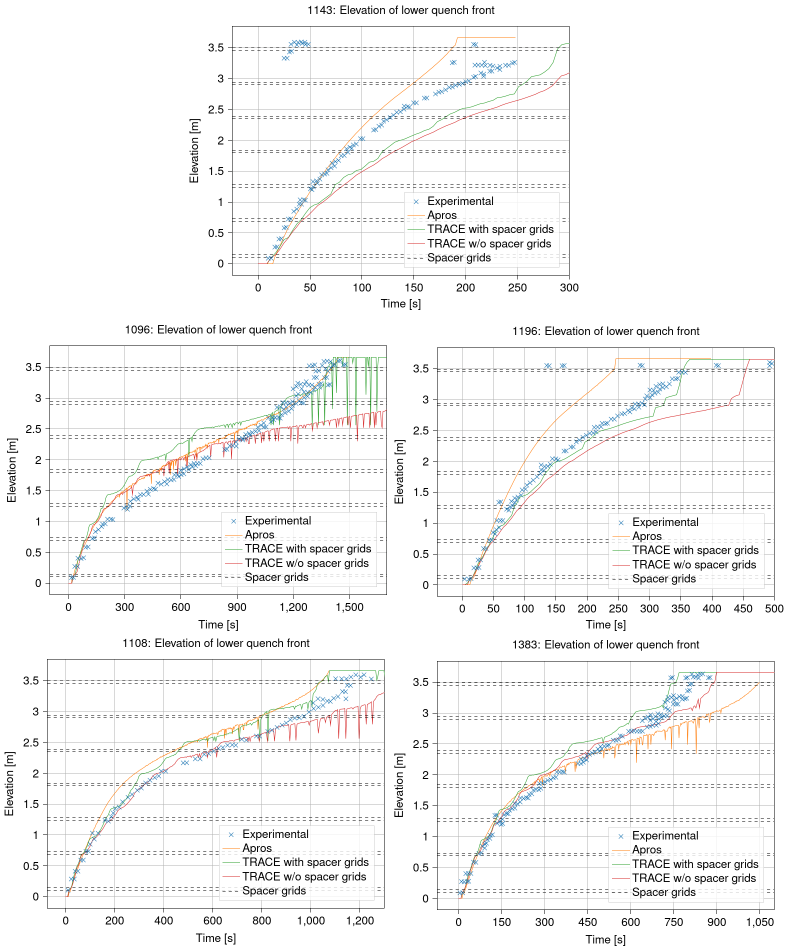

Figure 3. Lower quench fronts in the simulated cases.

Apros and TRACE model with spacer grids predicted the reflooding phenomena with a reasonable accuracy. As expected, the TRACE model with spacer grids provided an enhanced heat transfer compared to the model without spacer grids. Overall, in most cases Apros predicted the early stages of reflooding more accurately than TRACE. On the other hand, TRACE gave a better estimation for the total quench time. Both codes provided mainly conservative estimates for heater rod peak temperatures, but Apros generally gave a more accurate temperature profile behavior. TRACE significantly overestimated the peak temperatures, especially at higher elevations.

Assessment of Apros and TRACE against open phase RBHT reflooding experiments

In 2020 OECD/NEA RBHT project was starting in full with open phase experiment data open for project participants. The performed experiments focused on the impact of rod peak power, inlet subcooling and most notable, different reflooding rates and types such as oscillatory reflooding. Two experiments 9014 and 9015 had higher reflooding rates whereas seven experiments had low reflooding rates. In addition, two experiments 9011 and 9043 had extremely low reflooding rates. While these experiments can be used for code validation on their own, their other purpose was to provide modelling data in preparation for the incoming blind phase code benchmark.

These experiments were calculated with both Apros and TRACE (Hovi 2020a, Hovi 2020b). Machine learning was utilized and the Apros model was calibrated for the incoming benchmark according to these results. With Apros, also BEPU analysis was used for some of the cases. Normalized results are presented in Table 2, quench front progression in Figure 4 and one of the steam temperature measurements in Figure 5.

Table 2. Normalized Apros and TRACE peak cladding temperature (PCT) results.

Experiment	Apros				TRACE			
	PCT	PCT time	PCT elevation	PCT quench	PCT	PCT time	PCT elevation	PCT quench
9005	1.002	0.401	1.079	1.017	0.982	5.921	1.043	1.042
9011	0.966	1.317	1.074	1.145	1.004	0.944	1.149	N/A
9012	0.953	0.035	1.019	1.043	1.010	0.808	1.015	1.376
9014	1.007	0.780	1.079	0.860	0.982	1.007	1.043	1.183
9015	1.008	0.224	1.019	1.033	0.980	0.537	0.985	1.511
9021	0.963	0.386	1.019	1.063	1.015	0.603	1.015	1.013
9026	0.941	0.698	1.019	0.939	1.003	1.013	1.015	1.001
9027	0.953	0.596	1.019	0.960	1.008	0.975	1.015	1.006
9029	0.971	1.015	1.019	0.958	1.039	1.127	1.007	0.964
9037	1.023	0.488	1.019	0.993	0.989	5.131	0.985	1.019
9043	0.966	0.824	0.982	1.080	0.947	0.976	1.108	1.064

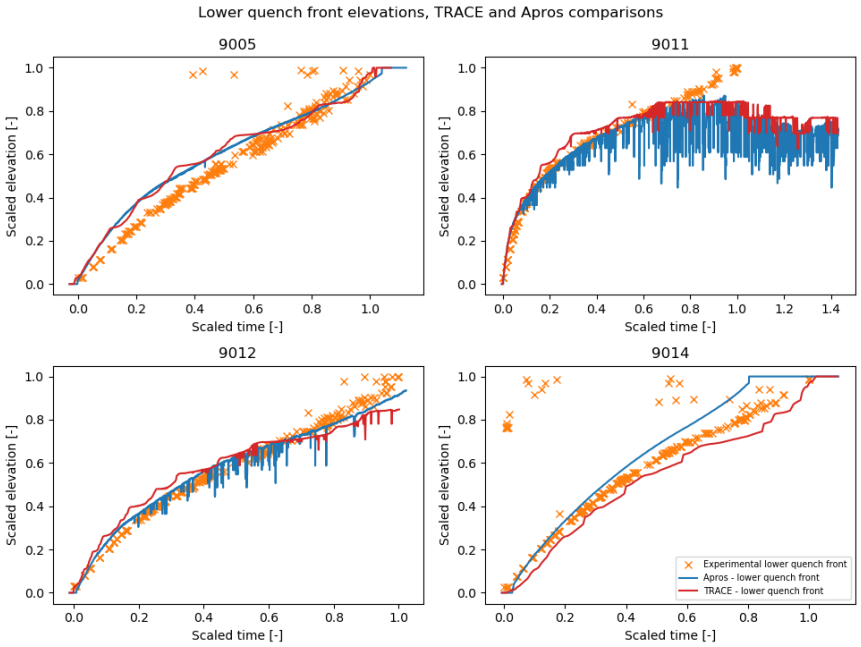

Figure 4. Quench front progression in some of the experiments.

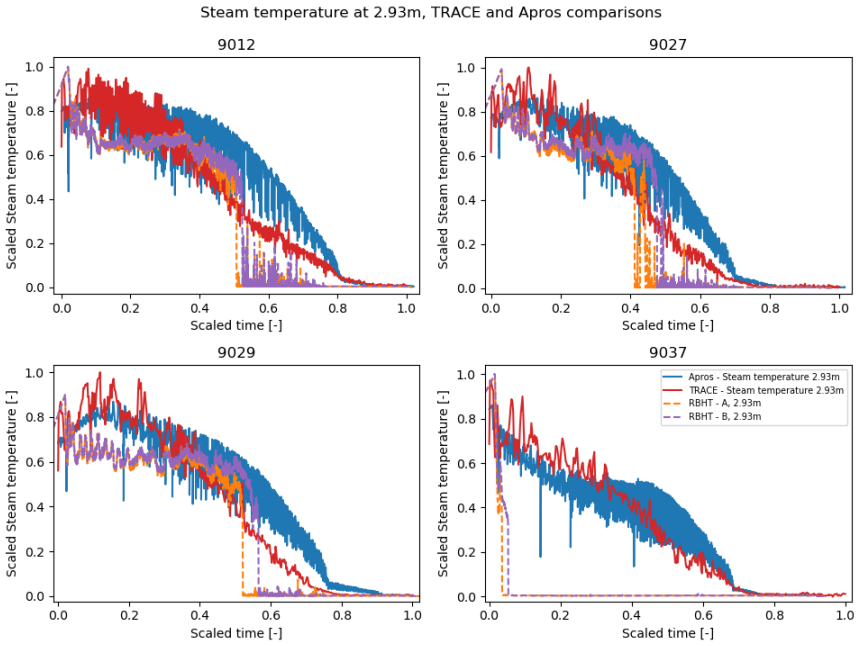

Figure 5. Steam temperature in some of the experiments.

The calibrated Apros model produced overall more accurate results. Quench front propagation and rod surface temperature estimations were good. As the benchmark will be participated only with Apros, the TRACE model did not go through similar calibration. The results, however, were still quite good. Especially steam exhaust rates and bundle pressure drop gave reasonably accurate estimations.

The RBHT project will continue in 2021 with a blind benchmark.

Analysis work on other test facilities

While the RBHT has been the analysis backbone of the project in the first two years, analysis work has progressed also with of some of the other test facilities. The original plan was to perform a coupled Apros-Fluent analysis with SAFIR2022 CFD4RSA on the newly modified PASI facility, located in Lappeenranta-Lahti University (Kouhia et al. 2018, Telkkä et al. 2020). However, as the CFD4RSA funding was postponed to 2021, only a part of the intended work was performed in 2020. The model has been modified and is ready for the coupled analysis (Hillberg, 2020). The experiment to be calculated in 2021 is VTT-01 (performed in SAFIR2022 PAHE), in which the goal was to observe the natural circulation behaviour of the PASI facility under different steam mass flow rate settings to the containment and how much condensate can be collected from the bottom of the containment vessel and from the walls of the containment vessel. In addition, the heat losses from the containment were under investigation.

Additionally, multiple PKL facility steady-state and IBLOCA experiments (Szogradi & Karppinen, 2020) and a double-ended LBLOCA experiment performed in FIX-II facility in Sweden (Hillberg, 2019), have been analysed with Apros. FIX-II facility and the Apros model are presented in Figure 6. As new critical flow correlations have been implemented in Apros in the last years, these were also tested but in this case the differences in results were minor (Figure 7). A master's thesis has also been started on critical flow modelling and it is expected to be finished in 2021. The thesis will focus on critical flow tests performed in the Swedish Marviken facility.

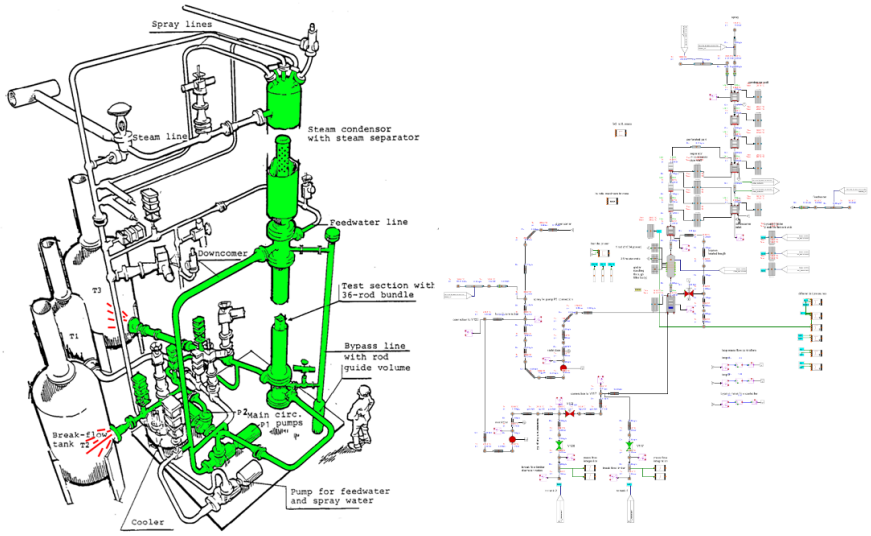

(a) (b)

Figure 6. (a) FIX-II facility (modelled parts in green) and (b) the Apros model.

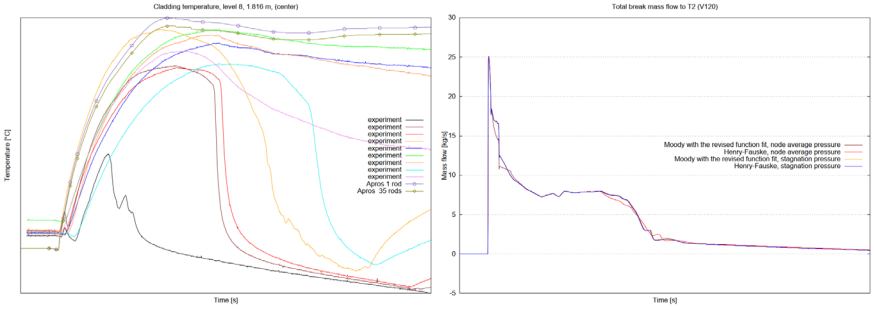

(a) (b)

Figure 7. (a) FIX-II 5052 Cladding temperatures. 3-dimensional flow in the bundle is clearly visible in the experimental data. (b) The effect of utilizing different critical flow correlations on break mass flow.

International cooperation

International cooperation is heavily represented in the project. Multiple research projects are being actively followed. In addition to the new validation data, these programs also contribute to knowledge transfer between organizations. The following programs or projects have been followed (Table 3) in the first two years of THACO:

- OECD/NEA Hydrogen Mitigation Experiments for Reactor Safety Phase 2 (HYMERES-2) is aimed on detailed analysis of the containment phenomenology during postulated severe accidents with the release and distribution of hydrogen. Also the participation fee of this project has been paid from THACO.
- OECD/NEA Rod Bundle Heat Transfer (RBHT) is a new experimental research project with an objective of conducting new experiments and evaluating system hydraulics codes in the simulation of reflood tests in a full height rod bundle for complex inlet flows. The facility is operated by Pennsylvania State University/U.S. Nuclear Regulatory Commission. This project has a strong emphasis in the analysis made within the first two years of THACO. Also the participation fee of this project is paid from THACO.
- OECD/NEA PKL-4 project investigated safety issues relevant for current PWR plants as well as for new PWR design concepts by means of systematic parameter studies on thermal-hydraulic phenomena and transient tests under postulated accident scenarios.
- OECD/NEA CSNI Working Group on Analysis and Management of Accidents (WGAMA) aims to advance the current understanding of the physical processes related to reactor safety.
- U.S. NRC's Code Applications and Maintenance Program (CAMP) is formed to exchange information on thermal-hydraulic safety related issues between U.S. NRC and its international partners. TRACE, PARCS, RELAP5 codes and the graphical interface SNAP are made available through this program.

Table 3. Type of representation in the international cooperation programs.

Project or program	Type of representation
OECD/NEA RBHT	MB member
OECD/NEA HYMERES-2	PRG member
OECD/NEA PKL-4	PRG member
OECD/NEA WGAMA	country representative
U.S. NRC CAMP	country contact person

References

Hillberg, S. 2019. Analysis of FIX-II experiment 5052 with Apros. Espoo: VTT. VTT research report. VTT-R-00914-19.

Hillberg, S. 2020. Apros analysis of PASI natural circulation experiment VTT-01. Espoo: VTT. VTT research report. VTT-R-00054-21.

Hovi, T. 2020a. Assessment of Apros against open phase RBHT reflooding experiments. VTT research report. VTT-R-01349-20.

Hovi, T. 2020b. Assessment of TRACE against open phase RBHT reflooding experiments. Espoo: VTT. VTT research report. VTT-R-00032-21.

Kouhia et al. 2018. INTEGRA 5/2018 General description of the PASI test facility, second edition. Lappeenranta: Lappeenranta-Lahti University of Technology LUT.

Leskinen, J., Hovi, T. 2020. Assessment of Apros and TRACE against RBHT reflooding experiments. Espoo: VTT. VTT research report. VTT-R-00033-20.

Szogradi, M., Karppinen, I. 2020. Analyses of PKL i1.1 LBLOCA parametric experiments with Apros. Espoo: VTT. VTT research report. VTT-R-00051-21.

Telkkä et al. 2020. PAHE 1/2020 - PASI tests for VTT projects. Lappeenranta: Lappeenranta-Lahti University of Technology LUT.

6. Mechanical Integrity

6.1 Advanced materials characterisation for structural integrity assessment (AMOS)

Sebastian Lindqvist, Laura Sirkiä, Pentti Arffman, Tommi Seppänen, Juha Kuutti, Jorma Hietikko

VTT Technical Research Centre of Finland Ltd
P.O. Box 1000, FI-02044 Espoo

Abstract

Advanced materials characterisation is required for fracture mechanical assessment of reactor pressure vessel and other safety class 1 components. One practical example is surveillance programs and the extension of the programs to cover modern requirements and long-term operation. In AMOS, these challenges are investigated through developing miniature testing techniques for C(T) specimens and arrest toughness, techniques for fracture mechanical testing during thermal transients and methods to account for the transferability. During 2019-2020, we carried out experimental testing and numerical analysis to develop quality criteria for miniature C(T) specimens, developed a new method to investigate the effect of thermal transients on fracture toughness in the ductile regime and reviewed the LTO performance of RPVs. During the upcoming years, the results will be post processed, in addition to performing more measurements to better understand the uncertainties and the connection to the structural integrity of the reactor pressure vessel.

Introduction

The structural analysis of nuclear power plant (NPP) safety class 1 components shall be based on fracture mechanics. The AMOS (Advanced materials characterisation for structural integrity) project focuses on development of analytical and experimental testing methods for fracture mechanical assessment of safety class 1 components, the reactor pressure vessel and the dissimilar metal welds of the pipe nozzles. The analyses of safety class 1 components are mandatory according to YVL E4 guidelines. The aim is to develop methods so that fracture can be explained, controlled, understood and predicted better than before. An important part of the project is also to train new experts to the field of fracture mechanics, where several retirements have occurred during the past years.

After introduction of fracture mechanics for safety analysis, the field has evolved, and different applications have emerged for assessing the structural safety. Firstly, the fracture toughness in the ductile-to-brittle transition region as a function of temperature can be described statistically with the Master Curve method. The Master

Curve enables a probabilistic description of material's lower boundary fracture toughness in the ductile-to-brittle transition region. Based on current testing practices, the fracture toughness is obtained with specimens with relatively deep cracks, loaded in bending, which causes a high constraint condition leading to a conservative estimate of the fracture toughness.

The progress of fracture mechanics has enabled the development of miniature specimen testing techniques. Miniature specimen test technique is crucial for ensuring that enough material is available to assess the effect of irradiation embrittlement on fracture toughness in surveillance programmes, considering reuse aspect, and for ensuring the cost-efficiency of the testing procedure.

For historical reasons, surveillance programmes are based typically on Charpy-V specimens. To obtain fracture toughness related data from tested Charpy-V specimens, miniature testing techniques or reconstitution techniques have been developed. Now, the miniature C(T) specimen testing technique based on fracuture mechanics is under development in several countries. The thickness of the specimens is 4 mm, figure 1. In Japan, USA, France and Russia, this technique has gained interest, since fracture mechanical data is required to demonstrate the safety for continued operation of the NPP fleets. The miniature C(T) specimen technique has been developed for the last 10 years. The method has been validated for base materials, welds, irradiated materials, and even for materials from different depth locations relative to the inside surface of the RPV. However, more development work is required to make the technique more applicable. Currently, the standards that are used for miniature C(T) specimens and the quality criteria that those standards include have been developed for 25 mm thick specimens, and can thus, be too strict for miniature specimens. If the quality criteria is not fulfilled, then the test result has to be discarded, which is unfavourable for surveillance programmes where there is restricted amount of material available.

In AMOS project, five topics related to analytical and experimental fracture mechanics were identified WP (work package) 1) Miniature C(T) specimens, WP 2) Shallow crack effects, WP 3) uctile tearing and transient loads, WP 4) Small specimen testing technique for obtaining crack arrest toughness, and WP 5) Use of fracture toughness for structural integrity and aging management.

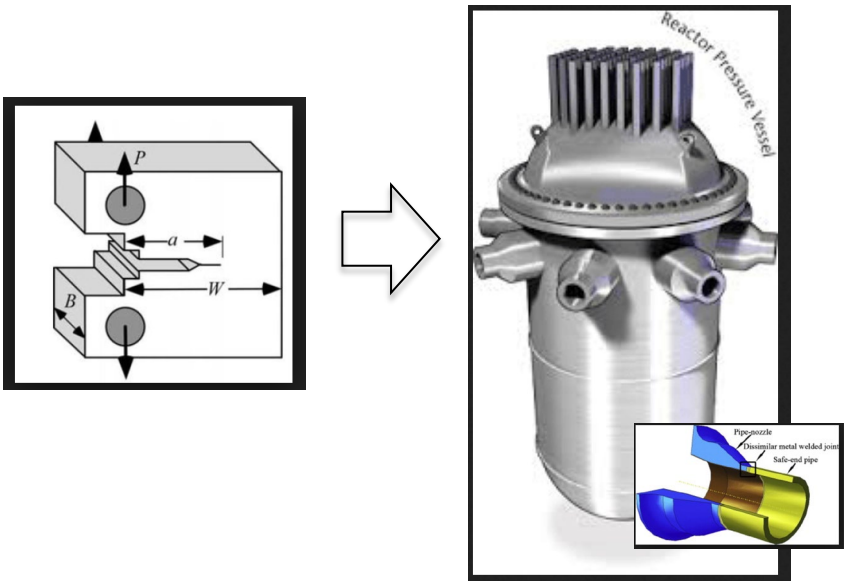

Figure 1. Transferability of fracture toughness results from specimens to component level.

Specific goals

In WP 1, the focus is on developing quality criteria for miniature specimens. The work will include experimental testing of miniature C(T) specimens to find out sufficient quality criteria. Also other miniature specimen testing techniques are investigated, but the focus is on miniature C(T) specimens. In the testing programme, the quality criteria for the C(T) specimens are investigated through varying the location of the pin-holes of the specimen, the manufacturing method of the side grooves and varying other critical dimensions of the specimen. Different measuring techniques to determine the displacement are also investigated. Metallography of the investigated specimens is required for a comprehensive analysis of the uncertainties. Also numerical simulations are required to develop quality criteria. The numerical work will include 2D and 3D simulations with FEM for materials with varying strength. In the simulations, the effect of crack curvature and variations in the C(T) specimen configuration are investigated. Since miniature C(T) specimen testing technique is the hottest topic internationally within the fracture mechanics community, the international activities in AMOS are planned for this work package, including participation to significant international forums like PVP, ASTM and IGRDM.

In WP 2, the focus is on developing a method accounting for the constraint effect in structural integrity analysis. The work will include experimental characterisation of the shape change in the Master Curve. A fracture toughness specimen geometry suitable for constraint testing will be identified and applied. And the effect of strength

on the obtained T0 and constraint will be investigated since radiation affects the strength of the material. Numerical simulations are required for making predictive models of the constraint as a function of load for different specimens and components. All of the mentioned results are required when in the final stage an improved engineering method is developed for assessing the effect of constraint on T0. In this work, metallography is required for identification of the initiation sites, and characterising the crack tip deformation condition. An important part of the work is collection of literature data for comparison with the results obtained in this investigation.

The focus in WP 3 is on developing a method for assessing the effect of transient loads on crack growth in the upper-shelf region and to investigate the ductile failure mechanisms. Experimental work will be performed to characterise the effect of decreasing and increasing load transients on tearing resistance at different load levels. The material behaviour under transients will also be validated for reactor pressure vessel steels. In addition, void growth behaviour in the ductile regime shall be investigated for round bar specimens and C(T) specimens.

In WP 4, the focus is on validating a model that enables characterisation of crack arrest toughness from instrumented Charpy-V specimens. The work will include experimental work on full-sized crack arrest specimens specially designed for crack arrest toughness measurements. The testing is done on three different materials with varying strength. The results will be compared to results of the same material obtained through instrumented impact toughness testing. Also more advanced crack arrest toughness testing methods, with smaller material consumption, will be used for characterisation of crack arrest toughness. Numerical simulations are required for calculating the stress intensity and the load condition of the test specimens. Metallography is required to get a deeper understanding of the conditions causing crack arrest and to investigate the effect of material variations.

In WP 5, the focus is on reviewing the methods applying fracture toughness for structural integrity analysis and aging management. The different methods used to assess the lower boundary curve, e.g. the Master Curve, in the ductile-to-brittle transition region are reviewed. Also the process to assess the experimental uncertainty in these analysis is described. In addition, a review is done of the different factors affecting the shift in transition temperature due to irradiation and thermal aging. The micromechanical reasons for materials to behave differently due to embrittlement are reviewed and the physics behind the developed irradiation embrittlement models are described. The work is planned to be an extension to the work done in FE-VAS. At the end of the project, the effect of the developed methods from this project on structural integrity and aging management are described. The work in this work package is based on existing literature.

Results 2019

D1.2.1, The effect of measuring the crack opening displacement from the load line vs. front face and the effect of side grooving of miniature specimens [1].

The field of structural analysis and fracture mechanics is developing and progressing all the time. At the moment, validating and studying the use of miniature size specimen test technique in surveillance programs is of great interest in several countries. The advantage of the use of miniature size C(T) specimens is among others reuse and material save.

In D1.2.1 AMOS 2019, the development of quality criteria for miniature size C(T) specimens was in focus. The usability, functionality as well as reliability of two different types of crack opening displacement measuring techniques and the effect of specimen side grooving was researched. The results were compared between miniature C(T) series themselves and to the results obtained with standard size 1T C(T) specimen.

The fracture toughness testing with miniature C(T) specimens was performed in several low test temperatures aiming to determine the transition temperature T_0. The test series consisted of two series of specimens, another series was side grooved, and another one was not. Based on results, it is justified to say in this case, that side grooving of miniature C(T) specimen has a negligible effect to what comes determination of transition temperature. The extraction location of miniature C(T) specimen seems to affect somewhat the results. When comparing results between miniature C(T) specimen and standard size 1T specimen, the T_0 is similar.

The comparison of crack opening displacement measurement results shows that either gage location is acceptable and accurate; whether gage is attached to the specimen front face or in the load line. Overall, both ways of measuring gives the very same T_0. COD_{LL} gages advantage is that it enables simpler test specimen shape, since there is no need for front face attaching.

The overall objective is to develop and validate quality criteria for miniature C(T) specimens and the results of this study supported this purpose. The results confirms the reliability of COD_{LL} gage usage and the negligible effect of side grooving; whether the crack opening displacement was measured with front face or load line attached gage or whether the specimen was side grooved or not, the effect for transition temperature T_0 was insignificant.

D3.1.1, The effect of temperature transients on fracture toughness [2].

The YVL guide E.4 requires that the risk for fast fracture is assessed in the upper shelf region. Fast fracture in the upper shelf area can occur by brittle fracture. In this case, the material has not been in the actual upper shelf temperature zone, but for example, rapid cooling has caused a shift in the ductile-to-brittle regime, and thus, brittle fracture can occur in the upper shelf area. The fracture toughness in the upper shelf area is determined with J-R curves. Presently, there is no data, nor predictions, regarding the J-R curve development during a decreasing thermal transient.

In D3.1.1 AMSO 2019, the effect of rapid cooling on J-R curves is investigated. Fracture toughness specimens of Laser 460MC Plus were cooled from 300 °C to the room temperature at a cooling rate of 2 °C/s determined at the center location of the specimen. The cooling rate is faster close to the surface. The cooling rate was selected to be in the same range as during a loss of coolant accident. The following was concluded: 1. No brittle fracture in the upper shelf region was

observed for the investigated material during the cooling transient. The transient can promote splitting observed in the specimens. 2. Based on the results, when doing structural integrity analyzes of thermal transients in the upper shelf region, it is recommendable to use the lowest fracture toughness properties in the investigated temperature range, if no other information is available.

These conclusions were done for a rolled steel with minimum fracture toughness at 200 °C and maximum at 300 °C. Thus further investigations should focus on investigating fracture toughness behavior of a RPV steel during a cooling transient in the upper shelf region. Typically, RPV steels have a different temperature dependence than the steel investigated in this study.

D4.1.1, Current state of crack arrest toughness characterisation [3].

Once initiated, a brittle crack propagates rapidly through material. However, if the crack driving force decreases and/or the crack advances to a region with higher fracture resistance, the crack growth may halt. This is called crack arrest. Crack arrest toughness is an interesting parameter from safety perspective, since it represents the minimum fracture toughness of a material. In contrast to weakest link initiation, crack arrest follows a principle of strongest link, but a single link is rarely able to halt an entire fracture. A sufficient amount of the crack must arrest locally for global effect. For these reasons the scatter of crack arrest toughness is essentially smaller and size effect minimal compared to fracture initiation toughness. Determination of static crack arrest toughness KIa is standardized in ASTM E1221. Measuring it, however, requires complicated tests and large specimens, something that is not possible in surveillance testing of nuclear power plant components. A better alternative for determination of KIa is therefore required, if it is intended to be used. Crack arrest toughness evaluation by means of instrumented Charpy impact testing seems like a promising future method for determination of the minimum fracture toughness of a ferritic steel. Other methods have also been suggested, each having their own advantages and disadvantages.

D5.2.1, Factors affecting the fracture toughness of surveillance specimens and RPVs [4].

Fracture toughness of surveillance specimens and reactor pressure vessels in western type light water reactors was reviewed. An evolving framework for fracture toughness requirements in structural integrity has existed since the 1970s. Significant mechanistic understanding of embrittlement phenomena is presented in the literature. Practical application of mechanisms into embrittlement models continues to evolve, based on accumulated experimental data. Research on decommissioned reactors provides the opportunity to study the RPV directly and more extensively than with surveillance programs. However, such research is scarcely available to date. Publicly available data suggests that the regulatory approach contains sufficient conservatism regarding the condition of the actual RPV. It is recommended that additional research be conducted on decommissioned reactors, not only to gain more confidence on the regulatory approach and transferability, but to also improve other aspects, such as neutron dosimetry and attenuation, which can eventually

more realistically quantify the inherent conservatism included in design and analysis.

Results 2020

D1.2.1, VTT report: Experimental investigations on the effect of pinhole location on fracture toughness [5].

This study, D1.2.1 AMOS 2020, focuses on researching the quality criteria for miniature C(T) specimens. Sufficient quality criteria is developed by experimental testing with miniature C(T) specimens. The quality criteria and applicability is investigated through varying the pin hole locations in order to obtain how great importance eccentric pinhole possess and does it affect to the measuring in any way.

In order to determine the transition temperature T0, the miniature C(T) specimen fracture toughness testing was performed with several low test temperatures inside an environmental chamber. Two series were tested; eccentric pinhole series and reference series. Obtained experimental test results show convergence between series and consequently, substantiates the postulate that miniature C(T) specimens even with eccentric pinhole locations gives a reliable outcome. Additionally, comparison of load-displacement chart slopes supports this assumption; slopes, either COD measured from load line or front face, amongst series are either identically or having no more than five percent of difference.

Numerical analysis of eccentric pinholes was performed through three different FE models; ‘nominal’, ‘mean’ and ‘max’, and was based experimental research data. In addition to the displacements and loading pin forces, the stress intensity factors, and J-integrals were evaluated from the simulation using the default Abaqus contour integral calculation routine. The simulated load line and front face measuring data was converted into stress intensity factors and J-integrals which allowed the evaluation of the accuracy of the standard formulae in the eccentric pinhole location case. Depending on the mode, the comparison of simulation result slopes gave a disparity between two to three percent. The disparity in the slopes affects the standard-based evaluation of the plastic work done to the specimen, and this affects the resulting J-integral which results differ between the simulation results and the standard-based predictions more than the stress intensity factors. However, the difference between the simulated J-integrals and those obtained with the ASTM E1921 formulae was approximately five percent, when the elastic simulations of the stress intensity factors were in good agreement with standard and deviated maximum of one point three percent. All in all, numerical analysis likewise substantiates the above-mentioned postulate on the effect of eccentric pinholes.

D1.6.1, NKS report: Test results on the fracture toughness behaviour in the ductile-to-brittle transition region, small and large specimens [6].

The objective of the work conducted in 2020 is to produce data for fracture mechanical analysis, and articles done in the upcoming years in AMOS and NKS project WPS-MAF. The fracture toughness of a ASTM A533 grade B class 1 plate was

characterized in the thickness direction. The results show that that the T_0 obtained with 15x30 SE(B) specimens is in the same range as the T_0 obtained with miniature 5x10 SE(B) specimens. The fracture toughness of the plate, 230 mm thick, is higher closer to the surface than at the centre, which agrees with previous investigations. Further metallography and post processing work is done to the 5x10 SE(B) specimens to analyse the differences to the 15x30 SE(B) specimens. These results are applied later for analyses of the effect of crack front curvature on fracture toughness.

D5.2.1, Embrittlement trend curves in Finland [7].

To evaluate embrittlement from neutron irradiation, Finnish regulations have required the use of surveillance programs in light water reactors since the 1970's. These are applied in the four operating reactors: two VVER-440s at Loviisa (LO1 and LO2) and two BWRs at Olkiluoto (OL1 and OL2). Same requirements apply to the EPR under construction (OL3) and VVER-1200 in licensing phase (FH1). In Finland the embrittlement trend curves are experimentally quantified with the use of the Master Curve or qualitatively using impact toughness. Application of the Master Curve has been a particular success for the operating VVER-440 reactors. In new builds, lessons learned from the past are applied to ensure that the degree of embrittlement remains low. Several decades of domestic research programs have aimed at, and continue to develop methods for improved application of fracture mechanics for RPVs.

Acknowledgement

We thank KIWA Inspecta and KTH for collaboration in WPS-MAF. We want to express our thanks to all reviewers of the AMOS deliverables and for the valuable comments.

References

[1] Sirkiä L. The effect of measuring the crack opening displacement from the load line vs. front face and the effect of side grooving of miniature specimens. VTT-R-00126-20 2020.

[2] Lindqvist S. Effect of cooling transient on J-R curve. VTT-R-01219-19 2019.

[3] Arffman P. Overview of crack arrest toughness KIa. VTT-R-00105-20 2020.

[4] Seppänen T. Factors affecting the fracture toughness of surveillance specimens and RPVs. VTT-R-01254-19. 2019.

[5] Sirkiä L, Kuutti J. Experimental investigations on the effect of pinhole location on fracture toughness. VTT-R-01183-20 2020.

[6] Lindqvist S, Peltonen V. NKS: Fracture toughness behaviour in the ductile-to-brittle transition region - small and large specimens and shallow and long cracks. VTT-R-00053-21 2021.

[7] Seppänen T, Lindqvist S. Embrittlement Trend Curves in Finland. DRAFT manuscript (24/11/2020) to be submitted to ASTM Symposium on Radiation ETCs 2021.

6.2 Effect of long-term operation on aging and environmentally assisted cracking of nuclear power plant component materials (ELIAS)

Caitlin Huotilainen[1], Pekka Nevasmaa[1], Petteri Lappalainen[1], Zaiqing Que[2], Ulla Ehrnsten[1], Iikka Virkkunen[2], Gaurav Mohanty[3]

[1]VTT Technical Research Centre of Finland Ltd
P.O. Box 1000, FI-02044 Espoo, Finland

[2]Aalto University
P.O. Box 11000, FI-00076 Finland

[3]Tampere University
FI-33014 Tampere, Finland

Abstract

During the first two years of the ELIAS project the main focus has been on reactor pressure vessel embrittlement mechanisms (2019) and reactor pressure vessel repair welding techniques and approaches (2019–2020). The reactor pressure vessel repair welding research work has been performed in close collaboration with the FEVAS Project.

Introduction

Nuclear power plants (NPP) must be operated in a safe and cost-effective manner. Central to the safety and reliability goals of these plants is effective materials degradation management. Effective materials degradation management must include the maintenance of operating plants, extension of the lifetime of plants, and choice and use of materials in new plants. (Wright 2017)

The long-term behaviour of the nuclear power plant component materials is of particular interest in Finland, because there are nuclear power plants that are at critical stages of their lifetime: either in the beginning of their operation or reaching the planning phase for lifetime extensions. Understanding of the materials' aging phenomena and the most important degradation mechanisms are of utmost importance in order to ensure safe plant operation and effective lifetime management for lifetimes that can reach 60 years or even beyond that.

The project focused on two main technical topics: (i) the identification of reactor pressure vessel (RPV) embrittlement mechanisms and (ii) the development of RPV repair welding techniques and approaches. In addition international collaboration and the dissemination of international projects to the Finnish community.

Identification of RPV Embrittlement Mechanisms

As the current fleet of NPPs approach the end of their original design lifetime, long-term operation (LTO) becomes an increasingly important topic and the integrity of safety-critical components must be ensured. While the RPV demonstrates excellent mechanical properties, in terms of hardness and fracture toughness and room and elevated temperatures in its “as fabricated” state, exposure to neutron irradiation can result in the embrittlement and, thus, degradation of the RPV base material and weld metal in the long term.

The embrittlement of pressure vessel materials consists of the hardening response from two separate mechanisms: (i) matrix damage (MD) mechanism and the (ii) formation of copper-rich precipitates (CRP). Neutron irradiation embrittlement is a result of three main mechanisms, i.e., matrix damage (vacancies and interstitials), segregation and formation of clusters, i.e., Cu-rich and MnNiSi -rich clusters. The dominating cluster type is dependent on the chemical composition of the material. Cu-rich clusters are frequently referred to as copper rich precipitates, CRPs, although they affect the properties of the RPV material also before becoming precipitates. CRP saturates at relatively low fluences (1×10^{19} n/cm^2, E > 1 MeV) and full saturation occurs before typical pressurized water reactor (PWR) end of life fluences. MD cannot be characterized by conventional microscopic methods as the size of the formations is beyond the resolution of small-angle neutron scattering, atom probe tomography, and transmission electron microscopy. Segregation of especially phosphorus to grain boundaries, and possibly also other surfaces (e.g. precipitates and inclusions), typically results in an increased amount of grain boundary cracking. MD formations are small in size and they anneal much faster than the CRPs and hence they can be separated by annealing studies.

During thermal annealing of an RPV material, most of these CRPs are dissolved back into matrix, while some of may grow larger (coarsening). The level (mechanical properties) of recovery depending on (i) the annealing temperature relative to the irradiation temperature, (ii) the annealing time, (iii) the impurity and alloying elements and (iv) type of product (e.g. plate, forging, weldment, etc.). Re-irradiation embrittlement is defined primarily by the MD term because the amount of Cu-rich cluster formation during re-irradiation is small. In low-Cu, high-Ni RPV materials, NiMnSi clusters are more decisive for the embrittlement, than Cu-rich clusters. Very little is known about the behavior of these clusters during annealing and re-irradiation.

The Russian norm for embrittlement (PNAE-G7-002-86) describes only total embrittlement, hence it does not separate MD, segregation and CRP. Further, it is an upper boundary description without confidence limits and the norm has not been revised since its first issue. The US power reactor embrittlement database (PR-EDB) including 855 transition temperature shift values has been recently reanalyzed (Easton et al. 2006). These analyses consist of MD and CRP terms, but the MD term can be considered incomplete, as it is based on data for low or no-copper materials. The full effect of MD can only be derived from annealing studies with real impurity content materials. The PR-EDB analysis also defines the flux effect for low

flux irradiations, which is relevant for boiling water reactors (BWR). The PR-EDB analysis is compared with the Irradiation Variable Database (IVAR) created by UC-Santa Barbara and Oak Ridge National Laboratory (ORNL) including tensile specimens of 33 alloys irradiated in well-controlled experiments. IVAR indicates the existence of a flux effect also for high flux irradiations, which is expected based on physical arguments (retardation of irradiation enhanced diffusion by recombination of primary defects).

Preliminary annealing studies were performed with several VVER440 materials approximately (Valo & Lappalainen 2015). The results are very promising but the analysis is restricted by the relatively small number of studied materials (12 samples) and the relatively large number of candidate variables and their combinations. A larger number of data points with varying P, Cu, Ni, Mn and Si contents and varying neutron fluence and fluence rates would enable increasing the parameters to be defined and would add confidence to the results. Preliminary annealing data give very good descriptions for the MD and CRP terms as a function of Cu, Ni, P, Mn and neutron fluence and Ni, Cu, P and neutron fluence.

In 2019, within the ELIAS project, studies on a larger set of specimens aiming to (i) increase the size of the database, (ii) include low flux data and (iii) widen the parameter range of the data were started. Specimens have been prepared from irradiated and tested Charpy V-notch (CVN) specimens, see Figure 1. Vickers hardness measurements (HV5) were performed to identify the initial condition, as well as any hardness gradients present in the materials, see Figure 2.

Future investigations will focus on (i) data analysis and the evolution of (ii) hardness and (iii) electrical resistivity as a function of annealing time (at 450 °C) and complementary microstructural characterizations. By employing these three complementary techniques information and insight to the embrittlement mechanism in RPV steels and welds can be obtained. Hardness measurements will provide information on changes and the evolution of mechanical properties, while resistivity measurements and microstructural characterizations will provide insight on the deformation of the crystal lattice of the material (e.g. due to the dissolution and/or precipitation of impurity elements in the matrix) and identify the impurities (precipitation, segregations) within the matrix as a function of annealing time, respectively.

(a) (b)

Figure 1. Photo of (a) a tested CVN specimen to be machined for investigations and (b) a 10 mm× 10 mm × 2 mm sample blank machined using electrical discharge machining (no hardness measurements performed yet).

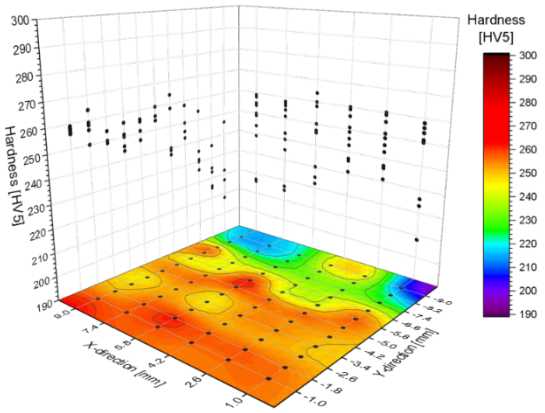

Figure 2. Representative reference hardness profile for a weld material sample presented as a contour map and as XZ and YZ reference point hardness value projections. Measured hardness indentations are shown as black dots on the map.

Development of RPV Repair Welding Methodology

As plants continue to age, there is an increased probability for the need of repairs due to extended exposure to a harsh environment (neutron flux, high temperature, high pressure, water chemistry). It is paramount that qualified and validated solutions are readily available, and that such methods are validated proactively, at a stage when they are not yet needed. In ELIAS, joint with FEVAS, a repair method for a postulated through cladding crack into the low alloy steel of a nuclear power plant's reactor pressure vessel has been investigated (Keinänen et al. 2020, Virkkunen et al. 2020, Huotilainen et al. 2021).

Repair welding (RW) is thought to represent the "worst-case" scenario where a postulated linear crack-like defect exists beneath the cladding and might extend across the interface into the RPV steel side. This postulated defect is then removed by machining, and the thereby machined groove will be filled by repair welding using a nickel-base superalloy filler metal and using mechanized/robotized arc welding process. While FEVAS focused on computational support for mock-up design and weld procedure tests, ELIAS performed the repair procedure design and characterization of the mock-up microstructures. The mock-up was welded at Aalto University as a joint effort between the projects.

In the project, a RW mock-up has been produced using an automated gas metal arc welding (GMAW) utilizing Cold Metal Transfer (CMT) method. As an alternative to conventional gas tungsten arc welding process, the use of automated GMAW-CMT mode offers many advantages, such as good weld quality, exceptionally stable arc, easy automation and very low heat input along with narrow heat-affected zone (HAZ). A postulated crack was excavated from a cladded and thermally embrittled

low alloy steel base material (BM) and repaired using a nickel base filler metal by gas metal arc welding-cold metal transfer. No pre-heating or post-weld heat treatment (PWHT) was applied, as it would be nearly impossible to apply these treatments in a reactor pressure vessel repair situation. One cladded plate was welded, meaning two excavations were filled, see Figure 3. One excavation was filled with 100 beads along the long side, while the second excavation was filled halfway (5 layers) the long side, followed by a 45° hatch pattern (6 layers) for a total depth of 40 mm.

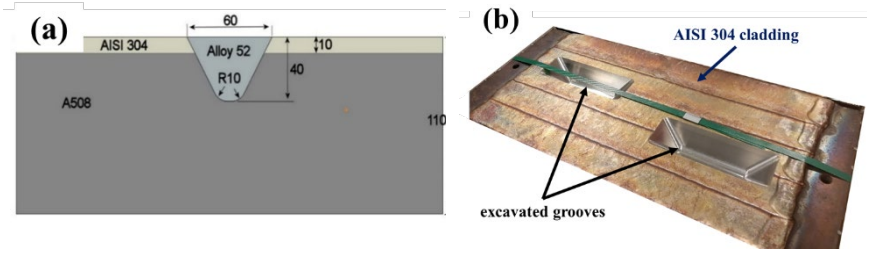

Figure 3. (a) Schematic diagram of the RW and (b) photograph of the two excavated grooves.

The mock-up RW was sectioned and a metallographic samples were prepared to study the weld quality and microstructure. Light optical microscopy (LOM) observations of the LAS HAZ can be seen in Figure 4. The HAZ is characterized by a coarse-grained structure of mixed lower-bainite and martensite, see Figure 4(a). There appears to be a band of upper-bainite and polygonal ferrite close to the weld interface. Near the LAS BM, a fine-grained area of bainite with some ferrite can be seen Figure 4(b). No indications of austenite were observed in the LAS HAZ. Therefore, it can be presumed that the HAZ has not experienced significant heating during the RW by GMAW-CMT. (Huotilainen et al. 2021)

The thermal embrittlement treatment of the LAS has resulted in significant changes in the ferritic steel's microstructure, compared to a typical as-supplied (quenched and tempered) LAS. The thermal embrittlement treatment has also led to coarsening of the grains, see Figure 4(c). The LAS is predominately bainite, and the long tempering time and slow cooling rate, may have favored secondary carbides and/or the re-precipitation of carbides and may have affected carbide coarsening. Some crack-like lack of inter-pass fusion defects and pores were observed in the RW. The observation of these defects indicates that further optimization of the RW parameters is required. Additional microstructural characterizations are required to completely assess the quality of the RW. (Huotilainen et al. 2021)

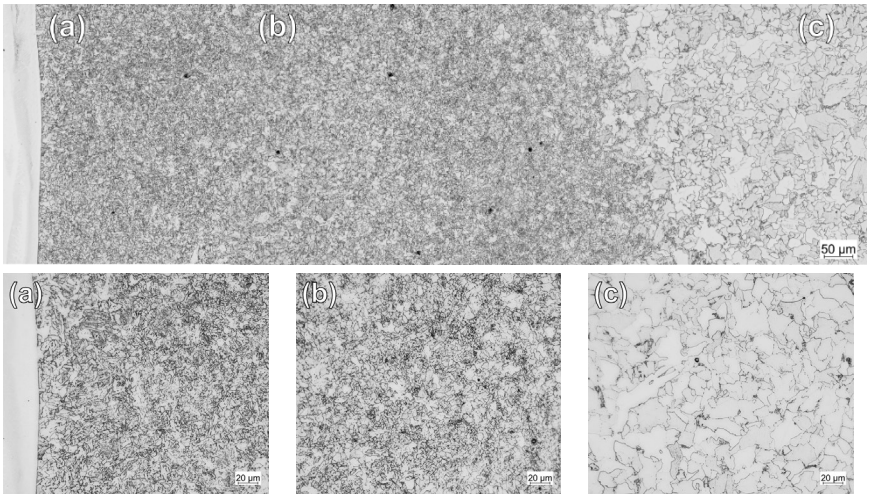

Figure 4. LOM images of the microstructure across the LAS HAZ of the 45°-hatch pattern RW after etching.

The hardness across the HAZ was measured by Vickers microhardness. Two loads were applied, (a) $HV_{0.3}$ and (b) $HV_{0.1}$, to evaluate the hardness in the LAS HAZ and very locally near weld interface, respectively. The results can be seen in Figure 5 (Huotilainen et al. 2021). A maximum hardness was measured locally in the LAS HAZ close to the FB. The hardness is within the acceptable range of values for a RW, even without the application of a pre-heating treatment or PWHT (Ohms et al. 2005, Bruomovsky et al. 2007, Yurioka & Horii 2006, Yu et al. 2014, Matejova, Jandova & Kask 2015).

In addition, micromechanical fracture toughness testing was performed on the RW produced in 2019 by Tampere University. This was the first time this method has been demonstrated on this material in Finland. A total of eight notched micro-cantilevers (≈10 µm × ≈2 µm ×≈2 µm) were ion-milled, in the WM and across the HAZ, and tested, see Figure 6. Data analysis of the fracture toughness behaviour of the HAZ is ongoing.

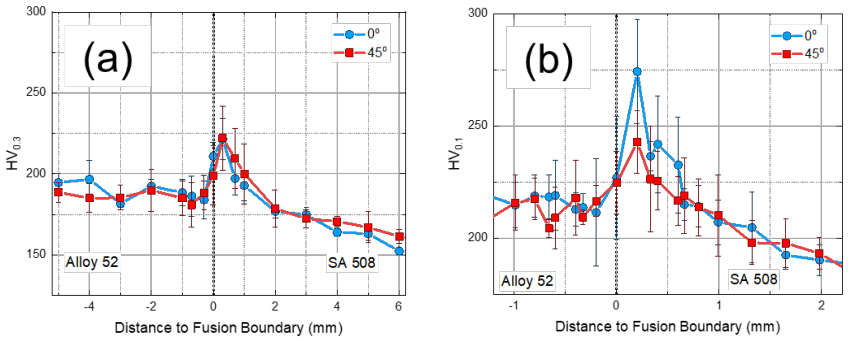

Figure 5. Measured microhardness ((a) $HV_{0.3}$ and (b) $HV_{0.1}$) across the HAZ of the RWs. The FB location is indicated by the dotted vertical line in the plots.

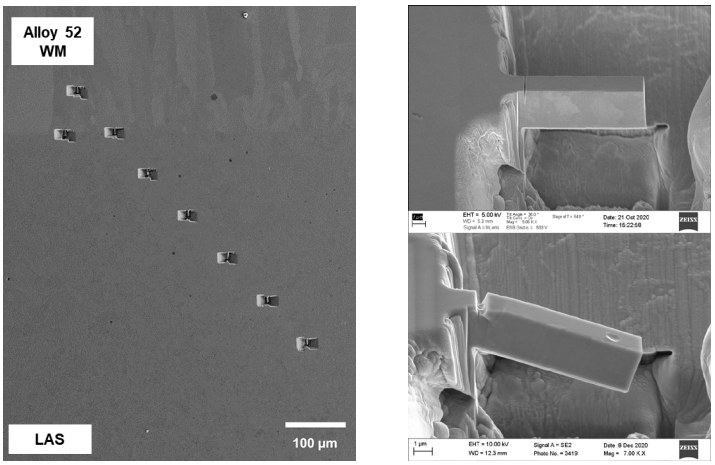

Figure 6. (left) Placement of microcantilevers in the RW and SEM images of micro-mechanical testing of the RW; (right-above) as-milled (focus ion beam) micro-cantilever before fracture mechanical testing and (right-below) post-test micro-cantilever.

The RW was simulated using a finite element method with in-house welding simulation methods. This work is described in more detail within the FEVAS Project.

Complementary experimental and numerical evaluations have been used to investigate a RW method for a postulated through cladding crack in to the RPV of an NPP using automated GTAW-CMT mode and a Ni-base superalloy weld metal. While the results are very promising, additional work is required in order to fully characterize the weld interface, investigate the welding residual stresses and fully

optimize the welding parameters, in terms of, for example, heat input, travel speed, bead placement, etc.

Closing remarks

This research presented here has been performed within the ELIAS project in 2019 and 2020. The ELIAS project will not continue in 2021, but the development of RPV repair welding methodology will continue the FENIX project.

Acknowledgements

The authors would also like to thank Taru Lehtikuusi (VTT), Johanna Lukin (VTT), Jari Lydman (VTT), Asta Nurmela (VTT), Hannu Hänninen (Aalto University), Mikko Peltonen (Aalto University), Henrik Sirén (Aalto University), Laura Tiainen (Aalto University), Mari Honkanen (Tampere Microscopy Center) and Aloshious Lambai (Tampere University) for their valuable contributions to this work.

References

Brumovsky, M., Brynda, J. & Ellinger, J. 2007. Welding Repair Procedure of Defects in WWER Reactor Pressure Vessels. Proceedings of the ASME 2007 Pressure Vessels and Piping Conference (PVP2007), 22–26 July 2007, San Antonio, Texas, USA, American Society of Mechanical Engineers, New York, pp. 907–911.

Eason, E.D, Odette, G.R., Nanstad, R.K. & Yamoto, T. 2006. A Physically Based Correlation of Irradiation-Induced Transition Temperature Shift for RPV Steels. ORNL/TM-2006/530.

Huotilainen, C. et al. 2021. Evaluation of an Alloy 52 / Cladded Carbon Steel Repair Weld by Cold Metal Transfer, PVP2021-61981. To be published in the Proceedings of the ASME 2021 Pressure Vessels & Piping Conference PVP2021, July 12-18, 2021, virtual conference.

Keinänen H. et al. 2020. A52M/SA52 Dissimilar Metal RPV Repair Weld: Evaluation of Different Techniques, PVP2020-21233, Proceedings of the ASME 2020 Pressure Vessels & Piping Conference PVP2020, July 20-24, 2020, virtual conference.

Matejova, M., Jandova, D. & Kasl, J. 2015. Structure Analyses of Experimental Welds Designed for Repair Welding of VVER 1000 Pressure Vessel, Key Engineering Materials, Vol. 647, pp. 131–140.

Ohms, C. et al. 2005. ENPOWER - Investigation by Neutron Diffraction and Finite Element Analysis on Residual Stress Formation in Repair Welds Applied

to Ferritic Steel Platers. Proceedings of the ASME 2005 Pressure Vessels and Piping Division Conference (PVP2005), 17–21 July 2005, Denver, Colorado, USA, American Society of Mechanical Engineers, New York, pp. 385–393.

PNAE-G7-002-86, Standards for Calculating the Strength of Equipment and Pipelines in Nuclear Power Plants, Energoatomizdat, Moscow.

Valo, M. & Lappalainen, P. 2015. Electrical resistivity response to annealing of VVER440-type weld material in irradiated, post-irradiation annealed and re-irradiated conditions, VTT Research Report VTT-R-00163-15. Espoo: VTT.

Virkkunen I. et al. 2020. A52M&SA52 Dissimilar Metal RPV Repair Weld: Experimental Evaluation and Post-weld Characterizations, PVP2020-21236, Proceedings of the ASME 2020 Pressure Vessels & Piping Conference PVP2020, July 20-24, 2020, virtual conference.

Wright, M. 2017. Preface of Proceedings of the 18th International Conference of Environmental Degradation of Materials in Nuclear Power Systems-Water Reactors. Portland, Oregon, USA, August 13-17, 2017.

Yu, L. et al. (2014). Hardness Prediction for Temper Bead Welding of Non-Consistent Layer Technique. In: 8th Int. Conf. on Processing & Manufacturing of Advanced Materials (THERMEC 2013), 2–6 December 2013, Las Vegas, USA, Materials Science Forum/Trans Tech. Publications, Switzerland.

Yurioka, N. & Horii, Y. (2006). Recent developments in repair welding technologies in Japan, Science and Technology of Welding and Joining, Vol. 11, pp. 255–264, No 3.

6.3 Extended lifetime of structural materials through improved water chemistry (ELMO)

Caitlin Huotilainen, Tiina Ikäläinen, Essi Jäppinen, Seppo Peltonen, Timo Saario, Konsta Sipilä, Aki Toivonen

VTT Technical Research Centre of Finland Ltd
P.O. Box 1000, FI-02044 Espoo

Abstract

Water chemistry applied in primary and secondary circuits have significant effect to the lifetime of the NPP components. Several water chemistry related research topics have been identified and included in the ELMO project. Hydrazine replacement study, enrichment of impurities and corrosion products in steam generators, lead assisted stress corrosion cracking of steam generator tubing and surveying on the existing information on SMR water chemistries have been included in the project. Useful results related on alternative scavenging chemicals for hydrazine have been obtained, as it was shown that there are sufficiently efficient scavenging chemicals available to be used during power operation. First estimates on the deposition and release of impurities on a simulated steam generator tube could be calculated from the unique experimental setup developed at VTT.

Introduction

The most important part of operating a nuclear power plant is ensuring radiation safety throughout the operating years. The integrity of the nuclear power plant structures, components and tubing, which act as radiation barriers, is degraded by various degradation and aging mechanisms. The primary reason for most of these mechanisms is material-environment interaction caused by contact with the process medium. This material-environment interaction can result in the manifestation of numerous different corrosion phenomena including stress corrosion cracking (SCC), wear, denting and pitting. Corrosion phenomena are linked to materials, component designs and the used water chemistry. Since especially for old plants, materials and designs are already selected, the easiest way to affect corrosion is to alter water chemistry. In fact, the prevalence of failures caused by corrosion has been closely associated to the water chemistry used. Therefore, water chemistry design and optimisation is a subject of the utmost importance.

The main objectives of the present project aim at developing knowledge on optimal PWR/VVER water chemistry programs. Following topics were studied:

- A justified alternative(s) for hydrazine replacement in the primary and secondary side both during outage (in SG preservation or fuel exchange) and power generation will be proposed

- Further development of experimental equipment simulating SG conditions and tools for evaluating kinetics of impurity enrichment and release will be presented
- Verification of zeta potential measurement results used in magnetite deposition studies
- Knowledge of PbSCC mechanisms will be strengthened and measures for PbSCC mitigation will be evaluated
- Measurement techniques for dissolution/removal of corrosion products in primary and secondary side cycles
- Research on water chemistry and corrosion problem aspects of SMRs will be initiated

Replacement chemicals for hydrazine

Hydrazine (N_2H_4) is generally used as an oxygen scavenger for corrosion control in both thermal and nuclear power plants. Although hydrazine is very effective in this application, it has been identified as a genotoxic carcinogen. The use of alternative chemicals such as nontoxic oxygen scavengers is therefore recommended. Several substances, including carbohydrazide, diethyl-hydroxylamine (DEHA), erythorbic acid (an isomer of ascorbic acid), hydroquinone and 2-butanone oxime (methyl-ethyl-ketoxime, MEKO) were studied in both laboratory and plant conditions. Although their reaction with oxygen has been exam- ined in some detail in a variety of conditions, no systematic comparative study in nuclear power plant steam generator conditions was reported.

The efficiency of several alternative oxygen scavengers to that of hydrazine in simulated PWR steam generator inlet conditions, both in terms of kinetics of their reaction with oxygen and interaction with 22K carbon steel (steam generator body material), were studied. Such comparison represents an important step in the process of selection of alternative oxygen scavengers for both nuclear and conventional power plant coolants. [Jäppinen et al 2021]

The initial rate of oxygen reaction at eight-fold excess of the scavenger estimated (see Figure 1) from both oxygen and redox sensors allows for the following ranking of additives: carbohydrazide (CH) > hydrazine ≈ erythorbic acid (EA) > diethyl-hydroxylamine (DEHA) >> methyl-ethyl-ketoxime (MEKO). Thus, carbohydrazide and to a certain extent erythorbic acid emerge as probable alternatives to hydrazine in the studied environment with respect to the initial rate of oxygen consumption.

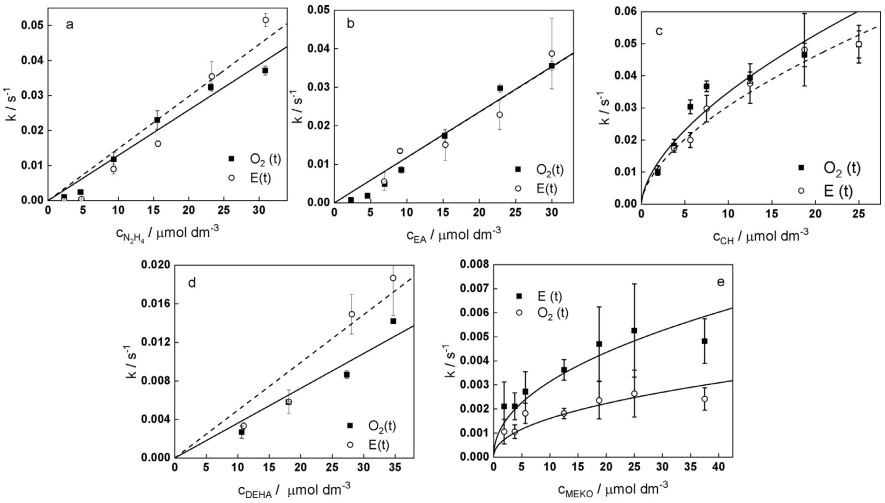

Figure 1. Reaction rate constant calculated for various oxygen scavenger chemicals as function of their concentrations.

The oxygen reaction is found to be first order with respect to hydrazine, erythorbic acid and DEHA. The order with respect to carbohydrazide is estimated to be 0.6, whereas that with respect to MEKO as 0.5. The increase of the rate of oxygen consumption with concentration is the fastest for carbohydrazide, i.e. the desired effect is the largest.

A pronounced decrease of the impedance magnitude at low frequencies upon addition of the oxygen scavengers to the electrolyte was observed (see Figure 2). This decrease is the most evident for EA, CH and DEHA, to a certain extent smaller for MEKO and the smallest for N_2H_4.

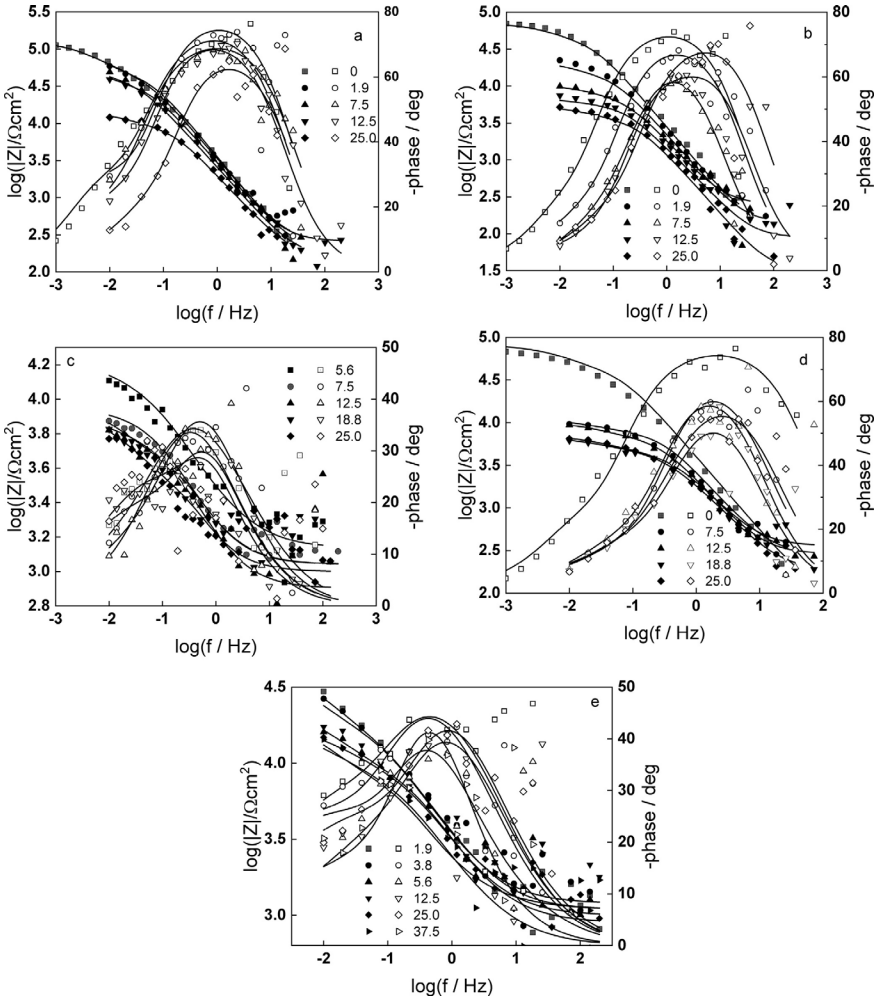

Figure 2. Electrochemical impedance spectra for 22K carbon steel as depending on the initial oxygen scavenger concentrations: (a) N_2H_4, (b) erythorbic acid, (c) carbohydrazide, (d) diethyl-hydroxylamine, (e) methyl-ethyl-ketoxime. Left vertical axis – impedance magnitude (fullsymbols), right vertical axis – phase shift vs. frequency (open symbols). Points – experimental values, solid lines – best-fit calculation according to the mixed-conduction model equations.

To discriminate between different processes responsible for this decrease, the EIS data for 22K steel were interpreted with the MCM in terms of film growth and restructuring, as well as charge transfer reactions at the film/solution interface. It can be concluded that the charge transfer reaction of scavengers is first order with respect to EA and CH, close to first order (with a power of 0.8) for DEHA, and 0.5 for MEKO. The order estimated for hydrazine is close to 2, i.e. the effect of this additive is considerably smaller.

The influence of scavengers on the reaction of film growth and dissolution (increase of the corrosion rate) is once again much more pronounced for the hydrazine alternatives (EA, CH and DEHA) than for hydrazine itself, indicating a much more effi- cient interaction of the alternative scavengers with the oxide layer on steel.

Enrichment of impurities on a simulated steam generator tube

The enrichment of impurities can occur in the steam generators of pressurized water reactors due to the intense boiling conditions prevailing within them. In this work, the deposition and release of chloride and sulphur based impurities were studied, with a special designed water circulation loop simulating the thermal-hydraulic heat transfer conditions in a steam generator. Alloy 690 tube samples were used to simulate steam generator tubing. In this setup, the water was fed over a cartridge heater on which A690 sample was mounted on. The cartridge heater would simulate the heat generated in the primary circuit and initiate boiling on the outer surface of the simulated steam generator tube. The conductivity of the in and out flowing water was monitored to detect deposition or release of charged particles (i.e. impurities). In-situ electrochemical impedance spectroscopy was used to characterize the evolution of the electrochemical system during non-boiling, boiling and after-boiling conditions. Inductively coupled plasma mass spectrometry analysis was used to measure the type and amount of deposited and released impurities.

It was shown that the deposition of the impurity is heavily dependent on the form in which the impurities are injected into the system (i.e. salt vs. acid). Deposition and release of impurities seemed to be initially linear, but for longer time scales, both phenomena followed a power-law type behaviour, as can be seen from Figure 2. From Figure 2 it can be seen how the conductivity is changed as, pH adjustment chemical and impurities are added into the water. In addition, it can be seen how the initiation of the boiling (increasing the cartridge heater temperature) causes the conductivity to drop as function of time. The decresing conductivity is correlated with the amount of depositing species. After the boiling is stopped, a rapid increase in conductivity can be seen after which the conductivity settles on a level before the boiling was initiated. At this stage, the release of deposited impurities is seen.

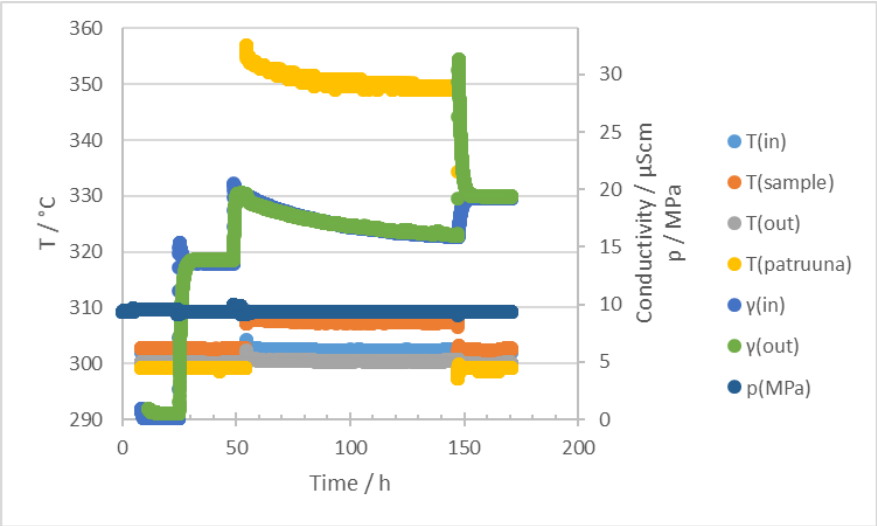

Figure 2. Deposition and release kinetic of the measured system when 2 ppm Cl (as NaCl) was added into the system.

The amount of depositing impurities was estimated to be 19 ppb/cm^2 for Cl and 11 ppb/cm^2 for SO_4 after roughly three days of boiling. The maximum deposition and release rates for the impurities were estimated to be 1,7 and 1,6 ppb/min×cm^2 for Cl and 1,50 and 0,93 ppb/min×cm^2 for SO_4, respectively. No remnants of the impurities were found on the sample surface during the post-test oxide characterization.

Electrochemical impedance spectroscopy (EIS) measurements were performed during the experiments to see if any differnecies between boiling and non-boiling conditions could be detected. EIS measurements revealed that four different physical processes are present in the system and the processes related to the double layer and solution properties were affected by boiling, as can be seen form intermediate frequencies in Figure 3. From this figure it can be seen that the impedance magnitude is affected by boiling. This is partially though to be yielded from the decreased surface area which is in contact with the electrolyte. The future work will include a more detailed analysis of the spectra to identify more detailed effects of boiling to corrosion behaviour of steam generator tubing materials.

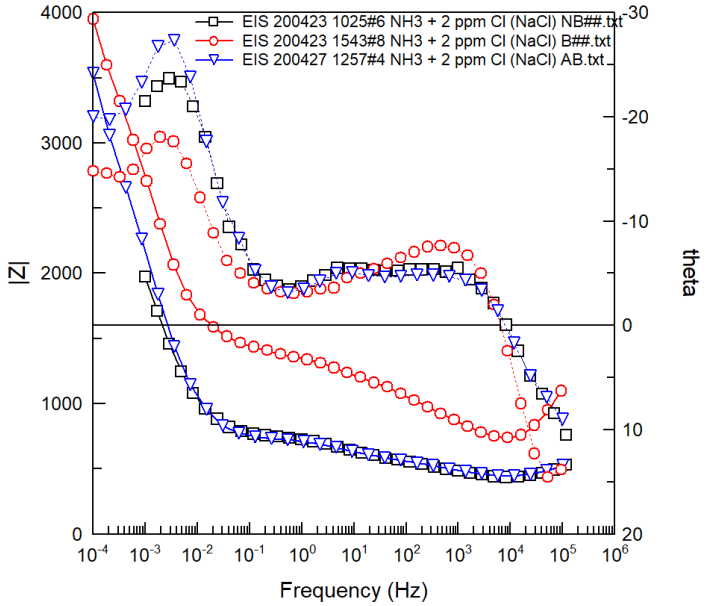

Figure 3. Measured impedance spectrum before boiling (NB), during boiling (B) and after boiling (AB) conditions when 2 ppm Cl was added as an impurity.

Zeta potential measurements on steam generator materials

Deposition of corrosion products may cause harmful degradation processes, such as stress corrosion cracking, in nuclear power plant steam generators. The exact deposition mechanism is still under debate and many interparticle forces may be involved in the deposition process. One of the possible forces is electrostatic double layer force, which according to model developed by UCTM and VTT [Bojinov et al 2020], may have very significant effect on deposition. The properties of the electrical double layer can be predicted by measuring the zeta potential of the double layer of the surface. In order to evaluate deposition effect of double layer forces, one must know the zeta potential of both depositing corrosion particles and the surfaces of the structural materials used in steam generators. The zeta potential of magnetite (corrosion product) has been previously measured at VTT in several NPP secondary side water chemistries (ammonia, ethanolamine, morpholine and octadecylamine) at temperature range between room temperature and steam generator operating temperature. During 2019 results for zeta potential measurements of a steam generator material (stainless steel AISI 316L) in ammonia and ammonia+octadecylamine water chemistries were obtained.

Measured zeta potential values in both environments and at all temperatures were in the vicinity of zero millivolts for stainless steel particles. This signals that there is no attracting nor repelling double layer force between magnetite particles and stainless steel surfaces but the deposition process in steam generator is

governed by other forces, such as van der Waals and gravitational forces and boiling. This probably is especially the case in ammonia water chemistry at steam generator operating temperature, because then also the magnetite particles have zeta potential of 0 mV, and by that the colloidal stability of particles is lost, and they start to flocculate and then deposit by interaction of van der Waals and gravitational forces.

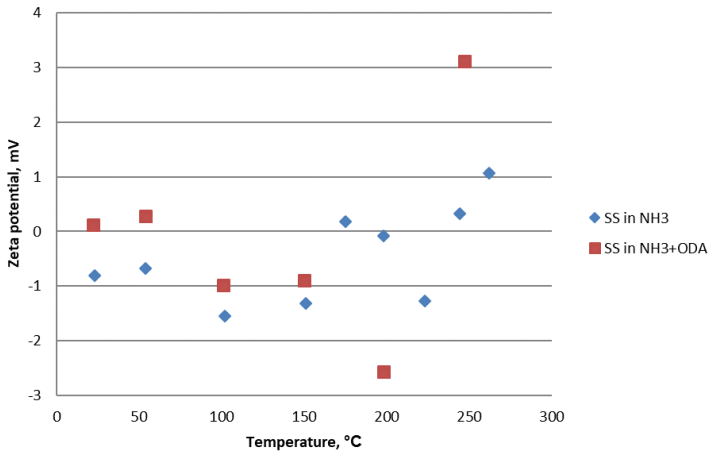

Figure 4. Zeta potential of stainless steel particles in ammonia+ODA solution as a function of temperature compared to results obtained in ammonia solution without ODA.

During 2020 the results of zeta potential measurements for magnetite particles in beginning of the cycle primary PWR chemistry (1000ppm B, 2 ppm Li) as a function of temperature. These values are compared to previously measured zeta potential values of magnetite in secondary side water chemistry controlled by ammonia.

Whereas in secondary chemistry zeta potential values of magnetite tend to approach zero millivolts at higher temperatures, in primary water chemistry, the zeta potential values seem to have a V-shaped curve, with its minimum being -208 mV measured at 161 °C. These results are compared to other reference data to verify the measurments results performed previously with the VTT's equipment.

Lead assisted stress corrosion cracking of A690 in alkaline crevice conditions

Lead assisted stress corrosion cracking of A690 in alkaline crevice solution was studied. Lead (Pb) addition (2.2 mmol kg-1, or 500 wppm) to the alkaline crevice environment studied in this work was found to affect markedly the electrochemical behavior of Alloy 690 tube material at 60°C and 278°C. In the current-voltage -curve, the anodic peak just above the corrosion potential increased in magnitude by a factor of ca. 3 upon the addition of Pb at 278°C (see Figure 5). On the other hand, the

impedance magnitude at the lower end of the frequency spectrum increased considerably in the passive range. Quantitative interpretation of the EIS data using a recent version of the MCM especially developed for Alloy 690 indicates that the oxidation processes at the alloy/inner layer interface are accelerated in the presence of Pb, however, the charge transfer reactions at the oxide/solution interface are slowed down. Further, significantly larger thicknesses are observed for films formed in the presence of Pb, as evidenced by both calculations based on EIS and estimations from compositional in-depth profiles measured by GDOES. The electronic properties of the oxide are also markedly influenced by Pb addition, as inferred by the significant differences in both absolute values and potential dependences of the space charge capacitance. The fracture strain of the Alloy 690 tube material studied in this work was found not to be affected by addition of 500 ppm of Pb into the alkaline crevice environment. The fracture surface appearance, as studied by scanning electron microscope (SEM) was found to be ductile. Based on the results gained, Alloy 690 tube material studied here appears to be not susceptible to SCC in the present crevice conditions at 278 °C, however, microscopic examinations are needed to confirm or disprove this statement. XPS analysis of the films on the strained and unstrained parts of the SSRT specimens exposed in the presence of Pb indicated the presence of Ni(II), Fe(II) and Fe(III), PbO and PbSO4 (the latter after 2–8 nm of sputtering). A notable difference with regard to the GDOES results on separate samples was the absence of Cr(III) at the surface (small quantities of Cr are observable after 8 nm of sputtering for the sample exposed at OCP). Concerning the cation composition of the surface and especially Pb(II) content, there is a semi-quantitative agreement between GDOES and XPS.

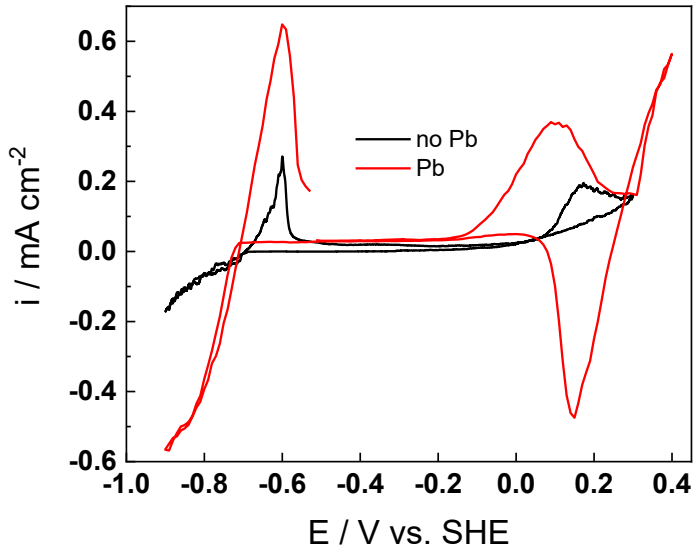

Figure 5. Current vs. potential curves (scan rate 0.167 mV s^{-1}) of Alloy 690 in the simulated crevice solution without and with Pb addition as PbO at 278 °C.

State of the art of monitoring the corrosion product dissolution and transport

The materials of the nuclear power plants are not insoluble at the power plant operating environment but are instead affected by different forms of corrosion. Corrosion products, like iron, nickel, chromium and copper compounds, are released to the process water as a result of corrosion. When these corrosion products move and re-deposit on surfaces, they can cause problems. In the primary circuit of a PWR the corrosion products are activated in the reactor core and then transported and deposited all over the primary circuit, which results in higher personnel radiation doses during maintenances. In the primary circuit, the corrosion products tend to deposit on the core region and the fuel assemblies influencing the core and the plant performance as well as the fuel integrity. In the secondary circuit, they deposit within the steam generator heat exchange tubes and on the surfaces of the steam generator components, enhancing the corrosion rates of the steam generators and lowering the thermal efficiency of the plant. One way of mitigating these processes is lowering the source term of the corrosion products: corrosion and corrosion product transport.

Several thermal, hydraulic and chemical parameters affect to the corrosion rates and the rates of corrosion product transport. In order to understand them better, plant operators and research facilities must have tools for monitoring the rates of corrosion product dissolution and transport, preferably in situ and on-line. This report provides an overview to the state-of-the art of corrosion rate and corrosion product monitoring. Several physical and electrochemical corrosion monitoring methods are presented as well as corrosion product monitoring methods based on grab sampling, integrated sampling, colorimetric methods, turbidity measurements, particle counters, acoustic detection and others.

Table 1. Summary on the corrosion product monitoring techniques.

Corrosion product monitoring	Strengths/weaknesses
Grab sampling	Traditional, easy and inexpensive/ No information about transients is gained, the representability might be poor
Integrated sampling	Better representability than grab sampling due larger sample amounts, easy to operate/ No in situ measurements
Colorimetric methods	Traditional technique /Low sensitivity, no in situ measurements
Turbidity methods	On-line, in-situ or sidestream method/ only qualitative, sensitivity might be poor
Particle counters	On-line method/ no in situ measurements
Acoustic detection	On-line method/ sensitivity might be poor
Dynamic light fluctuation particle monitor	On-line method, better sensitivity than particle counters/ only qualitative method
Dynamic light scattering	Method for particle size and size distribution/ No particle counting, no in situ measurements

SMR water chemistries - the state-of-the-art

Currently publicly available information on SMR water chemistries and structural materials are scarce, but based on the information found the water chemistries and structural materials are both similar to the ones used in generation III NPPs. Primary side chemistry seems to differ that in many cases there are not used soluble boron in reactivity control which is beneficial in corrosion point of view. Currently used PWR and VVER steam generator tubing materials have good corrosion resistance properties during normal operating periods. Minor concerns were listed when deviations to normal water chemistry is introduced.

References

Bojinov, M. Jäppinen, E. Saario, T. Sipilä, K. 2020. Identification of key parameters of magnetite deposition on steam generator surfaces - Modeling and preliminary experiments. Colloids and Surfaces A 586 (2020) 1242239.

Jäppinen, E., Ikäläinen, T., Lindfors, F., Saario, T., Sipilä, K., Betova, I., Bojinov, M. A comparative study of hydrazine alternatives in simulated steam generator conditions — Oxygen reaction kinetics and interaction with carbon steel. Electrochimica Acta 369 (2021) 137697. https://doi.org/10.1016/j.electacta.2020.137697

6.4 Fatigue and evolving assessment of integrity (FEVAS)

Juha Kuutti[1], Jarno Hiittenkivi[1], Heikki Keinänen[1], Pekka Nevasmaa[1], Ahti Oinonen[1], Tommi Seppänen[1], Henrik Siren[2], Iikka Virkkunen[2]

[1]VTT Technical Research Centre of Finland Ltd
P.O. Box 1000, FI-02044 Espoo

[2]Aalto University
P.O. Box 11000, FI-00076 AALTO

Abstract

The project FEVAS focuses on the structural integrity aspects of the pressure vessel and primary circuit with special emphasis on developing novel models, tools and techniques that help to ensure safe plant operation over the whole plant lifetime. The project has focused on the development of a F_{en} model to take into account the effect of the environment and temperature on the fatigue endurance of the primary circuit, conducted a study of surface crack behavior under cyclic thermal loads followed development of experimental and numerical techniques to capture it and developed techniques needed for the assessment of pressure-pulsation induced piping vibrations. Additionally, the project concentrated on the development of surface crack repair welding techniques through mock-up manufacturing, its material characterization and numerical simulations of the welding process.

Introduction

The emphasis of the FEVAS project is the research and development of the methods to assess the long-term structural integrity of the pressure vessel and primary circuit. The overarching aim of all research in the project to provide advanced and calibrated integrity assessment methods and input information required in these methods and to identify and quantify the uncertainties and errors of the structural integrity analyses performed to demonstrate the integrity of the primary circuit. The project improves the overall safety of NPPs by providing information on the state-of-the-art integrity assessment methods and their relations to conventional norm-based methods, including the inherent safety margins of the conventional methods.

The project focused in three topics: fluid-induced loads on piping, fatigue usage of primary circuit and development repair welding approaches.

Fluid-induced loads on piping

The coupling of primary water acoustics and piping vibrations is considered in the project. Suitable efficient analytical and numerical modelling capabilities are developed and the possible excitation sources are studied. The emphasis is on i) creating

understanding of the most important acoustic-structural phenomena in the primary circuit and ii) having efficient methods which can account for the fluid-structure-interaction (FSI) between the acoustics and the piping. The coolant water necessarily affects the dynamic behaviour of piping and components. At simplest, the effect can be modelled through the added mass. More complex two-way FSI effects result e.g. when the acoustic and structural natural frequencies are similar (Oinonen, 2019). For the coupled cases FSI modelling methods are necessary, such as 1D or 3D acoustic-structural codes or even coupled computational fluid dynamics (CFD) and structural analyse. A literature review was conducted on analytical and numerical methods for modelling coupled acoustic-structural piping vibrations. The current emphasis of the work is on 1D tools which enable efficient modelling of the whole circuit and on analytical methods which can be used for assessing the significance of different acoustic-structural phenomena.

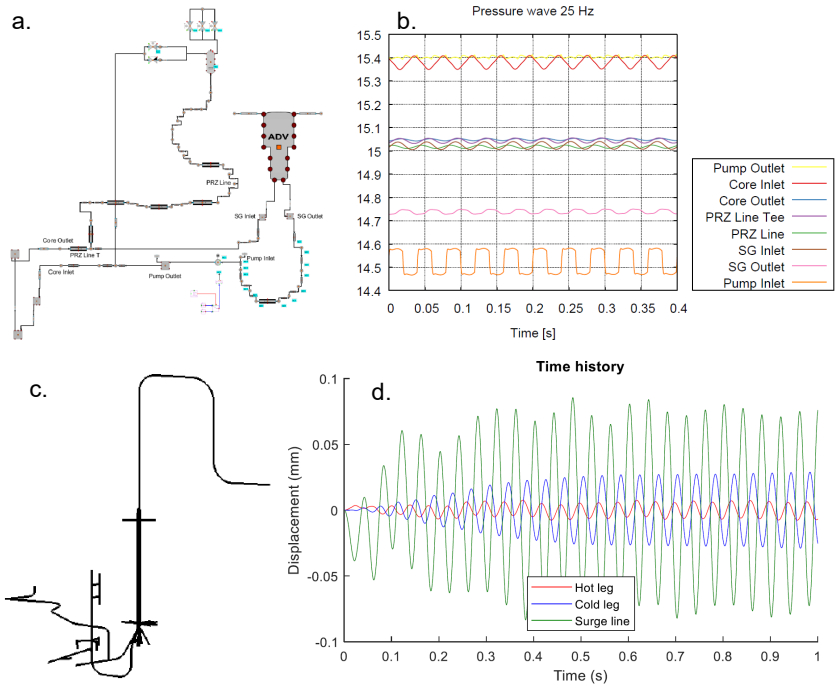

Figure 1. Apros model of a PWR primary circuit (a) and pump-induced pressures at different locations (b). Abaqus structural model of a PWR primary circuit (c) and vibration time histories in the model caused by pump pressure pulsations (d).

Apros was seen as a suitable modelling tool and it was used to calculate the acoustic pressure propagation in a PWR example primary circuit (Hiittenkivi 2019). Cyclic pressure pulsation was produced by the main circulation pump in the model. Figure 1a-b presents how the pressure propagates through the system and attenuates due to the flow resistances in the circuit. The amplitude of the pulsation generally

diminishes but some amplifying phenomena is observed at specific excitation frequencies. The excitations where then used as input for the structural piping vibrations analysis with Abaqus FE software (Kuutti & Hiittenkivi, 2020). Figure 1c-d shows the structural piping model and the resulting hot leg, cold leg and surge line vibrations. The assessment was performed one-way coupled such that the feedback effects of structural deformations were not considered in the thermal hydraulic assessment. The results show that this idealization was sufficient in the studied case as the structural vibration amplitudes remained low.

This part of the project also focused in combining new experimental NDT techniques with fracture mechanics simulations to study the behavior of a surface crack under cyclic thermal loading (Koskinen et al., 2021). As an improvement to conventional techniques, nonlinear ultrasound measurement techniques make it possible to detect partially closed cracks. Such a scenario may occur for example due to residual stresses or thermal contraction (Kuutti & Virkkunen, 2020). Together with the RACOON project, an experiment was performed where a surface crack in a thick steel plate was subjected to cyclic thermal loading. The specimen was instrumented with ultrasonic sensors, which performed on-line monitoring of the crack response during the loading. The scenario was simulated using the finite element method to obtain the crack opening displacements and contact pressure distributions on the crack face over the full loading cycle. Figure 2a-d shows the numerical predictions of the temperature history, crack opening displacements and contact stresses. The crack response signal measured using nonlinear ultrasonic techniques is shown in Figure 2e. The ultrasonic response is qualitatively in line with the crack opening state distribution.

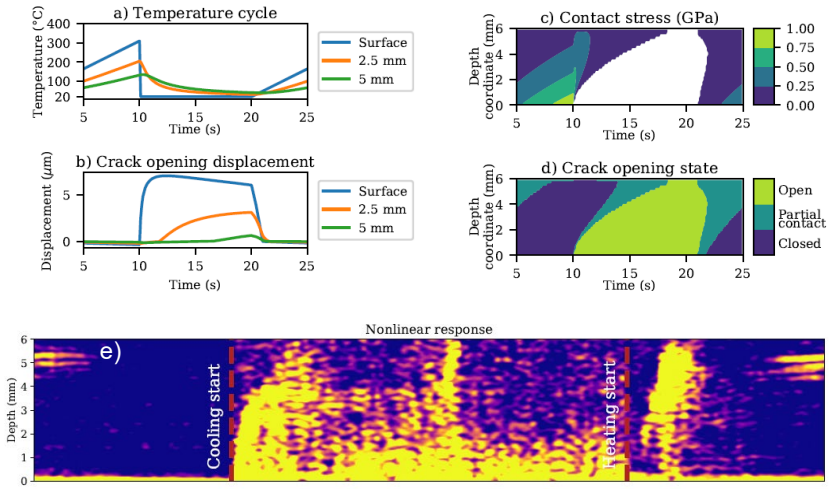

Figure 2. a-d: The temperature histories, crack opening displacement histories, contact stress and crack opening displacement over the load cycle obtained from the finite element simulation. e: Nonlinear ultrasonic response over the load cycle.

Fatigue usage of primary circuit

The project also focuses in the research on the environmental factor affecting the fatigue life of components subjected to the primary water environment and cyclic loading. Fatigue design curves are based on testing in air, but for four decades it has been observed that a reactor coolant environment degrades fatigue life. The greatest challenge in environmentally-assisted fatigue (EAF) has been quantifying the effect through a reduction factor, F_{en}. The work has two specific goals: to generate valid EAF data in support of a plastic strain rate based F_{en} model which can be applied in cumulative usage factor evaluation of plant components and to complete development of a relevant F_{en} model (Seppänen et al. 2019, 2020).

Environmental effects of LWR coolant need to be factored in when defining cumulative fatigue usage of primary circuit components. The basis is a set of codified design rules and fatigue design curves, based on experimental data. To accurately quantify environmental effects, the reference curve in air to which fatigue life in water is compared shall be as reliable as possible. Literature studies and accumulated data at VTT reveal that the use of common reference curves for a wide range of austenitic stainless steel alloys and temperatures is unreliable. Some design codes already include measures to consider this but ASME III is not yet among them. The ASME III design curve is adopted from NUREG/CR-6909 and contains no consideration for dependence of temperature or stainless steel grade.

Two different stainless steel grades, AISI 304L and 347, have previously been used in environmentally-assisted fatigue experiments at VTT. The experimental work in in FEVAS focused in providing additional baseline fatigue data for the development of the F_{en} model.

The results from the test series performed at 25 °C and 325 °C is shown in Figure 3. The project provided reference curves for the AISI 304L heat at room temperature and 325 °C to complement the curves already available for AISI 347. In Figure 4, demonstration of realistic environmental effect quantification is done using these reference curves as an alternative to the NUREG methodology. (Seppänen et al. 2019, 2020).

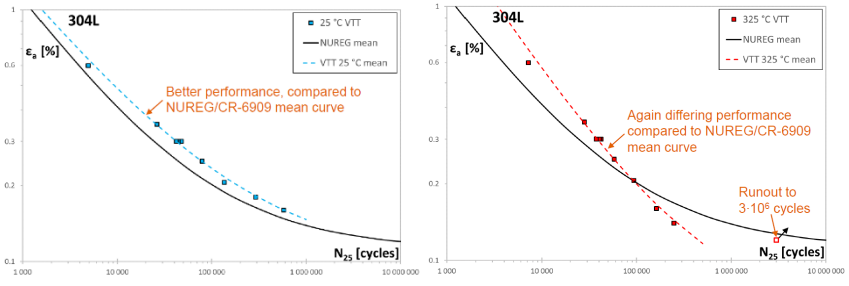

Figure 3. Low-cycle fatigue tests results for AISI304L at RT and 325 °C.

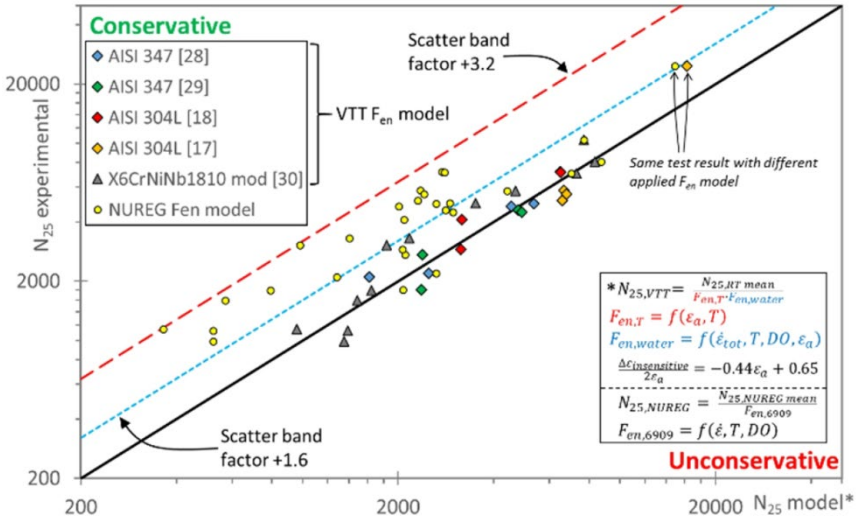

Figure 4. Fatigue life from application of VTT and NUREG F_{en} models.

Development of repair welding

As plants continue to age, there is an increased probability for the need of repairs due to extended exposure to a harsh environment (neutron flux, high temperature, high pressure, water chemistry). It is paramount that qualified and validated solutions are readily available, and that such methods are validated proactively, at a stage when they are not yet needed. In FEVAS (joint with ELIAS), a repair method for a postulated through cladding crack into the low alloy steel of a nuclear power plant's reactor pressure vessel has been investigated.

Repair welding is thought to represent a 'worst-case' scenario where a postulated linear crack-like defect exists beneath the cladding and might extend across the interface into the RPV steel side. This postulated defect is then removed by machining, and the thereby machined groove will be filled by repair welding using a nickel-base superalloy filler metal and using mechanised/robotised arc welding process. While FEVAS focused on computational support for mock-up design and weld procedure tests (Keinänen et al. 2020), ELIAS performed repair procedure design and characterization of the mock-up microstructure (Virkkunen et al. 2020). The mock-up was welded at Aalto University as a joint effort between the projects.

In the project, a repair weld mock-up was produced with CMT welding. As an alternative to conventional gas tungsten arc welding (GTAW) process, the use of automated gas metal arc welding (GMAW) utilizing Cold Metal Transfer (CMT) mode offers many advantages, such as good weld quality, exceptionally stable arc, easy automation and very low heat input along with narrow HAZ (Virkkunen et al., 2020). A postulated crack was excavated from a cladded and thermally embrittled low alloy steel material and repaired using a nickel base filler metal by gas metal

arc welding-cold metal transfer. No pre-heating or post-weld heat treatment was applied, as it would be nearly impossible to apply these treatments in a reactor pressure vessel repair situation. One cladded plate was welded (Figure 5), meaning two excavations were filled. One excavation was filled with 100 beads along the long side, while the second excavation was filled halfway (5 layers) the long side, followed by a 45° hatch pattern (6 layers) for a total depth of 40 mm.

The mock-up weld was sectioned and a metallographic sample prepared to study the weld quality. This part of the research and its results are described in more detail by the ELIAS project. (Huotilainen et al., 2021)

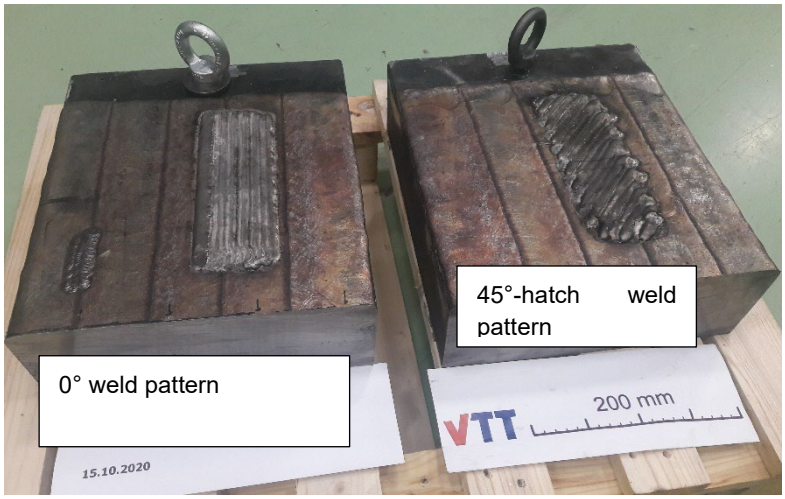

Figure 5. Repair weld mock-ups after welding.

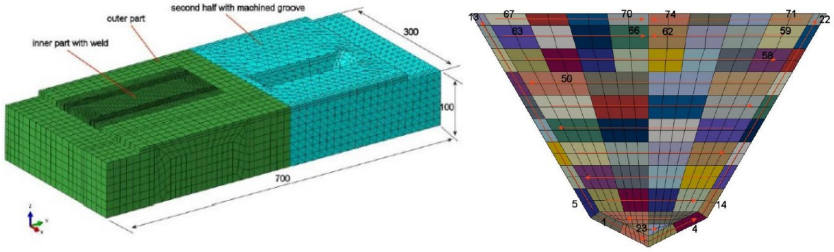

Figure 6. Finite element model for the mock-up welding simulation and bead order in the weld cross-section.

The welding was simulated with the finite element method using in-house welding simulation methods (Figure 6, Keinänen, 2019). The aim of the simulations was to scope the effects of different welding parameters and bead orders on the residual stresses, HAZ extent and cooling curves (Huotilainen et al. 2021). The computed longitudinal residual stresses show maxima at the surface of the weld, Figure 7. A

particular interest in the simulations was the computational prediction of the hardness distributions around the weld location. Based on an empirical correlation formulae and the simulated $t_{8/5}$ cooling time parameter, the as-welded hardness distribution in the base metal is shown in Figure 8.

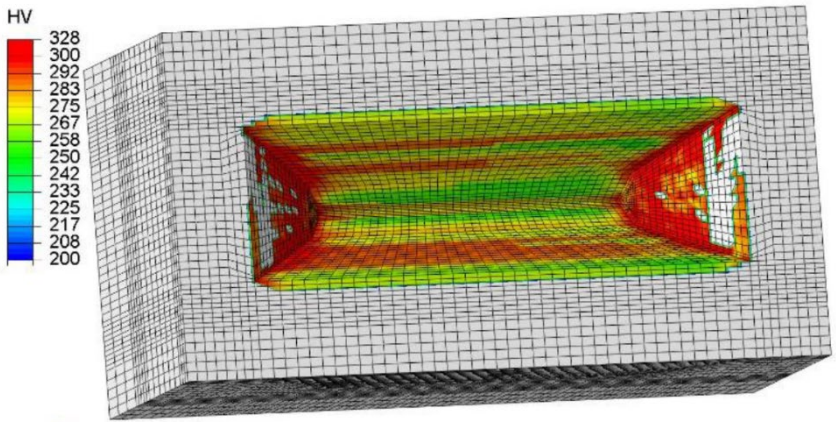

Figure 7. Hardness predictions in the base metal after welding as predicted from the $t_{8/5}$ cooling time.

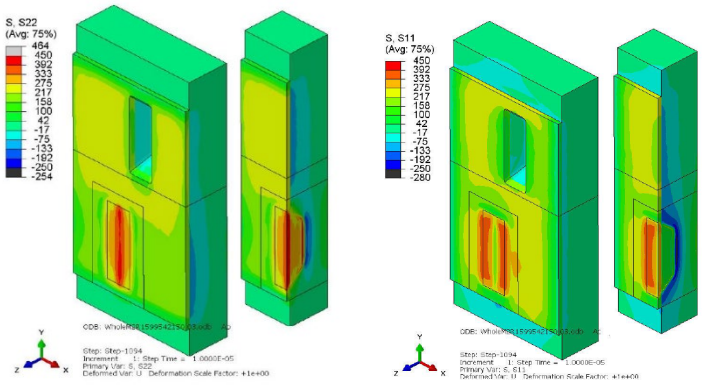

Figure 8. Computational prediction of the longitudinal (left) and transverse (right) weld residual stress distributions after welding at room temperature.

Experimental and numerical evaluations have been used to investigate a repair welding method for a postulated through cladding crack in to the RPV. The work will continue to fully characterize the weld interface, investigate the welding residual stresses and fully optimize the welding parameters along with the development of tools and methods to numerically simulate the welding process and predict the deformations and residual stresses.

Closing remarks

The research described above summarizes the accomplishments in the FEVAS project in 2019 and 2020. In 2021-2022, the work focuses solely in the development of repair welding thought the FENIX project.

References

Hiittenkivi, J. 2019. Vibration Induced by Pressure Waves in Piping. VTT Research Report VTT-R-01297-19. Espoo: VTT.

Huotilainen et al., 2021. Evaluation of an Alloy 52 / cladded carbon steep repair weld by cold metal transfer. Submitted to the ASME 2021 Pressure Vessels & Piping Conference PVP2021, PVP2021-61981, Virtual, Online.

Keinänen, H. 2019. Comparison between Abaqus Welding Interface and VTT in-house welding codes. VTT Research Report VTT-R-00519-19. Espoo: VTT.

Keinänen, K. et al. A52M/SA502 dissimilar metal RPV repair weld: Evaluation of different techniques, ASME 2020 Pressure Vessels & Piping Conference PVP2020, PVP2020-21233, August 3, 2020, Virtual, Online.

Koskinen, T., Kuutti, J., Virkkunen, I. & Rinta-aho, J. 2021. Online nonlinear ultrasound imaging of crack closure during thermal fatigue loading. Journal article manuscript in preparation.

Kuutti, J. & Hiittenkivi, H. 2020. An assessment of fluid-induced vibrations in a PWR primary circuit, Research Report VTT-R-01114-20. Espoo: VTT.

Kuutti, J. & Virkkunen, I., 2020. Crack closure behaviour of semicircular surface cracks subjected to cyclic thermal loads. Fatigue and Fracture of Engineering Materials and Structures, 2020, 43(12), pp. 3063–3067

Oinonen, A. 2019. Fluid-Structure-Interaction analysis for a water hammer loaded piping elbow, SMiRT-25 Conference, Charlotte, NC, USA, August 4-9, 2019.

Seppänen, T., Alhainen, J., Arilahti, E. & Solin, J. 2019. Strain-controlled low cycle fatigue of stainless steel in PWR water. ASME 2019 Pressure Vessels & Piping Conference PVP2019, July 14-19, 2019, San Antonio, Texas, USA.

Seppänen, T., Alhainen, J., Arilahti, E. & Solin, J. 2020. Grade and temperature dependent reference curves for realistic Fen quantification of austenitic stainless steels. ASME 2020 Pressure Vessels & Piping Conference PVP2020, PVP2020-21136, August 3, 2020, Virtual, Online.

Virkkunen, I. et al. A52/A502 dissimilar metal RPV repair weld: experimental evaluation and post-weld characterizations. ASME 2020 Pressure Vessels & Piping Conference PVP2020, PVP2020-21236, August 3, 2020, Virtual, Online.

6.5 Non-destructive examination of NPP primary circuit components and reliability of inspection (RACOON)

Tuomas Koskinen[1], Iikka Virkkunen[2], Oskari Jessen-Juhler[1], Jari Rinta-aho[1]; Oskar Siljama[2]

[1]VTT Technical Research Centre of Finland Ltd.
P.O. Box 1000, FI-02044 Espoo

[2]Aalto University of Technology
P.O. Box 11000, FI-00076 AALTO

Abstract

Non-destructive testing is vitally important in ensuring the safe and economic operation of aging nuclear power plants and other industrial systems. Reliable detection of service induced damage as early as possible allows for improved safety and effective maintenance. At the same time, finding flaws early pushes the NDT methods to the limits of detectability. Thus, effective estimation of NDE reliability is vital to successful application of NDE. While much progress has been made with NDE qualification, quantitative estimation of NDE reliability (namely, probability of detection, POD) is still not commonly used in the nuclear industry. The inspections vary, and providing sufficient empirical data for POD has remained infeasible.

In the RACOON project, inspection reliability and POD is studied with new tools (eFlaw's) that allow better empirical data gathering. Based on previous work, in the current project a first of a kind virtual round robin (VRR) with world-wide participation was conducted in collaboration with an international project. The target was the ultrasonic inspection of dissimilar metal welds (DMWs). The VRR demonstrated the capability and efficiency of the approach to determine NDT reliability and performance.

In addition to theoretical reliability, the consistency and repeatability of inspections are crucial to actual field reliability. In a short project ANDIE, now merged to the RACOON project, the application of machine learning to automated data analysis and defect detection was studied. Machine learning (ML) powered ultrasonic inspection has proven highly feasible approach to increase reliability, repeatability and efficiency of mechanized ultrasonic inspection. Originally short project ANDIE demonstrated the capability to use virtual flaws for training the ML models. In year 2020 the effect of different flaw types and sizes used in training the ML model was studied to have impact on detectability.

Introduction

Efficient and reliable NDE techniques support economical and safe operation of NPPs. The RACOON project, addressing "NDE on NPP primary circuit components,

machine learning and reliability in inspection" of the SAFIR2022 programme, works to improve the reiliability and efficiency of NDE methods with improved POD methodology, simulation and automated data analysis using machine learning. RACOON also participates to the Program for Investigation of NDE by International Collaboration (PIONIC), which is established to facilitate collaborative information sharing in the NDT of NPPs.

Better reliability estimation methods are necessary in order to develop NDT reliability. In the current project, inspection reliability is studied using novel technology called "eFlaws" or "virtual flaws". These allow unprecedented access to flawed data and make it possible to effectively study data analysis reliability. In the current project, a virtual round robin (VRR) was completed. Normal round robins are expensive and time consuming to conduct. The use of virtual data and the VRR approach enables the distribution of scan data simultaneously and efficiently all over the world. This agile distribution of inspection data instead using physical samples, allows faster results and larger distribution of samples with fraction of the cost of normal round robin exercise.

Novel NDT methods and simulation are studied to further understand the phenomena related to flaw detection. In addition, the additional goal for the simulation effort is to produce relevant models in order to produce ample flaw data for both reliability studies and for machine learning purposes.

The reliability and efficiency increase are studied with machine learning powered ultrasonic inspection. As virtual flaws enable the VRR, the same method allows generating ample enough data for teaching the ML model. The goal is to match and even exceed the performance of a human inspector for interpreting mechanized ultrasonic data. Machine learning powered ultrasonic inspection would decrease the data-analysis time drastically, increase repeatability of the inspection and increase the reliability of the inspection result. A master's thesis on using machine learning to detect flaws in austenitic stainless-steel welds was completed in 2020 (Siljama, 2020). A more detailed selection of the RACOON projects results are presented below.

NDT reliability assessment

In recent times, more and more of the inspections in the nuclear field are performed in a mechanized manner. This means, that the data acquisition and analysis, that were traditionally conducted simultaneously and interactively, are now separated to distinct steps. The analysis is often conducted in a different location after the data acquisition has been completed. This division can be carried over to the evaluation of NDT performance. While both successful data acquisition and evaluation are critical for the overall performance of the NDT, they can now be assessed separately. The quality of the data acquisition is, in general, far easier to evaluate. The potential sources of error include incorrect calibration of the equipment and failure to maintain sufficient probe coupling during scanning. These can often be evaluated without large mock-ups or representative flaws. In contrast, the data evaluation phase is

challenging to evaluate because the evaluation procedures vary and may include significant human judgement. Thus, they necessitate relevant data and, traditionally, large mock-ups. Consequently, the primary interest for international round robin is for the evaluation and comparison of the data evaluation phase.

Transportation of the round robin mock-ups all over the world to NDT laboratories is costly and a slow process. While the round robin exercise gives valuable insight on the capability of the used NDT methods and procedures, they are seldom conducted due to fiscal and time constraints.

The use of virtual flaws opened a possibility to conduct a virtual round robin exercise for mechanized data in a completely new way. The round robin was focused on the data analysis, where pre-acquired data was distributed around the world, making the exercise far more cost-effective than ever before. Moreover, as virtual flaws enable an ample flaw data generation a statistically meaningful sample could be generated to quantify the round robin performance with a POD. The VRR was divided into two phases, manufacturing, scanning and augmentation of the flaws (Virkkunen et al. 2019) and result analysis (Virkkunen et al. 2020).

For original scan data, a DMW mock-up provided by Swedish qualification Centre (SQC) through the PIONIC program and the mock-up was scanned with phased array TRL technique. The mock-up contained solidification cracks and an EDM notch, described in more detail in Figure 1. The axial flaw indications were considered as artefacts as the probe setup was not optimized for axial flaw detection and the virtual flaw technique allowed the removal of these signals as well.

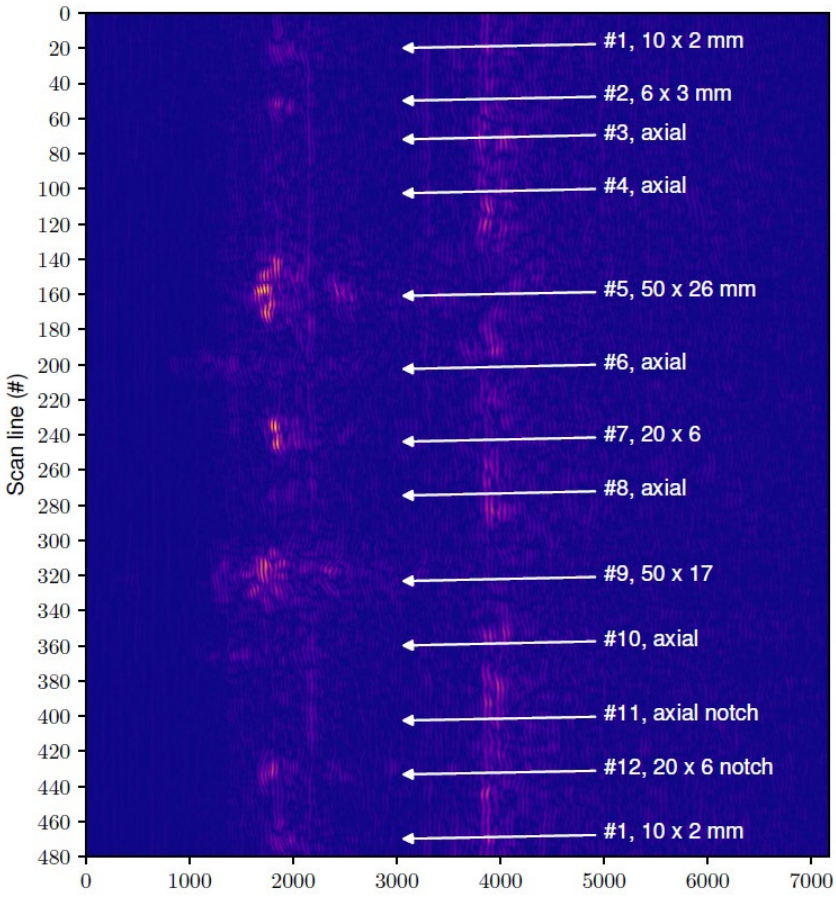

Figure 1. The original data showing the flaw indications, as acquired from the mock-up.

For POD purposes, the flaws in the mock-up where too large and decreasing the signal amplitude trough virtual flaws in excess deviates the signal too much from the original state. Thus, more flaws were generated through thermal fatigue to a separate DMW plates acquired from EPRI trough the PIONIC program. The flaw signals were extracted from the original weld data and implanted to generate 12 separate test data files containing 0 to 9 flaws each for analysis. The flaw files were the same for all participants, however the order of these files was shuffled to prevent information sharing between participants.

The participation for the VRR was good as 12 inspectors submitted back the results around the world. During the distribution and receiving the results, it was noted that, the inspection data is often linked to the software that produced it. While open formats for, e.g., ultrasonic data are available (Mienczakowski, 2015), they are unfortunately not yet widely adopted. This creates a major hindrance to the effective

use of NDT data in general, and conducting a virtual round robin is also affected by it. We can only hope, that in the near future, open formats will be more widely adopted. Certainly, virtual round robins as one of the many benefits of open data formats may speed their adoption. However, at present, no open format with sufficient adoption is available and thus any such round robin needs to select a used format which limits the participation to those teams that can effectively work with the selected file format.

The reported results can be seen in Table 1. The $a_{90/95}$ was estimated in two ways: the standard method and modified. As there are convergence issues for POD confidence bound estimation. This gave rise to unrealistic POD estimations i.e., the probability of finding zero-sized defect would be >0. This was amended by adding 20 synthetic misses with the size of 0 to the data to tie the detection probability to 0 at the flaw size of 0.

Table 1. Summary of the main results for VRR. The modified a90/95 is considered the best estimate for the value, due to convergence issues in estimation. False call rates are reported both as percentage in data and ASTM-E2862 compliant 95% confidence bound probability of false positives (PFP 95).

ID	Standard a90/95	Modified a90/95	False calls (count)	False call (%)	PFP 95 (%)
A		1.7	11	5%	8%
B	3.5	1.7	21	9%	13%
C	1.4	2.0	8	4%	6%
D	3.2	2.6	13	6%	9%
E	2.9	2.9	8	4%	6%
F	5.9	2.9	11	5%	8%
G	4.1	3.8	9	4%	7%
H		4.7	5	2%	5%
I	3.5	4.7	4	2%	4%
J	5.6	5.3	7	3%	6%
K	24.5	5.6	10	5%	8%
L	7.1	7.1	3	1%	3%

The results showed variance with $a_{90/95}$ ranging from 1.7 mm to 7.1 mm. For the two largest $a_{90/95}$ values the result can be explained with two large misses. The exact reason behind these misses were not found, as their signal-to-noise ratio was high enough for almost certain detection. This has been seen in other exercises as well, when the inspectors tend to miss the critical and large flaws while finding the smallest possible flaw.

False call performance was between 3% to 13%, with no clear link to the $a_{90/95}$ performance. However, as one inspection file was left completely flaw free, no inspector could determine the file completely flaw free. In fact, most of the false calls were made in this file. Moreover, 4 out of the 12 inspectors identified some files as flawless. The falsely flawless identified flaws did contain only small flaws with maximum equivalent flaw size below 3 mm.

The flaws are infrequent and most of the true data files inspected are flawless. Thus, making false calls in excess would hinder the inspection performance in actual inspection conditions. Therefore, this experimental setup does not fully represent the same inspections made in NPPs. This could be mitigated by increasing the number of flawless files and setting a limit to the number of false calls to discourage the inspectors to make false calls.

Simulation and Novel NDT

Ultrasonic simulation has been conducted in the WANDA project, predecessor to RACOON project (Jessen-Juhler, 2018, Koskinen et al. 2018) with CIVA simulation software. Simulation of NDT, particularly ultrasound testing, benefits the larger understanding of the conditions, phenomena and constraints around the inspection itself. Usually high approximation is more useful to understand the bigger picture in the inspection problem. However, CIVA simulation approximates the signal widely and for anisotropic situations such as austenitic stainless-steel weld or dissimilar metal weld, the approximation might be too vague for proper use in reliability exercises or as training data for machine learning (Koskinen et al. 2021).

Finite element method FEM was speculated to give more accurate approximation for flaw signal generation and simulation efforts were started in 2D in 2019. As flaw signal generation was successful in 2D (Jessen-Juhler et. al. 2019), the simulation model was extended to 3D shown in Figure 2 a). The simulations contained a simple phased array probe with 5 elements in a rexolite wedge. The wedge contained absorbing layers like a traditional wedge to reduce the noise from refracted ultrasonic waves. Unlike traditional ultrasonic probe, the transmitting and receiving elements do not have their own natural frequency, thus the recorded signal needs to be filtered digitally around this natural frequency to achieve the desired result. The material properties represented a homogeneous stainless-steel. The model was highly optimized with mirroring the geometry and limiting the element mesh to only on the areas of interest within the steel block.

The model was able to generate an A-scan show in Figure 2 b). The generated a signal resembles greatly a signal generated from an ultrasonic probe in a homogenous material. Even slight noise can be observed as in a real inspection, which has been unfeasible with CIVA simulations as the noise is generally randomly inflicted on the computation.

While both simulations in 2D and 3D were successful, the number of elements required made the computing time to exceed over 20 hours per single A-signal. As the simulated model was smaller than required for simulating a complete weld

inspection the computation would take even longer with Abaqus based solver. Therefore, the time required to simulate a B-scan would take multiple these A-scans to be any use for reliability and machine learning exercises would be too great.

The next step for the simulation effort is to find a solution for this computation time issue. One viable approach is to investigate other solvers, which might be more efficient in dealing with ultrasonic based problems.

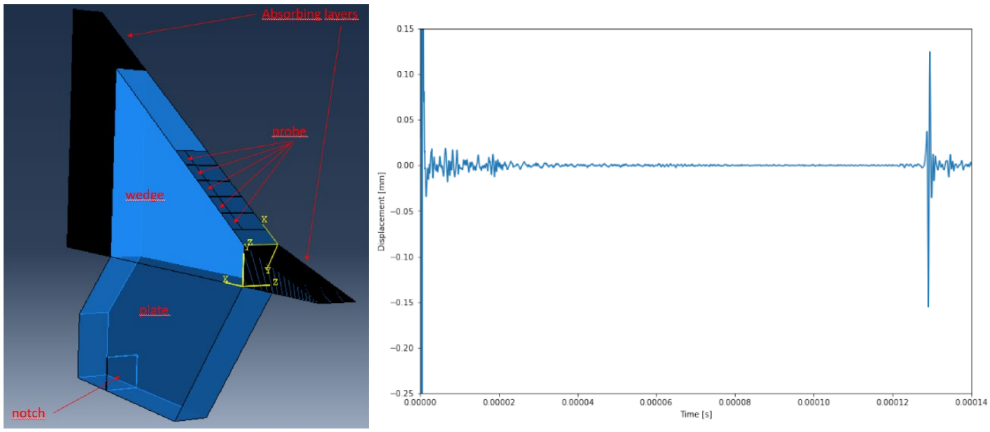

(a) b)

Figure 2. a) The 3D model geometry and setup b) The produced A-scan from 3D simulation

Surface acoustic wave (SAW) formation with phased array probe and a delay line was studied (Rinta-aho et al. 2019). While SAWs are an old concept, they can be utilized i.e., to inspect the integrity of coatings (Kauppinen, 1997). SAW is traditionally applied in immersion-based scans. This limits the type of components available for SAW type inspection. As modern phased array probes allow multitude of options on focusing the ultrasonic beam it is possible to adjust the focal laws with a delay line to generate SAW. Figure 3 a) demonstrates the method for SAW generation.

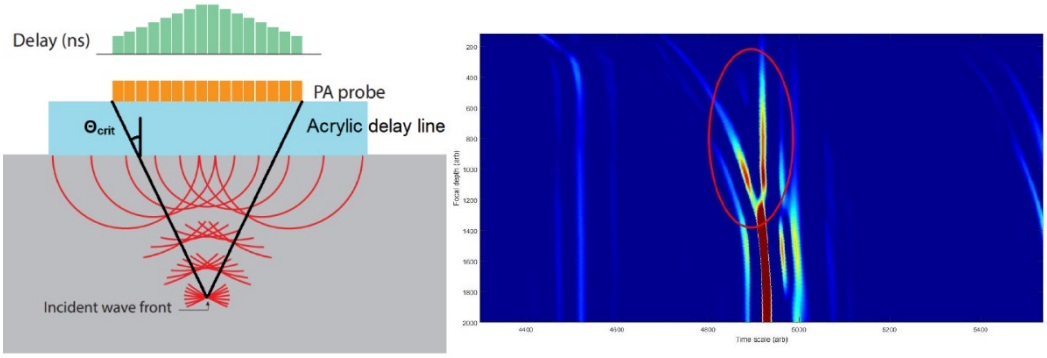

Figure 3. a) The PAUT and delay line setup in similar fashion as V(z) measurement. b) The wave split can be observed clearly from the scan

The initial idea behind focusing phased array focal laws trough a delay line comes from the V(z) measurement used in immersion. The focus point is moved vertically trough the focal laws until critical angle for SAW generation is achieved. The aperture of the probe needs to be large enough for the generated SAW to reach the receiver on the other end of the probe. In Figure 3 b) a wave split is clearly observed. This indicates the generation of SAW which could be then used to inspect the surface with reliably high accuracy.

Machine Learning Powered Ultrasonic inspection

ML powered ultrasonic inspection was originally studied as a small project ANDIE. The feasibility study showed the effectiveness of virtual flaws used for training the ML model (Virkkunen et al. 2021, https://doi.org/10.1007/s10921-020-00739-5). In addition, a research report was prepared (Koskinen et al. 2019) regarding the steps required how this new technology could be utilized in Finnish NPPs. The studies revealed that machine learning has the potential to change the NDT industry soon. The current state-of-the-art algorithms are powerful enough to match the skill of a human inspector or even surpass it in complex flaw detection tasks. Consequently, the use of machine learning presents a significant opportunity to make the in-service inspections more reliable, faster, and more economical.

As ANDIE was merged to RACOON in 2020 work began on more detailed research for ML powered ultrasonic inspection. The effect of flaw type used in training was studied in a DMW mock-up. The same used in the VRR exercise. (Koskinen et. al. 2021). The mock-up contained solidification cracks with varying sizes between 2 mm to 26 mm. There was also an EDM notch of 6 mm. The ML model was trained with different sets of available training data: All available flaws, only the small flaws used in training, only the medium flaws used in training, only the large flaws used in training and combination sets where the large flaws were not available for training and the small flaws were not available for training. Finally training set with only

medium sized solidification crack and only a medium sized EDM notch was available for training. In addition, CIVA simulated EDM notches were used for training the model.

The resulting POD curves, except for the model trained with simulated flaws can be seen in Figure 4. The performance achieved from the model trained with only the simulated flaws contained so much false calls, that no useful POD could be estimated. The flaw type has indeed an effect on the performance of the model. In addition, used flaw sizes effect the $a_{90/95}$ value considerably. The accuracy of the model can be adjusted trough the minimum flaw size used in training. This is highly convenient when optimizing the inspection result to detect the relevant flaw indications with high reliability. Moreover, the flaw type used in training should represent the real flaw signal in the process as much as possible. While the model was able to detect flaw types which were not used in the training, solidification cracks did miss the EDM notches constantly. On the other hand, the model trained with sets with EDM notch included or as an only flaw type managed to generalize to the solidification cracks in more efficient manner. This might be because of artefacts caused from the solidification process not caused in the process of manufacturing EDM notches.

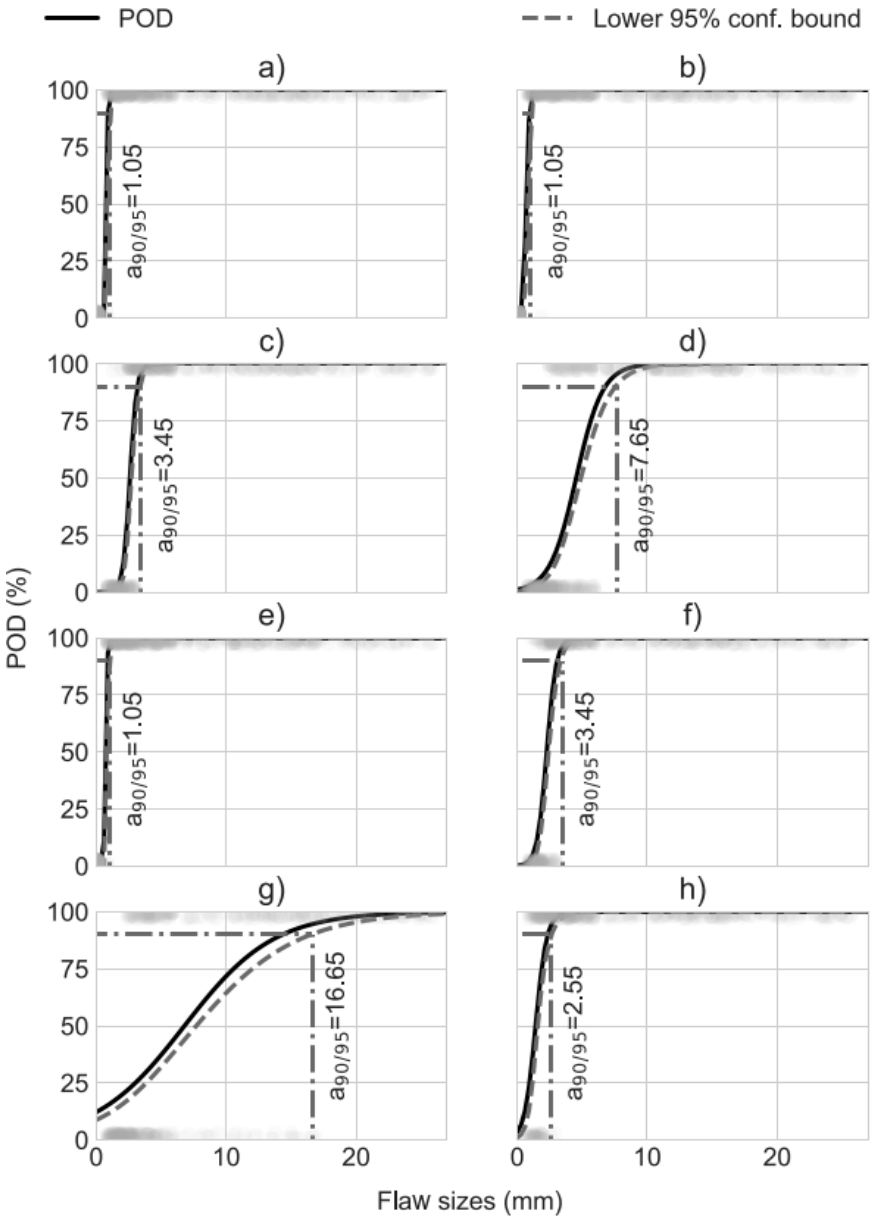

Figure 4. a) The POD curves for different training data combinations. a) All available flaws, b) Only small flaws used in training c) Only medium flaws used in training. d) Only large flaws used in training. e) Small and medium flaws used in training. f) Medium and large flaws used in training. g) Only medium sized solidification crack used in training. h) Only medium sized EDM notch used in training.

As the POD curves in Figure 4 were produced that an image was show to the model and it would evaluate whether the image contained a flaw. This was then evaluated as a hit, a miss or a false call regarding the true result. As this is not the way humans see the scan, the effectiveness needed to be demonstrated on real scan data. In Figure 5 there is a scan file from the VRR files, the same shown to human inspectors. The scan file was divided into pictures and shown to the model in scan order to produce prediction of the flaw locations. If the model would indicate more than 50% probability a flaw, the area would be marked as flawed. The performance, as already seen in Figure 4, was related to the flaw types available in training.

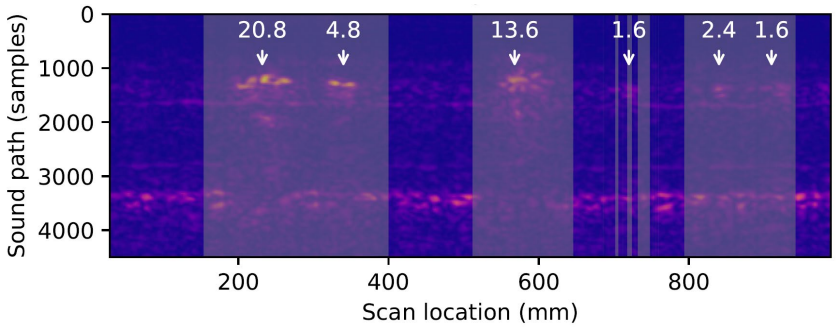

Figure 5. Model trained with only the largest flaws, 17 mm and 26 mm. The model's prediction is grey area and the white arrow points the flaw location and true flaw size. Only one of the two 1.6 mm flaws is difficult to find. No false calls.

The effectiveness of a ML model was studied with rich phased array data and austenitic stainless-steel weld with similar geometry usually seen in NPPs (Siljama et. al., 2020). The data represented the similar data which would be acquired from a traditional austenitic stainless-steel weld inspection in an NPP. The inspection angles used were 40° to 70° resulting in 31 channels per scan step. Total of 16 different thermal fatigue flaws with size range from 0.6 mm to 9 mm depth was manufactured to austenitic base material. These flaws were then virtually implanted to the three austenitic weld samples. While the weld free base material allowed more accurate flaw extraction and virtual implantation, the lack of weld meant there was no flaw interaction with the weld microstructure. The effect of this lack of interaction was studied by manufacturing thermal fatigue flaws to a set of three new welds.

A POD was evaluated with the flaws obtained from the base material flaw, but the flaws used for training were not used for POD evaluation. The POD curve can be seen in Figure 6. The a90/95 value achieved was 2.1 mm with false call rate of 2.3%. This result is in line with the human performance achieved from a DMW weld in the VRR exercise. Furthermore, the welds with manufactured thermal fatigue flaws were inspected by a human inspector and the trained model. The human inspector fared slightly better than the ML model by finding 9 out of 16 flaws, which one hit might have been a lucky false call. The ML model found 7 out of 16 flaws. For both the misses were related only to the smallest of flaws. However, the model

made only two false calls, which were resembling crack like indications in detail, whereas the human inspector made four false calls in total.

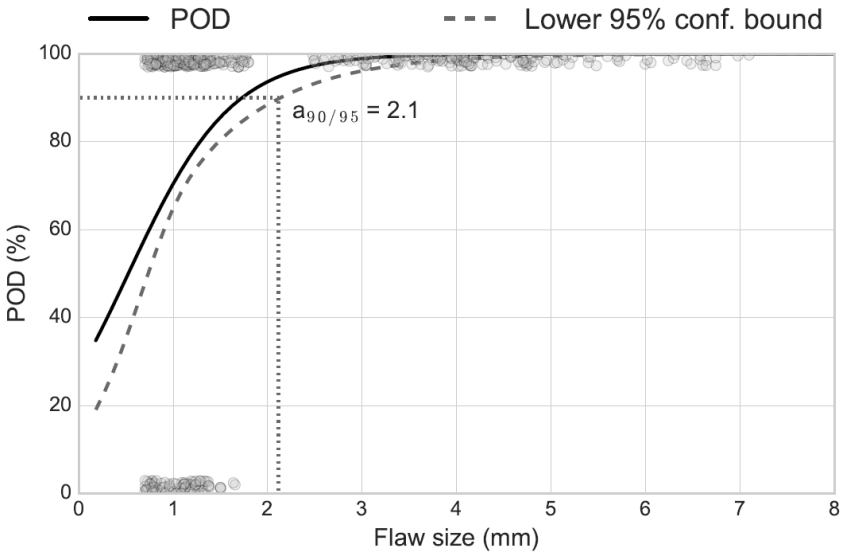

Figure 6. POD curve for the machine learning model trained to detect flaws in austenitic stainless-steel weld. The solid black line represents the POD value and the dashed grey line the lower 95% confidence bound. The model achieved $a_{90/95}$ value of 2.1 mm with a false call rate of 2.3%.

In conclusion, the ML model was fully capable of handling the same rich-data available for the human inspector with multiple angles and channels. As the data-analysis time is done in matter of seconds, this enables even more data driven inspection procedures. As more data can be collected from the inspection target with no rise in analysis time, there is potential for more accurate and reliable inspections with machine learning powered ultrasonic inspection.

Summary and conclusions

VRR was well received among participants. The results achieved were consistent and virtual flaws proved to be an effective way of generating the data for this exercise. The exercise showed how this VRR procedure could be conducted and how quickly results can be achieved as there is no requirement for moving the physical samples around the world. Moreover, this method shows promise for more effective qualification effort as well. Participant will get personal set of flaws and flaw locations every time, thus there is no urgent need for the data to be kept completely blind and secured. The value of this kind of exercise is to provide accurate info on the true

performance of the inspection. This information can be used for more accurate risk-informed in-service-inspections.

ML powered ultrasonic testing has the potential to change the data-analysis of mechanized ultrasonic data. The research has shown that the ML models are able to achieve human level performance. ML models can therefore produce more repeatable inspection results with a fraction of time normally used for inspecting the scanned data. As data-analysis time is no longer an issue the inspections can be designed in data-rich fashion, normally infeasible for a human inspector to go through. As data amount increases, reliability and confidence in the inspections can be driven even further.

Acknowledgement

Trueflaw Ltd. has contributed the virtual flaw (eFlaw) augmentation. Original weld samples have been acquired from SQC, PNNL and EPRI trough the PIONIC program and from Suisto Engineering. DEKRA has contributed scan data for the austenitic weld. All contributions are gratefully acknowledged.

References

Jessen-Juhler, O. 2018. Artificial flaw simulation in ultrasonic inspection of austenitic stainless-steel weld. Tampere University. 76 p.

Jessen-Juhler, O. Koskinen, T. & Virkkunen, I. 2019. Ultrasonic simulation with FEM, VTT research report VTT-R-01215-19.

Jessen-Juhler, O. Koskinen, T. & Virkkunen, I. 2020. Ultrasonic simulation with FEM in 3D, VTT research report VTT-R-01593-20.

Rinta-aho, J. Koskinen, T. & Jessen-Juhler, O. 2020. Generating and detecting surface acoustic waves using single phased array transducer. VTT research report VTT-R-00054-20, 11 p.

Siljama, O. 2020. Reliable defect detection using machine learning for ultrasonic inspection of nuclear power plant welds. Master's Thesis, Aalto University

Siljama, O. Koskinen, T. Jessen-Juhler, O. & Virkkunen, I. 2020. Automated flaw detection in multi-channel phased array ultrasonic data using machine learning, Unpublished: In review.

Kauppinen, P. (1997), The evaluation of integrity and elasticity of thermally sprayed ceramic coatings by ultrasound, VTT Publications 325, Finland

Koskinen, T. & Virkkunen, I. Hit / Miss POD With Model Assisted and Emulated Flaws, 2018, 12th European Conference on Non-Destructive Testing (ECNDT 2018), The e-Journal of Nondestructive Testing, Volume 23, issue 8.

Koskinen, T. Virkkunen, I. Rinta-aho, J. & Jessen-Juhler, O. 2019. Machine Learning for NDT in the Finnish Nuclear Industry. VTT research report VTT-R-00584-19, 23p.

Koskinen, T. Virkkunen, I. & Jessen-Juhler, O. 2021. The Effect of Different Flaw Data to Machine Learning Powered Ultrasonic Inspection, *J Nondestruct Eval, Accepted for publication.*

Mienczakowski, M. (2015). Multi-Frame Matrix Capture Common File Format (MFMC-CFF) Technical Specification. University of Bristol. Retrieved from https://www.bristol.ac.uk/media-library/sites/engineering/research/documents/Bristol%20MFMC-CFF%20Technical%20Specification%20-%20Draft%20For%20General%20Comment.pdf

Virkkunen, I., Koskinen, T. & Jessen-Juhler, O. 2019. Virtual round robin -progress report 2019. Espoo: Aalto University, 19 p.

Virkkunen, I., Koskinen, T. & Jessen-Juhler, O. 2020. Virtual round robin – a new opportunity to study NDT reliability. Unpublished: In review.

Virkkunen, I., Koskinen, T., Jessen-Juhler, O. & *Rinta-aho, J. 2021.* Augmented Ultrasonic Data for Machine Learning. *J Nondestruct Eval* **40,** 4. https://doi.org/10.1007/s10921-020-00739-5

6.6 Fatigue Management for LTO (FATIMA)

Tommi Seppänen[1], Jussi Solin[1], Jouni Alhainen[1], Esko Arilahti[1], Petri Lemettinen[2], Rami Vanninen[3], Erkki Pulkkinen[3]

[1]VTT Technical Research Centre of Finland Ltd
P.O. Box 1000, FI-02044 Espoo

[2]Fortum Power and Heat Oy
P.O. Box 100, FI-00048 FORTUM

[3]Teollisuuden Voima Oyj
Olkiluoto, FI-27160 Eurajoki

Abstract

The general objective of FATIMA is to go beyond existing state-of-the-art in fatigue management for long-term operation (LTO), accounting for environmental effects on fatigue life. As an alternative to existing practices, improved methods can be adopted through scientifically solid justification and international acceptance, which is the long-term goal of the project.

During the first year of FATIMA, international codes, standards and practices were reviewed for an up-to-date understanding of the state-of-the-art. International activities were started by participation in a collaboration group on environmentally-assisted fatigue issues. Experimental fatigue research was initiated in small scale during the first project year and will be scaled up during following years with material batches representative of Finnish nuclear power plants.

Introduction

The general objective of FATIMA project, which started in 2020, is to go beyond existing state-of-the-art in fatigue management for LTO, accounting for environmental effects on fatigue life. The main body of work is divided into three work packages, identified in Figure 1. They focus on international state-of-the-art and collaboration activities (WP1), environmentally-assisted fatigue (EAF) (WP2) and fatigue studies in air (WP3).

Successful R&D on material performance and ageing mechanisms has made it possible to refine specifications for materials and plant operation to exclude many failure scenarios, but cyclic strains caused by thermal transients cannot be excluded and fatigue remains a life limiting ageing mechanism. Mechanical loads and vibration excitation can also contribute to fatigue,

Monitoring and mitigation of Cumulative Usage Factor (normally for CUF ≤ 1) for fatigue is a challenge for long-term operation (LTO) and optimization of in-service inspection programs (RI-ISI). The priority of inspection correlates with codified

calculation of component usage (CUF). Improved realism in fatigue management allows maintaining high load factors and economic competitiveness for ageing plants without compromising safety. In addition, improved timing and focus of non-destructive evaluation or repair reduces radiation doses of personnel.

Fatigue Management is based on international practices, codes and standards. Improved methods can be adopted through scientifically solid justification and international acceptance, but consensus on current codes and state-of-the-art for environmentally-assisted fatigue (EAF) has been lost. Together with the debated and evolving F_{en} models for accounting the effects of reactor coolant water, ambiguity and volatility in fatigue assessment rules may cause uncertainty in long-term fatigue management of primary piping components.

Such uncertainty requires mitigation through responsible experimental research and development of science-based EAF models which remain compatible with the design codes and transferable to NPP components. This is the aim and long-term goal of FATIMA. As our research capacity is limited, opportunity for collaboration with major international stakeholders is an attractive route for discussion and wider acceptance of proposed methodologies.

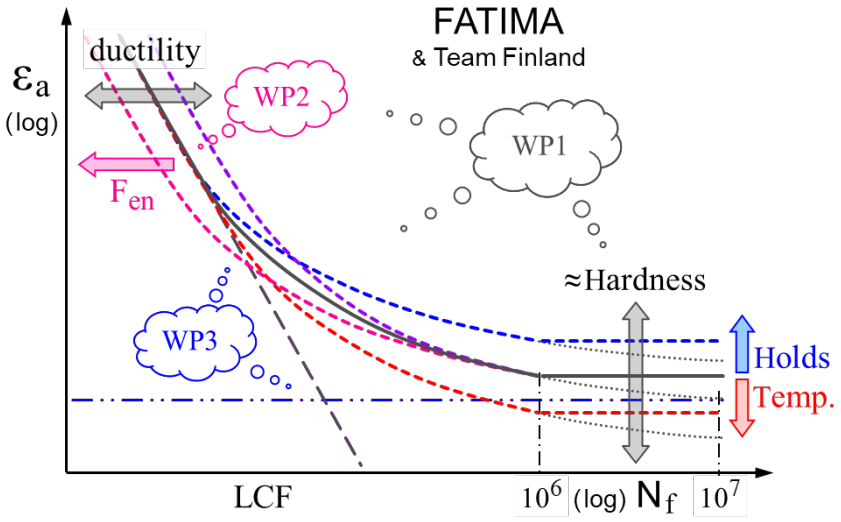

Figure 1. Research themes of FATIMA project.

Design Codes – common roots, but growing variations

The original ASME III, first published in 1963, served as a common root for all design codes and standards currently used for design and safety assessment of NPP primary loop pressure boundaries. The Finnish YVL Guide E.4 requires that the general safety level of ASME III shall be met, but also other Design Codes can be applied (e.g. RCC-M, KTA 3201.2, PNAE G-7-002-86).

Transferability of laboratory results to components in plants was a key target for the original ‘design by analysis’ fatigue assessment procedures, but ignored in some later adjustments. The current fatigue design curve for stainless steels in ASME Code section III is an example of this. The German KTA (2013) and Japanese JSME (ongoing) make clear distance to fatigue rules in ASME III (2010). The French RCC-M aims to maintain partial compatibility with ASME III, but with some corrective measures.

In 2020, the state-of-the-art review task was reported by Solin et al. (2020). The various challenges in management of fatigue and the evolving state-of-the-art in different codes, standards, rules and assumptions were discussed. The roots and current status of fatigue curves and design criteria applied in Finnish NPP’s were described in detail. A compilation of discussed design curves existing today are shown in Figure 2. The notable differences between the selected design codes are an interesting detail, when considering that all applicable design codes were originally rooted from the same ASME III code from 1963.

This task concluded that challenges remain in developing common understanding and practical application(s) for management of EAF while avoiding unnecessary conservatism without compromising safety and operability of reactors. It was suggested that collaboration between major stakeholders and contributors is needed, if harmonization of the design criteria and regulation is sought for internationally. The suggestion is also a direct reference to the collaboration activities within FATIMA.

The specific goal of collaboration activities is membership and active participation in an EAF R&D Collaboration Group, moderated by EPRI and formed by the major global stakeholders in EAF research. Meetings of the group are organized for ideation and discussion between leading experts in the world.

In 2020, Team Finland joint membership of VTT, Fortum and TVO entered the EAF R&D Collaboration Group as a new participant. The group has not been able to meet physically during 2020 but has kept discussion active by organizing online webinars, including an introductory presentation of Finnish EAF activities in the past and present. The motto of Team Finland is “*solution-oriented continuous improvement based on state-of-the-art and scientific approach for LTO*”.

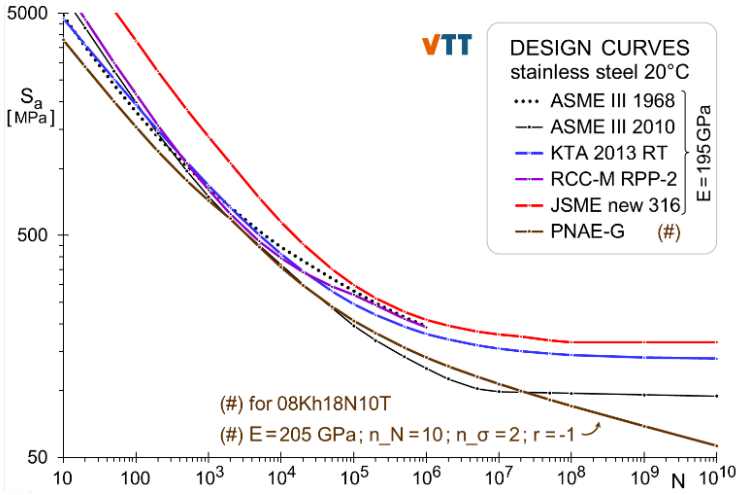

Figure 2. Design curves for stainless steels. (Solin et al. 2020)

Environmentally-Assisted Fatigue (EAF) in focus

Experimental programs on EAF started in USA and Japan about 50 years ago. Code-compatible test methods in relevant LWR coolant water environments were not available at that time and various nonstandard workaround methods were introduced. Transferability of results on environmental effects to codified component assessment was not considered as a first priority and as a consequence most of the laboratory data is not quantitatively comparable with the design criteria. From design point of view, the results remain qualitative and subject for discussion. Based on American and Japanese laboratory results, ANL prepared in 2007 a final report NUREG/CR-6909 which today is the default reference when discussing the the environmental fatigue correction factor, F_{en}.

Already the 2002 issue of regulatory guide YVL 3.5 had stated that "*influence of environment shall be accounted for in fatigue assessment*". The current guide YVL E.4 contains basically identical requirement, but referring to the Regulatory guide RG 1.207 of U.S. NRC. Potential other procedures shall be submitted to STUK for approval. Scientific evaluation of candidate 'other procedures' is an important mission for FATIMA, which will be focused on during the latter half of SAFIR2022.

Fatigue Design Curve

Debate over the fatigue reference and design curves has been a center of attention in international discussions for over a decade. During the 1990's and 2000's Argonne National Laboratory (ANL) compiled a wide collection of diverse fatigue data. 'Mean curves' were fitted to the collected data and an alternative design curve for stainless steel was proposed in multiple interim reports and concluding with the final

proposal in NUREG/CR-6909 report in 2007. NRC emphasized that it was not intended as replacement of the design curve given in ASME III and stated in regulatory guide RG 1.207 Rev. 0: "*This regulatory guide only applies to new plants, and no backfitting is intended or approved in connection with its issuance*." and "… *the design of the current fleet of reactors is satisfactory*." However, the proposed design curve replaced the previous one in ASME III in 2009.

The original data and regression model used by Langer for the ASME III design curve were ignored. As a result, the current ASME III design curve (since 2009) is based on a mix of relevant and irrelevant, valid and invalid data fitted to a model, which differs from the original code. Compatibility with the stress analysis part of the code has deteriorated and the reference curve is not representative for material batches relevant to NPP primary piping.

A particular focus area of FATIMA is in high cycle fatigue (HCF), where the historical and current design curves most notably differ. A return to design compatibility is ensured by standard experimental techniques applied on individually selected NPP material batches. An added benefit of assessing behaviour on a material batch level is a quantitative understanding of measured environmental effects, which may be evaluated against proposed models such as the one developed in SAFIR2018 FOUND and SAFIR2022 FEVAS projects.

As NPP components experience combinations of different thermal transients and mechanical loads, potential effects of variable amplitude loading need consideration. This is an area where major differences between ferritic and austenitic steels in HCF damage accumulation may occur, as suggested by limited in-house experimental results. Further clarification was sought in FATIMA by a test campaign on a well-characterized batch of AISI 347 stabilized stainless alloy. Firm conclusions of experimental work so far require supplemental results or more detailed investigation for confidence. Additional work is envisioned later in the FATIMA project.

References

Solin, J., Seppänen, T., Lemettinen, P., Vanninen, R., Pulkkinen, E. and Faidy, C. 2020. Codes, Standards, Rules and Assumptions on Environment Assisted Fatigue for Fatigue Management of Primary Piping, PVP2020-21501. Proceedings of the ASME 2020 Pressure Vessels and Piping Conference, Virtual, Online, July 20-24, 2020. 9 p.

7. Structures and Materials

7.1 Additive manufacturing in nuclear power plants (AM-NPP)

Alejandro Revuelta[1], Tuomas Riipinen[1], Mika Sirén[1], Antti Vaajoki[1], Zaiqing Que[1], Siddharth Jayaprakash[2]; Niklas Kretzschmar[2]; Mika Salmi[2]; Markus Korpela[3]

[1]VTT Technical Research Centre of Finland Ltd
P.O. Box 1000, FI-02044 Espoo

[2]Aalto University
P.O. Box 15500, FI-00076 Espoo

[3]Lapeenranta-Lahti University of Technology
P.O. Box 20, FI-53851 Lappeenranta

Abstract

The general objective of AM-NPP is to increase the knowledge of finnish stakeholders on the use of Addtive Manufacturing (AM), in particular Laser Powder Bed Fusion (L-PBF), therefore ensuring the safe use of additively manufactured metallic components in the nuclear sector. It is a technology which is showing a lot of applicability potential, e.g. in dealing with obsolescence in Nuclear Power Plants, but for which there is still little exposure to for both licensees and regulator. AM-NPP aims at closing this gap. The work developed during the different work packages aims at: Expanding standard procedures and deepen understanding of material-process-property relationships; contributing with scientific based facts to the introduction of AM in nuclear design codes; and, identifying safe ways of replacing obsolete components and realize new designs using AM. During the first two years of the project the focus has been on creating a roadmap of the use of AM in Finnish nuclear sector. Also, applicability of AM components and methods of quality control have been studied.

Introduction

Spare parts with additive manufacturing (AM, 3D printing) is a rising topic in different industries (Metsä-Kortelainen 2020). It has a potential for making spare parts on-demand, off- and onsite manufacturing and repairing existing parts (Salmi 2018, Chekurov 2017). It could also simplify the supply chains (Khajavi 2020). Based on different industries, distrust in quality, insufficient material and design knowledge among stakeholders and poor availability of design documentation on spare parts as the key barriers to adopting AM in the production of spare parts (Chekurov 2021).

Also, limited build chamber volumes and the need of post-processing are technical challenges (Kretzschmar 2018). In some industries, the delivery time of spares can be long can challenging. AM could shorten this delivery times and be a solution for long tails of company spare parts (Chekuroc 2018).

Due to the extremely long operating life of a nuclear power plant, power companies are facing the same problem as many other companies giving long service commitments for their products: how to ensure proper maintenance, repair and especially the availability of spare parts during the whole plant service life. Power plant maintenance is carried out during short annual service breaks. The maintenance is well planned, and many components have well scheduled exchange intervals either for the whole component or for part thereof. However, new, unexpected findings are also observed during the outage, and these may either require immediate action, or can be left as they are, for replacement or repair at a later stage, e.g. during the next outage. Some spare parts must thus be available during the outage, while others must have a reasonable delivery time. A well planned outage also include plans for both planned and possible repairs. However, there are many potential issues related to availability: very long lead times, lack of tooling needed to prepare the spare part, availability of appropriate contract manufacturer etc. One extremely potential answer to this demand are the extremely rapid developing and commercialising metal AM technologies, particularly powder-based processes that have matured on a wide front to production in extremely demanding applications, such as those of aerospace and medical industries. Additive manufacturing is also a very interesting in new reactor designs, e.g. small modular reactors (SMR).

Roadmap

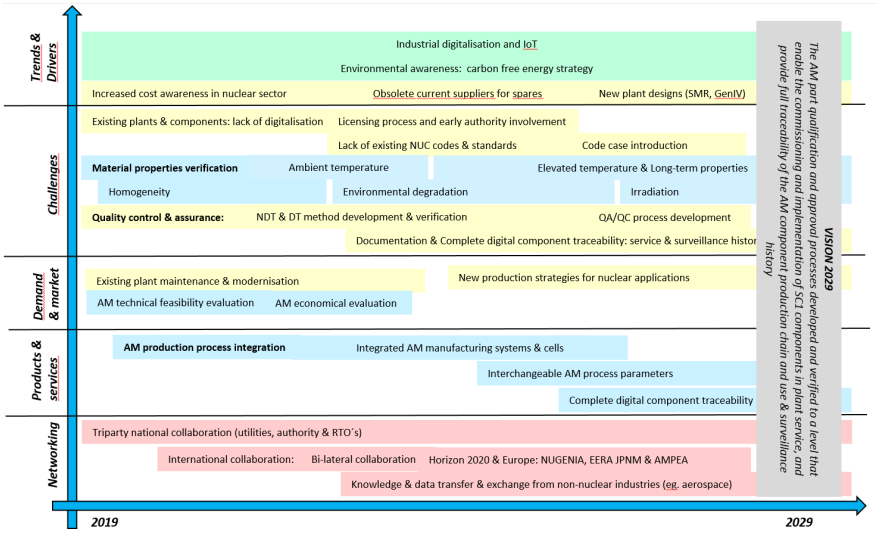

Figure 1. Overview of AM in nuclear power plants draft roadmap (Sirén, 2019).

The initial task in the AM-NPP project was ellaborating a draft of the roadmap for taking additively manufactured components in use in the Finnish nuclear energy sector. The final goal being introducing AM in nuclear design codes in Finland for 2029 at latest. In order to receive feedback from stakeholders, a workshop on this topic was arranged with participation of representatives of all licensees and also from the regulator. In this workshop, the state of the art of the technology was presented and attendants provided very constructive information regarding hopes and expectations (Korpela 2019). This information was the cornerstone of the work done on defining this initial draft of the roadmap. During the ellaboration of the roadmap it soon became evident that, instead an actual roadmap, the outcome will be rather a proposition or a basis for one. The reason is that there are a number of decisions to be made by the stakeholders that have a fundamental effect on the realisation of AM process application. On Figure 1, the overall schematic of the roadmap is presented and the different to be considered and their implementation is further developed in (Siren 2019).

Component Identification

Another relevant task of AM-NPP was analysing the feasibility of printing parts using AM for a few characteristic components which can be found in nuclear power plant facilities (Jayaprakash et al., 2019). The stakeholders provided some of these components as examples, and others were modelled similar to prototypical components found on literature:

- Valve seat: Part of an emergency pump system for NPPs categorized under safety class 2.
- Water impeller: Water pump impeller which had become obsolete and required replacement no longer commercially available. Based on literature and publicly available press releases.
- Thimble Plugging Device: A crucial element to place nuclear fuel in the reactor core. Based on literature and publicly available press releases.
- Bearing Housing: Housing used in on electric motors used in NPPs. Based on literature and publicly available press releases.

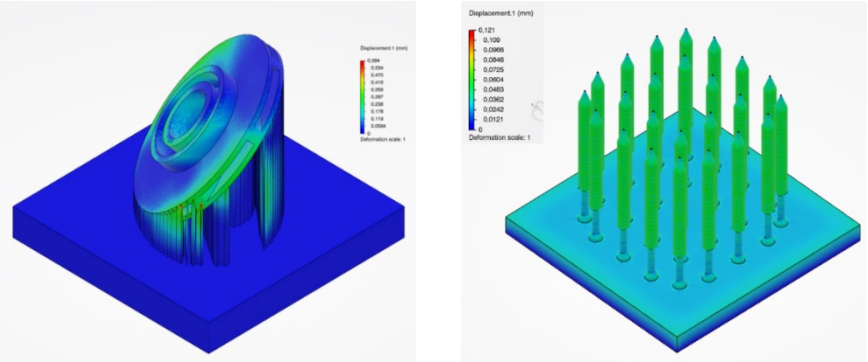

Figure 2. Example of simulations of representative AM components: a) water impeller, b) thimble plugging device (Jayaprakash et al., 2019).

The feasibility of these components was considered from both the technical point of view as well as from the safety perspective.

As an initial step, components have been assessed for printability of the component design. Even if AM provides great flexibility and potential for complexity, this is not guarantee that every component is printable. The screening has been performed using a software developed by Aalto University and using as an input part geometries and their material requirements. This process helps in gaining insights on design issues that impact the printing process, e.g., thing walls, and identifying potential postprocessing operations required to fulfil material quality requirements.

After this initial assessment was done, a simulation was performed to confirm printability of the parts and analyse displacements and associated re-coater collision risks that would induce print failure (Figure 2). The results of these simulations also contribute to gain insight on the necessity or redesign needs of support structures. As a result, it was identified that the valve impeller as initially configured for printing had a certain risk of collision; this would require a redesigned support structure, which would minimize the possible distortion.

Standardization

As of today, one of the major drawbacks for the adoption of additively manufactured components for critical applications is the need to ensure that those components are going to perform as expected, and that the whole quality assurance plan and quality control is carefully considered. This type of activities are typically supported by a collection of standards which provide instructions on what steps are required in order to ensure the proper level of quality. As L-PBF is still a relatively new manufacturing process, there is a certain level of fragmentation in the different standards as well as some significant gaps. This has been clearly identified as part of the roadmapping exercise done during the first year together with all the stackeholders of the AM-NPP project and during the second year of the project effort has been

made to clarify the status of the standardization landscape related to L-PBF manufacturing of AISI 316L material, especially in the nuclear context. As a result, a report has been published summarizing the main findings (Riipinen, 2020).

On Figure 3, a summary diagram of some of the main existing and incoming standards related to L-PBF is presented with a tentative organization around different stages of the manufacturing value chain for a component made of AISI 316L. And although some of the standards presented in Figure 3 are generic for any material, different materials will require the development of specific standards. In addition, none of these presented in Figure 3 are nuclear specific.

Two of the areas of special significance for the nuclear sector where there is still a gap in the existing standards, in addition to material behaviour under irradiation conditions, are fatigue and corrosion resistance properties (Riipinen 2020).

In 2019, the Nuclear Energy Institute published a roadmap for regulatory acceptance of advanced manufacturing methods in which it was described the existence of several ongoing code cases in the nuclear sector (Nuclear Energy Institute, 2019). In addition to these, there are several ongoing qualification activities done by European nuclear licensees to show the feasibility of AM in nuclear power plants. In 2020, the EURATOM project NUCOBAM (NUclear COmponents By Additive Manufacturing) as joint effort by industry, research institutes and academia to lay ground work for standardization efforts in the European Union in this field. As part of this project, different material experimental campaigns are being planned for material characterization; including behaviour of the material under irradiation conditions.

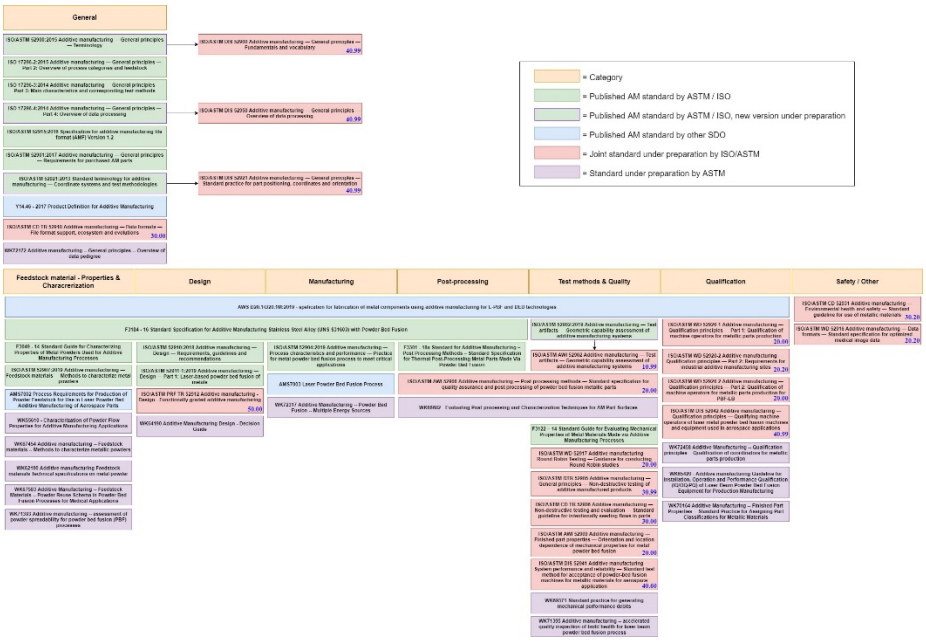

Figure 3. Overview of existing and incoming standards related to L-PBF of AISI 316L (Riipinen 2020).

It can be easily seen that despite the still limited number of published standards, there is a wide range of standards in draft phase covering most topics of the manufacturing chain. Standardization organizations are being very active and many of these drafts will become approved standards in the short future. Once these standards are agreed and final, they will support the quality assurance plans of components used in nuclear power plants and will increase the confidence of the authorities and regulators, and overall safety of NPPs using AM components. Additionally the certification process of a component will become easier and faster as well as having a reduced cost.

Quality Assurance and Control

In order to produce safe AISI316L components manufactured by L-PBF is necessary to have a very good understanding of the material properties that can be obtained from the process. Additionally, it is important to have solid quality assurance plans and quality control methods which will ensure that the performance of every component manufactured and put into service will be as expected.

Figure 4. Printed samples for quality evaluation (Riipinen 2020).

As part of AM-NPP, some of the key steps to be considered for ensuring a metallic component is printed with good quality, and thus with improved safety, are evaluated. Both from a general and practical level. These steps include, among others:

- Feedstock. Proper analysis and control of the raw material employed for the printing is the starting point of the manufacturing process. The material used has to ensure consistent values of powder chemistry, flowability and powder size distribution in addition to controlled storage conditions.
- Process monitoring. During recent years, several different systems to evaluate the progress of a build as the components are being printed have been developed. Although at the moment these process monitoring systems do not have closed loop control of the manufacturing process, they allow to analyze either in real-time or a posteriori the quality of a part with respect to a baseline/qualification component. These methods combined with possible Non Destructive Examinations, reduce the risk that a faulty part is accepted as valid. There are different types of process monitoring methods, being two of the most relevant the melt pool monitoring, which tracks the emissions of the melt pool continuously, and the so-called optical tomography, which analyse emissions of the whole building plate simultaneously typically from above the building plate.
- Non-Destructive Testing: Traditional NDT methods face difficulties for complex geometries making full use of the design freedom provided by AM. But, for many components, specially spare parts originally designed to be manufactured with a different process, they are still a valid testing method. For the most complex geometries, the X-ray Computed Tomography might be the only method technically capable of detecting flaws, especially in areas of difficult access.

It is concluded that in order to ensure the part quality and safety of the AM components used in the nuclear sector, a thorough part qualification framework should be in place. Especially considering the existing gaps in standardization.

To gain a hands on experience on how different quality control methods work together to improve the overall component quality and the variability of material properites within a manufactured batch, a set of 30 test cubes of 10x10x20mm was printed in an SLM125HL machine (125x125mm building platform) (Figure 4). All samples were printed with the standard parameters provided by the machine OEM and with powder previously analysed for chemical composition and particle size distribution. During manufacturing the process was monitored using a melt pool monitoring system (commercial PrintRite3D system from SigmaLabs Inc., with an approximate spatial resolution of 100µm) and a thermal camera (6 fps recoding).

After the build job was finalized and an initial analysis was performed on the process monitoring data, the most interesting samples were scanned with an X-Ray Computed Tomography system with an approximate voxel size of 8.4µm and the rest where sectioned and further analysed using optical microscopy.

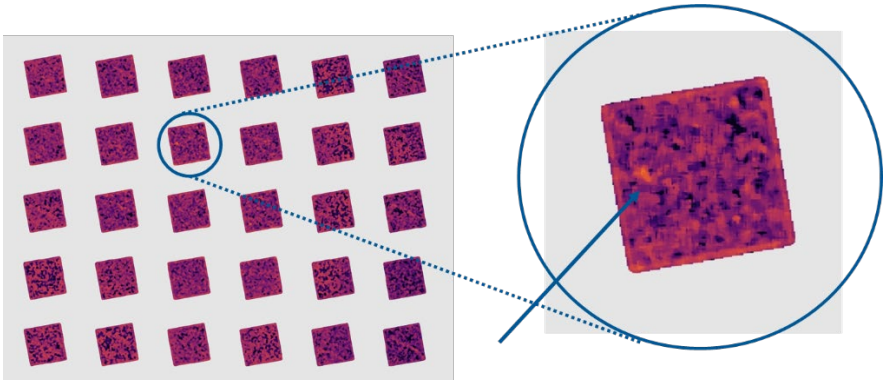

Figure 5. Example of defect prediction based on melt pool monitoring.

As this set of printed samples had simple geometries and well controlled and stable parameters, very few defects were detected by the MPM system, and a certain degree of manual evaluation by the final user was necessary. On Figure 5 an example of the prediction of a possible defect using this method is presented.

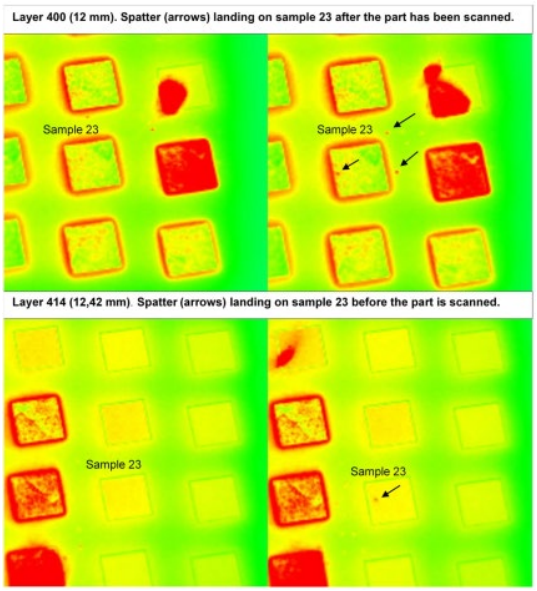

Figure 6. Infrared thermal image showing spatter during laser scanning near sample number 23 (Riipinen 2021). top) layer 400, bottom) layer 414.

Manual evaluation of the infrared images shows the existence of some spatter phenomena during the printing process which could lead to defects. In Figure 6 two sequential frames for two different layers is presented. In these images, it can be clearly seen the appearance of several hot spots which are indicative of spatter coming from the melt pool which could produce defects in the material.

Although X-Ray Computed Tomography is the NDT method which is better suited for the detection of small defects in complex metallic components, it is not completely hassle free. As it can be seen in Figure 7, even for a simple geometry as the one used in these experiments, there is a certain level of noise due to edge effects which can make more difficult the automated detection of defects. On the other hand, it still allows for an excellent level of detection of defects on a sample. Most defects detected in these samples had an average radius below 40µm. A few samples presented an increased number of defects on the top-most layers whose origin could not be determined. It was not possible to establish a correlation between the defects predicted by the process monitoring methods and the defects observed using µCT.

The porosity calculated using optical microscopy was small (<0,03%) and there was no correlation on porosity level versus position in the building platform.

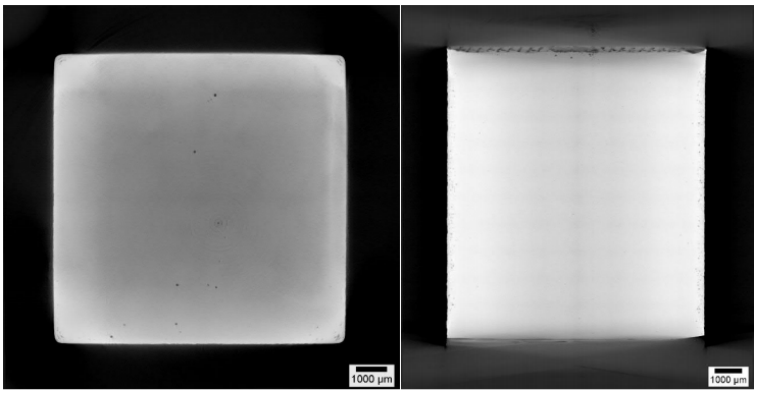

Figure 7. X-Ray Computer Tomography of one of the AISI316L samples. left) top view. right) vertical view (Riipinen 2021).

Although in this experimental work there was no clear correlation between the monitoring methods and the results of both NDT and optical microscopy examinations, it is important to remark that the final material had a very good overall density of >99.97%. This kind of comparative analysis should be repeated for a more representative component with more complex geometry which might be more likely to showcase defects. Is in that scenario where the potential of these process monitoring methods will better assessed.

Acknowledgements

The authors are grateful for the financial support received from the Finnish Nuclear Waste Managament Fund (VYR), Aalto University, Lappeenranta University, VTT Technical Centre of Finland Ltd. and Teollisuus Voima Oy. In addition, we would like to aknowledge the active participation of Fortum Oy, Teollisuus Voima Oy, Fennovoima Oy and STUK in sharing their insights about the additive manufacturing process and its future in Finnish nuclear power plants.

References

Metsä-Kortelainen, S., Reijonen, J., Riipinen, T., Vaajoki, A., Puukko, P., Salmi, M., Chekurov, S., Björkstrand, R., Kretzschmar, N., Akmal, J., Puttonen, T., & Partanen, J. 2020. New business from digital spare parts. VTT Technical Research Centre of Finland. https://doi.org/10.32040/2020.978-951-38-8827-5

Sirén, M. 2019. Additive Manufacturing in Finnish Nuclear Sector - Roadmap for implementation, VTT Research Report, VTT-R-01270-19.

Salmi, M., Partanen, J., Tuomi, J., Chekurov, S., Björkstrand, R., Huotilainen, E., Kukko, K., Kretzschmar, N., Akmal, J., Jalava, K., Koivisto, S., Vartiainen, M., Metsä-Kortelainen, S., Puukko, P., Jussila, A., Riipinen, T., Reijonen, J., Tanner, H., & Mikkola, M. 2018. Digital Spare Parts. VTT Technical Research Centre of Finland. http://www.vtt.fi/inf/julkaisut/muut/2018/DIVA_final_report.pdf

Kretzschmar, N., Chekurov, S., Salmi, M., & Tuomi, J. 2018. Evaluating the readiness level of additively manufactured digital spare parts: An industrial perspective. Applied Sciences, 8(10), 1837.

Chekurov, S., & Salmi, M. 2017. Additive manufacturing in offsite repair of consumer electronics. Physics Procedia, 89, 23-30.

Chekurov, S., Salmi, M., Verboeket, V., Puttonen, T., Riipinen, T., & Vaajoki, A. 2021. Assessing industrial barriers of additively manufactured digital spare part implementation in the machine-building industry: a cross-organizational focus group interview study. Journal of Manufacturing Technology Management.

Khajavi, S. H., Salmi, M., & Holmström, J. 2020. Additive Manufacturing as an Enabler of Digital Spare Parts. In Managing 3D Printing (pp. 45-60). Palgrave Macmillan, Cham.

Chekurov, S., Metsä-Kortelainen, S., Salmi, M., Roda, I., & Jussila, A. 2018. The perceived value of additively manufactured digital spare parts in industry: An empirical investigation. International Journal of Production Economics, 205, 87-97.

Korpela, M., Reijonen, J., Revuelta, A., Sirén, M. 2019. AM in Finnish Nuclear Sector - Workshop summary report, VTT Research Report, VTT-R-00741-19.

Jayaprakash, Siddharth, Kretzschmar, N., Korpela, M., Salmi, M., Revuelta, A. 2020. WP2 Report. Aalto University Technical report.

Riipinen, Tuomas. 2020. AM-NPP - Standarization in metal AM, VTT Research Report VTT-R-00617-20.

Riipinen, T., Revuelta, A., Vaajoki, A. 2021. AM NPP - Configuration of Melt Pool Monitoring for tracking material quality. VTT-R-00090-21

Nuclear Energy Institute. 2019. Roadmap for Regulatory Acceptance of Advanced Manufacturing Methods in the Nuclear Energy Industry. Available at: https://www.nei.org/resources/reports-briefs/roadmap-regulatory-acceptance-amm.

7.2 Critical studies in support of the ageing management of NPP concrete infrastructure (CONAGE)

Miguel Ferreira[1], Fahim Al-Neshawy[2], Edgar Bohner[1], Esko Sistonen[2];
Elina Huttunen-Saarivirta[1]

[1] VTT Technical Research Centre of Finland Ltd.
P.O. Box 1000, FI-02044 Espoo, Finland

[2] Aalto University, School of Engineering, Department of Civil Engineering
P. O. Box 12100, FI-00076 Aalto, Finland

Abstract

The research topics being addressed in the CONAGE project are strongly linked by key aspects of ageing management, where critical input is needed to support decision-based actions, whether related to inspection and maintenance actions on existing concrete infrastructure, or the design of new concrete infrastructures.

The research topics are divided into three work packages, addressing i) the non-destructive evaluation of NPP concrete infrastructure (WP1); ii) the risk of internal expansive reactions for NPP concrete infrastructure (WP2); and iii) steel liner and anchor corrosion in contact with concrete (WP3).

In the following sections, the research undertaken during the first two years of the project in each of the three work packages is briefly presented.

Introduction

Current Finnish nuclear power plants (NPP) have been designed for 40 years of operation. The concrete structures constructed before the starting of the NPP operation can be older than 45–50 years. There is evidence that ageing effects in some cases have been underestimated during the original design, construction and commissioning or have not been accurately taken into account during operation. It has also been recognized that the ageing of plants needs to be assessed, and an effective management strategy developed in a timely manner, to ensure the necessary technical basis for maintaining safety margins throughout the NPP operation [IAEA, 2016].

The CONAGE project addresses these ageing aspects of NPP structures, systems and components (SSC). The project identifies special aspects that are needed for long-term operation within the scope of ageing management. The topics of research addressed in this project are of interest not only for the concrete infrastructure of existing NPPs, but also especially for those in the design phase. According to an IAEA study, 90 % of all ageing problems are initiated in design phase [IAEA, 2016].

NPP ageing management programmes should have access to relevant concrete related R&D. This is fundamental since new developments may contradict assumptions made during a plant's design [IAEA, 2016] or highlight new issues previously unknown. Even though concrete has been extensively used as a construction material, the concrete used 40 years ago differs significantly from that commonly used today. The reinforced concrete structures of NPP (e.g. containment, spent fuel pools, water intake/outtake structures, foundations) perform multiple safety related functions (e.g. load carrying, radiation shielding and leak tightness). For many of these structures, it is neither technically nor economically feasible to have them replaced. For this reason, it is important that a comprehensive understanding of all possible ageing mechanisms, and their degradation consequence for the safety function of the structure, is achieved. This way, adequate considerations can be made during the design of existing NPPs, while mitigation measures can be planned for existing NPPs.

The research topics being addressed in CONAGE are strongly linked by key aspects of ageing management, where critical input is needed to support decision-based actions, whether related to inspection and maintenance actions on existing concrete infrastructure, or the design of new concrete infrastructures.

The research areas are divided into three main areas, addressing i) the non-destructive evaluation of NPP concrete infrastructure (WP1); ii) the risk of internal expansive reactions for NPP concrete infrastructure (WP2); and iii) steel liner and anchor corrosion in contact with concrete (WP3). In the following sections, the research undertaken during 2019–2020 is briefly presented.

The non-destructive evaluation of NPP concrete infrastructure

On-site assessment of the performance is a main challenge of existing concrete structures. Assessing of concrete structures ranges from visual inspection, non-destructive evaluation (NDE) to destructive testing where the concrete structure might be slightly or completely damaged and numerical analysis and/or simulation modelling of results. This workpackage (WP1) is mainly focusing on the NDE methods of NPP reinforced concrete structures.

The main objective of WP1 is to assess the structural integrity of thick-walled reinforced concrete structures of NPPs. The research work in WP1 includes the use of advanced NDE technologies and combination of testing methods to assess the structural integrity of thick-walled reinforced concrete structures.

This report presents two NDE approaches of the reinforced concrete mock-up wall: (i) combination of NDE techniques for the assessment of the compressive strength of concrete and (ii) the use of advanced NDE methods for the identification of general defects in mock-up wall.

Combined NDE for the Concrete Strength Evaluation.

The compressive strength of concrete structures is an important parameter to consider when determining a structures load bearing capacity. Assessment of concrete

strength of existing structures are mainly performed by destructive testing method. However, NDE are used to a certain extent to assess the compressive strength of concrete structures. The most popular used NDE methods for assessing concrete strength include rebound hammer and the ultrasonic pulse velocity (UPV).

The term “combined methods” refers to the use of two or more in situ test methods to estimate concrete strength. By combining results received by more than one method, a multivariable correlation can be established to estimate strength. Combined methods are reported [Samarin, 2004] to increase the reliability of the estimated strength.

The assessment of the in-situ compressive strength of concrete structures includes the following steps [D. Breysse *et al.*, 2017]: (i) selection of the NDE methods and drilling of the concrete cores, (ii) performing the NDE measurements and testing of the drilled cores, (iii) analysis and processing of the measurement and testing results and (iv) the derivation of strength estimation models.

The combined NDE techniques investigation was carried out on thick-walled reinforced concrete mock-up wall [Ferreira *et al.,* 2018] based on:

- Concrete specimens were taken from the concrete mix to determine the compressive strength at 28 and 91 days. The results were converted to the relative 150 mm cube strength.
- Compressive strength test for cored specimens according to the European standards [SFS-EN 12504-1, 2019].
- R-value rebound hammer (classic) and Q-value rebound hammer tests. The measurements were performed according to the European standards [SFS-EN 12504-2, 2019] and the compressive strength was predicted using the hammer manufacturer conversion equation.
- The UPV tests. The measurements were performed according to the European standards [SFS-EN 12504-4, 2004] and the compressive strength prediction equation was based on the test results of cored specimens.

A combined UPV and rebound hammer (SonReb) method is used to give a general relationship between compressive strength of concrete, rebound hammer number, and UPV. The basis of SonReb technique is given as tentative recommendations for *in situ* concrete strength estimation by combined non-destructive methods” published by RILEM Committee TC 43 CND [IAEA, 2002]. In SonReb method, the concrete compression strength is evaluated using Equation 1.

$$f_c = f_0 \cdot e^a \cdot V^b \cdot RN^c \qquad (1)$$

where:

$\mathrm{f_c}$ is the concrete compression strength, [MPa],
$\mathrm{f_0}$ is the unit conversion factor, [usually $\mathrm{f_0}$ = 1 MPa·s/m],
V is the ultrasonic pulse velocity [m/s],
RN is the rebound number (either R-value or Q-value) and
$\mathrm{a, b, c}$ are dimensionless correlation parameters that are obtained by the correlation with the destructive tests.

$$Ln(f_c) = a + b \cdot Ln(V) + c \cdot Ln(RN) \quad (2)$$

The SonReb method was used to esitmate the compressice strength of the reinforced concrete mock-up wall that was build in the WANDA Project [Ferreira *et al.,* 2018].The strength of the concrete mock-up wall was calculated using the following equation to combine the UPV and R-value rebound hammer measurements. The coefficient of determination R^2 for the equation is 0.886 [Al-Neshawy *et al.,* 2020].

$$f_c = 0{,}32035 \cdot V^{0{,}49282} \cdot {RN_R}^{0{,}27346} \quad (3)$$

Using the Q-value rebound hammer, the corresponding equation with coefficient of determination R^2 is 0,8466is.

$$f_c = 0{,}0507 \cdot V^{0{,}6138} \cdot {RN_Q}^{0{,}467} \quad (4)$$

The mix design of the concrete was based on the C35/45 compressive strength class and S3 consistency class. Maximum aggregate size used was 16 mm. The target temperature of the fresh concrete was 15 °C and the effective water-to-cement ratio was 0.47. The different materials used in the concrete were: Plus cement from Finnsementti – CEM II/B-M (S-LL) 42,5 N (Parainen), two aggregate fractions: 0/8 & 8/16 mm, and MasterGlenium SKY 600 superplasticizer (BASF). Two truck batches were delivered for the casting of the wall. The concrete batches details can be found in the research report [Al-Neshawy *et al.,* 2020].

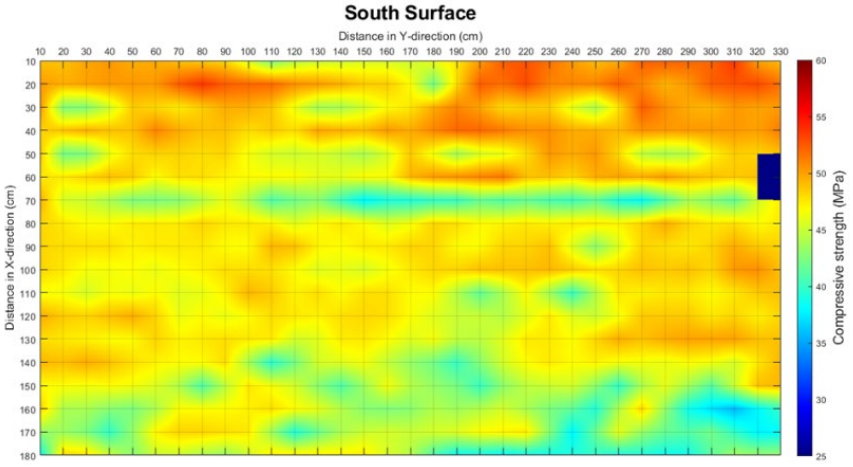

Figure 1. Compressive strength values received by combining the results of the UPV and R-value rebound hammer measurements.

Figure 1. presents the SonReb method results of a 283 points combination of UPV and R-value rebound hammer measurements. The average compressive strength of the measurements is 47 MPa with coefficient of variation CoV of 6.9%.

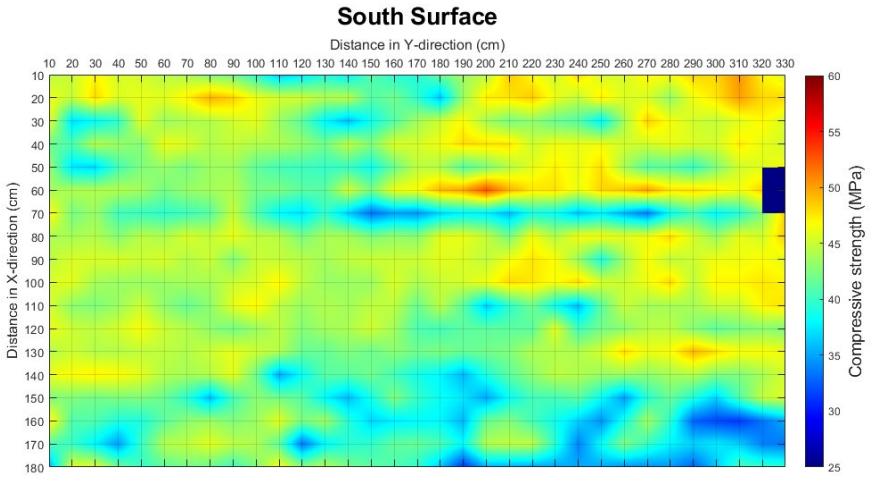

Figure 2. Compressive strength values received by combining the results of the UPV and Q-value rebound hammer measurements.

The results of UPV and the Q-value rebound hammer measurements for the same surface are represented in Figure 2. The average compressive strength of a combination of 267 meaurement points of UPV and Q-values was 43 MPa with coeffecient of variation of 9.1%.

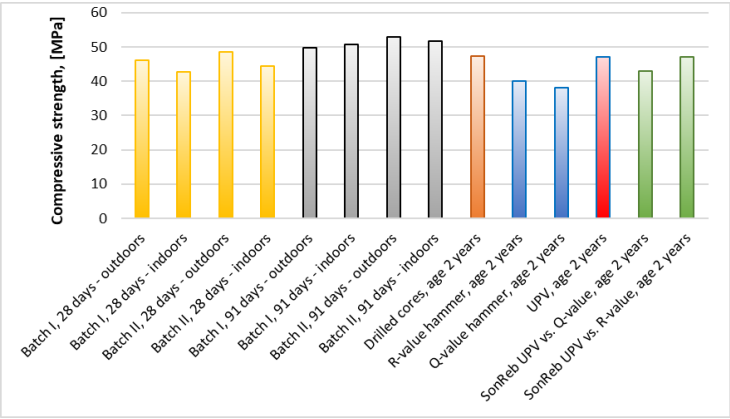

Figure 3. Average compressive strength results of the compressive strength test and the estimated values from NDT methods. The test results were converted to the relative 150 mm cube strength.

Figure 3 presents the prediction of compressive strength that carried out using combined NDE methods compared to the destructive testing methodologies. The results show that, compared to the cored samples strengths, the non-destructive method (SonReb) make it possible to improve the accuracy of the rebound hammer estimations of the concrete compressive strength *in situ.* As shown in Figure 3, the use of UPV, R-value rebound hammer and drilled sample gives the best probability of compressive strength prediction compared to the compressive test results cast and drilled specimens.

GPR for the identification of general defects in mock-up wall.

Ground Penetrating Radar (GPR) technique can be used to carry out imaging of reinforced concrete structure and make out assessment to the quality of concrete structure [Watt, 2007]. Interpretation of GPR data commonly helps to confirm the following main questions asked of a concrete structure:

- Concrete component thickness and reinforcement cover thickness (including variations from the original design)
- Existence, spacing, arrangement, and depth to embedded reinforcement
- Existence of other features such as prestressing cables, embedded conduits, and pipes

Condition information of the existing concrete structure can also be recovered using GPR, including the determination of the:

- Existence, location, and severity of voiding and honeycombing
- Existence and location of delamination/separation parallel to the surface
- Relative moisture content (laboratory testing still required for accurate measurement).

Limitations of GPR surveys include time intensive collection and the post processing of GPR data. Also, the presence of water will reflect/inhibit the passage of the radar pulse and thereby limit penetration and data quality. The depth range of GPR is limited by the electrical conductivity of the medium, the transmitted center frequency and the radiated power. As conductivity increases, the penetration depth decreases. Higher frequencies do not penetrate as far as lower frequencies but give better resolution. GPR technology is unable to determine the diameter of the target being located. As a rule of thumb, objects smaller than half the size of the wavelength cannot be detected. Larger objects may also not be detected, depending on the size and orientation. [Luodes, 2015; Sensors & software 2015).

The GPR survey was performed by scanning the surface of the thick-walled reinforced concrete wall. The GPR measurements using *GPR-Live scanner* (Proceq) were carried out on the the mock-up wall. The measurements were carried out on horizontal and vertical measurement tracks. The measurement track spacing was 5 cm in each case and the distance between the individual scans in the measuring direction was 4 mm. The position of the measuring tracks was determined by a grid template attached to the surface [Al-Neshawy, 2020].

Example of the result images from the data set taken on the east side of the test specimen are shown in Figure 4. In addition to the structural reinforcement layer, a conspicuous area measuring approx. 15 x 15 cm² is visible in the upper half of the image in the left depth section (depth range = 4–10 cm) (reflections from e.g. built-in components such as sensors, tendon heads, reinforcement or defects).

In the right depth section of the same dataset a further conspicuous area in the lower half of the picture is visible at a depth of 11–13 cm. This is also a clear reflection with a similar cause as mentioned above.

In summary, the GPR radar scanning system was used to take manual, area-wide measurements on the mock-up reinforced concrete wall. In the reconstructed data sets of each side surface the respective position of the existing structural reinforcement as well as conspicuous areas of e.g. tendon heads, built-in sensors, introduced defects or inhomogeneities were displayed.

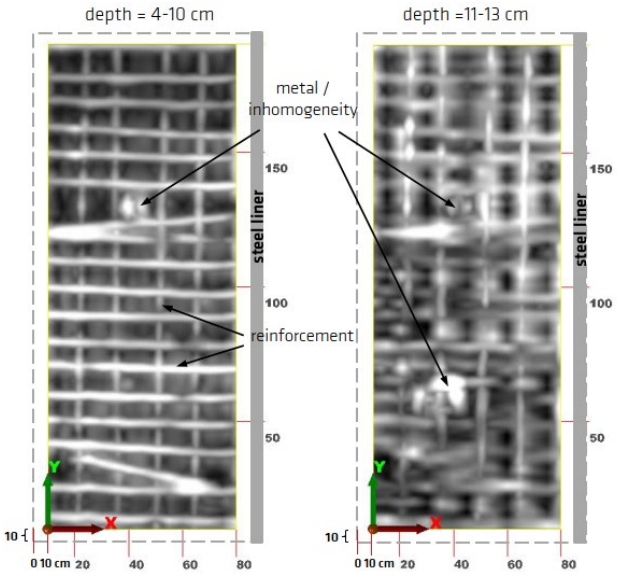

Figure 4. Depth sections from the reconstructed data set, captured with the GPR Live-system on the eastern side of the mock up wall (size of the measurement field = 80 cm x 180 cm) [Al-Neshawy, 2020].

Risk of internal expansive reactions of NPP concrete infrastructure

A significant number of problems related to concrete deterioration worldwide are due to the development of internal expansive reactions. These reactions diminish the affected structure's service life, may affect its function and, ultimately, can lead to its demolishing. Internal expansive reactions are mainly of two types: alkali-aggregate reaction (AAR) and delayed ettringite formation (DEF). Both deterioration

mechanisms cause the hardened concrete to expand and thereby progressively inducing tensile stresses and cracking. This influences the mechanical properties of concrete, which in turn reduces the structural capacity influencing its fragility. The research in this project focuses on AAR, or more specifically ASR (alkali-silica reactions, which are a subset of AAR that is more predominant in Finland) since it is more relevant to the Finnish utilities.

ASR related expansion in reinforced concrete structures has gained prominence in the recent past because of the widespread nature of the problem with in the nuclear community, and the potential adverse economic impacts that it may have [Snyder & Lwe, 2013; Chérnier et al., 2012, Manabe et al. 2018, Tang 2013]. Furthermore, the possibility of ASR occurrence in VTT's FiR 1 reactor containment structure [Orantie, 2014] and the many other documented cases in bridges and other infrastructure offer enough concern to address this issue in Finland.

For the occurrence of ASR, in addition to moisture, there should be enough alkalis and reactive aggregate. The source of alkalis can either be internal (constituent of the cement) or external (from the environment, e.g. from sea or ground water). Depending on the reactivity of the aggregate, concrete composition and the environment, damages can occur rapidly within the first years after construction, or slowly after decades. The cracking due to ASR leads to loss of function, durability, structural integrity and service life. ASR cannot be adequately stopped or repaired after it is found; only mitigated. NPPs and other nuclear infrastructures have been affected by ASR [Saouma & Hariri-Ardebili, 2014]. The risks are high in massive structures where a long service life is expected, if these are constructed with reactive materials. As well, certain structural members of nuclear facilities being exposed to increased temperature and humidity underlie a high damage probability. Since damages to nuclear structures can have large risks to the environment and society and are very costly to repair, strategies for preventing the use of improper concrete raw materials for the construction of new NPPs must be developed. Risk assessments regarding the inherent and residual swelling potential of the concrete subject to ASR needs to be assessed for existing NPP concrete structures, especial in the case of lifetime extension.

The main goal of this workpackage is to take initial steps in identifying the risk level of ASR for concrete used in Finnish NPPs. Furthermore, the project proposes to increase awareness of ASR as a potentially damaging mechanism and to initiate further actions to avoid ASR in newly planned or constructed nuclear structures. Subsequently, the gained knowledge on ASR in Finland will serve to increase the predictive accuracy when assessing service life extension of existing nuclear facilities and thus contributes to their operational safety in general.

The research conducted so far focuses on two aspects: i) Identify critical areas of Finnish NPP SSCs where ASR has the possibility to occur, based on concrete compositions and exposure conditions; and ii) study the reactiveness of aggregates used in the construction of Finnish NPPs.

With this research the project contributes significantly to the current state of knowledge concerning ASR performance in Finland.

Critical areas of Finnish NPP SSCs where ASR has the possibility to occur.

This study relies on information about the concreting history (constituents of the compositions used if available) and the existing exposure conditions to which the concrete infrastructure is subject to, provided by the utilities. This study is conducted to the component level, since a structure can be subject to unique variation in exposure (e.g. wall that is partially submerged). Key aspects considered are access to moisture, chemical composition of the concrete binder mixes, and geometry of the concrete elements.

The main reinforced concrete infrastructure of Finnish NPPs (OL1, OL2, OL3, LO1 and LO2) has been considered. Most of the information has been retrieved from the SERVICEMAN project [SAFIR 2010]. In addition, workshops were held with TVO and FORTUM to obtain additional insight and information to the NPPs in question. A detailed description of the work performed can be found in [Ferreira, 2019].

The exact compositions of the cement and supplementary cementious materials used has not been possible, so the study is based on published literature for the same or similar cement of the years in which the NPPs where built.

The potential for occurrence of ASR is based on assessing the combined risk of two of the three factors needed to occur simultaneously: sufficiently high alkali content and high moisture content. Only the sufficiently reactive aggregate factor is not known, and therefore not considered.

The potential for occurrence is defined as being either LOW, MEDIUM, or HIGH depending on factors related to the moisture content in the concrete and the potential alkali level due to the type of cement and environmental exposure conditions [Ferreira, 2019].

A factor that has not been explicitly considered is the effect of temperature. At higher temperatures, the increase in reactivity results in ASR end product more quickly, i.e., the expansive gel.

The choice of “Source of Alkalis” is not straight forward as cement types can have both high and low alkali content. For this reason, it is very important to know what was the exact chemical composition of the cement used as well as any additions added to the mix, and whether the alkalis in their chemical composition are chemically bound, or available to contribute to the alkalinity of the pore structure.

Table 2. Classification of the potential for occurrence of ASR of NPP’s reinforced concrete structures if the aggregate is found to be reactive [Ferreira, 2019].

Source of Alkalis*	**Factors affecting RH**	**CS<0.2m RH<70%**	**0.2m<CS<0.5m 70%<RH<80%**	**CS>0.5m RH>80%**
	Level	Low	Medium	High
CEM III	Low	LOW	LOW	MEDIUM
CEM I/II + SW CEM III + SW	Medium	LOW	MEDIUM	HIGH
CEM I, CEM II, CEM I/II + SW	High	MEDIUM	HIGH	(VERY) HIGH

SW – seawater; CS – thickness of the concrete structural element.

* – General indicator of cement types, but for confirmation exact binder composition should be known.

Table 2 presents the potential for occurrence of ASR on NPP reinforced concrete structures. By classifying, for a specific reinforced concrete structure/module, both the source of alkalis and the factors affecting relative humidity.

The results show that a large part of the concrete infrastructure of Finnish NPPs show medium to high potential of ASR occurrence, if the aggregate were to be found reactive [Ferreira, 2019]. This is due to the high alkali content in the concrete, and either the high relative humidity of the environment where the concrete element is situated, or due to the large cross section of the concrete element.

Reactiveness of aggregates used in the construction of Finnish NPPs.

Various aggregates used for the production of concrete structure of NPPs were received from Finnish utilities TVO and FORTUM for testing.

From FORTUM, six sand samples were taken from independent sand extraction pits. These sands have been used for the construction of different structural elements at the Loviisa NPP and in the KJT repository. These aggregate samples were subject to the RILEM AAR-2.2 test.

From TVO, eight rock samples taken from the surroundings of OL1 and OL2 where the excavated rock was used to make the aggregate for concrete were chosen to be tested for ASR. These aggregate samples were subject to the RILEM AAR-2.2 and the RILEM AAR-4.1 tests.

In the RILEM AAR-2.2 method, prisms are moulded from mortar prepared with the aggregate to be tested. Prism dimensions 160mm x 40mm x 40mm were chosen. The prisms were demoulded after 24 ± 2 h and their initial length measured. The specimens were then placed in water, transferred to an oven at 80 ± 2 °C for 24 h, removed from the water, surface dried, and the length measured immediately before the temperature has dropped substantially (zero reading). The specimens were then placed in containers with a 1 Mol NaOH solution already at 80 ± 2 °C, which were sealed and placed in an oven at 80 ± 2 °C. Length measurements were taken periodically. The duration of the test is usually 2 weeks, but these tests were extended to 5 weeks to check for delayed expansion. The cement used was a CEM I 52,5 R (Paraisten Pikasementti from Finnsementti), with a Na_2O_{EQ} = 1.77 %. This value exceeds the minimum requirement of 1.0 %. An absolute criterion for the interpretation of the results of AAR-2.2 have not yet been finally agreed, especially not for Finnish rock types. However, on the basis of trials carried out by RILEM on aggregate combinations of known field performance from various parts of the world, it seems that results in the test (after the standard 14-days, AAR-2.2) of less than 0.08 % are likely to indicate non-expansive materials, whilst results exceeding 0.16 % are likely to indicate expansive materials.

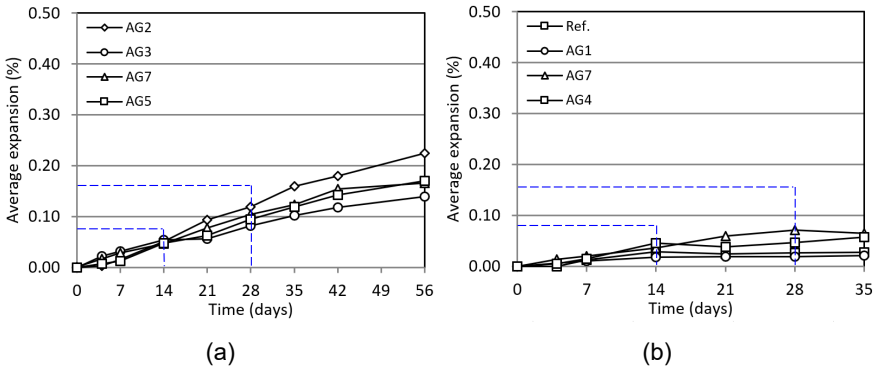

Figure 5. Expansion values for the AAR-2.2 test conducted on the sand aggregates from (a) Fortum [Ferreira, 2020b], and (b) TVO [Ferreira, 2020a].

The results of the tests for the FORTUM aggregate corroborate the petrographic analysis, and show expansion levels below 0.05 % at 14 days, and expansion levels below 0.012 % at 28 days. These results indicate that it is very likely that the FORTUM sands are non-expansive.

The results of the tests for the TVO aggregate show expansion levels below 0.05 % at 14 days, and expansion levels below 0.08 % at 28 days. These results indicate that it is very likely that the TVO rock aggregates are non-expansive.

In the RILEM AAR-4.1 method, prisms are moulded from concrete prepared with the aggregate to be tested. Prism size 285 mm x 75 mm x 75 mm was chosen. The prisms were demoulded after 24 ± 2 h and their initial length and weight are measured. The specimens were then placed in metallic containers with 35 ± 5 mm of water at the bottom. Each sealable container holds a maximum of three prisms. The sealed containers are placed inside an AAR reactor in which the temperature is at 60 ± 2 °C that contains an appropriate level of water to maintain 100% RH inside. Length measurements were taken periodically. The cement used was identical to that used in the RILEM AAR-2.2 tests. Criteria for the interpretation of the results of AAR-4.1 have not yet been finally agreed. However, on the basis of an initial assessment of the AAR-4.1 trials carried out by RILEM TC 191-ARP on aggregate combinations of known field performance from various parts of the world, it seems that a maximum expansion in the test of less than 0.03 % at 15 weeks indicates a non-reactive aggregate or aggregate combination.

The results of the tests for the TVO aggregate show expansion levels greater than 0.03 % at 15 weeks, therefore inconclusive in relation to the nature of their reactivity.

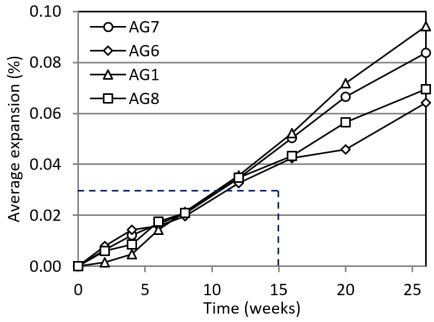

Figure 6. Expansion measurements for aggregate samples AG1, AG6, AG7 and AG8. The dotted line shows the expansion limit of 0.03 % at 15 weeks [Ferreira, 2020b].

Since the results show expansion above the 0.03 % at 15 weeks, and in the absence of local experience to the contrary, this indicates that it cannot be ruled out that the TVO rock aggregates are potentialy expansive. These results are surprising as they contradict the AAR-2.2 tests conducted on the same aggregates. For this reason, the AAR-2.2 tests are being repeated to confirm the result.

Steel liner and anchor corrosion

Age related degradation of steel components embedded or in direct contact with concrete structures is subject to research work focusing on the assessment of steel liner and anchor corrosion in particular. Corrosion experiments help to identify the electrochemical conditions and the mechanisms that allow for the corrosion of the steel liner plates at the interface of steel and concrete, i.e. in an area where the liner should be passive, thus protected from corrosion. Additional experiments will focus on corrosion and bond of anchors in concrete.

Steel liner corrosion

Corrosion of nuclear containment liners, pool liners and metallic anchors in contact with the concrete building structure has been observed at several occasions and at various NPPs globally [Petti et al.x, 2011]. Instances of steel liner corrosion have been reported also in Sweden and Finland (e.g. [Wegemar, 2006]). Figure 7 shows a corrosion damage in the steel liner, discovered in Ringhals 2 in 2004 [Aghili, 2007].

Steel liners can be embedded inside the concrete containment or pool walls, or they form the inner surface of the wall. The liner materials are usually carbon steel, galvanised steel or stainless steel. Corrosion has been detected at the inner surface of the liner plates (direct exposure to the containment interiors or the pool water), and where the plates are in direct contact with concrete (outer surface). Corrosion initiated on the outer surface has been associated with foreign material left embedded in the concrete, such as wood pieces or distance holders left in place at the time of concrete casting. Sometimes the cause of the corrosion was unclear, but

delamination of the steel plates from the concrete or liner bulging has been observed. At worst, corrosion has to penetrated the thick plates of the liner, or led to a significant decrease of the liner cross-section.

Figure 7. Corrosion damage in the steel liner from Ringhals 2 [Aghili, 2007].

Of particular interest is the corrosion at the outer surface of the liner in direct contact to the concrete. The challenge is that the liner surfaces in contact with concrete cannot be checked by visual inspections. The alkaline concrete should in principle cause passivation of the material and prevent any corrosion. However, according to the present understanding, the corrosion is initiated where the local pH at the steel/concrete or steel/foreign material interface drops below the value necessary to sustain passivity. The value is not a fixed quantity, as it depends, among other factors, on the concentration of aggressive species. Liner delamination and foreign materials in contact with the steel lead to the formation of a crevice. A macro cell is formed whereby the local anodic area, where active corrosion is occurring, is coupled to a large cathodic surface, in the presence of water or humidity. The passive sections of the liner as well as multiple layers of reinforcement bars and prestressed tendons in the containment or pool walls form the cathodic sites. Localised corrosion can propagate over a period of many years since the massive concrete structures have sufficient water content and the ionic conductivity necessary to support the electrochemical corrosion reactions.

A detailed understanding of the factors responsible for the appearance and extent of the corrosion, the corrosion localisation and the electrochemical mechanisms is still lacking, but crucial for predicting possible future incidences, identifying the corrosion locations and the extent of attack as well as establishing best mitigation procedures.

Experimental investigations aim for studying in detail and defining the corrosion mechanism of the steel plate and identifying which factors promote or impede the occurrence of corrosion. For this purpose concrete corrosion specimens were designed [Bohner & Huttunen-Saarivirta, 2020] and manufactured to allow for electrochemical measurements and further microscopy examinations during the course of the experiment.

The following two main corrosion scenarios have been presented in the literature review [Isotahdon et al., 2019] and will be subject of the experiments: 1) loss of passivity, i.e., activation, and 2) delamination-induced corrosion. A schematic representation of the experimental setups used in the investigation of each corrosion scenario is given in Figure 8.

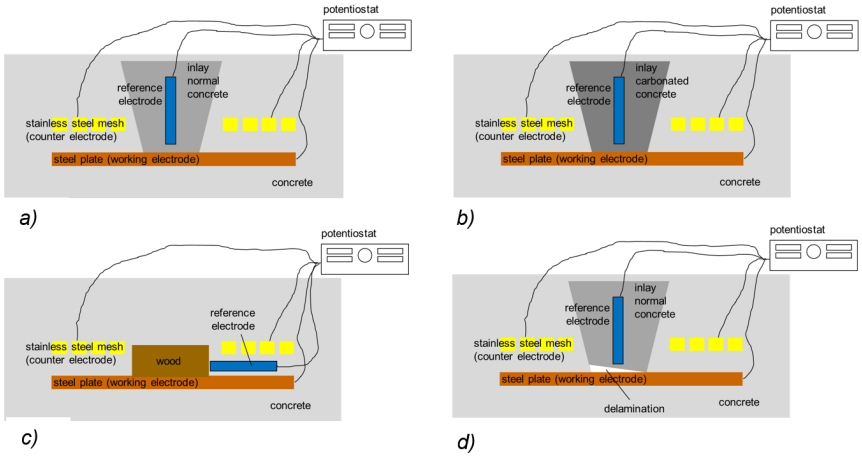

Figure 8. Schematic representation of the experimental setup for each corrosion scenario: a) Scenario 1, implemented with normal concrete; b) Scenario 1, implemented with carbonated concrete (low-pH concrete); c) Scenario 1, implemented with a piece of wood; d) Scenario 2, implemented with a gap between steel plate and concrete (delamination).

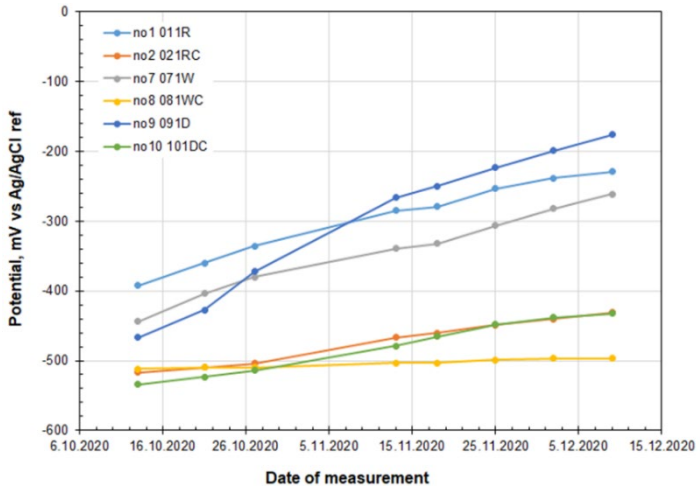

Figure 9. OCP records during first weeks of measurements. In the specimen identifiers, R refers to reference, C refers to chloride, W refers to wood and D refers to delamination.

During the corrosion tests, electrochemical measurements are performed regularly. The measurements involve open circuit potential (OCP) and linear polarization resistance (LPR) measurements. The electrochemical measurements with polarization, i.e., deviation from the equilibrium, are possible only for the cells consisting of working electrode (WE; steel plate), counter electrode (CE, stainless steel mesh) and reference electrode (RE; MnO2 electrode). In the case of OCP measurements, WE and RE are sufficient because they represent the equilibrium state. Figure 9 shows the preliminary results of OCP measurements. In all cases, the OCP values showed an increasing trend during the initial weeks of exposure. The potential values for the specimens 1, 7 and 9 were systematically higher than those for 2, 8 and 10 (see Figure 9). The results indicate that the specimens which contain chlorides featured lower overall potential levels than those without chlorides. Among the specimen types, those containing wood featured slightly lower potential values than the reference specimens and specimens with delamination.

Anchor corrosion

All cases where severe corrosion of the containment steel anchors was observed have been related to the presence of either chlorides or carbonated concrete. Furthermore, contact with different steel alloys increased galvanic corrosion. General corrosion, pitting corrosion, and stress corrosion cracking were found from the case studies. These are also present at NPP structures dealing with different anchor types (undercut, expansion, bonded), and steel materials (ordinary, galvanised, austenitic) [Isotahdon et al., 2019]. By decreasing the role of either exposure class, structural, or material properties, the service life of anchors can be increased. Chemical composition used in anchors plays an important role as a material property. Decreasing the moisture content at the concrete anchor interface is essential for the lower exposure class. Structural sealing at the surface of the concrete where anchor has been installed is vital for the ageing management.

The study on anchors focused on chemical composition and anchor types used based on a quesionaire sent to all Finnish utilities. Furthermore, it scoped especially on the propagation stage of corrosion. The study raised the need to increase knowledge of steel anchors with respect to the chemical composition of the used materials. Corrosion resistance is hugely dependent on the environmental factors or exposure classes and especially the coating and/or alloying elements in the steel. Further experimental studies should be made by taking into account the following variables: degradation mode (general corrosion, pitting, and hydrogen embrittlement stress cracking), steel grade (ordinary, galvanised, stainless steel), anchor type (expansion, undercut, bonded anchors), and exposure (carbonated, chlorides, stress state). Design and construction of the experimental setup based on the literature study is presented in Task 3.3 Anchor corrosion experiments, as part of WP3 Steel liner and anchor corrosion of this project [Sistonen, 2020a].

Three different kind of anchors were used; undercut, expansion (wedge), and bonded anchors [Sistonen, 2020b]. All anchors are from Hilti Oy Ltd, expect ordinary threaded rod produced by Etra Oy Ltd. Three steel material types of anchors were used; ordinary steel, hot dip or electro galvanised steel, and austenitic stainless

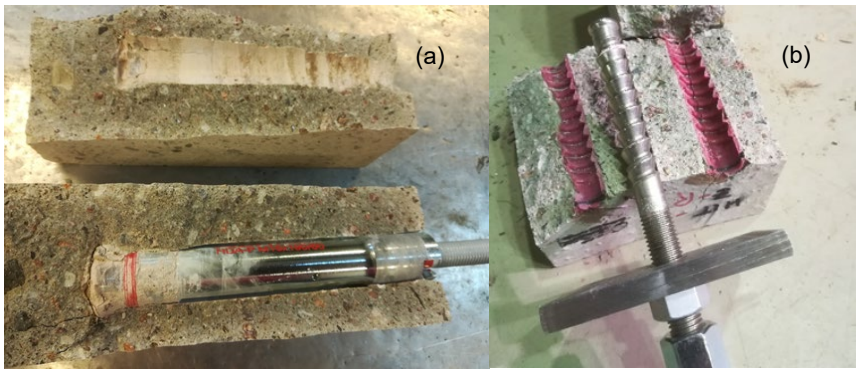

Figure 10. (a) Split undercut anchor specimen to perform situation after the maximum prestress force reached. (b) Example from pretesting to show failure along the anchor rod HIT-Z-R M16x175 when using two component epoxy resin (HIT-RE 500 V3/500/1) as a bonding chemical.

Table 3. Test results of pre-testing of anchor specimens.

Anchor type	Prestressing force [kN]	Torque moment [Nm]	Failure type (along the)	Remark
Expansion (Wedge) anchor [HST3]	>14.2	>30; <32	wedge anchor	Failure before the upper torque moment
Expansion (Wedge) anchor [HST3R]	>13.0	>26; <28	wedge anchor	Failure before the upper torque moment
Expansion (Wedge) anchor [HST-HCR]	>14.3	>32; <34	wedge anchor	Failure before the upper torque moment
Undercut anchor [HDA-P]	>46.1	>100	No visible cracking	Fixture plate with the dimensions of 100 × 100 × 10 mm^3
Undercut anchor [HDA-PF]	>45.4	>84; <92	undercut anchor	Failure before the upper torque moment
Undercut anchor [HDA-PR]	>46.5	>88; <92	undercut anchor	Failure before the upper torque moment
Chemical anchor (threaded rod) [DIN 975-8.8 St]	>60.7	>250; <300	bonded anchor	Failure before the upper torque moment
Chemical anchor (threaded rod) [AM 8.8]	>70.6	>250; <300	bonded anchor	Failure before the upper torque moment
Chemical anchor (anchor rod) [HIT-Z-R]	>45.2	>130; <140	bonded anchor/punching cone/anchor rod debonded from the epoxy	Failure before the upper torque moment

steel (the grade of steel AISI 304 (A2), AISI 316 (A4), 1.4529 (A6) (Hilti, 2010). Ordinary steel anchors were used for reference purposes. The specimens were cast on 25th June 2020 with self-compacting concrete provided by Ruskon Betoni Etelä Oy Ltd. The self-compacting concrete mixture requirements were compressive strength class of C30/C37, consistency class SF2, and target air content of 3.0%. The water-to-binder ratio was 0.51. Anchors were hit or installed to the drilled and cleaned holes of cured concrete slabs on August, and September 2020. Thereafter, specimens were sawn from the slabs with the dimensions of 68-82 × 150 × 220 mm^3 on August, and September 2020. Pretesting of one specimen from all anchor types for determining the tensile force as a function of the torque moment were made on August, and September 2020 (Figure 10). Test results of pretesting of anchor specimens are presented in Table 3. Note that only one anchor per one type were pretested.

Drying of the specimens in the ovens at the temperature of 45-55 °C were carried out on October, and November 2020. Thereafter, the anchor specimens were exposed to accelerated carbonation in the chamber, in which the atmosphere contained approximately 4.5-5 vol% CO_2 and had app. 55% RH and temperature T equal to 22 °C. Accelerated carbonation started on November 2020.

Final remarks

The results of CONAGE project can be exploited by all Finnish NPP's both operating and under construction and the information can be shared with foreign partners. The relevance of the objectives for NPPs, regulators, and the construction industry in general, is intrinsically linked to the correct understanding of deterioration mechanisms, their nature and consequences, how to address them in the design phase of new NPPs, and how to assess their current state and mitigate occurrence. As a result, it is expected that:

- Changes can be suggested to the current design procedure to take into account a performance based approach to design of new concrete structures and the assessment of existing concrete structures.
- Utilities will benefit from increased service life of their infrastructure. This is quite significant because the repercussions are directly linked to the sustainability of the sector: reduction in the consumption of natural resources; reduction in the production of construction and demolition waste; reduction in the production of CO2 as a result of the previously mentioned factors;
- The risk for ASR in Finnish NPP concrete structures can be assessed and preliminary insight on avoidance of reactive material for the construction of new nuclear structures can be provided.
- Improved RI-ISI of liner and anchor bolt corrosion because of better understanding of the damage mechanisms and the likelihood of their occurrence.
- New knowledge for the education of new engineers (expert in NDE) for the Finnish NPPs and industry.

Acknowledgement

The authores woud like to acknowledge the funding received from SAFIR 2022, The Finnish Research Programme on Nuclear Power Plant Safety 2019 – 2022.

References

Aghili, B. 2007. Ageing aspects of Concrete Containments from a Regulatory Point of View. Transactions, SMiRT 19, Toronto, August 2007. Paper # H02/3. 6 p.

Al-Neshawy, F., Ahmed, H., Puttonen, J., 2020. Defining concrete compressive strength by combining the results of different NDT methods. Research report, AALTO-R-001-2020.

Al-Neshawy, F., 2020. Ground Penetrating Radar (GPR) for use on thick-walled concrete structure. Research report, AALTO-R-002-2020.

Breysse, D., et al. (2017). Non destructive assessment of in situ concrete strength: comparison of approaches through an international benchmark. Materials and Structures/Materiaux et Constructions, 50(2), 1–17.

Bohner, E., Huttunen-Saarivirta, E. 2020. Report on the test setup for steel liner corrosion experiments. SAFIR2022 Conage Project, Deliverable 3.2.1. Research Report VTT-R-00069-20. March 2020, Espoo, Finland. 13 p.

Chénier, J-O., et al., 2012. An approach regarding AMP for concrete containment structure at the Gentilly-2 NPP. Pro. 33rd Annual Conf. of the Canadian Nuclear Society, Saskatoon, Canada, June 10 -13, 2012, Vol. 1, 234-259.

Ferreira, M., Sjöblom, V., Al-Neshawy, F., Ojala, T., 2018. Final Report for the Construction of a Non-Destructive Evaluation mock-up. Research report VTT-R-02769-18. 49p. VTT Technical Research Centre of Finland Ltd.

Ferreira, M., 2019. Assessment of the potential of AAR occurrence in NPP concrete structures. SAFIR 2022 - CONAGE Project, VTT Research Report VTT-R-00982-19, VTT Technical Research Centre of Finland Ltd. 34p.

Ferreira, M., 2020b. Acquiring field experience concerning AAR in NPPs – Aggregates from Loviisa & Olkiluoto. SAFIR 2022 - CONAGE Project, VTT Research Report VTT-R-01287-20. VTT Technical Research Centre of Finland Ltd.

Ferreira, M., 2020a. Acquiring field experience concerning AAR in NPPs – Aggregates from Olkiluoto. SAFIR 2022 - CONAGE Project, VTT Research Report VTT-R-00022-2, 28p. VTT Technical Research Centre of Finland Ltd.

Godart, B., Divet, L., 2013. Lessons learned from structures damaged by delayed ettringite formation and the French prevention strategy. V Int. Conference on Forensic Engineering, Institution of Civil Engineers, France. 12 p.

Hilti. 2010. Corrosion Aspects of Fastening Systems. 35 p. Cited 17.11. 2020. Access: www.hilti.co.nz/medias/sys_master/h49/h55/9176913051678/Hilti_Bro sch_Korrosion_en_2010-final.pdf

IAEA, 2016. Ageing Management of Concrete Structures in Nuclear Power Plants. Nuclear Energy Series No. NP-T-3.5, Internat. Atomic Energy Agency. 372 p.

IAEA, 2002. Guidebook on non-destructive testing of concrete structures (Issue 17). IAEA–TCS–17, International Atomic Energy Agency. Vienna.

Isotahdon, E., Bohner, E., Huttunen-Saarivirta, E., Sistonen, E. 2019. Corrosion of steel liners and anchors in concrete. VTT Research report VTT-R-01011-19. VTT Technical Research Centre of Finland Ltd. 49 p. + app. 7 p.

Luodes, H. (2015). Ground penetrating radar and assessment of natural stone. Geological Survey Of Finland – GTK. Report of Investigation 223. 48p.

Manabe, R., Kawae, H., Ogawa, K., Matsuura, M., 2018. Maintenance management of turbine generator foundation affected by Alkali-silica reaction. Journal of Advanced Concrete Technology 16(4):179-190.

Orantie, K. 2014. FiR 1 tutkimusreatorin betonisen suojakuoren lujuusominaisuuksien ja mikrorakenteen tutkimukset tarjouksen. VTT O-157037-14. VTT Expert Services Oy. 31 p.

Petti, J. P., et al., 2011. Nuclear Containment Steel Liner Corrosion Workshop. Final Summary and Recommendation. Report. Sandia Report SAND2010-8718. Sandia National Laboratories.

SAFIR 2010. The Finnish Research Programme on Nuclear Power Plant Safety 2007–2010. http://virtual.vtt.fi/virtual/safir2010/

Samarin, A., 2004. Combined Methods. In V. M. Malhotra & N. J. Carino (Eds.), Handbook on Nondestructive Testing of Concrete.

Saouma, V., Hariri-Ardebili, M., 2014. A proposed aging management program for ASR in a NPP. Nuclear Engineering and Design, Vol.277, 248-264.

Sensors & Software Inc. (2015). Concrete Scanning with GPR – Guidebook. 33p.

SFS-EN 12504-1 (2019). Testing concrete in structures. Part 1: Cored specimens. Taking, examining and testing in compression. CEN.

SFS-EN 12504-2 (2019). Testing concrete in structures — Part 2: Non-destructive testing — Determination of rebound number. CEN.

SFS-EN 12504-4 (2004). Testing concrete. Part 4: Determination of ultrasonic pulse velocity. CEN.

Sistonen, E. 2020a. Report on experimental setup of anchor corrosion tests. Aalto Research Report, AALTO-R-001-2020. Espoo 2020. 13 p. Espoo, 16.04.2020.

Sistonen, E. 2020b. Status Report on anchor corrosion experiments. Aalto Status Research Report, AALTO-R-001-202x. Espoo 2020. 41 p. Espoo, 10.11.2020.

Snyder, K.A., Lwe, H.S. 2013. Alkali-Silica Reaction Degradation of Nuclear Power Plant Concrete Struc-tures: A Scoping Study. NISTIR 7937 National institute of Satndards and Technology. Washington, USA. 48 p.

Tang, T.M., 2013. Concrete Degradation of the Containment of Tihange 2 NPP in Belgium, OECD NEA/CSNI – WGIAGE – Concrete subgroup, 08 April 2013.

Watt, D. S., 2007. Building Pathology - Principles & Practice. Blackwell Publishing.

Wegemar, B., 2006. Corrosion failure of a BWR embedded reactor containment liner. Journal de Physique IV, Vol. 136, Issue 1, pp. 257-262.

7.3 Modelling of aged reinforced concrete structures for design extension conditions (CONFIT)

Kim Calonius[1], Alexis Fedoroff[1], Miguel Ferreira[1], Ludovic Fülöp[1], Kari Kolari[1], Jari Rinta-aho[1]; Tuomas Koskinen[1], Tommi Seppänen[1], Ari Vepsä[1], Oskari Jessen-Juhler[1], Reijo Kouhia[2], Jani Vilppo[2]

[1]VTT Technical Research Centre of Finland Ltd
P.O. Box 1000, FI-02044 Espoo

[2]TUNI Tampere University
Kalevantie 4, 33014 Tampereen yliopisto

Abstract

Two different types of constitutive material models have been developed during the two first years of this project. The first one is Concrete Damaged Plasticity (CDP) model that has been available in Abaqus Finite Element (FE) code and used at VTT for many years. It was further extended and calibrated in the project in 2019. This user-extended CDP model is especially suitable for hard impact simulations. The second one is so-called tensorial damage model that captures the effect of crack initiation and growth on the continuum response. Beside the stress-state, the mechanical response of cracked material depends strongly on the opening and closure of micro-cracks, called unilateral effect. The effect is of importance in the vibration problems. This is the only material model type that describes damage-induced anisotropy and has not been available in any FE code. It was further developed and implemented to Abaqus during 2020. The user-extended CDP model has now been partly validated against different types of material tests. The same calibration and validation process will be conducted for the other model in the future.

The implications of material ageing for structural performance assessment and especially for numerical modelling of reinforced concrete structures has been studied. This information has been summarized, focusing on stressors, degradation mechanisms, potential failure modes, and in-service inspection methods. Calculation models have been collected for the estimation of the ageing and deterioration effects on the key mechanical properties. These provide inputs for mechanical properties in structural models that take into account the ageing and deterioration of concrete in NPP structures

Introduction

The protective walls, containment and civil structures of Nuclear Power Plants (NPPs) are mainly reinforced concrete (RC) structures. Long term operation of NPPs requires structural integrity assessment of aged concrete structures in YVL design extension conditions (DEC) e.g. external hazards like earthquakes and wide

body aircraft crashes. These DEC have been introduced recently in NPP design in Finland. The DEC loads are considerably higher than the earlier design basis loads (DBL).

An airplane crash (APC) on safety related structures, in spite of its low probability, has for a long time been recognized as a relevant loading case, especially in designing plants to areas with heavy air traffic. STUK regulation Y/1/2016 (STUK, 2016) requires that the nuclear plant design takes into account large airliner crashes, as well as resulting fires and explosions. Nonlinear numerical modelling has been used for several years in APC simulation. However, the concrete material models used in the simulations have usually been validated only for certain types of experimental tests. Therefore, there is a need for a more universal material model which is more firmly based on physical phenomena and adequate for different types of loading cases, e.g. soft/hard impacts, earthquakes and resulting vibrations. Additional themes that require closer focus are the ageing of concrete and the scaling and strain rate effects. Ageing of concrete has not been previously taken into account in DEC assessment. The material study including ageing and degradation mechanisms involves collaboration between structural analysis and concrete material experts at VTT.

Structural analyses of these phenomena require nonlinear numerical analysis. In order for the results of these numerical analyses to be reliable, the applicability of the used methods and models should be validated experimentally and analytically. At VTT, computational methods and tools for analysing behaviour of reinforced concrete structures under impact load have been developed and validated within projects belonging to the previous SAFIR programs since year 2003. International impact testing projects (IMPACT 1-4), carried out at VTT, have provided unique and valuable experimental data for this work. It is clear that substantial improvement of the material model capabilities should be introduced to increase reliability of the models aiming to prove performance at DEC stage. Also, the increase in computational capacity enables larger calculation models which are needed for highly nonlinear numerical simulations. This continuous increase demands continuous development of material models and analysis approaches. The material model development involves collaboration with Tampere University (TUNI).

Material model development (shown in Figure 1) is a trial and error process, which aims at finding the most appropriate mathematical description, such that the response of the model matches the response obtained from a number of experimental stress-strain situations. Due to the challenges that arise in the calibration of the material model against appropriate test results, it is of paramount importance to conduct proper validation simulations. In these small-scale validation simulations, the experimental test setup is modelled as accurately as possible using finite elements, and the measured macroscopic quantities are then compared to the simulated ones. In order to rule out artefacts due to discretization, a sensitivity study on the element mesh size has to be performed.

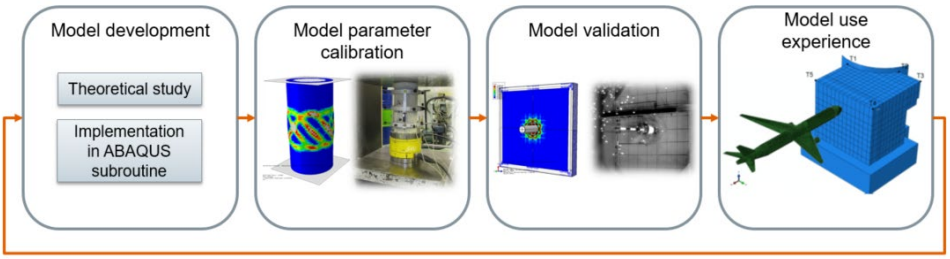

Figure 1. Concrete material model development chart.

The goal of the project is to develop understanding of the material modelling of concrete in the nonlinear domain by improving the use of existing material models, developing new material models and using calibration tests to stand at the basis of the development. Relatively new concrete material testing and measurement methods (such as DIC and ultrasonic methods) have also been further developed in the project. The expected result is a validated user-friendly analysis tool for reinforced concrete structures under design extension conditions (DEC), which takes the effect of ageing into account and gives more reliable results than the previous analysis tools. Methods and modelling techniques developed and validated here can directly be applied in safety assessment and design analyses of aged reinforced structures of NPPs under design extension conditions.

User-extended Abaqus Concrete Damaged Plasticity model for hard impact simulations

The Concrete Damaged Plasticity (CDP) model available in Abaqus finite element software has been implemented based on a theory developed in (Lubliner, et al., 1989) for monotonic loading cases and later enhanced in (Lee & Fenves, 1998) to encompass static cyclic behaviour. In order to extend the CDP model to dynamic behaviour, it is necessary to introduce rate dependency of concrete in the material model parameters. Based on the assumption that concrete compression strength increases with hydrostatic pressure, and that concrete tensile strength increases with strain rate, a VSDFLD Abaqus user subroutine has been written. This user-extended CDP model is described in (Fedoroff, et al., 2019). In addition to confinement pressure dependency of compressive strength and rate dependency of tensile strength, in hard missile impact simulations it is necessary to formulate an algorithm for element removal as a means to materialize fragmentation of concrete during the impact process. The element removal algorithm is described in (Fedoroff & Calonius, 2020) and it is validated against experimental hard missile impact benchmark tests. The core of the work done for the implementation of the user-extended CDP model has been conducted in SAFIR2018 ERNEST project. Figure 2 shows an example where concrete confinement, shear cone formation and finally fragmentation of concrete can be observed.

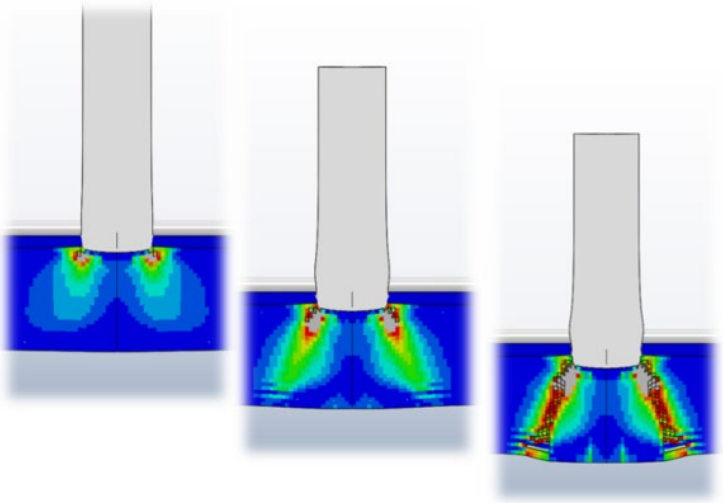

Figure 2. Example of hard missile impact simulation.

The development and validation of the user-extended CDP model continued in 2019 in the SAFIR CONFIT project. The focus was set on material model parameter calibration as described in (Calonius, et al., 2019). The proposed strategy for the material model parameter calibration is based on an iterative process where various concrete material tests (uniaxial compression, three point bending, split-tensile test, etc.) are simulated. At the end of each iteration, the model parameters are updated in order to obtain, on the next iteration a stress-strain curve that matches the experimental one. The CDP model parameters are generated using an Excel-VBA script by entering values for Eurocode material parameters (such as stiffness modulus, compressive strength, tensile strength, fracture energy, etc.) as well as values for confinement pressure and strain rate dependencies.

The results of the model parameter calibration simulations are shown in Figure 3 for the uniaxial compressive case, in Figure 4 for the three point bending case and in Figure 5 for the split tensile case. It can be noticed that for the uniaxial compressive test the experimental material parameter values (compressive strength, stress at maximum) generate a good initial estimate for the CDP material parameter values, which means that the iteration converges rapidly. However, the three point bending test and split tensile test simulations need more iterations in order to converge. Some corresponding experimentally tested specimen are shown in Figure 6.

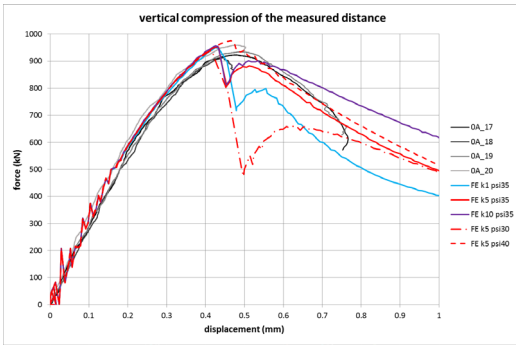

(a) Simulation vs. experimental stress-strain curves

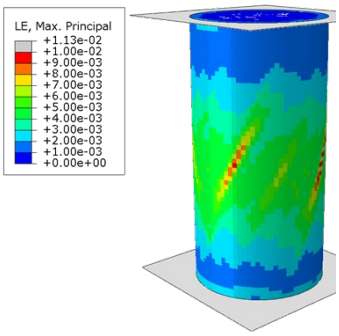

(b) Crack formation during the simulation

Figure 3. Uniaxial compression test simulation.

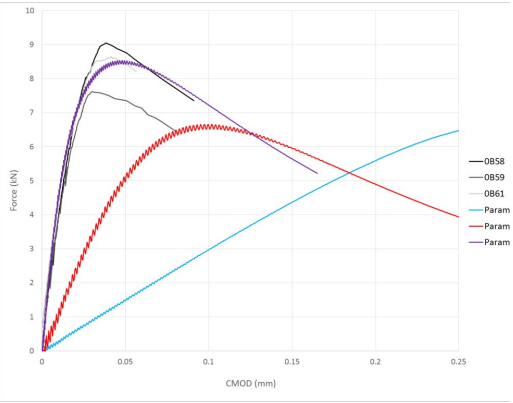

(a) Simulation vs. experimental stress-strain curves

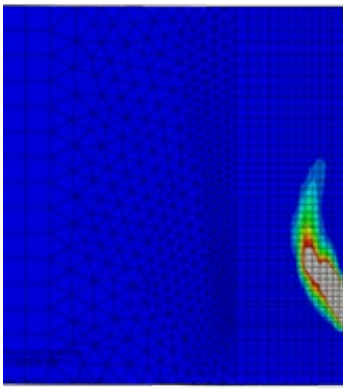

(b) Crack formation during the simulation

Figure 4. Three point bending test simulation.

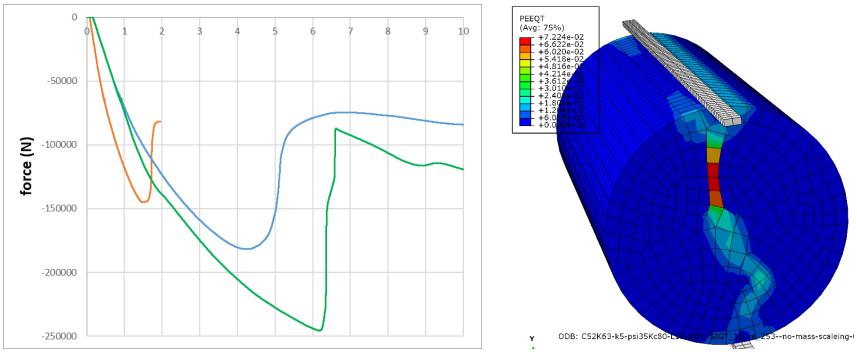

(a) Simulated force-time curves

(b) Crack formation during the simulation

Figure 5. Split tensile test simulation.

(a) 0A20 (b) 0B58 (c) 0A24

Figure 6. Tested 0% AE specimen in (a) uniaxial compression test, (b) three-point bending test and (c) split tensile test (Fülöp and Niemelä, 2018).

In addition to the development and validation of the user-extended CDP model, some novel non-destructive concrete testing methods were evaluated in the context of the CONFIT project. Digital Image Correlation (DIC) was tested in a concrete cube compressive test and compared to strain gauge measurement results, Figure 7, and to Abaqus simulation results using the CDP material model, Figure 8.

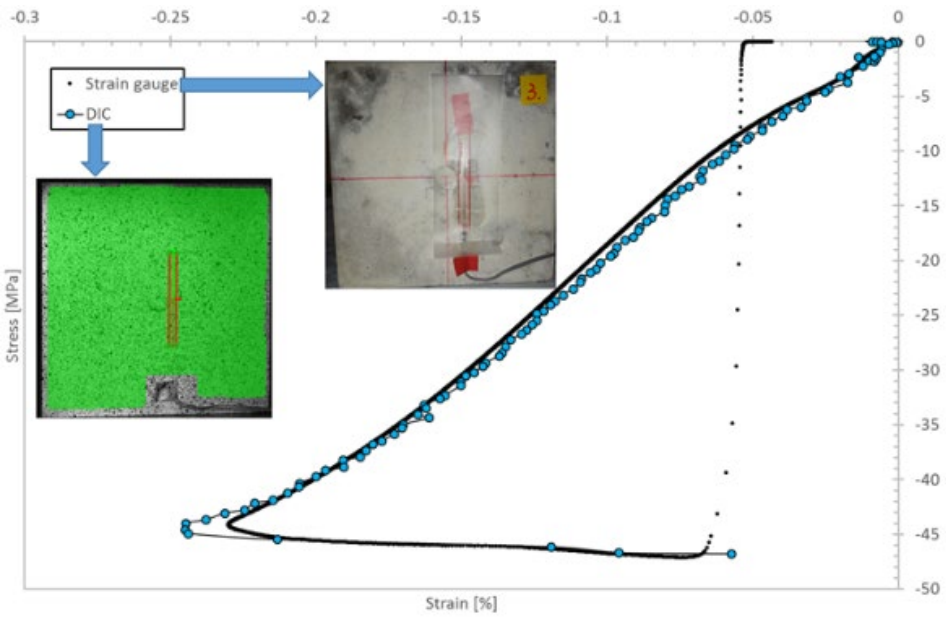

Figure 7. Comparison of vertical strain measurement results with a strain gauge and Digital Image Correlation.

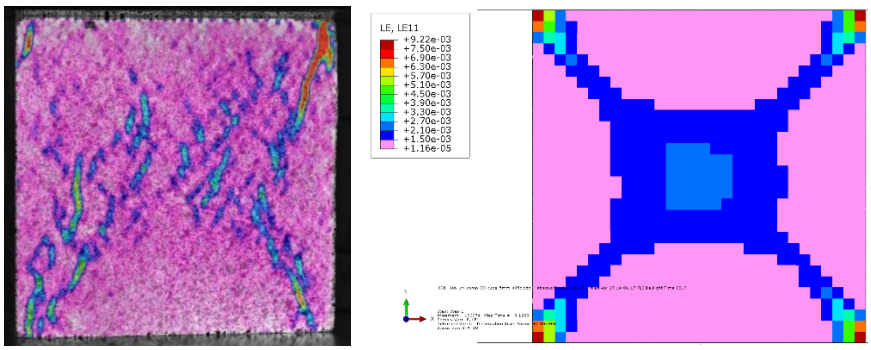

(a) DIC strain field (b) Abaqus CDP simulation strain field

Figure 8. Comparison of strain fields DIC vs. simulation.

Further, ultrasound methods were experimented on concrete cube specimens in order to find out p-wave and s-wave sound velocity in virgin and damaged concrete (Figure 9). As shown in (Brown, 2001), the measurements of p-, and s-waves in six directions of a chamfered cube of a given material enable the measurement of the 9 components of the orthotropic stiffness matrix. Because concrete is a porous

material, which attenuates acoustic waves very effectively, the so called pitch-catch method has to be used for sound velocity determination. The pitch-catch method consists in applying an emitting sensor and a receiving sensor on opposite sides of the specimen. Due to internal delay in the electronics, the pitch-catch method has to be first calibrated on a specimen with known sound velocity.

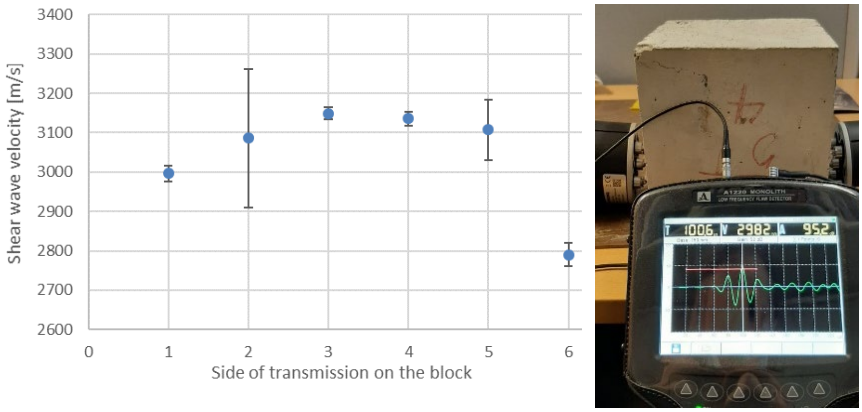

(a) s-wave velocity measurements (with unknown offset value that needs to be determined by calibration)

(b) pich-catch measurement

Figure 9. Wavespeed measurements on damaged concrete cube specimen.

Tensorial damage model for anisotropic concrete behaviour

Modeling of concrete structures under extreme loadings as explosion and impact is challenging. Both the material and geometric non-linearities have to be considered in the modelling. The ultimate failure of structures can be described as a continuous process of damage initiation, propagation and fragmentation.

In the simulation, it is extremely important that the failure pattern during the damage evolution is correctly described by the model. That is not the case in classical continuum models – the models target on the modelling of ultimate stress state and often neglect the associated failure patterns. Brittle kind of materials like concrete, natural rocks and natural ice tend to fail by axial splitting along the direction of uniaxial loading shown in Figure 10. As discussed by Schreyer (2007) the classical stress criteria do not have the flexibility to reflect the failure modes for various of stress states and “none predicts axial splitting”.

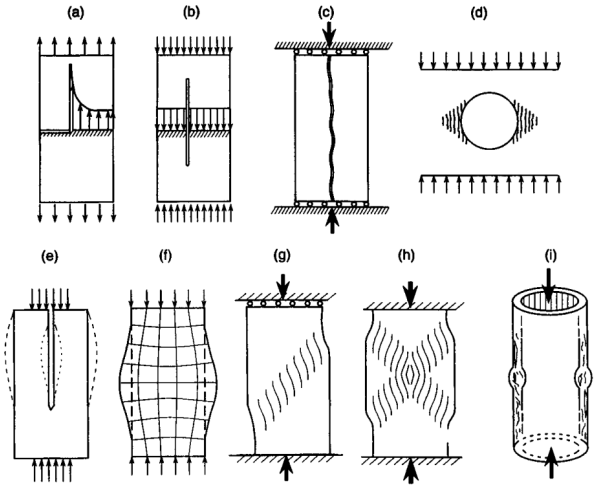

Figure 10. Global mechanisms of brittle compressive fracture as described by Bazant and Xiang (1997). Under uniaxial loading the failure mode is axial splitting along the direction of compression (c).

Formulation of the anisotropic tensorial damage model is done by specifying two potential functions, the specific Gibbs free energy and the dissipation potential. The isotropic potential functions are written in terms of invariants forming a functional, i.e. irreducible basis having two symmetric second-order tensor variables, namely the stress tensor and the damage tensor, which resembles the crack density tensor of Kachanov (1992). Therefore, the magnitude of the components of the damage tensor are not limited above, which makes numerical implementation somewhat simpler than using the standard definition of damage as a ratio of damaged to the undamaged area.

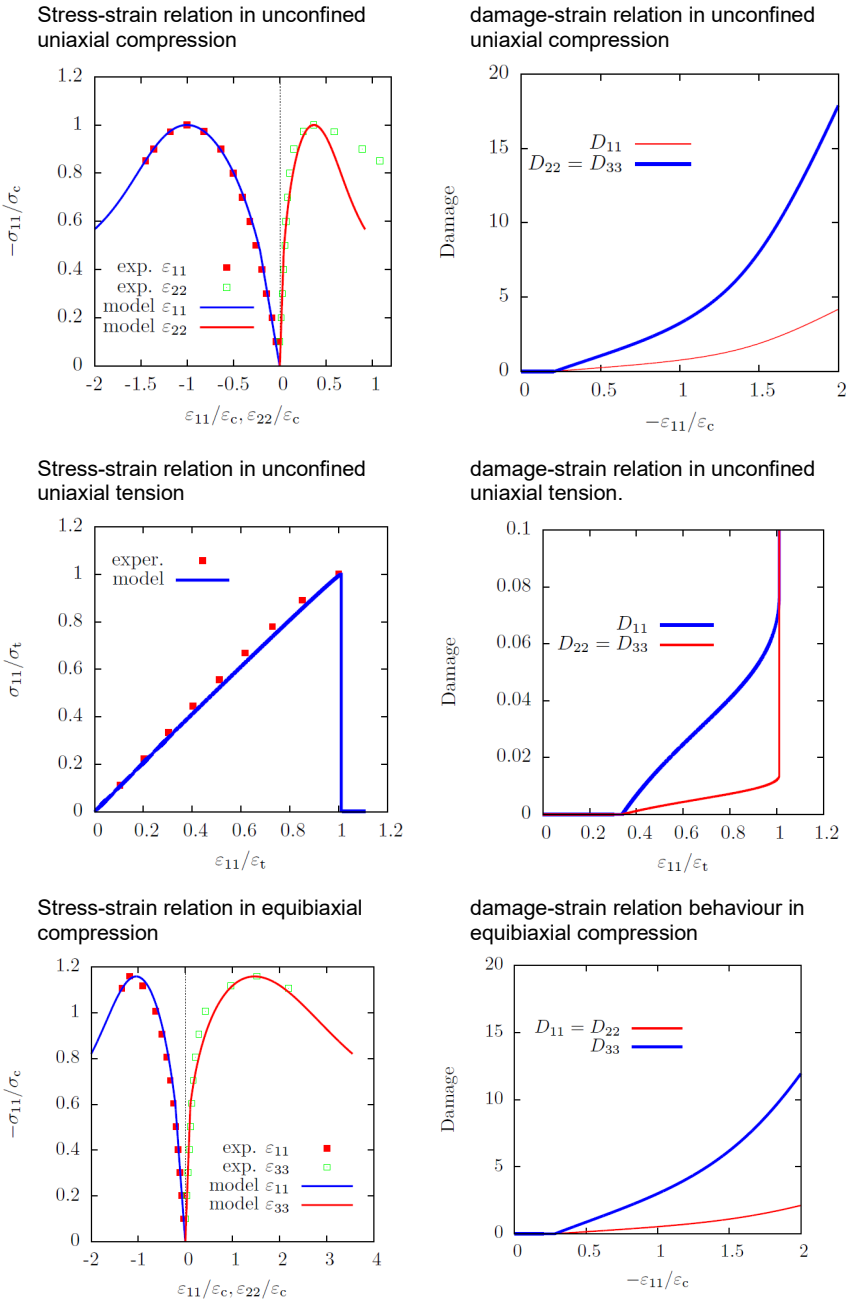

Figure 11. Stress-strain relations and damage evolutions in different directions predicted by the model under different types of loading schemes.

The specific Gibbs free energy is constructed to represent linear elastic solid in undamaged states. Furthermore, only linear terms of the damage tensor are retained, thus the “crack” interaction is not taken into account. Hardening and softening is modelled using a single internal variable. The dissipation potential is chosen in accordance to the famous Ottosen (1977) failure criterion, which captures the relevant features in concrete failure. The formulation is basically non-associated, however, the formulation follows closely the one for the standard dissipative solid. An additional convenient feature is that the material parameters of the model can be obtained in a closed form solution from standard material tests results: uniaxial compression/tension, equibiaxial compression and one extra point on the compressive meridian.

In Figure 11 the model predictions, stress-strain relations and damage evolutions, are shown in unconfined compression/tension and equibaxial compression. Correspondence to the well-known experimental results by Kupfer et al. (1969) is good. It can also be seen from the damage-strain curves that the model is able to capture the correct failure mode.

Effects of ageing on reinforced concrete

Reinforced concrete structures used in NPPs are used for varying applications and environments. The long-term reliability of NPP safety-related concrete structures depends on the ability of these structures to withstand the time-dependent deterioration. Experience has shown that concrete is a durable material. However, faulty design, use of unsuitable materials, improper workmanship, exposure to aggressive environments, excessive structural loads, accident conditions and a combination of the above factors can compromise its performance (Naus et al., 1996).

Many factors complicate the contribution of ageing effects to the residual life of the NPP safety-related concrete structures. Uncertainties arise due to differences in design codes and standards for components of different ages and lack of past measurements and records. During the exploitation phase, detection, inspection, surveillance, and maintenance methods or programs may be inadequate. In addition, there may be limitations in the applicability of time-dependent models for quantifying the contribution of ageing to concrete structures (Naus et al., 1996).

Concrete long-term reliability can be improved by limiting the exposure of the concrete structures to deteriorating effects, and by periodic inspection and maintenance procedures. The ageing research of concrete structures is to not only identify and mitigate the time-dependent deterioration mechanism on concrete, but also understand the implica-tion for structural performance and characterise this performance in material models.

A degradation factor, or stressor, can be defined as an agent or stimulus resulting from construction or pre-operation and operation conditions that can result in the ageing process and failure of the structure. Different materials within the concrete structure are affected by different types of stressors (USNRC, 2013).

The implications of material ageing for structural performance assessment and especially for numerical modelling of reinforced concrete structures have been studied. The four main constituents of reinforced concrete (concrete, mild steel reinforcement, prestressing steel and steel liner) and their likely stressors have been reviewed. This information, focusing on stressors, degradation mechanisms, potential failure modes, and in-service inspection methods is reported in (Ferreira & Fülöp, 2020).

The study provides a review of the current state of understanding of the effect of stressors on the material and mechanical properties that are currently used in concrete modelling. Focus has been on mechanical properties of concrete as a function of the “loading” conditions. Figure 12 illustrates an example of the effect of ageing, i.e., accumulated neutron fluence, on the compressive strength of concrete.

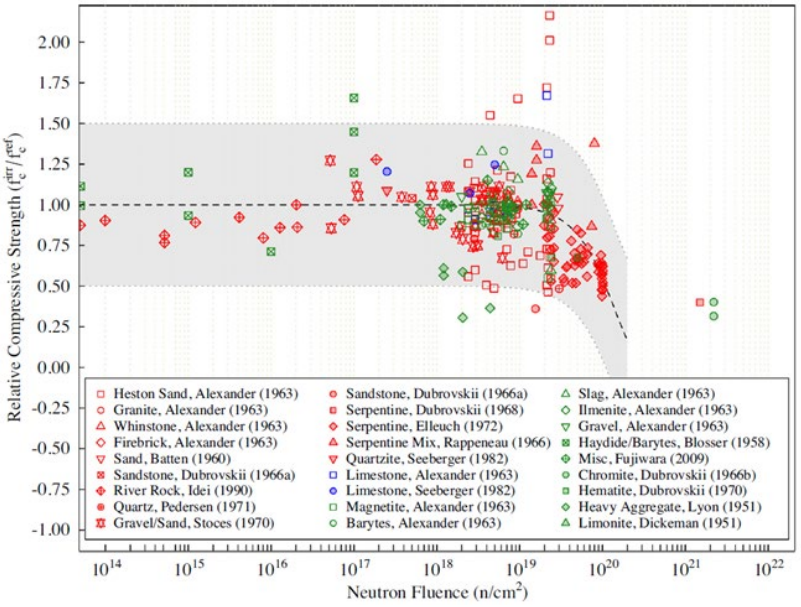

Figure 12. Relative compressive strength of concrete and mortar specimens versus neutron fluence. The neutron spectrum and specimen temperature vary between experiments. A decrease in compressive strength above 2×1019 n/cm2 is suggested (Le Pape et al., 2016).

Generally, it is concluded that models exist for estimating the effect of aging and deterioration on a large number of mechanical properties (e.g. compressive strength, tensile strength, modulus of elasticity, etc.). Hence, the use of “as-new” properties for estimating performance of existing NPP structures should be critically revised. Aged concrete and its respective time-dependent properties should be considered in performance estimation for NPPs to accidental loads or DEC conditions.

References

Bažant, Z. & Xiang, Y. 1997. Size Effect in Compression Fracture: Splitting Crack Band Propagation. Journal of Engineering Mechanics / Volume 123 Issue 2 - February 1997. DOI:10.1061/(ASCE)0733-9399(1997)123:2(162)

Brown, R. J. 2001. Relationships between the velocities and the elastic constants of an anisotropic solid possessing orthorombic symmetry, s.l.: CREWES project.

Calonius, K. et al. 2019. Calibration of Abaqus CDP model parameters. Oulu, Proceedings of the 32nd Nordic Seminar on Computational Mechanics.

Fedoroff, A., Calonius, K. & Kuutti, J. 2019. Behavior of the abaqus CDP model in simple stress states. Rakenteiden Mekaniikka (Journal of Structural Mechanics), pp. 52(2), 87-113.

Fedoroff, A. & Calonius, K. 2020. Using the abaqus CDP model in impact simulations. Rakenteiden mekaniikka (Journal of Structural Mechanics), pp. 53(3), 180-207.

Ferreira, M. & Fülöp, L. 2020. Understanding the effect of ageing and deterioration of reinforced concrete on its durability and mechanical performance. SAFIR 2022 - CONFIT Project, VTT Research Report VTT-R-01115-20, 90 p.

Fülöp, L. & Niemelä, M. 2018. Excessively air entrained concrete - Characterization of the basic mechanical properties, VTT-R-06996-18.

Kachanov, M. 1992. Effective elastic properties of cracked solids: critical review of some basic concepts. Applied Mechanics Review 45, 304–335. doi: https://doi.org/10.1115/1.3119761

Kupfer, H., Hilsdorf, H. & Rüsch, H. 1969. Behaviour of concrete under biaxial stresses. Journal of the American Concrete Institute 66, 656–666. doi: https://doi.org/10.14359/7388

Lee, J. & Fenves, G. L. 1998. Plastic-damage model for cyclic loading of concrete structures. J. Eng. Mech., pp. 892-900.

Le Pape, Y., Giorla, A. & Sanahuja, J. 2016. Combined Effects of Temperature and Irradiation on Concrete Damage. Journal of Advanced Concrete Technology, volume Vol.14, pp 70-86.

Lubliner, J., Oliver, J., Oller, S. & Oñate, E. 1989. A plastic-damage model for concrete. Int. J. Solids Structures, pp. 299-326.

Naus, D., Oland, C. B. & Ellingwood, B. 1996. Report on Aging of concrete containment structures in nuclear power plant. s.l.: U.S. Nuclear Regulatory Commission, 1996. p. 300. NUREG/CR-6424, BNL-NUREG-13148.

Ottosen, N. 1977. A failure criterion for concrete. Journal of the Engineering Mechanics, ASCE 103, 527–535.

Schreyer, H.L. 2007. Modelling surface orientation and stress at failure of concrete and geological materials. International Journal for Numerical and Analytical Methods in Geomechanics 31, 147–171. doi: https://doi.org/10.1002/nag.557, arXiv:nag.2347.

Säteilyturvakeskus. 2016. Regulation on the Safety of a Nuclear Power Plant. Helsinki: s.n., 2016. STUK Y/1/2016.

USNRC (United States Nuclear Regulatory Commission). 2013. NUREG/CR-7153, Volume 4 – Expanded Materials Degradation Assessment (EMDA): Aging of Concrete and Civil Structures. p. 137. ORNL/TM-2013/532.

7.4 Safety criteria and improved ageing management research for polymer components exposed to thermal-radiative environments (SAMPO)

Harri Joki[1], Jari Rinta-Aho[1], Konsta Sipilä[1], Jukka Vaari[1], Anna Bondesson[2]; Mohit Pushp[2]; Jason Ryan[2]; Henrik Toss[2]

[1]VTT Technical Research Centre of Finland Ltd
P.O. Box 1000, FI-02044 Espoo

[2]RISE Research Institutes of Sweden
Box 857, 501 15 Borås, Sweden

Abstract

In SAMPO project several research topics related to polylmeric components ued inside NPP containments are included. The project contains three different work packages, which comprise of task with similar topics. The first work package is related to acceptance criterion and safety margin assessment. Here, work is focused on providing improved estimation for lifetimes of critical polymer components, studying the sensitivity of polymer properties to additive content and methods to verify polymer quality and setting up safety margins for O-rings. The results of this WP indicate the importance on setting acceptance criterion based on the functional property. Also improvements in polymer quality management is developed as techniques for on-site quality analysis are provided. The second work package focuses on improving ageing management of polymer components. Here within important research topics are online condition monitoring techniques as well as sensitive analysis methods and improving the interpretation of non-destructive testing data. Promising results have been obtained for the use of online monitoring methos such as microcalorimetry and permittivity measurements. Further development have been made in developing non-destructive cable condition monitoring methods and analysing the ageing of such cables by the means of molecular dynamics simulations. The third work package is solely on international cooperation, improving the knowledge transfer between the research community and industry and following international trends on polymer based components used in NPPs.

Introduction

SAMPO project focuses on safe long-term use of polymer components and improving their ageing management. This is done by studying ageing mechanisms of polymers, determining how to set acceptance criterion properly and providing robust tools for condition monitoring. These topics become more relevant as the original planned lifetime of the plants is approaching and extension is considered. Safety criteria assessment and ageing management needs to be at sufficient level in order

to prevent premature component breakdown and avoiding endangering the overall safety.

Lifetime estimation on sealing and membrane

The aim of this task is trying to identify critical components and to investigate the possibilities to obtain such components from plants under decommissioning or during maintenance, including material data.

The workshops that were held at Ringhals NPP and Forsmark NPP have been the main method to identify critical and interesting materials for further investigating. In a first stage focus was set on Ringhals because of their upcoming decommission of two reactors but during the decommissioning time it will be hard to get out materials because critical components will still be in used in the reactors for several years to come. Discussion of materials of special interest for the project were also held at the SAMPO workshop at Fortum, Espoo in November 27-28th 2019.

For investigating residual lifetime of the chosen and obtained materials some testing has been initiated. This initial investigation of the materials has included testing of hardness, tensile strength, and elongation at break.

The materials used for this tests were:

Neoprene membranes from Ringhals NPP: Ringhals has collected membranes from earlier revisions and the collection contains several membranes of similar type and of similar conditions and time in use.

- Outtake was made in September 2018
- They have been in the plant for 8 years (which is maintenance interval)
- There is membranes of three dimensions 40, 19 and 17.5 cm in diameter

Reinforced EPDM seal between structure joints from TVO (**Olkiluoto)**.

- Installed in 2005, planned lifetime until 2025
- Exposure temperature 45 °C, during power operation in nitrogen atmosphere, after outage it has been stored in air
- Installed in L-shape
- Should withstand LOCA, the LOCA profile would be some time at 2,4 bar and 95°C followed by some time at 3,7 bar and 170 °C

The membranes and the joint seal were reinforced so the rubber material was cut off and punched into dumbbells. Tensile testing was made according to ISO 37 with type 2 dumbbell on a Zwick Z1 tensile tester at a rate of 500mm/min and with a clip-on extensometer. The hardness was measured according to ISO 48-2 on a Bareiss Digitest Hardness Tester equipped with an IRHD-m measuring device.

The seal material was heat aged in 120 °C for 45 days. Which is equivalenet to 20 years service life in 45 °C.

Membrane

For the 17.5 cm membrane there were some difference in the test results between the samples, one can see that the membranes with the same first digit is more alike each other, they were placed in the same bag and thus taken from the same environment

For the 19 cm membrane the result was more similar between the samples

TVO seal

Not much difference after ageing

The aging was made in air which is tougher for the material than the nitrogen atmosphere it is used in the plant

Setting up safety margins for O-rings 2020

This task primarily aims to attain usage lifetimes for rubber O-rings which are present in critical functional capacities in Nuclear Powerplants (NPPs). SAMPO 2019 focused upon verification of COMRADE results and was successful in doing so. SAMPO 2020 focuses on utilising model materials to attain material failure, further verifying methods and better representing average power plant material.

Rubber O-rings can be found in some critical components such as pumps and pipe connections. If these pipes were to fail, a so-called ‘loss of coolant accident’ (LOCA) could occur. This could obviously be disastrous to the Powerplant and surroundings.

Ethylene Propylene Diene Monomer (EPDM) was supplied by James Walker Ltd. Two grades are present and defined here as ‘top-level’, which is the same material as used in COMRADE and SAMPO 2019, and ‘bad’ which is a bespoke material fabricated from James Walker for SAMPO.

Compression set and leak test

Compression set test was performed on standard test specimen of cylindrical shape with a diameter 13 ± 0.1 mm and a thickness 5,6 ± 0,2 mmm according to ISO 815-1. The standard test specimens were cut from the rubber sheets with a standard cutting mould. Three test specimens were placed between the plates of one compression device with the spacers with a height of 1.4 mm. The bolts were tightened so that the percentage of the compression was 75% of the original thickness. In total, three assembled compression devices were papered for EPDM and nitrile sample, respectively. The compression was performed in air. Leak test rigs had O-rings compressed to approximately 20%.

Previous work in 2019 focused on the overall verification of the data attained in the prior project COMRADE, i.e. the method used in COMRADE (measurement on O-rings), and the standardised method for measuring compression set (cylindrical cut-outs from a sheet). This experimentation showed that the data is reliable in both circumstances. In Task 1.3 2020, work has been undertaken on compression set of a model material provided by James Walker (JW), at a level which has been described by JW as 6/10 (denoted 'bad' material), where the material measured in SAMPO 2019 is considered at top levels, 9-10/10. The purpose of this was two-fold. Firstly, we wanted to assure that a material could reach failure, unlike the prior COMRADE project, where the top level material was used, and failure was rare – thus casting into doubt at time whether the experiment was at fault, or if the material was just simply that good. Secondly, it is unknown whether power plants will at all times use top level material, so experimentation upon a more realistic, yet still proficient material, was deemed wise.

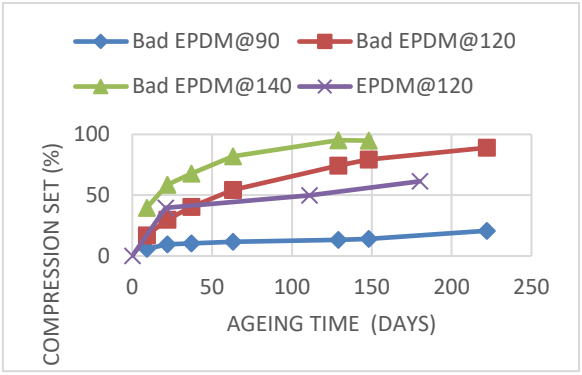

Figure 1. Data of compression set for model 'bad' material, and one set of data of top-level material at 120 °C for comparison.

Experimentation moved on to compression set within leak test rigs, having verified compression in this manor is appropriate. During a symposium summarising 2019 data for stakeholders, it was brought to our attention that the 'old' test rigs may not be deemed satisfactory enough for duplicating the environment that O-rings find themselves in inside a power plant. Thus, the rigs were redesigned as per figure 2, where one can see a groove has been cut out for the ring to sit within, compared to the 'old' test rig with much more empty space in the centre. Compression set is underway for EPDM material within both leak test rig designs, and the data can be found in figure 3. The data follows the expected trend, with raising temperature, a higher compression set is attained. The testing will continue to attain more data points. Note that leak testing has been performed at the 2 latter time points as per figure 3, no leaks were detected except for the 'old' rig, at 140 °C. For the first of the two time points the leak was detected under low pressure (~5 Bar) and once the operating pressure for the test was attained (~60 Bar), the leak was no longer

detected. It could be deduced that the higher pressure allowed the O-ring to attain a tighter seal within the test rig. For the last point, the rig was leaking continuously and could not hold any higher pressure.

Figure 2. O-ring test rigs. Left: old test rig from COMRADE. Right: new test rig re-designed for SAMPO.

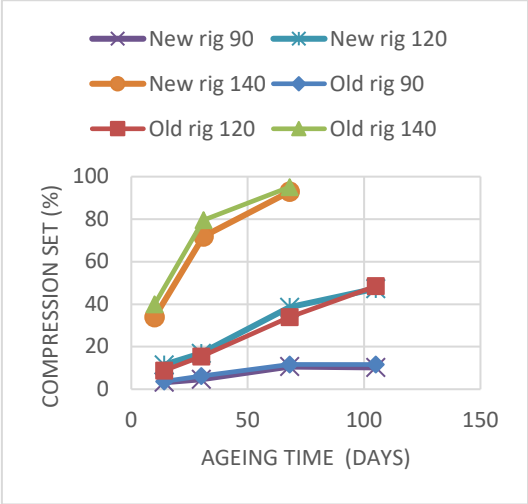

Figure 3. Compression set of model 'bad' EPDM material within test rigs, both 'old' and redesigned.

Stress-relaxation

Testing was performed in duplicate for each temperature (90, 120, 140 °C). The samples were compressed initially to 75% and the force was measured continuously until 50 % of initial force was reached (test of samples in 90 °C was discontinued before reaching 50%).

Stress relaxation was conducted to determine failure (F_{50}, 50% compression) for the model 'bad' material, EPDM. The values of which can be found in table 1.

Table 1. EPDM material: time for F_{50}, failure, at 50% compression.

Temperature	Sample no	Time to F_{50} [days]
120 °C	1	89
	2	134
140 °C	1	19
	2	23

The values follow an expected trend that at higher temperature the material fails sooner. It should be noted that the EPDM being run at 90 °C has reached only ~90% compression as of 150 days (Figure 4). Top-level EPDM rubber, as determined in COMRADE, gave for 140 °C an F_{50} of 49 days. Whereas, for 120 °C, compression reached 75% after 58 days.

Based on this, following conclusions could be made on experimental data:

- Expected trends are present for all data – higher temperature leads to greater/faster failure.
- Model 'bad' material performs worse, as expected, than the top-level material from SAMPO 2019 and COMRADE before.
- The model 'bad' material is important as it better represents the average material in use at a power plant. Additionally, allowing for shorter test times whilst working with similar degradation mechanisms.
- The new rig seems to hold against leakage longer than the old rig.
- Perhaps more experimentation should be performed on commercial grade material, which JW denotes as being a 2-3/10 level material. Stress-relaxation particularly would be useful to determine key aging points in the material. This could lead to the use of a material that allows for shorter testing time, which ties in with WP2 requirements.

Methods for polymer quality verification at on-site

Additives are used to improve processability of the polymers as well as their material properties. In task 1.2 the aim is to identify important additives and provide suitable methods for their analysis for on-site purposes. The most important additives in the case NPP cable insulators and sealants would be those, which have an effect to their functional properties and hinder the ageing. In this sense antioxidants, plasticizers (for elastomers) and certain colorants would be relevant, as they are known to contribute to the ageing process. In 2019 it was shown that various methods for additive analysis were exist and they provide various possibilities to examine polymeric materials. Several methods are able to qualitatively and/or quantitatively analyze additives that are important for the polymer material properties and ageing behaviour. However, to be able to use many of the methods with their full capacity, high level of expertise is required. The applicability of the methods for on-site use

may be limited due to their complexity in sample preparation phase and high equipment purchase cost.

During 2020 the various previously identified analysis methods were more closely examined in order to identify the most suitable ones for on-site quality verification [Joki et al 2021]. For this purpose various criterion were developed to identify the most applicable methods for on-site measurements. The most important criteria were related to analysis sensitivity (methods needs to be capable to measure something relevant), sample preparation (minimized sample preparation phase, preferably none) and analysis and equipment related limitations (applicability to wide range of polymers, equipment size, portability and cost). Based on this comparision of the methods, DSC and FTIR were identified to be suitable for antioxidant analysis and combined TGA and EDS for filler analysis.

A small scale test were performed with the identified methods in order to show their cababilites to distinguish a poor material from a good material. For antioxidant analysis aged and unaged polyethylene samples were tested. The ageing of samples were performed at 100°C for 40 weeks. DSC and FTIR both could distinguish aged PE sample from unaged sample. OIT measured with DSC decreased from 180 minutes to 10 minutes indicating a heavy antioxidant depletion in the material due to ageing (see Figure 4). Similarly carbonyl group peak height was clearly affected by ageing, indicating formation of carbonyl groups due to ageing (see Figure 5).

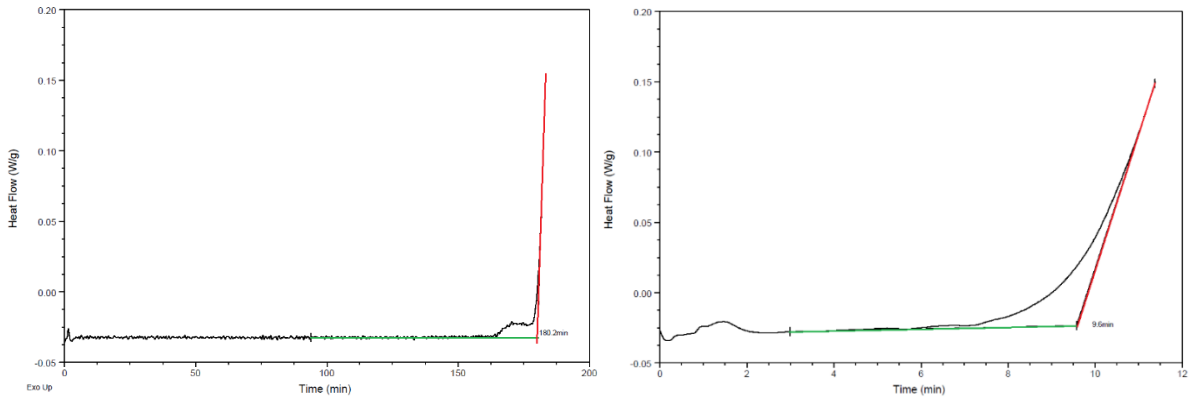

Figure 4. OIT measured with DSC. Unaged polyethylene on left side and sample aged for 40 weeks at 100°C on right side.

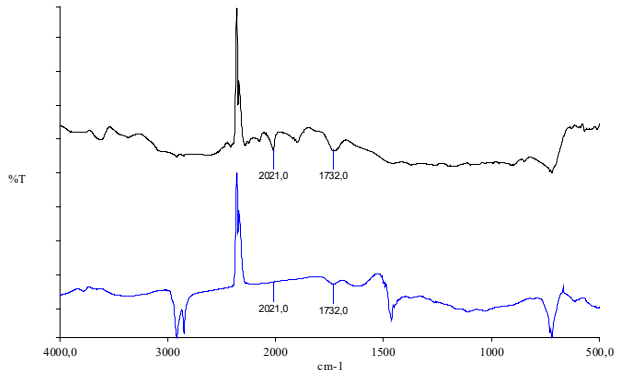

Figure 5. The measured FTIR spectra for unaged (black curve) and aged (blue curve) samples.

TGA analysis were performed on two different size EPDM samples in order to estimate the effect of sample size on analysis results. According to the analysis, roughly 40% of the sample was non-volatile below 800 °C. The EDS analysis performed on the ash revealed more the presence of carbon, sulphur and zinc, as shown in Table 2. Sulphur is probably the curing agent, but zinc may have various functions. Here zinc is assumed to be used as a processing aid. Thus, when the S and Zn contents are taken into account, it can be estimated that the filler content of these specific samples were 37,8% for the smaller sample and 38,3% for the larger sample.

The small scale tests performed with each method showed that DSC and FTIR would be suitable methods for AO analysis while combined TGA and ESD should suit well for filler analysis. A small scale test was performed to estimate the applicability of the identified methods for on-site use. OIT and FTIR measurements were clearly capable to distinguish the aged and unaged PE samples from each other. Additional measurements would be required to show whether they can provide quantitative results with sufficient accuracy.

The combined TGA and EDS provided the carbon black content of the EPDM rubber tested. Additional non-volatile additives could be detected as well by EDS and it makes the filler analysis more accurate. The resolution of both methods need to be confirmed with further measurements with custom made materials.

Table 2. EDS results for the smaller and larger EPDM sample after the TGA. W% = weight percentage and A% = atomic percentage.

	Smaller sample		**Larger sample**	
Element	**W%**	**A%**	**W%**	**A%**
C	94.39	98.71	94.56	98.76
S	1.06	0.42	0.97	0.38
Zn	4.55	0.87	4.47	0.86

Online condition monitoring techniques - Dielectric Properties

The goal of this study was to assess if the accelerated ageing performed within the project induced measurable dielectric changes in some of the rubber materials and, if possible, identify specific frequency regions with more pronounced as well as systematic changes. We also wanted to investigate the feasibility of the concept of online monitoring of dielectric changes in similar rubber materials over extended periods of time.

As the frequency region of interest is unknown for any new material under investigation a broad band measurement method is needed. For this reason, a coaxial probe was chosen for the dielectric characterization of the materials. The coaxial probe is in principle a monopole antenna sensor, albeit not the type of antenna sensor we hope to see implemented as a result of this work. Instead of incorporating the antenna in or on the material the dielectric probe is pressed against the material.

Measurements on aged samples

Measurements have been performed on provided EPDM samples that were cut out from the same piece of test material after which they were put through accelerated ageing to different degrees.

Measurements were performed for three unaged samples and four samples aged at 140 °C for 6 months, of which two were also irradiated in cycles between ageing. The probe was disconnected from the samples and then reconnected between measurements to ensure measurements were performed at more than one specific sample location. This also helps in ruling out that the variation in results between samples could simply be due to differences in the contact between probe and sample.

Before the first measurement the cable was placed in a fixed position to the extent possible. The measurement set-up was then calibrated for the entire measured frequency spectrum using air, milli-Q water and a short as reference points. The placement of the measurement equipment unfortunately turned out to be sub-optimal and it is difficult to rule out cable drift due to other activities in the vicinity of the measurement set-up. This may also be one reason why it was difficult to realize a good calibration for the lower frequencies.

A simple mean over all measurements made on each sample/sample group is presented below. Material pre-irradiation appears to have very little effect on the results for the samples aged at 140 °C. This is consistent with the results from the mechanical studies. A slight increase in the real part of the permittivity could indicate an increased density of dipoles. There appear to be no clear frequency shifts for the peaks of the imaginary part of the permittivity. Without knowing the exact blend of the rubber material under test it is difficult to make any statement on if the results are plausible or not.

Looking at the data on a log-log scale there appears to be a shift in the dominant polarization mechanism at 6–10 GHz for this specific material, seen as a more

pronounced reduction in the real part of the permittivity over those frequencies as well as what looks like a corresponding peak in the imaginary part of the permittivity in that same frequency interval. If the changes seen in the data is in fact due to the ageing mechanisms it appears that the ageing at higher temperatures affect the entire spectra, while the lower temperature aging only appears to affect the lower frequencies. This could indicate a possibility to use different frequencies for identification of different types of ageing.

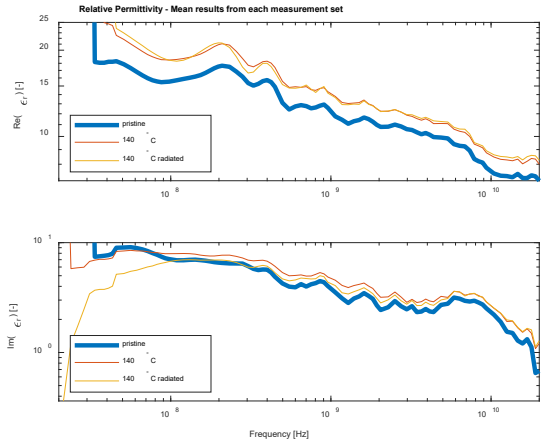

Figure 6. The measured dielectric response for the aged samples.

Online measurements

Online measurements were performed on a sample placed in a climate chamber for accelerated ageing.

The measurement probe was inserted into a climate chamber set at 50 °C. This temperature was chosen as it was the highest temperature for which there appeared to be no risk of damaging the measurement probe available to us. The probe was calibrated in position, at the intended measurement temperature, with air, milli-Q water and an electrical short as references (references also heated to the measurement temperature). The probe and sample were pressed together and fixated, using a sample holder made of PTFE, to achieve good and consistent contact between probe and sample throughout the measurement cycle. The Vector Network Analyzer used to sweep and record the frequency response of the probe and sample was programmed to perform one measurement sweep approximately every hour for 1001 hours, resulting in a total measurement/ageing cycle of a little more than 44 days.

The measured relative permittivity as function of frequency taken approximately every hour for a total of 44 days was plotted together with the colour axis indicating progression in time [days]. In most of the investigated frequency span it appears

that the relative permittivity increases as time progresses. At this timescale the change is quite small, and the rate of change is highest at the start of the measurement series. The overall trend appears to be consistent with the results observed for the samples aged at 140 °C although the change seen at this timescale might be too small to draw any definite conclusion. At around 5 GHz the imaginary part of the permittivity appears to go below zero. This is likely not a true result, but rather an effect of reaching a Fabry-Perot resonance as the sample at this point is ¼ wavelength thick (~5–6 mm). The measurement set-up used here is thus not valid at these frequencies. Measurements on samples of a different thickness would be helpful to realize correct characterization over the entire spectrum.

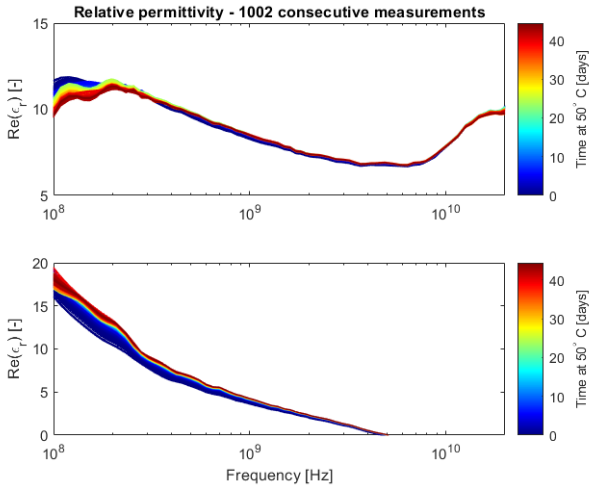

Figure 7. The measured dielectric response in online measurements.

Measurement results achieved can be seen as indications that the permittivity might prove a useful indicator for aging monitoring of some polymeric materials. To better determine the effect of ageing on the permittivity of the material measurements either need to be performed over very extended periods of time or at higher temperatures for a more accelerated ageing process. For this to be possible it would be beneficial to acquire a probe and/or probe system which is more robust and may function at higher temperature and have better handling of cable drift and sample contact variations.

As it has not been possible yet to identify any specific frequency region of interest, for the materials provided, frequency specific antenna sensor design and simulation has been postponed.

Sensitive analysing techniques

Isothermal microcalorimetry is used to age the different polymeric materials at different temperatures for different time duration. The corresponding heat flows (exotherm or endotherm) were measured while the materials have been aged.

IMC measurements were performed as per the standard test procedure recommended by the manufacturer. Steel ampoules along with the samples were held in the calorimeter for 15 min so that both the steel ampoule and sample will be in thermal equilibrium with the calorimeter. After 15 min of preheating, the ampoules were placed into the calorimeter and the measurement was started. Even though the steel ampoules along with the samples were preheated as aforesaid, the slight difference between the temperature of the ampoules and calorimeters can produce results with higher uncertainty. Therefore, 45 min of the heat flow values obtained using IMC, from the start of the experiments were not considered.

SEM technique is used for the elemental analyses for the selected aged samples. SEM instrument: ZEISS SEM Supra 40vp, equipped with Oxford Instruments EDX detector X-Max with 50 mm^2 window was used in this study. EPDM samples were attached to a circular stub using double sticking carbon tape. These stubs were then mounted on a circular sample holder and inserted in the vacuum chamber. For SEM imaging an acceleration voltage of 1 kV was used in high vacuum condition (around 1 x 10^{-6} mbar in the chamber), working distance around 3.5 mm, aperture 30 µm. Detector SE2 (Scattered Electron). While running EDX the voltage was increased to 15 kV and a low vacuum condition was required (around 35 Pa = 0.35 mbar) as the samples were not covered with a conducting film. Working distance around 8.5 mm, aperture 60 µm. Software used for EDX mapping was AZtec version 4.3 (Oxford Instruments). VPSE (Variable Pressure Secondary Electron) detector for SEM-images together with EDX-maps.

As shown in the Figure 9, the normalised heat flow from non-aged EPDM is significantly higher than the aged EPDM. This is expected because EPDM aged at 120 °C has already been exposed the higher temperatures than IMC test.

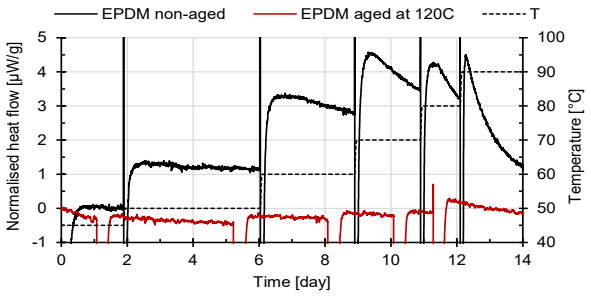

Figure 8. Normalised heat flow (µW/g) for EPDM non-aged and EPDM already aged at 120 °C. The IMC test was conducted at six different temperatures 45 °C, 50 °C, 60 °C, 70 °C, 80 °C and 90 °C for two weeks. Temperature steps are shown by a dotted line.

It can also be seen that reactivity (Normalised heat flow) for non-aged EPDM has increased at 50 °C, 60 °C and 70 °C in comparison to 45 °C. This is expected because thermal power should increase with the increase in temperature provided the mechanism responsible for thermal degradation remains the same. However, a noticeable reduction in the reactivity is seen at 80 °C in comparison to 70 °C. This indicates a change in the mechanism. The positive values of normalized heat flow for non-aged EPDM indicate exothermic processes and negative values for the aged EPDM indicate endothermic processes or lack of thermal degradation in presence of air.

Figure 9 shows the normalised heat flow (µW/g) for commercial grade rubbers without and with reinforcement. The IMC test was conducted at six different temperatures 45 °C, 50 °C, 60 °C, 70 °C, 80 °C and 90 °C. The heat flow values have increased with the increase in the temperature. The normalised heat flow is higher in reinforced in comparison the without reinforced commercial grade rubber material.

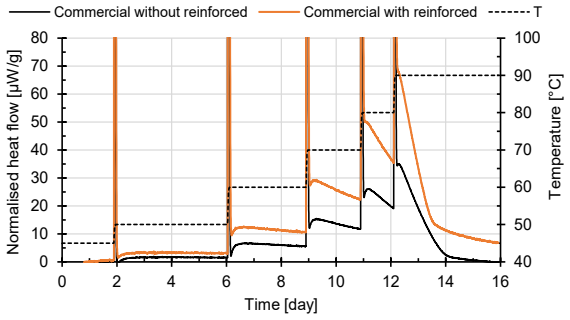

Figure 9. Normalised heat flow (µW/g) for commercial grade rubbers without and with reinforcement. The IMC test was conducted at six different temperatures 45 °C, 50 °C, 60 °C, 70 °C, 80 °C and 90 °C. Temperature steps are shown by a dotted line.

Three different model materials were tested at different temperatures as shown from Figures 10 and 11. The normalised heat flow (µW/g) for good material in the form of an O-ring are in agreement with the non-aged EPDM shown in Figure 10. For the 'bad' material in the form of an O-ring and a cutting from a rubber sheet, the normalised heat flow (µW/g) were lower at 50 °C and 60 °C in comparison to the good material O-ring. The normalised heat flow remains below zero at 70 °C, and 80 °C for both 'bad' materials. In comparison to the exothermic heat flow at 50 °C, 60 °C values at 70 °C, and 80 °C can be considered as endothermic for both 'bad' materials.

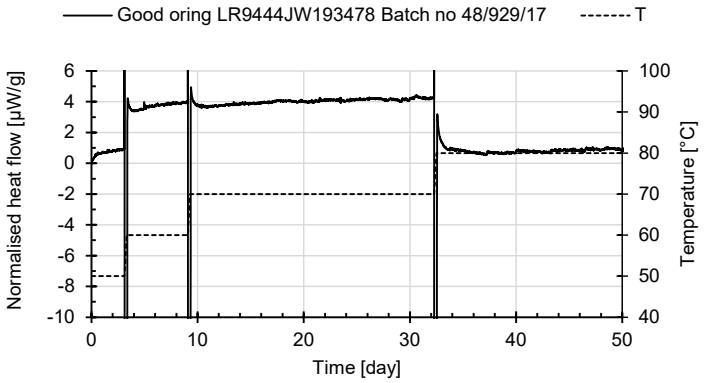

Figure 10. Normalised heat flow (mW/g) for good O-rings measured at 50 °C, 60 °C, 70 °C, and 80 °C. Temperature steps are shown by a dotted line.

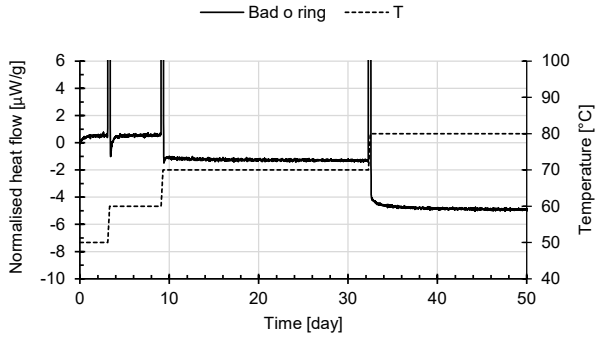

Figure 11. Normalised heat flow (mW/g) for 'bad' O-rings measured at 50 °C, 60 °C, 70 °C, and 80 °C. Temperature steps are shown by a dotted line.

SEM-EDX testing should be considered for qualitative analysis. First, two SEM-EDX analysis on fresh EPDM sample are presented, followed by aged EPDM (after IMC test 45–90 °C). The SEM measurement highlighted a difference between the unaged and aged materials and has provided an interesting change on the aged EPDM (after IMC test 45–90 °C) in comparison to the fresh EPDM. Figure 14 shows a SEM image for fresh EPDM using 100 µm magnification.

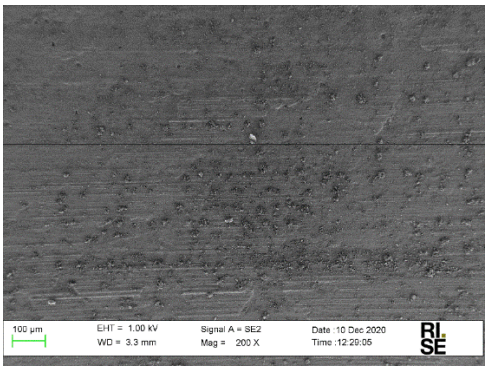

Figure 12. SEM image for fresh EPDM using 100 µm magnification.

EDX analysis as shown in Figure 15 indicates the presence of different elements on the surface. Carbon is shown on the picture to the left in a first row (C Kα1_2). Similarly, symbol O in O Kα1 stands for oxygen, S in S Kα1 for sulphur, Ca in Ca Kα1 for calcium, Cu in Cu Lα1,2 for copper and Zn in Zu Lα1,2 for Zinc. As it can be seen that carbon, oxygen and zinc are evenly distributed on the surface of the fresh EPDM rubber. Sulphur (S) is shown by the shiny yellow dots and image indicates the presence of S in the material, which is expected.

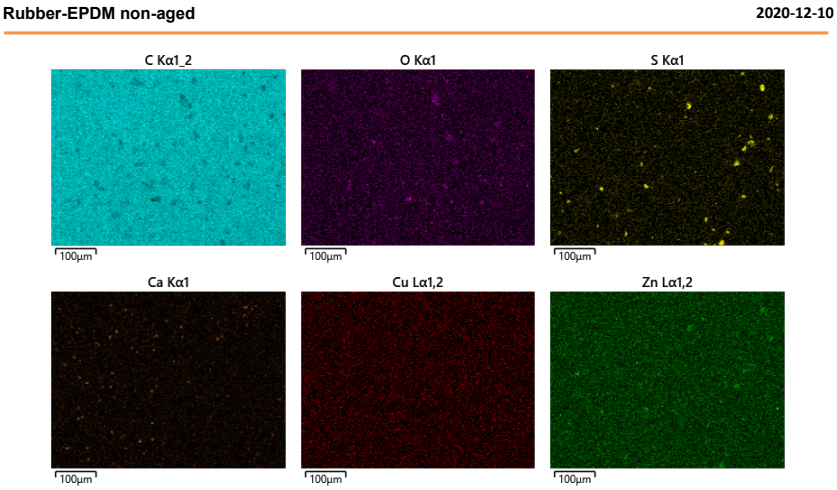

Figure 13. EDX analyses of the EPDM samples.

IMC tests have provided valuable information about the reactivity of the polymeric materials:

- The migration of antioxidants for example can be seen online in a real time.

- The heat flow signal closer to the real operating temperatures can been seen.
- The SEM analysis has provided a valuable information (migration and oxidation of antioxidant) which can be linked to the lower values of activation energy obtained at lower temperatures for example 60, 70 and 80 °C in comparison to the higher temperatures 90, 100 and 125 °C.

Improved interpretation of non-destructive testing data

One of the goals in SAMPO is to develop computational methods to assist in interpreting non-destructive testing data for polymeric NPP components. Molecular dynamics simulations can be applied in correlating the ageing effects in material to non-destructively measured material parameters. For example, ultrasonic technique seems to be well compatible with MD simulations. MD simulations has shown that the parameters required for sound velocity calculation, i.e. Young's modulus, Poisson's ratio and density values, could be extracted for PE and XLPE by mimicking standardized tensile test, as shown in Figure 14. However, the first simulations performed indicated that there is a discrepancy between the computationally predicted and literature values.

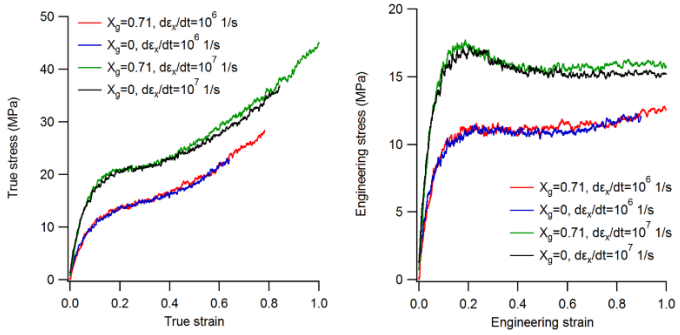

Figure 14. Simulated stress-strain curves for the PE (blue and black curves) and XLPE (red and green curves) systems. X_g stands for gel fraction, and $d\varepsilon_x/dt$ for strain rate in x direction.

During 2020 the material model was improved in order to obtain more accurate predictions [Rinta-Aho et al, 2021]. Firstly, the model was improved by taking into account the polydispersity of the chains that arises from the catalytic polymerization process. Secondly, it was verified that using united atom approach provided similar results as all-atom approach, justifying the use of the computationally much more affordable united-atom approach in interpretation of ultrasonic data.

The introduction of the polydisperse system yielded in improvements of the ageing model. Crystallinity degree increases as chain scission is induced in the amorphous phase, which is along with the experimental data found in literature. In

addition, the prediction of mechanical parameters (elastic modulus, Poisson's ratio, density, and sound velocity) as function of ageing seem to be possible with improved accuracy compared to the previously used monodisperse system.

Further development of ultrasound and DSC techniques for cable condition monitoring were continued in 2020. Aged PE and XLPE samples were measured in order to demonstrate the sensitivity of the methods. However, it seemed that even after 40 weeks of ageing the measurable material properties, i.e. ultrasound velocity and crystallinity degree did not change. However, the elongation at break values did decrease, as can be seen from Figure 15. It is interesting to see that the material remains its elasticity while its ability to withstand plastic deformation decreases. This explains why the ultrasound or crystallinity degree values stayed constant during this ageing period. Further clarification is required on the ageing mechanism to explain the results or predict when the changes in the elasticity begin to be seen.

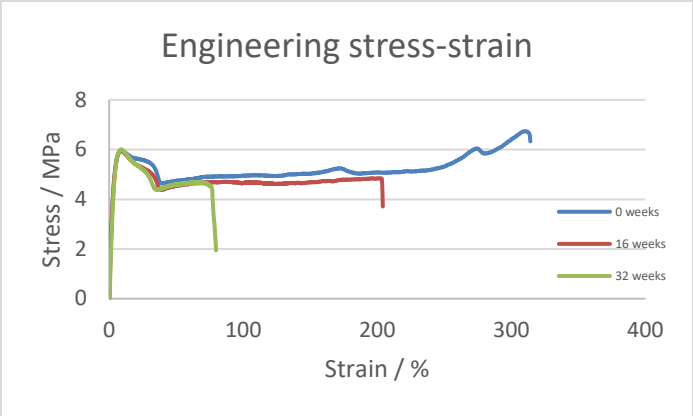

Figure 15. Engineering stress-strain curves for individual PE samples after 0, 16 and 32 weeks of ageing.

References

Joki, H., Sipilä, K. 2021. Identifying suitable methods for on-site polymer quality verification. VTT-R-00072-21. 14 pp.

Rinta-Aho, J., Sipilä, K., Vaari, J. 2021. Studying the ageing of polyethylene by using non-destructive testing methods and molecular dynamics simulations. VTT-R-00005-21. 20 pp.

8. Severe Accidents

8.1 Analytical severe accident research (ANSA)

Anna Korpinen, Tuomo Sevón, Veikko Taivassalo, Sara Ojalehto, Mikko Ilvonen, Jukka Rossi

VTT Technical Research Centre of Finland Ltd
P.O. Box 1000, FI-02044 Espoo

Abstract

In the frame of this project, national competence in the area of severe accidents has been further improved and the tools and methods in use have been validated in their intended purposes.

Third versions of VTT's MELCOR models for the Fukushima unit 2 and unit 3 accidents were developed. The reactor water level measurement systems were added to the models to have more information on the progress of the accidents. Measured pressures are reproduced well.

Models were developed to assess the hydrogen behaviour in the containment on more profound level. Especially was focused on developing a model for the combustion of ultra-lean hydrogen mixtures as those are more probable in the containment than richer ones. The computational results are mainly in a good agreement with experimental results.

To have an in-depth understanding of the phenomena affecting heat transfer in a crucible type core catcher, a CFD model was developed to simulate heat transfer in an externally cooled, homogeneous molten corium pool. The results agreed well with SIMECO-2 pre-test analysis conducted by Li (2016).

Pool scrubbing experiments for CsI aerosol and CH_3I considering the effect of NaOH and $Na_2S_2O_3$ were analysed with ASTEC. For CsI aerosols, ASTEC results seem to be very sensitive to particle size and the effect is larger on globular regime. At jet regime, the behaviour of analytical DF results is reverse to experimental results when considering the effect of inlet flow rate.

An international code benchmark was participated to compare VTT's in-house codes VALMA and ARANO with well-known international code packages for off-site dispersion and dose assessment. The results were well comparable wih the results of other participants.

Fukushima accident analyses

The Fukushima accident provides a unique opportunity for obtaining more information about the progress of severe accidents and their prevention and mitigation. Analyzing the accidents was started already in 2012 and since then, models for the

three units are continuously developed further when new information is received (Sevón, 2015; 2017).

The third versions of VTT's MELCOR models for the Fukushima unit 2 and unit 3 accidents were developed (Sevón, 2019; 2020a; 2020b). Compared to the second versions, detailed plant data from the OECD BSAF-2 project was utilized, making it possible to eliminate most of the uncertainties related to unknown dimensions of the plant. Now, most of the remaining uncertainties are related to physical and chemical models and nodalization in MELCOR, and uncertain boundary conditions, like the water injection rate with the fire engine and locations of various leaks. In addition, the reactor water level measurement systems were added to the models. The measurement system is based on measuring the pressure difference between two water-filled pipelines that were connected to the reactor. The measurements were distorted by boiling of water in the measurement system.

Unit 2 calculation reproduces the measured pressures well. This required manual tuning of the RCIC (Reactor Core Isolation Cooling) flow rates and flooding rate of the torus room with water from the tsunami. Drywell pressure during the accident is presented in Figure 1. Camera inspections have shown that the reactor lower head has failed and debris has been ejected to the pedestal. This could be reproduced by shifting the fire engine pump curve to lower pressures, so that the water injection did not succeed until 14 h after the start of the fire engine. To reproduce the measured reactor water level measurement at unit 2, was assumed a small safety relief valve gasket leak to the drywell, starting 78.5 h after the earthquake.

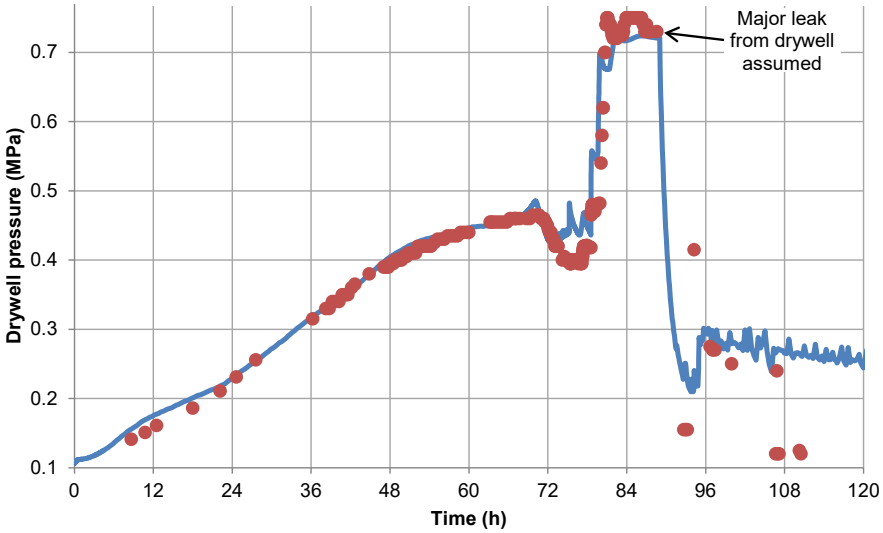

Figure 1. Measured and calculated drywell pressure during the Fukushima unit 2 accident.

Unit 3 calculation reproduced the measured reactor and containment pressures fairly well. This required manual tuning of the flow rates of the steam-driven cooling systems. A small leak from the recirculation pump seal to the drywell was assumed, starting 6 h 20 min after the earthquake, in order to reproduce the measured pressure increase.

At unit 3, the reactor water level measurement could be reproduced well as illustrated in Figure 2 by assuming that the reactor depressurization at 42.2 h was caused by automatic depressurization system (ADS) actuation, and that a leak of superheated steam from the steam line to the drywell started at the same time. ADS alone could not explain the distorted measurements. However, the calculations could not rule out a steam line failure as a reason for the depressurization, instead of ADS actuation.

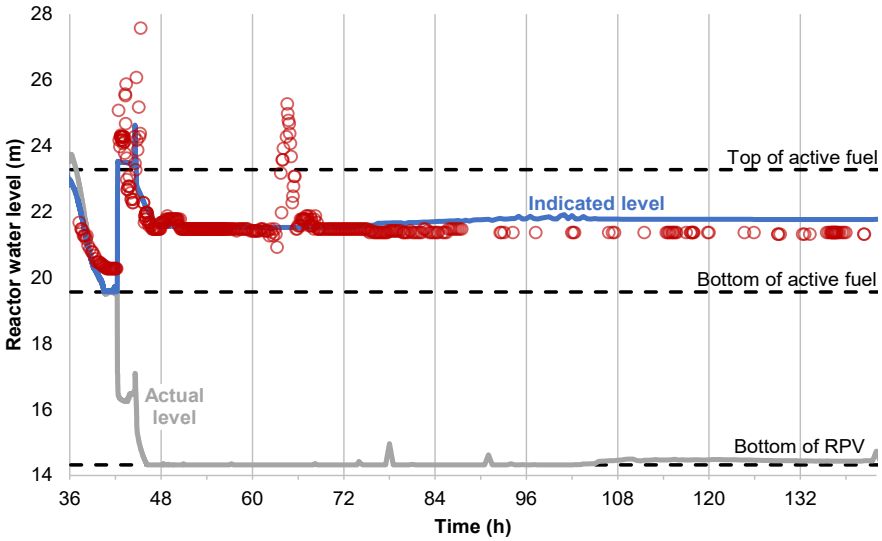

Figure 2. Water level in the reactor at unit 3. The grey line shows the actual calculated level, the blue line is the level indicated by the simulated measurement system, and the red circles are raw measurement data.

Hydrogen behaviour in the containment

Containment is the last safety barrier preventing the release of fission products and therefore ensuring the integrity of the containment is extremely important. Hydrogen combustion constitutes a risk to the containment but first hydrogen migration should be assessed to estimate the timing for the formation and composition of a flammable mixture.

A benchmark exercise on THAI TH-32 experiment was performed to study the applicability of the OpenFOAM modelling framework in predicting hydrogen behaviour in a containment and to study the efficiency of natural convection in eroding

light gas stratification. In the experiment, helium was used as a simulant for hydrogen. An applicable OpenFOAM solver and turbulence model were tested in a simplified geometry. Once a body-fitted polyhedral mesh was created for the THAI vessel, the warming and migration stages of the experiment were computed. Preliminary results for the helium concentration are in a good agreement with the experimental data.

Lean hydrogen mixtures are actually more probable than richer ones despite their analyses are less conclusive. VTT's model for the combustion of lean hydrogen mixtures has been developed further and extended to ultra-lean hydrogen concentrations close to the limit of flammability. The combustion model is implemented in the CFD-code Fluent as user defined functions.

The performance of the revised modelling framework was tested by computing eight THAI combustion experiments with downward and upward flame propagations (Taivassalo, 2020). In these experiments, the volume fraction of hydrogen in air varies from 7 to 11.8 %. The computational results are mainly in a good agreement with experimental results. The model reflects the influences of changes in the experimental conditions even quantitatively. Considering the complexity of the hydrogen combustion and the number of phenomena involved in these experiments the agreement is remarkable. An example of comparison of computational and experimental first flame arrival times is in Figure 3.

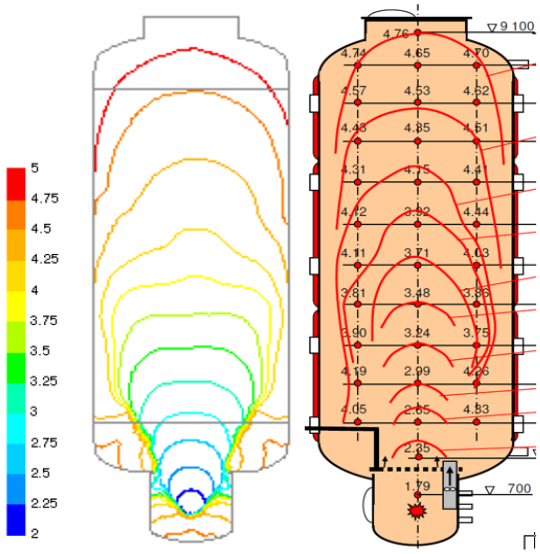

Figure 3. Computational (a) and experimental (b) first flame arrival time on a vertical cross-section for Test HD-3 with 9.01 vol-% for H_2.

In order to improve predictivity and reliability of combustion modelling, experimental results were further analyzed to determine the characteristics of a key model parameter (Taivassalo, 2021). Computation of hydrogen-air deflagrations are commonly based on the tracking of the propagation of a flame front. Wrinkling of the flame front complicates the numerical simulations especially in lean mixtures. As wrinkling increases the area of the reacting surface and thus the flame speed, it cannot be ignored in analyzing combustion. Detailed modelling of a wrinkled flame front would however require so dense spatial discretization that it is not computationally applicable when considering hydrogen combustion in large reactor containments. The influence of the subgrid-scale wrinkling is commonly incorporated by means of the wrinkling factor.

A number of models has been developed for the wrinkling factor in turbulent flows but the wrinkling factor is less comprehensively characterized in conditions without the turbulence-dominated wrinkling. Especially in lean hydrogen-air mixtures, the influence of the intrinsic instabilities and buoyancy on the wrinkling factor is important but poorly quantified.

If the volume fraction of hydrogen in air is more than about 10 %, the wrinkling factor does not vary significantly. In leaner mixtures close to the flammability limit, the wrinkling factor features a more complex behavior. Unfortunately the experimental data on these conditions is sparse because buoyancy complicates the utilization of deflagration experiments performed in spherical vessels.

In the performed study, the wrinkling factor is determined from the flame propagation in ultra-lean hydrogen-air mixtures in large-scale experiments. Measured data from combustion experiments performed in the THAI vessel is applied to evaluate the wrinkling factor as a function of time. Two components contributing the total wrinkling factor were identified. The first component increases relatively fast after the ignition and is a constant throughout the combustion process. This component is probably present in all lean hydrogen-air mixtures and its magnitude likely depends on the hydrogen concentration especially in lean mixtures. The contribution of the second component is significant in ultra-lean hydrogen-air mixtures. The second component increases almost linearly as a function of the pressure and dominates at high pressures.

Passive safety features

Proper functioning of the passive safety features under all circumstances will be ensured after validating the models against suitable experiments and developing reliable modelling practices. To have an in-depth understanding of the phenomena affecting heat transfer in a crucible type core catcher, the analyses should be made with a CFD-based tool.

The work was started by building an OpenFOAM model capable of simulating heat transfer in an externally cooled, homogeneous molten corium pool (Ojalehto, 2021). In order to validate the model, a SIMECO-2 experiment was simulated, and the results were compared to a pre-test analysis conducted by Li (2016).

Additionally, the effect of the mesh resolution and the mushy zone coefficient on the results were studied.

Higher mesh resolution and smaller cell size near the top surface resulted into higher peak of the heat flux, higher surface temperature, and a smoother flow field in the top region. Lower mesh resolution resulted into lower flow velocity near the crust surface, which also reduced the magnitude of the wall heat flux in that area. Mushy zone coefficient has a significant effect on the wall heat flux, crust/mushy zone thicknesses, and the pool temperature.

The final results were in a good agreement with the pre-test analysis by Li (2016). The most notable differences were the enhanced heat transfer in the upper part of the pool (Figure 4) and the thicker mushy zone (Figure 5) resulted by the OpenFOAM model. The most probable reason for the differences was the definition of the liquid fraction. In order to decrease uncertainties in these parameters, the solidification and thermophysical models should be modified to include an option for a custom temperature dependence for the liquid fraction.

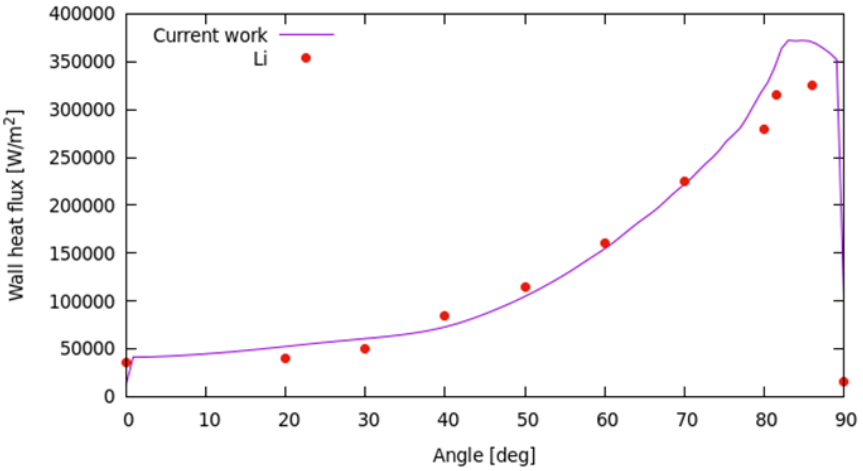

Figure 4. Comparison of the local wall heat fluxes along the pool angle.

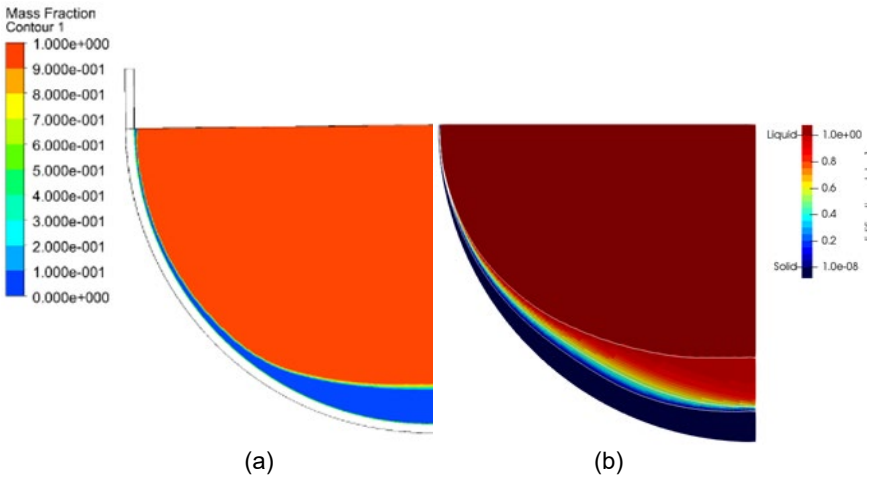

Figure 5. Comparison of the crust thicknesses: (a) result from the pre-test analysis by Li (2016), cropped for consistency, and (b) OpenFOAM model prediction.

Pool scrubbing

The final objective of severe accident management is to minimize the potential source term to the environment. An important mechanism in mitigating fission product release from the containment is pool scrubbing. Experiments in the SAFIR2022 MANTRA project aim at completing the experimental matrix for the effect of pool depth, flow rate into the pool and pool chemistry both for particulate and gaseous iodine species. These experiments provide excellent validation data for the integral codes.

Experiments for CsI aerosol and CH_3I considering the effect of NaOH and $Na_2S_2O_3$ were analysed with ASTEC V2.1.1.6 (Kärkelä et al., 2020). Experimental and analytical Decontamination Factor (DF) results for CsI were in a good agreement at the globular injection regime (Figure 6). The effect of NaOH seemed to be negligible. When the pool inlet flow reached the jet regime (69 l/min and 103 l/min), the analytical and experimental values started to differ more, analytical results being overly conservative. Further analyses for CsI aerosol (Kärkelä et al., 2021) showed, that experimental DF values increase with increasing inlet flow rate at the jet regime whereas analytical DF values decrease with increasing inlet flow rate not depending on the regime. So, the behaviour of the analytical results is reverse to the experimental results. The same outcome at the jet regime has been confirmed also by Herranz et al. (2018).

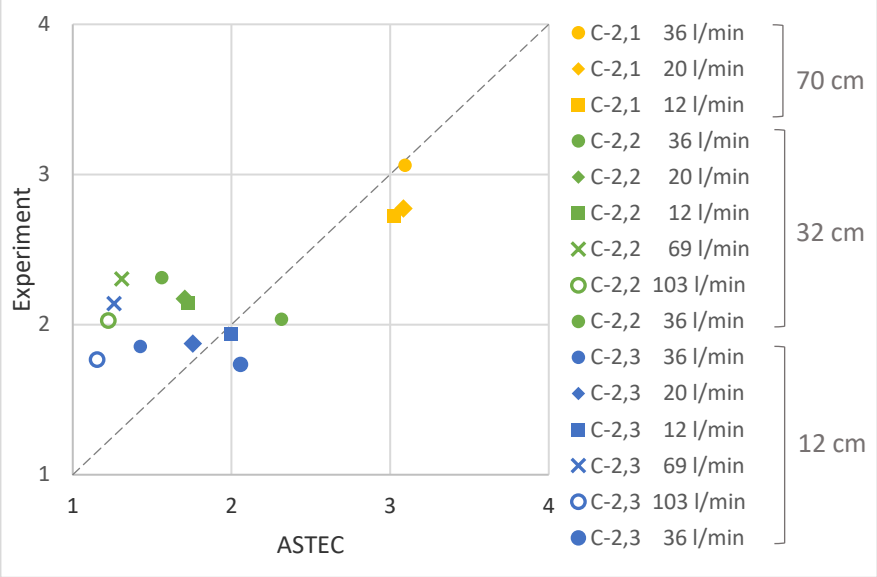

Figure 6. Comparison of the analytical and experimental results for CsI with NaOH added to the pool. Five different N_2 inlet flow rates and three different pool depths were examined. N_2 inlets 69 l/min and 103 l/min are on the jet regime.

As the results seemed to differ more with larger particles (Kärkelä et al., 2021), especially on the globular regime, a simple sensitivity study was performed for the ASTEC input parameters related to particle size distribution. The effects of geometric mean diameter (dg) and standard deviation of the first distribution (GSD) to the DF were studied on globular and jet regimes. Results on the jet regime are in Figure 7. It can be confirmed, that increasing geometric mean diameter and increasing standard deviation increase DF notably. The behaviour have somewhat similar trend on globular and jet regimes, but the resulted DF values are smaller on the jet regime. ASTEC results seem to be very sensitive to particle size and the effect is larger on globular regime.

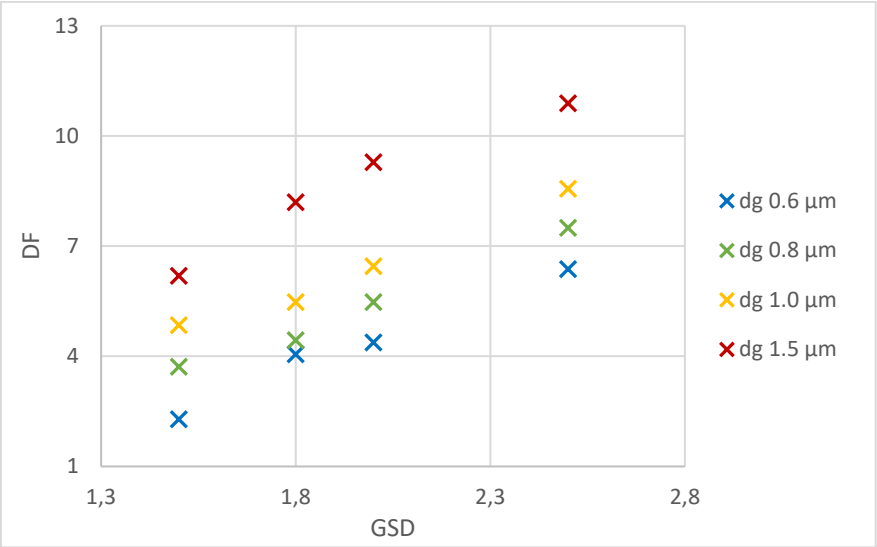

Figure 7. The effects of geometric mean diameter (dg) and standard deviation (GSD) to the DF on globular regime (N_2 inlet flow rate 24 l/min).

Experimental and analytical DF results for CH_3I were in a good agreement for a pure water pool (Kärkelä et al., 2020). In the experiments was observed that $Na_2S_2O_3$ could enhance trapping of CH_3I. Unfortunately, this effect could not be reproduced in the model by adding a chemical reaction either between $Na_2S_2O_3$ and dissolved CH_3I or $Na_2S_2O_3$ and I^-. Only increasing the individual mass transfer coefficient in the liquid side increased trapping of CH_3I. This must result from the way pool scrubbing phenomenon is modelled in ASTEC. It seems, that chemical reactions are not taking place at the bubble-water interface “during pool scrubbing”, but after the products are fully transferred into aqueous phase.

Environmental consequences

Severe accidents have shown that understanding of dispersion and exposure phenomena are needed for all-encompassing nuclear safety. Assessing the transport of radioactive release to evaluate the environmental consequences is especially important for defining the necessary protective actions. The physical phenomena are complicated, and they can be modelled by codes featuring various levels of sophistication.

A lot of verification and validation effort is needed to check the reliability of the codes being developed. Therefore, an international code benchmark BARCO (Benchmarking on Assessment of Radiological COnsequences) was participated to compare VTT’s in-house codes VALMA and ARANO with well-known international code packages for off-site dispersion and dose assessment. The benchmark was

based on a hypothetical release scenario from the Ukrainian Rivne NPP, which has two VVER-440/213 and two VVER-1000/320 reactors operating. A real weather scenario, with dispersion direction towards EU area, was chosen.

ARANO results are more limited than VALMA, because only time-independent (i.e. final, after cloud passage) radiation doses are readily available. Expectedly, ARANO predicted higher maximum doses than VALMA for the 24 hours long release, because only VALMA uses the realistic spread of wind direction, which comes from numerical weather prediction through the SILAM model. Total dose produced by VALMA is presented in Figure 8.

In comparison to the results of other participants, ARANO and VALMA results were well within the range of the 'bunch' of the result values. VALMA predicted lower dose rates near the source, but also higher dose rates at longer ranges. These results were explained by the dispersion data: data points at very close vicinity of source were not included, and at longer ranges was predicted some rain (causing wet deposition), which was not seen by other models.

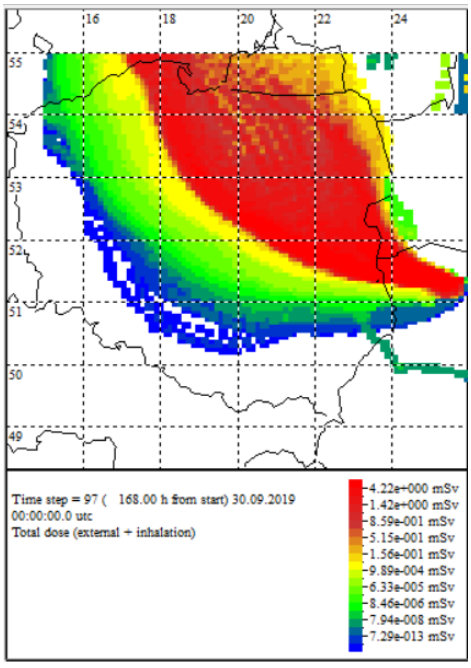

Figure 8. Total dose produced by VALMA taking into account external dose and inhalation (integration time is one week). Release source is at Rivne NPP in Ukraine and the plume is transported westward over Poland.

References

Herranz, L.E., Iglesias, R., Fontanet, J. 2018. Mitigation of source term in suppression pools: Large uncertainties in predictability. Annals of Nuclear Energy, Volume 120, p. 509-515.

Kärkelä, T., Korpinen, A. & Gouëllo, M. 2020. Pool Scrubbing of Gaseous and Particulate Iodine. Espoo: VTT. VTT Research Report VTT-R-00201-20. 34 p.

Kärkelä, T., Korpinen, A. & Gouëllo, M. 2021. Pool Scrubbing of CsI Aerosol. Espoo: VTT. VTT Research Report VTT-R-00175-21. 22 p.

Li, Y, 2016. CFD Pre-test Analysis of SIMECO-2 Experiment. Stockholm: KTH Royal Institute of Technology. 77 p.

Ojalehto, S. 2021. Computational Fluid Dynamics Analysis of Heat Transfer in Nuclear Reactor Core Melt Pool. Master's Thesis. 65 p.

Sevón, T. 2015. A MELCOR model of Fukushima Daiichi Unit 1 accident. Annals of Nuclear Energy, Volume. 85, p. 1–11.

Sevón, T. 2017. Fukushima Unit 1 Accident Modeling with MELCOR, Version 3. VTT Research Report VTT-R-04046-17. 43 p.

Sevón, T. 2019. Fukushima Unit 2 Accident Modeling with MELCOR, Version 3. Espoo: VTT. VTT Research Report VTT-R-01274-19. 64 p.

Sevón, T. 2020a. Analysis of reactor water level measurements during the Fukushima unit 2 accident. Nuclear Engineering and Design, Volume 366, paper 110760.

Sevón, T. 2020b. Fukushima Unit 3 Accident Modeling with MELCOR, Version 3. Espoo: VTT. VTT Research Report VTT-R-01242-20. 61 p.

Taivassalo, V. 2020. On modelling combustion of ultra-lean hydrogen-air mixtures. Espoo: VTT. VTT Research Report VTT-R-00226-20. 47 p.

Taivassalo, V. 2021. On the wrinkling characteristics of flames in laminar premixed ultra-lean hydrogen-air mixtures. Article draft.

8.2 Mitigation and analysis of fission products transport (MANTRA)

Teemu Kärkelä, Mélany Gouëllo, Ilona Lindholm, Unto Tapper, Tuomo Sevon

VTT Technical Research Centre of Finland Ltd
P.O. Box 1000, FI-02044 Espoo

Abstract

The aim in the MANTRA project during 2019–2022 is to investigate the transport and chemistry of gaseous and particulate fission products in severe accident conditions. In 2019–2020, the main focus was on the behaviour of iodine, caesium and tellurium, which are highly radiotoxic and the mitigation of their possible source term is of utmost importance. It was observed that the fission product deposits on the reactor coolant system (RCS) surfaces act as an important source of gaseous iodine, which can enhance the iodine source term. The tellurium transport was related to the oxidizing or reducing conditions in the RCS. The containment spray system was efficient in removing the airborne tellurium species. The pool scrubbing of fission product aerosols was notable and the decontamination factor increased significantly in the jet regime (high flow rates). Further actions to consider the long-term severe accident management issues were also taken. The follow-up of OECD/NEA STEM-2, BIP-3 and ESTER projects was carried out.

Introduction

In Fukushima Daiichi nuclear plant cooling of the reactor cores at units 1, 2 and 3 was lost due station black out. Since the cooling could not be restored in time, fuel damage took place in all three reactors and fission products were partly released from the core. As expected in a such severe accident, a high contribution to the source term to the environment was from iodine isotopes. In case of the Chernobyl accident, a high release of fission products to the environment took place and fission products (FPs) were spread e.g. across the continent of Europe.

Traditionally, it has been assumed that in a severe accident most iodine would be released from the fuel. Release to the containment would take place mostly as aerosol particles with gaseous fraction of about 5%. Concerning studies on iodine chemistry in the primary circuit, it is typically assumed that caesium iodide is the main iodine compound formed in the reactor coolant system. This assumption leads to a low release of gaseous iodine into the containment, because the current severe accident (SA) integral codes do not take into consideration the effect of FP deposits chemical reactions on the primary circuit surfaces. Also, the previous studies have mainly focused on the reactions taking place in the gas phase [Gouëllo et al., 2013; Grégoire et al., 2012]. However, the importance of surface reactions as a source of volatile iodine is even increased at the late phase of accident when the

thermalhydraulic conditions of the circuit are changing, as it has also been verified in the SAFIR2018 CATFIS and SAFIR2022 MANTRA projects [Gouëllo et al., 2018; Miyahara et al., 2020].

After being released from the reactor core the FPs, including tellurium, are transported to the containment through the reactor coolant system. In the RCS, the FPs released from the core are subjected to the surrounding prevailing conditions (e.g., oxidizing, reducing) and significantly lower temperatures than in the core. The change of conditions enables the FPs to condense and form aerosols of different composition and size. Once the FPs have reached the containment, they are exposed to various removal processes. One of the important safety features is the containment spray system (CSS), which removes both aerosols and gaseous species from the containment atmosphere and flushes them down to the sump. Although tellurium source term has been relatively well studied in terms of its release behavior from the core, the reactions and behavior of tellurium species following the core release still remain unclear.

Pool scrubbing is an important phenomenon in mitigating the source-term to the environment by retention of fission products passing through water pools of containment building. The majority of the experimental studies related to pool scrubbing have been conducted in 1980s and 1990s in order to establish suitable mod-els for predicting the pool decontamination efficiency under reactor-typical conditions. Results from past research on pool scrubbing showed that both experimental data on fission products retention in water pools as well as related model predictions were affected by large uncertainty bands, which make application to reactor cases questionable. Particularly, the retention of fission products in pools at high temperatures and high gas flow rates through the pool are not well-understood.

Long-term severe accident management address physical and chemical processes in a severely damaged nuclear power plant after the period of 72 hours or after the plant has reached the safe stable state. The maintenance of safe stable state requires continuous decay heat removal, sub-criticality and prevention of uncontrolled leakages of radioactive material from the containment. The lessons learnt e.g. from the Fukushima accident need to be exploited.

Both OECD/NEA STEM-2 (Source Term Evaluation and Mitigation Issues) and OECD/NEA BIP-3 (Behaviour of Iodine) projects were followed-up and the projects ended in 2019. As a continuation, the follow-up of a new, four-year OECD/NEA ESTER (Experiments on Source Term for Delayed Releases) project started in 2020.

Primary circuit chemistry of iodine and caesium

After fission products have been released from the overheated and molten fuel, they are transported through the reactor coolant system and fission products will reach areas at lower temperature. As a consequence, vapour condensation and particle nucleation processes takes place in the gas flow. If vapour condensation takes place close to the surfaces of primary circuit, a layer of condensate can be formed

on it. Particles in the gas flow may also deposit on the circuit surfaces together with control rod and structural materials. The set-up of the EXSI-PC experimental facility used for the studies on iodine and caesium chemistry in the primary circuit conditions is presented in Figure 1. Inactive materials have been used to simulate fission products. The precursor materials were CsI, CsOH, I_2 and H_3BO_3.

For the first set of experiments, I_2 vapour was generated by the sublimation of molecular iodine pellets. The gaseous I_2 passed above an evaporation crucible filled with CsOH aqueous solution and placed inside the furnace.

During the second set of experiments, CsI particles were generated by nebulization of a concentrated caesium iodide aqueous solution and then passed through a Thermal Gradient Tube (TGT). The gaseous H_3BO_3 was generated by vaporisation from a crucible placed inside the furnace.

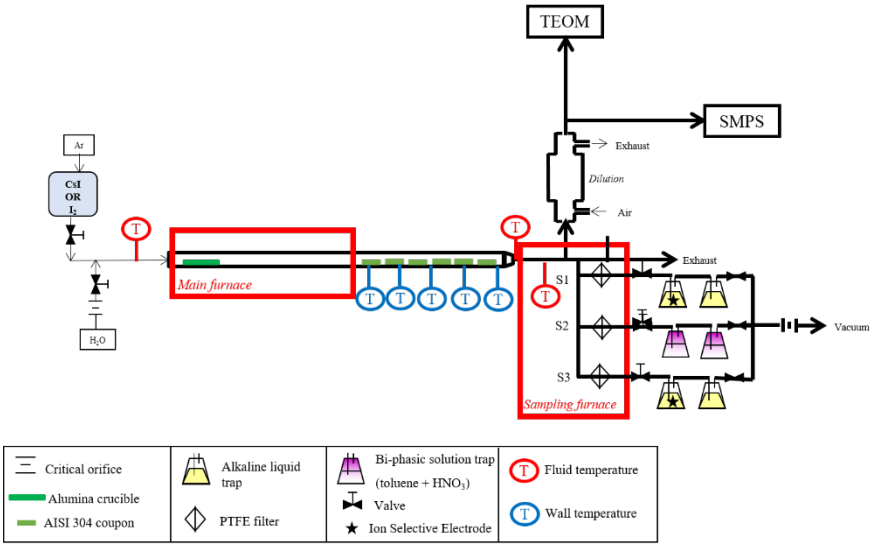

Figure 1. Schematics of the EXSI-PC experimental facility.

The evaporation crucible containing the precursor material was placed in a tube inside the reaction furnace. The furnace tube used in the experiments was made of stainless steel (AISI 304), which was pre-oxidized before the experiment. The furnace was heated to 700 °C. The carrier gas was then fed into the heated furnace, where the source materials reacted with each other, with gas and with the surface of the crucible. Reaction products were then transported with the gas flow through four sampling lines:

(1) A first line headed for aerosol on-line measurement. Upstream from the online aerosol measurement devices, the flow was diluted in order to decrease the concentration of the produced particles low enough for the instrumentation as well to decrease the temperature of the flow below 313 K. The particle number size distributions were measured with a TSI Scanning

Mobility Particle Sizer (SMPS), with series 3080 platform, series 3081 Differential Mobility Analyser (DMA) and series 3775 Condensation Particle Counter (CPC). The aerosol mass concentration was monitored by Tapered Element Oscillating Microbalance Series 1400a (TEOM).

(2) A second line was used to sample particles and gaseous species. The line was equipped with a polytetrafluroethylene (PTFE) membrane filter (hydrophobic, poral grade 5.0 µm, 47 mm, Mitex®) and two liquid traps assembled in series. They were filled with a solution of 0.1 M sodium hydroxide (NaOH) in water (150 ml). During the test, the first liquid trap was equipped with the Ion Selective Electrode (ISE) in order to monitor on-line the concentration of iodine. After the test, the solutions and the leachants from filters (50 ml) were analysed by Inductively Coupled Plasma Mass Spectrometry (ICP-MS). The analyses were performed with a Thermo Fisher Scientific HR-ICP-MS Element2 apparatus. This line was used for the first 20-minute sampling (S1).

(3) A third line was used with a similar configuration as the second line, except the nature of the liquid traps. The liquid traps were filled with an immiscible solution composed of aqueous phase (nitric acid, pH=3; 50 ml) and an organic phase (toluene; 100 ml) in order to selectively separate hydrogen iodide (HI) from molecular iodine (I_2). Due to its non-polarity, molecular iodine is expected to be trapped in the organic phase while hydrogen iodide would stay in the aqueous phase. This line was used for the second 20-minute sampling (S2). The quantification of molecular iodine in toluene was carried out by UV-visible spectroscopy using a Perkin Elmer spectrophotometer model Lambda 900.

(4) The last line had the same configuration as the second line. This line was used for the third 20-minute sampling (S3).

Table 1 describes the test matrix and conditions.

Table 1. Experiments conducted on primary circuit chemistry of iodine and caesium during the past two years.

Exp.	Precursor	Carrier gas composition	Other
MANTRA-1	I_2	Ar/H_2O (86.7/13.3 vol-%)	Reference experiment for I_2 behaviour
MANTRA-2	CsOH	Ar/H_2O (86.7/13.3 vol-%)	Reference experiment for CsOH behaviour
MANTRA-3	I_2	Ar/H_2O (86.7/13.3 vol-%)	
	CsOH		
MANTRA-3bis	I_2	Ar/H_2O (86.7/13.3 vol-%)	
	CsOH		
MANTRA-4	I_2	Ar/H_2O (86.7/13.3 vol-%)	
	CsOH		

Exp.	Precursor	Carrier gas composition	Other
MANTRA-5	CsI particles	Ar/H_2O (86.7/13.3 vol-%)	Deposition phase (i.e. “phase 1”)
MANTRA-6	H_3BO_3 gas	Ar/H_2 (95/5 vol-%)	Blank behaviour
MANTRA-7	CsI particles	Ar/H_2O (86.7/13.3 vol-%)	Deposition phase (i.e. “phase 1”)
MANTRA-7_Re	Deposited CsI	Ar/H_2 (95/5 vol-%)	Reaction/vaporisation phase (i.e. “phase 2”)
MANTRA-8	CsI particles	Ar/H_2O (86.7/13.3 vol-%)	Deposition phase (i.e. “phase 1”)
MANTRA-8_Re	Deposited CsI + H_3BO_3 gas	Ar/H_2 (95/5 vol-%)	Reaction/vaporisation phase (i.e. “phase 2”)

The first set of experiments with I_2 and CsOH has confirmed the formation of CsI particles [Gouëllo, 2019]. From the second set of experiments, it was highlighted that the deposited CsI partlcles were subjected to revaporization process in Ar/H_2 atmosphere; gaseous iodine was released from the deposits. When H_3BO_3(g) was present in the carrier gas (Ar/H_2), the percentage of gaseous iodine released was higher, see Figure 2. The interpretation of the SMPS and TEOM results [Gouëllo, 2021] also suggested that the presence of H_3BO_3(g) would then have an influence on the transport of the deposited/condensed CsI as it showed different behaviour than during revaporisation/resuspension under Ar/H_2.

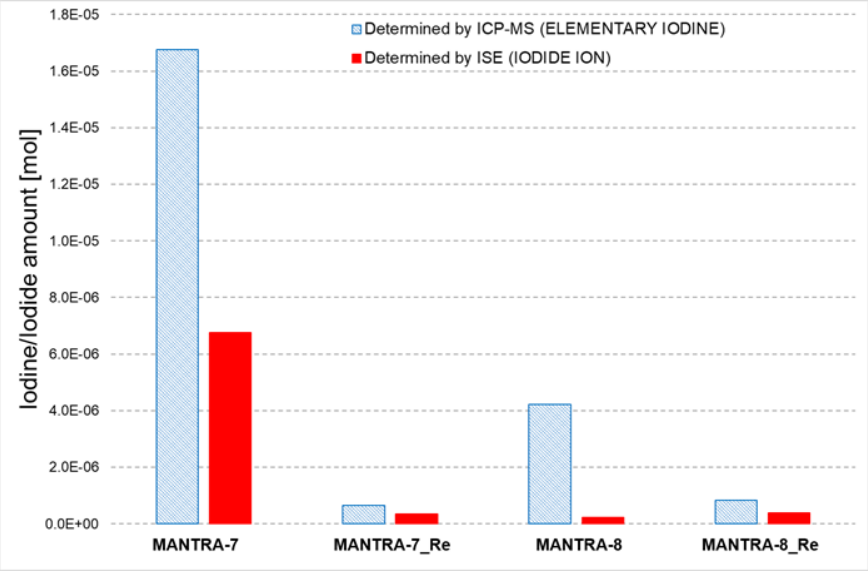

Figure 2. Amount of gaseous iodine transported during the second set of experiments [Gouëllo, 2021].

In parallel to the experimental work, analytical work was initiated in 2019. It consisted in validating the models implemented in the SOPHAEROS module (version v2.1.1.6) of the Accident Source Term Evaluation Code (ASTEC) [Cousin et al., 2008] on the basis of a comparison with the obtained experimental results. As a first step, comparison was made with the experimental data of several experiments performed previously under Ar/H_2O atmosphere [Gouëllo, 2021]. The analytical work has highlighted good agreement on the behaviour of compounds between SOPHAEROS models and the experimental results obtained for pure compounds (I_2, CsI). However, it has shown discrepancies when another compound was considered in the chemical system. Especially looking at the release of gaseous iodine, the amount of gaseous iodine was systematically underestimated, see Figure 3. This stresses the need to take into account condensed-phase reactions in the SOPHAEROS code in future.

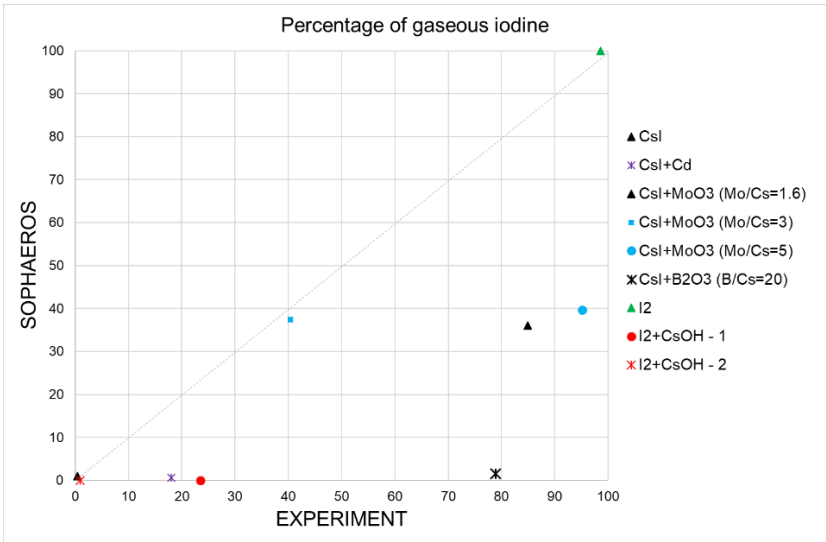

Figure 3. Comparison of the ASTEC/SOPHAEROS V2.1.1.6 results to the experimental values for the percentage of gaseous iodine [Gouëllo, 2021].

Tellurium transport in the RCS and mitigation by the containment spray system

The radiotoxic tellurium has two main features, which emphasize its safety importance: 1) tellurium is highly volatile and 2) the decay products consist of iodine. As the behaviour of tellurium after being released from fuel is not fully understood, a study to improve the knowledge was initiated. These experiments covering the transport of tellurium in the RCS and the mitigation of airborne tellurium species using a containment spray system were conducted using the experimental facilities

of VTT in collaboration between VTT, Chalmers University of Technology and Oslo University as part of NKS-R activity.

The transport of tellurium in primary circuit conditions was investigated [Espegren et al., 2020]. Metallic tellurium precursor was exposed to oxidizing and reducing conditions at ca. 1200 °C. The release and transport of gaseous and aerosol species was examined. As an example, a micrograph of the formed tellurium containing aerosol is shown in Figure 4.

The metallic tellurium precursor was released and transported with a rather constant rate in a dry or humid nitrogen atmosphere. In case of an air atmosphere, the transport of tellurium was notably higher at first. However, the metallic tellurium seemed to be oxidised by the oxygen in the course experiments. It led to a reduction of tellurium release. The fraction of tellurium transported through the model primary circuit (in comparison to the release) was the highest in the air atmosphere, see Figure 5.

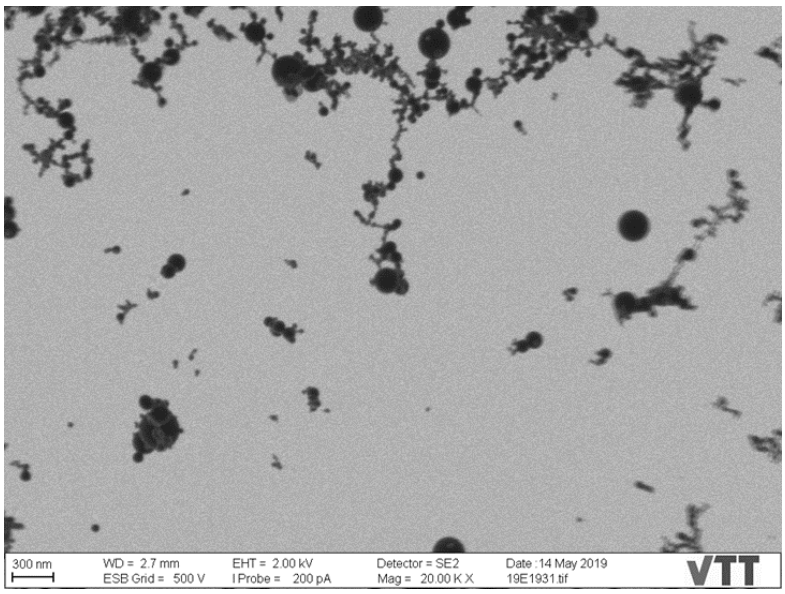

Figure 4. Micrograph of tellurium containing aerosol – precursor TeO_2 vaporized in a dry air atmosphere at ca. 1200 °C. A significant fraction of the analyzed particles were long agglomerate chains composed of primary particles with a diameter of less than 100 nm

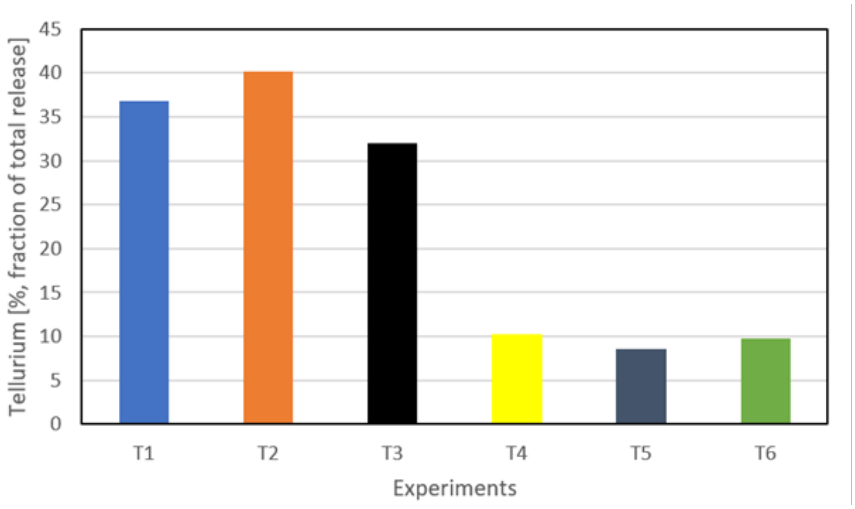

Figure 5. Fraction of tellurium transported through the model primary circuit (in comparison to the release) was higher in the air atmosphere (Experiments T1 to T3) than in the nitrogen atmosphere (Experiments T4 to T6). The temperature of the circuit decreased from ca. 1200 °C to 30 °C in the experiments.

The retention of tellurium aerosols (Te, TeO_2) by a containment spray system model was also examined [Kärkelä et al., 2020]. Tellurium dioxide and metallic tellurium precursors were exposed to oxidizing and reducing conditions. The chemistry of spray droplets was varied from water to alkaline borate solutions. The removal efficiency was derived.

The water droplets were efficient in trapping the airborne particles. Further increase in the trapping efficiency was observed when the chemistry of droplets was varied, see Figure 6. The removal efficiency was high for TeO_2 and Te in an air atmosphere, but the removal efficiency for metallic tellurium decreased in an nitrogen atmosphere.

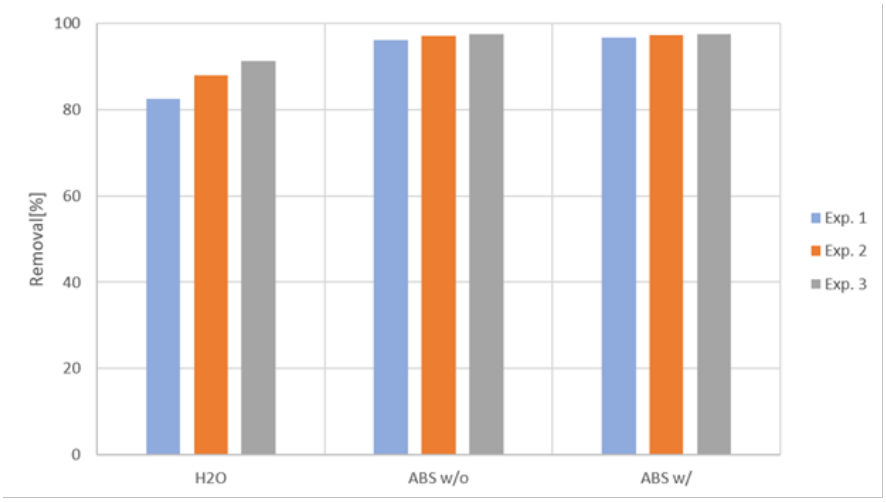

Figure 6. Removal efficiency of a containment spray system model for tellurium dioxide particles in an air atmosphere. The water droplets were efficient in trapping the airborne particles. Further increase in the trapping efficiency was observed when the chemistry of droplets was varied using alkaline borate solutions.

Pool scrubbing of CsI aerosol

The water pools of containment building may act as important sinks for the fission products by trapping the radiotoxic species from the gas flow directed into the pool. However, most of the existing information on this phenomenon is based on the data of experiments performed at low temperatures and low flow rates into the pool. Therefore, the current models for this phenomenon in the severe accident analysis codes are also lacking of data and thus, the models are not able to simulate the pool scrubbing in detail.

As part of MANTRA, several series of experiments have been performed using CsI, I_2 and CH_3I as precursors [Kärkelä et al., 2020; Kärkelä et al., 2021]. The pool temperature has ranged from low pool temperatures up to 70 °C. The gas flow rate into the pool has been varied from the low (globular regime) to high (jet regime) flow rates. The pool depth has ranged from 10 cm to 70 cm. The performed experiments have been simulated using the ASTEC code in the SAFIR2022 ANSA project.

For the CsI aerosol experiments in 2019–2020, the obtained decontamination factor was in a range from 2 to 4 in the globular regime and it increased up to ca. 12 in the jet regime (at the studied conditions), see Figure 7.

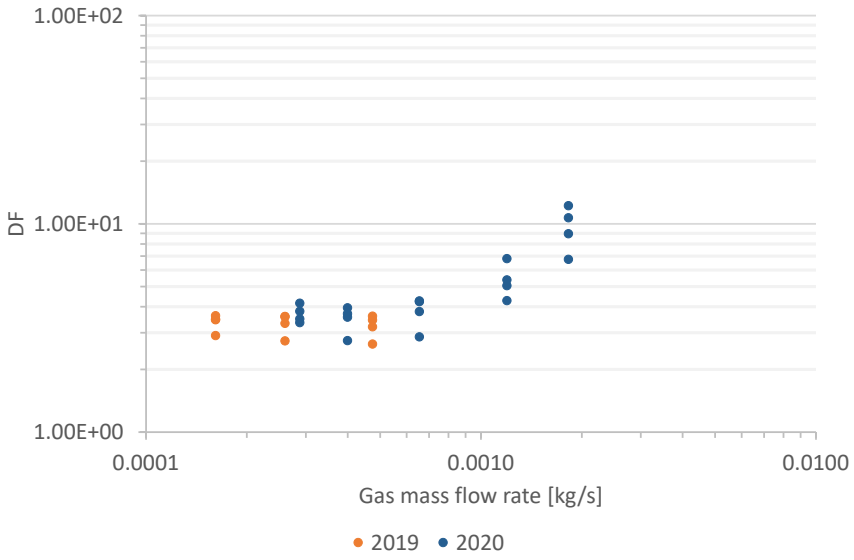

Figure 7. Decontamination factor results for CsI aerosol (VTT studies in 2019 and 2020). The decontamination factor (DF) results are given as a function of gas mass flow rate into the pool (jet regime > 0.001 kg/s).

Related to the NUGENIA TA2.4 area IPRESCA project dedicated to (gaseous and aerosol FP) pool scrubbing research, MANTRA is coordinating a task on gaseous iodine retention in the pool. The project includes over 30 international organizations around the world.

Long-term severe accident management

In the long-term severe accident management study during 2019, the key outcomes and recommendations of OECD/NEA, IAEA, US DOE and EU SARNET working groups or projects was reviewed and a limited scope overview of recent Fukushima-related journal articles from the past three years for the background information was summarized. To recognize useful and sustainable research topics close discussions with all Finnish utilities and STUK were carried out. The long-term accident management research topics that are interesting for the Finnish NPPs were identified and listed. The behaviour of caesium was emphasized.

In 2020, the goal was to investigate (based on the published literature during 2010's) what is the chemical form and morphology of caesium contamination after a severe accident [Lindholm, 2020]. The post-accident investigations at and around the Fukushima plant site provide a broad scope of information. Where applicable, the observations and outcomes obtained from Fukushima were compared with the Chernobyl accident data. In addition to characterization of contamination, the study addressed the latest developments in the clean-up methods of caesium

contamination. The study also supports thinking of aspects related to long-term severe accident management.

The follow-up of OECD/NEA STEM-2, BIP-3, ESTER projects

The follow-up of both four-year OECD/NEA STEM-2 and three-year BIP-3 projects [OECD, 2017] continued until 2019. The OECD/NEA STEM-2 project composed of two experimental main topics: ruthenium transport in primary circuit conditions (as also studied in the SAFIR2018 CATFIS project) and behaviour of particulate iodine on containment surfaces. The OECD/NEA BIP-3 project focused especially on the adsorption and desorption phenomena of gaseous inorganic and organic iodine on the painted containment surfaces. The four-year OECD/NEA ESTER project follow-up started in 2020 [OECD, 2021]. The objective is on the delayed releases due to chemical remobilisation from high temperature (reactor coolant system) fission product deposits (as also studied in the SAFIR2022 MANTRA project). Another objective in the ESTER project is to study the iodine reactivity (I_2 and IOx) with organic compounds, which may be present in the containment atmosphere. The aim is to assess the source of organic iodine formation, other than iodine-paint interaction. Another important part of the ESTER project is to compare the performance of various severe accident analysis codes and the user effect.

References

Cousin, F., Dieschbourg, K., Jacq, F., 2008. New Capabilities of Simulating Fission Product Transport in Circuits With ASTEC/SOPHAEROS v. 1.3. Nucl. Eng. Des. 238, 2430–2438. https://doi.org/https://doi.org/10.1016/j.nucengdes.2008.03.018

Espegren, F., Kärkelä, T., Pasi, A.-E., Tapper, U., Kučera, J., Lerum, H.V., Omtvedt, J.P., Ekberg, C., 2020. Tellurium transport in the RCS under conditions relevant for severe nuclear accidents, Submitted to Progress in Nuclear Energy.

Gouëllo, M., Mutelle, H., Cousin, F., Sobanska, S., Blanquet, E., 2013. Analysis of the iodine gas phase produced by interaction of CsI and MoO_3 vapours in flowing steam, Nuclear Engineering and Design 263, 462-472.

Gouëllo, M., Hokkinen, J., Kärkelä, T., Auvinen, A., 2018. A Scoping Study of Chemical Behaviour of Caesium Iodide in Presence of Boron in Condensed Phase (650 °C and 400 °C) under Primary Circuit Conditions. Nucl. Technol. 203, 66–84. https://doi.org/https://doi.org/10.1080/00295450.2018.1429111

Gouëllo, M., 2019. Experiments and ASTEC Analyses on Iodine and Caesium Chemistry Report VTT-R-01244-19. Espoo, Finland.

Gouëllo, M., 2021. Progress report of the Experiments and ASTEC Analysis on Iodine and Caesium Chemistry Report VTT-R-00042-21. Espoo, Finland.

Grégoire, A.-C., Mutelle, H., 2012. Experimental study of the [Mo, Cs, I, O, H] and [B, Cs, I, O, H] systems in the primary circuit of a PWR in conditions representative of a severe accident, In the proceedings of NENE2012 conference, Ljubljana, Slovenia.

Kärkelä, T., Pasi, A.-E., Espegren, F., Sevón, T., Tapper, U., Ekberg, C., 2020. Tellurium retention by containment spray system, Submitted to Annals of Nuclear Energy.

Kärkelä, T., Korpinen, A. & Gouëllo, M., 2020. Pool Scrubbing of Gaseous and Particulate Iodine. Espoo: VTT. VTT Research Report VTT-R-00201-20. 34 p.

Kärkelä, T., Korpinen, A. & Gouëllo, M., 2021. Pool Scrubbing of CsI Aerosol. Espoo: VTT. VTT Research Report VTT-R-00175-21. 22 p.

Lindholm, I., 2020. Literature survey on radiocesium source term in severe accidents - chemistry, morphology and clean-up, VTT-R-01248-20.

Miyahara, N., Miwa, S., Gouëllo, M., Imoto, J., Horiguchi, N., Sato, I., Osaka, M., 2020. Experimental Study on Transport Behavior of Cesium Iodide in the Reactor Coolant System under LWR Severe Accident Conditions [WWW Document]. J. Nucl. Sci. Technol. https://doi.org/https://doi.org/10.1080/00223131.2020.1782281

OECD, 2017: https://www.oecd-nea.org/jcms/pl_32256/nea-joint-projects

OECD, 2021: https://www.oecd-nea.org/jcms/pl_46387/new-joint-project-experiments-on-source-term-for-delayed-releases-ester

9. Research Infrastructure

9.1 Barsebäck reactor pressure vessel material used for true evaluation of embrittlement (BRUTE)

Ulla Ehrnstén, Pentti Arffman, Jari Lydman, Noora Hytönen, Zaiqing Que

VTT Technical Research Centre of Finland Ltd
P.O. Box 1000, FI-02044 Espoo

Abstract

The objective of the BRUTE Excellence SAFIR2022 project is twofold, i.e., to perform mechanical and microstructural investigations of Barsebäck 2 boiling water reactor (BWR) reactor pressure vessel (RPV) materials in irradiated and thermally aged conditions. These results are used for determination of the compatibility of the surveillance program, used to assess the influence of ageing and assessment of the structural integrity of the RPVs, with the results of the real RPV material.

The other main objective is to pioneer the new infrastructure in the Centre for Nuclear Safety, CNS, VTT. Building a new national infrastructure is a huge undertaking, and has been supported by several SAFIR and VTT projects. BRUTE is taking the CNS infrastructure into final use, and lessons learned are used also in future projects.

The pioneering and validation work has resulted in accreditation of all mechanical test methods at CNS, after overcoming smaller and bigger challenges. The material investigations have resulted in high-quality results on mechanical properties and microstructure, improving the understanding of irradiation induced embrittlement and factors affecting brittle fracture initiation.

Introduction

The objective of the BRUTE Excellence SAFIR2022 project is twofold, i.e., to perform mechanical and microstructural investigations of Barsebäck 2 boiling water reactor (BWR) reactor pressure vessel (RPV) materials in irradiated and thermally aged conditions and to pioneer the new infrastructure in the Centre for Nuclear Safety, CNS, VTT.

Determining the compatibility of the surveillance programs, used to assess the influence of ageing and assessment of the structural integrity of the RPVs, using results obtained from real RPV materials, is highly important, as the RPV is the most important component of a nuclear power plant. Having access to material from a real component is unique. The BREDA project in Sweden, the Barsebäck Research and Development Arena, has planned, executed and funded the cutting of the trepans, and is a prerequisite for the BRUTE project.

Eight trepans with a diameter of 200 mm and full RPV wall thickness (~130–160 mm) were cut from the B2 RPV in April 2018, both from the beltline welds, subjected to thermal load and neutron irradiation during the 27 years of operation, as well as from the vessel head, subjected only to thermal load. Materials from surveillance programmes and from accelerated irradiation to mimic about 200 years of operation are also available as well as data from earlier test campaigns. This makes the material selection unique.

Validation of methods

Validation of mechanical test methods has been a major undertaking during the first two years of the BRUTE project, though simultaneously making progress on mechanical testing using the validated methods. The microstructural methods were validated early, and therefore the microstructural investigation could be started from the beginning of BRUTE. Cutting is a huge undertaking in BRUTE, dealing with trepans nearly 30 kg in weight. Electric discharge machining (EDM) was selected as the main cutting method as part of the design phase for the CNS [1].

The validation of microstructural investigation methods comprised of validating Light Optical Microscopy (LOM), Scanning electron microscopy (SEM) with attached detectors such as Energy dispersive X-ray spectroscopy (EDS) and backscattered electron diffraction (EBSD), and hardness measurements. The two aforementioned methods were calibrated for magnification with ascertain resolution and so forth as part of the installation and training.

The hardness measurement validation was performed as part of the accreditation efforts in 2018. The effect of surface quality was additionally evaluated with the expected outcome that EDM cutting, or fine lathe cutting is not sufficient but polishing is required to obtain results, which are not affected by the surface preparation [2].

The cutting processes were validated using dummy steel material with similar dimensions as the trepan. The main cutting method is EDM. In 2019, EDM was simultaneously subject to optimisation work as part of the SAFIR2022 LABWAST project, especially concerning the water circulation system. The object was to minimize contamination of the water circulation system, and different possibilities were evaluated before deciding on the filter system. The cutting accuracy and surface quality was determined and both fulfil the set requirements.

Preparations for handling the 30 kg trepans, Figure 1a, exceeding the size used in the design for CNS has included lifting and movement trials using magnet lifters and dummy trepans (shaft pieces with same dimensions as the trepans), Figure 1b. A jig for the EDM was designed and manufactured, delivered, assembled and tested, Figure 1c. A dummy trepan was then cut into three pieces using EDM to evaluate the cutting speed and cutting and surface quality.

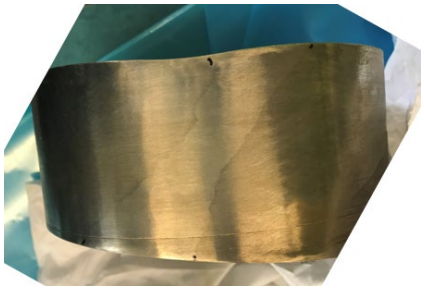

(a)

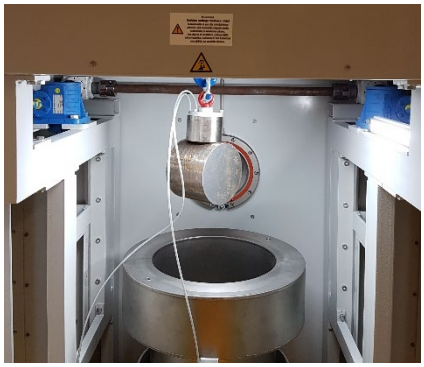

(b)

(c)

Figure 1. (a) Appearance of a ∅200 mm, 40 kg trepan, (b) training moving a dummy trepan in and from a transportation cask, (c) and cutting of a dummy trepan using the designed jig and the new EDM.

After the cutting procedure was validated, cutting plans were prepared for the first two trepans, and specimens were cut, Figure 2.

Mechanical test validation has been performed for tensile testing using flat, sub-size specimens compared to standard size, impact toughness testing using Charpy V-notch (CVN) specimens and fracture toughness testing. Accreditation was achieved for all methods in 2019, and validation of fracture toughness testing using miniature compact tension (C(T)) specimens, which are cut from tested CVN specimen halves, was performed in 2020 [3,4].

The impact test validation was performed using SSAB UHB steel with a tensile and yield strength of about 640 MPa / 340 MPa. It had been used in a national comparison test with more than ten participants. The comparison was done compared to the accredited VTT Research Hall laboratory data, and the results were within ±2σ standard deviation.

(a)

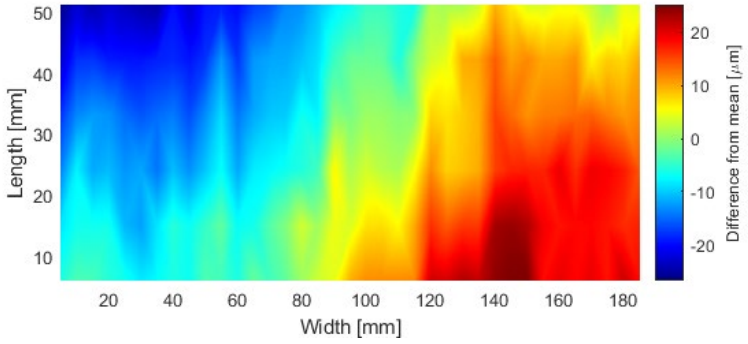

(b)

Figure 2. (a) Appearance of a 10 mm thick slice cut using EDM from a ∅200 mm, 40 kg dummy trepan, (b) and results from surface evenness measurements.

The tensile test validation was performed using Laser 460MC Plus hot-rolled cold-forming steel plate, from which miniature tensile test specimens where cut perpendicular to the rolling direction using EDM from different depths of the plate. 10 specimens were tested at room temperature and the results were compared to a similar test series performed at the accredited VTT Research Hall laboratory, Table 1. As can be seen from the table, the strength values are in good correlation.

Table 1. Tensile test verification results.

	ReH (MPa)	**ReL (MPa)**	**Rp0.2 (MPa)**	**Rm (MPa)**
VTT CNS	482	464	479	580
St. dev.	12	9	11	11
VTT RH	486	480	480	597
St. dev.	12	9	10	13

The validation of fracture toughness testing using miniature C(T) specimens encompassed in the validation were pre-test measurements, fatigue pre-cracking, proper testing, fracture surface imaging as well as data analysis following ASTM E1921-19 [5]. The validation was performed with two different materials, i.e., NESC-1 project material and CRIEPI material from an earlier round-robin. Both are well-characterised materials, and therefore considered to be suitable for the validation.

Two different set-ups for crack opening displacements (COD), i.e., front-face clips and later load-line clips, as depicted in Figure 3, where used.

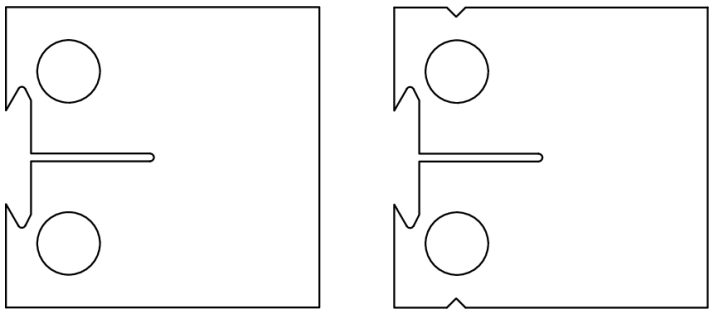

Figure 3. An illustration of the two miniature tensile specimens models utilized in validation tests. The model on the left (a) is used in NESC specimens and the one on the right (b) with both clip gage slots is used in CRIEPI specimens.

When testing NESC material, it was hypothesized that some specimens might have been extracted too close to the cladding. Indeed, this seemed to be the case since the results had large variance and the ensuing Master Curve had a high reference temperature T_0. These specimens were omitted from any further measurements and analyses. Since the homogeneity of the material is compromised, it is inapplicable for validation purposes. The incomplete Master curve reference temperature T_0 obtained for NESC-1 material was +79.7±9.3 °C, compared to +68 °C of the original project value, the difference of which exceeds one standard deviation. The displacement curves are, though consistent.

On the other hand, the complete T_0 obtained for CRIEPI material was -116.7±7.9 °C, in comparison to -109 °C of previous VTT tests and -101 °C of original CRIEPI tests. Both datasets were deemed inhomogeneous and the reference temperatures after inhomogeneity-related conservatism were 85.5 °C and -113.7 °C, respectively, Figure 4. Quality assurance was performed by analysing the key-curve behaviour, and the load-displacement curves follow the trends well, as depicted for the NESC material in Figure 5.

The tests and analyses demonstrate that CNS testing facilities are capable of high quality Master Curve testing. After some challenges were handled, the load-displacement curves have been consistent and the ensuing Master Curves

correspond with reference data. Furthermore, supplementary measurements such as dimensions and fracture surfaces, Figure 6, can be made with good accuracy.

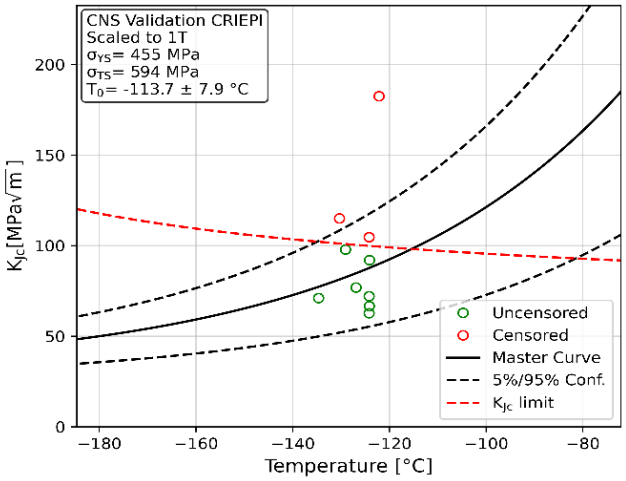

Figure 4. Master Curve of CRIEPI material. The reference temperature estimate is obtained through inhomogeneous dataset analysis.

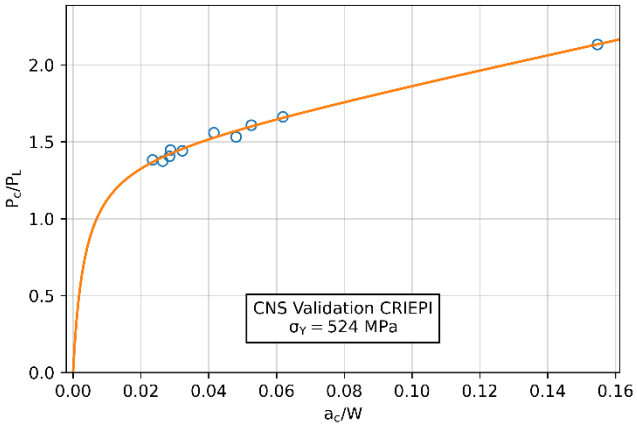

Figure 5. Key-curve behaviour of CRIEPI material.

Figure 6. Picture showing the appearance of a CRIEPI specimen after testing.

The B2 RPV trepans

Several trepans were cut from the decommissioned Barsebäck 2 RPV as part of the BREDA project, Figure 7. The planning, preparatory work, including trial cuts of mock-ups, and the execution of the cutting is a vast undertaking, requiring both large funding, good collaboration between stakeholders, including the radiation safety authority and excellent technical skills and is simultaneously a huge in-kind contribution to SAFIR2022. The trepans were successfully cut from the RPV, from the head and beltline areas, and delivered to the Ringhals plant, were the cladding was removed by milling. This was first done on the non-irradiated trepans from the RPV head (RPVH), which were subsequently delivered to VTT in March 2019, before repeating the procedure on the beltline trepans, before sending them to VTT in February 2020.

The head is a forging SA 508 Class 2 and the vessel is a plate metal SA 533 Grade B Class 1. The weld joints are made using high-Ni, high Mn and low Cu weld filler materials. The same materials are used in most Nordic RPV´s, such as B1, O2, O3, OI1, OI2, F1, F2, F3, R3 and R4 and the materials are thus very relevant. The chemical composition of the B2 weld metal is presented in Table 2.

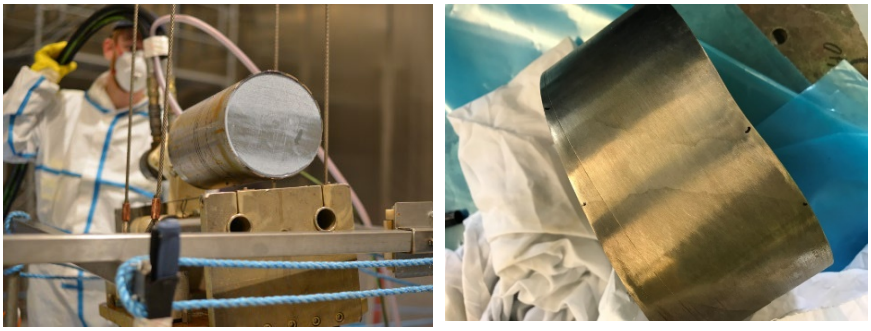

(a) (b)

Figure 7. A picture showing a newly cut trepan from the B2 RPV (a), and a close-up of a trepan from the RPVH (b).

Table 2. Chemical composition of the B2 weld metal (wt.%)

C	Si	Mn	P	S	Cr	Mo	Ni	Cu	Co
0.084	0.22	1.53	0.011	0.004	0.13	0.45	1.47	0.064	0.008

Cutting of trepans

Cutting is a major task in the project, and high-quality specimens is a pre-requisite for high-quality results. EDM was selected as the main cutting method during the design phase of the CNS. The requirements for high-quality cutting comprise of accuracy, high enough surface quality, as well as optimised waste handling.

Before cutting could start, the exact location of the welds in the trepans were identified, and this information was used for preparation of cutting plans. The welds in the RPVH trepans were inclined, which was taken into consideration in the cutting plans. Cutting started with making the trepan smaller to fit into the EDM gap. This was achieved by cutting of side-slabs, which were used for microstructural investigations. Slices from the trepans were cut first, and these slices were then used for cutting of tensile specimens and impact toughness specimens, Figure 8. The same procedures were used for cutting of the RPV beltline trepans. Each beltline trepan has been subjected to a different fluence during operation. The trepan #6, with the highest measured surface dose rate was selected as the first trepan for further investigations.

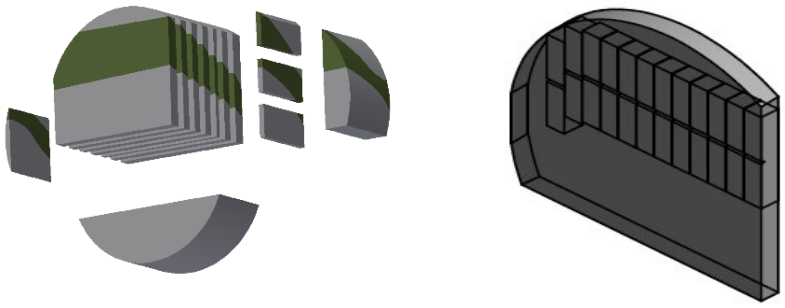

(a) (b)

Figure 8. (a) Cutting plans showing main cuts, including cuts of side slabs for metallographic investigations, and (b) impact test specimens from a RPVH trepan.

After finished impact toughness testing, the fracture surfaces are removed from a selection of the specimens, and miniature C(T) specimens are prepared from the remaining weld metal in the specimens, as depicted in Figure 9, and used for fracture toughness testing.

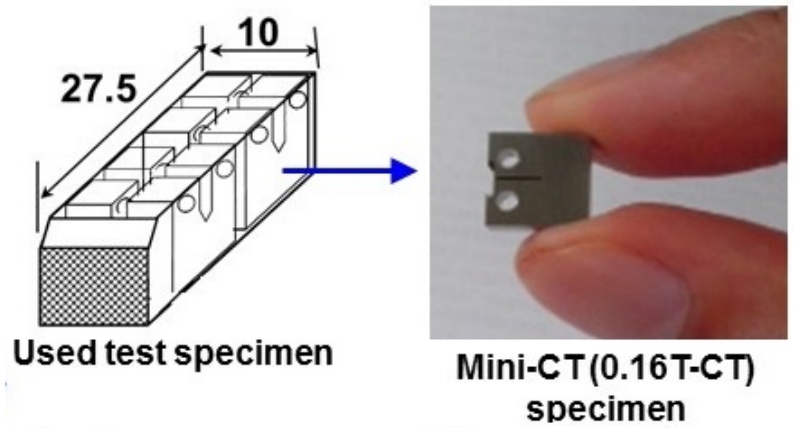

Figure 9. Schematic presentation of miniature C(T) specimens from a tested CVN specimen half.

Tensile and impact toughness of the RPVH weld metal

Tensile tests on the RPVH weld metal was performed at four different temperatures between room temperature and +300 °C with Zwick Z250 universal testing machine in accordance to tensile testing standard ISO 6892. Laser extensometer Zwick LaserXtens was utilized for elongation measurement. A temperature chamber is

installed in the test frame. After the test the fracture surfaces were measured an optical microscope. Analysis of all test data was done in MATLAB. [5] Impact toughness testing in T-S orientation were performed with a 300J instrumented impact hammer according to ISO standards 148:2016 and 14556:2015. [6]

The results showed similar values as the base-line results, Figure 10(a). Analyses of the impact toughness test results included impact energy and crack arrest force transition curve determinations as well as correlation evaluation between impact energy and lateral expansion and shear fracture appearance. The acquired transition temperatures of T_{41J} is -75 °C. When compared to the baseline results, representing the same weld metal in as-welded condition, the results indicate that the transition temperature does not shift due to thermal embrittlement (280 °C for 28 years), Figure 10(b). However, impact toughness in the upper shelf region, i.e. the ductile region, is lower than in the reference condition. As the data in the upper shelf region was observed to deviate from the expected linear correlation between the impact energy and lateral expansion, the scatter in this data is considered large, and should be treated with caution.

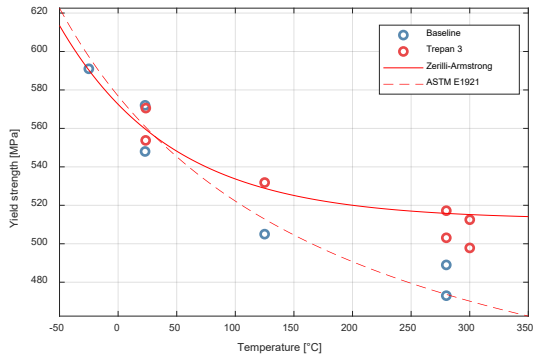

(a)

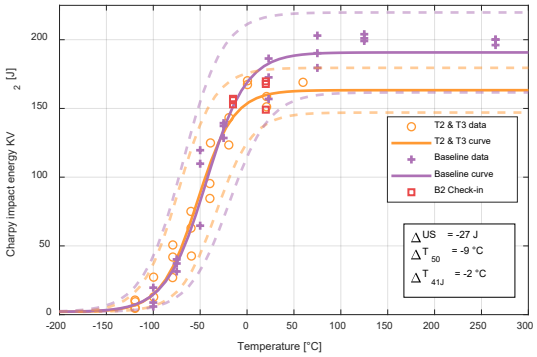

(b)

Figure 10. Tensile (a) and impact (b) test results on the RPVH SAW weld metal from the RPVH trepans.

Both the tensile and impact toughness testing proved demonstrated the VTT´s new facilities, machines and personnel at the CNS are capable of high quality testing. Tensile and impact toughness testing has also been performed in the beltline weld metal, and the results are under evaluation. These results have further proved the CNS capabilities to perform high-quality investigations on irradiated materials.

Hardness of the RPVH weld metal

The RPVH hardness and microstructure (reported below) was investigated in a Master Thesis in 2019. [7] The Vickers hardness measurements of the RPVH weld metal were performed according to the standard SFS-EN ISO 6507-1:2018. The hardness was measured through-wall using two different loads, i.e., HV10 and HV1, and across the weld, focusing on the fusion line area. After the hardness

measurements had been performed, the polished slice was etched to reveal the microstructure, and the location of the hardness indents in the microstructure was determined. The results from the through-wall hardness measurements are shown in Figure 11. The hardness is lower next to the inner surface of the trepan, in the heat affected zone (HAZ) formed from welding of the stainless steel cladding on the inner surface of the RPV. The average hardness is 215 HV10, and no remarkable difference between the as-welded and re-heated microstructure in the weld is observed. The hardness is higher in the HAZ of plate, with highest values next to the fusion line, Figure 12. Similar measurements have been performed in the belt-line weld metal, and the results are under evaluation.

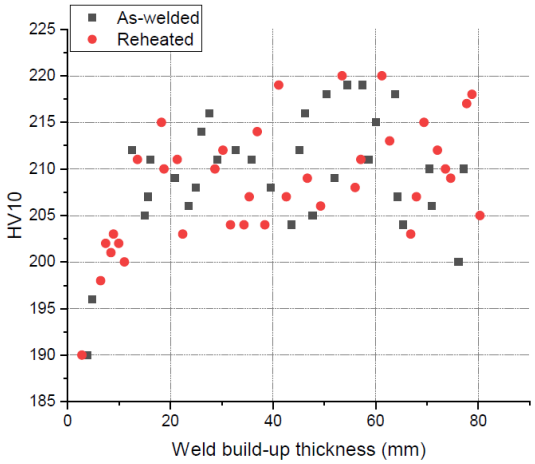

Figure 11. HV10 results through the wall thickness in the cross-section investigated separately for the as-welded and reheated regions in the weld.

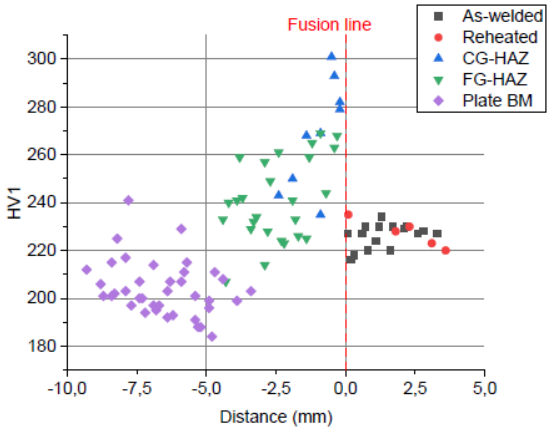

Figure 12. HV1 results across the weld-plate fusion line.

Microstructure of the RPVH weld metal

The investigations revealed that the main part of the weld was made using submerged arc welding (SAW), while the outmost part was made using manual metal arc welding (MMA). Acicular ferrite dominated the as-welded microstructure with some grain boundary ferrite between the columnar grains. Polygonal ferrite dominated the reheated microstructure from welding the consequent weld bead, with some grain boundary ferrite and acicular ferrite, which was confirmed also using electron back-scattered diffraction (EBSD), Figure 13 [8].

Fracture specimens from impact toughness tests at low temperatures were subjected to fractographic investigations to determine the primary initiation site for brittle fracture, Figure 14. On all investigated brittle specimens, the cleavage fracture initiated at an inclusion in the weld metal, and there is a correlation between particle size and impact toughness energy, Figure 15, i.e., specimens with larger initiator particles result in relatively lower impact energies when tested at the same temperature. An expected correlation between the distance of initiation and the impact toughness energy was also observed [9, 10]. The primary fracture site can be determined in all specimens tested in the lower part of the transition curve, at and below 41 J reference impact toughness energy, but not above, due to the change of the fracture mechanism, and hence the changes in the fracture appearance, showing that the value 41 J, commonly used for determination of the ductile to brittle transition temperature is a good choice.

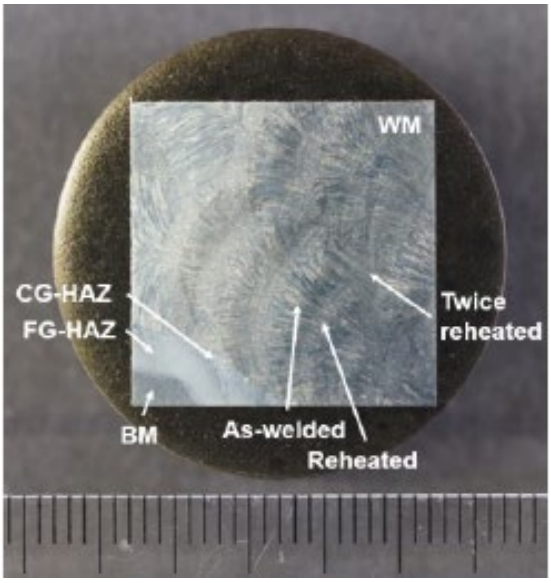

(a)

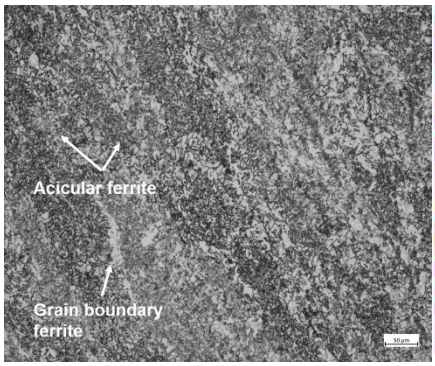

(b)

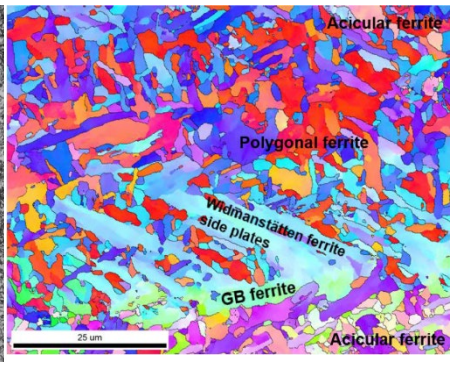

(c)

Figure 13. (a) Macro- and (b and c) microstructure of the SAW weld using light (b) optical microscope (c) and SEM/EBSD.

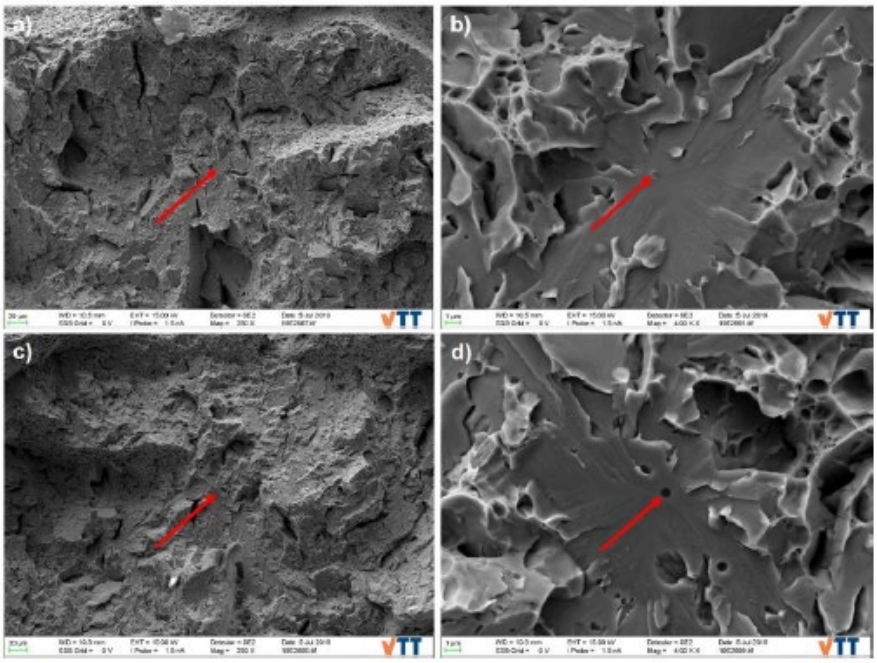

Figure 14. Primary initiation site in the two specimens halves of an impact toughness test specimen.

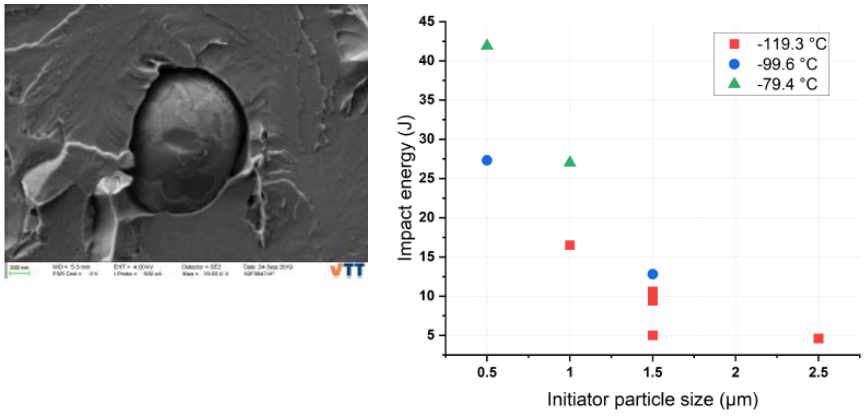

(a) (b)

Figure 15. Initiation particle (a) and correlation between particle size and impact toughness energy. [10]

Particle interface debonding is observed in the specimens in the lower part of the transition curve, where the plastic flow is limited. Debonding is normally associated with void nucleation during plastic deformation, when a second-phase particle remains more or less intact. The plastic strain breaks the interatomic bonding between the matrix and the particle instead of breaking the inclusion. The large inclusions increase the local inhomogeneity, which promotes debonding. The interface debonding may initiate a microcrack in the surrounding brittle material and propagate as macroscale cleavage fracture at low temperatures. Hence, multiple active mechanisms are needed to explain the behaviour for aged materials since traditional methodology, i.e., Griffith's theory with failure of an inclusion is not enough without the parallel mechanisms such as debonding of particles and/or grain boundary.

According to the semi-quantitative EDS analysis made on the primary initiation sites, the particles at the crack initiation sites are mostly multiphase oxides. The main detected elements were Mn, Si and Al, which are alloying elements in the ferritic weld metal. The multiphase oxide inclusions fulfil the Griffith criterion of brittle fracture initiation. The particle may be brittle due to the intrinsic crystal structure or preceding small defects within the inclusion. Therefore, the inclusion is likely to crack in the presence of plastic strain and further initiate a cleavage fracture. In case of more ductile oxy-sulphides, debonding at the interfaces between uncracked inclusions and weld metal matrix can induce further brittle fracture. Debonding can be concluded to be a result of mild thermal ageing, which is too small to affect the mechanical properties but strong enough to cause debonding rather than particle cracking at the brittle fracture initiation site. However, the effect of thermal ageing below 300 °C on debonding caused microcracking still requires further studies [8].

Similar investigations were performed on the specimens used for fracture toughness testing. The investigations of the FT specimen fracture surfaces show that the distribution of the initiation sites are concentrated toward the middle of the specimens, which is in accordance with expectations, taking the stress state along the specimen width into account. The initiation does not always occur at the deepest point of the pre-fatigue crack, Figure 16. Similar to the CVN specimens, there is a correlation between the distance from the notch or pre-crack tip, and the mechanical properties, i.e., the impact energy or the fracture toughness. Specimens with higher fracture toughness values have their initiation sites further away from the pre-fatigue crack tip. Also the amount of ductile crack growth is longer when the fracture toughness is higher.

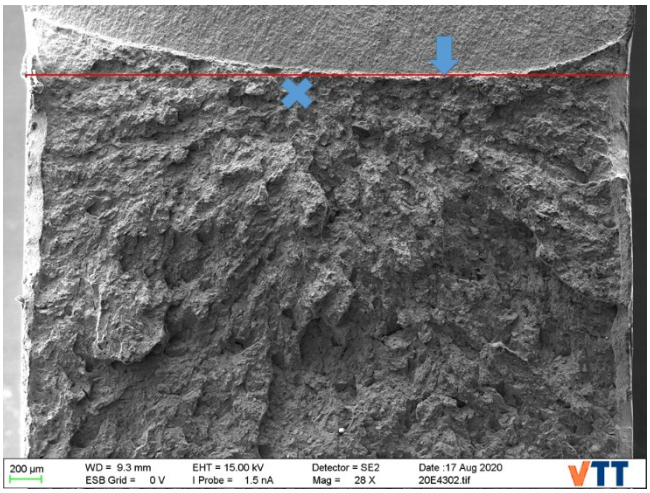

Figure 16. The location of the primary initiation site for the brittle fracture is seldom at exactly the same location as the deepest point of the pre-fatigue crack.

Two types of initiation sites were observed, i.e., cracked and debonded particles, Figure 17. The initiating particle sizes are larger than the average particle size. Similar to the CVN specimens, specimens with lower toughness values showed larger initiating particle sizes. Concerning the microstructure, which macroscopically consists of as-welded and reheated zones with different microstructures, lower fracture toughness values were observed when the prefatigue crack tip is in the reheated microstructure.

The microstructure of the beltline weld has been investigated, and the results show mainly similar microstructures compared to the RPVH weld metal [11]. Further, more detailed investigations are ongoing.

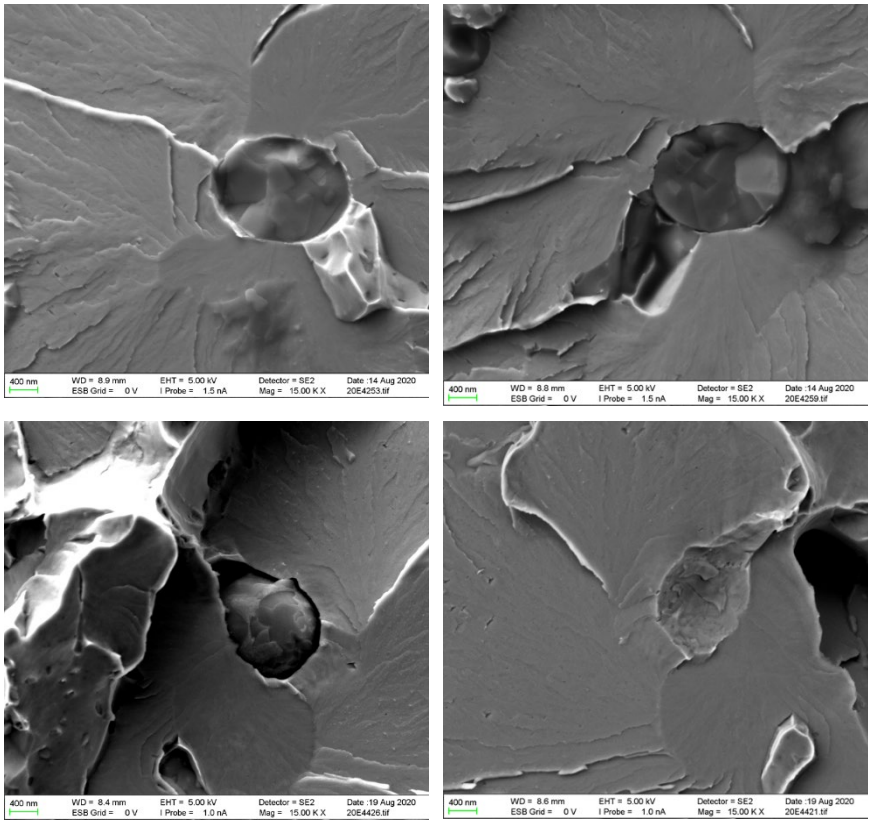

Figure 17. Broken (upper two pictures), and debonded (lower two pictures) particles at the brittle fracture primary initiation sites.

Stakeholder activities

The main stakeholders for BRUTE are the Finnish stakeholder group with members from the Finnish NPPs and STUK, the BREDA advisory group, with members from Finnish and Swedish NPPs, authorities and Energiforsk, who manages the BREDA project, and technical experts, especially at Ringhals NPP, KTH and Chalmers. The progress of BRUTE is reported and discussed in dedicated meetings to the different stakeholder groups. Dissemination of the results has further been promoted through presentation of the results at seminars, where also related work, performed at e.g. KTH and Chalmers, has been presented. The results have also been presented international meetings, one in Japan and one in Sweden (Kärnteknik 2019).

The seminar “Reactor pressure vessel embrittlement seminar for the BREDA – BRUTE project” in 2018 was very successful with high-class presentations from senior experts and doctoral students and with good discussions, and more than 30

participants from Finland and Sweden, Figure 18. A second seminar was arranged in 2020 as a webinar, with about 50 participants. Also here, presentations were given by the BRUTE project team members, but also by others performing related research at KTH and Chalmers on the same weld metal. The topics of these presentations included e.g. atom probe results on thermally aged and irradiated weld metal, presented by postdoc Kristina Lindgren, Chalmers, and on the further development of the weakest link model, developed by Magnus Boåsen in his PhD thesis, by the doctoral student Daniela Klein from KTH.

Two researchers, one from KTH and one from Chalmers, visited CNS in February 2020 just before the outbreak of the pandemic, for further annealing studies on specimens with similar weld metal as the B2 RPV weld metal.

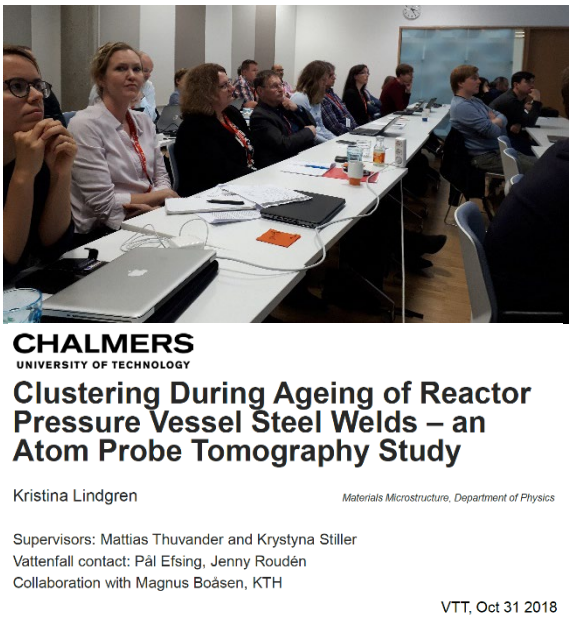

Figure 18. More than 30 participants participated in the BRUTE RPV embrittlement seminar in 2018, and listened to talks, including that by K. Lindgren, KTH, summarising her thesis work.

Acknowledgements

SAFIR2022 (especially reference group 8), Ringhals AB, the BREDA project, and NKS (Nordisk Kärnsäkerhet) are acknowledged for the opportunity, support and funding. The project team is acknowledged for high quality work and diligence.

References

[1] Reports from the SAFIR REHOT and RADLAB projects.

[2] Ehrnstén, U. Evaluation of surface requirement for hardness measurements in BRUTE. VTT Research Report VTT-R-06879-18.

[3] Ehrnstén, U. et al. Validation of mechanical test methods for the BRUTE project. VTT research report, VTT-R-00793-19.

[4] Arffman, P. and Saarinen, J. Validation of fracture mechanical testing at CNS using miniature compact tension specimens, VTT Research Report VTT-R-01174-20.

[5] Arffman, P. Tensile test results from B2 RPV head SAW weld metal. VTT research report, VTT-R-00073-20.

[6] Arffman, P. Impact test results from B2 RPV head SAW weld metal. VTT research report, VTT-R-00942-19.

[7] Hytönen, N: Effect of microstructure on brittle fracture initiation in a reactor pressure vessel weld metal, Tampere University, November 2019.

[8] Que, Z. and Ehrnstén, U. Characterisation of B2 RPVH materials using EBSD. VTT research report, VTT-R-01054-19.

[9] Lydman, J. et al. Fractography and microstructural characterization of Barsebäck 2 RPV head weld W28 miniature fracture toughness specimens. VTT-R-01451-20.

[10] Hytönen, N. et al., Effect of microstructure on brittle fracture initiation in a thermally aged boiling water reactor pressure vessel head. International Journal of Minerals, Metallurgy and Materials, https://doi.org/10.1007/s12613-020-2226-6.

[11] Hytönen, N. et al. Microstructural investigations of beltline weld metal. VTT-R-00027-21.

9.2 Infrastructure development at LUT safety research laboratory (IDEAL)

Joonas Telkkä, Elina Hujala, Lauri Pyy

LUT University
P.O. Box 20, FI-53851 Lappeenranta, Finland

Abstract

The general objective of the IDEAL project (2019–2022) is to develop the experimental thermal hydraulic infrastructure at LUT University nuclear safety research laboratory. The project comprises maintenance of the existing thermal hydraulic test facilities, development and upgrade of the instrumentation and data acquisition capabilities, as well as development of the new modular integral test facility, MOTEL. The motivation for the project is in providing state-of-the-art experimental thermal hydraulic capabilities, which benefit the whole Finnish nuclear community. The maintained and upgraded facilities are used in other important SAFIR-, industrial- and EU-funded safety research projects. Enhancement of the measurement capabilities enables production of high-quality data for understanding the thermal hydraulic phenomena and for the development and validation of computational tools, such as CFD codes. Procurement and implementation of novel measurement techniques promote the growth of expertise on the field of experimental thermal hydraulics and offer topics for master's and bachelor's theses. Maintenance of the facilities and expertise enables rapid solution of problems that arise in the Finnish nuclear power plants. Upgrade of the process control, computational and data storage systems enables better handling and filing of the large amounts of experimental data.

Introduction

In the SAFIR2014 research programme, the research project ELAINE was launched for the enhancement of measurement instrumentation available for the thermal hydraulic experiments in LUT University. Significant milestones in the project were the acquisitions of a particle image velocimetry (PIV) measurement system, wire-mesh sensor (WMS) electronics and a system of three modern high-speed cameras (HSC). In addition to acquisitions of experimental hardware, a new data storage system for the experimental data (EDS) was developed and taken into active use. In addition, one important task in the project was the maintenance of the (PWR) PACTEL test facility in order to secure its operability and availability for the experiments.

In the SAFIR2018 programme, the INFRAL project was launched in 2015, and it aimed for the further development of the techniques related to the advanced measurement techniques and their applications. The goal was to build good in-house expertise in the use of the acquired techniques to facilitate the needs of

computational modellers in the future experiments in the best way technically possible. Further, the goal of the INFRAL project was to secure the operability of the PACTEL test facilities and to launch a study on the new major test facility to prepare for the post-PACTEL era.

The IDEAL project was launched in 2019 to continue the LUT thermal hydraulic infrastructure development work done within ELAINE and INFRAL. The IDEAL project is divided into five different work packages. The first work package (Development of instrumentation) includes activities that are related to the use of advanced measurement techniques in the LUT laboratory. These techniques include PIV, WMS, high-speed cameras, optic fibers for longitudinal temperature distribution measuring, and ultrasonic flow meters. The second work package (Maintenance of test facilities) aims on the maintenance of test facilities such as (PWR) PACTEL, MOTEL and PASI, and it comprises also the yearly inspections, calibrations and other maintenance actions in the lab. Planning and creating a component stock, as well as planning and preparation of the laboratory power upgrade are part of the work package, too.

The third work package (Process control and computational systems) was a new addition to the infrastructure development project compared to the previous ELAINE and INFRAL projects. The work package includes renewing of the laboratory's field and process instrumentation, upgrade of the computation servers and enlargement of the available experimental data storage space.

The fourth work package (Development of the MOTEL test facility) continues the work initiated in INFRAL to develop the LUT laboratory's new large-scale test facility, MOTEL (MOdular TEst Loop). The work package includes the assembling and erecting of the first version of the facility, the design (and construction) of the next MOTEL vesions, as well as the shakedown and characterizing experiments of the facility. By means of this work, MOTEL will be ready for use in other research projects. The fifth work package (Project management) includes the tasks related to the project management and participation to the reference group meetings and seminars. International co-operation is included in this work package, too.

IDEAL is essentially an infrastructure development project. Thus, a large share of the project funding during the previous two years has been allocated to materials and supplies, especially concerning the server procurements in WP3 and the building of MOTEL in WP4. Nevertheless, as reported in the following chapters, a significant amount of scientific research has been done within the project.

Development of instrumentation

The WP1 of IDEAL concerns the development of advanced measurement techniques, such as particle image velocimetry, wire-mesh sensors, high-speed cameras and the related pattern recognition technology, optic fibers for longitudinal temperature distribution measurement and ultrasonic flow meters.

In 2019, the main focus for PIV was in literary work as there were no measurements involved within the SAFIR-related projects. The theoretical background

survey and feasibility study for high-speed PIV (HS-PIV) was stared, partly as a summer trainee work. An inventory of all PIV and high-speed camera and other imaging equipment was conducted in 2019.

The high-speed PIV study was finalized in 2020. The study is summarized in the following paragraphs.

Earlier, it was considered that choosing between high spatial resolution or high temporal resolution was a compromise that has to be made when executing PIV measurements. However, with the recent developments in high-speed imaging, high-speed Particle Image Velocimetry can also offer high spatiality. The HS-PIV technique allows the measurement of turbulent quantities in transient flows. High speed measurements both in time and space also allow the measurements of acceleration fields. The HS-PIV technique is simply conducted as a normal PIV measurement but using higher repetition laser unit (or continuous wave laser) and high-speed cameras (HS-cameras) for image acquisition. The HS-PIV technique can offer a kilohertz temporal resolution with a multiple megapixel spatial resolution depending on the hardware used. Naturally, high spatial resolution HS-cameras are still very expensive, so there are still compromises in the final composition of a HS-PIV system, depending on the budget. In addition, the amount of RAM drives the HS-camera price up, but it gives a possibility to make either longer measurements or more measurements without the need for uploading the captured images to the system computer. For the laser units, the repetition rate and the pulse energy are the defining factors of the price. The faster the laser with higher laser pulse energy, the more expensive it will be if using pulsed.

Previously, the LUT laboratory has used PIV in many occasions in different thermal hydraulic studies, e.g. in direct contact condensation (DCC) experiments with blowdown or sparger pipes in the PPOOLEX facility, as well as for particle size measurements of nozzles with a Shadowgraphy extension of the PIV system. In addition, several non-SAFIR related studies have been conducted over the years. The current PIV system was acquired in late 2011 and it is a so-called slow-speed PIV system with the measurement frequency of 7 Hz, later 15 Hz after the upgrade of the existing system with the LaVision sCMOS cameras in 2017.

The existing system has a high spatial resolution capable of measuring thousands of velocity vectors within a measurement area in the range of tens of centimeters per side (the size is naturally dependent on the wanted spatial resolution). So far, it has been found out that the temporal resolution of the current system is not always ideal, as the timescales of turbulent and other thermal hydraulic phenomena are very short. For example, the rapid condensation of a steam slug in the SEF-POOL facility occurs in a millisecond timeframe. In addition, measuring transient conditions or keeping constant ambient conditions for long time frames in large test facilities, like PPOOLEX, is challenging. Thus, one advantage of a HS-PIV system would be the possibility to gather time-averaged data samples faster. In other words, the existing slow-speed PIV system can be mainly used in time-averaging of vector velocity fields in constant ambient conditions. The flow measurement infrastructure of LUT Nuclear Engineering is capped due to this limitation. With a HS-PIV system, it would be possible to extend the flow measurements to wider array of

thermal hydraulic studies where the optical requirements for the PIV measurement are met.

The minimum requirement for updating the existing PIV system to a high-speed use is a new laser unit with a higher repetition rate. In addition, the Programmable Timing Unit (PTUX) needs to be upgraded for the high-speed use. PTUX synchronizes camera(s) with laser pulses. The currently used measurement and analysis software DaVis 10 is suitable for the HS-PIV use without upgrades. LUT Nuclear Engineering has acquired Phantom Miro M310 high-speed cameras previously for the pattern recognition purposes and they could be used as a part of the system. A hardware registration for the Phantom Miro M310 is needed for DaVis 10. Phantom Miro M310 is equipped with a 1280x800 pixel sensor with a maximum image acquisition rate of 3200 fps resulting in a throughput of 3.2 Gpx/s (gigapixels per second). The camera is equipped with 12 GB RAM. This enables a 1.6 kHz measurement frequency in a PIV use for roughly 3.75 seconds in total. Or, total of 6000 image pairs with a chosen frequency as the sensor is roughly the size of one megapixel.

The preliminary plan for HS PIV system has been ongoing with the help of LaVision, the prior supplier of the existing PIV system, on behalf of the laser unit and auxiliary system updates. For a possible upgrade of HS cameras, talks with Citius Imaging Ltd Oy have been ongoing. Both companies have also supplied preliminary quotations in order to have the sense of the overall budget needed for a HS PIV system. As stated above, using the existing Miro M310 HS cameras is possible, but high-speed cameras with a better spatial resolution, RAM and throughput can offer a better result. In addition, the future needs of pattern recognition analysis will take part in deciding the need for the upgrading of the HS cameras.

It was decided in the autumn of 2020 that the purchase of a high-speed PIV system will take place later since there are more important procurements to be made in the project in 2021. Thus, the possible procurement shifts to the future.

Within the LUT infrastructure development projects, high-speed cameras have been used to support data analyses of various condensation experiments. A pattern recognition algorithm has been created and developed with the high-speed camera measurement results. In 2019, the cameras were applied to sparger experiments in the SEF-POOL test facility (experiments of the SAFIR SPASET project). The pattern recognition algorithm was improved in 2019 using the HSC data from the 2018 SEF-POOL experiments. A conference paper based on this analysis was written and presented in the NURETH-18 (the 18th International Topical Meeting on Nuclear Reactor Thermal Hydraulics) conference in Portland, USA in August 2019 (Hujala et al., 2019).

In 2019, a dissertation named “Quantification of large steam bubble oscillations and chugging using image analysis” was finalized and presented by Elina Hujala with due permission for public examination and criticism on the first of November 2019 at LUT University. D.Sc. (Tech.) Mikko Lemmetty from TVO acted as an opponent and Professor Juhani Hyvärinen acted as a custos. The dissertation was approved with distinction in the academic council of LUT School of Energy Systems at 20th of November 2019 (Hujala, 2019).

In the dissertation, a pattern recognition-based image analysis algorithm for vertical vent pipes was designed and developed. The direct contact condensation experiment (DCC-05) of the LUT University's PPOOLEX test facility was used as a reference test. The algorithm consists of three parts: pre-processing, where all image processing takes place, pattern recognition, where the edges of the bubbles are detected, and post-processing, where all images are analyzed, and data collected. The algorithm evaluates basic properties of large steam bubbles, such as volume, surface area, surface velocity and acceleration, and different frequencies.

Frequency analysis was also conducted in the DCC-05 case. The analysis showed two main frequencies: 53 Hz and 126 Hz. The algorithm was also applied to computational fluid dynamics (CFD) simulations, where the algorithm was used to determine critical wavelengths of condensation driven Rayleigh-Taylor instability in succession to establish the most suitable grid density for the simulations. A frequency analysis was also performed for the CFD simulation cases and compared to the results of the algorithm. This is illustrated in Figure 1.

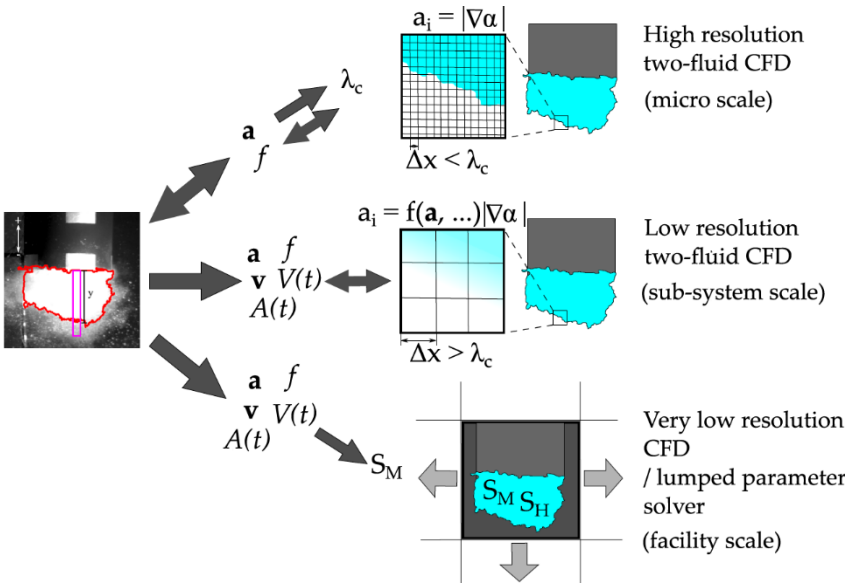

Figure 1. Validation data from image analysis for different scale numerical DCC models.

The algorithm was extended to cover cases where multiple bubbles travel at the same time in the frame being analyzed. The extended algorithm tracks multiple bubble properties in the same image. The evaluation of surface velocities and acceleration were also improved.

The algorithm works well in evaluating volume, surface area, velocities and accelerations of large steam bubbles. The research verified that even from moderate quality video material, it is possible to acquire high quality quantitative data, if the

frame rate of the video had been high enough and the most obtrusive objects could be filtered out from it. The algorithm can help to understand phenomena that underlay the design of BWR safety systems.

In 2020, a plan for the further high-speed camera testing with stand-alone HSC measurements focusing only on the cameras to be conducted in 2021 was made. In 2020, an extempore test was carried out to prepare for the 2021 studies. In this test, pressurized air was injected into the water of the SEF-POOL test facility. Short test shots were recorded using a single camera. Either the flow rate of the pressurized air or the temperature of the pool water was not measured. With the pressurized air, clearly defined bubbles were produced. Because of the small flow rate, the air does not mix the water, and the background of the images stays clear and calm. The clear bubbles with an even background gives a good starting point for the error estimation and image analysis. The conducted test showed that the SEF-POOL test facility is an appropriate base when testing the features of the HSC system. Thus, there is no need for a separate test facility for this purpose. Also, an improved backlight proved to be better than the lighting used in the SEF-INF experiments.

In 2021, separate experiments for the algorithm development purposes will be conducted. The experiments should be made using both pressurized air and steam. Steam injection should be horizontal, but pressurized air can also be injected in a vertical direction. Because the algorithm development requires large steam bubbles, a bubbling condensation oscillation mode is needed. This determines the temperature of the water quite hot, over 353 K. The experiment will start by finding a reasonable camera resolution. The minimum frame rate is 1000 fps. If the bubbles fit well to the image area and some movement can be seen, and there is not too much extra background visible, the resolution is appropriate. After this, the resolution will be constant during the experiment. Different frame rates will be tested between 1000 fps and 7000 fps (approximately). 6000 fps should be suitable, if the length of the video is at least one second.

At first, a good filming conditions are tested. When the filming conditions are considered adequate, each feature of the camera will be tested separately (white balance, aperture etc.). At least one second of video will be recorded for each test. All tests should be repeated using pressurized air. The flow rate of the air and the temperature of the water should be known. The flow rate will be fixed the way that the bubbles are separated. From the results of the experiments, the pattern recognition-based image analysis algorithms will be improved, and at least one journal article will be written.

The studies with the axial wire-mesh sensor develop at LUT, named AXE, have been conducted during the previous years in the HIPE test facility. In 2019, a conference paper based on the results of the AXE void fraction measurements in swirling two-phase flow was published and presented in the SWINTH-2019 (the Specialist Workshop on Advanced Instrumentation and Measurement Techniques for Experiments related to Nuclear Reactor Thermal Hydraulics and Severe Accidents) workshop in Livorno, Italy in October 2019 (Telkkä et al., 2019).

The results presented in the paper from the axial sensor measurements with both 30° and 60° swirl generators together with the comparative measurements with the

traditional radial WMS (TRAD) reveal that the axial sensor is not able to produce reliable enough void fraction data. The axial sensor produces void fraction values, which are significantly lower than those measured with the TRAD sensor. Also, the shapes of the void fraction profiles differ from the traditional sensor data. The axial sensor produces much more asymmetric void fraction distributions compared to the radial sensor. This results from the intrusive character of the AXE sensor, especially its leading edge, which significantly disturbs the swirling flow.

The previous studies of the performance of the axial sensor with non-swirling flow showed that the AXE sensor was able to produce reliable void-fraction data. In non-swirling flow, the void fraction distributions were qualitatively very similar for both the axial and radial sensors (Ylönen & Hyvärinen, 2015, Telkkä et al., 2018). It was concluded in the earlier studies that the axial sensor can be applied to the measurement of non-swirling two-phase flows, for the sensor did not cause an irrecoverable redistribution of the flow in the performed tests (Ylönen & Hyvärinen, 2015, Telkkä et al., 2018). The studies presented in the SWINTH-2019 paper clearly indicated that when the two-phase flow is transformed into a swirling flow, the intrusive structure of the sensor becomes significant, and the sensor is not able to produce reliable void fraction data anymore.

The studies related to the WMS techniques will continue within the IDEAL project. One issue will be to further study the possibility of purchasing and applying a high pressure/temperature capable WMS. The new LUT integral test facility, MOTEL, is one possible target of application for such a sensor at some point in the future.

The optic fiber technique was tentatively tested in 2019 in the passive heat removal test facility, PASI, in the natural circulation experiment NC-03, which was conducted within the SAFIR2022 PAHE project. The fiber was placed in the water pool of PASI in order to see the temperature profile in the tank. In the testing, the measurement system worked but didn’t provide reliable temperature data. The temperature values measured with the fiber were larger than those measured with reference thermocouples (TC). The difference increased as a function of temperature: the higher the temperatures were, the bigger the difference to the TC measurements was. Significant differences were observed. Figure 2 presents an example of temperature data from the optic fiber and a reference thermocouple as a function of time during the experiment. Five short measurement sets were taken with the optic fiber from the locations of the thermocouples.

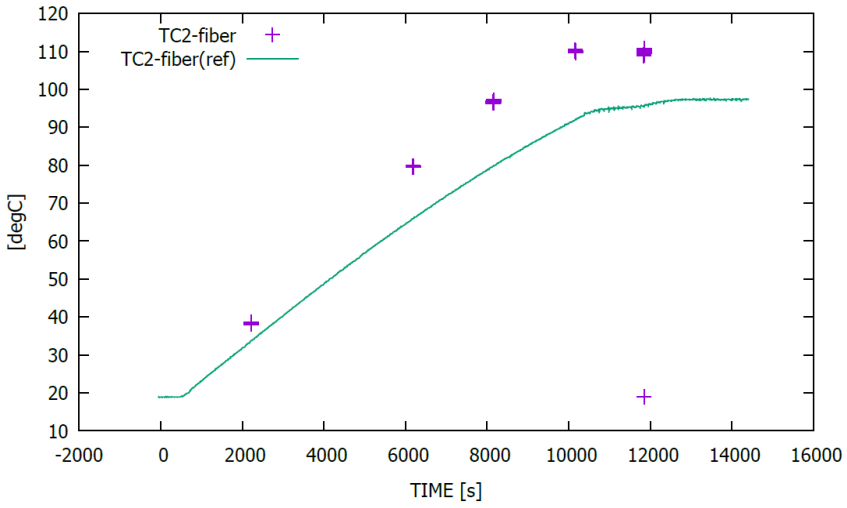

Figure 2. Temperature data from the optic fiber (TC2-fiber) and the reference thermocouple TC2 (TC2-fiber(ref)) as a function of time during the PASI NC-03 experiment.

The reason for the difference between the measurements was considered to be the bends of the thin steel capillary pipes (outer diameter 3 mm), inside of which the fiber was placed. The bends affect the thermal expansion, which is exploited in the temperature measurement in the optic fiber technique. Thus, the accuracy of the measurements suffers.

In 2020, the fibers were further tested as a bachelor's thesis work (Kinnunen, 2020). The measurement set-up was simpler water pool measurement with both a straight fiber and fibers bent to U-curves. In the work, the effect of the capillary pipe curves of different radiuses was studied. In addition, the aim was to study the effect of vibration to the measurement accuracy since there was indication from the previous measurements that vibration may affect the results. The vibration was executed by means of shaking the measurement set-up before the measurement. Also, the effect of temperature was studied: all measurements were conducted with "cold" water (~10–20 °C) and "hot" water (~50 °C). The spatial resolution used in the measurements was 0.65 mm, which is the highest possible with the current system. The measurements were conducted inside the water pool of the HIPE (Horizontal and Inclined Pipe Experiments) test facility in the LUT laboratory. Figure 3 presents the fibers (inside capillary pipes) placed inside the water pool.

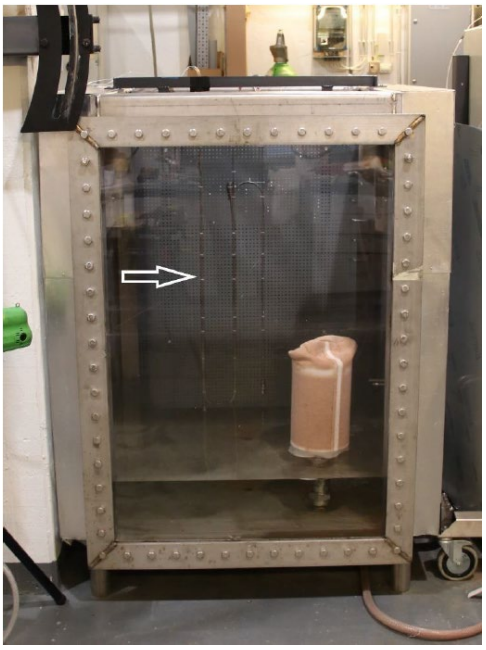

Figure 3. Optic fibers placed inside the water pool of the HIPE test facility.

Two series of measurements were conducted in the work. The first series was done with three fibers: one straight fiber, one fiber with one U-curve with a 97 mm diameter, and one fiber with two U-curves with 97 mm diameters. The second series was done with one fiber with six U-curves with tighter, 43 mm diameters. Each used fiber was a five-meter-long fiber, and the ends of the fibers were used in the measurements. Thermocouples were used to gain reference temperature data in both measurement series. An example of the measurement results is shown in Figure 4. In the figure, the gray dots are moving average values of the optic fiber temperature data with the spatial resolution of 0.65 mm. The red dots are the reference thermocouple measurement values. The black dots are the optic fiber temperature values in the locations of the thermocouples.

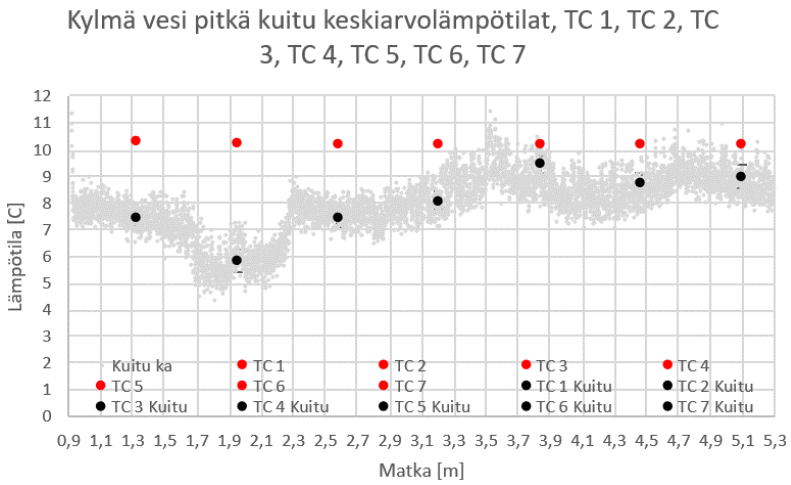

Figure 4. Example of measurement results with optic fiber with six bends in cold water.

The example figure above shows really large differences between the fiber and thermocouple measurements. It also shows that the deviation of the fiber measurement is approximately 2 °C in this case. Further, we can see that the effect of the bends on the measurement result is difficult to interpret from the results.

The gained results show in general that the fibers still give data, which differs relatively much from the reference thermocouple measurements. Based on the results of the work, there seems not to be a clear indication on which factors affect the results most (bends, temperature, length of the fiber…). Therefore, the testing of the fibers must be further continued in the future at least with measurements with different spatial resolutions. So far, the measurements have been conducted with the maximum resolution, which probably causes larger deviation of the temperature data. In general, it seems that the optic fiber technique is not suitable for really accurate temperature measurement, but rather for rougher 1D distribution measurement where the interest is more on temperature gradients on certain lengths (for example height of a pool, length of a steam generator tube etc.), and where the accuracy of the measurement doesn't play so big role. Kinnunen (2020) presents the results of the above-described study in more detail.

The ultrasonic flow meters were initially tested in the above-mentioned PASI natural circulation experiment NC-03 in 2019. In these measurements, one flow meter was attached on the outer surface of each of the 15 PASI heat exchange tubes in the tube parts outside the PASI containment vessel. Figure 5 presents the working principle of the ultrasonic flow meter. The sensors *a* and *b*, which are attached on the outer surface of the flow channel, work alternatively to send and receive ultrasonic pulses. The sound waves travelling with the flow (*ab*) move faster than those travelling against it (*ba*). The flow rate is determined from the difference of these pulses.

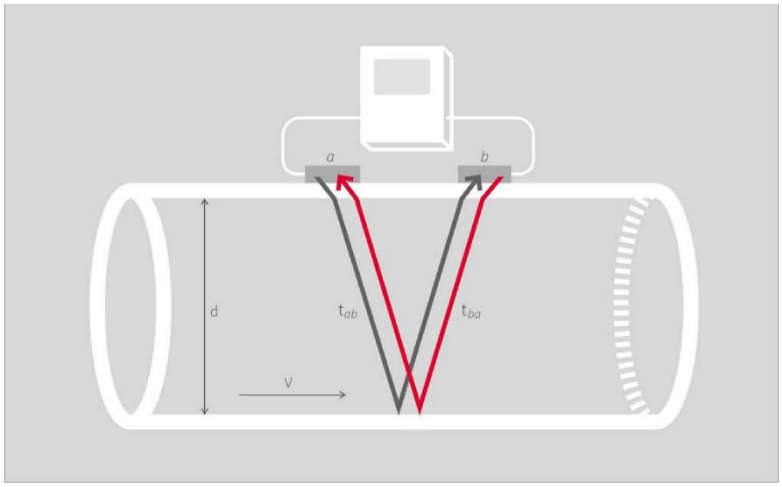

Figure 5. Working principle of the ultrasonic flow meter.

The results of the testing in 2019 were not convincing. Figure 6 shows the results of these measurements. The figure presents the PASI loop (downcomer) flow rate and the combined flow rates of the 15 ultrasonic flow meters during the whole duration of the NC-03 experiment. The period from the beginning to approximately 10 000 s was single-phase natural circulation with a steady loop flow rate. From ~10 000 s begins the phase of two-phase flow natural circulation, during which the loop flow strongly oscillates.

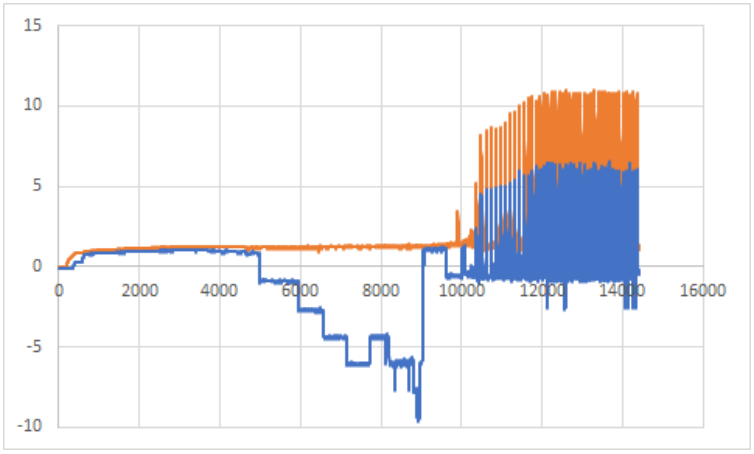

Figure 6. PASI downcomer flow rate (orange curve) [kg/s] and the combined flow rates of the 15 ultrasonic flow meters (blue curve) [kg/s] as a function of time during the PASI NC-03 experiment.

The results show that the ultrasonic flow meters provided relatively reliable flow rate data during the first approximately 5000 seconds of the NC-03 experiment. The sum of the measured flow rates of the ultrasonic flow meters almost equals to the PASI downcomer flowrate measured with a magnetic flow meter. After that, there are significant differences in the results between the measurement techniques. The reason for this is presumably the fact that the flow rates after 5000 s were between the laminar and turbulent flow areas. The ultrasonic flow measuring technique assumes the measured flow to be either laminar or turbulent, and the flow areas between those provide imprecise flow rate data.

The testing of the ultrasonic flow meters was continued in 2020 in a separate test set-up to prepare for the use in the annular downcomer of the MOTEL test facility. A mock-up of the annular downcomer space, a rectangular flow channel with a 3.5 cm x 51.5 cm cross-sectional area, was attached to the HIPE test facility water tank. The water was circulated from the water tank to the flow channel and back. The testing set-up is presented in Figure 7. The flow meter is attached on the surface of the flow channel, as it will be attached on the surface of the MOTEL downcomer.

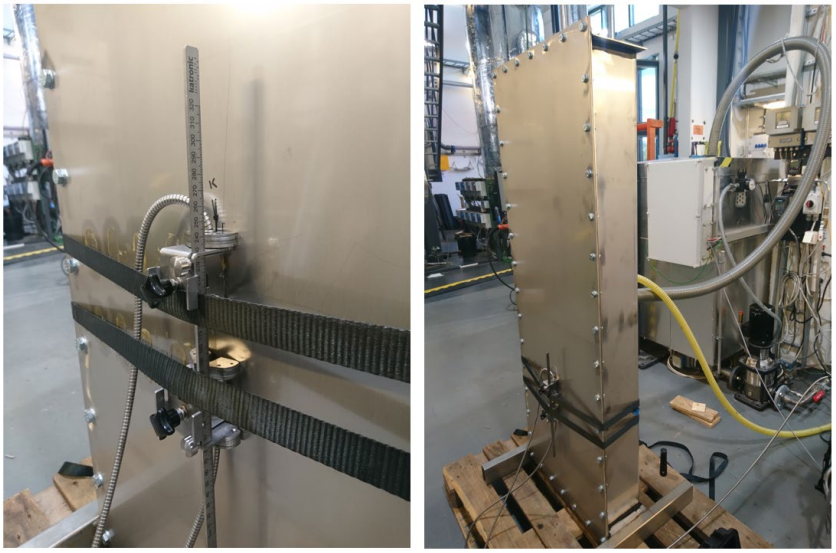

Figure 7. Ultrasonic flow meter testing set-up attached to the HIPE test facility.

The testing was conducted in atmospheric pressure and temperature. The challenge in this measurement configuration is that the flow meter assumes circular flow channel (the diameter of the channel is put in the meter before measuring). Therefore, a correction factor has to be used in order to correct the measurement data to correspond the situation in the annular downcomer space. The effect of the curvature of the MOTEL downcomer was considered negligible. The flow meter assumes round channel cross-section ($\pi d^2/4$). In this case, the flow channel is rectangular (assumed measurement area d^2). Thus, the correction factor $4/\pi$ was used in this

case. Measurements were conducted on various lateral locations of the flow channel. Example of the results is shown in Figure 8.

The reference flow velocity data was measured from the HIPE test facility flow channel as volumetric flow. This was converted into velocity, assuming that the flow is evenly distributed inside the mock-up flow channel. This was one uncertainty in this study since there was no information on how the flow was distributed in the channel. The reference velocity data is shown with the blue line in the figure below ("Velocity average"). The raw ultrasonic flow meter measurement data is shown with the red line ("Katronic average"). The data corrected with the correction factor is shown with the green line ("Korjattu"). The data in the figure are moving averages to smoothen the deviation of the data.

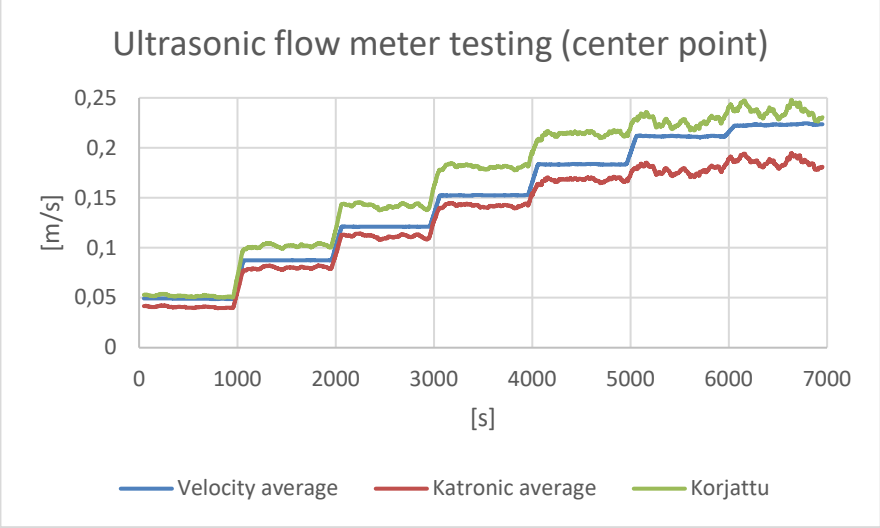

Figure 8. Ultrasonic flow meter testing result from the center point of the flow channel (50 s moving average).

Based on the results of this testing, it is difficult to draw clear conclusions on how accurately the ultrasonic flow meters measure the flow velocity. It can be seen in the figure above that at some velocity levels the correction factor corrects the measured velocity to correspond the reference velocity. Nevertheless, at some velocity levels the effect of the correction factor is opposite – the corrected values differ even more from the reference velocity than the raw data. The results seem to differ according to the lateral location of the flow meter, too. In addition, as mentioned above, the reference velocity is very much assumed/approximated, thus any clear conclusions are hard to draw. These initial results are promising, though, because the magnitude of the measurement result seems to be correct.

The testing of the ultrasonic flow meters will continue in 2021 with eliminating certain assumptions made. The most important improvement is to gain reliable

reference velocity data from the mock-up channel modeling the annular downcomer. This will be done by means of making the flow channel presented in Figure 7 transparent and adding the PIV measurement system to the set-up in order to measure reliable reference flow velocity data. With a transparent flow channel and PIV, it can be also studied how evenly the flow is distributed inside the flow channel in practice. This testing will be executed as a bachelor's thesis work supervised by the LUT laboratory personnel.

Maintenance of test facilities

The WP2 of IDEAL includes continuous maintenance work in the laboratory, as well as the yearly maintenance actions, which are carried out in the nuclear safety research laboratory in order to ensure availability of the test facilities for thermal hydraulic experiments that are conducted within other research projects, such as PATE, PAHE and SPASET, as well as within non-SAFIR research projects.

In summer 2019, the annual outage was conducted. Calibration of pressure and pressure difference transducers of the (PWR) PACTEL and PASI test facilities was performed using Beamex MC5 calibrator, which has internal pressure calibration components, and which is annually calibrated by the manufacturer. The PPOOLEX facility's air humidity meter (Vaisala) was calibrated by the manufacturer.

In 2019, the PASI facility steam supply system was renewed. In the PASI experiments conducted earlier, steam supply to the containment vessel was executed by means of an external steam supply system. In the natural circulation experiment NC-03 of the SAFIR2022 PAHE project, the used external system was able to use only a part of its nominal power for the steam production, and it was not able to produce completely dry steam. Hence, it was decided that in the future PASI experiments, this kind of steam supply system will not be used, but the steam for the experiments will be produced with the PACTEL facility. During the summer 2019, a steam line was built from PACTEL, which is located in the old LUT laboratory building, to PASI, which is located in the new laboratory building. Hence, there is no need for a rental, moveable steam supply system anymore.

During the annual outage in summer 2020, the transducers were calibrated. Calibrations of pressure and pressure difference transducers of the (PWR) PACTEL, MOTEL and PASI test facilities were performed using Beamex MC5 calibrator, which has internal pressure calibration components, and which is annually calibrated by the manufacturer. The PPOOLEX facility's air humidity meter (Vaisala) was calibrated and serviced by the manufacturer and then installed to the PASI facility.

The periodical pressure vessel inspection was performed for the (PWR) PACTEL facility in 2020. It consisted of internal inspection for core section and service inspection for the facility itself. The opening pressures of the PACTEL safety valves were tested separately in a test bench.

In 2020, a new Coriolis flow meter was acquired and installed to the PACTEL accumulator 2 injection line. Also, a new Vortex flow meter was acquired and installed as a replacement to the main flow meter in the PACTEL downcomer line.

In 2020, The main safety valve of the PACTEL facility was changed to new one during the spring. This was required in the previous pressure vessel inspection. During this operation, the condition of the accompanying rupture disc was inspected and found to be intact. This inspection was also done for the rupture disc of the pressurizer.

Part of the compressed air system was renewed, and new shutoff valves were installed in order to minimize the use of compressed air during non-activity periods of the PACTEL facility. Also, some of the valve actuators and pilot valves were either fixed or swapped for new components. These modifications were made to significantly reduce the amount of compressed air wasted.

Renewal of the electrical systems of the laboratory has begun in 2020. To enhance safety, residual current protection devices were installed, and the selectivity of the electrical networks were improved. In the next stage, some of the cabling will be rerouted in order to relieve the overloading of the cable routing.

In WP2, also 3D laser scanning of the PASI test facility was conducted in 2020. The purpose of this was that with the results of the scanning the accurate pipeline diameters for the test facility in the SolidWorks model would be gained. The heat exchanger and the riser and downcomer lines of PASI were scanned, and the results are not fully convincing. It seems that when scanning bright surfaces with lots of “interference sources” (thermo couple wires etc.), the result is not perfect. The gained data should be processed more in order to use it to support the design and scaling of test facilities.

The work package 2 includes also a planning of a component stock in the laboratory. The idea behind the component stock is to ensure the functionality of the existing test facilities and thus reduce the off-production and repairs time in case of component breaks, to ensure the laboratory’s ability to construct new testing systems that require components with long delivery times without any delays and to have a variety of sensors for different applications with different working principles. Based on the needs, a preliminary list of components was written in 2019. Components include mechanical components, instruments and components for maintenance. In 2020, 20 k€ out of 30 k€ allocated to the procurement of the components was moved to WP4, because the MOTEL facility needed new signal converters for the heating elements, and thus also new measuring cards had to be acquired. The old measurement cards will be left for the component stock and can be used in the future. No procurements have been made to the component stock, yet.

The upgrade of power transformers has been prepared for already several years in order to increase the electrical power available for the thermal hydraulic experiments. Currently the maximum power available is 1 MW, and the aim is to increase the power into approximately 2.5 MW. The upgrade process has been delayed from the original schedule due to the complexity of the upgrading process. The options for the upgrade are being studied in the many organizations involved. In addition to the three affected laboratories of LUT School of Energy Systems, also Suomen

Yliopistokiinteistöt as the owner of the buildings, Lappeenrannan Energia as the power provider, as well as electrical system design consultants are part of the process. In 2019, new initiation concerning the power upgrade was made for the 2019 LUT University's internal investment program. The options to execute the upgrade are either to add a new power transformer or replace the old transformer by a new bigger one. The process proceeded in 2020. The LUT investment program granted 150 k€ for the task. The preliminary estimation of the costs (used in the LUT investment application) was 200 k€. Current cost estimation is at least 200 k€ for the power upgrade. 50 k€ is budgeted in IDEAL for 2021 to complement the LUT investment funding.

Process control and computational systems

The third work package was a new addition to IDEAL compared to the previous infrastructure development projects. The work package includes renewal of the laboratory's field and process instrumentation, upgrade of the high-performance computing (HPC) infrastructure and enlargement of the available storage space for measurement and calculation data.

The field instrumentation of the LUT laboratory will be renewed during SAFIR2022. In 2019, the necessary components were purchased: a safety valve to the PWR PACTEL primary side, a Coriolis flow meter to the accumulator line, a Vortex flow meter to the downcomer line, three pressure transducers and twelve differential pressure transducers. So far, the Coriolis flow meter and the Vortex flow meter have been installed. The process instrumentation will be renewed later in the future.

The amount of data from the experiments in the LUT laboratory has been expanding due to advanced and high-speed measurement capabilities. Similarly, the use of modern computational tools, such as CFD, to support and supplement experiments produces large data sets. The current EDS storage system is not suitable for large data files. Thus, enlargement of the data storage space has been planned and executed within the IDEAL project. The storage of data will be done tripartitely in the future: the first stage is the data space of the measurement computers and HPC servers; the second stage for large amounts of data will be a new centralized data space located in conjunction of the HPC servers; the third stage is the EDS system for the traditional data plus a new FairData cloud service for data to be stored for longer time. This system is illustrated in Figure 9.

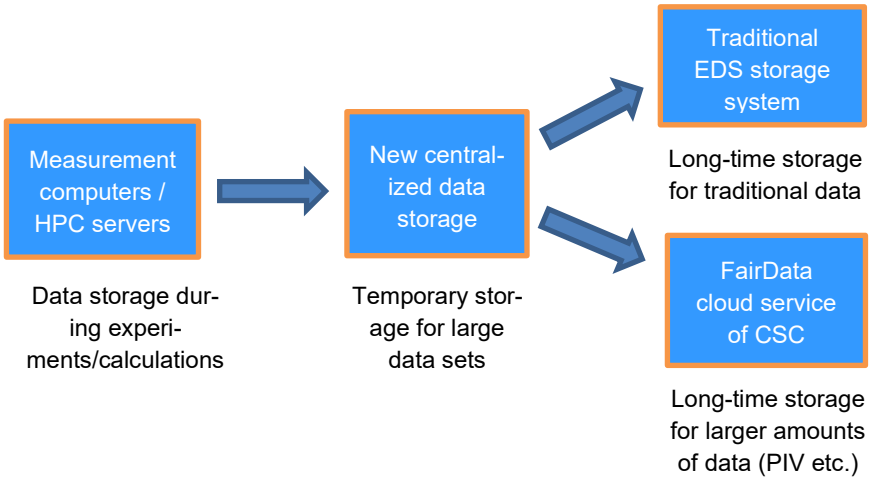

Figure 9. Data storage system of the LUT laboratory.

In addition, upgrade of the HPC infrastructure is realized jointly within IDEAL and an internal investment project of LUT. This includes increasing the capacities of the cooling and power supply systems and replacing outdated computing hardware with newer. IDEAL contributes to the planning of the overall work and to a part of the computing hardware investment. Planning of the server room modifications including cooling and power supply systems and the corresponding tendering process for these contracts was completed during the summer 2020. The construction works and acquisition of cooling and UPS equipment realized with LUT internal budget were completed by the end of 2020. New computing hardware were purchased in late 2020 and their installations will continue in 2021.

The new data storage servers were purchased in 2020 at the same time with the computation servers. The installation work of the data servers will continue in 2021, too. Filing of the old test data is also included in the task of data storage space enlargement. The filing has been initiated and it will continue in 2021.

Development of the MOTEL test facility

The WP4 deals with the development of the new modular integral test facility, MOTEL (MOdular TEst Loop). The first version of the MOTEL test facility is a model of a small modular reactor (SMR), and the design resembles to that of NuScale's SMR. Figure 10 presents a general view of MOTEL, and Figure 11 presents a cross-sectional view of the facility. The first configuration of MOTEL is comprised of three interchangeable modules that can be detected in Figure 10: the core module, the steam generator and the pressurizer.

Regarding the design of MOTEL, the design of the heater element (core module) was emphasized, in particular. Traditionally, in integral test facilities the heater

element is long and thin in order to have the height scaling 1:1 compared to the reference power plant in question. With MOTEL, the intention was to break this rule. The core section of MOTEL was made wider and shorter than usually in order to study both axial and radial flow phenomena inside the core. The SMR design enabled to design the core this way.

The fuel rod bundle geometry in MOTEL does not accurately model any existing plant type, although MOTEL is loosely based on NuScale's SMR design. The MOTEL core is a general representation of a fuel rod bundle. The core is comprised of 132 electrically heated heating rods and 16 instrumentation rods. The heated length of a single heating rod is 1830 mm. The diameter of a single rod is 19.05 mm, and the maximum heating power of one rod is 7.5 kW. Hence, the maximum heating power of the facility is 990 kW. The axial power distribution of the core is cosine-shaped, likewise in real NPP cores. The radial power distribution of the core is adjustable with 12 power segments. The arrangement of the heating rods is in a rectangular grid, which is more practical concerning instrumentation and investigation of flow phenomena inside the core. The core module of the test facility can be swapped to a different setup, if needed. Thus, it can be replaced in the future with a core representing a specific reactor core design.

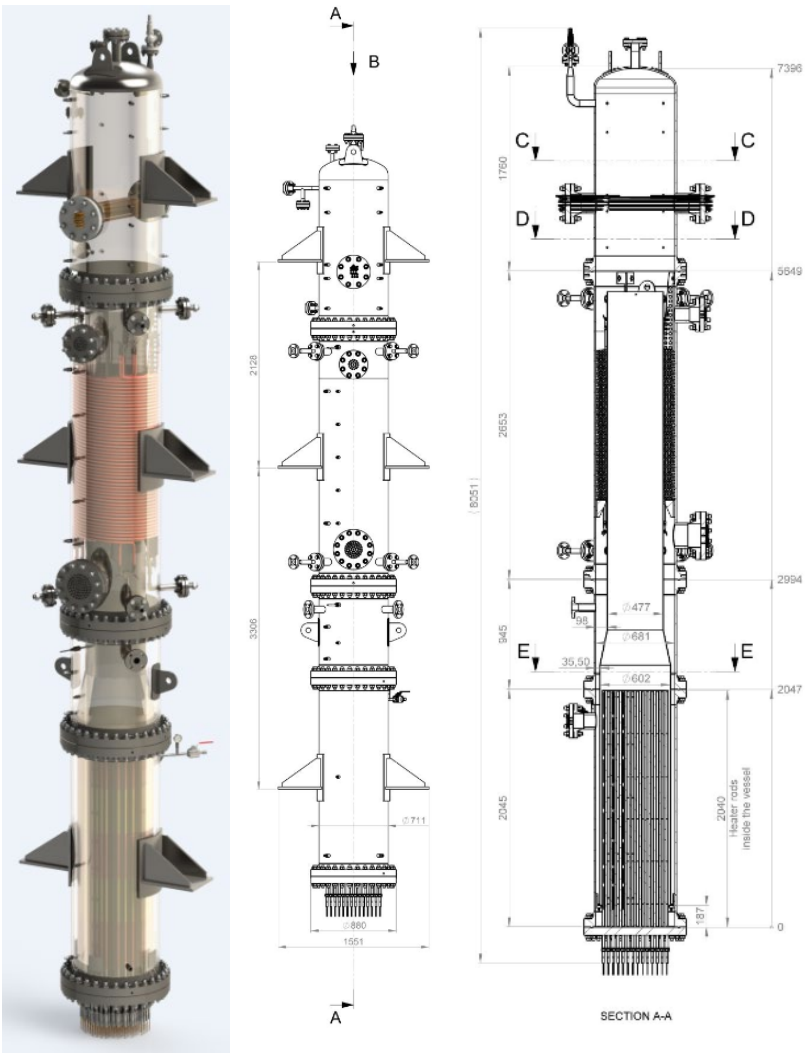

Figure 10. General view and the dimensions of the MOTEL test facility. The three changeable modules can be detected: core module, steam generator and pressurizer.

An essential and unique feature of NuScale's SMR design is the helical coil steam generator, whose behavior is one of the key interests regarding the experimental activities with MOTEL's first version. A special characteristic of this type of steam generator is that boiling happens inside the steam generator tubes, whereas the primary water flows outside the tubes. The MOTEL steam generator is comprised of 16 steam generator tubes. Half of the tubes circulate clockwise and the other half counterclockwise.

The pressurizer is located at the top part of the test facility. The pressurizer has two heating elements (30 kW heating power each) to adjust the pressure inside the test facility. There is a relief valve at the top of the pressurizer.

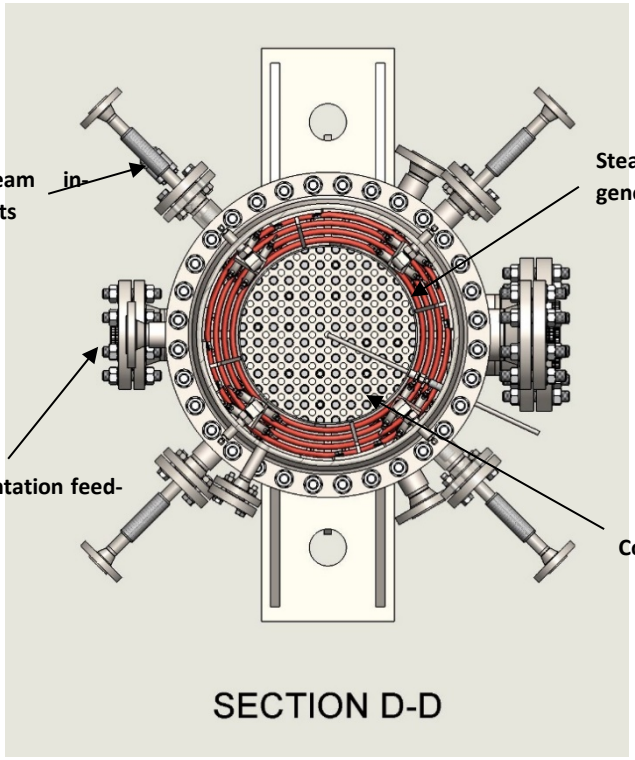

Figure 11. Cross-sectional view of MOTEL viewed from above (section D-D in Figure 10).

In 2019, the MOTEL framework and the facility itself were erected in the laboratory. All the components were assembled, and instrumentation was installed. The final insulation and pipeline/valve works were done in 2020. Figure 12 shows the facility assembling in the laboratory.

Figure 12. The MOTEL facility assembling in the LUT laboratory.

The first version of MOTEL represents a SMR; hence, the whole primary circuit is located inside a single pressure vessel. The system operates by natural circulation, and thus no pumps are needed to circulate the primary water. As the water heats up in the core section, it rises in the riser located in the center of the vessel. Once the heated water reaches the top of the riser, it flows down inside the annular downcomer space through the steam generator tubes where the heat is transferred to the secondary side. After the SG the cooled water continues in the annular downcomer located in the outer edge of the vessel. The cooler water has a higher density, and it is driven by gravity to the bottom of the vessel, where the water heats up again in the core section. The secondary side water is pumped into the steam generator tubes where the boiling happens. The secondary water enters the SG tubes through four inlet collectors. Four SG tubes are connected to each collector. The generated steam is directed out of the test facility via four outlet collectors,

respectively. Feedwater is highly purified, and its conductivity is measured online to prevent the build-up of limescale.

The total height of the MOTEL test facility is 7.7 m, and the diameter of the vessel is approximately 700 mm. The riser inner diameter is 477 mm, and the width of the annular downcomer is 100 mm. The design pressure of the facility is 40 bar, and the design temperature is 250 °C. Table 1 summarizes the main characteristics of the facility.

Table 1. Main characteristics of the MOTEL test facility.

Characteristics	MOTEL
Total height [m]	7.7
Main diameter [mm]	~700
Maximum primary pressure [bar]	40
Maximum secondary pressure [bar]	40
Maximum temperature [°C]	250
Number of helical steam generator tubes	16
Maximum heating power [kW]	990
Number of heating rods	132
Heated length of the heating rods [mm]	1830
Diameter of the heating rods [mm]	19.05
Number of instrumentation rods	16
Number of dummy rods	145
Main material of the components	Stainless steel
Insulation material / thickness [mm]	Mineral wool / 120

The shakedown tests of MOTEL were conducted in December 2020. The purpose of these tests was to ensure that all the facility systems including the process control and data acquisition systems work as expected. In the shakedown test, the power feed systems and the steam generator operation were tested. In addition, the functioning of the measurement systems was checked.

After the shakedown test, the official commissioning test of MOTEL was conducted. This test can be considered as a second part of the shakedown tests. In the commissioning test, the operation of the pressure-related safety equipment as mandated by the Finnish law was tested. The safety automation against over-pressurization of the facility as well as the core overheating protection system were tested. Kotro et al. (2020) present the more detailed description and the results of the MOTEL shakedown tests.

As the commissioning test was successfully conducted, the official operating license of MOTEL was granted, and the facility is ready for the characterizing experiments. These include a heat loss experiment, a pressure loss experiment and an experiment characterizing natural circulation. The characterizing experiments will take place in early 2021.

Project management

The work package 5 includes the tasks related to the project management and participation to the reference group meetings and seminars. Also, international co-operation activities are a part of the work package.

International co-operation is essentially fulfilled by taking part in SILENCE, an international network for owners of thermal hydraulic test facilities all around the world. Networking and maintaining good communication with other test facility operators is very important and may produce valuable co-operations and participations to the international research projects. In June 2019, three researchers from LUT attended the SILENCE network meeting, which was held at LUT University, Lappeenranta. In 2020, the meeting was originally scheduled for March, but due to the worldwide Covid-19 situation, it was postponed and arranged as a remote meeting in June.

References

Hujala, E., Tanskanen, V., Patel, G. & Hyvärinen, J. 2019. Image analysis of bubbling mode condensation oscillations in horizontal saprger. Proceedings of the 18th International Topical Meeting on Nuclear Reactor Thermal Hydraulics (NURETH-18), Portland, U.S., August 18-23, 2019. 12 p.

Hujala, E. 2019. Quantification of large steam bubble oscillations and chugging using image analysis. Doctoral dissertation, LUT University, 2019.

Kinnunen, S. 2020. 1D temperature distribution measuring in the HIPE test facility water tank with fiber optic cable. Bachelor's thesis, LUT University, 2020.

Kotro, E., Pyy, L., Räsänen, A. & Telkkä, J. 2020. Shakedown tests of MOTEL. Research Report IDEAL 2/2020, LUT University, Nuclear Engineering, 2020. 27 p.

Telkkä, J., Jämsén, S. & Hyvärinen, J. 2019. Defining void fraction with axial wire-mesh sensor in a swirling two-phase flow. Proceedings of the Specialist Workshop on Advanced Instrumentation and Measurement Techniques for Experiments related to Nuclear Reactor Thermal Hydraulics and Severe Accidents (SWINTH-2019), Livorno, Italy, October 22-25, 2019. 16 p.

Telkkä, J., Ylönen, A., Hyvärinen, J. and Varju, T. 2018. Estimation of velocity fields from the axial wire-mesh sensor data. Nuclear Engineering and Design 336 (2018), 34-44. 11 p.

Ylönen, A. & Hyvärinen, J. 2015. Study of Two-Phase Pipe Flow using the Axial Wire-Mesh Sensor. Proceedings of the 16th International Topical Meeting on Nuclear Reactor Thermal Hydraulics (NURETH-16), Chicago, U.S., August 30-September 4, 2015. 10 p.

9.3 Participation in the Jules Horowitz Reactor Project (JHR2022)

Caitlin Huotilainen, Ville Tulkki, Pekka Moilanen, Petri Kinnunen, Seppo Hillberg

VTT Technical Research Centre of Finland Ltd.
P.O. Box 1000, FI-02044 Espoo

Abstract

During the first two years of the JHR2022 project, the main focus has been on participation in the Jules Horowitz Reactor Project through the three working groups (fuel, materials and technology), upgrading MeLoDIE devices (mechanical loading device for irradiation experiments) and the participation in related international collaboration and research program, including the OECD/NEA Framework FIDES Program, the Horizon2020 coordination and support action JHOP2040 and a secondee exchange at CEA-Cadarache.

Introduction

Over the past forty years, materials testing reactors (MTR) have provided essential and invaluable support to the both the nuclear industry and researchers. As the existing fleet of MTRs continues to age, they are faced with an increasing probability of shut-down, due to outdated safety standards, and the likelihood that their experimental capabilities are no longer able to respond to current needs and requirements for the qualification of new fuels and materials. The Jules Horowitz Reactor (JHR), a new European materials testing reactor (MTR), is currently under construction at the Commissariat à l'Énergie Atomique et aux Énergies Alternatives (CEA) Cadarache research center in France. A drawing of the JHR can be seen in Figure 1. The JHR has been labeled as a European Strategic Forum Research Infrastructure (ESFRI) and will become a major part of European nuclear research infrastructure (NRI).

Finland is participating in the construction of the JHR with a 2 % in-kind contribution. This in-kind contribution includes the delivery of experimental systems/devices: (i) the underwater gamma spectrometry and X-ray radiography (UGXR) and (ii) hot cell gamma spectroscopy and X-ray radiography (HGXR) non-destructive examination (NDE) test benches and (iii) a Mechanical Loading Device for Irradiation Experiments (MeLoDIE). This in-kind contribution gives Finland the opportunity to both use and directly benefit from the research performed in the JHR, which includes results of future experimental campaigns.

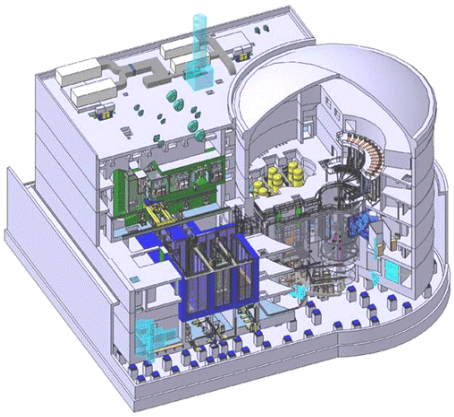

Figure 1. The Jules Horowitz Reactor.

The JHR is designed to (i) provide a high neutron flux, (ii) run highly instrumented experiment, (iii) support advanced modeling needs and (iv) operate experimental devices capable of simulating the environment, in terms of coolant chemistry, pressure, temperature and neutron flux, and respond to the experimental needs of water reactors, gas cooled thermal or fast reactors, sodium fast reactors, etc. Even though the JHR construction is currently ongoing, the planning of experimental needs and devices has already begun.

Additionally, as successful irradiation campaigns require planning, sample preparation, transfer of the samples and rig configuration prior to performing the actual test, the first experimental projects must be planned and prepared for during the span of SAFIR2022. In order to prepare for experimental needs and plan for operation, the JHR consortium has created three internal working groups (WG) - the (i) Fuel WG (FWG), (ii) Materials WG (MWG) and (iii) Technology WG (TWG). The role of these working groups is to determine the experimental needs of JHR and plan the future experiments. VTT actively participated in all three WGs, thus ensuring that the national interests are brought forward and considered by the consortium and its future actions and endeavors. The WGs hold meetings at least two times per year and, in spring, the annual JHR Technical Seminar is arranged. At this seminar, the outcomes of the WG meetings and the progress of in-kind contributions are presented and reviewed.

To assist with gaining experience within the JHR consortium, several projects utilizing existing experimental capabilities have been planned by the consortium. This includes on the structural materials side the acquisition of a JHR Archive Material and preparation of the round robin/benchmarking test campaign and upgrades to the MeLoDIE (Mechanical Loading Device for Irradiation Experiments) devices for instrumented in-core testing of nuclear fuel cladding. On the fuel side, a proposal for a fuel irradiation experiment will be built around the OECD/NEA Framework for Irradiation Experiments (FIDES) Programme.

JHR Collaboration and Activities 2019-2020

The planning of future experiments in the JHR takes place in three working groups (WG): fuel (FWG), materials (MWG) and technology (TWG). The objectives of the WGs is to advise the governing board on possible topics of interest for JHR programs by identifying experimental needs, planning future experiments and developing experimental devices and capabilities based upon needs.

The ninth Annual Seminar was held on April 3-5, 2019 in Cadarache, France. The seminar was preceded by the first edition of the JHR School. Over the course of three days, the JHR School covered a number of topics, including an introduction to research reactors, the scientific needs for nuclear fuel and materials research, the JHR specifications, modeling tools and support for research and materials testing reactors (including core physics and thermal hydraulics), an overview of the French safety requirements for a new MTR, the JHR design guidelines and associated challenges with the development of modern and highly instrumented experimental devices. Two persons from Finland participated in the JHR School.

The FWG, MWG and TWG held parallel meetings, during the ninth Annual JHR Technical Seminar and in fall 2019, the three WGs held meetings at the Joint Research Centre (JRC) in Petten, The Netherlands.

In October 2019, a publication and presentation on the JHR capabilities, Finnish contribution and the available experimental devices at the start of operation was made at the Nuclear Science and Technology Symposium (SYP2019) in Helsinki, Finland (Huotilainen et al. 2019). The available experimental devices at the start of operation included: MADISON, ADELINE and MICA, in addition to the hot cells and non-destructive examination benches. MADISON (Multi-rod Adaptable Device for Irradiations of experimental fuel Samples Operating in Normal conditions) and ADELINE (Advances Device for Experimenting up to Limits Irradiated Nuclear fuel Elements) will be located in the reflector area and be dedicated to the study and evaluation of nuclear fuel behavior under normal and off-normal operating conditions, respectively (JHR 2019). The MADISON device can be used for short- and long-term studies and the ADELINE device is designed to investigate fuel behavior during power ramps. The MICA (Material Irradiation CApsule) is dedicated to materials investigations, e.g. changes in material properties due to neutron irradiation, temperature and possibly stresses. Its design is based upon the NaK capsules previously used in the Osiris Reactor at CEA-Saclay (Saclay, France). The MICA capsule will be located in the center of a fuel element in the reactor core (JHR 2019).

From October 2019 through March 2020, Seppo Hillberg (VTT) participated in a secondee exchange at CEA-Cadarache. The topic of his secondement was the development of non-destructive inspection methods for the evaluation of JHR irradiation test devices. According to the French regulations, non-destructive inspection of test devices must be performed every forty months. The main focus of his work was to determine where and how the investigations should be performed on the welds of the ADELINE test device and ultrasonic (volumetric) and the eddy current (surface C-scan) non-destructive inspection methods were investigated. Some conclusions from the first stage of this work included (i) the need for two inspection

methods – i.e. eddy current for surface examination coupled with volumetric ultrasonic inspection for the body, (ii) the most suitable location for inspection being the storage pool, (iii) some level of automation is required, (iv) the possible difficulties in performing corrosion inspections in some.

Due to the exceptional situation in 2020, the 10th Annual JHR Technical Seminar was canceled. The next Technical Seminar is planned in spring 2021, and will most likely be a virtual event. Despite the difficult situation in 2020, the three WGs remained active and motivated in their work and have organized a number of virtual meetings and teleconferences. In 2020, the major focus of the MWG has been the planning of the JHR Archive Material (JAM) Programme, set to benchmark the specific neutron spectrum of JHR and preparing the guidelines for the JAM Programme, in terms of material specifications and as-supplied characterizations, irradiation campaign conditions and requirements, along with post-irradiation examinations are being developed. The focus of the FWG has been on planning the participation in the FIDES Framework Programme.

JHOP2040

The JHR Operation Plan 2040 (JHOP2040) Project is a Horizon 2020 coordination and support action. This project was submitted in fall 2019 in response to the call text “NFRP-16: Roadmap for use of Euratom access rights to Jules Horowitz Reactor experimental capacity” and received a positive funding decision in spring 2020. The project’s kick-off was postponed from spring 2020 to September 2020 and the project’s duration is thirty-months. JHOP2040 is coordinated by Petri Kinnunen (VTT). The consortium is made up of ten partners from seven countries that are part of the JHR consortium, see Figure 2. [JHOP 2020]

The main goal of this project is to create the Roadmap for the first fifteen years of operation of the JHR, while ensuring the effective use of Euratom access rights. The roadmap will, firstly, make a detailed plan for the first four year of operation, i.e. the first research program cycle in JHR considering the available experimental devices and capabilities at the start of operation, and, secondly, the entire roadmap will take into consideration the evolving list of available experimental devices and capabilities and industry needs.

The main objectives are to (i) both strengthen and widen the JHR research network, (ii) make full use of the JHR capacity through collaboration with potential users, (iii) create the Roadmap for the first four years of operation and (iv) create the roadmap for the next eleven years of operation, from the start of the first irradiations.

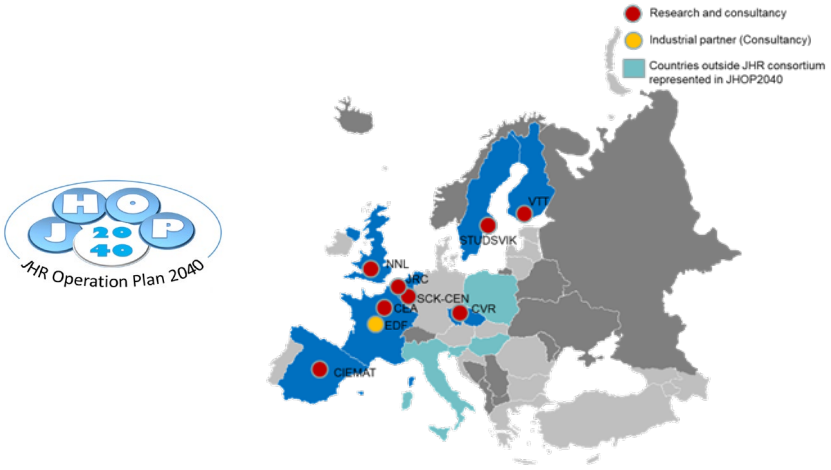

Figure 2. JHOP2040 consortium members, Euratom member states and nuclear institutions represented in the project.

FIDES Programme

The preparations for the kick-off of the FIDES Programme began with a meeting in September 2019. This meeting was attended remotely by VTTers. During this meeting the first three Joint Experimental Programmes (JEEP) presented and the draft agreements were reviewed. The presented JEEPs were (i) the Power to Melt and Manoeuvrability (P2M) JEEP, (ii) the MIR-LOCA (loss of coolant accident tests in the MIR reactor) JEEP and (iii) the In-pile Creep Studies of ATF Claddings (INCA) JEEP.

The P2M Project will address long lasting power transients without scram that may potentially lead to fuel centerline melting, if the ramp level is sufficiently high and moreover lead to high stresses the cladding. The fuel volume change at incipient fuel melting and fission gas release from fuel melting would be investigated and testing would take place in BR2 (SCK·CEN, Belgium).

The goal of the MIR-LOCA Project is to obtain new experimental data on the behavior of VVER-1000 fuel rods, containing Gadolinia doped fuel under LOCA conditions and the verification safety analysis codes in VVERs. Similar tests have been performed in the past.

The motivation for the INCA Project is to perform in-pile qualification testing for advanced technology fuels (ATF) and obtain information on their creep behavior. Testing will be performed in LVR-15 at CVR in Rez, Czech Republic. This project would be carried out in two phases: (1) irradiation in the high dpa OKaP rig and subsequent post-irradiation examinations of the claddings, followed by (2) in-pile testing using an upgraded MeLoDIE device for deployment in LVR-15. The kick-off

of the INCA Project took place in December 2019. Finland is participating in the INCA JEEP and the specific contributions will be detailed in the following section.

Since the preparations for the kick-off were started, additional virtual meetings have been held, including the FIDES Establishment Board meeting in June 2020. Jorma Aurela (TEM) and Ville Tulkki (VTT) were nominated for Finland's representatives in the FIDES Programme as Administrative Contact Person and Technical Contact Person, respectively. Significant progress was made with preparation of the final FIDES Agreement in 2020 and it was distributed for signature in fall 2020. Moreover, virtual technical meetings have been held focusing on the planning and initiation of the experimental work within the JEEPs. The progress of the FIDES Framework Programme establishment and the technical JEEPS, specifically the P2M and INCA projects, are being followed within the JHR2022 project.

MeLoDIE Upgrades and the Role of MeLoDIE in INCA

To respond to the need for instrumented material tests in the JHR, CEA has developed, in collaboration with VTT (in-kind project 2009-2015) the MeLoDIE I test device (Guimbal et al. 2011). MeLoDIE I is an instrumented in-reactor creep experiment for fuel cladding tube specimen under controlled bi-axial loading in the Osiris research reactor in Saclay, France. (Guimbal et al. 2011)

The irradiation was performed in one of the core positions of the Osiris reactor using the CHOUCA capsule filled with NaK. The MeLoDIE I loading device is part of the sample holder. The targeted test temperature was 350 °C, and the internal pressure of the zirconium tubular sample was approximately 160 bar. A closed Helium circulation loop has been designed to generate needed continuous Helium flow rate for the pneumatic servo controlled pressure adjusting loops of the MeLoDie I device. Two separate control systems have been built into the helium circuit. One of the systems controls the four pressures used to perform the test. Another control system has been built for reactor safety with programmable logic control (PLC) controlled automatic closing valves, see Figure 3. (Moilanen 2004, Guimbal et al. 2011)

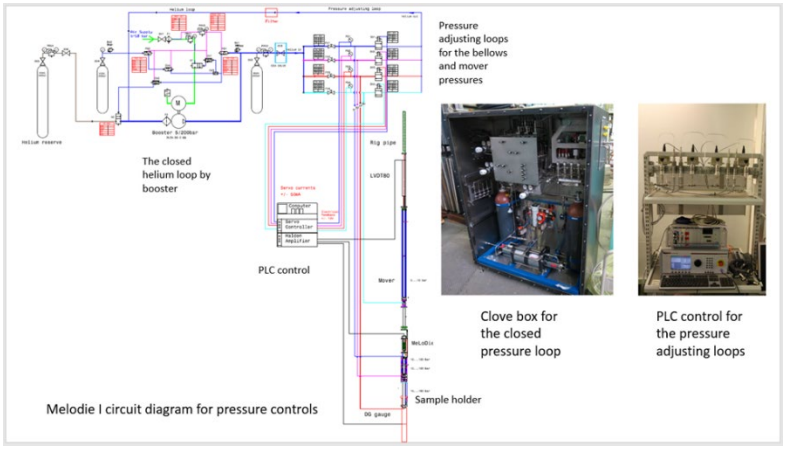

Figure 3. Schematic figure of the MeLoDIE I testing system (Moilanen 2004, Guimbal et al. 2011)

An upgraded MeLoDIE device will be used within the FIDES INCA JEEP. This project focuses on the assessment of the irradiation induced cladding creep properties of advanced and traditional nuclear fuel cladding materials, e.g. standard and optimized Zr alloys and ATF, including coated claddings. The creep behavior of selected nuclear fuel cladding materials will be studied in irradiation experiments planned in the LVR-15 reactor at CVR in Rez, Czech Republic, first, using their high-dpa OKaP rig, and then using the highly instrumented and advanced MeLoDIE test device.

The MeLoDIE II device is currently being upgraded and designed for deployment in the LVR-15, based upon the lessons learned from the use of the MeLoDIE I devices. The main focus of the re-design is on optimizing the structure of the loading frame to make it simpler, lighter (due to gamma heating) and stronger. Moreover, the re-design of the diameter gauge (DG) device is an important part of the design of the MeLoDIE II device. In addition, the positions of the thermocouples, pressure pipes and mover parts of the diameter gauge have been made during the re-design. The MeLoDIE II device with main tubes, wires and components and the mover posts for the DG can be seen in Figure 4 and Figure 5, respectively. (Moilanen 2020)

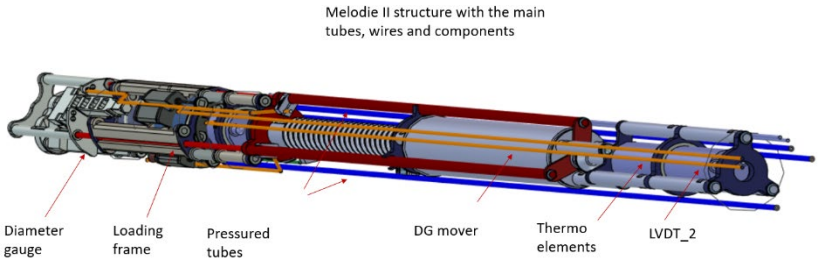

Figure 4. Schematic figure of MeLoDIE II with (a) the main tubes, wires and components (Moilanen 2020).

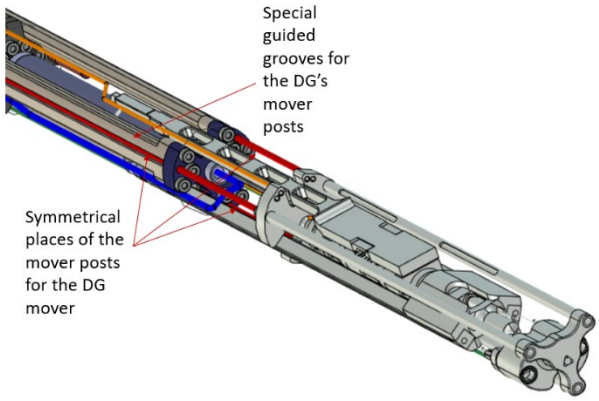

Figure 5. Schematic figure of MeLoDIE II with the mover posts locations with the DG device).

Finite element modeling (FEM) calculations were performed to assess the loading frame and compared it to the MeLoDIE I structure. These calculations revealed that with the slightly lighter device, the stress resistance of MeLoDIE II is considerably improved with regards to MeLoDIE I device. In addition, the DG mover system has been improved. In the MeLoDIE I device, during the Osiris experiments, bellows of the mover device were pressurized externally, resulting in frictional forces during movement. In the upgrades, the device is now pressurized internally and has been rotated. This results in the transfer posts of the DG being shortened, and the frictional forces can be controlled more precisely with adjustable clearances.

The project has explored ways to make the device better compared to the already tested version of MeLoDIE I. Particular attention has been paid to improving the structure of the equipment, maintaining and inspecting the operation of the helium gas loops, and improving the operation of the mover equipment as well as calibration of the pneumatic loading units, bellows. The continued development of the MeLoDIE II device, for its eventual installation in the LVR-15 reactor is part of the In-pile Creep Studies of ATF Claddings (INCA) Project in the OECD/NEA FIDES

Programme. Based on the experience gained, MeLoDIE III equipment should be designed for the reactor needs of the Jules Horowitz reactor.

Acknowledgements

The authors would like to thank all members of the JHR Consortium and Fuel, Materials and Technology Working Groups for their dedication to the JHR. In addition, the authors would like to thank Petri Kotiluoto (VTT) and Alejandro Revuelta (VTT) for the contributions to this work and the Finnish stakeholders (Business Finland, Fortum, TVO and Fennovoima) for their support of the JHR Consortium and the construction of new European NRI.

References

Guimbal, P., Villard, J-F., Auclair, M., Carassou, S., Moilanen, P., Huotilianen, S., Patalainen, M. & Tähtinen, S. 2011, Status of the MeLoDie experiment, RRFM11, 20-24 March 2011, Rome, Italy.

Huotilainen C., Tulkki, V., Moilanen, P., Kinnunen P., Kotiluoto, P. Revuelta, A. & Bignan G. 2019. Jules Horowitz Reactor – the Future of European Materials Testing Reactor, Proceedings of the Nuclear Science and Technology Symposium – SYP2019, 30-31 October, 2019, Helsinki, Finland.

JHR Operation Plan 2040, 2020. Retrieved on February 13, 2021 from www.jhop2040-h2020.eu/.

JHR 2019. MADISON, ADELINE and MICA Device testing specifics. Retrieved on June 11, 2019 from http://www-rjh.cea.fr/irradiation-devices.html.

Moilanen, P. 2004. Pneumatic servo-controlled material testing device capable of operating at high temperature water and irradiation conditions, Doctoral thesis, VTT Industrial Systems, Espoo, VTT Publications: 532. ISBN 951-38-6384-0; 951-38-6385-9.

Moilanen, P. 2020. Status of the MeLoDIE I and MeLoDIE II Experiments - Advanced Devices for Online Biaxial Study of the Irradiation Creep of LWR Cladding in Test Reactor Core. VTT Research Report VTT-R-01476-20. Espoo: VTT.

9.4 Pre-emptive reduction of radiological laboratory legacy waste (LABWAST)

Wade Karlsen

VTT Technical Research Centre of Finland Ltd
P.O. Box 1000, FI-02044 Espoo

Abstract

The infrastructure renewal of the radiological research infrastructure hosted by VTT is embodied in the new VTT Centre for Nuclear Safety. Initiated a decade ago, the renewal has proceeded well, and valuable assets have been built-up to enable high-level nuclear safety research in Finland. The renewal work reached a crescendo in the SAFIR and KYT 2018 programmes, where the focus was on constructing, equipping and licensing the new facility. The LABWAST project in the first year of the current SAFIR and KYT programs focused on taking the new facilities into full operation, with commissioning and ramp-up of operations for both reactor safety and final repository research. The LABWAST project in particular already looked to the future and eventual decommissioning of the facilities, with a particular focus on efforts to better utilize existing research materials, and developing effective means of handling the radioactive waste generated over the long term during the operation of the facilities. Simultaneously, the investment aid project RADINFRA carried out the last remaining procurements over the 2019-2020 period, mainly related to supporting facilities for handling, storage, and transport of specimens and waste.

Introduction

The LABWAST project executes the renewal of the radiological research infrastructure hosted by VTT, embodied in the new VTT Centre for Nuclear Safety. Initiated a decade ago, the infrastructure renewal has proceeded well, and valuable assets have been built-up to enable high-level nuclear safety research in Finland. The renewal work reached a crescendo in the RADLAB project of the SAFIR2018 and KYT2018 programs, with construction and licensing of the new VTT Centre for Nuclear Safety, and expansion of the license in 2018 to include the new hot cell facilities.

The VTT CNS and its hot cell facility is a national infrastructure hosted by VTT, and is considered an important element in fulfilling the national requirements for independent competencies for domestic nuclear power generation. As such, from 2016 onward, the Finnish State Nuclear Waste Management Fund (VYR) has supported the renewal of the radiological laboratory research infrastructure via three instruments: 1) the research and infrastructure instrument, generally comprised mainly of personnel, travel and associated research execution expenses; 2) a special allocation for supporting the VTT Ltd. Centre for Nuclear Safety radiological

laboratory facility expense (RADCNS), and 3) a special allocation for supporting the VTT Ltd. Centre for Nuclear Safety radiological laboratory equipment investment expenses as investment aid (RADINFRA). All three instruments have been jointly supported by the SAFIR2018 (nuclear power plant safety) and KYT2018 (nuclear waste management) research programs.

The largest equipment investment was the hot cells enabling safe handling and orderly storage of activated and contaminated materials, shown in Figure 1. The other equipment investments have primarily focused on devices for materials testing and examination activities related to assessing the structural integrity of the materials from which safety-critical components are fabricated, and analyzing deficiencies and failures of such materials that may emerge during regular inspection campaigns. The latter in particular require rapid-response availability of appropriate equipment and resources, to minimize plant shut-down time. In consideration of the co-funding by the KYT program, and reflecting the broader applicability of the VTT CNS laboratories in the nuclear sector, several devices have also been procured for bentonite studies, analytical radiochemistry, and aerosol research. These are described in the Proceedings of the SAFIR 2018 Final Seminar.

Figure 1. The new hot cells of the VTT Centre for Nuclear Safety were installed in 2017 during the SAFIR2018 program.

Additional project activities have included the design, fabrication and installation of self-built research facilities, and materials and waste-handling and storage facilities, as well as the full laboratory infrastructure commissioning and ramp-up of operations for both reactor safety and nuclear waste management research. The LABWAST project in particular already looked to the future and eventual

decommissioning of the facilities, with a particular focus on efforts to better utilize existing research materials, and to develop effective means of handling the radioactive waste generated over the long term during the operation of the facilities. The latter goal is in line with the expectation set forth in the Final Report of the National Cooperation Group on Nuclear Waste Management" (L. Kumpula, O. Slant, 2019-09-02; Publications of the Ministry of Economic Affairs and Employment 2019:45)

Specific activities in LABWAST

With the aim to facilitate *sustainable* research of radioactive materils, the LABWAST project carried out activities in legacy waste mitigation, effective utilization of finite hot material, and advancing hot analytical radiochemistry. In parallel, the RADINFRA project carried out procurements for several new pieces of equipment.

Legacy waste mitigation:

The LABWAST project explored several different approaches for minimizing the accumulation of radioactive legacy waste over the operational lifetime of the new facility. In addition to an overall review and assessment of decontamination and waste handling approaches, work focused on the three most challenging areas from the radioactive waste management perspective: the cutting and grinding debris produced during metallographic specimen preparation, the treatment of chemicals associated with metallographic processes, and the cutting-debris separation water loop of the electric-discharge machine (EDM).

Insight into the sources and mitigation of legacy waste was acquired by reviewing documentation of the decommissioning of the Otakaari 3 facilities, and identifying contamination-reduction opportunities to implement in the new facilities. An extensive literature review was carried out on decontamination and waste reduction methods, including experiences presented at the International Working Group on "Hot Laboratories and Remote Handling" annual meetings over the past few decades. The assessment resulted in a comprehensive report reviewing decontamination and waste reduction approaches with relevance to mitigating the accumulation of legacy waste in the new hot cell facilities, and applicable also in other facilities handling radioactive materials [Karlsen, W.].

Metallography waste:

For safe handling of fine debris-type of waste generated during cutting and grinding, a specific practical study was carried out in conjunction with work that involved cutting and grinding some 100 dpa Flux Thimble Tube material harvested from an operating PWR (Figure 2). The material had a Co-60 specific activity of 1.7 GBq/g. By conducting a fastidious measurement and clean-up routine following the in-cell cutting and grinding work, useful insight was gained regarding the relationship between waste generation and the hot cell decontamination process.

The liquids generated in microscopy procedures were also evaluated. The electropolishing solution used with the highly radioactive FTT material, as well as activated water from filtering out grinding and sawing debris from that material, were collected for further analysis of radioactivity, and for testing waste handling methods. Through a subcontract funded by the RADINFRA investment aid, paths were then identified for safely neutralizing radioactive acid solutions (including the particularly challenging case of perchloric acid), and their sedimentation for subsequent evaporation and cementation for safe interim storage as waste.

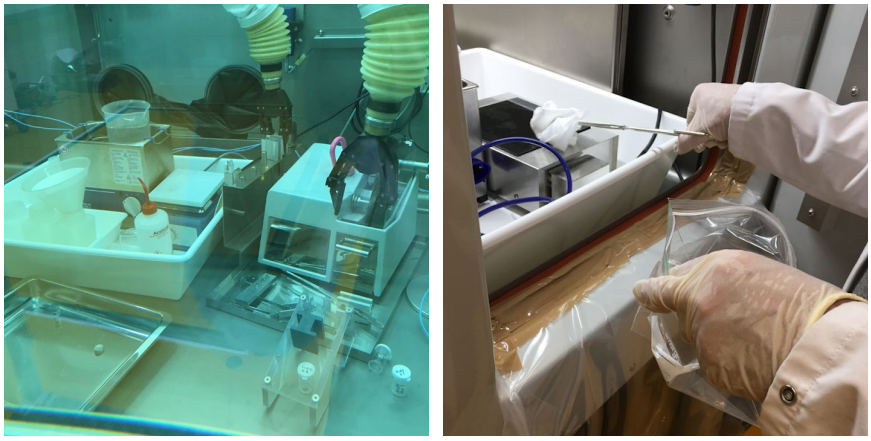

Figure 2. Cutting and grinding procedures when preparing microscopy specimens in the hot cells is a significant source of contamination and associated waste when cleaning up afterwards.

Electric discharge machining waste:
Regarding the radioactive waste generated in the EDM cutting process, a study was carried out to characterize the debris collected from different parts of the water circuit, as well as debris adhered to the spent anode wire. The debris separation system is intended to remove the radioactive EDM cutting debris to yield clean, significantly less active water for the circuit (Figure 3) [Karlsen, W., Leporanta, J., Tapper, U.]. The results were used to guide design of safe handling processes for these two waste streams.

As a part of the effort to develop the EDM debris separation circuit, a series of piloting trials were carried out involving centrifuging, automatically reversible permanent filtration, and magnetic separation. The piloting led to the ultimate decision to abandon the involvement of such additional devices in favor of simply utilizing disposable filter cartridges that are merely significantly smaller than the large OEM filter cartridges. This approach was found to improve the overall reliability of the cutting performance of the EDM, particularly in heavy cutting circumstances like that of sectioning RPV trepans (work that is featured in the SAFIR 2022 BRUTE project). Subsequent design refinement efforts and filter trials were carried out by VTT in

2020, ultimately yielding a design that is being fabricated on a subcontract made possible by RADINFRA investment aid.

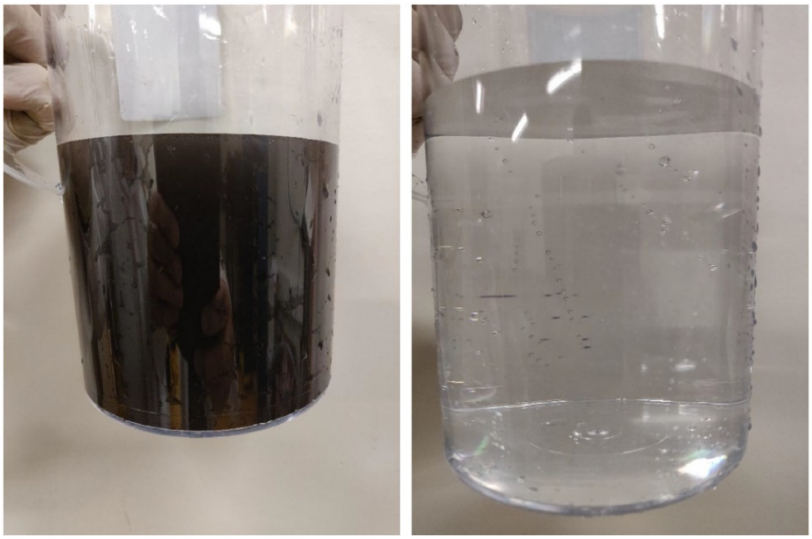

Figure 3. With the electric discharge machine operational, emphasis was placed on improving the debris separation circuit, resulting in a decision to utilize filtration to remove the particles and yield clear water. This is essential when machining radioactive materials. [Karlsen, W., Leporanta, J., Tapper, U.]

Effective utilization of finite hot material:

With an aim to utilize the radioactive specimen materials more effectively, the LABWAST project also developed in-cell specimen preparation and mechanical testing methods to facilitate reusing tested materials and minimize rejections. Effective use of test materials is particularly important for life extension propositions involving limited amounts of available reactor pressure vessel (RPV) surveillance materials.

An important milestone was the arrival and installation of the CNC milling device in the transport reception cell (Figure 4). The device features pressure-feedback clamping control for precisely fixing surveillance capsules of various sizes. The machining performance of the device was tested, particularly regarding the capability to make the small holes required for mini-CT specimens. The device testing has been carried out focusing on validating the methods required for the SAFIR2022 BRUTE project, and its subsequent testing for reliably machining specimens. Exercises were also successfully carried out to open a monolithic surveillance capsule (like that for an EPR), as well to open the strand of small surveillance capsules (like that of VVERs). Testing of reactor pressure vessel surveillance materials are essential for demonstrating the structural integrity of the RPV [Tähtinen, S., Leporanta, J.].

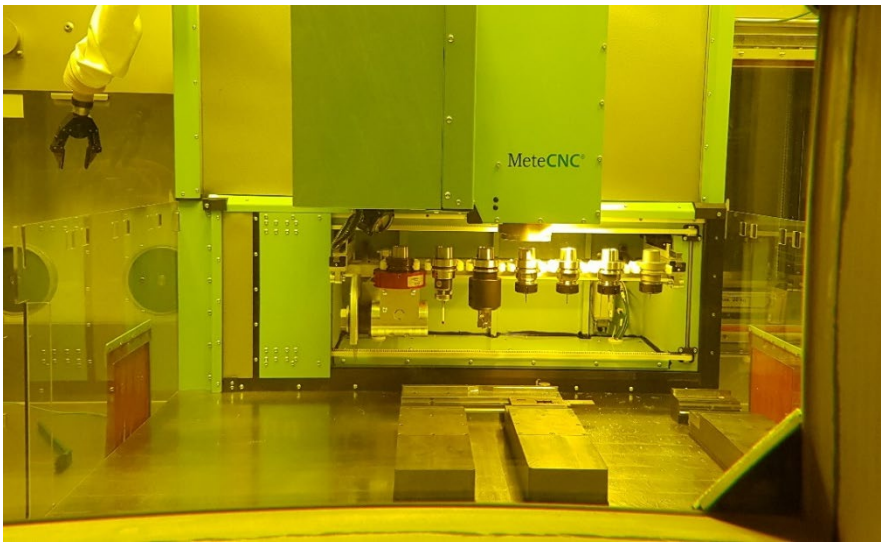

Figure 4. An important milestone was the arrival and installation of the CNC milling device in the transport reception cell in Q2/2019. [Tähtinen, S., Leporanta, J.]

In the area of mechanical testing methods, improvement in the testing capabilities was carried out, and then round-robin campaigns were carried out for both tensile and Charpy impact testing. The round-robin tests included the associated steps involving in-cell EDM cutting to prepare test specimens, quantifying the specimen dimensions by using the in-cell optical measurement device, and utilizing the non-contact laser extensometer to measure the specimen strain in tensile tests, and found that VTT devices perform satisfactorily. Reliable mechanical testing is essential both from the perspective of efficacy of the data produced, and minimization of specimen waste from rejected tests. The amount of material available with the desired neutron irradiation characteristics relevant to the operating plant is finite and the in-plant irradiation accumulation is impossible to repeat more quickly with certainty of its representativity [Arffman, P.].

Finally, the test-specimen reconstitution process was demonstrated using the in-cell EDM and electron beam welding devices (Figure 5). The specimen reconstitution is an essential method for generating additional test specimens with the same irradiation profile by using the broken pieces of specimens already tested. To improve the validation of reconstituted specimens, an infrared camera was procured for on-line monitoring of thermal input during electron beam welding. Thermal input control is essential for preventing impact to the as-irradiated condition when reconstituting specimens. Likewise, a laser engraving system was procured, and several VTT hot cell workers were then trained in its use. The device was then installed in the same hot-cell as the electron beam welder (EBW), where it can be used to label new specimens created using the EDM in the adjacent cell, and or e.g. reconstituted with the EBW [Tähtinen, S., Jokipii, M, Leporanta, J.].

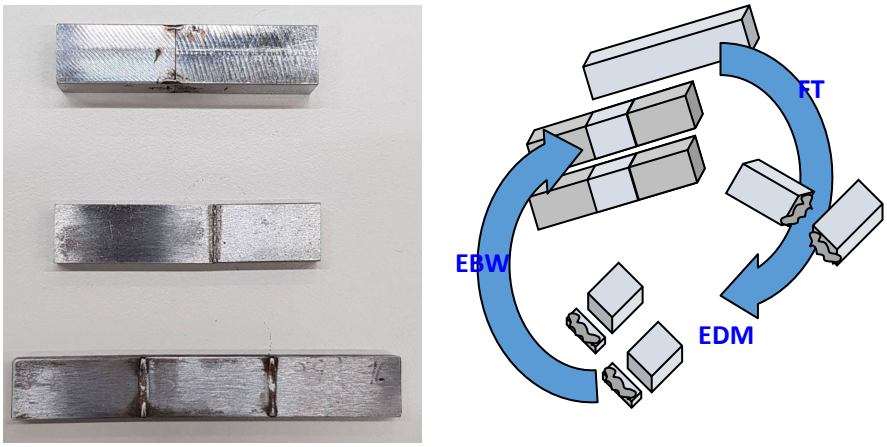

Figure 5. The readiness of the in-cell electric discharge machine and electron beam welder was demonstrated for reconstituting spent test specimens into new test specimens for RPV surveillance materials. This is a valuable tool when considering reactor life-time extension. [Tähtinen, S., Jokipii, M, Leporanta, J.]

Advances in hot analytical radiochemistry:

The LABWAST project also placed effort on developing the effective utilization of the new hot analytical radiochemistry and aerosol laboratory equipment. At the same time, the renewal of the iodine filter testing system was executed.

In the spring of 2019 a training course was held at VTT for users of the inductionally-coupled plasma optical emission device that was procured with RADINFRA investment aid in 2018. The course was hosted by VTT with Agilent Technologies, and 4 VTT people participated, as did 4 of Agilent's own employees, and 2 from SSAB. Optical emission spectrometry is an important radiochemistry analytical tool for analyzing the composition of specimens in the liquid or liquefied state, including of different isotopes [Leskinen, A.].

An alpha spectrometer that was also procured with RADINFRA investment aid in 2018, but delivered at the end of the year, was taken into use in 2019. Several VTTers were trained in its use. Then effectiveness and energy calibrations were carried out, and baseline background measurements were carried out for all four specimen chambers. In the latter part of the year, the capabilities of the alpha-spectrometer were demonstrated for accurately measuring the alpha-emitting isotopes of a material by carrying out benchmark tests with certified reference materials from the IAEA, with a Po-210 analysis kit. Many of the heavier isotopes in the nuclear fission chain decay by emitting alpha particles, so alpha spectrometry is an important radiochemistry analytical method in characterizing nuclear materials [Lavonen, T.].

Once new DustTrak aerosol measurement devices were delivered to VTT, the performance of four different aerosol measurement devices were evaluated for the measurement of CsI aerosol. CsI is a main representative aerosol in a severe nuclear power plant accident. The comparison tests showed that the devices are in quite good agreement on the number and mass concentration of the measured aerosol. A report was compiled detailing the methods and results. The experimental methods are important in developing better models for simulating severe accidents in operating nuclear power plants [Kärkelä, T., Gouëllo, M.,].

Finally, following delays in equipment delivery for the iodine laboratory, work accelerated on the fabrication of the new set-up towards the end of 2019, and it was then completed in 2020 with VTT internal resources. The facility is shown in Figure 6. The components of the new iodine set-up have been procured using RADINFRA investment aid. The iodine laboratory is an important asset for conducting the tests required to demonstrate the efficacy of the isotope-capture resins of the exhaust stacks of operating nuclear power plants.

Figure 6. The fabrication of the radioactive iodine generation set-up was completed in 2020.

Other procurements by the RADINFRA investment aid:

While the LABWAST project in 2019 and VTT's own self-funded projects have focused on carrying out the work related to procuring, nuclearizing, installing, and taking into use devices in the infrastructure renewal program, several different procurements have also been made over the 2019-2020 period utilizing the RADINFRA investment aid instrument. These are highlighted in the next paragraphs.

Hot-cell devices for reactor materials studies

Several devices were procured for installation in the hot cells. Many of the devices are related to mechanical testing, whether specimen preparation, testing, or post-test examination. Mechanical testing is essential when verifying the structural integrity of the materials that a reactor is constructed of. Other devices are related to the preparation and examination of metallographic specimens. Metallographic examination is important when conducting failure analyses, and also when examining material microstructure and microchemical features and the consequences of irradiation.

As mentioned in conjuction with demonstrating the reconstitution process for reactor pressure vessel materials, a laser engraving system was procured (Figure 7). Several VTT hot cell workers were trained in its use. The device was then installed in the same hot-cell as the electron beam welder (EBW). The device enables precise, clean, durable marking of specimens with minimal damage. By using a higher power setting, the laser can also be used for cutting out shapes in thin metal sheets, which is useful in preparing things like specimens for reactor dosimetry.

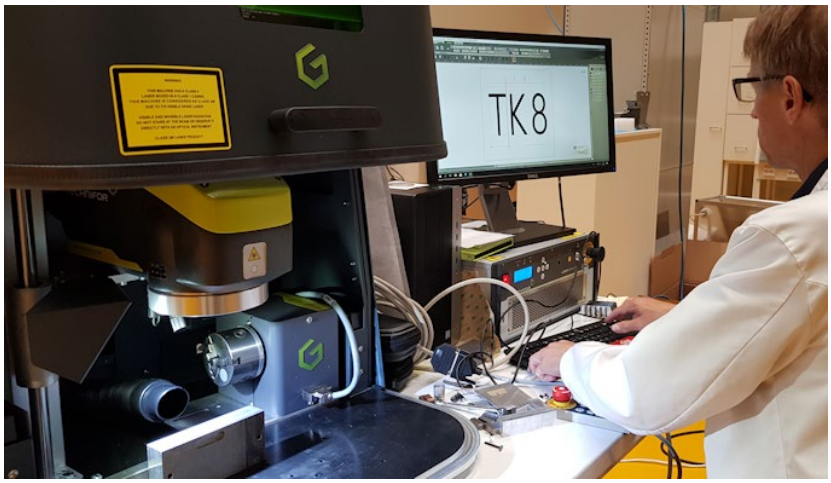

Figure 7. A laser engraving system was procured which enables precise, clean, durable marking of specimens with minimal damage.

An annealing furnace was procured for materials testing, and adaptions to it were made for utilizing it in a locally-shielded position. The furnace was utilized by the SAFIR2022 ELIAS project as part of a study into the effects of annealing on the radiation-induced hardening of reactor pressure vessel materials.

As part of the effort to improve the overall quality and reliability of the mechanical testing, an alignment tool was procured for the tensile testing machine, and a temperature probe calibration device was procured for enabling in-house calibrations. Both proper alignment and accurate temperature measurement are important aspects for producing representative mechanical test results, and since the mechanical testing equipment is located in the hot cells and used with radioactive materials, external service providers are not really an option.

Another important aspect of mechanical testing is post-test quantification of the fracture behavior by examining the fracture surface. As his bachelors thesis, Topias Käyhkö completed the remotely-operated fracture surface recording and quantification set-up. The completely tailored device utilizes a hexapod multi-axial positioning platform for ensuring precise specimen orientation, and digital imaging through a concentric lens set-up for capturing undistorted images that can be directly and accurately quantified (Figure 8). Both the hexapod device itself, and the custom design and building of the device were executed using RADINFRA investment aid funds. The work led to the Bachelor thesis “Murtopintojen kuvausjärjestelmän suunnittelu” [Käyhkö, T.] The device is installed in the dimension-measurement hot cell.

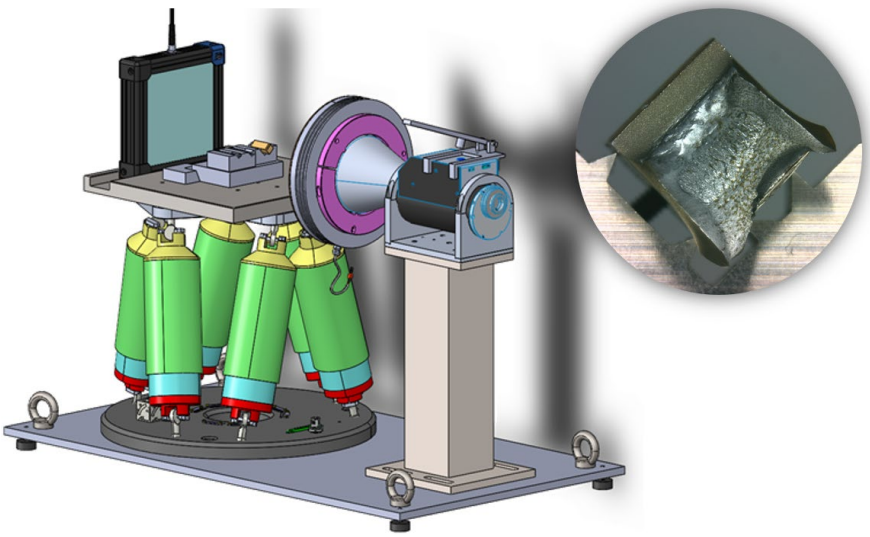

Figure 8. For examining the fracture surface of tested specimens, a tailored device was designed and fabricated which utilizes a hexapod multi-axial positioning platform for ensuring precise specimen orientation, and digital imaging through a concentric lens set-up for capturing undistorted images that can be directly and accurately quantified. [Käyhkö, T.]

Several hot-cell metallography devices were also procured and installed in the new hot cells. These included two stereo macroscopes, two devices for grinding and polishing metallography specimens, and an electro-hydraulic hot mounting press for metallographic specimens. The equipment completes the capabilities to produce cross sections of irradiated materials for subsequent examination and analysis of the microstructure by light microscopy and scanning electron microscopy. Performing cross-sectional metallography is essential when conducting failure analyses and when trying to understand the relationship between material microstructure and consequent mechanical performance, whether in question is an aged plant material, or a novel new material being considered for nuclear applications.

Laboratory devices for nuclear material and radiochemistry studies

Besides the hot cells, the CNS laboratory has many rooms for locating other pieces of equipment that require only small specimens, and thus only small quantities of radioactivity, or which otherwise relate to nuclear sector research. Besides those mentioned already in earlier sections, several other new devices were also procured with RADINFRA investment aid during 2019 and 2020.

Complementing the other capabilities for analysing reactor structural materials, a glow-discharge optical emission spectrometer (GD-OES) was procured in Q1/2020. The device is to be used in accurate measurement of trace elements of solid materials, such as the carbon content distribution in RPV materials (a goal of the SAFIR2022 BRUTE project). The device is also capable of producing depth profiles from the surface, such as the composition of oxides formed on primary circuit stainless steel materials.

A gradient ion chromatography system was also delivered in Q1/2020. The device can be used on its own for anion analysis, or connected to the high-resolution inductionally-coupled plasma mass spectrometer that is installed in the CNS cleanroom facility, for full ionic speciation analyses. Ion speciation analyses is the process of separating and quantifying different molecular versions of a compound, which can exhibit very different physiochemical properties, including varying toxicities.

As an addition to the triaxial mechanical testing facility for bentonite clay studies, a sophisticated linear voltage displacement transducer (LVDT) package was procured. The set-up enables well-controlled, on-line monitoring of triaxially-loaded geomaterials. It is used in several different projects, including the KYT2022 BROCTIO project studying bentonite behavior for nuclear waste final repository applications.

A remotely-operated, high-temperature tube furnace was procured and installed in the nuclear material handling area of the CNS (Figure 9). The device is designed to enable fabrication of unirradiated nuclear fuel and fuel-analogue ceramic materials in a very controlled manner. It involves strict control of oxygen and hydrogen contents in the atmosphere. Understanding the nuclear fuel pellet fabrication process and its research is an import part of research around nuclear fuel behavior in operation. The microstructure of the fuel in the beginning determines its thermomechanical behavior in the reactor. The furnace will be used for sintering fuel pellets in a controlled manner to separate important phenomena. [Heikinheimo, J.]

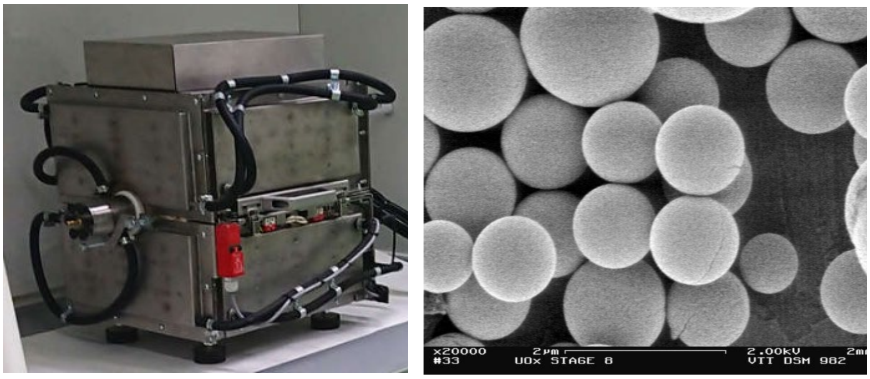

Figure 9. The high-temperature tube furnace was procured to enable fabrication of unirradiated nuclear fuel and fuel-analogue ceramic materials, for studies seeking to understand the nuclear fuel pellet fabrication processes, which can impact the performance of the fuel during operation. [Heikinheimo, J.]

Auxiliary devices for hot laboratory operations

While research and testing of radioactive materials of the nuclear sector is the primary aim of the CNS hot cells and hot laboratory facilities, there are numerous supporting activities that are required for the laboratory to operate in a safe, organized, and responsible fashion. Beyond those mentioned in the earlier sections, several other equipment procurements have also been made with RADINFRA investment aid for some of the supporting funtions.

In 2019 a gamma spectrometer was procured for the transport reception cell located in the basement of the CNS. It was installed on a mobile base so that it can be positioned at the rear of the transport reception cell 3.1, at a special aperture in the rear wall of the cell. On the inside of the cell, a custom-fabricated, movable specimen tray was installed that enables specimens of various geometries to be raised up in front of the aperature for collection of their gamma spectrum. The device is used for measuring the gamma-emitting isotopes of incoming and outgoing radioactive materials shipments, and can also be used for a first assessment of any unknown sources that may be brought to the CNS in collaboration with nuclear security response experts.

For use with many of the analytical devices, in 2019 a mobile shielding wall with a built-in shielding window was procured. As a generic device, it is used as local shielding when handling small specimens for different analytical devices, like the hydrogen analyzer. This enables added operator protection when utilizing analytical devices with specimens having elevated radioactivities.

A particularly significant milestone at the end of 2019 was the placing of an order for a custom-designed, certified A-Type irradiated materials road transport cask with Daher GmbH. The order was placed after a long and complicated tendering process, and with the recommendation of the SAFIR2022 Steerging Group 4. The

complete package includes the Type A certified cask, its auxiliary equipment (e.g. lifting beam and lifting lugs, standing frame and transport and turning frame), and two IP-2 standard dimension shipping containers for carrying the cask and its equipment by truck. The planned delivery date was the end of 2020. During 2020 the auxiliary equipment and containers were fabricated, the quality management plan (QMP) for fabrication of the cask according BAM-GGR 016 for type A /IP-2 casks was submitted to the authority for review and gained approval. The QMP included modelling and accompanying drop tests of a 1:3 model of the cask (Figure 10). However, an accident at the Daher GmbH factory in November 2020 led to the need for manufacturing a totally new cask body. The expectation is that the new cask will be finished and delivered by June 2021.

Figure 10. Certification of Daher GmbH's quality management plan for the A-Type road transport cask for irradiated materials invoved conducting drop tests of 1:3 model of the cask during Q3/2020.

Another procurement in 2020 was upgrading of the radioactive materials database system. The first version was procured in 2016–2017, and is used to facilitate the orderly storage of specimens and other radioactive materials in the CNS. Via the database, physical materials can be logged with their radioactivity, isotope make-up, and precise current location in the storage cell or other location in the laboratory, and associated with customers (owners) and projects, and additional attached information such as photos or documents. As specimens have been moved from the storage cell of the old Otakaari 3 facilities, to the new radioactive materials storage cell in the CNS, their pertinent information has been logged into the new radioactive materials database system. This has provided an opportunity to identify needed modifications to make the system more fit for purpose. A prioritized list of needs was then used for a subcontract to execute improvements to the system. The upgraded

system was then deployed successfully at the beginning of 2021, including migration of all the contents of the existing database into the new upgraded system.

Finally, as part of the on-going effort to develop a safe and reliable auxiliary water circuit for handling the radioactive debris produced by the EDM, a series of subcontracts were carried out with Platom Oy over the course of 2019-2020. As already introduced above, VTT conducted a series of piloting trials involving centrifuging, automatically reversible permanent filtration, and magnetic separation, which ultimately led to the decision to abandon the involvement of such additional devices in favor of simply utilizing disposable filter cartridges that are merely significantly smaller than the large OEM filter cartridges. In parallel to VTT's trials, the contracts with Platom produced a series of design iterations for the hardware and control systems for the alternatives being explored. The final design concept was reached in Q4/2020. As illustrated in Figure 11, it is comprised of a bank of three debris filters and one resin filter, featuring self-closing filter containers and means for dewatering the filters with compressed air. The system enables integral operation with the EDM and safe filter handling for changing the filters out. Platom Oy is fabricating the system along with a new stainless steel EDM pool and a spent anode wire collection system, with planned delivery of all components by the end of Q2/2021. Following system testing, VTT will take responsibility for designing and fabricating the needed shielding an remote handling devices for handling the debris-filled filters and activated resins.

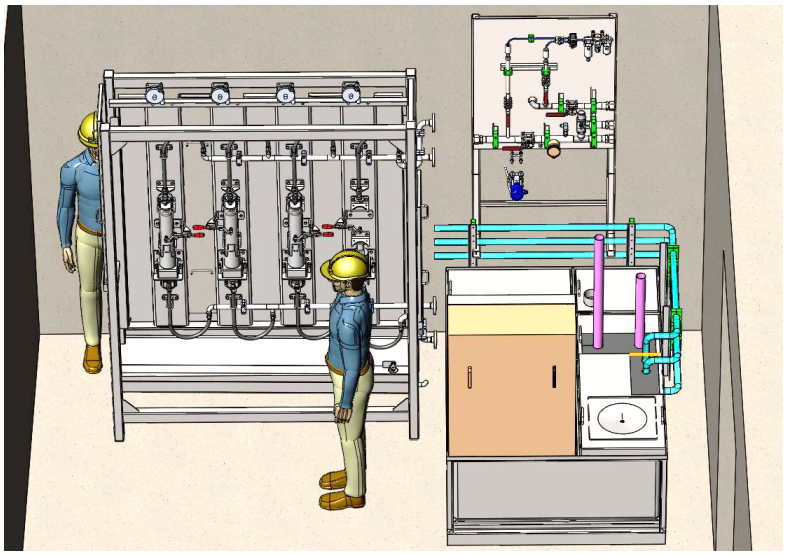

Figure 11. The final design concept for the EDM auxiliary water loop for debris separation is comprised of a bank of three debris filters and one resin filter, featuring self-closing filter containers and means for dewatering the filters with compressed air. It is being fabricated on a subcontract with Platom Oy.

Summary and conclusions

Having been initiated a decade ago, the nuclear materials research and testing infrastructure renewal embodied in the VTT Centre for Nuclear Safety has proceeded well, and valuable assets have been built-up to enable high-level nuclear safety research in Finland. In the first two years of the SAFIR- and KYT2022 programs the LABWAST project (2019) and RADINFRA investment aid project have made significant strides in taking the new infrastructure into operation for testing and research, and carried out the last procurements of scientific devices and key supporting infrastructure. The research and testing capacity is already being utilized in over 50 different jointly funded and contract research and testing projects. The projects represent the entire spectrum of the nuclear power plant lifecycle, from materials-issues of new-build powerplants through aspects of aging of materials in long-term operation, and from decommissioning challenges through spent fuel final repository issues. In addition to continuing to expand the utilization of the new facility in research and testing, the work that was initiated in the LABWAST project will continue to seek sustainable waste management and interim storage solutions for the operational waste associated with the research and testing activities.

Acknowledgment

VTT wishes to acknowledge the important support of the Finnish Nuclear Waste Management Fund, VYR for making the infrastructure renewal financially possible.

References

Karlsen, W. “Radiological laboratory commissioning (RADLAB)” in SAFIR2018 – The Finnish Research Programme on Nuclear Power Plant Safety 2015–2018 Final Report, J. Hämäläinen & Vesa Suolanen (eds.) ISBN 978-951-38-8682-0, VTT Technology 349, ISSN-L 2242-1211, ISSN 2242-122X (Online) DOI: 10.32040/2242-122X.2019.T349, Copyright © VTT (2019), pp. 471-498.

Karlsen, W., Review of advanced waste reduction approaches, VTT Report VTT-R-01239-19, 2019, 31p.

Karlsen, W., Leporanta, J., Tapper, U., Efficacy of EDM debris separation system, VTT Report VTT-R-01253-19, 2020, 33p.

Tähtinen, S., Leporanta, J. Functionality of remote-controlled CNC milling machine in hot cell, VTT Report VTT-R-00886-20, 26p.

Tähtinen, S., Jokipii, M, Leporanta, J., Report on reconstitution technique at the CNS hot cells, VTT Report VTT-R-00056-20, 2020, 12p.

Arffman, P., Iskukokeet referenssimateriaalilla, VTT Report VTT-R-01186-19, 2019, 8p.

Arffman, P., Mekaanisen testauksen vertailukokeet YTT:ssa 2019, VTT Report VTT-R-01187-19, 2019, 17p.

Lavonen, T., Functionality report of alpha spectrometer, VTT Report VTT-R-01148-19, 2019, 21p.

Kärkelä, T., Gouëllo, M., Comparison of online aerosol measurement devices using CsI aerosol, VTT Report VTT-R-00063-20, 18p.

Käyhkö, T., ”Murtopintojen kuvausjärjestelmän suunnittelu” Bachelors Thesis, Metropolia https://www.theseus.fi/handle/10024/260870

Myllykylä, E., Helosuo, K., KURSSIRAPORTTI ICP-OES 51XX käyttäjäkurssi 16-17.4.2019 (VTT)

Leskinen, A., Functionality report of ICP-OES Device, VTT Report VTT-R-04334-18, 2018, 76p.

Karlsen, W., New VTT Hot Cells in Operation, Suomalaisen Ydintekniikan Päivät 2019- SYP2019. https://ats-fns.fi/fi/suomalaisen-ydintekniikan-paivat/proceedings-2019

Heikinheimo, J., High-Temperature Experimental Techniques for Nuclear Fuel Separate Effect Tests, Suomalaisen Ydintekniikan Päivät 2019- SYP2019. https://ats-fns.fi/fi/suomalaisen-ydintekniikan-paivat/proceedings-2019

Series title and number

VTT Technology 383

Title	**SAFIR2022 – The Finnish Research Programme on Nuclear Power Plant Safety 2019–2022** Interim Report
Author(s)	Jari Hämäläinen & Vesa Suolanen (eds.)
Abstract	The Finnish Research Programme on Nuclear Power Plant Safety 2019–2022, SAFIR2022, continues a series of Finnish national research programmes in nuclear energy that started in 1989. The programmes were initially carried out separately in the fields of operational aspects of safety (YKÄ 1990–1994, RETU 1995–1998) and structural safety (RATU 1990–1994, RATU2 1995–1998, OHA 1995–1998), and then in combined programmes (FINNUS 1999–2002, SAFIR2003–2006, SAFIR2010 2007–2010, SAFIR2014 2011–2014, SAFIR2018 2015–2018). Simultaneously research has been carried out in the national nuclear waste management programmes (KYT2022 runs in parallel with SAFIR2022). SAFIR2022 consists of four main research areas: (1) Overall safety and systemic approach to safety; (2) Reactor safety; (3) Structural safety and materials; and (4) Research infrastructure. Research has been carried out in 36 projects that are guided by eight reference groups. The research results of the projects are published in scientific journals, conference papers and research reports. The programme management structure consists of the Management Board, four steering groups managing the research areas, eight reference groups, and programme administration. SAFIR2022 Management Board has representatives of the Radiation and Nuclear Safety Authority (STUK), the Ministry of Economic Affairs and Employment (MEAE), Fennovoima Oy, Fortum, Teollisuuden Voima Oyj (TVO), Technical Research Centre of Finland Ltd (VTT), Lappeenranta-Lahti University of Technology (LUT), Aalto University (Aalto), Tampere University (TAU) and the Swedish Radiation Safety Authority (SSM). Research in the programme has been carried out by VTT, LUT, Aalto, Finnish Meteorological Institute (FMI), Finnish Institute of Occupational Health (FIOH), TAU and RISE Research Institutes of Sweden. A few subcontractors have also contributed to the work in the projects. This report has been prepared by the programme management in cooperation with the project leaders and project staff. More information on SAFIR2022 can be found on the programme website http://safir2022.vtt.fi
ISBN, ISSN, URN	ISBN 978-951-38-8743-8 ISSN-L 2242-1211 ISSN 2242-122X (Online) DOI: 10.32040/2242-122X.2021.T383
Date	March 2021
Language	English
Pages	472 p.
Name of the project	The Finnish Nuclear Power Plant Safety Research Programme 2019-2022, SAFIR2022
Commissioned by	MEAE
Keywords	nuclear safety, safety management, nuclear power plants, human factors, safety culture, automation systems, control room, nuclear fuels, reactor physics, core transient analysis, thermal hydraulics, modelling, severe accidents, structural safety, construction safety, risk assessment, research infrastructure
Publisher	VTT Technical Research Centre of Finland Ltd P.O. Box 1000, FI-02044 VTT, Finland, Tel. 020 722 111, https://www.vttresearch.com

SAFIR2022 – The Finnish Research Programme on Nuclear Power Plant Safety 2019–2022

Interim Report

ISBN 978-951-38-8743-8
ISSN-L 2242-1211
ISSN 2242-122X (Online)
DOI: 10.32040/2242-122X.2021.T383

VTT beyond the obvious